

**Contributing Editor**

**ABDULLAH A. AL-BADR**

**Founding Editor**

**KLAUS FLOREY**



# Azithromycin

**Ahmed H.H. Bakheit<sup>\*</sup>, Badraddin M.H. Al-Hadiya<sup>†</sup>,  
Ahmed A. Abd-Elgalil<sup>‡</sup>**

<sup>\*</sup>Department of Pharmaceutical Chemistry, College of Pharmacy, King Saud University, Riyadh, Kingdom of Saudi Arabia

<sup>†</sup>Department of Pharmaceutical Chemistry, College of Pharmacy, Taif University, TAIF, KSU

<sup>‡</sup>Research Center, College of Pharmacy, King Saud University, Riyadh, Kingdom of Saudi Arabia

## Contents

Background	2
1. Description	2
1.1 Nomenclature	2
1.2 Formulae	3
1.3 Elemental analysis	4
1.4 Appearance	4
2. Methods of Preparation of Azithromycin	4
3. Physical Characteristics	5
3.1 Specific optical rotation	5
3.2 Ionization constant	6
3.3 Solubility characteristics	6
3.4 Partition coefficient	6
3.5 Particle morphology	6
3.6 Crystallographic properties	7
3.7 Hygroscopicity	7
3.8 Thermal methods of analysis	9
3.9 Spectroscopy	12
3.10 Mass spectrometry	17
4. Methods of Analysis	17
4.1 Compendial methods of analysis	17
4.2 Electrochemical methods of analysis	24
4.3 Spectroscopic methods of analysis	25
4.4 Chromatographic methods of analysis	28
4.5 Determination in body fluids and tissues	30
5. Stability	30
6. Clinical Applications	33
6.1 An overview	33
6.2 Antimicrobial spectrum susceptibility	33
6.3 Mechanism of action	33
6.4 Resistance to macrolides	34
6.5 Actions other than antimicrobial effects	34

6.6	Clinical uses and dosing	35
6.7	ADME profile	35
6.8	Side effects	36
6.9	Drug interactions	36
References		36



## BACKGROUND

A team of researchers at the Croatian pharmaceutical company Pliva, led by Dr. Slobodan Đokić, discovered azithromycin in 1980. It was patented in 1981. Pfizer launched azithromycin under Pliva's license in other markets under the brand name Zithromax in 1991. After several years, the U.S. Food and Drug Administration approved AzaSite, an ophthalmic formulation of azithromycin, for the treatment of eye infections [1].



## 1. DESCRIPTION

### 1.1. Nomenclature

#### 1.1.1 Systematic chemical names [2–5]

(2*R*,3*S*,4*R*,5*R*,8*R*,10*R*,11*R*,12*S*,13*S*,14*R*)-13-(2,6-dideoxy-3-*C*-3-*O*-dimethyl- $\alpha$ -*L*-ribo-hexopyranosyloxy)-2-ethyl-3,4,10-trihydroxy-3,5,6,8,10,12,14-heptamethyl-11-(3,4,6-trideoxy-3-dimethylamino- $\beta$ -*D*-xylo-hexopyranosyloxy)-1-oxa-6-aza-cyclopentadecan-15-one dehydrate.

(2*R*,3*S*,4*R*,5*R*,8*R*,10*R*,11*R*,12*S*,13*S*,14*R*)-2-ethyl-3,4,10-trihydroxy-3,5,6,8,10,12,14-heptamethyl-15-oxo-11-{[3,4,6-trideoxy-3-(dimethylamino)- $\beta$ -*D*-xylo-]oxy}-1-oxa-6-azacyclopentadec-13-yl 2,6-dideoxy-3-*C*-methyl-3-*O*-methyl- $\alpha$ -*L*-ribo-hexopyranoside.

(2*R*,3*S*,4*R*,5*R*,8*R*,10*R*,11*R*,12*S*,13*S*,14*R*)-13-[(2,6-dideoxy-3-*C*-methyl-3-*O*-methyl- $\alpha$ -*L*-ribo-hexopyranosyl)oxy]-2-ethyl-3,4,10-trihydroxy-3,5,6,8,10,12,14-heptamethyl-11-[[3,4,6-trideoxy-3-(dimethylamino)- $\beta$ -*D*-xylo-hexopyranosyl]oxy]-1-oxa-6-azacyclopentadecan-15-one.

(2*R*,3*S*,4*R*,5*R*,8*R*,11*R*,13*S*,14*R*)-11-(((2*S*,3*S*,4*S*,6*R*)-4-(dimethylamino)-3-hydroxy-6-methyltetrahydro-2*H*-pyran-2-yl)oxy)-2-ethyl-3,4,10-trihydroxy-13-(((2*R*,4*R*,5*S*,6*S*)-5-hydroxy-4-methoxy-4,6-dimethyltetrahydro-2*H*-pran-2-yl)oxy)-3,5,6,8,10,14-hexamethyl-1-oxa-6-azacyclopentadecan-15-one.

*N*-methyl-11-aza-10-deoxo-10-dihydroerythromycin A; 9-deoxo-9a-methyl-9a-aza-homoerythromycin A; CP-62993; XZ-450; Azitrocin; Sumamed; Trozocina; Zithromax; Zitromax.

### 1.1.2 Nonproprietary names

Generic [6]: azithromycin

Synonyms [2–7]: Atsitromysiini; Azithromycine; Azithromycinum; Azitromicina; Azitromicinas; Azitromisin; Azitromycin; Azytromycyna; CP-62993; XZ-450; Azithramycine; Azithromycin Dihydrate; Azithromycine [French]; Azithromycinum [Latin]; Azitromicina [Spanish].

### 1.1.3 Proprietary names [3,7,8]

Azacid<sup>®</sup> (Biosen: TR); Azitromin<sup>®</sup> (Farmasa: BE); Azitromax<sup>®</sup> (Pfizer: NO); Azro<sup>®</sup> (Eczacibasi: TR); Cronopen<sup>®</sup> (Elea: AR); Hemomycin<sup>®</sup> (Hemofarm: YU); Misultina<sup>®</sup> (Microsules: AR); Mixoterin<sup>®</sup> (Roux-Ocefa: AR); Sumamed<sup>®</sup> (Pliva: CZ, HR, PL); Triamid<sup>®</sup> (Beta: AR); Zifin<sup>®</sup> (Pratapa: ID); Zithrax<sup>®</sup> (Dankos: ID); Zithromax<sup>®</sup> (Pfizer: NL); Zitromax<sup>®</sup> (Pfizer: AR, BE, LU, TR); Zitrotek<sup>®</sup> (Pfizer: TR);

*Dihydrate*: Arzomicin<sup>®</sup> (Sintyal: AR); Azadose<sup>®</sup> (Pfizer: FR); Azatek<sup>®</sup> (Biosen: TR); Azithral<sup>®</sup> (Alembic: IN); Azitrin<sup>®</sup> (Andromaco: AR); Azitro<sup>®</sup> (Deva: TR); Azitrocin<sup>®</sup> (Pfizer: MX); Azitrocin<sup>®</sup> (Roerig: IT); Azitromax<sup>®</sup> (Pfizer: NO,SE); Azitromicina Richet<sup>®</sup> (Richet: AR); Azitrotek<sup>®</sup> (Deva: TR); Aziwok<sup>®</sup> (Wockhardt: IN); Azomax<sup>®</sup> (Kocak: TR); Azro<sup>®</sup> (Eczacibasi: TR); Cronopen<sup>®</sup> (Elea: AR); Goxal<sup>®</sup> (Pharmacia: ES); Ribotrex<sup>®</sup> (Pierre Fabre: IT); Toraseptol<sup>®</sup> (Lesvi: ES); Triamid<sup>®</sup> (Beta: AR); Trozocina<sup>®</sup> (Sigma-Tau: IT); Ultreon<sup>®</sup> (Pfizer: DE); Vinzam<sup>®</sup> (Funk: ES); Zentavion<sup>®</sup> (Vita: ES); Zistic<sup>®</sup> (Bernofarm: ID); Zithromax<sup>®</sup> (Bayer: DE); Zithromax<sup>®</sup> (Mack: DE); Zithromax<sup>®</sup> (Pfizer: AT, AU, CA, CH, FI, FR, ID, IE, IN, PT, UK, US); Zitromax<sup>®</sup> (Pfizer: BE, BR, DK, ES, IT).

## 1.2. Formulae [2,3]

### 1.2.1 Empirical formula, molecular weight, CAS number

	Empirical formula	Molecular weight	CAS number
Anhydrous azithromycin	$C_{38}H_{72}N_2O_{12}$	748.984	83905-01-5
Monohydrate azithromycin	$C_{38}H_{72}N_2O_{12}H_2O$	767.02	121479-24-4
Azithromycin dihydrate	$C_{38}H_{72}N_2O_{12}2H_2O$	785.0	117772-70-0

### 1.2.2 Structural formula

See Figure 1.1



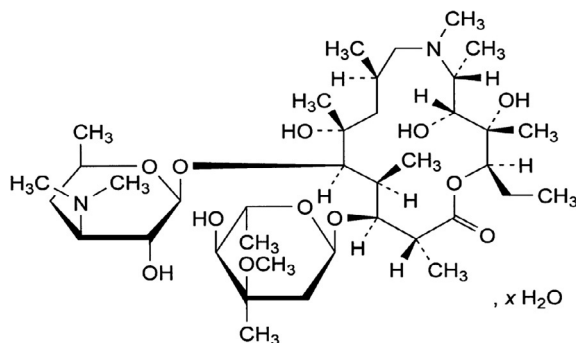


**Figure 1.1** Structural formula of azithromycin hydrate.

### 1.3. Elemental analysis

The theoretical elemental composition of azithromycin is as follows [5]:

Carbon: 60.94 %; Hydrogen: 9.69%; Nitrogen: 3.74%; Oxygen: 25.63%

### 1.4. Appearance [2]

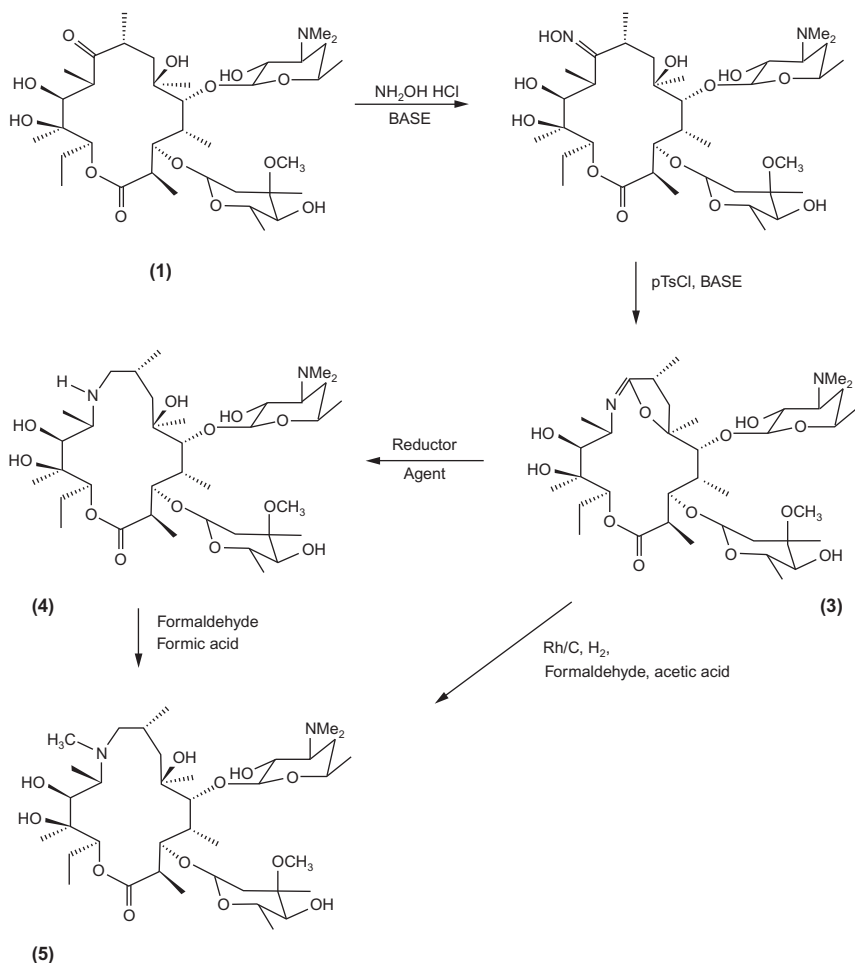
A white or almost white powder.



## 2. METHODS OF PREPARATION OF AZITHROMYCIN

Azithromycin (**5**) was prepared from erythromycin A [9,10] by treating the erythromycin (**1**) in methanol with hydroxylamine hydrochloride and a base at reflux temperature for 10 h to form oxime (**2**). The oxime was isolated, purified, and subjected to Beckmann's rearrangement to obtain the intermediary (6,9-iminoether) (**3**) (Scheme 1.1) in aqueous acetone in the presence of *p*-toluenesulfonyl chloride and base for 2 h at 5 °C (and 2 h more at room temperature). The iminoether was reduced to the secondary amine (**4**) with sodium borohydride in methanol [11,12] or by catalytic hydrogenation in the presence of platinum dioxide and acetic acid as solvents [13].

Another alternate synthetic method for azithromycin is reported [14] The iminoether (**3**) was prepared in single step (Scheme 1.2) from erythromycin A (**1**), by treating the erythromycin A (**1**) solution in acetone with *O*-mesitylene-sulfonylhydroxylamine, to form the mesitylenesulfonyloxime “*in situ*” from erythromycin A, which was treated with an aqueous base (sodium bicarbonate) at 0 °C, and then the intermediary 6-9-iminoether (**3**) (Scheme 1.2) was produced by a Beckmann's rearrangement. The iminoether (**3**) was reduced with reductive methylation using common techniques [15] to obtain azithromycin (**5**).



**Scheme 1.1** Beckmann's rearrangement to obtain the intermediary (6,9-iminoether) for preparation of Azithromycin.

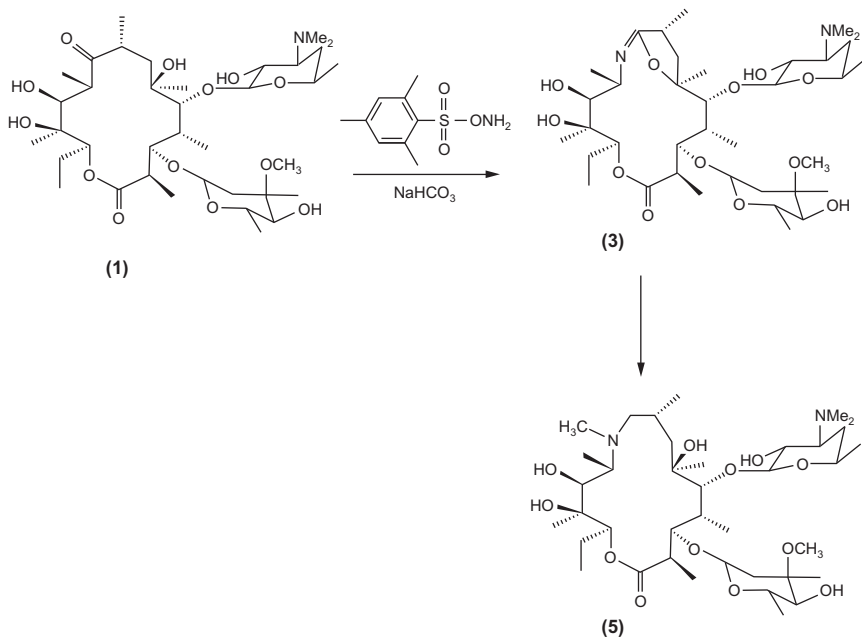
Azithromycin is a semisynthetic 15-membered macrolide antibiotic, which is derived from erythromycin A by a sequence of oximation, Beckmann rearrangement, reduction, and N-methylation [16–19]. Rengaraju *et al.* [20] improved process for preparing nonhygroscopic azithromycin dehydrate.



### 3. PHYSICAL CHARACTERISTICS

#### 3.1. Specific optical rotation [5,21]

$[\alpha]^{20} -45^\circ$  to  $-49^\circ$  (anhydrous substance) (C = 1 in anhydrous ethanol R)  
 $[\alpha]^{20} -37^\circ$  (C = 1 in  $\text{CHCl}_3$ )



**Scheme 1.2** An alternate synthetic method for Azithromycin.

### 3.2. Ionization constant [22]

$$\text{p}K_a = 7.34$$

### 3.3. Solubility characteristics [21]

Azithromycin is practically insoluble in water and freely soluble in anhydrous ethanol and methylene chloride.

### 3.4. Partition coefficient

The octanol/water partition coefficient ( $K_{ow}$ ) of azithromycin was 0.65 at 20 °C and pH 7 [23]. Adsorption isotherm studies indicated that the thermodynamic data revealed that the adsorption of azithromycin on the surface of zinc was endothermic, spontaneous, and consistent with the adsorption model of Langmuir [24].

### 3.5. Particle morphology

Gandhi *et al.* [25] viewed the commercial sample, dehydration and monohydration of azithromycin by scanning electron microscopy (Jeol electron

microscope, D-6000, Japan). The samples were sputter coated with gold before examination, and they found that the internal crystal structure appears to be the same, as is evident from the similar enthalpy of fusion for all three samples [26].

### 3.6. Crystallographic properties

#### 3.6.1 Single crystal structure

Data were collected at room temperature using Bruker X-ray diffractometers equipped with copper radiation and graphite monochromators. Structures were solved using direct methods. The SHELXTL computer library provided by Bruker AXS, Inc. facilitated all necessary crystallographic computations and molecular displays (SHELXTL™ Reference Manual, Version 5.1, Bruker AXS, Madison, WI, USA) [14].

The molecular structure of the anhydrous crystalline azithromycin obtained is shown in Figure 1.2, and the structure was elucidated by single crystal X-ray diffraction, finding that it coincides with the anhydrous crystalline form, with a tetragonal crystal system and the space group  $P4_22_12$ . These and other crystallographic data from the diffraction analysis are compared with data reported for the dihydrated crystalline form. A displays peaks at 9.3, 13.0 and 18.7 degrees of 2-theta [27].

#### 3.6.2 X-ray powder diffraction pattern [28]

The X-ray powder diffraction pattern of azithromycin has been measured using a Bruker D5000 diffractometer (Madison, Wis.) equipped with copper radiation, fixed slits (1.0, 1.0, 0.6 mm), and a Kevex solid state detector. The pattern obtained is shown in Figure 1.3, and Azithromycin dehydrate displays peaks at 7.2, 7.9, 9.3, 9.9, 11.2, 12.0, 12.7, 13.0, 14.0, 15.6, 16.0, 16.4, 16.8, 17.5, 18.2, 18.7, 19.1, 19.8, 20.5, 20.9, 21.2, 21.6, 21.8, and 24.0, the data was collected from 3.0 to 40.0 degrees in 2-theta using a step size of 0.04 degrees and a step time of 1.0 seconds.

### 3.7. Hygroscopicity

Azithromycin was found to exhibit pseudopolymorphism and can exist as monohydrate and dihydrate. The anhydrous form of AZI seemed to be unstable since it converted to dihydrate on storage at room temperature. On the other hand, monohydrate in the presence of moisture can convert

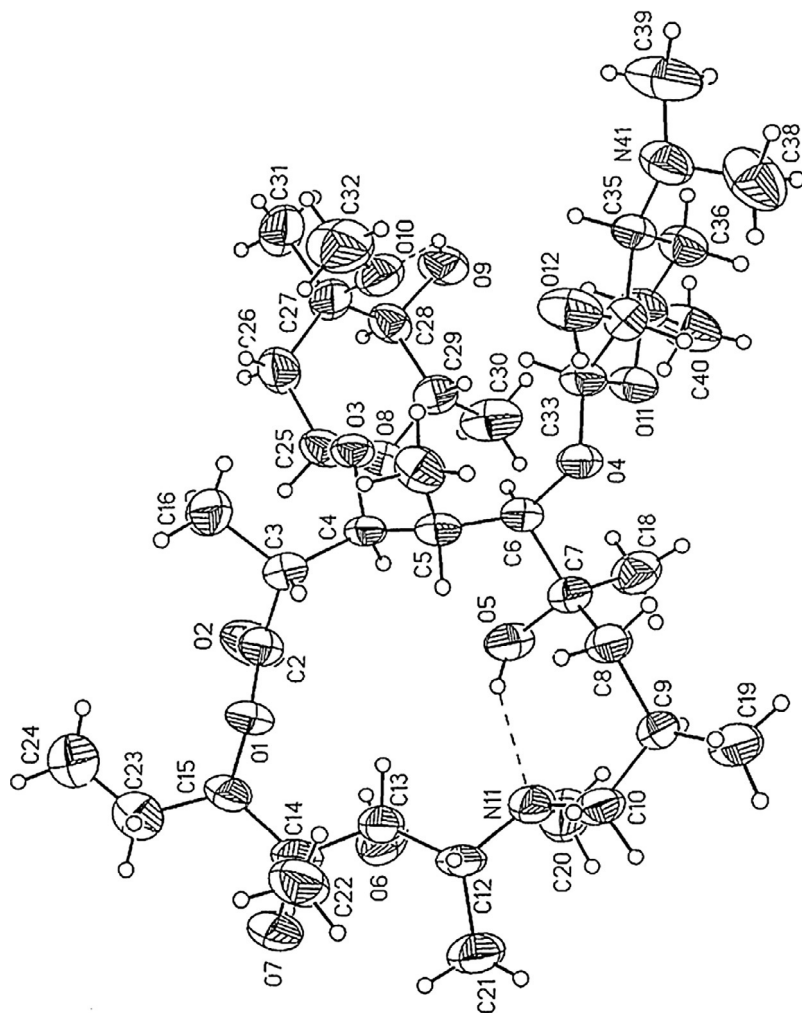


**Figure 1.2** An X-ray crystal structure of the crystalline anhydrous azithromycin.

to the more stable dihydrate form. Therefore, the most stable form of AZI is dehydrate [25].

Allen *et al.* [29] found that azithromycin was obtained as hygroscopic monohydrate when it was prepared by crystallization from ethanol and water, and nonhygroscopic dehydrate azithromycin was prepared by crystallization from tetrahydrofuran and aliphatic ( $C_5$ – $C_7$ ) hydrocarbon in the presence of at least two molar equivalents of water.

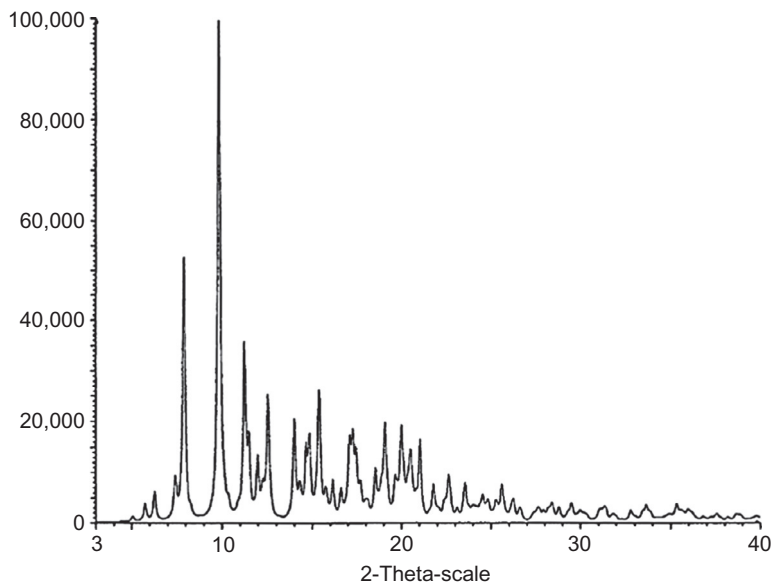


**Figure 1.3** An experimental powder X-ray diffraction pattern of azithromycin dehydrate [8].

### 3.8. Thermal methods of analysis

#### 3.8.1 Melting behavior

The melting range of azithromycin crystals is between 113 and 115 °C [5].

#### 3.8.2 Differential scanning calorimetry [25]

The differential scanning calorimetry (DSC) thermogram of azithromycin was recorded on a DSC (Mettler, Toledo DSC 821 Switzerland) using Mettler Star system. The curve shown in Figure 1.4 was collected from 0 to 250 °C with nitrogen purging (80 ml/min), and using a heating rate of 10 °C/min. DSC thermograms of anhydrous, dehydrate, and monohydrate are shown in Figure 1.4, and the thermal characteristics are shown in Table 1.1.

#### 3.8.3 Thermogravimetric analysis

Thermogravimetric analysis was carried out using TGA (Mettler, LMI JM Switzerland) apparatus. The samples (1–5 mg) were placed in aluminum pans and heated up to 250 °C at a rate of 1 °C/min under nitrogen purge (40 ml/min). The TGA thermogram obtained with the AZC sample is given in Figure 1.5. This thermogram exhibited the transition from the dihydrate to the anhydrous form of azithromycin. The observed weight loss

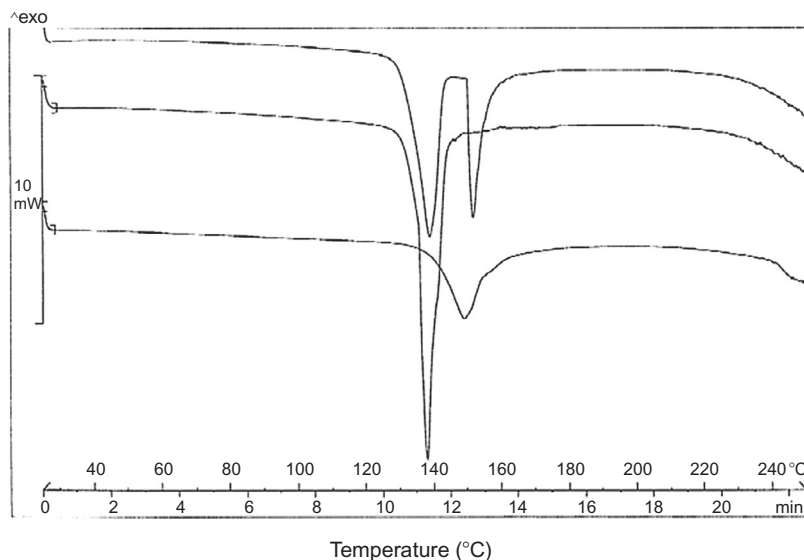


**Figure 1.4** DSC thermograms of different forms of AZI. Upper curve depicts the commercial sample of AZI; middle curve shows the endotherm of dihydrate (DH) and lower curve shows the endotherm of monohydrate (MH). The thermograms were generated using a sealed pan.

**Table 1.1** Thermal analysis and KFT of different forms of AZI

Sample name	DSC analysis		Water content	
	Temperature range (°C)	Heat fusion (J/g)	TGA (%)	KFT (%)
<i>Anhydrous azithromycin</i>	132.29–143.09	62.73 ± 7.13	4.452 ± 0.18	4.57 ± 0.03
	149.83–155.48	30.41 ± 2.93		
<i>Monohydrate azithromycin</i>	134.65–155.48	92.99 ± 8.58	4.155 ± 0.41	4.35 ± 0.28
<i>azithromycin dihydrate</i>	139.88–156.31	92.83 ± 2.41	2.472 ± 0.41	2.39 ± 0.79

of 4.38% corresponded to the stoichiometric weight loss of two water molecules [30].

Gandhi *et al.* [25] were found a stoichiometric weight loss of two water molecules (theoretical weight loss 4.58%) for CS and DH by TGA, while MH showed a weight loss corresponding to one molecule of water (theoretical weight loss 2.29%) as shown in Figure 1.6. The results were in good

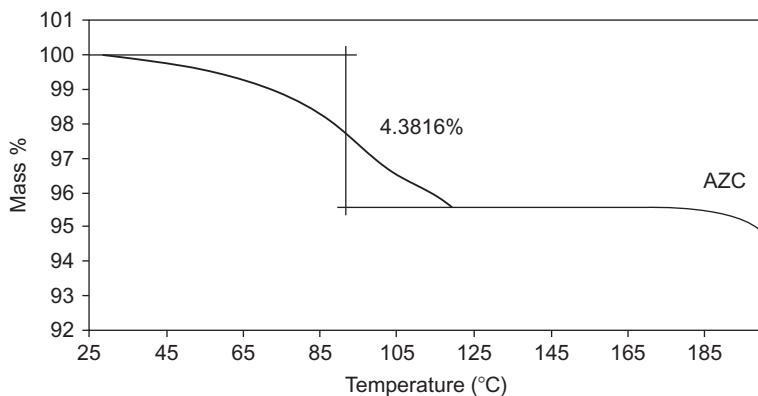


Figure 1.5 TGA thermogram of AZC.

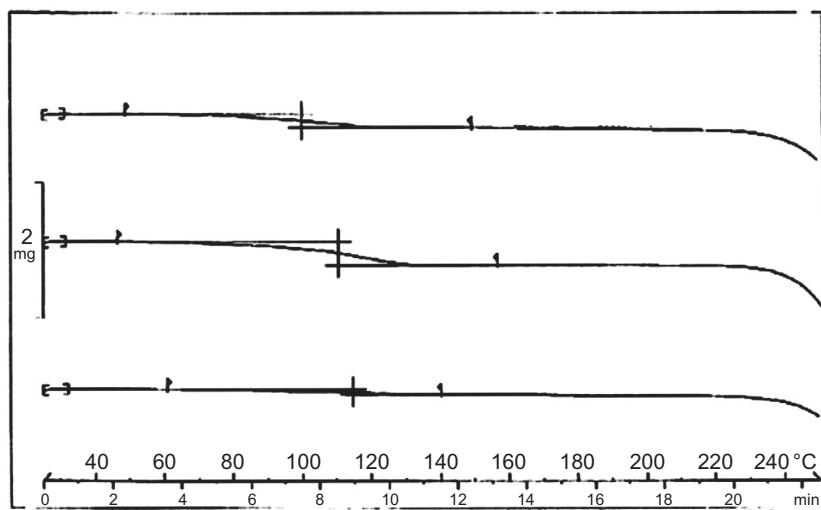


Figure 1.6 TGA thermograms of different forms of AZI. Upper curve indicates stoichiometric weight loss of two water molecules in CS, middle curve indicates weight loss of two water molecules in DH, and lower curve indicates weight loss of one water molecule in MH.

agreement with those found by Karl Fischer titration KFT as shown in Table 1.1.

### 3.8.4 Karl Fischer titration (KFT) [25]

Water content in different forms of AZI was determined using a Karl Fischer titrimeter (Metrohm, 716 DMS, Switzerland). Samples (20–25 mg) were



accurately weighed and quickly transferred to the titration vessel containing anhydrous methanol.

### **3.8.5 Boiling point, enthalpy of vapor, flash point, and vapor pressure**

The calculated value of the boiling point of azithromycin under a pressure of 760 mmHg was 822.1 °C. The enthalpy of vapor calculated value was 135.99 KJ/mol. The value of flash point was found to be 451 °C, and the vapor pressure was calculated to be  $251 \times 10^{-31}$  mmHg at 25 °C [31].

## **3.9. Spectroscopy**

### **3.9.1 UV/Vis spectroscopy**

The ultraviolet spectrum of azithromycin dihydrate in methanol and mobile phase (methanol: acetonitrile: phosphate buffer pH 6.7: tetrahydrofuran, 15:25:60:2.5, v/v) shown in Figure 1.7. The figures were recorded using a double beam Model GBC 916UV VIS spectrophotometer (GBC Scientific Equipment Pty Ltd., Melbourne, Victoria, Australia). The values of wavelength maximum in nanometer ( $\lambda_{\text{max}}$ ) are 201.6 nm on methanol and 199.2 nm on mobile phase. The spectra of azithromycin in methanol (Figure 1.7A) and mobile phase (Figure 1.7B) were shown below.

### **3.9.2 Vibrational spectroscopy [32]**

The infrared absorption spectrum of azithromycin is shown in Figure 1.8. It was obtained in a KBr disc using a FT-IR Nicolet<sup>®</sup> Imoact 410 instrument, infrared spectrophotometer. The principal peaks were 3561, 3496, 13344, 1282, 1269, 1251, and 1083.

### **3.9.3 Nuclear magnetic resonance spectrometry [33]**

#### **3.9.3.1 <sup>1</sup>H NMR spectrum [33]**

The <sup>1</sup>H nuclear magnetic resonance (NMR) spectrum of AZI was recorded using an internal deuterium lock at ambient probe temperatures on the following instruments: Bruker DPX-400 (400 MHz), Bruker Avance DRX-400 (400 MHz), Bruker Avance 500 BB-ATM (500 MHz), and Bruker Avance 500 Cryo Ultrashield (500 MHz). An internal reference of  $\delta_{\text{H}}$  7.26 was used for the residual CHCl<sub>3</sub> in CDCl<sub>3</sub>. Data are represented as follows: chemical shift (in ppm to the nearest 0.01 ppm), integration, multiplicity (s, singlet; d, doublet; t, triplet; q, quartet; m, multiplet), coupling constant (*J* in Hz to the nearest 1 Hz), and assignments, which were determined either on the basis of unambiguous chemical shift or coupling pattern,

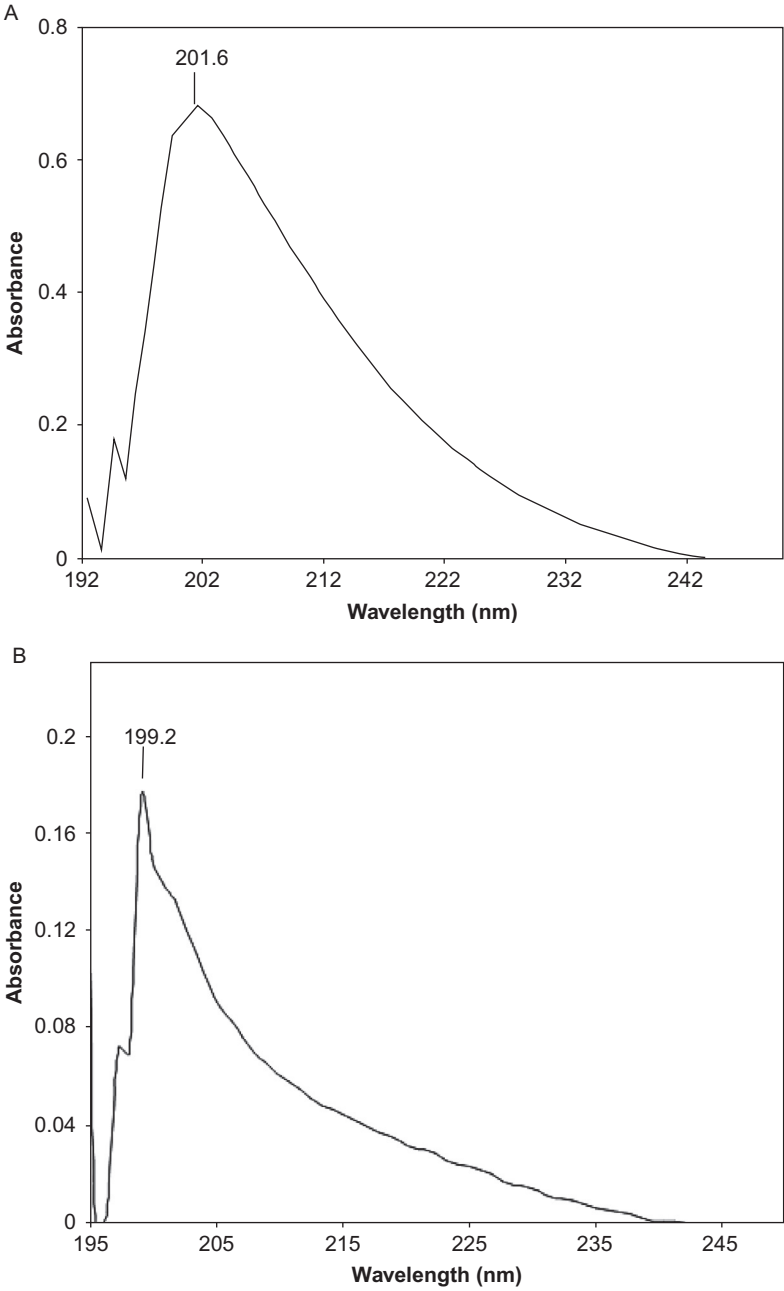


**Figure 1.7** (A) The ultraviolet spectrum of AZI dihydrate in methanol. (B) The ultraviolet spectrum of AZI dihydrate in mobile phase.

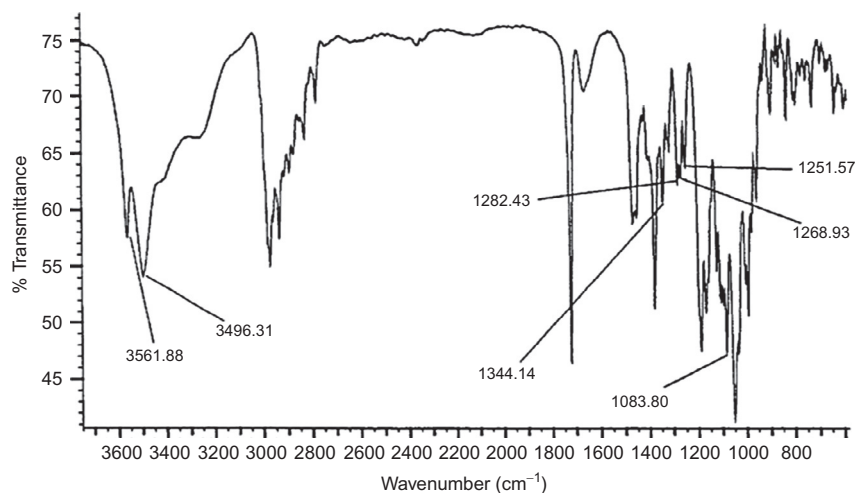


**Figure 1.8** Infrared absorption spectrum of azithromycin.

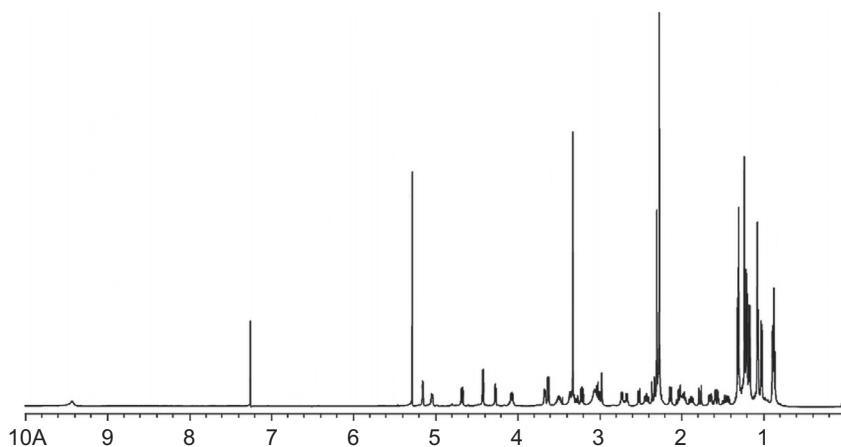


**Figure 1.9** Full <sup>1</sup>H NMR spectrum of azithromycin in CDCl<sub>3</sub>.

by patterns observed in 2D experiments (<sup>1</sup>H–<sup>1</sup>H COSY and HMQC) or by analogy to fully interpreted spectra for related compounds.

Azithromycin is shown in [Figure 1.9](#) (full <sup>1</sup>H NMR spectrum). The assignments for the observed bands are provided in [Table 1.2](#).

### 3.9.3.2 <sup>13</sup>C NMR spectrum [33]

The <sup>13</sup>C NMR spectrum of azithromycin was recorded by broadband proton spin decoupling at ambient probe temperature using an internal

**Table 1.2** Assignments for the resonance bands observed in the  $^1\text{H}$  NMR spectrum of azithromycin in  $\text{CDCl}_3$ See [Figure 1.10 reference 33](#)

Chemical shift (ppm)	Number of protons	Multiplicity and coupling constant (J)	Assignment
9.44	1		(1H, $\text{C}_2\text{—OH}$ )
5.13	1	Doublet (5 Hz)	$\text{C}_1''\text{—H}$
4.74	1	Doublet (6 Hz)	$\text{C}_{11}\text{—OH}$
4.68	1	Doublet of doublets (10 Hz)	$\text{C}_{13}\text{—H}$
4.43	1	Doublet (7 Hz)	$\text{C}_1'\text{—H}$
4.29	1	Doublet of doublets (5, 2 Hz)	$\text{C}_3\text{—H}$
4.08	1	Doublet of quartet (10, 6 Hz)	$\text{C}_5'\text{—H}$
3.68	1	Doublet (5 Hz)	$\text{C}_{11}\text{—H}$
3.65	1	Doublet (7 Hz)	$\text{C}_5\text{—H}$
3.55–3.47	1	Multiple	$\text{C}_5'\text{—H}$
3.35	1	Singlet	$\text{C}_{12}\text{—OH}$
3.34	3	Singlet	$\text{C}_3'\text{—OCH}_3$
3.23	1	Doublet of doublets (10, 7 Hz)	$\text{C}_2'\text{—H}$
3.03	1	app. triplet (10 Hz)	$\text{C}_4'\text{—H}$
2.89	1	Singlet	$\text{C}_6\text{—OH}$
2.78–2.72	1	Multiple	$\text{C}_2\text{—H}$
2.69	1	Quartet (7 Hz)	$\text{C}_{10}\text{—H}$
2.52	1	Doublet (10 Hz)	$\text{C}_9\text{—H}$
2.46–2.41		Multiple	$\text{C}_3'\text{—H}$
2.35	1	Doublet (15 Hz)	$\text{C}_2'\text{—H}$
2.31	3	Singlet	$\text{C}_1\text{—H}_3$
2.28	6	Singlet	$\text{C}_3'\text{—N}(\text{CH}_3)_2$
2.15	1	Doublet (11 Hz)	$\text{C}_4'\text{—OH}$
2.07–1.95	2	Multiple	$\text{C}_4\text{—H}$ and $\text{C}_8\text{—H}$

*Continued*

**Table 1.2** Assignments for the resonance bands observed in the  $^1\text{H}$  NMR spectrum of azithromycin in  $\text{CDCl}_3$ —cont'd

Chemical shift (ppm)	Number of protons	Multiplicity and coupling constant (J)	Assignment
2.02	1	Doublet (10 Hz)	$\text{C}_9\text{—}\underline{\text{H}}$
1.93–1.85	1	Multiple	$\text{C}_{13}\text{—}\underline{\text{CH}_2}\text{—CH}_3$
1.79	1	Doublet (15 Hz)	$\text{C}_7\text{—}\underline{\text{H}}$
1.67–1.63	1	Multiple	$\text{C}_4'\text{—}\underline{\text{H}}$
1.58	1	Doublet of doublets (15, 5 Hz)	$\text{C}_2''\text{—}\underline{\text{H}}$
1.51–1.43	1	Multiple	$\text{C}_{13}\text{—}\underline{\text{CH}_2}\text{—CH}_3$
1.32	3	Doublet (5 Hz)	$\text{C}_5''\text{—}\underline{\text{CH}_3}$
1.31	3	Singlet	$\text{C}_6\text{—}\underline{\text{CH}_3}$
1.24	3	Singlet	$\text{C}_3''\text{—}\underline{\text{CH}_3}$
1.26–1.21	2	Multiple	$\text{C}_7\text{—}\underline{\text{H}}$ and $\text{C}_4'\text{—}\underline{\text{H}}$
1.22	3	Doublet (6 Hz)	$\text{C}_5'\text{—}\underline{\text{CH}_3}$
1.19	3	Doublet (7 Hz)	$\text{C}_2\text{—}\underline{\text{CH}_3}$
1.08	1	Doublet (7 Hz)	$\text{C}_{10}\text{—}\underline{\text{CH}_3}$
1.08	3	Singlet	$\text{C}_{12}\text{—}\underline{\text{CH}_3}$
1.04	3	Doublet (7 Hz)	$\text{C}_4\text{—}\underline{\text{CH}_3}$
0.90	3	Doublet (7 Hz)	$\text{C}_8\text{—}\underline{\text{CH}_3}$
0.89	3	Triplet (7 Hz)	$\text{C}_{13}\text{—CH}_2\text{—}\underline{\text{CH}_3}$

deuterium lock. All chemical shift values are reported in ppm to the nearest 0.01 ppm. An internal reference of  $\delta_{\text{C}}$  77.0 was used for  $\text{CDCl}_3$ . Assignments were supported by DEPT editing and determined either on the basis of unambiguous chemical shift, by patterns observed in 2D experiments (HMQC) or by analogy to fully interpreted spectra for related compounds.

Azithromycin is shown in [Figure 1.11](#) (full  $^{13}\text{C}$  NMR spectrum). The assignments for the observed bands are provided in [Table 1.3](#), which are consistent with the 13 carbon contents of azithromycin.

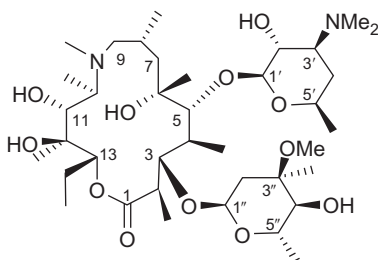


**Figure 1.10** AZI proton assignment.

### 3.10. Mass spectrometry [34]

The mass spectrum of azithromycin was obtained utilizing A Thermo Scientific TSQ Quantum mass spectrometer systems feature HyperQuad quadrupoles. The MS analysis was performed with electro-spray ionization (ESI) interface in both negative and positive ion modes.

*TSQ Quantum Ultra AM Instrument Conditions:* Ionization mode and source: Positive and negative ESI; electrospray voltage: (+) 3.5 kV, (–) –2.5 kV; sheath gas: 1; auxiliary gas: 0; ion transfer tube temperature: 270 °C; ion transfer tube offset: 35 V; tube lens offset: 77 V; collision energy: 25 eV (famotidine), 23 eV (azithromycin); collision pressure: 1.2 mTorr; Q1/Q3 resolution: 0.1 Da FWHM; accurate mass mode: internal; micro scans: 2.

**Figure 1.12** shows the detected mass fragmentation pattern of azithromycin. The major peaks in the spectrum occur at  $m/z$  749, 591, 574, 434, 158.

For protonated azithromycin, elimination of  $H_2O$  and successive loss of the two sugar moieties were the major fragmentation pathways. The CID mass spectrum of the  $[M - H]^+$  of azithromycin was very similar to that of the protonated species and showed successive loss of the two sugar moieties as the major dissociation pathways as shown in **Figure 1.13**.

## 4. METHODS OF ANALYSIS

### 4.1. Compendial methods of analysis

#### 4.1.1 Identification

##### 4.1.1.1 IR spectrum of Azithromycin

The IR spectra of the drug were obtained in the solid state using 90 g/l solutions in methylene chloride [21,34]

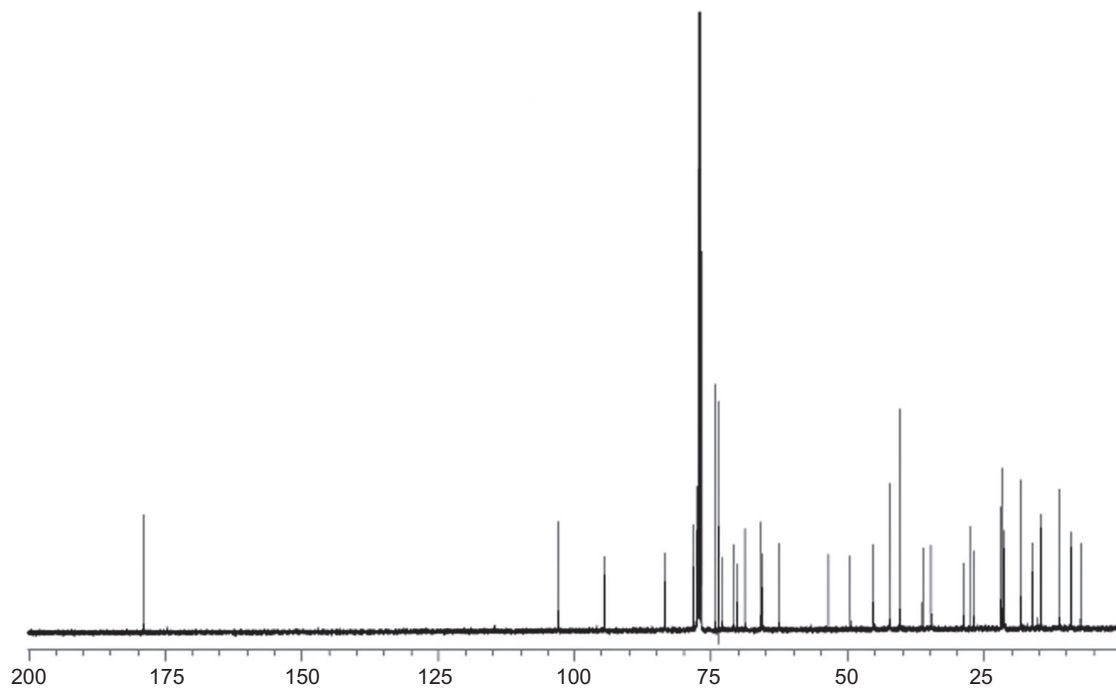


**Figure 1.11** Full  $^{13}\text{C}$  NMR spectrum of azithromycin in  $\text{CDCl}_3$ .

**Table 1.3** Assignments for the resonance bands observed in the  $^{13}\text{C}$  NMR spectrum of azithromycin

Chemical shift (ppm)	Assignments	Chemical shift (ppm)	Assignment
178.9	( $\underline{\text{C}}_1$ )	42.3	(2C, $\underline{\text{C}}_4$ and $\underline{\text{C}}_7$ )
102.9	( $\underline{\text{C}}_1'$ )	40.3	( $\text{C}_3' - \text{N}(\underline{\text{CH}}_3)_2$ )
94.5	( $\underline{\text{C}}_1''$ )	36.2	( $\underline{\text{C}}_1$ )
83.3	( $\underline{\text{C}}_5$ )	34.7	( $\underline{\text{C}}_2''$ )
78.1	( $\underline{\text{C}}_4''$ )	28.7	( $\underline{\text{C}}_4'$ )
77.6	( $\underline{\text{C}}_3$ )	27.6	( $\text{C}_6 - \underline{\text{CH}}_3$ )
77.4	( $\underline{\text{C}}_{13}$ )	26.7	( $\underline{\text{C}}_8$ )
73.6	( $\underline{\text{C}}_6$ )	22.0	( $\text{C}_8 - \underline{\text{CH}}_3$ )
73.6	( $\underline{\text{C}}_{11}$ )	21.6	( $\text{C}_3'' - \underline{\text{CH}}_3$ )
72.9	( $\underline{\text{C}}_3''$ )	21.3	( $\text{C}_5' - \underline{\text{CH}}_3$ )
70.8	( $\underline{\text{C}}_2'$ )	21.3	( $\text{C}_{13} - \underline{\text{CH}}_2$ )
70.1	( $\underline{\text{C}}_9$ )	18.2	( $\text{C}_5'' - \underline{\text{CH}}_3$ )
68.7	( $\underline{\text{C}}_5'$ )	16.2	( $\text{C}_{12} - \underline{\text{CH}}_3$ )
65.9	( $\underline{\text{C}}_3'$ )	14.6	( $\text{C}_2 - \underline{\text{CH}}_3$ )
65.5	( $\underline{\text{C}}_5''$ )	11.2	( $\text{C}_{13} - \text{CH}_2 - \underline{\text{CH}}_3$ )
62.4	( $\underline{\text{C}}_{10}$ )	9.0	( $\text{C}_4 - \underline{\text{CH}}_3$ )
49.4	( $\text{C}_3'' - \text{O}\underline{\text{CH}}_3$ )	7.3	( $\text{C}_{10} - \underline{\text{CH}}_3$ )
45.3	( $\underline{\text{C}}_2$ )		

#### 4.1.1.2 HPLC drug chromatogram

The principal peak in the HPLC drug chromatogram obtained with test solution was similar in retention time and size to the principal peak in the chromatogram obtained with reference solution [21,34].

#### 4.1.2 Impurity Analysis [47]

The specified impurities (A, B, C, D, E, F, G, H, I, K, J, L, M, N, O, and P) of azithromycin were determined using liquid.



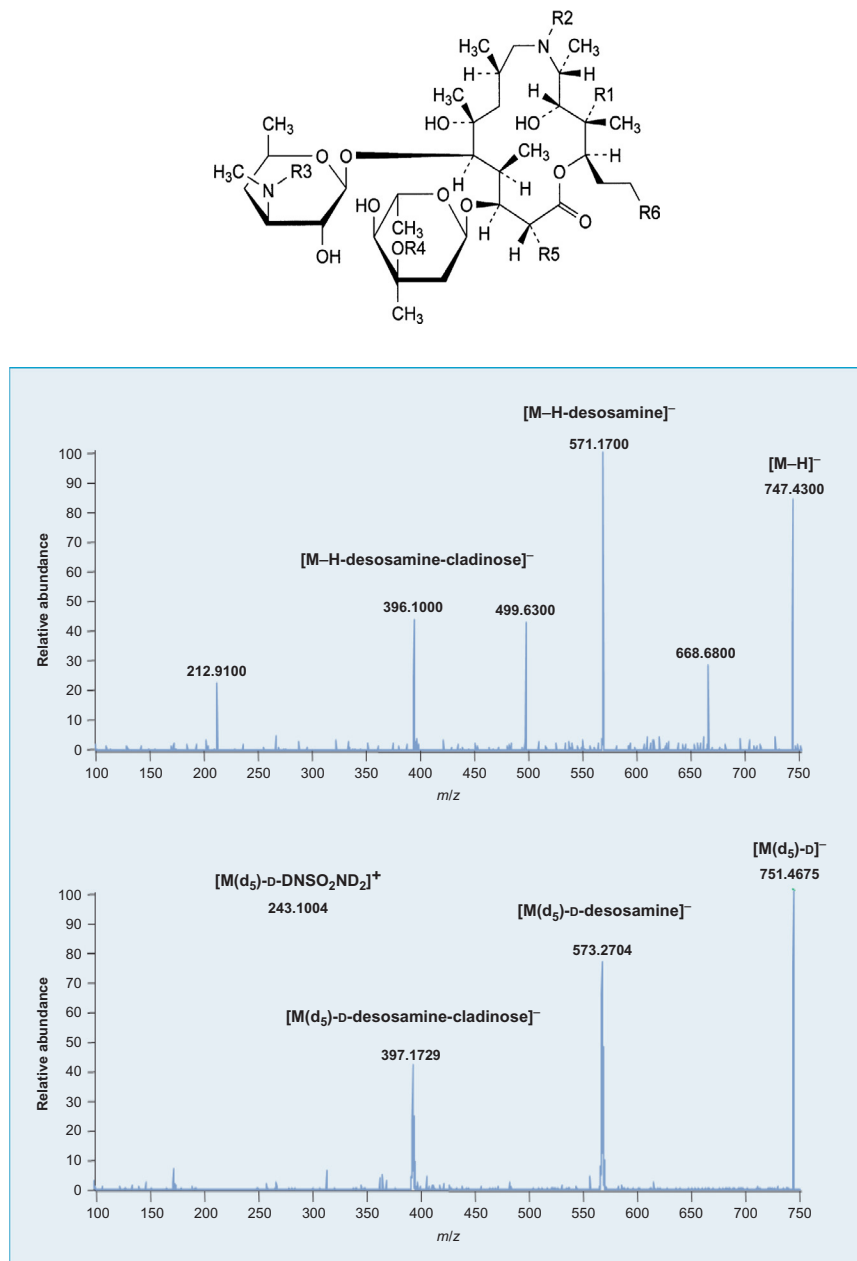


**Figure 1.12** Negative ion ESI mass spectra of azithromycin (MW = 748): CID product ion spectra (MS/MS) of  $[M - H]^-$  at  $m/z$  747 and the fully exchanged  $[M(d_5)-D]^-$  at  $m/z$  751. Deuteration was achieved by liquid phase H/D exchange method. MS and MS/MS experiments were performed on a TSQ Quantum Ultra AM mass spectrometer.

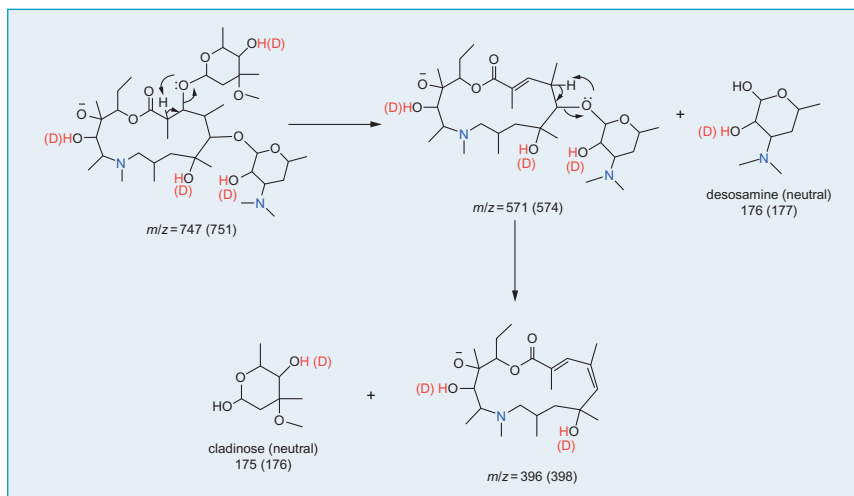
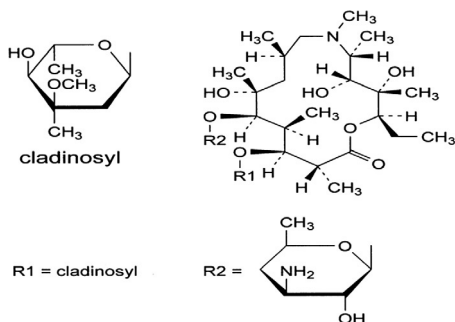
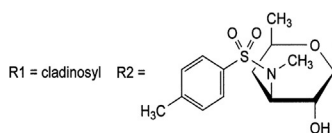


**Figure 1.13** Proposed CID fragmentation mechanisms for the major fragment ions from deprotonated azithromycin at  $m/z$  747 determined from H/D exchange patterns, high-resolution mass measurements, and MS/MS experiments. Numbers in parentheses refer to deuterated fragmentations. The proposed site of deprotonation is based on the most acidic proton of the lactone ring.

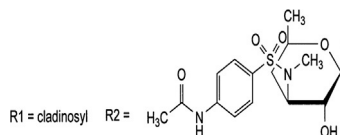
- (A)  $R_1 = \text{OH}$ ,  $R_2 = R_6 = \text{H}$ ,  $R_3 = R_4 = R_5 = \text{CH}_3$ : 6-demethylazithromycin,  
 (B)  $R_1 = R_6 = \text{H}$ ,  $R_2 = R_3 = R_4 = R_5 = \text{CH}_3$ : 3-deoxyazithromycin (azithromycin B),  
 (C)  $R_1 = \text{OH}$ ,  $R_2 = R_3 = R_5 = \text{CH}_3$ ,  $R_4 = R_6 = \text{H}$ : 3''-O-demethylazithromycin (azithromycin C),  
 (D)  $R_1 = \text{OH}$ ,  $R_2 = R_3 = R_4 = \text{CH}_3$ ,  $R_5 = \text{CH}_2\text{OH}$ ,  $R_6 = \text{H}$ : 14-demethyl-14-(hydroxymethyl)azithromycin (azithromycin F),  
 (F)  $R_1 = \text{OH}$ ,  $R_2 = R_4 = R_5 = \text{CH}_3$ ,  $R_3 = \text{CHO}$ ,  $R_6 = \text{H}$ : 3'-N-demethyl-3'-N-formylazithromycin,  
 (I)  $R_1 = \text{OH}$ ,  $R_2 = R_4 = R_5 = \text{CH}_3$ ,  $R_3 = R_6 = \text{H}$ : 3'-N-demethylazithromycin,  
 (O)  $R_1 = \text{OH}$ ,  $R_2 = R_3 = R_4 = R_5 = R_6 = \text{CH}_3$ : 2-desethyl-2-propylazithromycin,



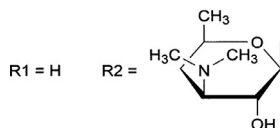
(E) 3'-(*N,N*-didemethyl)azithromycin (aminoazithromycin),



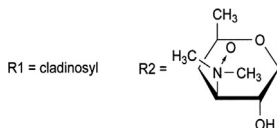
(G) 3'-*N*-demethyl-3'-*N*-[(4-methylphenyl)sulphonyl]azithromycin,



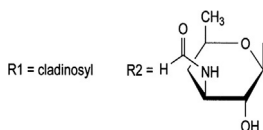
(H) 3'-*N*-[[4-(acetamino)phenyl]sulphonyl]-3'-*N*-demethylazithromycin,



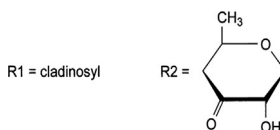
(J) 13-*O*-decladinosylazithromycin,



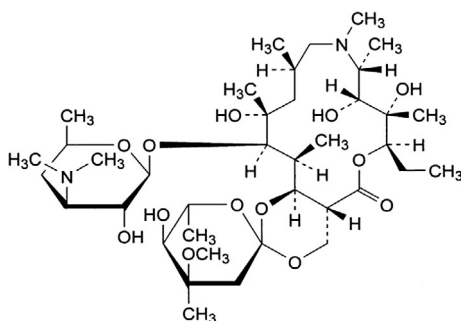
(L) azithromycin 3'-*N*-oxide,



(M) 3'-(*N,N*-didemethyl)-3'-*N*-formylazithromycin



(N) 3'-de(dimethylamino)-3'-oxoazithromycin,



(K) C<sub>14</sub>, 1''-epoxyazithromycin (azithromycin E),  
Unknown structure.

### 4.1.3 Other tests

#### 4.1.3.1 Water [47]

1.8–6.5%, determined on 0.200 g.

#### 4.1.3.2 Sulphated ash [47]

Maximum 0.2%, determined on 1.0 g.

#### 4.1.4 Assay method [47]

##### 4.1.4.1 Liquid chromatography

Solution A: Mix 60 volumes of acetonitrile R1 and 40 volumes of a 6.7 g/l solution of dipotassium hydrogen phosphate R adjusted to pH 8.0 with phosphoric acid R.

- Test solution: Dissolve 53.0 mg of the substance to be examined in 2 ml of acetonitrile R1 and dilute to 100.0 ml with solution A.
- Reference solution (a): Dissolve 53.0 mg of azithromycin CRS in 2 ml of acetonitrile R1 and dilute to 100.0 ml with solution A.
- Reference solution (b): Dissolve 5 mg of the substance to be examined and 5 mg of azithromycin impurity A CRS in 0.5 ml of acetonitrile R1 and dilute to 10 ml with solution A.
- Column size:  $l=0.25$  m,  $\varnothing=4.6$  mm; stationary phase: octadecylsilyl vinyl polymer for chromatography R ( $5\text{ }\mu\text{m}$ ); temperature:  $40\text{ }^{\circ}\text{C}$ .
- Mobile phase: Mix 60 volumes of acetonitrile R1 and 40 volumes of a 6.7 g/l solution of dipotassium hydrogen phosphate R adjusted to pH 11.0 with a 560 g/l solution of potassium hydroxide R.
- Flow rate, 1.0 ml/min; UV spectrophotometry detection at  $\lambda$  210 nm; injection, 10  $\mu\text{l}$ ; run time, 15 min; retention time of Azithromycin, 10 min; resolution: minimum 3.0 between the peaks of impurity A and azithromycin.

## 4.2. Electrochemical methods of analysis

### 4.2.1 Voltammetry

Studies on the electrochemical oxidation and determination of azithromycin on glassy carbon and modified glassy carbon electrodes have been frequently published. The voltammetric determination of azithromycin at a carbon paste electrode [48], the adsorptive stripping voltammetric determination of azithromycin at a glassy carbon electrode modified by electrochemical oxidation [49], and the voltammetric assay of azithromycin in pharmaceutical dosage forms [50] have been published. Also, studies on the electrochemical oxidation of azithromycin and its interaction with bovine serum albumin [51], identification of azithromycin by abrasive stripping voltammetry [52], and the mathematical modeling of the electrode process of azithromycin using cyclic voltammetry at a hanging mercury drop electrode [53] can be found in the literature. There is also some data concerning a validated LC method for *in vitro* analysis of azithromycin using

electrochemical detection with dual glassy carbon electrodes operating in the oxidative screen mode [37]. The electro-chemical oxidation of azithromycin using voltammetry and *in situ* FTIR spectroscopy to obtain mechanistic information about the overall process on a platinum electrode in acetonitrile has also been reported [54].

Avramov *et al.* [55] examined the oxidative properties and assay of azithromycin at a gold electrode in neutral electrolyte using cyclic linear sweep voltammetry. The maximum value of the current of the oxidation peak of pure azithromycin and azithromycin from tablet dosage form (Hemomycin<sup>®</sup>, Hemofarm, Vrsac, Serbia and Montenegro) at 0.6 V versus SCE in 0.05 M NaHCO<sub>3</sub> and in a mixture methanol–0.05 M NaHCO<sub>3</sub> (1:1) at a scan rate of 50 mV s<sup>-1</sup> is a linear function of the concentration in the range of 0.235–0.588 mg/cm<sup>3</sup>. HPLC analysis of the bulk of electrolyte confirmed the data obtained by analysis of the values of the current peak concerning the concentration of antibiotic in the investigated concentration range.

For the determination of the azithromycin concentration, only the first cycle was recorded, which will be presented later for different concentrations. It is obvious from the cyclic voltammograms of pure azithromycin in 0.05 M NaHCO<sub>3</sub> (Figures 1.14)

#### 4.2.2 Coulometry

A variant of the Karl Fischer water determination was described [25]. By heating the drug substance, the contained water was transferred into a titration cell by a carrier gas. The automated system consisted of an oven sample processor and a coulometer.

### 4.3. Spectroscopic methods of analysis

#### 4.3.1 Spectrophotometry

Azithromycin was determined in its pharmaceutical dosage forms by the formation of an ion pair between this drug and an inorganic complex of (Mo (V)-thiocyanate) followed by its extraction with dichloroethane. This ion-association complex shows an orange color and exhibits a maximum absorbance at 469 nm [56].

Su-Ying [57] established a UV spectrophotometry method to determine the contents of azithromycin tablets quickly and exactly. The concentration of azithromycin was determined according to related drug dissolubility standard procedures in pharmacopoeia. Ethanol and 0.1 mol/L hydrochloric

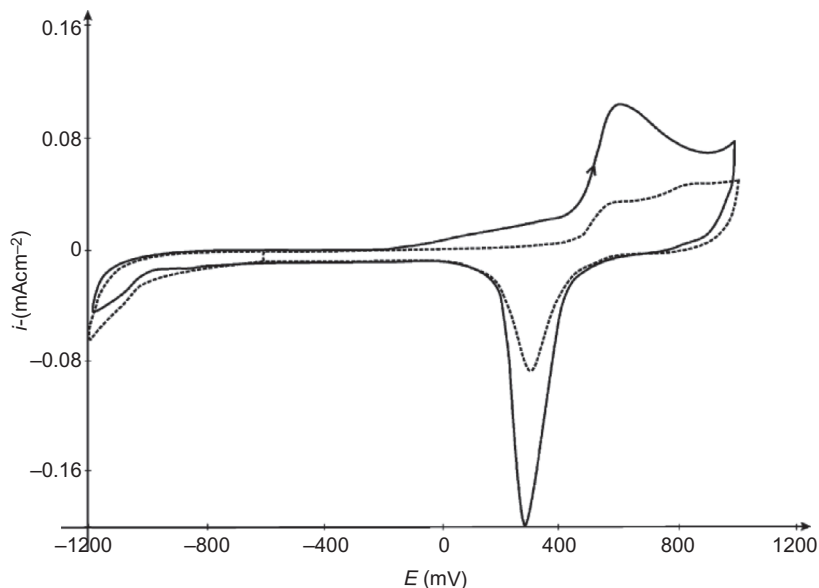


**Figure 1.14** Cyclic voltammogram of an Au electrode in 0.05 M  $\text{NaHCO}_3$  (---) and after the addition of  $0.588 \text{ mg/cm}^3$  of pure azithromycin dihydrate, 30th sweep (full line), sweep rate: 50 mV/s.

acid were used as dilute solvents and  $75 \rightarrow 100$  sulfuric acid was used as colored solvent. The samples were analyzed at the wavelength of 482 nm.

Huakan *et al.* [58] developed a spectrophotometric method for the determination of azithromycin based on the charge transfer reaction between azithromycin as donor and alizarin as acceptor in ethanol solution. The composition ratio and stability constant of charge transfer complex were 1:1 and  $4.8 \times 10^3$ , respectively. The apparent molar absorptivity of complex at 546 nm is  $5.79 \times 10^3 \text{ L mol}^{-1} \text{ cm}^{-1}$ .

Suhagia *et al.* [59] developed a simple and sensitive spectrophotometric method for the determination of azithromycin in its pharmaceutical dosage forms. In the method, azithromycin is oxidized with potassium permanganate to liberate formaldehyde, which is determined *in situ* using acetyl acetone, in the presence of ammonium acetate. An yellow colored chromogen was obtained, having an absorption maxima at 412 nm. The method is found to be linear in the concentration range of  $10\text{--}75 \text{ }\mu\text{g/ml}$ , with regression coefficient of 0.9978.

Shu-xia *et al.* [60] established a method for the determination of azithromycin tablets dissolution based on charge-transfer reaction with alizarin red. Methods of the dissolution test were conducted, using phosphate

buffer solution as medium, with a stirring speed of 100 rpm/min. The solution was withdrawn after 45 min. The absorbance of dissolution solutions was measured at 538 nm. Dissolution limit is 75% of the labeled amount. Result Good linear correlation was achieved at the range of 50–250  $\mu\text{g/ml}$  azithromycin ( $r=0.9996$ ).

Paula *et al.* [61] proposed a new method for simple and fast spectrophotometric determination of azithromycin in pharmaceutical formulations. The method is based on the charge transfer reaction between the azithromycin and quinalizarin in methanol medium. In order to achieve maximum sensitivity, the effect of some chemical variables such as the type of solvent, reagent concentration, and reaction time was evaluated. The reaction was characterized in terms of stability of the product formed and its stoichiometry, and the apparent molar absorptivity and association constant were derived. Best conditions for the analytical determination of azithromycin were observed in methanol medium with a quinalizarin concentration of 50  $\text{mg L}^{-1}$ . At these conditions, the radical anion (absorbing species) was formed in the medium immediately after mixing of the reagents and showed maximum absorption at 564 nm. The method presented a limit of detection of 0.35  $\text{mg L}^{-1}$  and a limit of quantification of 1.2  $\text{mg L}^{-1}$ .

Sayed *et al.* [62] developed two simple, accurate, precise, and rapid spectrophotometric and conductometric methods for the estimation of erythromycin thiocyanate(I), clarithromycin (II), and azithromycin dihydrate(III) in both pure and pharmaceutical dosage forms. The spectrophotometric procedure depends on the reaction of rose Bengal and copper with the cited drugs to form stable ternary complexes which were extractable with methylene chloride, and the absorbances were measured at 558, 557, and 560 nm for (I), (II), and (III), respectively. The conductometric method depends on the formation of an ion-pair complex between the studied drug and rose Bengal.

Ashour *et al.* [63] developed and validated new, simple, and rapid spectrophotometric for the assay of two macrolide drugs, azithromycin (AZT) and erythromycin (ERY), in pure and pharmaceutical formulations. The method was based on the reaction of AZT and ERY with sodium 1,2-naphthoquinone-4-sulphonate in alkaline medium at 25 °C to form an orange-colored product of maximum absorption peak at 452 nm.

#### 4.3.2 Spectrofluorimetry

El-Rabbat *et al.* [64] described a simple spectrofluorometric method for the analysis of four macrolide antibiotics. The method is based on the condensation of 10% (w/v) malonic acid and acetic acid anhydride under



the catalytic effect of tertiary amine groups of the studied macrolides. The relative fluorescence intensity of the condensation product was measured at 397/452 nm (excitation/emission) for azithromycin dihydrate and at 392/445 nm (for clarithromycin, erythromycin ethylsuccinate, and roxithromycin).

Almeida *et al.* [65] proposed a fluorescence method for azithromycin determination in pharmaceutical formulations. The method is based on the synchronous fluorescence ( $\Delta\lambda = 30$  nm, 482 nm) produced when azithromycin is derivatized in strong acidic medium (9.0 mol L<sup>-1</sup> HCl).

Khashaba [66] analyzed the macrolides (erythromycin, erythromycin esters, azithromycin dihydrate, clarithromycin, and roxithromycin) by a simple spectrofluorimetric method based on the oxidation by cerium (VI) in the presence of sulfuric acid and monitoring the fluorescence of cerium (III) formed at  $\lambda_{\text{ex}}$  255 nm and  $\lambda_{\text{em}}$  348 nm.

#### 4.3.3 Colorimetry

Hunfeld *et al.* [67] used a newly developed colorimetric microdilution method to analyze the activity of 12 antimicrobial agents against nine *Borrelia burgdorferi* isolates, including all three genospecies pathogenic for humans. In addition, *in vitro* antimicrobial resistance patterns of *Borrelia valaisiana* and *Borrelia bissettii* tick isolates were investigated. The applied test system is based upon color changes that occur in the presence of phenol red and result from the accumulation of nonvolatile acid produced by actively metabolizing spirochetes. After 72 h of incubation, minimal inhibitory concentrations (MICs) were determined from the decrease of absorbance by software-assisted calculation of growth curves. MIC values were lowest for azlocillin (MIC,  $\leq 0.125$   $\mu\text{g/ml}$ ), ceftriaxone (MIC range,  $\leq 0.015$ – $0.06$   $\mu\text{g/ml}$ ), and azithromycin (MIC range,  $\leq 0.015$ – $0.06$   $\mu\text{g/ml}$ ). Whereas tobramycin (MIC range, 8–64  $\mu\text{g/ml}$ ) exhibited little activity, spectinomycin (MIC range, 0.25–2  $\mu\text{g/ml}$ ) showed *in vitro* antimicrobial activity against *B. burgdorferi*.

Haleem *et al.* [68] developed a simple, accurate, and rapid spectrophotometric method for the estimation of azithromycin by the acidic hydrolysis of the drug with sulfuric acid and monitoring the absorbance at 482 nm.

### 4.4. Chromatographic methods of analysis

#### 4.4.1 Electrophoresis

Kumar *et al.* [69] described the use of AZM as a chiral selector for the enantiomeric separations of five chiral drugs and one amino acid (tryptophan) in

capillary electrophoresis (CE). The enantioseparation is carried out using polar organic mixtures of acetonitrile (ACN), methanol (MeOH), acetic acid, and triethylamine as run buffer. The influences of the chiral selector concentration, ACN/MeOH ratio, applied voltage, and capillary temperature on enantioseparation are investigated. The results shown that AZM is a viable chiral selector in CE for the enantioseparation of the type of chiral drugs investigated.

Lebedeva *et al.* [70] described successful use of macrolide antibiotic azithromycin for enantioseparation of tetrahydrozoline. The procedure was proposed for the analysis of tetrahydrozoline in pharmaceuticals. Linearity was achieved in the concentration range  $5 \times 10^{-2}$  to 1 mg/ml. The azithromycin stability in the background electrolyte and the antibiotic adsorption on the fused-silica capillary were studied. Best enantioseparation with resolution factor 1.6 was achieved in less than 10 min.

#### 4.4.2 Thin-layer chromatography

Kwiecień *et al.* [71] established a thin-layer chromatographic (TLC) method with densitometric detection for quantification of azithromycin in pharmaceutical preparations. Silica gel plates with fluorescence indicator F<sub>254</sub> were used with chloroform–ethanol–ammonia 6:14:0.2 (v/v) as mobile phase. Chromatograms were visualized by spraying with 1:4 (v/v) sulfuric acid–ethanol and heating at 120 °C for 5 min. Scanning and densitometric analysis was performed at 483 nm. The  $R_F$  of azithromycin under these conditions was 0.53. The method was characterized by high sensitivity (LOD = 40 ng/zone and LOQ = 80 ng/zone), wide linear range (from 0.08 to 1.2 µg/zone,  $r = 0.9965$ )

Khedr *et al.* [72] described a validated stability-indicating TLC method of the analysis of azithromycin (AZT) in bulk and capsule forms. Both AZT potential impurity and degradation products can be selectively and accurately estimated in both raw material and product onto one precoated silica–gel TLC plate 60F<sub>254</sub>. The development system used is *n*-hexane–ethyl acetate diethylamine (75:25:10, v/v/v). The separated bands are detected as brown to brownish red spots after spraying with modified Dragendorff's solution. The  $R_F$  values of AZT, azaerythromycin A, and the three degradation products are 0.54, 0.35, 0.40, 0.20, and 0.12, respectively.

#### 4.4.3 High-performance liquid chromatography

Liquid chromatography with UV detection has been already employed for the analysis of azithromycin in azithromycin tablets [39], raw material, and

azithromycin tablets [36,73]. A high-performance liquid chromatography (HPLC) method with UV detector was developed for the determination of azithromycin and other related compounds, impurities, degradation products in raw material as well as in new pharmaceutical formulations: dry suspension and capsules. Validation of the method was performed according to the requirements of USP for assay determination, which included accuracy, precision, specificity, linearity, and range.

An HPLC method was developed that confirmed the photodegradation of azithromycin in environmental waters, under simulated solar radiation [74].

A stability-indicating HPLC method has been described for azithromycin in raw materials, capsules, and suspension [75].

Other HPLC methods for the analysis of AZI in raw material, dosage forms, and biological samples that have been reported in the literature are listed in Table 1.4.

#### 4.5. Determination in body fluids and tissues

Azithromycin concentrations versus time profiles in extracellular space of muscle and subcutaneous adipose tissue, also in plasma and white blood cells, were determined at days 1 and 3 of treatment as well as 2 and 7 days after end of treatment. Of all compartments, azithromycin concentrations were highest in white blood cells, attesting for intracellular accumulation. However, azithromycin concentrations in both soft tissues were markedly lower than in plasma both during and after treatment. Azithromycin concentrations were measured by subinhibitory at all time points in both soft tissues and at the large majority of observed time points in plasma [76].



### 5. STABILITY

El-Gindy *et al.* [75] developed a validated stability-indicating HPLC method for the analysis of azithromycin (AZ) and its related compounds in raw materials and capsules. The stability of AZ was studied under accelerated acidic, alkaline, and oxidative conditions. The major peak detected from the degradation of AZ in alkaline and acidic conditions was decladinosylazithromycine, while azithromycin N-oxide was detected from the oxidative degradation. Long-term stability studies for capsule and oral suspension were also carried out.

**Table 1.4** HPLC methods for the analysis of azithromycin

Column	Sample matrix	Mobile phase composition	Detection	References
Gamma-alumina	Raw material	Phosphate buffer–acetonitrile, adjusted to pH 11.0 with potassium hydroxide	Amperometric guard: +0.70 V screen: +0.85 V	[35]
LiChroCART <sup>®</sup> C <sub>18</sub> , 5 µm	Raw material	Phosphate buffer–acetonitrile–methanol, adjusted to pH 8.0 with phosphoric acid	UV 215 nm	[36]
Nova-Pack C <sub>18</sub> , 4 µm	Raw material	Ammonium acetate–acetonitrile–methanol tetrahydrofuran, mobile phase pH 7.2–7.4	Amperometric guard: +0.7 V screen: +0.8 V	[37]
XTerra RP C <sub>18</sub> , 5 µm	Raw material	Phosphate buffer–water–acetonitrile, adjusted to pH 6.5 with potassium hydroxide	UV 215 nm	[38]
Phenomenex Synergi <sup>®</sup> C <sub>18</sub> , 4 µm	Raw material, dosage forms	Gradient elution, phosphate buffer–acetonitrile–methanol, adjusted to pH 7.0 with potassium hydroxide	UV 210 nm	[39]
YMC-Park ODS-AP C <sub>18</sub> , 5 µm	Rat's plasma	Phosphate buffer–acetonitrile, adjusted to pH 7.2 with potassium hydroxide	Amperometric detect: +0.95 V	[40]

*Continued*

**Table 1.4** HPLC methods for the analysis of azithromycin—cont'd

Column	Sample matrix	Mobile phase composition	Detection	References
Nova-Pack C <sub>18</sub> , 4 µm	Human tears and plasma	Phosphate buffer–sodium perchlorate–acetonitrile–methanol, adjusted to pH 7.0 with phosphoric acid	Amperometric guard: +0.7 V screen: +0.85 V	[41]
Radial-Pak Resolve Silica cartridge, 5 µm	Rat's blood plasma, serum, and human urine	Ammonium acetate–acetonitrile–methanol, adjusted to pH 7.0 with acetic acid	Coulometric guard: +0.90 V	[42]
C <sub>18</sub> (250 mm × 4.6 mm, 5 µm)	Azithromycin syrup	Acetonitrile –0.067 mol L <sup>-1</sup> K <sub>2</sub> HPO <sub>3</sub> (pH adjusted to 6.5) (40:60)	UV 210 nm	[43]
ODS-C <sub>18</sub> column (150 mm × 4.6 mm, 5 µm)	Eye drops	Acetonitrile and 0.1 mol L <sup>-1</sup> KH <sub>2</sub> PO <sub>4</sub> as the mobile phase (30:70)	UV 215 nm	[44]
CAPCELL PAK C <sub>(18)</sub> MGIIcolumn (250 mm × 4.6 mm, 5 µm)	Azithromycin capsules	Acetonitrile phosphate buffer (to dissolve dipotassium hydrogen phosphate 8.7 g diluting to 1000 ml with water, and adjust pH to 8.2 with phosphoric acid) (60:40)	UV 210 nm	[45]
Dikma Technologies Diamonsil C <sub>18</sub> column (150 mm × 4.6 mm, 5 µm)		Ammonium dihydrogen phosphate (0.045 M, pH 3.0 adjusted by phosphoric acid):acetonitrile 47:15 (v/v)	UV 210 nm	[46]

Moreno *et al.* [77] were developed a stability study of azithromycin in ophthalmic preparations by submission to different types of light, temperature, and pH, using the biodiffusion assay (cylinder  $3 \times 3$ ) for the quantifications. *Bacillus subtilis*, ATCC 9372, was used as test organism. The used concentration range was of 50–200 µg/ml.



## 6. CLINICAL APPLICATIONS

### 6.1. An overview

Azithromycin is the member of macrolide antibiotics. It is semisynthetic derivatives of erythromycin. Azithromycin differs from erythromycin by the addition of a methyl-substituted nitrogen atom into the lactone ring. This structural modification improved acid stability and tissue penetration and broaden the spectrum of activity. Macrolides generally cover a wide range of Gram-positive and Gram-negative bacterial species including intracellular pathogens such as *Chlamydia* and *Legionella*. They express their antibiotic activity by binding to the 50S ribosome subunit and inhibit protein synthesis [78,79].

Azithromycin pharmacology and therapeutics aspects were given below in more details.

### 6.2. Antimicrobial spectrum susceptibility

Azithromycin is less active against Gram-positive bacteria than erythromycin but is considerably more effective against some Gram-negative organisms such as *Haemophilus influenzae*, *Moraxella catarrhalis* as well as having activity against some of the Enterobacteriaceae such as *Escherichia coli* and *Salmonella* and *Shigella* species; Also activity against *Legionella pneumophila*, *B. burgdorferi*, *Mycoplasma pneumoniae*. Also it is owes enhanced activity against *Mycobacterium avium-intracellulare*, as well as against some protozoa (e.g., *Cryptosporidium*, and *Plasmodium* species, an excellent action against *Toxoplasma gondii*, killing the cysts). Azithromycin more active than erythromycin against *Chlamydia trachomatis* and *Ureaplasma urealyticum*, [79,80].

### 6.3. Mechanism of action

It is a bacteriostatic agent that inhibits protein synthesis by binding reversibly to 50S ribosomal subunits of sensitive microorganisms. Cells are considerably more permeable to the unionized form of the drug, which probably explains the increased antimicrobial activity at alkaline pH [79].

## 6.4. Resistance to macrolides

Generally, resistance to macrolides results from the following mechanisms:

- Drug efflux by an active pump mechanism
- Ribosomal protection by inducible or constitutive production of methylase enzymes, mediated by expression of (ermA), (ermB), and (ermC), which modify the ribosomal target and decrease drug binding
- Hydrolysis by esterases produced by Enterobacteriaceae
- Chromosomal mutations that alter a 50S ribosomal subunit protein (found in *B. subtilis*, Campylobacter species, mycobacteria, and Gram-positive cocci) [79].

## 6.5. Actions other than antimicrobial effects

- Studies were indicated the activity of azithromycin as promising medication for the treatment of gastroparesis and gastrointestinal dysmotility [81,82].
- One study showed that azithromycin may be effective against late-onset asthma [83].
- Azithromycin has been shown to be effective against malaria when used in combination with artesunate or quinine. Azithromycin–artesunate, even when given only once daily for 3 days, and azithromycin–quinine, given 3 times daily, are safe and efficacious combination treatments for uncomplicated falciparum malaria, and they deserve additional study in special patient populations [84].
- *Ischaemic heart disease*: Macrolide antibacterials, including azithromycin, clarithromycin, and roxithromycin, have been investigated in the prevention of ischaemic heart disease, based on a suggested link between atherosclerosis and infection with *Chlamydia pneumoniae* (*Chlamydia pneumoniae*). Although preliminary results from some pilot studies were promising, longer-term studies in large numbers of patients were disappointing and none of the three macrolides decreased ischemic events or provided clinical benefit; indeed, in one study, an unexpected increase in cardiovascular mortality was seen in those taking clarithromycin [79,86,87].
- *Gingival hyperplasia*: Azithromycin improves cyclosporin-associated gingival hyperplasia, especially when administered early in the process [88].
- *Cystic fibrosis*: Long-term azithromycin is widely used in cystic fibrosis, with evidence demonstrating a reduction in lung function decline and exacerbation rate. This immunomodulatory therapy probably disrupts *Pseudomonas aeruginosa* biofilm growth [89].

## 6.6. Clinical uses and dosing

Clinically, azithromycin used for many as follows: respiratory-tract infections, otitis media, skin and soft-tissue infections, uncomplicated genital chlamydial infections and nongonococcal urethritis, mild or moderate typhoid due to multiple-antibacterial-resistant organisms, prophylaxis of group A streptococcal infection and as prevention therapy of bacterial endocarditis in patients undergoing dental procedures who are at high risk for endocarditis, pertussis, mycobacterial infections [79,88,90].

- Treatment or prophylaxis of *Mycobacterium avium-intracellulare* infection in AIDS patients requires higher doses: 600 mg daily in combination with one or more other agents for treatment, or 1200 mg once weekly for primary prevention.
- Azithromycin is useful in the treatment of sexually transmitted diseases, especially during pregnancy when tetracyclines are contraindicated. The treatment of uncomplicated nongonococcal urethritis presumed to be caused by *C. trachomatis* consists of a single 1-g dose of azithromycin. This dose also is effective for chancroid [79].
- Azithromycin (1 g per week for 3 weeks) is an alternative regimen for the treatment of *granuloma inguinale* or *lymphogranuloma venereum* [79].
- Uncomplicated genital chlamydial infections and nongonococcal urethritis, 1 g as a single dose [90].
- Typhoid, 500 mg once daily for 7 days [90].

## 6.7. ADME profile

Azithromycin administered orally is absorbed rapidly and distributes widely throughout the body, except to the brain and cerebrospinal fluid. Peak plasma concentrations occur 2–3 h after an oral dose. A 500-mg loading dose will produce a peak plasma drug concentration of ~0.4 g/ml. When this loading dose is followed by 250 mg once daily for 4 days, the steady-state peak drug concentration is 0.24 g/ml. Azithromycin also can be administered intravenously, producing plasma concentrations of 3–4 g/ml after a 1-h infusion of 500 mg. Absorption from capsules, but not tablets or suspension, is reduced by food. Azithromycin's unique pharmacokinetic properties include extensive tissue distribution and high drug concentrations within cells (including phagocytes), resulting in much greater concentrations of drugs in tissue or secretions compared to simultaneous serum concentrations. Tissue fibroblasts act as the natural reservoir for the drug *in vivo*. Data from animal studies indicate that azithromycin crosses the placenta. Protein



binding is 50% at very low plasma concentrations and less at higher concentrations. Azithromycin undergoes some hepatic metabolism (demethylation) to inactive metabolites, but biliary excretion is the major route of elimination. Only 12% of drug is excreted unchanged in the urine. The elimination half-life ( $t_{1/2}$ ), 40–68 h, is prolonged because of extensive tissue sequestration and binding [79,85].

## 6.8. Side effects

Anorexia, dyspepsia, flatulence, dizziness, headache, drowsiness, convulsions, arthralgia, and disturbances in taste and smell; rarely constipation, hepatitis, hepatic failure, syncope, insomnia, agitation, anxiety, asthenia, paraesthesia, hyperactivity, thrombocytopenia, haemolytic anaemia, interstitial nephritis, acute renal failure, photosensitivity, tooth and tongue discoloration [90].

## 6.9. Drug interactions

- Azithromycin, generally appear to be free of drug interactions. Caution is advised, nevertheless, when using azithromycin in conjunction with drugs known to interact with erythromycin [80].
- Giving azithromycin with antacids containing aluminum or magnesium salts can reduce the rate, but not the extent, of its absorption; azithromycin should be given at least 1 h before or 2 h after the antacid [85].
- Azithromycin serum concentrations are markedly increased when it is given with nelfinavir [85].
- Azithromycin capsules should not be administered with food because it will result in reduced absorption.
- Azithromycin possibly enhances anticoagulant effect of coumarins [90].
- Azithromycin possibly increases plasma concentration of theophylline [90].

## REFERENCES

- [1] Z. Banić Tomišić, The story of azithromycin, *Kemija u Industriji* 60 (12) (2011) 603–617.
- [2] Martindale the Complete Drug Reference, 36th, the Pharmaceutical Press, 207.
- [3] <http://en.wikipedia.org/wiki/Azithromycin>.
- [4] <http://www.rxlist.com/zithromax-drug.htm>.
- [5] The Merck Index, 12th, 1996, Merck & CO., Inc., USA. 157.
- [6] [http://www.who.int/selection\\_medicines/committees/expert/19/applications/azithromycin\\_21\\_ac\\_ad.pdf](http://www.who.int/selection_medicines/committees/expert/19/applications/azithromycin_21_ac_ad.pdf).
- [7] <http://www.drugbank.ca/drugs/db00207>.
- [8] Z.J. Li, A.V. Trask, Crystal forms of azithromycin, 2005, U.S. Patent No. 6,977,243.

- [9] S. Turchetta, P. Massardo, P. Casellato, Process for preparing high purity azithromycin, 2003, U.S. Patent Application 10/516,719.
- [10] S.P. Singh, S.M.J. Mukarram, M. Purohit, A.R. Khan, Process for preparation of anhydrous azithromycin, 2008, U.S. Patent Application 12/184,051.
- [11] M. Bayod-Jasanada, R.J. Carbajo, F. Lopez-Ortiz, Synthesis of 9-deoxy-9a-aza-9a-homoerythromycin A 11,12-hydrogen borate and azithromycin 11,12-hydrogen borate. A new procedure to obtain azithromycin dihydrate, *J. Org. Chem.* 62 (21) (1997) 7479.
- [12] S. Djokić, G. Kobrehel, G. Lazarevski, N. Lopotar, Z. Tamburašev, B. Kamenar, A. Nagl, I. Vicković, Erythromycin series. Part 11. Ring expansion of erythromycin A oxime by the Beckmann rearrangement, *J. Chem. Soc. Perkin Trans. 1* (1986) 1881–1890.
- [13] B.V. Yang, M. Goldsmith, J.P. Rizzi, A novel product from Beckmann rearrangement of erythromycin A 9 (E)-oxime, *Tetrahedron Lett.* 35 (19) (1994) 3025–3028.
- [14] J.A. De La Torre Garcia, F.F. Andrade, J.M.F.L. Ochoa, Single-step process for preparing 7, 16-deoxy-2-aza-10-0-cladinosil-12-0-desosaminil-4, 5-dihydroxy-6-ethyl-3, 5, 9, 11, 13, 15-hexamethylbicycle (11.2.1) hexadeca-1 (2)-en-ona and obtaining a new form of 9-deoxy-9a-methyl-9a-aza-9a-homoerythromycin A, 2003, U.S. Patent 6,528,492.
- [15] S.H. Pine, B.L. Sanchez, Formic acid-formaldehyde methylation of amines, *J. Org. Chem.* 36 (6) (1971) 829–832.
- [16] J.S. Davies, E. Hunt, I.I. Zomaya, The chemistry of erythromycin. Reactions of erythromycin A imine and its 6-methyl ether with aldehydes and hydrazines, *J. Chem. Soc. Perkin Trans. 5* (1990) 1409–1414.
- [17] Y. Ni, Z. Sun, Recent progress on industrial fermentative production of acetone–butanol–ethanol by *Clostridium acetobutylicum* in China, *Appl. Microbiol. Biotechnol.* 83 (3) (2009) 415–423.
- [18] H.A. Kirst, Recent Progress in the Chemical Synthesis of Antibiotics, Springer, Heidelberg, 1990, pp. 39–63.
- [19] S. Mutak, Azalides from azithromycin to new azalide derivatives, *J. Antibiotics* 60 (2) (2007) 85–122.
- [20] S. Rengaraju, Process for the preparation of non-hygroscopic azithromycin dihydrate, 2002, U.S. Patent Application 10/050,897.
- [21] European Pharmacopoeia. ed. t. edition. vol. 16. 2005. 1649.
- [22] S. Babić, A.J.M. Horvat, D. Mutavdžić Pavlović, M. Kaštelan-Macan, Determination of  $pK_a$  values of active pharmaceutical ingredients, *TrAC Trends Anal. Chem.* 26 (11) (2007) 1043–1061.
- [23] Material Safety Data Sheet, 2012. <http://www.greenstonellc.com/pdfs/MSDS/AZITHROMYCIN%20TABLETS%20250MG%20AND%20500MG%20-%20MSDS.pdf>.
- [24] S. Odoemelum, E. Ogoko, B. Ita, N. Eddy, Inhibition of the corrosion of zinc in H<sub>2</sub>SO<sub>4</sub> by 9-deoxy-9a-aza-9a-methyl-9a-homoerythromycin A (azithromycin), *Portugaliae Electrochim. Acta* 27 (1) (2009) 57–68.
- [25] R. Gandhi, O. Pillai, R. Thilagavathi, B. Gopalakrishnan, C.L. Kaul, R. Panchagnula, Characterization of azithromycin hydrates, *Eur. J. Pharm. Sci.* 16 (3) (2002) 175–184.
- [26] A.K. Tiwary, G.M. Panpalia, Influence of crystal habit on trimethoprim suspension formulation, *Pharm. Res.* 16 (2) (1999) 261–265.
- [27] Z.H. Zhang, T.S. Li, T.S. Jin, J.X. Wang, A simple and efficient procedure for deprotection of tetrahydropyranyl ethers catalysed by expansive graphite†, *J. Chem. Res. Synopses* 3 (1998) 152–153.
- [28] Z.J. Li, A.V. Trask, Crystal forms of azithromycin, 2006, Google Patents.
- [29] D.J.M. Allen, K.M. Nepveux, Azithromycin dihydrate, in European Patent, 1992, EP 0298650.

- [30] S. Timoumi, D. Mangin, R. Peczalski, F. Zagrouba, J. Andrieu, A.H. Abadi, Stability and thermophysical properties of azithromycin dihydrate, *Arab. J. Chem.* (2010). <http://www.sciencedirect.com/science/article/pii/S1878535210002297>.
- [31] <http://www.chemspider.com/chemical-structure.2278824.html>.
- [32] M.S.B. Jasanada, I.L. Garcia, F.F. Mari, Azithromycin preparation in its noncrystalline and crystalline dihydrate forms, 2002, U.S. Patent 6,451,990.
- [33] F.G. Glansdorp, R.J. Spandl, J.E. Swatton, O. Loiseleur, M. Welch, D.R. Spring, Using chemical probes to investigate the sub-inhibitory effects of azithromycin, *Org. Biomol. Chem.* 6 (22) (2008) 4120–4124.
- [34] A. Kamel, K. Colizza, G. Pgrd, C.T.P. Jeanville, T.F. Scientific, Mechanisms of Ion Formation for Famotidine and Azithromycin Using Hydrogen/Deuterium Exchange and High Resolution Mass Measurements, Application Note: 374.
- [35] L. Tong, P. Eichhorn, S. Pérez, Y. Wang, D. Barceló, Photodegradation of azithromycin in various aqueous systems under simulated and natural solar radiation: Kinetics and identification of photoproducts, *Chemosphere* 83 (3) (2011) 340–348.
- [36] A. Khedr, M. Sheha, Quantitative thin-layer chromatographic method of analysis of azithromycin in pure and capsule forms, *J. Chromatogr. Sci.* 41 (1) (2003) 10–16.
- [37] R.A. Shawabkeh, M.F. Tutunji, Mathematical modelling of the electrode process of azithromycin using cyclic voltammetry at hanging mercury drop electrode, *Sensors* 2 (11) (2002) 436–446.
- [38] A. El-Gindy, K.A. Attia, M.W. Nassar, N.M. Al Abasawi, M. Al-Shabrawi, Optimization and validation of a stability-indicating RP-HPLC method for determination of azithromycin and its related compounds, *J. AOAC Int.* 94 (2) (2011) 513–522.
- [39] A. Kwiecień, J. Krzek, Ł. Biniek, TLC-densitometric determination of azithromycin in pharmaceutical preparations, *JPC* 21 (3) (2008) 177–181.
- [40] U. Pharmacopeia. 32, 2009. in US Pharmacopeial Convention, Rockville, MD.
- [41] F. Kamau, H. Chepkwony, J. Ngugi, D. Debremaeker, E. Roets, J. Hoogmartens, Isocratic liquid chromatographic method for the analysis of azithromycin and its structurally related substances in bulk samples, *J. Chromatogr. Sci.* 40 (9) (2002) 529–533.
- [42] C. Taninaka, H. Ohtani, E. Hanada, H. Kotaki, H. Sato, T. Iga, Determination of erythromycin, clarithromycin, roxithromycin, and azithromycin in plasma by high-performance liquid chromatography with amperometric detection, *J. Chromatogr. B Biomed. Sci. Appl.* 738 (2) (2000) 405–411.
- [43] D.A. Raines, A. Yusuf, M.H. Jabak, W.S. Ahmed, Z.A. Karcioglu, A. El-Yazigi, Simultaneous high-performance liquid chromatography analysis of azithromycin and two of its metabolites in human tears and plasma, *Ther. Drug Monit.* 20 (6) (1998) 680–684.
- [44] L. Ke, Z. Yajie, Determination of azithromycin and azithromycin capsules by HPLC [J], *China Pharm.* 1 (2010) 041.
- [45] Y.H. Kim, J.V. Pothuluri, C.E. Cerniglia, Voltammetric investigation of macrolides by an HPLC-coulometric assay, *J. Pharm. Biomed. Anal.* 38 (3) (2005) 390–396.
- [46] H. Yan, H. Yuan, Determination of azithromycin in azithromycin syrup by HPLC [J], *Anhui Med. Pharm. J.* 1 (2009) 014.
- [47] British Pharmacopoeia. vol. 1. 2005, the stationery office on behalf of the medicine and health care products Regulatory Agency (MHRA), pp. 192–194.
- [48] M.A.R. Gaur, J. Gan, P. Hansal, K. Harper, R. Mannan, A. Panchal, K. Patel, M. Patel, N. Patel, J. Rana, A. Rogowska, *British Pharm.* (2009) 469–477.
- [49] O.A. Farghaly, N.A. Mohamed, Voltammetric determination of azithromycin at the carbon paste electrode, *Talanta* 62 (3) (2004) 531–538.
- [50] B. Nigovic, Adsorptive stripping voltammetric determination of azithromycin at a glassy carbon electrode modified by electrochemical oxidation, *Anal. Sci.* 20 (4) (2004) 639–643.
- [51] B. Nigović, B. Šimunić, Voltammetric assay of azithromycin in pharmaceutical dosage forms, *J. Pharm. Biomed. Anal.* 32 (1) (2003) 197–202.

- [52] W. Yunhua, J. Xiaobo, H. Shengshui, Studies on electrochemical oxidation of azithromycin and its interaction with bovine serum albumin, *Bioelectrochemistry* 64 (1) (2004) 91–97.
- [53] Š. Komorsky-Lovrić, B. Nigović, Identification of 5-aminosalicylic acid, ciprofloxacin and azithromycin by abrasive stripping voltammetry, *J. Pharm. Biomed. Anal.* 36 (1) (2004) 81–89.
- [54] R. Gandhi, C. Kaul, R. Panchagnula, Validated LC method for in-vitro analysis of azithromycin using electrochemical detection, *J. Pharm. Biomed. Anal.* 23 (6) (2000) 1073.
- [55] J.A.R.L. Ortiz, O.P. Marquez, J. Marquez, In: *Proceedings of the 2001 Joint International Meeting—The 200th Meeting of the Electrochemical Society Inc. and the 52nd Annual Meeting of the International Society of Electrochemistry*, San Francisco, CA, 2001, pp. 2–7 (Abs# 1192).
- [56] M. Avramov Ivić, S. Petrović, D.Ž. Mijin, P. Živković, I. Kosović, K. Drljević, M. Jovanović, Studies on electrochemical oxidation of azithromycin and Hemomycin<sup>®</sup> at gold electrode in neutral electrolyte, *Electrochim. Acta* 51 (12) (2006) 2407–2416.
- [57] M. Rachidi, J. Elharti, K. Digua, Y. Cherrah, A. Bouklouze, New spectrophotometric method for azithromycin determination, *Anal. Lett.* 39 (9) (2006) 1917–1926.
- [58] M. Su-Ying, Determination of the contents of azithromycin tablets with UV spectrophotometry [J], *J. Pediatr. Pharm.* 4 (2007) 020.
- [59] L. Huakan, Z. Yanqing, W. Yuhua, K. Janfeng, Spectrophotometric determination of azithromycin based on the charge transfer reaction between azithromycin and alizarin, *Chin. J. Anal. Chem.* 32 (5) (2004) 598–600.
- [60] B. Suhagia, S. Shah, I. Rathod, H. Patel, K. Doshi, Determination of azithromycin in pharmaceutical dosage forms by spectrophotometric method, *Indian J. Pharm. Sci.* 68 (2) (2006) 242.
- [61] T. Shu-Xia, J. Ye, X. Zan, C. Tai-Mei, Z. Xing-Ru, Spectrophotometric determination of azithromycin tablets dissolution by charge-transfer complex with alizarin red, *Chin. J. Antibiot.* 30 (9) (2005) 533.
- [62] C.E.R. De Paula, V.G.K. Almeida, R.J. Cassella, Novel spectrophotometric method for the determination of azithromycin in pharmaceutical formulations based on its charge transfer reaction with quinalizarin, *J. Braz. Chem. Soc.* 21 (9) (2010) 1664–1671.
- [63] R.A. Sayed, W.S. Hassan, M.Y. El-Mammli, A. Shalaby, New spectrophotometric and conductometric methods for macrolide antibiotics determination in pure and pharmaceutical dosage forms using rose Bengal, *J. Spectrosc.* 7 (2013) 13–26, V 2013, ID2 14270, p.13. <http://dx.doi.org/10.1155/2013/214270>.
- [64] S. Ashour, R. Bayram, Novel spectrophotometric method for determination of some macrolide antibiotics in pharmaceutical formulations using 1,2-naphthoquinone-4-sulphonate, *Spectrochim. Acta A Mol. Biomol. Spectrosc.* 99 (2012) 74–80.
- [65] N. El-Rabbat, H.F. Askal, P.Y. Khashaba, N.N. Attia, A validated spectrofluorometric assay for the determination of certain macrolide antibiotics in pharmaceutical formulations and spiked biological fluids, *J. AOAC Int.* 89 (5) (2006) 1276–1287.
- [66] V.G. Almeida, V.S. Braga, W.F. Pacheco, R.J. Cassella, Fluorescence determination of azithromycin in pharmaceutical formulations by using the synchronous scanning approach after its Acid derivatization, *J. Fluoresc.* 23 (1) (2013) 31–39.
- [67] P.Y. Khashaba, Spectrofluorimetric analysis of certain macrolide antibiotics in bulk and pharmaceutical formulations, *J. Pharm. Biomed. Anal.* 27 (6) (2002) 923–932.
- [68] K.P. Hunfeld, P. Kraiczy, T. Wichelhaus, V. Schäfer, V. Brade, New colorimetric microdilution method for in vitro susceptibility testing of *Borrelia burgdorferi* against antimicrobial substances, *Eur. J. Clin. Microbiol. Infect. Dis.* 19 (1) (2000) 27–32.
- [69] D. Haleem, E. Shireen, M. Haleem, W. Kaye, U. Bailer, G. Frank, A. Wagner, S. Henry, Degradation studies of azithromycin and its spectrophotometric determination in pharmaceutical dosage forms, *Pak. J. Pharm. Sci.* 19 (2) (2006) 98–103.

- [71] A.P. Kumar, J.H. Park, Azithromycin as a new chiral selector in capillary electrophoresis, *J. Chromatogr. A* 4 (9) (2011) 1314–1317.
- [72] M.V. Lebedeva, G.A. Bulgakova, A.F. Prokhorova, E.N. Shapovalova, M.G. Chernobrovkin, O.A. Shpigun, Azithromycin for enantioseparation of tetrahydrozoline in NACE, *Chromatographia* 76 (7–8) (2013) 375–379.
- [73] L. Miguel, C. Barbas, LC determination of impurities in azithromycin tablets, *J. Pharm. Biomed. Anal.* 33 (2) (2003) 211–217.
- [74] P. Zubata, R. Ceresole, M.A. Rosasco, M.T. Pizzorno, A new HPLC method for azithromycin quantitation, *J. Pharm. Biomed. Anal.* 27 (5) (2002) 833–836.
- [75] N. Kovačić-Bošnjak, J. Marincel, N. Lopotar, G. Kobrehel, Reversed-phase HPLC analysis of the semisynthetic macrolide antibiotic azithromycin, *Chromatographia* 25 (11) (1988) 999–1003.
- [76] Z.Y. Yang, L. Wang, X. Tang, Determination of azithromycin by ion-pair HPLC with UV detection, *J. Pharm. Biomed. Anal.* 49 (3) (2009) 811–815.
- [77] S. Pan, X. Xiao, Y. Wang, Y. Yin, X. Zhu, Comparison of HPLC and microbiological methods in the detection of azithromycin in eye drops [J], *Northwest Pharm. J.* 3 (2011) 011.
- [78] P. Matzneller, S. Krasniqi, M. Kinzig, F. Sörgel, S. Hüttner, E. Lackner, M. Müller, M. Zeitlinger, Blood, tissue and intracellular concentrations of azithromycin during and after end of therapy, *Antimicrob. Agents Chemother.* 28 (2013) 28.
- [79] A.D.H. Moreno, M.F.C.D. Silva, H.R.N. Salgado, Stability study of azithromycin in ophthalmic preparations, *Braz. J. Pharm. Sci.* 45 (2009) 219–226.
- [80] L.L. Brunton, L.L. Brunton; associate editors, B.A. Chaber, B.C. Knollmann Goodman and Gilman's *The Pharmacological Basis of Therapeutics*, 12th ed., 2011.
- [81] S.S. Martindale, *The complete drug reference*, 36th ed., Pharmaceutical press, London, 2009.
- [82] L.L. Brunton, H.P. Rang, M.M. Dale, J.M. Ritter, R.J. Flower, Rang & Dale *Pharmacology*, 6th ed., Churchill Livingstone 2011, 2007.
- [83] B. Moshiree, R. McDonald, W. Hou, P.P. Toskes, Comparison of the effect of azithromycin versus erythromycin on antroduodenal pressure profiles of patients with chronic functional gastrointestinal pain and gastroparesis, *Dig. Dis. Sci.* 55 (3) (2010) 675–683.
- [84] P. Chini, P.P. Toskes, S. Waseem, W. Hou, R. McDonald, B. Moshiree, Effect of azithromycin on small bowel motility in patients with gastrointestinal dysmotility, *Scand. J. Gastroenterol.* 47 (4) (2012) 422–427.
- [85] *Wikipedia*. [cited 2013 25/5]; Available from: *Wikipedia*: <http://en.wikipedia.org/wiki/Azithromycin>.
- [86] D.L. Hahn, Treatment of *Chlamydia pneumoniae* infection in adult asthma: a before-after trial, *J. Fam. Pract.* 41 (4) (1995) 345–351.
- [87] H. Noedl, S. Krudsood, K. Chalermratana, U. Silachamroon, W. Leowattana, N. Tangpukdee, S. Looreesuwan, R.S. Miller, M. Fukuda, K. Jongsakul, S. Sriwichai, J. Rowan, H. Bhattacharyya, C. Ohrt, C. Knirsch, Azithromycin combination therapy with artesunate or quinine for the treatment of uncomplicated *Plasmodium falciparum* malaria in adults: a randomized, phase 2 clinical trial in Thailand, *Clin. Infect. Dis.* 43 (10) (2006) 1264–1271.
- [88] E. Gomez, M. Sanchez-Nunez, J.E. Sanchez, C. Corte, S. Aguado, C. Portal, J. Baltar, J. Alvarez-Grande, Treatment of cyclosporin-induced gingival hyperplasia with azithromycin, *Nephrol Dial Transplant* 12 (12) (1997) 2694–2697.
- [89] K. Hurt, D. Bilton, Cystic fibrosis, *Medicine* 40 (5) (2012) 273–276.
- [90] Joint Formulary Committee, *British National Formulary*, 57th ed., British Medical Association and Royal Pharmaceutical Society of Great Britain, London, 2009.



# Cefdinir

**Abdullah A. Al-Badr, Fahad A. Alasseiri**

Department of Pharmaceutical Chemistry, College of Pharmacy, King Saud University, P.O. Box 2457, Riyadh, Saudi Arabia

## Contents

1. Description	42
1.1 Nomenclature	42
1.2 Formulae	42
1.3 Elemental analysis	43
1.4 Appearance	43
2. Uses and Applications	43
3. Methods of Preparation	43
4. Physical Characteristics	54
4.1 Ionization constant	54
4.2 Solubility	54
4.3 X-ray powder diffraction	54
4.4 Thermal methods of analysis	54
5. Spectral Properties	55
5.1 Ultraviolet spectroscopy	55
5.2 Vibrational spectroscopy	55
5.3 Nuclear magnetic resonance spectrometry	59
5.4 Mass spectrometry	60
6. Methods of Analysis	60
6.1 Compendial methods	60
6.2 Spectrophotometric methods	92
6.3 Polarographic method	94
6.4 Voltammetric methods	95
6.5 Chromatographic methods	96
7. Pharmacokinetics	102
8. Stability	106
Acknowledgments	108
References	108



## 1. DESCRIPTION

### 1.1. Nomenclature

#### 1.1.1 Systematic chemical names

- (6*R*,7*R*)-7-[[*(Z)*-(2-Amino-4-thiazolyl)(hydroxyimino)acetyl]amino]-3-ethenyl-8-oxo-5-thia-1-azabicyclo[4.2.0]oct-2-ene-2-carboxylic acid.
- Syn-7-[2-(2-amino-4-thiazolyl)-2-hydroxyiminoacetamido]-3-vinyl-3-cephem-4-carboxylic acid.
- (–)(6*R*,7*R*)-7-[2-(2-amino-4-thiazolyl)glyoxylamido]-8-oxo-3-vinyl-5-thia-1-azabicyclo[4.2.0]oct-2-ene-2-carboxylic acid 7<sup>2</sup>-(*Z*)-oxime.
- 7-[(2-Amino-1,3-thiazol-4-yl)-2-[(*Z*)-hydroxyimino]acetamido]-3-vinyl-3-cephem-4-carboxylic acid.
- 7β-[2-(2-aminothiazol-4-yl)-2-(*Z*)-hydroximinoacetamido]-3-vinyl-3-cephem-4-carboxylic acid.
- 5-Thia-1-azabicyclo[4,2,0]oct-2-ene-carboxylic acid, 7-[[*(2*-amino-4-thiazolyl)(hydroxyimino)acetyl]amino-]-3-ethenyl-8-oxo-, [6*R*-[6α, 7β(*Z*)]]-; [1,2].

#### 1.1.2 Non-proprietary names

Cefdinir, FK 482, BMV-28488

#### 1.1.3 Proprietary names

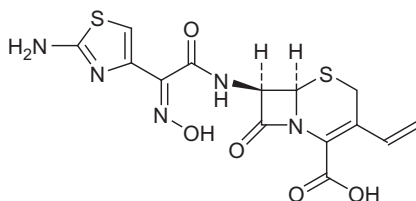
Omnicef<sup>®</sup>, Cefzon<sup>®</sup>

## 1.2. Formulae

### 1.2.1 Empirical formula, molecular weight, and CAS number

$C_{14}H_{13}N_5O_5S_2$	395.42	91832-40-5
-------------------------	--------	------------

### 1.2.2 Structural formula



### 1.3. Elemental analysis

C 42.53%, H 3.31%, N 17.71, O 20.23%, S 16.22%

### 1.4. Appearance

White to slightly brownish-yellow solid [1].



## 2. USES AND APPLICATIONS

Cefdinir is a third-generation oral cephalosporin antibiotic similar to cefixime. It is reported to be much more active *in vitro* than cefixime against *Staphylococcus aureus* and *Enterococcus faecalis*, but it is less active against *Enterobacteriaceae*. It is given by mouth in a usual dose of 600 mg daily as a single dose or in two divided doses. Children may be given 14 mg/kg body-weight daily up to a maximum of 600 mg. Doses should be reduced in patients with renal impairment (with a creatinine clearance of less than 30 mL/min) to 300 mg once daily [2–7].



## 3. METHODS OF PREPARATION

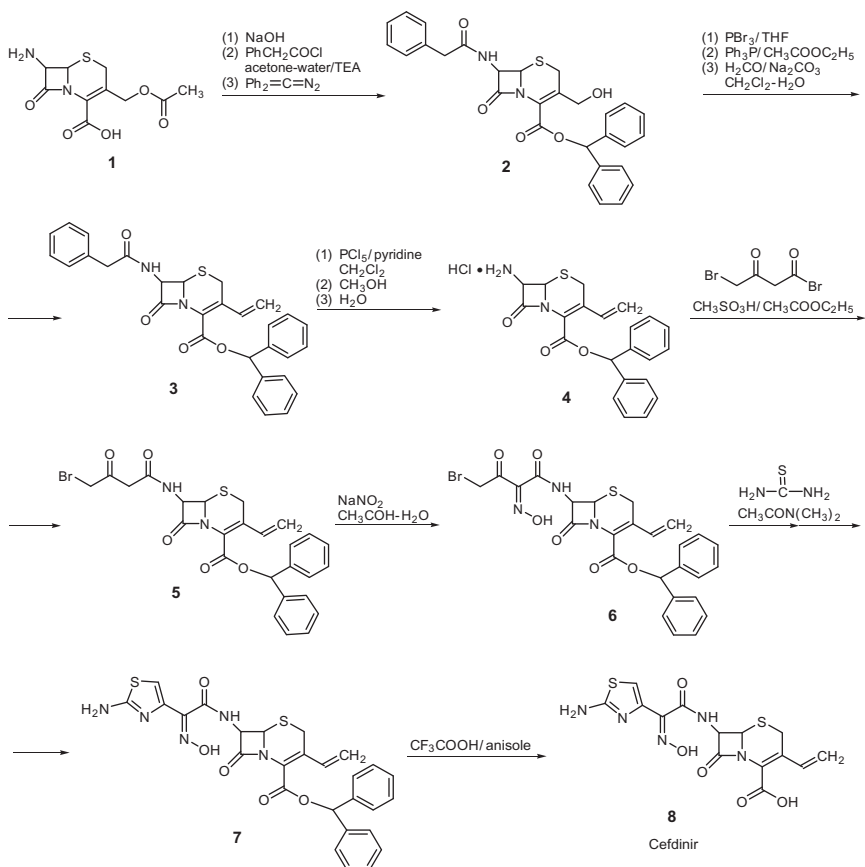
Gonzalez *et al.* [8] described the synthesis of cefdinir which is reported in the literature [9–13] as follows.

7-Aminocephalosporanic acid **1** was treated with sodium hydroxide and was then reacted with phenyl acetyl chloride in acetone, water, and triethylamine and finally by diphenyldiazomethane to give the diprotected compound **2**. The alcohol **2** was treated with phosphorous tribromide in tetrahydrofuran and then by triphenyl phosphine in ethyl acetate and finally by formaldehyde in sodium carbonate and dichloromethane in water to yield the 3-ethenyl compound **3**. Compound **3** was reacted with phosphorous pentachloride in pyridine and dichloromethane. The product obtained was treated with methanol and water to form **4**. The amino group in **4** was acylated with 4-bromoacetoacetyl bromide and methane sulfonic acid in ethyl acetate, and compound **5** is produced. Compound **5** reacted with sodium nitrite in acetaldehyde and water to yield **6**. The latter compound **6** was cyclized by reaction with thiourea in *N,N*-dimethylacetamide to produce **7**. Compound **7** reacted with trifluoroacetic acid in anisole to give the free acid, cefdinir **8**, Scheme 2.1.



Gonzalez *et al.* [8] prepared sodium 2-(2-tritylaminothiazol-4-yl)-(Z)-2-(tritylhydroximino)acetate **6** as an intermediate compound for the synthesis of cefdinir.

Ethyl aceto acetate **1** was treated with sodium nitrite in acetic acid and water to give ethyl-2-hydroximino-3-oxobutyrates **2**. The oxime **2** was treated with sulfonyl chloride in acetic acid to yield the 4-chloro derivative **3**. Compound **3** was cyclized with thiourea to give **4**. The product **4** was protected with triphenyl methyl chloride, triethylamine in chloroform to produce **5**. Compound **5** was hydrolyzed to give sodium 2-(2-tritylaminothiazol-4-yl)-(Z)-2-(trityloximino)acetate **6**. Compound **6**, was treated with benzhydryl-7-amino-3-vinyl-3-cephem-4-carboxylate

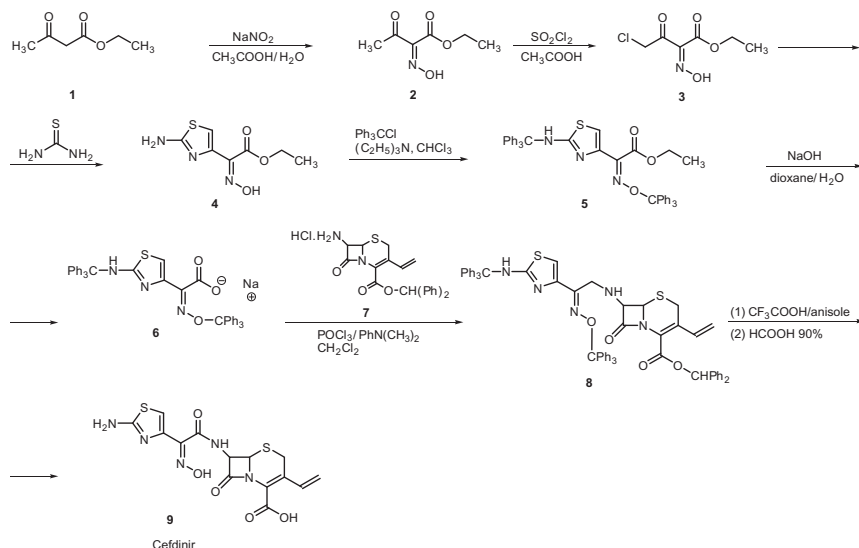


Scheme 2.1 Synthesis of cefdinir according to the reported methods [9–13].

hydrochloride **7** in phosphorous oxychloride, dimethylaniline, and dichloromethane to produce **8**. Compound **8** was treated with trifluoroacetic acid, anisole, and formic acid to produce cefdinir **9** (Scheme 2.2).

Gonzalez *et al.* [8] overcame the drawbacks of using the diketene during the synthesis of cefdinir by the literature methods [9–13] as follows.

7-Aminocephalosporanic acid **1** was hydrolyzed by sodium hydroxide and hydrochloric acid to the alcohol **2**. The 7-amino group in compound **2** was protected by treatment with phenylacetic acid, phosphorous oxychloride, dimethylformamide, tetrahydrofuran, and then by bistrimethylsilyl acetamide in tetrahydrofuran. The carboxylic acid group was esterified with diphenyldiazomethane to give the 4-diphenyl methyl ester **3**. Compound **3** was treated with phosphorous tribromide in tetrahydrofuran then with triphenylphosphine in ethyl acetate and finally by formaldehyde in sodium carbonate, dichloromethane, and water to yield the 3-ethenyl compound **4**. Compound **4** was treated with phosphorous pentachloride in pyridine and dichloromethane and in methanol and water to produce the 7-amine hydrochloride **5**. Reaction of **5** with sodium 2-(2-tritylaminothiazol-4-yl)-2-(trityloxyimino)acetate **6** and phosphorous oxychloride and dimethylaniline in dichloromethane produced **7**.



**Scheme 2.2** The modified synthesis of cefdinir [8].

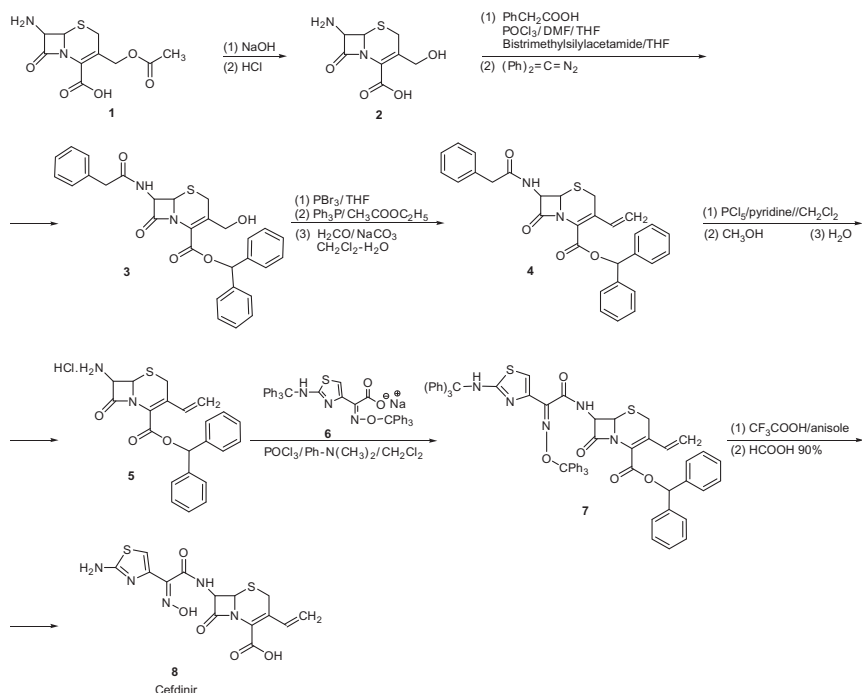
Compound **7** was deprotected by treatment with trifluoroacetic acid in anisole and then with 90% formic acid to give cefdinir **8** (Scheme 2.3).

Takaya *et al.* [10] prepared cefdinir according to the following.

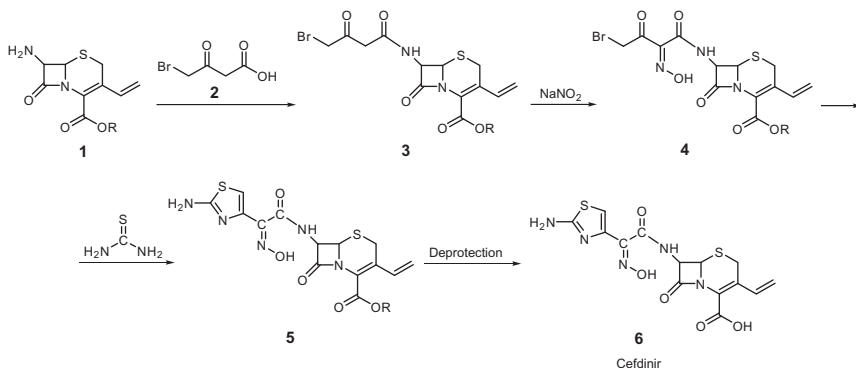
7-Amino-3-vinyl-3-cephem-4-carboxylic acid ester **1** was acylated with 4-bromo-3-oxobutanoic acid **2** to obtain the acylated product **3**. Compound **3** was treated a sodium nitrite to give the oxime **4**. Compound **4** was cyclized with thiourea to produce the 2-aminothiazole **5**. Cefdinir **6** was obtained from compound **5** after the removal of carboxylic acid protecting group, Scheme 2.4.

Kamachi *et al.* [12] described the following method for the preparation of cefdinir.

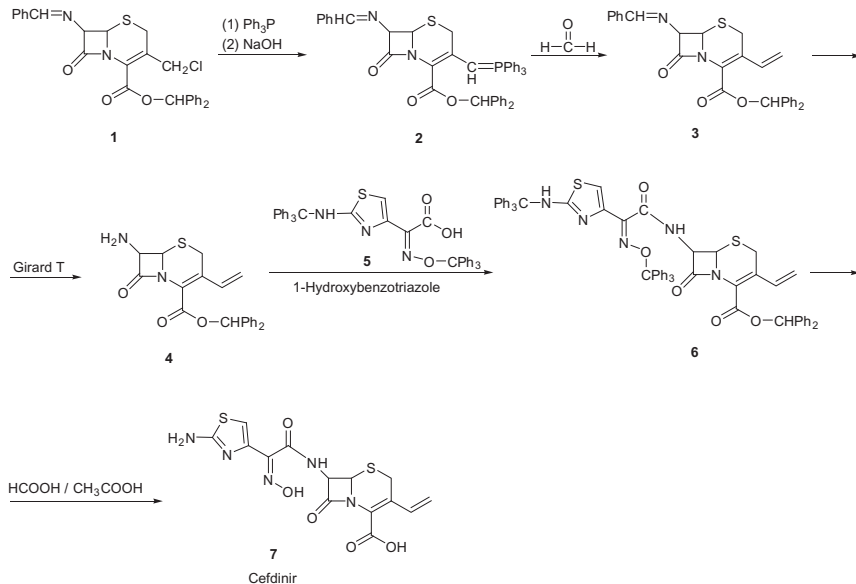
Diphenylmethyl-7-benzylidene-3-cephem-3-chloromethyl-4-carboxylate **1** was treated with triphenylphosphine followed by aqueous sodium hydroxide to produce the yield **2**. The Wittig reaction with formaldehyde was carried out to afford the product **3**, which was without isolation, treated with Girard T reagent to yield **4**. Compound **4** was acylated with



Scheme 2.3 Synthesis of cefdinir [8].



**Scheme 2.4** Synthesis of cefdinir [10].



**Scheme 2.5** Synthesis of cefdinir [12].

(*Z*)-2-(2-(2-tritylaminothiazol-4-yl)-2-trityloximino acetic acid **5** by the active ester method using 1-hydroxybenzotriazole to afford **6**. Deblocking of **6** with formic acid–acetic acid yield cefdinir **7**, [Scheme 2.5](#).

Lee *et al.* [14] used the following procedure for the preparation of cefdinir.

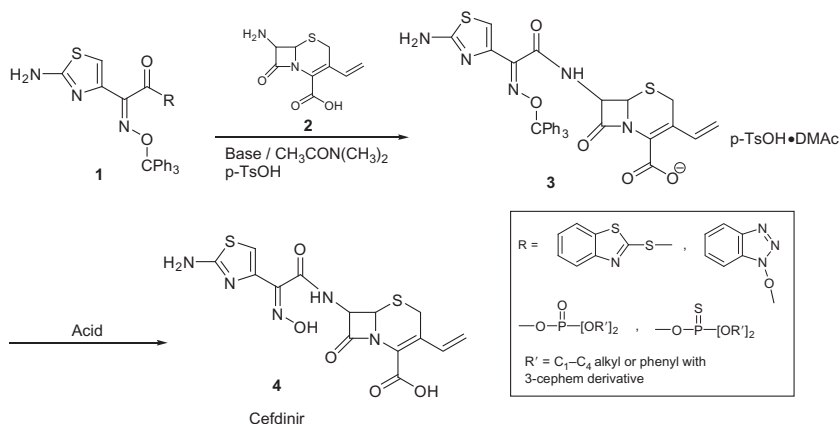
Reaction of substituted 2-(2-amino-4-thiazolyl)-2-trityloxyimino acetyl **1** with 7-amino-3-vinyl-3-cephem-4-carboxylic acid **2** in base, and *N,N*-dimethylacetamide and *p*-toluene sulfonic acid gives 7-[2-(2-amino-4-thiazolyl)-2-trityloxyimino-acetamido]-3-vinyl-3-cephem-4-carboxylic acid salt **3**. After removal of the trityl protecting group and hydrolysis, cefdinir **4** is produced (Scheme 2.6).

Kumar *et al.* [15] described the following method for the preparation of cefdinir.

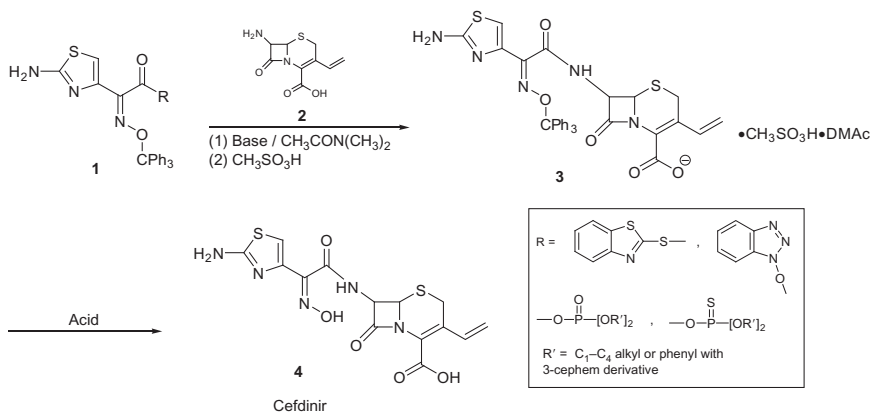
Reaction of substituted 2-(2-amino-4-thiazolyl)-2-trityloxyimino acetyl **1** with 7-amino-3-vinyl-3-cephem-4-carboxylic acid **2** in base, *N,N*-dimethyl acetamide and methyl sulfonic acid gives 7-[2-(2-amino-4-thiazolyl)-2-trityloxyimino-acetamido]-3-vinyl-3-cephem-4-carboxylic acid salt **3**. After removal of the trityl protecting group and hydrolysis, cefdinir **4** is produced (Scheme 2.7).

Moralikrishna *et al.* [16] reported the following method for preparation of cefdinir.

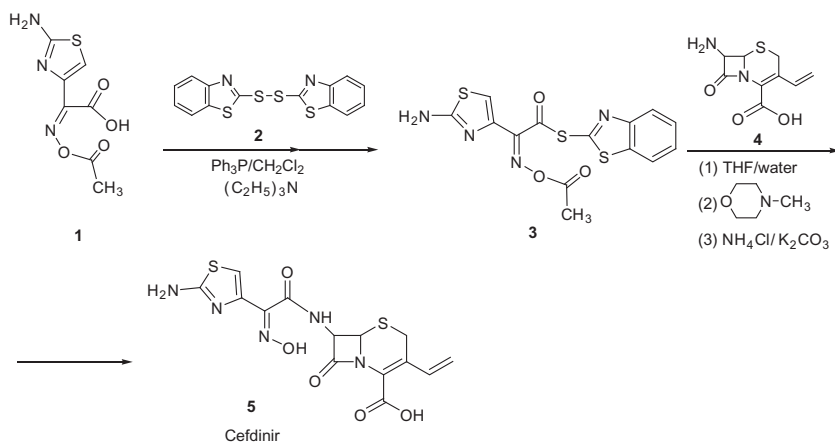
(*Z*)-2-(2-amino-4-thiazolyl)-2-acetoxyimino acetic acid **1** was treated with triphenyl phosphine and bis-(benzothiazol-2-yl)disulfide **2** and was taken in dichloromethane and stirred for ½ h at 15–20 °C. Triethylamine was added and reaction was monitored by HPLC and the product **3** was obtained. Compound **3** was treated with 7-amino-3-vinyl-3-cephem-4-carboxylic acid **4** and was taken in aqueous tetrahydrofuran and *N*-methyl morpholine was added. Ammonium chloride was added and hydrolysis was carried out by potassium carbonate solution to obtain cefdinir **5**, Scheme 2.8.



Scheme 2.6 Synthesis of cefdinir [14].



**Scheme 2.7** Synthesis of cefdinir [15].

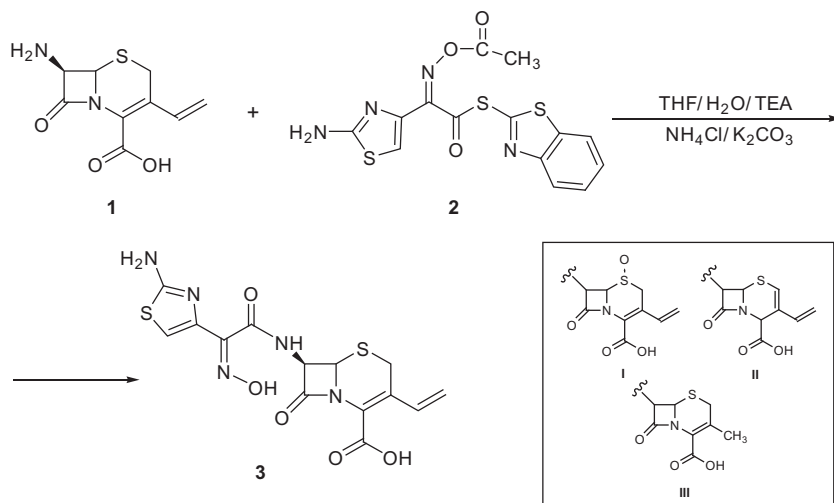


**Scheme 2.8** Synthesis of cefdinir [16].

Rao *et al.* [17,18] prepared cefdinir by the condensation of 7-amino-3-vinyl-3-cephem-4-carboxylic acid **1** with 2-(2-aminothiazol-4-yl)-2-((Z)-acetyloxyimino)-thioacetic acid benzothiazolyl-2-thioester **2** according to Scheme 2.9. The authors isolated and elucidated and characterized three impurities from the bulk of cefdinir namely: the *s*-oxide **I**, the ceph-2-em isomer **II**, and the 3-methyl analog **III** of cefdinir **3**.

Singh *et al.* [19] outlined the preparation of cefdinir as follows.

The condensation of 2-(2-aminothiazol-4-yl)-2-((Z)-trityloxyimino)-thioacetic acid benzothiazolyl-2-thioester **1** with 7-amino-3-vinyl-3-cephem-4-carboxylic acid **2** by means of tributylamine in *N,N*-dimethyl



**Scheme 2.9** Synthesis of cefdinir [17,18].

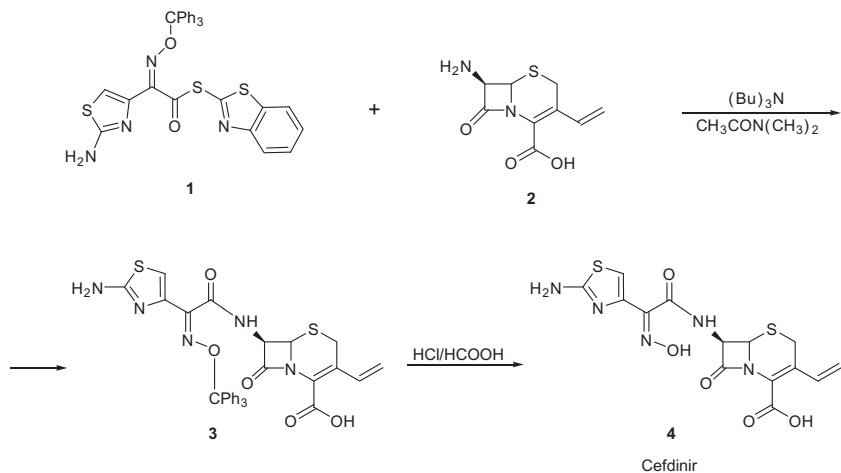
acetamide gives the corresponding amide **3** which is diprotected by means of HCl and formic acid to provide cefdinir **4**, [Scheme 2.10](#).

Kawabata *et al.* [20] described a method for the preparation of cefdinir as follows.

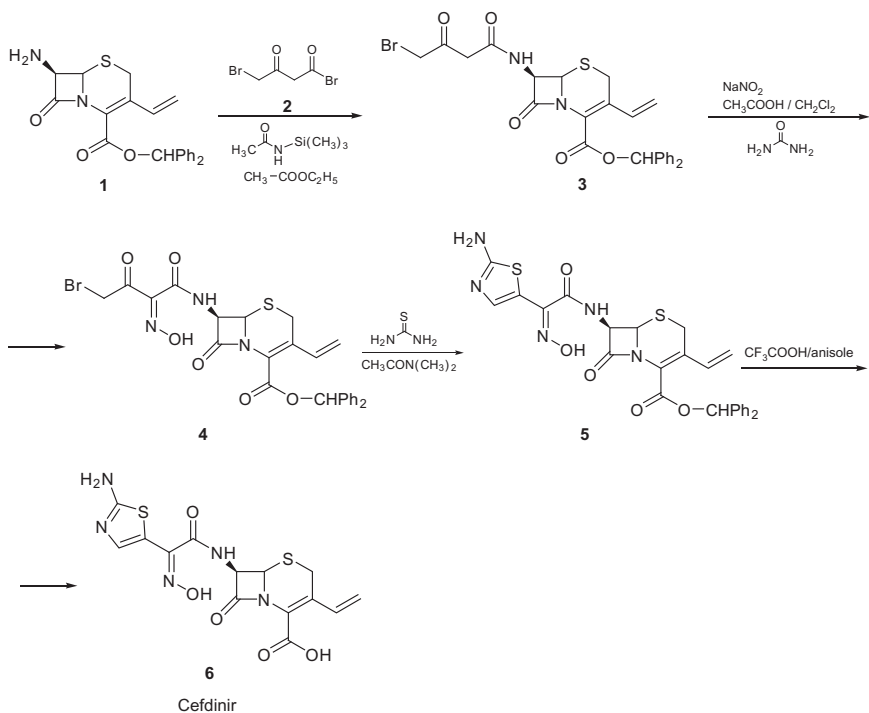
The condensation of benzhydryl-7-amino-3-vinyl-3-cephem-4-carboxylate **1** with 4-bromoacetoacetyl bromide **2** by means of trimethylsilylacetamide in ethyl acetate gives benzhydryl-7-(4-bromoacetoacetamido)-3-vinyl-3-cephem-4-carboxylate **3** which by reaction with sodium nitrite-acetic acid in dichloromethane and then with urea is converted to benzhydryl-7-(4-bromo-2-(hydroxyimino)acetoacetamido)-3-vinyl-3-cephem-4-carboxylate **4**. The cyclization of **4** with thiourea in dimethylacetamide affords benzhydryl-7-[2-(2-aminothiazol-4-yl)-2-(hydroxyiminoacetamido)]-3-vinyl-3-cephem-4-carboxylic acid salt **3** which is finally hydrolyzed with trifluoroacetic acid-anisole to give cefdinir **6**, [Scheme 2.11](#).

Sakane and Kazuo [21] prepared cefdinir as described in Spanish patent ES-2013828 as follows.

Sodium 2-(2-aminothiazol-4-yl)-2-hydroxyimino acetate **1** was converted to (*Z*)-2-(2-amino-4-thiazolyl)-2-acetyloxyimino acetic acid **2** and compound **2** was converted into the corresponding acid chloride hydrochloride **3**, via reaction with phosphorus pentachloride and **3** was condensed



Scheme 2.10 Synthesis of cefdinir [19].



Scheme 2.11 Synthesis of cefdinir [20].

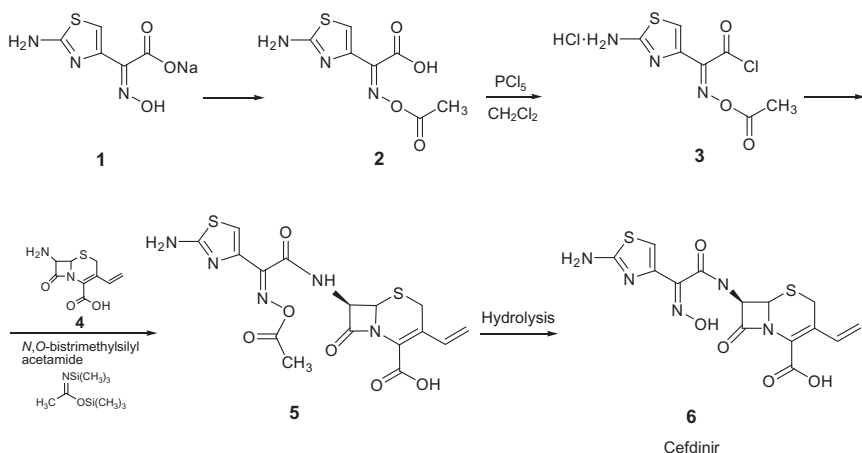


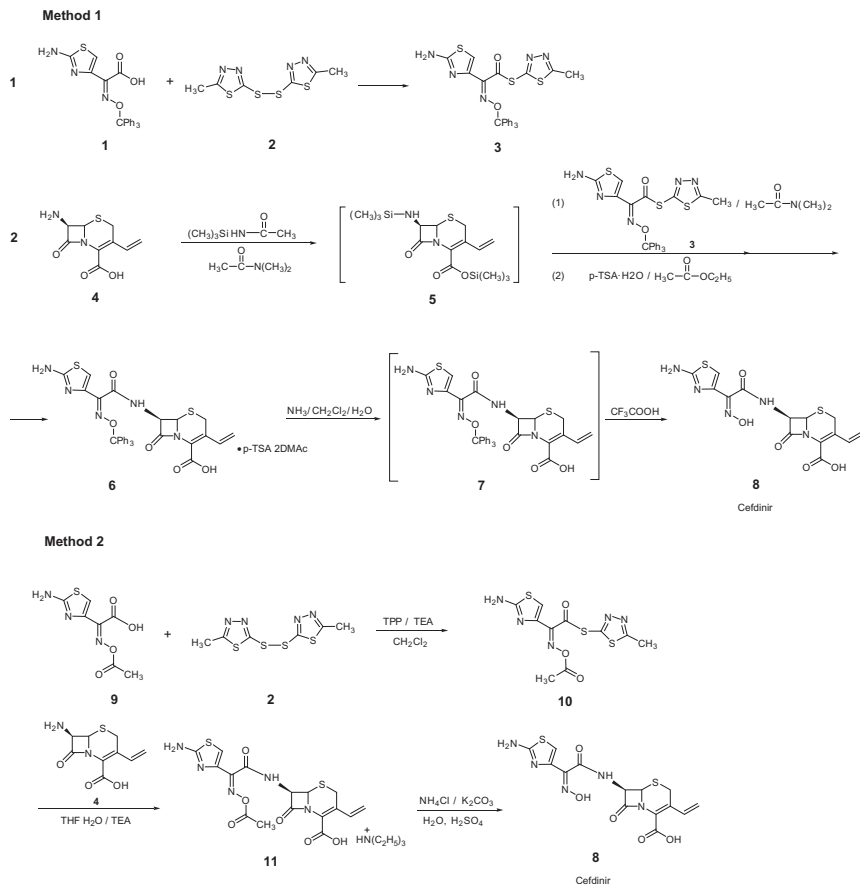
with 7-amino-3-vinyl-3-cephem-4-carboxylic acid **4** to yield O-acetyl derivative **5** which was deprotected to produce cefdinir **6**, [Scheme 2.12](#).

Rao *et al.* [22] synthesized two new compounds namely: 2-mercapto-5-methyl-1,3,4-thiadiazolyl-(Z)-2-(2-amino-4-thiazolyl)-2-trityloxyiminoacetate **3** and 2-mercapto-5-methyl-1,3,4-thiadiazolyl-(Z)-2-(2-amino-4-thiazolyl)-acetyloxyimino acetate **10** and used them (methods 1 and 2) for the preparation of cefdinir. Compound **3** was prepared by the reaction of (Z)-2-(2-amino-4-thiazolyl)-2-trityloxyimino acetic acid **1** with bis-(5-methyl-1,3,4-thiadiazol-2-yl)disulfide **2**. Similarly compound **10** was prepared by the reaction of (Z)-2-(2-amino-4-thiazolyl)-2-acetoxyimino acetic acid **9** with bis-(s-methyl-1,3,4-thiadiazol-2-yl)-disulfide **2**. In method 1, 7-amino-3-vinyl-3-cephem-4-carboxylic acid **4** was treated with *N*-trimethyl silyl acetamide and *N,N*-dimethylacetamide and the product obtained **5** was treated with compound **3** to give **6**. Compound **6** was treated with ammonia in dichloromethane and water and the intermediate compound **7** was produced. After the removal of protecting group from **7** by trifluoroacetic acid, cefdinir **8** was produced.

In method 2, compound **10** was treated with compound **4** in tetrahydrofuran, water, and triethylamine to give the intermediate **11** which was treated with ammonium chloride and sodium carbonate and after hydrolysis with aqueous sulfuric acid, cefdinir **8** was produced, [Scheme 2.13](#).

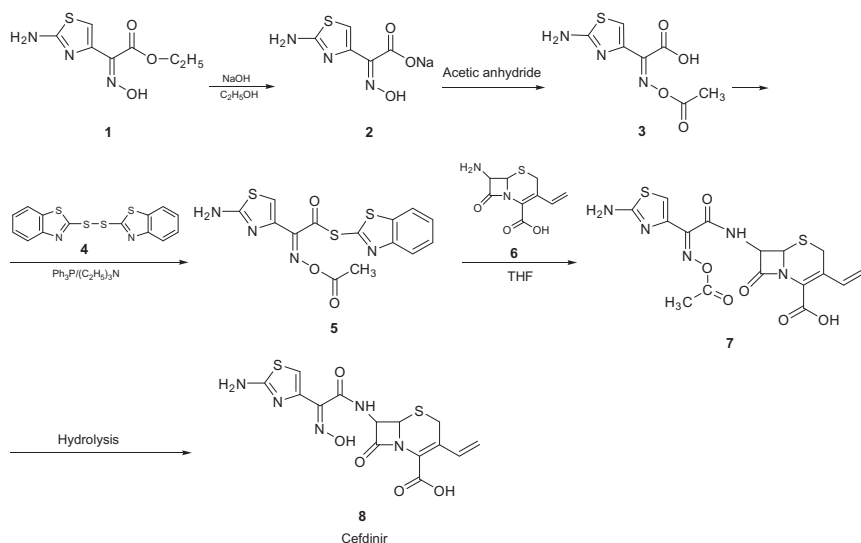
Dandala *et al.* [23] reported the following method for the synthesis of cefdinir.





**Scheme 2.13** Synthesis of cefdinir (methods 1 and 2) [22].

Ethyl (*Z*)-2-(2-amino-4-thiazolyl)-2-hydroxyimino acetate **1** is treated with aqueous sodium hydroxide in ethanol to yield the corresponding sodium salt **2**. Compound **2** was acetylated to yield (*Z*)-2-(2-amino-4-thiazolyl)-2-acetyloxyimino acetic acid **3**. Condensation of **3** with bis-(benzothiazol-2-yl) disulfide **4** in the presence of triphenylphosphine and a base gives 2-mercaptobenzothiazolyl-(*Z*)-2-(2-amino-4-thiazolyl)-2-acetyloxyiminoacetate (*O*-acetyl thioester) **5**. Compound **5** when treated with 7-amino-3-vinyl-3-cephem-4-carboxylic acid **6** in tetrahydrofuran compound **7** was produced. After the hydrolysis of compound **7**, cefdinir **8** was obtained, [Scheme 2.14](#).



Scheme 2.14 Synthesis of cefdinir [23].



## 4. PHYSICAL CHARACTERISTICS

### 4.1. Ionization constant

pKa: 8.70

### 4.2. Solubility

Slightly soluble in dilute hydrochloric acid, sparingly soluble in 0.1 M pH 7 phosphate buffer [2].

### 4.3. X-ray powder diffraction

The X-ray powder diffraction pattern of cefdinir was performed using Simmons XRD-5000 diffractometer. Figure 2.1 shows the X-ray powder diffraction pattern of cefdinir which was obtained on a pure sample of the drug substance. Table 2.1 shows the values for the scattering angles (deg,  $2\theta$ ), the interplanar  $d$ -spacing ( $\text{\AA}$ ), and the relative intensities.

### 4.4. Thermal methods of analysis

#### 4.4.1 Melting point

170 °C (dec) [1].

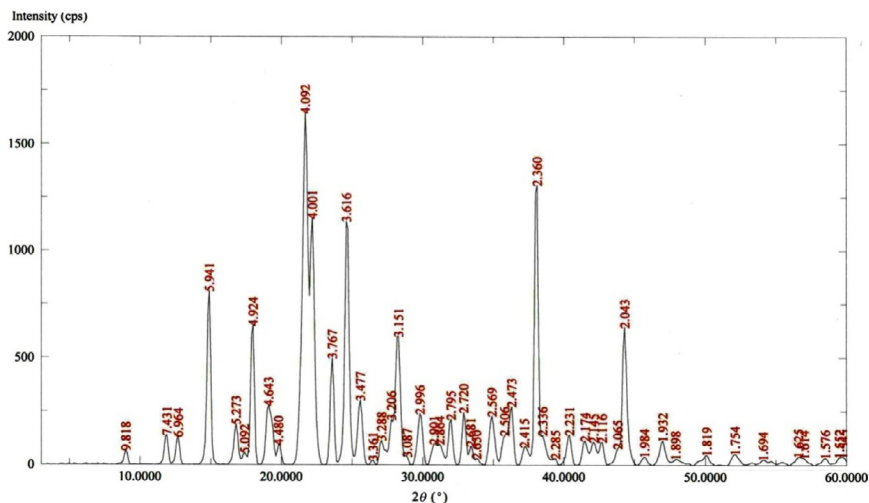


Figure 2.1 The X-ray powder diffraction pattern of cefdinir.

#### 4.4.2 Differential scanning calorimetry

The differential scanning calorimetry (DSC) studies were carried out using differential scanning calorimeter equipped with anointer cooler (Shimadzu DSC-60, Shimadzu Corporation, Koyoto, Japan). Indium/zinc standard were used to calibrate the temperature and enthalpy scale. The samples were hermetically sealed in an aluminum pans and heated at a constant rate of 10 °C/min over a temperature range of 25–300 °C. Inert atmosphere was maintained by purging nitrogen gas at a flow rate of 50 mL/min. The DSC thermogram is shown in Figure 2.2.



## 5. SPECTRAL PROPERTIES

### 5.1. Ultraviolet spectroscopy

The ultraviolet absorption spectrum of cefdinir in ethanol was recorded using a Shimadzu ultraviolet–visible spectrophotometer 1601 PC. The ultraviolet spectrum is shown in Figure 2.3 and cefdinir exhibited three maxima at 200.5, 223.5, and 287 nm.

### 5.2. Vibrational spectroscopy

The infrared absorption spectrum of cefdinir was obtained in a KBr pellet using a Perkin Elmer infrared spectrophotometer is presented in Figure 2.4. The principal peaks and their assignments are listed in Table 2.2.

**Table 2.1** The X-ray powder diffraction pattern for cefdinir

Scattering angle (° 2θ)	d-Spacing (Å)	Relative intensity (%)	Scattering angle (° 2θ)	d-Spacing (Å)	Relative intensity (%)
9.00	9.8176	66	38.100	2.3600	1308
11.900	7.4308	140	38.500	2.3364	140
12.700	6.9645	131	39.400	2.2851	31
14.900	5.9407	810	40.400	2.2308	141
16.800	5.2729	189	41.500	2.1741	113
17.400	5.0924	55	42.100	2.1445	108
18.000	4.9240	650	42.700	2.1158	107
19.100	4.6468	277	43.800	2.0652	79
19.800	4.4802	95	44.300	2.0430	643
21.700	4.0920	1645	45.700	1.9836	38
22.200	4.0010	1152	47.000	1.9317	112
23.600	3.7667	497	47.900	1.8975	28
24.600	3.6158	1137	50.100	1.8192	46
25.600	3.4768	301	52.100	1.7540	51
26.500	3.3607	21	54.100	1.6938	25
27.100	3.2877	115	56.600	1.6248	39
27.800	3.2065	212	57.000	1.6143	32
28.300	3.1509	600	58.500	1.5764	33
28.900	3.0869	38	59.500	1.5523	36
29.800	2.9957	239	59.800	1.5452	36
30.800	2.9006	98	61.900	1.4978	23
31.200	2.8644	96	64.500	1.4435	109
32.000	2.7945	213	77.600	1.2293	209
32.900	2.7201	245	81.700	1.1777	106
33.400	2.6805	89	98.200	1.0191	26
33.800	2.6497	31	98.500	1.0168	21
34.900	2.5687	228	110.900	0.9352	65
35.800	2.5061	140	111.400	0.9324	35
36.300	2.4728	273	115.400	0.9113	55
37.200	2.4150	84	115.800	0.9093	34

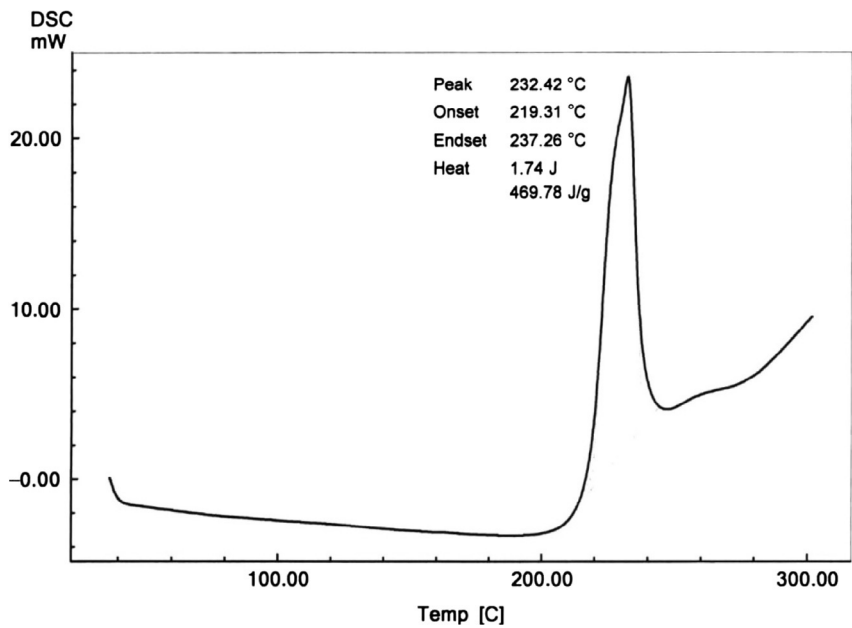


Figure 2.2 The differential scanning calorimetry thermogram of cefdinir.

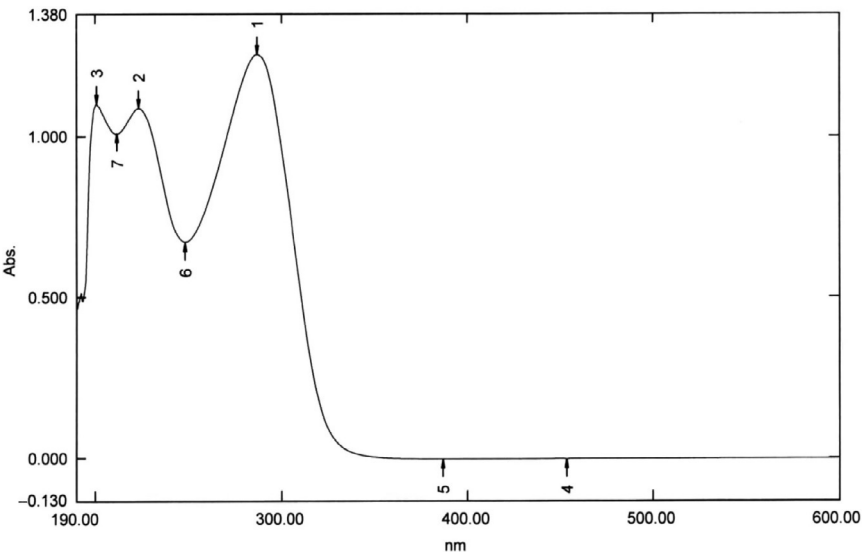


Figure 2.3 The ultraviolet spectrum of cefdinir in ethanol.

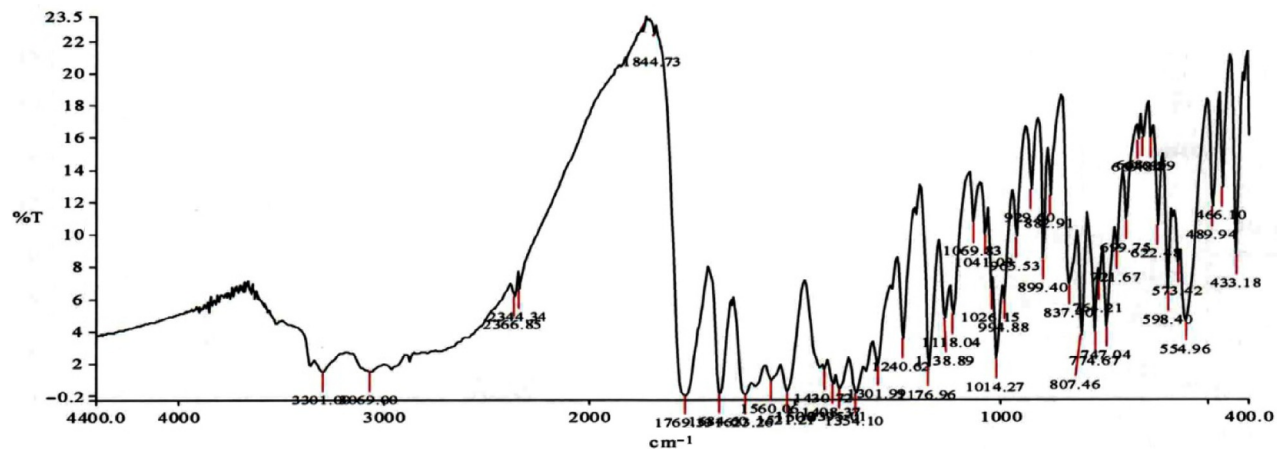
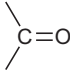
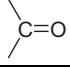


Figure 2.4 The Infrared spectrum of cefdinir (KBr disc).

**Table 2.2** The vibrational assignments of cefdinir infrared absorption bands

Frequency (cm <sup>-1</sup> )	Assignment
3302, 3170	–NH–
2980	CH aliphatic
1784	β-Lactam 
1668	Amide 
1520	–NH–
11611, 1429	Acid 
1350, 1334	NH <sub>2</sub>
1010	NO

### 5.3. Nuclear magnetic resonance spectrometry

The <sup>1</sup>H and <sup>13</sup>C NMR spectra of cefdinir were recorded with a Bruker instrument 200 Spectrometer (200 MHz). Chemical shifts were expressed in parts per million with respect to the tetramethylsilane (TMS) signal for <sup>1</sup>H and <sup>13</sup>C NMR.

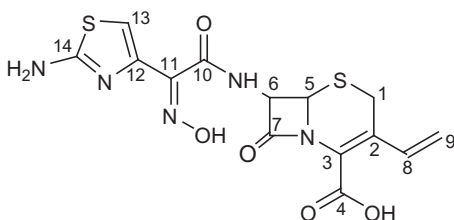
#### 5.3.1 <sup>1</sup>H NMR spectra

The <sup>1</sup>H spectra of cefdinir were recorded with a Bruker 200 spectrometer (200 MHz). Chemical shifts were expressed in parts per million with respect to the TMS signal. The corresponding spectral assignment of <sup>1</sup>H NMR spectra of cefdinir is listed in [Table 2.3](#). The <sup>1</sup>H NMR spectra of cefdinir were dissolved in DMSO-d<sub>6</sub> and are shown in [Figures 2.5–2.7](#), and the COSY spectrum is shown in [Figure 2.8](#).

#### 5.3.2 <sup>13</sup>C NMR Spectra

The <sup>13</sup>C NMR spectra of cefdinir were recorded with a Bruker spectrometer (200 MHz). Chemical shifts were expressed in parts per million with respect to the TMS signal. The corresponding spectral assignment for the <sup>13</sup>C NMR spectra of cefdinir is listed in [Table 2.4](#). The <sup>13</sup>C NMR spectra of cefdinir dissolved in DMSO-d<sub>6</sub> are shown in [Figures 2.9 and 2.10](#) and HMBC and HSQC spectra are shown in [Figures 2.11 and 2.12](#), respectively.



**Table 2.3** The proton-nuclear magnetic resonance assignments for the spectrum of cefdinir

Chemical shift (ppm relative to TMS)	Number of protons	Multiplicity (s, singlet; d, doublet; dd, double doublet; m, multiplet; q, quartet)	Assignment (proton at carbon number)
3.56, 3.83	2	ABq	1
5.20	1	d	6
5.32	1	d	9 <i>cis</i>
5.60	1	d	9 <i>trans</i>
5.81	1	dd	5
6.68	1	s	13
6.92	1	dd	8
7.14	2	s	–NH <sub>2</sub>
9.50	1	d	–NHCO
11.34	1	s	–NOH

## 5.4. Mass spectrometry

The mass spectrum of cefdinir was carried out using an Agilent 6410 triple quadrupole LC/MS in the negative mode. Figure 2.13 shows the mass fragmentation pattern of the drug substance and Table 2.5 lists the assignments of the mass fragments.



## 6. METHODS OF ANALYSIS

### 6.1. Compendial methods

#### 6.1.1 Japanese pharmacopeia methods [24]

##### 6.1.1.1 Cefdinir

Cefdinir contains not less than 900 µg (potency) per mg. The potency of cefdinir is expressed as mass (potency) of cefdinir (C<sub>14</sub>H<sub>13</sub>N<sub>5</sub>O<sub>5</sub>S<sub>2</sub>).

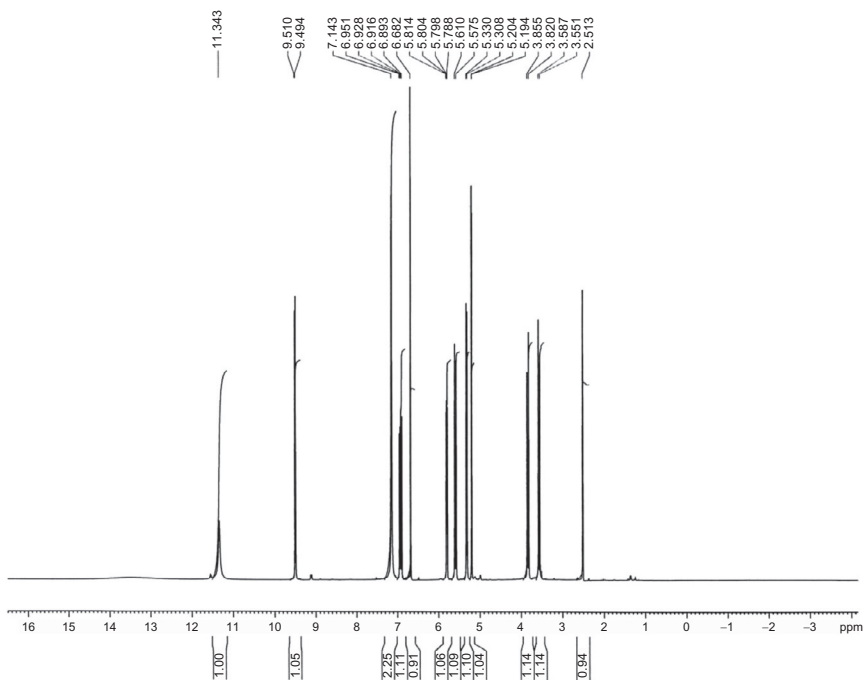


Figure 2.5 The  $^1\text{H}$  NMR spectrum of cefdinir.

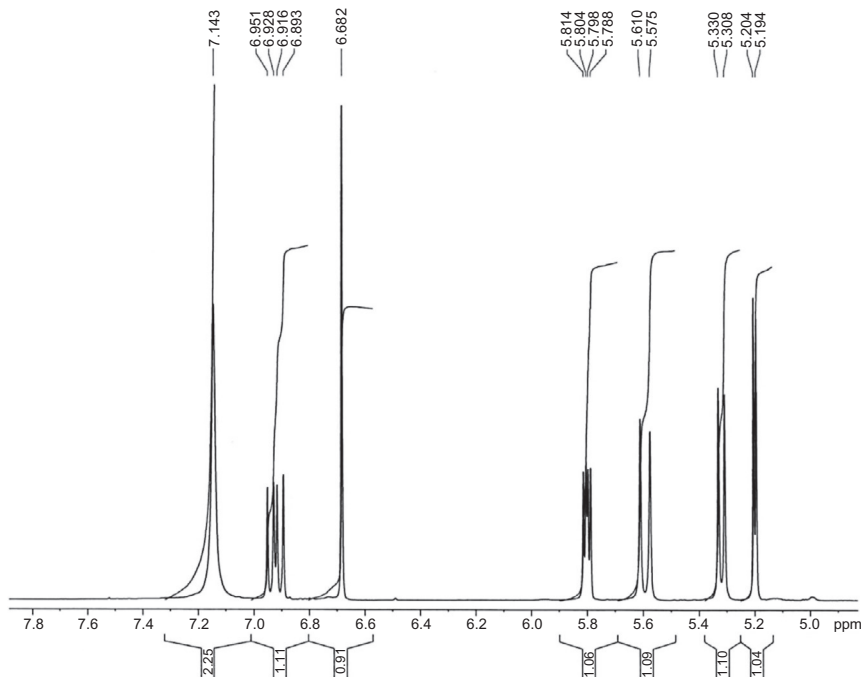
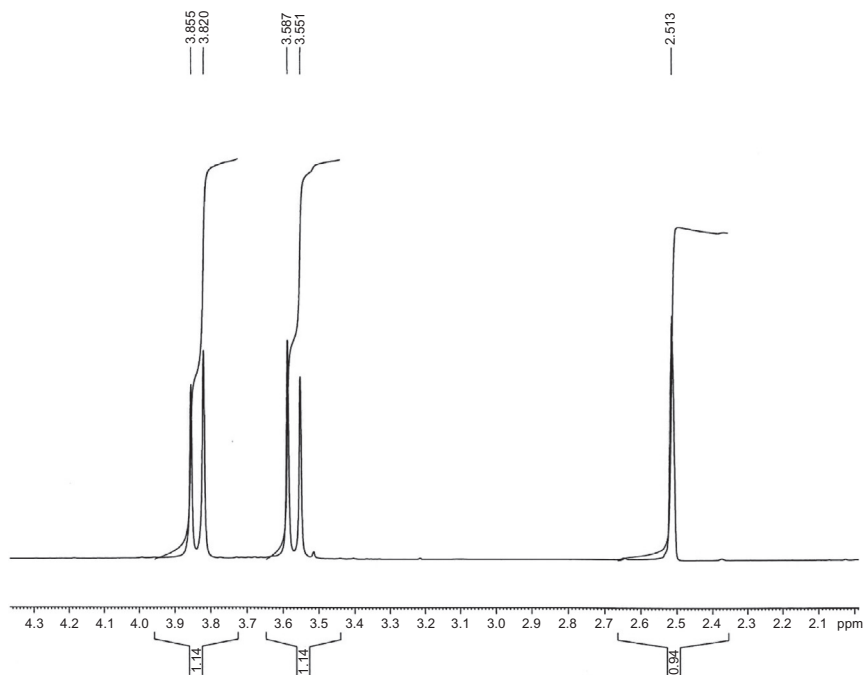


Figure 2.6 The expanded  $^1\text{H}$ -NMR spectrum of cefdinir (5.0-7.4 ppm) in  $\text{DMSO-d}_6$ .



**Figure 2.7** The expanded  $^1\text{H}$ -NMR spectrum of cefdinir (2.4–4.0 ppm) in  $\text{DMSO-d}_6$ .

**Description:** Cefdinir occurs as a white to light yellow crystalline powder.

It is practically insoluble in water, in ethanol (95%), and in diethyl ether. It dissolves in 0.1 mol/L phosphate buffer solution, pH 7.0.

### Identification

(1) Determine the absorption spectra of solutions of Cefdinir and Cefdinir Reference Standard in 0.1 mol/L phosphate buffer solution, pH 7.0 (1 in 100,000) as directed under the ultraviolet–visible spectrophotometry, in the general method <2.24>, and compare these spectra: both spectra exhibit similar intensities of absorption at the same wavelengths.

(2) Determine the infrared absorption spectra of Cefdinir and Cefdinir Reference Standard as directed in the paste method under the infrared spectrophotometry, in the general method <2.25>, and compare these spectra: both spectra exhibit similar intensities of absorption at the same wave numbers.

(3) Determine the spectrum of a solution of cefdinir in a mixture of deuterated dimethyl sulfoxide and heavy water for nuclear magnetic resonance spectroscopy (4:1) (1 in 10), using TMS for nuclear magnetic

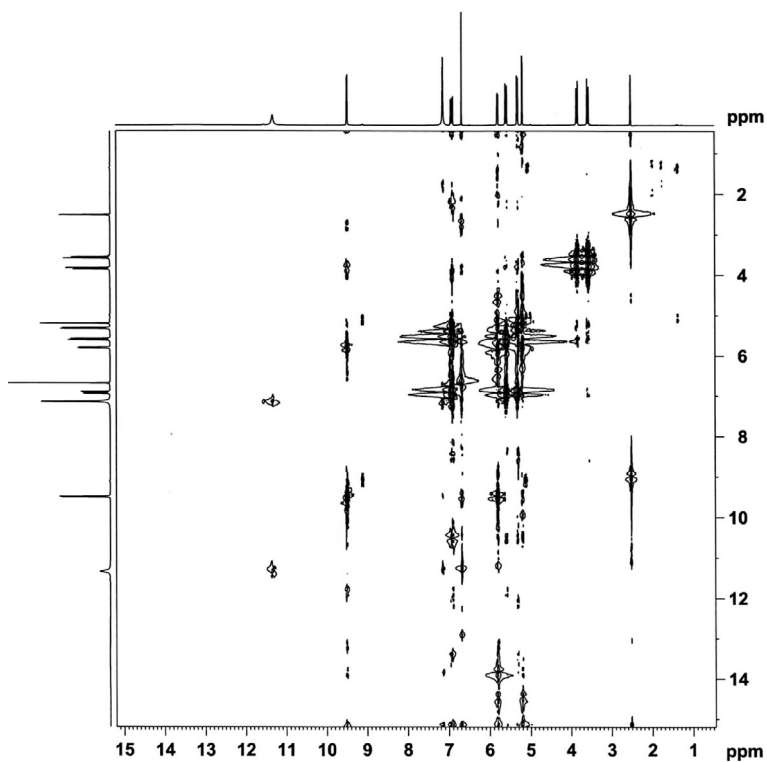
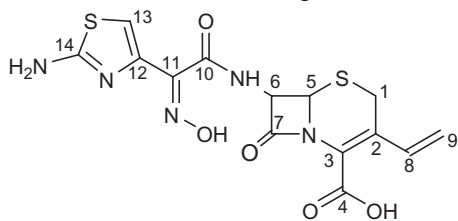


**Figure 2.8** The COSY  $^1\text{H}$  NMR spectrum of cefdinir in  $\text{DMSO-d}_6$ .

**Table 2.4** The  $^{13}\text{C}$  nuclear magnetic resonance assignments for the spectrum of cefdinir



Chemical shift (ppm relative to TMS)	Assignment at carbon number	Chemical shift (ppm relative to TMS)	Assignment at carbon number
23.22	1	131.98	8
57.86	5	142.84	12
58.76	6	147.38	11
106.82	13	163.23	4
117.20	9	163.77	7
124.22	2	163.91	10
125.40	3	168.20	14

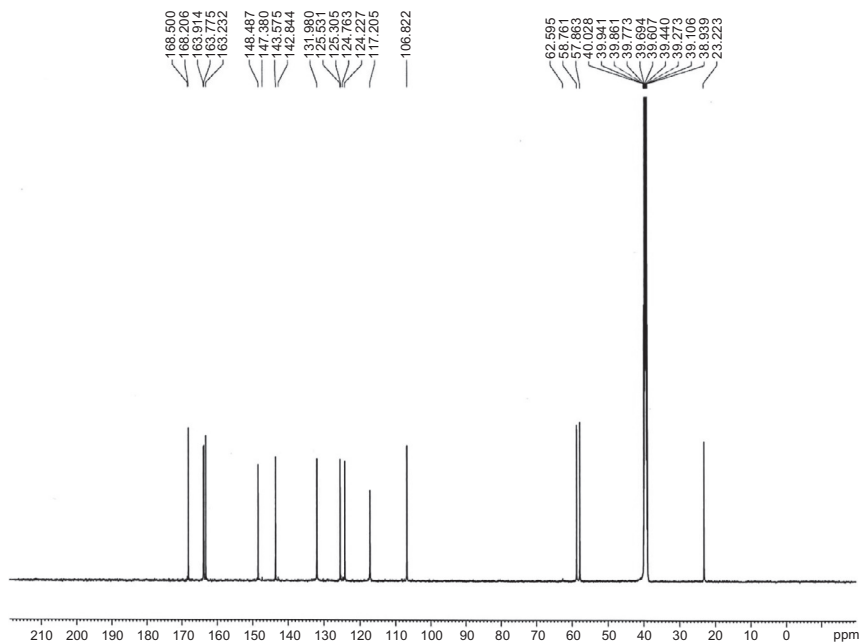


Figure 2.9 The  $^{13}\text{C}$  NMR spectrum of cefdinir in  $\text{DMSO-d}_6$ .

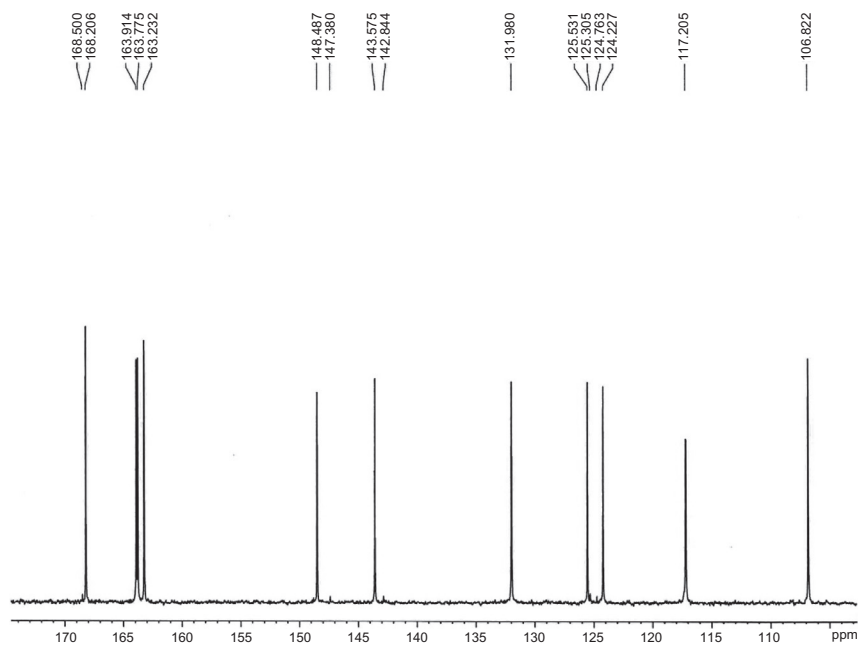


Figure 2.10 The expanded  $^{13}\text{C}$  NMR spectrum of cefdinir in  $\text{DMSO-d}_6$ .

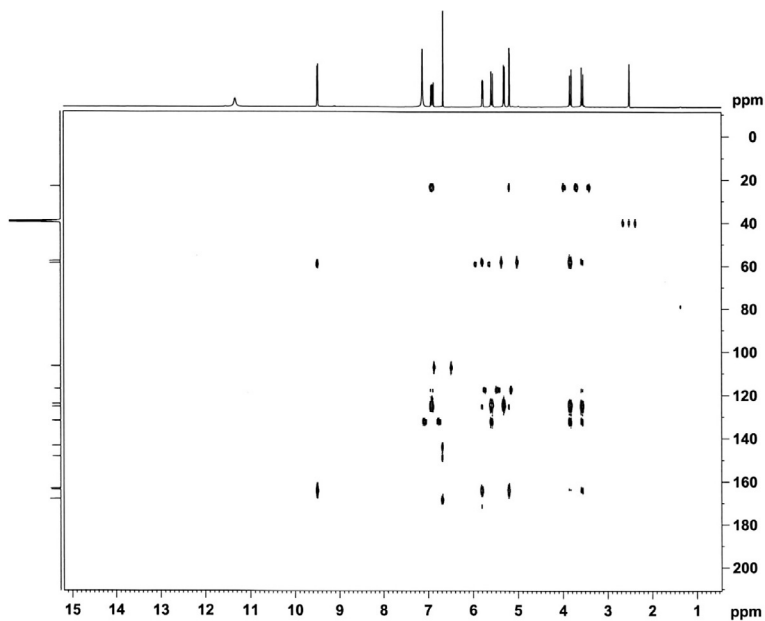


Figure 2.11 The HMBC NMR spectrum of cefdinir in DMSO-d<sub>6</sub>.

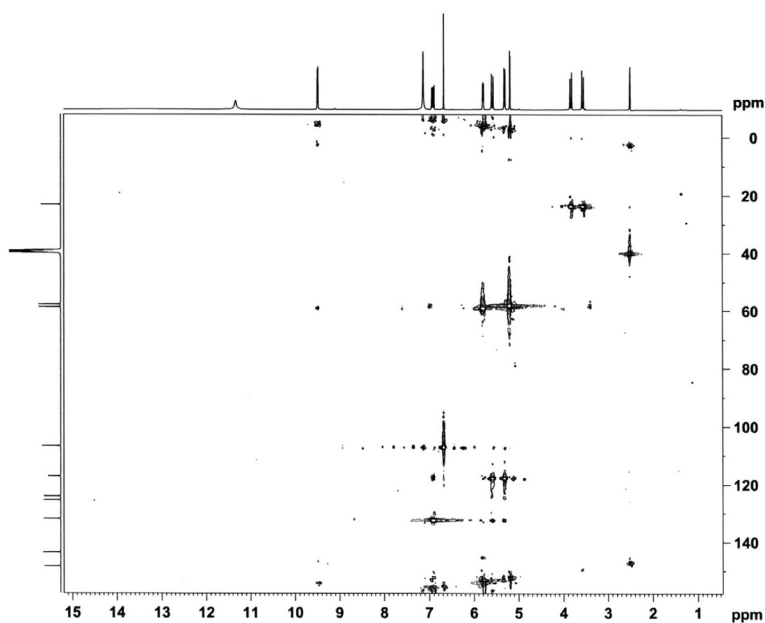
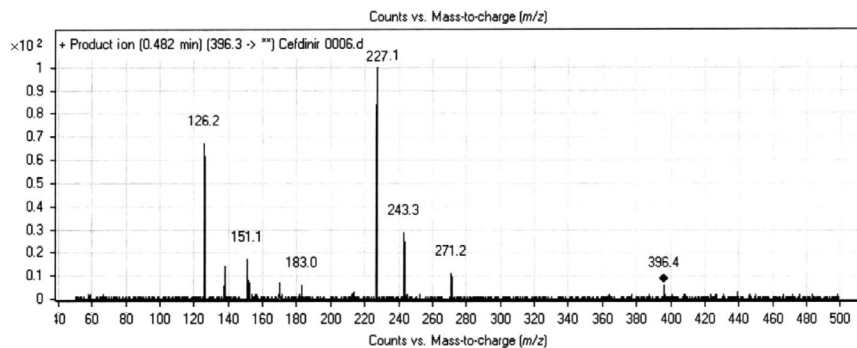
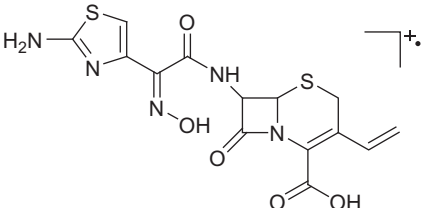
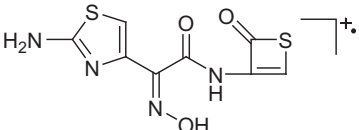
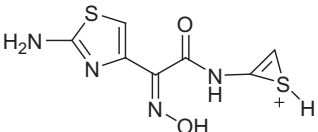
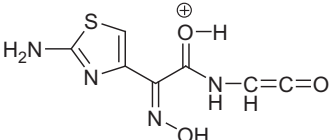


Figure 2.12 The HSQC NMR spectrum of cefdinir in DMSO-d<sub>6</sub>.

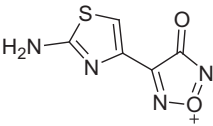
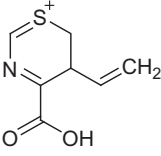
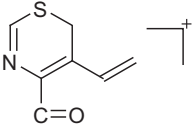
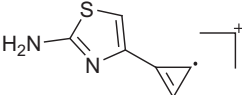
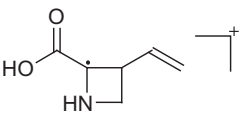


**Figure 2.13** The mass spectrum of cefdinir.

**Table 2.5** Summary of assignment for the fragmentation ions observed in the mass spectrum of cefdinir

$m/z$	Relative intensity (%)	Fragment Formula	Ions
395	8	$C_{14}H_{13}N_5O_5S_2$	
271	12	$C_8H_7S_2N_4O_3$	
243	30	$C_7H_7S_2N_4O_2$	
227	100	$C_7H_7S_1N_4O_3$	

**Table 2.5** Summary of assignment for the fragmentation ions observed in the mass spectrum of cefdinir—cont'd

<i>m/z</i>	Relative intensity (%)	Fragment	
		Formula	Ions
183	6	C <sub>5</sub> H <sub>3</sub> N <sub>4</sub> SO <sub>2</sub>	
170	8	C <sub>7</sub> H <sub>8</sub> NSO <sub>2</sub>	
152	18	C <sub>7</sub> H <sub>6</sub> SNO	
137	13	C <sub>6</sub> H <sub>5</sub> SN <sub>2</sub>	
126	68	C <sub>6</sub> H <sub>8</sub> NO <sub>2</sub>	

resonance spectroscopy as an internal reference compound, as directed under the nuclear magnetic resonance spectroscopy, in the general method <2.21> (<sup>1</sup>H): it exhibits multiple signals, A at around δ5.0–6.1 ppm and B at around δ6.4–7.5 ppm. The ratio of integrated intensity of each signal, A:B is about 2:1.

**Absorbance:** Carry out this test according to the general method <2.24>  $E_{1\text{cm}}^{1\%}$  (287 nm): 570–610 (50 mg, 0.1 mol/L phosphate buffer solution, pH 7.0, 5000 mL).

**Optical rotation:** Carry out this test according to the general method <2.49>  $[\alpha]_D^{20}$ : –58 to –66° (0.25 g, 0.1 mol/L phosphate buffer solution, pH 7.0, 25 mL, 100 mm).

**Purity: (1)** Heavy metals, carry out this test according to the general method <1.07>—Proceed with 2.0 g of cefdinir according to Method 2



and perform the test. Prepare the control solution with 2.0 mL of Standard Lead Solution (not more than 10 ppm).

(2) Related substances—Dissolve about 0.1 g of cefdinir in 10 mL of 0.1 mol/L phosphate buffer solution, pH 7.0. Pipet 3 mL of this solution, add tetramethylammonium hydroxide TS, pH 5.5, to make exactly 20 mL, and use this solution as the sample solution. Perform the test with 10  $\mu$ L of the sample solution as directed under the liquid chromatography, in the general method <2.01> according to the following conditions: determine the areas of each peak by the automatic integration method and calculate the amounts of their peaks by the area percentage method; the amount of E-isomer having the relative retention time 1.5 to cefdinir is not more than 0.8%, and the amount of total peak areas other than cefdinir is not more than 3.0%.

*Operating conditions*

Detector: An ultraviolet absorption photometer (wavelength: 254 nm).

Column: A stainless steel column 4.6 mm in inside diameter and 15 cm in length, packed with octadecyl silanized silica gel for liquid chromatography (5  $\mu$ m in particle diameter).

Column temperature: A constant temperature of about 40 °C.

Mobile phase A: To 1000 mL of tetramethylammonium hydroxide TS, pH 5.5, add 0.4 mL of 0.1 mol/L disodium dihydrogen ethylenediamine tetraacetate TS.

Mobile phase B: To 500 mL of tetramethylammonium hydroxide TS, pH 5.5 add 300 mL of acetonitrile for liquid chromatography and 200 mL of methanol, and add 0.4 mL of 0.1 mol/L disodium dihydrogen ethylenediamine tetraacetate TS.

Flowing of the mobile phase: Control the gradient by mixing the mobile A and B as directed in the following table.

Time after injection of the sample (min)	Mobile phase A (Vol. %)	Mobile phase B (Vol. %)
0–2	95	5
2–22	95 $\rightarrow$ 75	5 $\rightarrow$ 25
22–32	75 $\rightarrow$ 50	25 $\rightarrow$ 50
32–37	50	50
37–38	50 $\rightarrow$ 95	50 $\rightarrow$ 5
38–58	95	5

Flow rate: 1.0 mL/min. The retention time of cefdinir is about 22 min under this condition.

Time span of measurement: About 40 min after injection of the sample solution.

#### *System suitability*

Test for required detection: Pipet 1 mL of the sample solution, add tetramethylammonium hydroxide TS, pH 5.5, to make exactly 100 mL, and use this solution as the test solution for system suitability. Pipet 1 mL of the test solution for system suitability, add tetramethylammonium hydroxide TS, pH 5.5, to make exactly 10 mL. Confirm that the peak area of cefdinir obtained from 10  $\mu$ L of this solution is equivalent to 7–13% of that obtained from 10  $\mu$ L of the test solution for system suitability.

System performance: Dissolve 0.03 g of Cefdinir Reference Standard and 2 mg of cefdinir lactam ring-cleavage lactones in 3 mL of 0.1 mol/L phosphate buffer solution, pH 7.0, add tetramethylammonium hydroxide TS, pH 5.5, to make 20 mL. When the procedure is run with 10  $\mu$ L of this solution under the above operating conditions, peak 1 and peak 2 of cefdinir lactam ring-cleavage lactones separated into four peaks, cefdinir, peak 3, and peak 4 of remaining cefdinir lactam ring-cleavage lactones are eluted in this order. Relative retention time of peak 3 of cefdinir lactam ring-cleavage lactone to the retention time of cefdinir is not less than 1.09. The number of theoretical plates and the symmetry factor of the peak of cefdinir are not less than 7000 steps and not more than 3.0, respectively.

System repeatability: When the test is repeated  $3 \times$  with 10  $\mu$ L of the test solution for system suitability under the above operating conditions, the relative standard deviation of the peak areas of cefdinir is not more than 2.0%.

**Water** Carry out this test according to the general method <2.48> not more than 2.0% (1 g, volumetric titration, direct titration). Use a mixture of formamide and methanol for water determination (2:1 instead of using methanol alone for water determination).

**Assay** Weigh accurately an amount of Cefdinir and Cefdinir Reference Standard equivalent to about 20 mg (potency), dissolve each in 0.1 mol/L phosphate buffer solution, pH 7.0, to make exactly 100 mL, and use these solutions as the sample solution and the standard solution. Perform the test with 5  $\mu$ L of the sample solution and the standard solution as directed under Liquid Chromatography <2.01> according to the following conditions, and calculate the peak areas,  $A_T$  and  $A_S$ , of cefdinir of the solutions.

$$\text{Amount}[\mu\text{g}(\text{potency})] \text{ of cefdinir } (\text{C}_{14}\text{H}_{13}\text{N}_5\text{O}_5\text{S}_2) = W_s \times \frac{A_T}{A_S} \times 1000$$

$w_s$  = Amount [mg (potency)] of Cefdinir Reference Standard.

#### *Operating conditions*

Detector: An ultraviolet absorption photometer (wavelength: 254 nm).

Column: A stainless steel column 4.6 mm in inside diameter and 15 cm in length, packed with octadecylsilanized silica gel for liquid chromatography (5  $\mu\text{m}$  in particle diameter).

Column temperature: A constant temperature of about 40 °C.

Mobile phase: To 1000 mL of tetramethylammonium hydroxide TS, pH 5.5, add 0.4 mL of 0.1 mol/L disodium dihydrogen ethylenediamine tetraacetate TS. To 900 mL of this solution, add 60 mL of acetonitrile for liquid chromatography and 40 mL of methanol.

Flow rate: Adjust the flow rate so that the retention time of cefdinir is about 8 min.

#### *System suitability*

System performance: Dissolve 2 mg of Cefdinir Reference Standard and 5 mg of cefdinir lactam ring-cleavage lactones in 10 mL of 0.1 mol/L phosphate buffer solution, pH 7.0. When the procedure is run with 5  $\mu\text{L}$  of this solution under the above operating conditions, peak 1 and peak 2 of cefdinir lactam ring-cleavage lactones separated into four peaks, cefdinir, peak 3 and peak 4 of remaining cefdinir lactam ring-cleavage lactones are eluted in this order. The resolution between the peak 2 of cefdinir lactam ring-cleavage lactone and that of cefdinir is not less than 1.2. The number of theoretical plates and the symmetry factor of the peak of cefdinir are not less than 2000 steps and not more than 1.5, respectively.

System repeatability: When the test is repeated 6  $\times$  with 5  $\mu\text{L}$  of the standard solution under the above operating conditions, the relative standard deviation of the peak areas of cefdinir is not more than 1.0%.

**Containers and storage:** Containers—Tight containers. Storage—Light-resistant containers.

#### 6.1.1.2 Cefdinir capsules

Capsules contain not less than 90.0% and not more than 110.0% of the labeled amount of cefdinir ( $\text{C}_{14}\text{H}_{13}\text{N}_5\text{O}_5\text{S}_2$ ; 395.41).

**Method of preparation:** Prepare as directed under capsules, with cefdinir.

**Identification:** To an amount of the contents of Cefdinir capsules, equivalent to 10 mg (potency) of cefdinir according to the labeled amount, add 100 mL of 0.1 mol/L phosphate buffer solution, pH 7.0, exposure to ultrasonic waves for 1 min, and filter. To 2 mL of the filtrate, add 0.1 mol/L phosphate buffer solution, pH 7.0, to make 20 mL, and determine the absorption spectrum of this solution as directed under ultraviolet–visible spectrophotometry, in the general method <2.24>: it exhibits maxima between 221 and 225 nm and between 285 and 289 nm.

**Uniformity of dosage unit:** Carry out this test according to the general method <6.02>. It meets the requirement of the Mass variation test.

**Dissolution:** Carry out this test according to the general method <6.10>. Perform the test according to the following method: it meets the requirement.

Perform the test with one capsule of Cefdinir capsules at 50 revolutions per minute according to the Paddle method using a sinker, using 900 mL of second fluid for dissolution test as the dissolution medium. Withdraw 20 mL or more of the dissolution medium 30 min after starting the test for a 50-mg capsule or 45 min after for a 100-mg capsule and filter through a membrane filter with pore size of not more than 0.5  $\mu\text{m}$ . Discard the first 10 mL of the filtrate, pipet  $V$  mL of the subsequent filtrate, add second fluid for dissolution test to make exactly  $V'$  mL so that each mL contains about 56  $\mu\text{g}$  (potency) of cefdinir according to the labeled amount, and use this solution as the sample solution. Separately, weigh accurately about 28 mg (potency) of Cefdinir Reference Standard and dissolve in second fluid for dissolution test to make exactly 100 mL. Pipet 4 mL of this solution, add second fluid for dissolution test to make exactly 20 mL, and use this solution as the standard solution. Perform the test with exactly 20  $\mu\text{L}$  each of the sample solution and standard solution as directed under Liquid Chromatography, in the general method <2.01>, and determine the peak areas,  $A_T$  and  $A_S$ , of cefdinir. The dissolution rate of a 50-mg capsule in 30 min is not less than 80% and that of a 100-mg capsule in 45 min is not less than 75%.

$$\text{Dissolution rate (\%)} \text{ with respect to the labeled amount of cefdinir} \\ (C_{14}H_{13}N_5O_5S_2) = W_S \times (A_T/A_S) \times (V/V') \times (1/C) \times 180$$

where  $W_S$  is the amount [mg (potency)] of Cefdinir Reference Standard;  $C$  is the labeled amount [mg (potency)] of cefdinir ( $C_{14}H_{13}N_5O_5S_2$ ) in one capsule.

*Operating conditions*

Proceed as directed in the Assay under Cefdinir.

*System suitability*

System performance: When the procedure is run with 20  $\mu\text{L}$  of the standard solution under the above operating conditions, the number of theoretical plates and the symmetry factor of the peak of cefdinir are not less than 2000 and not more than 2.0, respectively.

System repeatability: When the test is repeated  $6 \times$  with 20  $\mu\text{L}$  of the standard solution under the above operating conditions, the relative standard deviation of the peak area of cefdinir is not more than 1.0%.

**Assay** Weigh accurately not less than five Cefdinir capsules, take out the contents, and powder. Wash the empty capsules with a little amount of diethyl ether, if necessary, allow to stand at a room temperature to vaporize the adhering diethyl ether, and weigh accurately the mass of the capsules to calculate the mass of the contents. Weigh accurately an amount of the contents, equivalent to about 0.1 g (potency) of cefdinir according to the labeled amount, add 70 mL of 0.1 mol/L phosphate buffer solution, pH 7.0, shake for 30 min, and add 0.1 mol/L phosphate buffer solution, pH 7.0, to make exactly 100 mL. Centrifuge this solution at 3000 revolutions per minute for 10 min, pipet 4 mL of the supernatant liquid, add 0.1 mol/L phosphate buffer solution, pH 7.0, to make exactly 20 mL, and use this solution as the sample solution. Separately, weigh accurately an amount of Cefdinir Reference Standard, equivalent to about 20 mg (potency), dissolved in 0.1 mol/L phosphate buffer solution, pH 7.0, to make exactly 100 mL, and use this solution as the standard solution. Proceed as directed in the Assay under Cefdinir.

$$\begin{aligned} \text{Amount [mg(potency)] of cefdinir (C}_{14}\text{H}_{13}\text{N}_5\text{O}_5\text{S}_2) \\ = W_S \times (A_T/A_S) \times 5 \end{aligned}$$

where  $W_S$  is the amount [mg (potency)] of Cefdinir Reference Standard.

**Containers and storage:** Containers—Tight containers.

**6.1.1.3 Cefdinir fine granules**

Cefdinir Fine Granules contain not less than 93.0% and not more than 107.0% of the labeled amount of cefdinir ( $\text{C}_{14}\text{H}_{13}\text{N}_5\text{O}_5\text{S}_2$ : 395.41).

**Method of preparation:** Prepare to finely granulated form as directed under Powders, with cefdinir.

**Identification:** To an amount of Cefdinir Fine Granules, equivalent to 10 mg (potency) of cefdinir according to the labeled amount, add 100 mL of 0.1 mol/L phosphate buffer solution, pH 7.0, exposure to ultrasonic waves for 1 min, and filter. To 2 mL of the filtrate, add 0.1 mol/L phosphate buffer solution, pH 7.0, to make 20 mL, and determine the absorption spectrum of this solution as directed under ultraviolet–visible spectrophotometry, in the general method <2.24>: it exhibits maxima between 221 and 225 nm and between 285 and 289 nm.

**Uniformity of dosage units:** Carry out this test according to the general method <6.02>. The granules in single-unit container meet the requirement of the Mass variation test.

**Dissolution:** Carry out this test according to the general method <6.10>. Perform the test according to the following method: it meets the requirement.

Perform the test with an accurate amount of Cefdinir Fine Granules, equivalent to about 0.1 g (potency) of cefdinir according to the labeled amount, at 50 revolutions per minute according to the Paddle method using 900 mL of second fluid for dissolution test as the dissolution medium. Withdraw 20 mL or more of the dissolution medium 30 min after starting the test, and filter through a membrane filter with a pore size not exceeding 0.5  $\mu\text{m}$ . Discard the first 10 mL of the filtrate and use the subsequent filtrate as the sample solution. Separately, weigh accurately about 28 mg (potency) of Cefdinir Reference Standard and second fluid for dissolution test to make exactly 50 mL. Pipet 4 mL of this solution, add second fluid for dissolution test to make exactly 20 mL, and use this solution as the standard solution. Perform the test with exactly 20  $\mu\text{L}$  each of the sample solution and standard solution as directed under Liquid Chromatography in the general method <2.01>, and determine the peak areas,  $A_T$  and  $A_S$ , of cefdinir. The dissolution rate in 30 min is not less than 75%.

Dissolution rate (%) with respect to the labeled amount of cefdinir

$$(\text{C}_{14}\text{H}_{13}\text{N}_5\text{O}_5\text{S}_2) = (W_S/W_T) \times (A_T/A_S) \times (1/C) \times 360$$

where  $W_S$  is the amount [mg (potency)] of Cefdinir Reference Standard,  $W_T$  is the amount (g) of sample,  $C$  is the labeled amount [mg (potency)] of cefdinir ( $\text{C}_{14}\text{H}_{13}\text{N}_5\text{O}_5\text{S}_2$ ) in 1 g.

*Operating conditions*

Proceed as directed in the Assay under Cefdinir.

### *System suitability*

System performance: When the procedure is run with 20  $\mu\text{L}$  of the standard solution under the above operating conditions, the number of theoretical plates and the symmetry factor of the peak of cefdinir are not less than 2000 and not more than 2.0, respectively.

System repeatability: When the test is repeated  $6 \times$  with 20  $\mu\text{L}$  of the standard solution under the above operating conditions, the relative standard deviation of the peak area of cefdinir is not more than 1.0%.

**Particle size** Carry out this test according to the general method  $\langle 6.03 \rangle$ . It meets the requirement of fine granules of the Powders.

**Assay** Powder, if necessary, and weigh accurately an amount of Cefdinir Fine Granules, equivalent to about 0.1 g (potency) of cefdinir according to the labeled amount, add 70 mL of 0.1 mol/L phosphate buffer solution, pH 7.0, shake for 30 min, and add 0.1 mol/L phosphate buffer solution, pH 7.0, to make exactly 100 mL. Centrifuge at 3000 revolutions per minute for 10 min, pipet 4 mL of the supernatant liquid, add 0.1 mol/L phosphate buffer solution, pH 7.0, to make 20 mL, and use this solution as the sample solution. Separately, weigh accurately an amount of Cefdinir Reference Standard, equivalent to about 20 mg (potency), dissolve in 0.1 mol/L phosphate buffer solution, pH 7.0, to make exactly 100 mL, and use this solution as the standard solution. Proceed as directed in the Assay under Cefdinir.

Amount [mg (potency)] of cefdinir ( $\text{C}_{14}\text{H}_{13}\text{N}_5\text{O}_5\text{S}_2$ ) =  $W_S \times (A_T/A_S) \times 5$

where  $W_S$  is the amount [mg (potency)] of Cefdinir Reference Standard.

**Containers and storage:** Containers—Tight containers. Storage—Light-resistant containers.

## **6.1.2 United States pharmacopeia methods [25]**

### **6.1.2.1 Cefdinir**

Cefdinir contains not less than 960  $\mu\text{g}/\text{mg}$  and not more than 1020  $\mu\text{g}/\text{mg}$  of  $\text{C}_{14}\text{H}_{13}\text{N}_5\text{O}_5\text{S}_2$ , calculated on the anhydrous basis.

**Packaging and storage:** Preserve in tight, light-resistant containers.

**USP Reference standards:**  $\langle 11 \rangle$ —USP Cefdinir RS, USP Cefdinir-Related Compound A RS.

### **Identification**

**A: Infrared Absorption** Carry out the infrared test according to the general procedure  $\langle 197\text{M} \rangle$ . The infrared absorption spectrum of a potassium bromide dispersion of it, previously dried, exhibit maxima only as the same wavelength as that of similar *Preparation of USP Cefdinir RS*.

**B:** The retention time of the major peak in the chromatogram of the *Assay preparation* corresponds to that in the chromatogram of the *Standard preparation*, as obtained in the *Assay*.

**Specific rotation:** Carry out this test according to the general method <781S> between  $-61^{\circ}$  and  $-67^{\circ}$ , at  $20^{\circ}\text{C}$ .

*Test solution:* 10 mg/mL, in *Buffer solution* as prepared in the *Assay*.

**Water, Method 1:** Carry out this test according to the general method <921>: not more than 2.0% (anhydrous) or not less than 4.0% and not more than 8.0% (monohydrate), using a mixture of formamide and methanol (2:1) as the solvent.

**Residue on ignition:** Carry out this test according to the general method <281>: not more than 0.1%.

*Heavy metals, Method II:* Carry out this test according to the general method <231>: 0.001%.

### Related compounds

*Buffer solution, Tetramethylammonium hydroxide solution, and 0.1 M Edetate disodium solution*—Proceed as directed in the *Assay*.

*Solution A*—To 1000 mL of *Tetramethylammonium hydroxide solution*, add 0.4 mL of 0.1 M *Edetate disodium solution* then filter and degas.

*Solution B*—To 500 mL of *Tetramethylammonium hydroxide solution*, add 300 mL of acetonitrile, 200 mL of methanol, and 0.4 mL of 0.1 M *Edetate disodium solution* then filter and degas.

*Mobile phase*—Use variable mixtures of *Solution A* and *Solution B* as directed for *Chromatographic system*. Make adjustments if necessary (see *System Suitability* under *Chromatography*, in the general method <621>).

*System suitability solution A*—Transfer 1 mL of the *Test solution* to a 100-mL volumetric flask, dilute with *Tetramethylammonium hydroxide solution* to volume, and mix.

*System suitability solution B*—Transfer 1 mL of *System suitability solution A* to a 10-mL volumetric flask, dilute with *Tetramethylammonium hydroxide solution* to volume, and mix.

*System suitability solution C*—Transfer about 30 mg of USP Cefdinir RS and 2 mg of USP Cefdinir-Related Compound A RS to a 20-mL volumetric flask, dissolve in 3 mL of *Buffer solution*, dilute with *Tetramethylammonium hydroxide solution* to volume, and mix.

*Test solution*—Transfer about 100 mg of cefdinir, accurately weighed, to a 10-mL volumetric flask, dissolve in and dilute with *Buffer solution* to volume, and mix. Transfer 3 mL of this solution to a 20-mL volumetric flask, dilute with *Tetramethylammonium hydroxide solution* to volume, and mix. [Note—Inject this solution immediately.]



*Chromatographic system* (see *Chromatography*, in the general method <621>)—The liquid chromatography is equipped with a 254-nm detector and a 4.6-mm × 15-cm column that contains packing L1. The column temperature is maintained at 40°. The flow rate is about 1 mL/min. The chromatograph is programmed as follows.

Time (min)	Solution A (%)	Solution B (%)	Elution
0–2	95	5	Isocratic
2–22	95 → 75	5 → 25	Linear gradient
22–32	75 → 50	25 → 50	Linear gradient
32–37	50	50	Isocratic
37–38	50 → 95	50 → 5	Linear gradient
38–58	95	5	Isocratic

Chromatograph *System suitability solution A* and *System suitability solution B* and record the peak responses as directed for *Procedure*: the peak response of cefdinir in *System suitability solution B* is about 7–13% of that obtained from *System suitability solution A*. Chromatograph *System suitability solution C* and record the peak responses as directed for *Procedure*: cefdinir-related compound A elutes with four peaks. The relative retention times are not less than 1.1 for the third peak of cefdinir-related compound A and 1.0 for cefdinir; the column efficiency, determined from the cefdinir peak, is not less than 7000 theoretical plates; the tailing factor for the cefdinir peak is not more than 3.0; and the relative standard deviation for replicate injections, based on the cefdinir peak, is not more than 2.0%.

*Procedure*—Inject a volume (about 10 µL) of the *Test solution* into the chromatograph, record the chromatogram, and measure all the peak responses. Continue the chromatogram for 40 min. Calculate the percentage of each impurity in the portion of cefdinir taken by the formula:

$$100(r_i/r_s)$$

in which  $r_i$  is the peak response for each impurity and  $r_s$  is the sum of the responses of all the peaks. The limits for the impurities are specified in Table 2.6.

### Assay

*Buffer solution*—Dissolve about 7.1 g of anhydrous dibasic sodium phosphate in 500 mL of water (*Solution A*). Dissolve about 6.8 g of monobasic

**Table 2.6** The limits for impurities of cefdinir, 1

Impurity	Relative retention time	Limit (w/w, %)
Impurity A <sup>a</sup>	0.10	0.5
Impurity B <sup>b</sup>	0.12	0.5
Impurity C <sup>c</sup>	0.74	0.7
Cefdinir-related compound A (four peaks) <sup>d</sup>	0.85, 0.93, 1.11, 1.14	0.7 (total for all four peaks)
Impurity E <sup>e</sup>	1.22	0.5
Impurity F <sup>f</sup>	1.36	0.5
Impurity G <sup>g</sup>	1.51	0.7
Impurity H (two peaks) <sup>h</sup>	1.61, 1.64	0.5 (total for both peaks)
Individual unknown impurity	—	0.2
Total impurities	—	3.0

<sup>a</sup> N-[(Z)-2-(2-aminothiazol-4-yl)-2-(hydroxyimino)acetyl]glycine.  
<sup>b</sup> (Z)-2-(2-aminothiazol-4-yl)-N-(2,2-dihydroxyethyl)-2-(hydroxyimino)acetamide.  
<sup>c</sup> (6R,7R)-7-[(Z)-2-(2-aminothiazol-4-yl)-2-(hydroxyimino)acetamido]-3-ethenyl-8-oxo-5-thia-1-azabicyclo[4.2.0]oct-2-ene-2-carboxylic acid.  
<sup>d</sup> 2(R)-2-[(Z)-2-(2-aminothiazol-4-yl)-2-(hydroxyiminoacetamido)]-2-[(2RS,5RS)-5-methyl-7-oxo-2,4,5,7-tetrahydro-1H-furo[3,4-d][1,3]thiazin-2-yl]acetic acid.  
<sup>e</sup> (Z)-2-(2-aminothiazol-4-yl)-2-(hydroxyimino)-N-{(3RS,5aR,6R)-3-methyl-1,7-dioxo-1,3,4,5a,6,7-hexahydroazeto[2,1-b]furo[3,4-d][1,3]thiazin-6-yl}acetamide.  
<sup>f</sup> (6R,7R)-7-(4-hydroxyisoxazole-3-carboxamido)-8-oxo-3-vinyl-5-thia-1-azabicyclo[4.2.0]oct-2-ene-2-carboxylic acid.  
<sup>g</sup> (6R,7R)-7-[(E)-2-(2-aminothiazol-4-yl)-2-(hydroxyiminoacetamido)]-8-oxo-3-vinyl-5-thia-1-azabicyclo[4.2.0]oct-2-ene-2-carboxylic acid.  
<sup>h</sup> (Z)-2-(2-aminothiazol-4-yl)-2-(hydroxyimino)-N-{[(2RS,5RS)-5-methyl-7-oxo-2,4,5,7-tetrahydro-1H-furo[3,4-d][1,3-thiazin-2-yl]methyl}acetamide.

potassium phosphate in 500 mL of water (*Solution B*). Add appropriate amounts of *Solution A* and *Solution B* (approximately 2:1 v/v) to obtain a mixture having a pH of 7.0.

*Tetramethylammonium hydroxide solution*—To 10 mL of tetramethylammonium hydroxide (10%), add 990 mL of water and adjust with dilute phosphoric acid (1 in 10) to a pH of 5.5.

0.1 M *Edetate disodium solution*—Dissolve 37.2 g of edetate disodium in 1000 mL of water and mix.

*Mobile phase*—Prepare a filtered and degassed mixture of *Tetramethylammonium hydroxide solution*, acetonitrile, methanol, and 0.1 M

*Edetate disodium solution* (900:60:40:0.4). Make adjustments if necessary (see *System Suitability* under *Chromatography*, in the general method <621>).

*System suitability solution*—Dissolve accurately weighed quantities of USP Cefdinir RS and USP Cefdinir-Related Compound A RS in *Buffer solution* to obtain a solution having a known concentration of about 0.2 mg/mL of USP Cefdinir RS and 0.5 mg/mL of USP Cefdinir-Related Compound A RS.

*Standard preparation*—Dissolve an accurately weighed quantity of USP Cefdinir RS in *Buffer solution*, dilute quantitatively, and stepwise if necessary, with *Buffer solution* to obtain a solution having a known concentration of about 0.2 mg/mL.

*Assay preparation*—Transfer about 20 mg of cefdinir, accurately weighed, to a 100-mL volumetric flask, dissolve in and dilute with *Buffer solution* to volume, and mix well.

*Chromatographic system* (see *Chromatography*, in the general method <621>)—The liquid chromatography is equipped with a 254-nm detector and a 4.6-mm  $\times$  15-cm column that contains 5- $\mu$ m packing L1. The flow rate is about 1 mL/min. The column temperature is maintained at 40°. Chromatograph the *System suitability solution* and record the peak responses as directed for *Procedure*: cefdinir-related compound A elutes with four peaks. The resolution,  $R$ , between the second peak of cefdinir-related compound A and cefdinir is not less than 1.2 and the tailing factor for the cefdinir peak is not more than 1.5. Chromatograph the *Standard preparation* and record the peak responses as directed for *Procedure*: the relative standard deviation for replicate injections is not more than 1.0%.

*Procedure*—Separately inject equal volumes (about 5  $\mu$ L) of the *Standard preparation* and the *Assay preparation* into the chromatograph, record the chromatograms, and measure the responses for the major peaks. Calculate the quantity, in  $\mu$ g, of  $C_{14}H_{13}N_5O_5S_2$  in each mg of cefdinir taken by the formula:

$$P(C_S/C_U)(r_U/r_S)$$

in which  $P$  is the purity, in  $\mu$ g/mg, of USP Cefdinir RS;  $C_S$  is the concentration, in mg/mL, of USP Cefdinir RS in the *Standard preparation*;  $C_U$  is the concentration, in mg/mL, of Cefdinir in the *Assay preparation*; and  $r_U$  and  $r_S$  are the peak responses obtained from the *Assay preparation* and the *Standard preparation*, respectively.

#### 6.1.2.2 Cefdinir capsules

Cefdinir capsules contain not less than 90.0% and not more than 110.0% of the labeled amount of  $C_{14}H_{13}N_5O_5S_2$ .

Packaging and storage—Preserve in tight, light-resistant containers, and store at controlled room temperature.

**USP Reference standards:** <11>—USP Cefdinir RS, USP Cefdinir-Related Compound A RS, USP Cefdinir-Related Compound B RS.

### Identification

**A: Ultraviolet Absorption:** Carry out this test according to the general method <197U>—0.1 M Phosphate buffer solution—Prepare as directed in the Assay.

*Blank solution:* 0.1 M Phosphate buffer solution.

*Standard solution*—Prepare a solution containing about 0.01 mg/mL of USP Cefdinir RS in 0.1 M Phosphate buffer solution.

*Sample solution*—Prepare a solution containing an amount equivalent to about 0.01 mg/mL of cefdinir in 0.1 M Phosphate buffer solution, and pass through a suitable filter.

*Procedure*—Compare the spectrum obtained from the *Sample solution* using a 1-cm cell to that obtained from the *Standard solution*, using the *Blank solution* to zero the instrument: the UV absorption spectrum of the *Sample solution* exhibits maxima and minima at the same wavelengths as that of a *Standard solution* concomitantly measured.

**B:** The retention time of the major peak in the chromatogram of the *Assay preparation* corresponds to that in the chromatogram of the *Standard preparation*, as obtained in the *Assay*.

**Dissolution:** Carry out this test according to the general method <711>.

*Medium:* 0.05 M phosphate buffer, pH 6.8, 900 mL.

*Apparatus 2:* 50 rpm.

*Time:* 30 min.

*Standard solution*—Dissolve an accurately weighed quantity of USP Cefdinir RS in *Medium* to obtain a solution having a concentration of about 0.33 mg/mL.

*Test solution*—Pass a portion of the solution under test through a Suitable 0.45- $\mu$ m filter. If necessary, dilute a portion of each filtered sample with *Medium* to obtain a solution that has a theoretical concentration of about 0.33 mg/mL of cefdinir, considering complete release of the label claim.

*Blank solution*—Dissolve one empty gelatin capsule shell in 100 mL of *Medium*, dilute with *Medium* to 900 mL, and filter if necessary.

*Procedure*—Determine the amount of  $C_{14}H_{13}N_5O_5S_2$  dissolved by UV absorption at the wavelength of maximum absorbance at 290 nm on portions of the *Test solution*, in comparison with the *Standard solution*, using a 1-cm cell and *Blank solution* as blank. Calculate the percentage of  $C_{14}H_{13}N_5O_5S_2$  dissolved by the formula:

$$\frac{A_U \times C_S \times D \times 900 \times 100}{A_S \times L}$$

in which  $A_U$  and  $A_S$  are the absorbance's obtained from the *Test solution* and the *Standard solution*, respectively;  $C_S$  is the concentration, in mg/mL, of the *Standard solution*;  $D$  is the dilution factor of the *Test solution*; 900 is the volume, in mL, of *Medium*; 100 is the conversion factor to percentage; and  $L$  is the capsule label claim, in mg.

**Tolerances**—Not less than 80% (Q) of the labeled amount of  $C_{14}H_{13}N_5O_5S_2$  is dissolved in 30 min.

**Uniformity of dosage units** Carry out this test according to the general method <905>: meet the requirements.

### Related compounds

#### *M Phosphate buffer solution*

**Solution A**—Dissolve 14.2 g of sodium phosphate, dibasic, anhydrous, in water, and dilute with water to 1000.0 mL.

**Solution B**—Dissolve 6.8 g of potassium phosphate, monobasic, in water, and dilute with water to 500.0 mL.

**Solution C**—Combine 1000 mL of *Solution A* with 500 mL of *Solution B*. Verify the pH of  $7.0 \pm 0.1$ , and adjust, if necessary using *Solution A* or *Solution B*.

**Dilute phosphoric acid solution**—Dilute phosphoric acid (1 in 10) with water and mix.

**0.1 M Disodium ethylenediamine tetraacetate (EDTA)**—Transfer about 3.72 g of disodium ethylenediamine tetraacetate into a 100-mL volumetric flask. Dissolve in and dilute with water to volume and mix.

**0.1% Tetramethylammonium hydroxide solution**—Dilute 20 mL of tetramethylammonium hydroxide (10% in water) with water to make 2000 mL and mix. Adjust with *Dilute phosphoric acid solution* to a pH of  $5.5 \pm 0.1$ .

**Mobile phase A**—Transfer 0.4 mL of 0.1 M EDTA to 1000 mL of 0.1% Tetramethylammonium hydroxide solution and mix.

**Mobile phase B**—Mix 250 mL of 0.1% Tetramethylammonium hydroxide solution, 150 mL of acetonitrile, and 100 mL of methanol. Add 0.2 mL of 0.1 M EDTA and mix.

**Mobile phase**—Use variable mixtures of *Mobile phase A* and *Mobile phase B* as directed in the *Chromatographic system*.

**Standard solution 1**—Dissolve an appropriate amount of USP Cefdinir RS in 0.1 M Phosphate buffer solution (*Solution C*) to obtain a solution having a

known concentration of about 0.75 mg/mL of USP Cefdinir RS. Dilute with 0.1% *Tetramethylammonium hydroxide solution* an appropriate amount of this solution, stepwise, if necessary, to obtain a solution having a known concentration of about 15 µg/mL.

*Standard solution 2*—Dissolve an appropriate quantity of USP Cefdinir-Related Compound A RS in 0.1% *Tetramethylammonium hydroxide solution* to obtain a solution having a known concentration of about 0.04 mg/mL.

*Standard solution 3*—Dissolve an appropriate quantity of USP Cefdinir-Related Compound B RS in 0.1% *Tetramethylammonium hydroxide solution* to obtain a solution having a known concentration of about 0.04 mg/mL.

*Resolution solution*—Transfer about 37.5 mg of accurately weighed USP Cefdinir RS into a 25-mL volumetric flask. Add about 10 mL of 0.1 M *Phosphate buffer solution*. Add 5.0 mL of each of *Standard solution 2* and *Standard solution 3* and dilute with 0.1% *Tetramethylammonium hydroxide solution* to volume.

*Test solution*—Transfer an accurately weighed portion of the contents of 20 opened capsules, equivalent to about 300 mg of cefdinir, into a 200-mL volumetric flask. Dissolve in 30 mL of 0.1 M *Phosphate buffer solution* (*Solution C*) and dilute with 0.1% *Tetramethylammonium hydroxide solution* to volume to obtain a solution having a known concentration of about 1.5 mg/mL of cefdinir.

*Chromatographic system* (see *Chromatography*, in the general method <621>)—The liquid chromatography is equipped with a 254-nm detector and a 4.6-mm × 150-mm column that contains 5-µm packing L1. The temperature of the *Test solution* is maintained at 4 ± 3°, and the column temperature is maintained at 40 ± 0.5°. The flow rate is about 1 mL/min. The chromatograph is programmed as follows for a run time of about 60 min.

Time (min)	Mobile phase A (%)	Mobile phase B (%)	Elution
0–2	95	5	Isocratic
2–22	95 → 75	5 → 25	Linear gradient
22–32	75 → 50	25 → 50	Linear gradient
32–37	50	50	Isocratic
37–38	50 → 95	50 → 5	Linear gradient
38–58	95	5	Isocratic

*Procedure*—Separately inject equal volumes (about 10  $\mu\text{L}$ ) of the *Resolution solution*, *Standard solution 1*, and the *Test solution* into the chromatograph, record the chromatograms, and measure the peak responses: the resolution between the cefdinir peak and the third peak of cefdinir-related compound A (lactam ring-cleavage lactones) is not less than 1.5; the tailing factor of cefdinir-related compound B is not more than 1.5; and the relative standard deviation for the cefdinir peak response in replicate injections of *Standard solution 1* is not more than 2.0%. The approximate relative retention times and the relative response factors for each of the related substances compared to cefdinir are given in [Table 2.7](#). Calculate the percentage of each individual specified and unspecified impurity in the portion of Capsules taken, using the formula:

$$\left(\frac{100}{F}\right)\left(\frac{C_S}{C_U}\right)\left(\frac{r_U}{r_S}\right)$$

in which  $C_S$  is the concentration, in mg/mL, of USP Cefdinir RS in *Standard solution 1*;  $C_U$  is the concentration, in mg/mL, of cefdinir in the *Test solution*;  $r_U$  is the peak response of each impurity obtained from the *Test solution*;  $r_S$  is the peak response of cefdinir obtained from *Standard solution 1*; and  $F$  is the relative response factor as mentioned in [Table 2.7](#) for each impurity. The specified and unspecified impurities meet the limits specified in [Table 2.7](#).

### Assay

*0.1 M Phosphate buffer solution*—Dissolve 10.65 g of dibasic sodium phosphate and 3.40 g of monobasic potassium phosphate in 750 mL of water. Adjust with phosphoric acid or sodium hydroxide to a pH of  $7.0 \pm 0.05$  and dilute with water to 1000 mL.

*Citric acid buffer solution*—Dissolve 7.0 g of citric acid monohydrate in 1000 mL of water and adjust with phosphoric acid to a pH of  $2.0 \pm 0.05$ .

*Mobile phase*—Mix 1000 mL of *Citric acid buffer solution* with 111 mL of methanol and 28 mL of tetrahydrofuran. Make adjustments if necessary (see *System Suitability* under *Chromatography*, in the general method <621>).

*Standard preparation*—Accurately weigh a known amount of USP Cefdinir RS into a suitable volumetric flask. Dissolve in 0.1 M *Phosphate buffer solution* to obtain a solution having a known concentration of about 0.05 mg/mL of cefdinir.

*Assay preparation*—Transfer an accurately weighed portion of the contents of 20 opened Capsules, equivalent to about 100 mg of cefdinir, into

**Table 2.7** The limits for impurities of cefdinir, 2

Related substance	Approximate relative retention time	Relative response factor	Limit of quantitation (% of cefdinir)	Limit (%)
Impurity VIII	0.10	1.1	0.1	NMT 0.5
Impurity IV	0.13	1.1	0.1	NMT 0.5
Impurity XIV	0.36	1.0	0.05	NMT 0.2
Impurity V	0.46	1.5	0.05	NMT 0.7
Impurity B <sup>a</sup>	0.77	1.0	0.05	NMT 0.3
Impurity XI	0.75	1.0	0.05	NMT 0.7
Cefdinir-related compound A	0.85	1.5	0.1	NMT 2.5
(Lactam ring-cleavage lactones-a) <sup>b</sup>	0.94	1.5	0.1	—
Cefdinir-related compound A (Lactam ring-cleavage lactones-c) <sup>b</sup>	1.11	1.5	0.1	—
Cefdinir-related compound A (Lactam ring-cleavage lactones-d) <sup>b</sup>	1.14	1.5	0.1	—
Impurity VI	1.18	1.1	0.05	NMT 0.2
Impurity I	1.23	1.2	0.05	NMT 1.0
Cefdinir-related compound B <sup>b</sup>	1.28	1.1	0.05	NMT 0.2
Impurity XIII	1.37	1.4	0.05	NMT 0.5
Impurity E <sup>a</sup>	1.44	1.0	0.05	NMT 0.5

*Continued*



**Table 2.7** The limits for impurities of cefdinir, 2—cont'd

Related substance	Approximate relative retention time	Relative response factor	Limit of quantitation (% of cefdinir)	Limit (%)
Impurity XV	1.49	1.0	0.05	NMT 0.2
Impurity VII	1.51	1.1	0.05	NMT 0.7
Impurity IIIa <sup>c</sup>	1.62	1.3	0.05	NMT 1.0
Impurity IIIb <sup>c</sup>	1.64	1.3	0.05	—
Impurity D <sup>a</sup>	1.82	1.0	0.05	NMT 0.2
Individual unidentified impurities	N/A	1.0	N/A	NMT 0.2
Total unidentified impurities <sup>d</sup>	N/A	N/A	N/A	NMT 1.0
Total impurities	N/A	NIA	N/A	NMT 5.0

<sup>a</sup>Impurity B, Impurity D, and Impurity E are unidentified impurities.

<sup>b</sup>RS II is a mixture of four isomers designated as RS IIa, RS IIb, RS IIc, and RS IId. The sum of all values is reported and the total limit for all four isomers combined is 2.5%.

<sup>c</sup>RS III is a mixture of two isomers designated as RS IIIa and RS IIIb. The sum of both values is reported and the total limit for both isomers combined is 1.0%.

<sup>d</sup>The total unidentified impurities limit includes the percentage total of unidentified impurities B, D, and E and any other individual unidentified impurities.

a suitable volumetric flask. Dissolve in and dilute with 0.1 M *Phosphate buffer solution* to obtain a solution having a known concentration of about 0.05 mg/mL of cefdinir.

**Resolution solution**—Accurately weigh a known amount of USP Cefdinir RS and *m*-hydroxybenzoic acid into a suitable volumetric flask. Dissolve in 0.1 M *Phosphate buffer solution* to obtain a solution having a known concentration of about 0.05 mg/mL of cefdinir and about 0.175 mg/mL of *m*-hydroxybenzoic acid.

**Chromatographic system** (see *Chromatography*, in the general method <621>)—The liquid chromatography is equipped with a 254-nm detector and a 3.9-mm × 150-mm column that contains 4-μm packing L1. The flow rate is maintained at about 1.4 mL/min. Chromatograph the *Resolution*

*solution* and record the peak area response as directed for *Procedure*. The resolution between cefdinir and *m*-hydroxybenzoic acid is greater than 3.0; the tailing factor of the cefdinir peak is not more than 2.0; and the relative standard deviation for replicate injections of the *Standard preparation* is not more than 1.0%.

**Procedure**—Separately inject equal volumes (about 15 µL) of the *Standard preparation* and the *Assay preparation* into the chromatograph, record the chromatograms, and measure the responses for the major peaks. Calculate the percentage of cefdinir (C<sub>14</sub>H<sub>13</sub>N<sub>5</sub>O<sub>5</sub>S<sub>2</sub>) based on the label claim, in the portion of Capsules taken by the formula:

$$100 \left( \frac{C_S}{C_U} \right) \left( \frac{r_U}{r_S} \right)$$

in which  $C_S$  is the concentration, in mg/mL, of cefdinir in the *Standard solution*;  $C_U$  is the concentration of cefdinir in the *Assay preparation*; and  $r_U$  and  $r_S$  are the peak responses of cefdinir in the *Assay preparation* and the *Standard preparation*, respectively.

### 6.1.2.3 Cefdinir for oral suspension

Cefdinir for Oral Suspension contains not less than 90.0% and not more than 110.0% of the labeled amount of C<sub>14</sub>H<sub>13</sub>N<sub>5</sub>O<sub>5</sub>S<sub>2</sub>. It may contain one or more suitable buffers, flavors, preservatives, stabilizing agents, sweeteners, and suspending agents.

**Packaging and storage**—Preserve in tight, light-resistant containers, and store at controlled room temperature.

**Labeling**—The label specifies the directions for the constitution of the powder and states the equivalent amount of C<sub>14</sub>H<sub>13</sub>N<sub>5</sub>O<sub>5</sub>S<sub>2</sub> in a given volume of Oral Suspension after constitution.

**USP Reference standards:** According to the general method <11>—*USP Cefdinir RS*, *USP Cefdinir-Related Compound A RS*, *USP Cefdinir-Related Compound B RS*.

#### Identification

**A: Thin-Layer Chromatographic Identification Test**, carry out this test as directed in the general method <201>.

0.1 M *Phosphate buffer solution*—Prepare as directed in the *Assay*.

*Standard solution*—Transfer an appropriate amount of *USP Cefdinir RS* into a suitable volumetric flask. Dissolve in and dilute with methanol and

0.1 M *Phosphate buffer solution* (75:25) to obtain a solution containing a known amount of about 0.6 mg/mL of USP Cefdinir RS.

*Test solution*—Mix a portion of constituted Oral Suspension equivalent to about 125 mg of cefdinir in a 100-mL volumetric flask with 50 mL of 0.1 M *Phosphate buffer solution* and dilute with methanol to volume. Pass a portion through a suitable 0.45- $\mu$ m filter. Transfer 5.0 mL of the filtrate to a 10-mL volumetric flask and dilute with methanol to volume.

*Procedure*—Separately apply 10  $\mu$ L of the *Test solution* and the *Standard solution* to a suitable thin-layer chromatographic plate (see *Chromatography*, in the general method <621>) coated with a 0.25-mm layer of chromatographic silica gel, preconditioned with *n*-hexane-tetradecane solution (95:5), and allow the spots to dry. Place the plate in a chamber equilibrated with a solvent mixture consisting of methanol and water (80:20), and develop the chromatogram in the same solvent system until the solvent front has moved about 15 cm. Remove the plate from the developing chamber, allow the solvent to evaporate, and visually locate the spots under a short-wavelength UV light: the *RF* value of the principal spot obtained from the *Test solution* corresponds to that obtained from the *Standard solution*.

**B:** The retention time of the main peak in the chromatogram of the *Assay preparation* corresponds to that in the chromatogram of the *Standard preparation*, as obtained in the *Assay*.

**Dissolution:** Carry out this test as directed in the general procedure <711>.

*Medium:* 0.05 M phosphate buffer, pH 6.8, 900 mL.

*Apparatus 2:* 50 rpm.

*Time:* 30 min.

*Standard solution*—Dissolve an accurately weighed quantity of USP Cefdinir RS and dilute with *Medium*, quantitatively, and stepwise, if necessary, to obtain a solution having a concentration of about 0.14 mg/mL.

*Test solution*—Transfer 5 mL, by weight, of the reconstituted Oral Suspension into the vessel. After the appropriate time withdraw a portion of the solution under test and pass through a suitable 0.45- $\mu$ m filter. Dilute with *Medium* a portion of each filtered sample as necessary to obtain a solution having a concentration of about 0.14 mg/mL of cefdinir.

*Procedure*—Determine the amount of  $C_{14}H_{13}N_5O_5S_2$  dissolved by employing UV absorption at the wavelength of maximum absorbance at about 290 nm on portions of the *Test solution* in comparison with the *Standard solution*, using *Medium* as blank. Calculate the percentage of cefdinir dissolved by the formula:

$$\frac{A_U \times C_S \times d \times D \times 900 \times 100}{A_S \times W_U \times L}$$

in which  $A_U$  and  $A_S$  are the absorbance's obtained from the *Test solution* and *Standard solution*, respectively;  $C_S$  is the concentration, in mg/mL, of cefdinir in the *Standard solution*;  $d$  is the density, in mg/mL, of the Oral Suspension obtained by dividing the weight of Oral Suspension taken by 5 mL;  $D$  is the dissolution factor used, if necessary, to prepare the *Test solution*; 900 is the volume, in mL, of *Medium*; 100 is the conversion factor to percentage;  $W_U$  is the weight, in mg, of Oral Suspension taken; and  $L$  is the label claim, in mg.

**Tolerances**—Not less than 80% (Q) of the labeled amount of  $C_{14}H_{13}N_5O_5S_2$  is dissolved in 30 min.

**Uniformity of dosage units:** Carry out this test as directed in the general method <905>—For Oral Suspension packaged in single-unit containers: meets the requirements.

**Deliverable volume:** Carry out this test as directed in the general method <698>—For Oral Suspension packaged in multiple-unit containers: meets the requirements.

**pH:** When this test is carried out as directed in the general method <791>—Between 3.5 and 4.5.

**Loss on drying:** This experiment should be carried out as directed in the general method <731>—Dry about 1 g of powder over phosphorous pentoxide in a vacuum oven not exceeding 5 mm of mercury at 70° for 4–4.5 h: it loses not more than 1.0%.

### Related compounds

#### *M Phosphate buffer solution*

**Solution A**—Dissolve in and dilute with water 14.2 g of anhydrous dibasic sodium phosphate to 1000.0 mL.

**Solution B**—Dissolve in and dilute with water 6.8 g of monobasic potassium phosphate to 500.0 mL.

**Solution C**—Mix 1000 mL of *Solution A* with 500 mL of *Solution B*. Verify a pH of  $7.0 \pm 0.1$ .

**Dilute phosphoric acid solution**—Dilute phosphoric acid with water (1 in 10) and mix.

**0.1 M Disodium ethylenediaminetetraacetate (EDTA)**—Transfer about 3.72 g of disodium ethylenediaminetetraacetate into a 100-mL volumetric flask. Dissolve in and dilute with water to volume and mix.

0.1% *Tetramethylammonium hydroxide solution*—Dilute 20 mL of tetramethylammonium hydroxide (10% in water) with water to make 2000 mL and mix. Adjust with *Dilute phosphoric acid solution* to a pH of  $5.5 \pm 0.1$ .

*Mobile phase A*—Transfer 0.4 mL of 0.1 M EDTA to 1000 mL of 0.1% *Tetramethylammonium hydroxide solution* and mix.

*Mobile phase B*—Mix 250 mL of 0.1% *Tetramethylammonium hydroxide solution*, 150 mL of acetonitrile, and 100 mL of methanol. Add 0.2 mL of 0.1 M EDTA and mix.

*Mobile phase*—Use variable mixtures of *Mobile phase A* and *Mobile phase B* as directed in the *Chromatographic system*.

*Standard solution 1*—Dissolve an appropriate amount of USP Cefdinir RS in 0.1 M *Phosphate buffer solution (Solution C)* to obtain a solution having a known concentration of about 0.75 mg/mL of USP Cefdinir RS. Dilute with 0.1% *Tetramethylammonium hydroxide solution* an appropriate amount of this solution, stepwise, if necessary, to obtain a solution having a known concentration of about 15  $\mu\text{g/mL}$ .

*Standard solution 2*—Dissolve an appropriate quantity of USP Cefdinir-Related Compound A RS in 0.1% *Tetramethylammonium hydroxide solution* to obtain a solution having a known concentration of about 0.04 mg/mL.

*Standard solution 3*—Dissolve an appropriate quantity of USP Cefdinir-Related Compound B RS in 0.1 M *Phosphate buffer solution* to obtain a solution having a known concentration of about 0.04 mg/mL.

*Resolution solution*—Transfer about 37.5 mg of accurately weighed USP Cefdinir RS into a 25-mL volumetric flask. Add about 10 mL of 0.1 M *Phosphate buffer solution*. Add 5.0 mL of each of *Standard solution 2* and *Standard solution 3* and dilute with 0.1% *Tetramethylammonium hydroxide solution* to volume.

*Test solution*—Transfer a volume of constituted Oral Suspension equivalent to about 150 mg of Cefdinir into a 100-mL volumetric flask. Dissolve in 30 mL of 0.1 M *Phosphate buffer solution (Solution C)* and dilute with 0.1% *Tetramethylammonium hydroxide solution* to volume.

*Chromatographic system* (see *Chromatography*, in the general method <621>)—The liquid chromatography is equipped with a 254-nm detector and a 4.6-mm  $\times$  150-mm column that contains 5- $\mu\text{m}$  packing L1. The *Test solution* is maintained at a temperature of  $4 \pm 3^\circ$ , and the column temperature is maintained at  $40 \pm 0.5^\circ$ . The flow rate is about 1 mL/min. The chromatograph is programmed as follows for a run time of about 60 min.

Time (min)	Mobile phase A (%)	Mobile phase B (%)	Elution
00–02	95	5	Isocratic
02–22	95 → 75	5 → 25	Linear gradient
22–32	75 → 50	25 → 50	Linear gradient
32–37	50	50	Isocratic
37–38	50 → 95	50 → 5	Linear gradient
38–58	95	5	Isocratic

**Procedure**—Separately inject equal volumes (about 10 µL) of the *Resolution solution*, *Standard solution 1*, and the *Test solution* into the chromatograph, record the chromatograms, and measure the peak responses: the resolution between the cefdinir peak and the third peak of cefdinir-related compound A is greater than 1.5; the tailing factor of cefdinir-related compound B is not more than 1.5; and the relative standard deviation for the cefdinir peak response in replicate injections of *Standard solution 1* is not more than 2.0%. The approximate relative retention times and the relative response factors for each of the related compounds compared to cefdinir are given in [Table 2.8](#). Calculate the percentage of individual specified and unspecified impurities in the portion of Oral Suspension taken by the formula:

$$(100/F)(C_S/C_U)(r_U/r_S)$$

in which *F* is the relative response factor for each impurity, as mentioned in [Table 2.8](#); *C<sub>S</sub>* is the concentration, in mg/mL, of USP Cefdinir RS in *Standard solution 1*; *C<sub>U</sub>* is the concentration, in mg/mL, of cefdinir in the *Test solution*; *r<sub>U</sub>* is the peak response of each impurity obtained from the *Test solution*; and *r<sub>S</sub>* is the peak response of cefdinir obtained from *Standard solution 1*. The specified and unspecified impurities meet the limits specified in [Table 2.8](#).

### Assay

**1 M Phosphate buffer solution**—Dissolve 10.65 g of anhydrous dibasic sodium phosphate and 3.40 g of monobasic potassium phosphate in 750 mL of water. Adjust with phosphoric acid or sodium hydroxide to a pH of 7.0 ± 0.05 and dilute with water to 1000 mL.

**Citric acid buffer solution**—Dissolve 7.0 g of citric acid monohydrate in 1000 mL of water and adjust with phosphoric acid to a pH of 2.0 ± 0.05.

**Table 2.8** The limits for impurities of cefdinir, 3

Related compound	Approximate relative retention time	Relative response factor	Limit of quantitation (% of cefdinir)	Limit (%)
Impurity VIII	0.10	1.1	0.1	NMT 0.5
Impurity IV	0.13	1.1	0.1	NMT 0.6
Impurity XIV	0.36	1.0	0.05	NMT 0.2
Impurity V	0.46	1.5	0.05	NMT 0.3
Impurity B <sup>a</sup>	0.77	1.0	0.05	NMT 0.2
Impurity XI	0.75	1.0	0.05	NMT 0.7
Cefdinir-related compound A <sup>b</sup> (Isomer a)	0.85	1.5	0.1	NMT 3.3
Cefdinir-related compound A <sup>b</sup> (Isomer b)	0.94	1.5	0.1	—
Cefdinir-related compound A <sup>b</sup> (Isomer c)	1.11	1.5	0.1	—
Cefdinir-related compound A <sup>b</sup> (Isomer d)	1.14	1.5	0.1	—
Impurity VI	1.18	1.1	0.05	NMT 0.2
Impurity I	1.23	1.2	0.05	NMT 0.8
Cefdinir-related compound B	1.28	1.1	0.05	NMT 0.2
Impurity XIII	1.37	1.4	0.05	NMT 0.5
Impurity E <sup>a</sup>	1.44	1.0	0.05	NMT 0.2
Impurity XV	1.49	1.0	0.05	NMT 0.2
Impurity VII	1.51	1.1	0.05	NMT 1.2
Impurity IIIa <sup>c</sup>	1.62	1.3	0.05	NMT 1.1
Impurity IIIb <sup>c</sup>	1.64	1.3	0.05	—
Impurity D <sup>a</sup>	1.82	1.0	0.05	NMT 0.2

**Table 2.8** The limits for impurities of cefdinir, 3—cont'd

Related compound	Approximate relative retention time	Relative response factor	Limit of quantitation (% of cefdinir)	Limit (%)
Individual unidentified impurities	N/A	1.0	0.05	NMT 0.2
Total unidentified impurities <sup>d</sup>	N/A	N/A	N/A	NMT 0.9
Total impurities	N/A	N/A	N/A	NMT 6.2

<sup>a</sup>Impurity B, Impurity D, and Impurity E are unidentified impurities.  
<sup>b</sup>Cefdinir-related compound A is a mixture of four isomers designated as lactam ring-cleavage lactones a, b, c, and d. The sum of all values is reported, and the total limit for all four isomers combined is 3.3%.  
<sup>c</sup>Impurity III is a mixture of two isomers designated as Impurity IIIa and Impurity IIIb. The sum of both values is reported, and the total limit for both isomers combined is 1.5%.  
<sup>d</sup>The total unidentified impurities limit includes the percentage total of unidentified impurities B, D, and E and any other unidentified impurities detected.

*Mobile phase*—Mix 1000 mL of *Citric acid buffer solution* with 111 mL of methanol and 28 mL of tetrahydrofuran. Make adjustments if necessary (see *System Suitability* under *Chromatography*, in the general method <621>).

*Standard preparation*—Accurately weigh a known amount of USP Cefdinir RS into a suitable volumetric flask. Dissolve in 0.1 M *Phosphate buffer solution* to obtain a solution having a known concentration of about 0.05 mg/mL of cefdinir.

*Assay preparation*—Quantitatively transfer the contents of each bottle of constituted Oral Suspension into a suitable flask and dilute with 0.1 M *Phosphate buffer solution* to obtain a solution having a concentration of about 0.05 mg/mL of cefdinir.

*Resolution solution*—Accurately weigh known quantities of USP Cefdinir RS and *m*-hydroxybenzoic acid into a suitable volumetric flask. Dissolve in 0.1 M *Phosphate buffer solution* to obtain a solution having a known concentration of about 0.05 mg/mL of cefdinir and about 0.175 mg/mL of *m*-hydroxybenzoic acid.

*Chromatographic system* (see *Chromatography*, in the general method <621>)—The liquid chromatography is equipped with a 254-nm detector and a 3.9-mm × 150-mm column that contains 4-μm packing L1. The flow rate is maintained at about 1.4 mL/min. Chromatograph the *Resolution solution* and record the peak response as directed in the *Procedure*. The resolution between cefdinir and *m*-hydroxybenzoic acid is greater



than 3.0; the tailing factor of the cefdinir peak is not more than 2.0; and the relative standard deviation for replicate injections of the *Standard preparation* is not more than 1.0%.

**Procedure**—Separately inject equal volumes (about 15  $\mu\text{L}$ ) of the *Standard preparation* and the *Assay preparation* into the chromatograph, record the chromatograms, and measure the responses for the major peaks. Calculate the percentage of cefdinir ( $\text{C}_{14}\text{H}_{13}\text{N}_5\text{O}_5\text{S}_2$ ) in the portion of Oral Suspension taken by the formula:

$$100(C_S/C_U)(r_U/r_S)$$

in which  $C_S$  is the concentration, in mg/mL, of cefdinir in the *Standard solution*;  $C_U$  is the concentration of cefdinir in the *Assay preparation*; and  $r_U$  and  $r_S$  are the peak responses of cefdinir in the *Assay preparation* and the *Standard preparation*, respectively.

## 6.2. Spectrophotometric methods

Shah and Pundarikakshudu [26] developed two simple and sensitive spectroscopic methods in the UV and visible region for the estimation of cefdinir in pharmaceutical dosage forms. In method A, cefdinir showed absorption maximum at 287 nm in 0.1 M phosphate buffer (pH 7). In method B, the drug reacted with Folin–Ciocalteu reagent under alkaline conditions forming a blue colored chromogen having absorption maximum at 720 nm. The methods obey Beer's law in the concentration range of 3–17 ng/mL and 4–20  $\mu\text{g/mL}$ , respectively. The methods are statistically evaluated for accuracy and precision.

Sankar *et al.* [27] described a simple and sensitive ultraviolet spectrophotometric method for the determination of cefdinir in pure drug substance and in pharmaceutical formulations. The drug exhibits a maximum at 225 nm and the method obeys Beer's law at the concentration range of 5–25  $\mu\text{g/mL}$ . The method was extended to the determination of pharmaceutical preparation and there is no interference from any common pharmaceutical additives.

Patil and Kasture [28] developed a new spectrophotometric method for the estimation of cefdinir from capsule formulations. The spectra the drug showed maximum at 282 nm. The statistical analytical of data indicated a high level of precision for the method as evidenced by low value of coefficient of variation (0.017%). The coefficient of correlation was highly significant (0.999608). The plot clearly showed a straight line passing

through the origin. The assay method was validated by low values of percent relative standard deviation ranging from 0.57 to 0.91 and standard error ranging from 0.33 to 0.52, indicating accuracy and precision of the methods. The accuracy of the method was further proved by excellent recovery data. The reproducibility of the results confirmed the ruggedness of the method.

Sankar *et al.* [29] developed a simple spectrophotometric method for the determination of cefdinir in pure form and in its pharmaceuticals. It is based on formation of red complex with ferric chloride and 2,2'-bipyridyl having absorption maxima at 530 nm. The chromogen obeys Beer's law in the concentration range of 0.5–2.5  $\mu\text{g/mL}$ .

Sankar *et al.* [30] developed two simple and sensitive visible spectrophotometric methods (A and B) for the estimation of cefdinir in pure and in pharmaceutical dosage forms. Method A is based on the oxidation followed by complexation between the cefdinir and 1,10-phenanthroline in presence of ferric chloride to form a blood red colored chromogen with  $\lambda_{\text{max}}$  at 520 nm. In method B, cefdinir reacts with Folin–Ciocalteu reagent an alkaline media to form a blue colored chromogen at  $\lambda_{\text{max}}$  at 710 nm. Beer's law is obeyed in the concentration range of 0.3–2.4  $\mu\text{g/mL}$  and 1.5–7.5  $\mu\text{g/mL}$  for methods A and B, respectively. Results obtained are reproducible and are statistically validated and are suitable for the analysis of cefdinir in bulk and in pharmaceutical dosage forms.

Singh *et al.* [31] described a nonextractive spectrophotometric method for the content assay of cefdinir in formulations. The method is based on complexation of cefdinir and iron under reducing conditions in a buffered medium (pH 11) to form a magenta colored donor–acceptor complex ( $\lambda_{\text{max}} = 550 \text{ nm}$ ; apparent molar absorptivity = 3720 L/mol/cm). No other cephalosporins, penicillins, and common excipients interfere under the test conditions. The Beer's law is followed in the concentrations range 8–160  $\mu\text{g/mL}$ .

Narala and Saraswathi [32] described three spectrophotometric methods (A, B, and C) for the determination of cefdinir. The methods are based on the oxidation of the drug with Fe(III) and the estimation of the Fe(II) produced after chelation with either 1,10-phenanthroline or 2,2'-Bipyridyl or potassium ferricyanide at 512, 510, and 700 nm. The Beer's law was obeyed in the concentration range of 2–8, 8–24, and 4–12  $\mu\text{g/mL}$  for cefdinir for the method A, B, and C, respectively. The results of the methods were validated statistically and applied to the determination of cefdinir in bulk and in pharmaceutical formulations without any interference from excipients.

Gouda *et al.* [33] developed and validated two spectrophotometric methods for the determination of cefdinir in bulk drug and in its pharmaceutical formulations. The first method is based on the reaction of cefdinir with 1,2-naphthoquinone-4-sulfonic acid sodium (NQS) in an alkaline medium (pH 11) to form an orange colored product that was measured at 490 nm. The second method depends on hydrolysis of cefdinir using 0.5 M sodium hydroxide at 100 °C and subsequent reaction of the formed sulfide ion with 4-chloro-7-nitrobenzo-2-oxa-1,3-diazole (NBD-Cl) to form a yellow-colored chromogen measured at 390 nm. Different variables affecting the reactions of cefdinir with both 1,2-naphthoquinone-4-sulfonic acid sodium and 4-chloro-7-nitrobenzo-2-oxa-1,3-diazole (e.g., sodium hydroxide concentration hydrolysis time, NQS and NBD-Cl concentrations, and diluting solvent) were studied and optimized. Under optimum condition, good linear relationship with good correlation coefficient was found in the range of 10–80 and 5–30 µg/mL for NQS and NBD-Cl, respectively. The limit of the assay detection and quantitation ranged from 1.097 and 0.280 and 3.656 and 0.934 µg/mL for NQS and NBD-CL, respectively. The accuracy and precision of methods were satisfactory. The method is simple, convenient and was applied for the analysis of cefdinir in pharmaceutical formulations and the recovery percent ranged from 99.25% to 100.20%.

Suganthi *et al.* [34] developed a simple, accurate, and sensitive spectrofluorimetric procedure for the estimation of cefdinir containing heterocyclic fused ring structure, in 1 M sodium hydroxide at 95° for 1 h, which shows strong fluorescence having excitation and emission wavelength 262 and 530 nm, respectively. Linear relationship for fluorescence intensity was obtained in the range of 0.2–1 µg/mL. The method was statistically validated and applied to the determination of cefdinir in pharmaceutical dosage form.

### 6.3. Polarographic method

Jain *et al.* [35] investigated the electrochemical behavior of cefdinir and two irreversible well-defined cathodic peaks were observed. From the electrochemical response, the main reduction steps were related to the reduction of the C=N and C=C groups. A fully validated, sensitive, and reproducible square-wave cathodic absorptive stripping voltammetric procedure has been developed for the trace determination of the bulk drug, pharmaceutical formulation, and in human urine, at the mercury electrode.

The optimal experimental parameters for the drug assay were accumulation potential  $-0.3$  V (vs. Ag/AgCl, 3 M KCl), accumulation time 15 s, frequency = 120 Hz, pulse amplitude = 0.07 V, and scan increment = 10 mV in phosphate buffer pH 2. The first peak current showed a linear dependence with the drug concentration over the range  $1.88 \times 10^{-8}$  to  $12 \times 10^{-8}$  M. The achieved limit of detection and limit of quantification were  $5 \times 10^{-9}$  M (0.2 ng/mL) and  $1.7 \times 10^{-9}$  M (0.67 ng/mL), respectively. The procedure was applied to the assay of the drug in capsules form with mean percentage recoveries of 99.7. Applicability to assay the drug in urine samples was illustrated. The peak current was linear, with the drug concentration in the range 0.08–0.7 ng/mL of the urine.

#### 6.4. Voltammetric methods

Jain *et al.* [36] studied the voltammetric behavior of cefdinir in different surfactant media; anionic, neutral, and cationic surfactants over the pH range 2.5–12 in phosphate buffer (0.2 M). Addition of cationic surfactant (citrimide) to the cefdinir-containing electrolyte enhanced the reduction current signal while the anionic surfactant (sodium lauryl) and neutral surfactant (Tween-20) showed an opposite effect. The reduction process was irreversible over the entire pH range studied (2.5–12). The mechanism of reduction has been postulated on the basis of controlled potential electrolysis, coulometry, and spectral analysis. An analytical method with adequate precision and accuracy was developed for the determination of cefdinir in linear concentration range  $2 \times 10^{-4}$  to  $1 \times 10^{-5}$  mol/L with detection limit  $0.3 \times 10^{-6}$  mol/L. The analysis of cefdinir in its pharmaceutical formulation resulted in mean recoveries of 99% and 98% for both the reduction peaks.

Tao *et al.* [37] developed an electrochemical method for the determination of cefdinir by differential pulse voltammetry. Adding cefdinir solution into 0.2 mol/L sodium hydroxide solution and the degradation products of cefdinir was determined by differential pulse voltammetry from  $-0.1$  to  $-1$  V. In a supporting electrolyte of 0.05 mol/L sodium hydroxide solution, a sensitive reductive peak of degradation product was attained at  $-0.52$  V. A linear relationship was held between the peak current and the concentration of cefdinir in the range from  $4 \times 10^{-8}$  to  $4 \times 10^{-7}$  mol/L and from  $4 \times 10^{-7}$  to  $4 \times 10^{-6}$  mol/L, and the detection limit was  $3 \times 10^{-8}$  mol/L. The method is accurate, reproducible, reliable, and may be used for the determination of cefdinir.

Dong *et al.* [38] studied the electrochemical behavior of the degradation products of cefdinir in a 0.05 mol/L of sodium hydroxide solution by linear sweep voltammetry and cyclic voltammetry. The results indicate that the C=N bond in the oxime group was reduced. A saturated adsorption amount of  $1.32 \times 10^{-10}$  mol/cm<sup>2</sup> at mercury electrode was obtained. The adsorption coefficient  $\beta$  was  $1.56 \times 10^5$  L/mol. Gibbs standard energy of adsorption  $\Delta G^\circ$  at 25° was  $-29.63$  kJ/mol and the number of electrons transferred  $n$  was 2. A method for the determination of cefdinir by differential pulse voltammetry was used. The reduction peak currents of the cefdinir's degradation products were found to be linear in a concentration range of  $4 \times 10^{-7}$  to  $4 \times 10^{-6}$  mol/L and that of  $4 \times 10^{-8}$  to  $4 \times 10^{-7}$  mol/L, respectively. The detection limit was found to be  $3 \times 10^{-8}$  mol/L, under the optimized conditions. The applicability of this approach was illustrated by the determination of cefdinir in capsules. The mechanism about the degradation of cefdinir in 0.2 mol/L sodium hydroxide was discussed by UV spectrophotometry.

## 6.5. Chromatographic methods

### 6.5.1 High-performance liquid chromatographic methods

Okamoto *et al.* [39] described a validated HPLC method used for the determination of cefdinir and its related substances. The method which is specific and stability-indicating provided a linear response with concentration. The system and method precision, expressed as relative standard deviations, were not greater than 1%, and the reproducibilities within and between laboratories were acceptable for the assay method. The procedure can quantitate related substances greater than approximately 0.05% of the principal cefdinir peak.

Wang [40] established an HPLC method for the determination of cefdinir and its related substances. A C<sub>18</sub> column (25 cm  $\times$  4.6 mm, 5  $\mu$ m) was used. The mobile phase was a mixture of 0.025 mol/L diammonium hydrogen phosphate adjusted to pH 5 with phosphoric acid and acetonitrile (89:11). The ultraviolet detection wavelength was 225 nm. The method proved to be selective for the separation of cefdinir, its byproducts, degradation products, and E-isomer. The method is simple, selective, and suitable for the determination of cefdinir and its impurities.

Qian *et al.* [41] established a high-performance liquid chromatographic method for the determination of cefdinir in capsules. A C<sub>18</sub> column (15 cm  $\times$  4.6 mm, 5  $\mu$ m), keeping at temperature of 25 °C was used. The mobile phase was a mixture of 0.029 mol/L diammonium hydrogen

phosphate (adjusted to pH 5 with phosphoric acid) and acetonitrile (86:14) and a flow rate of 0.5 mL/min with the detection wavelength at 286 nm. The injection volume was 20  $\mu$ L. The standard curve was linear over the range of 10–100  $\mu$ g/mL with the correlation coefficient of 0.9999. The average recovery was 100.19%.

Hadad *et al.* [42] developed and validated a simple and reliable liquid chromatographic method for the determination of cefdinir in human urine and capsule samples. The chromatographic separation was achieved on C<sub>18</sub> column using mobile phase consisting of potassium dihydrogen phosphate (10 mM, pH 4.5)–acetonitrile (90:10). Quantitation was achieved with ultraviolet detection at 285 nm, based on peak area with linear calibration curve at a concentration range of 0.7–39  $\mu$ g/mL. The method was applied for the establishment of an urinary excretion pattern after oral dose.

Mashelkar and Renapurkar [43] described a stability-indicating HPLC method for the quantitative determination of cefdinir. The drug was separated on a Inertsil C<sub>18</sub> HPLC column using mobile phase consisting of a mixture of 0.02 M ammonium formate buffer pH 4.5 (solvent A) and organic modifier methanol (solvent B). The method was LCMS compatible and can be used to identify the degradation products. The mass spectrum provides the identity of the degradation products formed and proves the specificity of the method and demonstrates the stability-indicating power of the method. Degradation studies were performed on the bulk samples of cefdinir under acidic conditions (using 1 N HCl), basic conditions (0.05 NaOH), neutral conditions, oxidation (0.1% hydrogen peroxide), thermal (105 °C) and photolytic conditions (UV light at 254 nm). Degradation was observed under hydrolytic (acidic and basic), oxidative, and photolytic stress conditions. The method was validated with respect to linearity, accuracy, precision, and robustness.

Shahed *et al.* [44] validated a reversed-phase HPLC method with UV detection to determine cefdinir concentrations in human serum samples and applied to determine the pharmacokinetic parameters of cefdinir in healthy Bangladeshi male volunteers. The mobile phase is consisting of a mixture of 0.2 M sodium dihydrogen phosphate buffer (pH  $3.2 \pm 0.05$  adjusted with *o*-phosphoric acid) and methanol at a ratio of 70:30 was pumped at a flow rate of 1 mL/min through the C<sub>18</sub> column at room temperature and the chromatographic separation was monitored at a wavelength of 254 nm with a sensitivity of 0.0001 AUFS. Cefaclor was used as internal standard. The method is selective and linear for cefdinir concentrations

ranging from 0.05 to 5  $\mu\text{g/mL}$  for serum samples. The method is accurate and precise for pharmacokinetic and bioequivalence studies of cefdinir.

Snali *et al.* [45] determined the  $\text{pK}_a$  value of cefdinir precisely in water and methanol–water binary mixture (20% v/v) using spectrophotometric titration and high-performance liquid chromatography, respectively. The chromatographic procedure has been developed for the determination of cefdinir in drug formulation. This method was validated for specificity, precision, linearity, range, accuracy, limit of detection, and limit of quantitation as per the ICH guidelines. The method can be used for routine analysis of the drug and as an alternative tool for drug quality control laboratories.

Li *et al.* [46] developed a high-performance liquid chromatography coupled with online solid-phase extraction (SPE) and ultraviolet detection for the determination of cefdinir in beagle dog plasma. After simple pre-treatment for plasma with 6% perchloric acid, a volume of 100  $\mu\text{L}$  upper layer of the plasma sample was injected into the self-made online SPE extraction. The analytes were retained on the trap column (Lichrospher  $\text{C}_{18}$ , 4.6 mm  $\times$  3.7 cm, 25  $\mu\text{m}$ ) and the biological matrix was washed out with the solvent (20 mM potassium dihydrogen phosphate adjusted to pH 3) at a flow rate of 2 mL/min. By rotation of the switching valve, the target analytes could be eluted from trap column to analytical column in the pack-flush mode by the mobile phase (methanol:acetonitrile:20 mM potassium dihydrogen phosphate adjusted pH 3 (11.25:6.75:82) at a flow rate of 1.5 mL/min), and then separated on the analytical column (Ultimate<sup>TM</sup> XB  $\text{C}_{18}$ , 5 cm  $\times$  4.6 mm, 5  $\mu\text{m}$ ). The complete cycle of the online SPE preconcentration, purification, and HPLC separation of the analytes was 4 min. The UV detection was performed at 286 nm. The method showed good performance in terms of specificity, linearity, detection and quantification limits, precision, and accuracy. The method was applied to the analysis of the drug in beagle dog plasma to support the preclinical pharmacokinetic trials.

Sankar *et al.* [47] developed a simple, fast, and precise reversed-phase high-performance liquid chromatographic method for estimation of the cefdinir in bulk and in pharmaceutical dosage forms. The analysis was carried out using a Partisil  $\text{C}_{18}$  octadecylsilane column (15 cm  $\times$  4.6, 5  $\mu\text{m}$ ) in isocratic mode, with mobile phase comprising acetonitrile and water in the ratio 60:40 (v/v). The flow rate was 1 mL/min and effluents were monitored at 240 nm. The retention time of cefdinir was 1.9 min. The method produced linear response in the concentration range of 0.5–50  $\mu\text{g/mL}$  and the percentage recovery ranged from 98.6 to 100.15. The method was

convenient and reproducible for the analysis of cefdinir in the pharmaceutical dosage form.

Gandhimathi *et al.* [48] developed a simple, efficient, and reproducible reversed-phase HPLC method for the determination of cefdinir in capsules. The eluent was done using a mobile phase consisting of 0.01 N potassium dihydrogen phosphate, pH 6.9, and methanol (80:20) on Water's Spherisorb ODS 4.6 mm  $\times$  15 cm analytical column with flow rate of 1 mL/min with detection at 285 nm. An external standard calibration method was employed for quantitation. The eluent time was 2 min. The linearity range was 5–10  $\mu$ g/mL for cefdinir.

Mehta *et al.* [49] developed a stability-indicating reversed-phase liquid chromatographic method for the determination of cefdinir in its different dosage forms (capsules and suspensions). The method is optimized by analyzing the placebo preparation, formulations, and degraded samples of the drug substance according to the international conference on Harmonization. The method can separate the drug from its degradation products formed under stress conditions along with pharmaceutical ingredients such as preservatives. The method was used to determine cefdinir in capsules and Insta-use suspensions. The method was found to be linear for a concentration range of 6–14  $\mu$ g/mL. Average recoveries obtained with the method were 99.3% and 99.6% for Insta-use suspension and capsules, respectively. The method is simple, fast, specific, stability-indicating, precise, and robust.

Zhao *et al.* [50] developed a reversed-phase HPLC method for the determination of the content of cefdinir in human plasma. Arilin was chosen as the internal standard and the plasma samples were prepared by protein precipitating using trichloroacetic acid. Chromatographic separation was achieved with a Nucleodur C<sub>18</sub> reversed-phase column (25 cm  $\times$  4.6 mm, 5  $\mu$ m), mobile phase was 0.025 mol/L ammonium dihydrogen phosphate (pH 3) and acetonitrile (90.5:9.5) and flow rate was 1 mL/min. The detection wavelength was set at 286 nm. The results showed that the calibration curve was linear over a concentration range of 0.05–2  $\mu$ g/mL. The relative standard deviation of intra-day was 3.7–5.9% and for inter-day was 3.5–5.7%. The recovery of cefdinir was 65–72.4%. The method which is sensitive, accurate, and convenient had low limit of quantitation and well reproducibility and can be applied to the pharmacokinetic study of cefdinir in human plasma.

Hamrapurkar *et al.* [51] developed and validated a stability-indicating reversed-phase high-performance liquid chromatographic method for the determination of cefdinir in the presence of its degradation products as



per International Conference on harmonization guidelines. The analysis was performed on a Waters RP Spherisorb C<sub>18</sub> column (25 cm × 4.6 mm, 5 μm). A mobile phase consisting of water (pH adjusted to 3 with orthophosphoric acid):acetonitrile:methanol (13:5:2) was used. The flow rate was 1 mL/min. The separation was performed at room temperature. Detection was carried out at 286 nm, using a photodiode array detector. The method was statistically validated for linearity accuracy, specificity, limit of detection, and limit of quantitation. The specificity of the method was ascertained by forced degradation studies, by acid and alkali degradation, oxidation, photolysis, and heat of hydrogenation.

Khan *et al.* [52] developed and validated an isocratic reversed-phase high-performance liquid chromatographic method for the simultaneous determination of cefdinir and cefixime in human plasma, after optimization of various chromatographic conditions and other experimental parameters. Sample preparation is based on a simple extraction procedure consisting of deprotonation and extraction with three parts of 6% trichloroacetic acid aqueous solution followed by volume make up with the aqueous component of the mobile phase obtained best recoveries of the two analytes. Samples were separated on a Supelco Discovery HS C<sub>18</sub> (15 cm × 4.6 mm, 5 μm) analytical column protected by a Perkin Elmer C<sub>18</sub> (3 cm × 4.6 mm, 10 μm) guard cartridge. The mobile phase, methanol:acetonitrile (50:50):0.05% trifluoroacetic acid (19:81), operated at 50 °C column oven temperature was pumped at a flow rate of 2 mL/min and the column eluents were monitored at a wavelength of 285 nm. The method demonstrated acceptable values for selectivity, linearity, recovery, precision, sensitivity, stability of solution, and robustness. The method was applied to a pharmacokinetic study in healthy volunteers.

Narala and Saraswathi [53] developed two reversed-phase high-performance liquid chromatographic methods for the determination of cefdinir in pharmaceutical dosage forms. The methods were carried out in an isocratic mode using Kromosil C<sub>18</sub> column (25 cm × 4.6 mm, 5 μm) with mobile phase comprised of methanol and 0.025 M potassium dihydrogen phosphate buffer (75:25) at a flow rate of 1 mL/min, with effluent detection at 285 nm for cefdinir. The retention time was found to be 2.97 min for cefdinir. Linearity was obtained in the concentration range of 20–100 μg/mL for cefdinir. The methods are accurate, precise, and suitable for the analysis of the drug in pharmaceutical dosage form.

Sakamoto *et al.* [54] described a microbiological assay and HPLC method for the determination of cefdinir in biological fluids. The drug was assayed

by paper disk, cup, and agar-well method using *Providencia stuartii* ATCC 43665 and *Providencia stuartii* ATCC 43664 (a sensitive mutant of *P. stuartii* ATCC 43665) and antibiotic medium Number 1 (Difco). *P. stuartii* ATCC 43665 was used for assaying high concentrations of cefdinir ( $>0.13 \mu\text{g/mL}$ ) and *P. stuartii* ATCC 43664 for lower concentrations. The lowest detectable concentration of cefdinir in human plasma was  $0.016 \mu\text{g/mL}$  for the cup-plate and agar-well method and  $0.03 \mu\text{g/mL}$  for the disc-plate method using *P. stuartii* ATCC 43664. Plasma and urine levels of cefdinir in human after oral administration were detected by HPLC. The detection limits in plasma and urine were 0.4 and  $0.5 \mu\text{g/mL}$ , respectively.

### 6.5.2 High-performance liquid chromatography/mass spectrometric methods

Chen *et al.* [55] developed a sensitive and selective liquid chromatography–tandem mass spectrometric method for the analysis of cefdinir in human plasma. After a simple protein precipitation using trichloroacetic acid, the posttreatment samples were applied to a prepacked RP-18 Waters SymmetryShield column interfaced with a triple quadrupole tandem mass spectrometer. Positive electrospray ionization was employed as the ionization source. The mobile phase consisted of methanol–water–formic acid (25:75:0.075). The analyte and the internal standard, cofaclor, were both detected by the use of selected reaction monitoring mode. The method was linear in the concentration range of 5–2000 ng/mL. The lower limit of quantification was 5 ng/mL. The intra- and inter-day relative standard deviation across three validation runs over the entire concentration range was less than 4.3%. The accuracy determined at three concentrations (36, 360, and 1800 ng/mL for cefdinir) ranged from 99.6% to 106.7% in terms of recovery. The chromatographic run time for each plasma sample was less than 3 min. The method was applied for the evaluation of pharmacokinetic profiles of Cefdinir capsule in 12 healthy volunteers.

Rao *et al.* [56] developed a robust and sensitive solid-phase extraction followed by liquid chromatography–electrospray ionization (LC–ESI) mass spectrometric method for the determination of cefdinir and other antibiotics in surface waters. The sample recoveries on Oasis HLB cartridge were found to be  $>80\%$ . Identification was carried out by LC–ESI–MS/MS. The positive ion ESI mass spectra containing the peaks of quasi molecular ions  $[\text{M} + \text{H}]^+$  allowed the determination of the molecular masses whereas the fragment ions obtained by MS/MS of  $[\text{M} + \text{H}]^+$  ions permitted the structural

assignments. Quantification was carried out by selective ion monitoring using the quasi molecular ion  $[M+H]^+$  of the parent compounds. The detection and quantification limits were found to be in the range of 0.6–8.1 and 2–24  $\mu\text{g/L}$ , respectively. The surface of waters of different lakes and tanks of Hyderabad, India, were found to contain a few antibiotics.



## 7. PHARMACOKINETICS

Cefdinir exhibits broad range *in vitro* activity against Gram-positive and Gram-negative aerobes. It is stable to hydrolysis by many of the common  $\beta$ -lactamases. The pharmacokinetic parameters of the drug in children are similar to those obtained in adults using similar  $\text{mg/m}^2$  doses (300, 600 mg in adults = 7.14 mg/kg in children, respectively) [57].

The terminal elimination half-life  $t_{1/2}$  of cefdinir increases in patients with chronic renal failure to  $11 \times$  that of healthy controls. Hemodialysis effectively removes cefdinir and  $t_{1/2}$  during hemodialysis decreases to one sixth of that in tests without dialysis but is still longer than in healthy subjects. 100 Mg of the drug once a day is sufficient dose for hemodialysis patient [58].

A cefdinir dosage of 25 mg/kg once daily would be ineffective for treatment of acute otitis media caused by penicillin-nonsusceptible *Streptococcus pneumonia* strain [59].

Cefdinir is administered orally to patients with chronic renal failure undergoing continuous ambulatory peritoneal dialysis to investigate changes in serum concentration, excretion rate into the dialysate and serum protein binding of cefdinir. The serum concentration level of cefdinir was found to be dose dependent in patients given the drug for 4–14 day. Cefdinir inhibited 90–100% of the clinical isolates such as *S. aureus*, *S. epidermidis*, *E. coli*, and its antibacterial activity was stronger than that of amoxicillin and cofactor against clinical isolates [60].

The relative bioavailability and bioequivalence of cefdinir dispersible tablets were studied in healthy volunteers. The pharmacokinetic parameter of the test and reference dispersible tablets was bioequivalent [61].

The pharmacokinetic interaction between cefdinir and captopril or quinapril was studied in rats. Captopril and quinapril and/or their metabolites have a major impact on the disposition of cefdinir in rats, probably by competition at the plasma protein binding level and at the tubular anionic carrier level. This mechanism also is relevant in humans [62].

The pharmacokinetic and clinical effects of 5% and 10% fine granules of cefdinir were studied in the pediatric field. The results showed that blood concentration and urinary excretion of cefdinir in children was studied in the fasting and the nonfasting state. Data showed that blood concentration of the drug depended on the dose level. Clinical effects of cefdinir on various infections were studied in a number of children who were treated with 5% fine granules of cefdinir and in children with 10% fine granules of cefdinir. Granules were administered at daily doses of 9–18 mg/kg in three divided portions. Clinical efficacy rates in children of the 5% granules and in another group of the 10% granule group from whom causative bacteria were isolated were 94.9% and 96.2%, respectively. The appropriate dose levels of cefdinir for pediatric infection ranged from 9 to 18 mg/kg a day, divided in three portions [63].

The clinical efficacy and side effects of cefdinir was evaluated in children treated with cefdinir. The dosage of the drug ranged from 8.1 to 15.9 mg/kg/day with treatment continued for 2–10 days. Twenty-eight of children were evaluated for efficacy, 10 patients with tonsillitis, 3 with scarlet fever, 4 with lower respiratory infections, 2 with otitis media, 2 with cervical lymphadenitis, 3 with urinary tract infection, 4 with skin and soft tissue infections and 2 with viral disease. Clinical responses were excellent in 14 patients, good in 12, fair in 1, and poor in 1 with an efficacy rate of 92.9% [64].

Cefdinir was evaluated for its efficacy and safety in four male children of age 9–13 years. The drug was given orally to three of them at a dose of 3 mg/kg. Peak plasma level of 0.71  $\mu\text{g/mL}$ , 0.78  $\mu\text{g/mL}$ , and 0.45  $\mu\text{g/mL}$  were attained in the three children respectively, at 4 h after dosing. Half-lives of the drug in serum were 1.78, 1.48, and 2.23 h, respectively. The 12 h urine recovery rates were 17.4%, 28.1%, and 6.2%. When the drug was given orally to the remaining child at a dose of 6 mg/kg, the peak plasma level was attained at 4 h after dosing with level of 1.16  $\mu\text{g/mL}$ .  $T_{1/2}$  was 1.78 h. The 12 h urinary recovery of rate of cefdinir was 15%. The drug was given orally to 26 patients of different bacterial infections, the responses were excellent in 15, good in 8, fair in 1, and poor in 2. The drug is useful for the treatment of bacterial infections in pediatrics [65].

The pharmacokinetics, bacteriological, and clinical studies of cefdinir 10% fine granules were performed in pediatrics. Plasma concentration and urinary excretions of the drug 5% and 10% fine granules were investigated on three pediatric patients with ages 5–13 years administered with a drug in fasting state at a dose level of 3 mg/kg using a cross over method.

Average plasma concentrations in a group of patients administered with 5% fine granules peaked at 3 h after administration with level of  $1.05 \pm 0.29 \mu\text{g/mL}$  and decreased to  $0.12 \pm 0.05 \mu\text{g/mL}$  at 8 h with a half-life of  $1.48 \pm 0.09 \text{ h}$ . The overall efficacy rate was 100%. Bacteriological effects against organisms; *S. aureus* and *S. agalactiae* were eradicated and the overall eradication rate was 90% [66].

The antibacterial activities of cefdinir against *S. aureus*, *S. pyogenes*, *S. pneumonia*, *Haemophilus influenzae*, *Branhamella catarrhalis*, *E. coli*, and *Klebsiella pneumoniae* were studied in comparison with those of cefaclor, cefixime, and amoxicillin. The results showed that the drug has high antibacterial activities against these organisms. The activity of the drug against Gram-positive bacteria was similar to those of amoxicillin and was lower than those of cefaclor and cefixime. Absorption and excretion blood concentration and urinary excretion rates of cefdinir 5% and 10% granules and 100 mg capsule were determined. The data of 10% granules of cefdinir were similar to those of cefdinir 5% granules. Urinary recovery rates in the first 8 h ranged from 6.85% to 39.2% with 3 mg/kg and 6.08–25.5% with 6 mg/kg of the drug [67].

Cefdinir was administered to eight children and concentration of the drug in plasma and urine and the urinary recovery rates of the drug were determined. The results obtained are: mean plasma peak levels of the drug were observed at 2 h after administration in the before-meal group and 4–5 h after administration in the after-meal group, mean peak value of 0.88 and 0.5  $\mu\text{g/mL}$ , respectively. Mean half-life were 1.61 h in the before-meal group and 2.54 h in the after-meal group. Mean urinary peak concentrations of the drug were observed during 2–4 h after dosing in the before-meal group and 6–8 h in after-meal group with values of 93.3 and 44.8  $\mu\text{g/mL}$ . Good clinical effects were obtained with an efficacy of 100% in nine patients with six diseases due to bacterial infection. Good bacteriological effects against two strains of *S. pyogenes*, two strains of *E. coli*, and one strain of *H. influenzae* with an eradication rates of 100% [68].

The antibacterial activities and the oral absorption efficiencies were studied with regard to cefdinir and other 3-vinyl cephalosporins with various seven acyl side chains. Cefdinir showed excellent antibacterial activity and good oral absorption in rats. *In vitro* and *in vivo* antibacterial activities, the affinity for PBPs and the stability of the  $\beta$ -lactamases revealed that cefdinir had well-balanced antimicrobial activities against Gram-positive and Gram-negative bacteria and good biological properties. The pharmacokinetics of the drug in the healthy volunteers showed that serum

concentration and half-life were good enough to make cefdinir an effective drug. The mechanism of the intestinal absorption of the drug and related oral cepheems are discussed and a hypothesis for the molecular recognition by the carrier protein in the intestine is proposed [69].

The clinical effectiveness and the pharmacokinetics of cefdinir were examined in pediatric patients. Plasma concentration and urinary excretion of the drug after administration of 5% fine granules were investigated in four children at a dose level of 6 mg/kg. Average plasma concentrations peaked at 4 h after administration at 0.99  $\mu\text{g/mL}$  with a half-life of 2.12 h. The first 24-h urinary recovery of the drug in three children averaged 22%. Clinical effects were excellent in 16, good in 7, and overall efficacy rate of 100%. The organisms were 12 strains of *S. pyogenes*, 4 of *H. influenza*, 5 of *H. parainfluenzae*, 1 of *E. coli*, and 1 of *Salmonella*. The bacteriological effects were rated as “eradicated” for 19 strains and unchanged for 4 with an eradication rate of 82.6%. No side effects were observed. The drug is useful for the treatment of bacterial infections of pediatrics [70].

Cefdinir is primarily eliminated by the kidney. The drug renal transport mechanisms were studied in the erythrocyte-free isolated perfused rat kidney. To study cefdinir renal transport mechanisms, inhibition studies were conducted by copper-fusing cefdinir with inhibitors of the renal organic anion (Probenecid), organic cation (tetraethylammonium), or dipeptide (glycylsarcosine) transport system. The drug concentration in biological samples was determined using RP-HPLC. Difference between treatments and controls were evaluated using analysis of variance and Dunnett’s test. The excretion ratio for cefdinir was 5.94, a value indicating net renal tubular secretion. Anionic cationic, and dipeptide transport inhibitors all significantly affected cefdinir excretion ratio [71].

Comparison between the pharmacokinetics/pharmacodynamic properties of cefdinir and other antibiotics against common bacteria of community acquired infections and evaluate the recommended regimens was performed. The antibacterial activities of three agents against 238 clinical isolates were determined by standard agar dilution test and the pharmacokinetics of these antibiotics in male healthy volunteers were conducted in Latin-square manner. The time over MIC of serum antibiotics concentrations was calculated with pharmacokinetic equation and MIC. The time over MIC of cefdinir after 100 mg oral administration meets with the clinical requirement in most infections [72].

Cefdinir was evaluated for its efficacy, safety, and pharmacokinetics in 13 children. Plasma concentration peaked at 3–4 h of the administration

of 3 mg/kg of the drug with  $C_{\max}$  ranging from 0.57 to 0.89  $\mu\text{g/mL}$  except 1 case in which the absorption of the drug was poor. Recovery rates in urine averaged at 13.4% with a large individual variation. Ten children with 12 bacterial infections were treated with 9 mg/kg/day of cefdinir fine granules. Clinical responses were good in 10 patients and fair in 1 patient, with an efficacy rate of 90.9% [73].

Cefdinir is safe and effective for treating skin infections caused by *S. aureus* and *S. pyogenes* and many Gram-negative pathogens. The pharmacokinetic, dosing schedule, adverse event profile, and efficacy data for cefdinir in adults and pediatrics populations in the treatment of the uncomplicated skin structure infections [74].

The administration of cefdinir to healthy subjects after high protein diet and L-phenylalanine load was studied to explore the induction of intestinal peptide transporter. Six healthy subjects had normal protein and high protein diets and L-phenylalanine for 12 days in a randomized three-way cross-over study. A single dose of cefdinir (100 mg) was given on the 13th day. Serial plasma samples were collected and measured by HPLC. Urinary urea nitrogen levels were increased by high protein. Plasma trough Phenylalanine levels were increased. However,  $C_{\max}$ ,  $T_{\max}$ ,  $\text{AUC}_{\text{last}}$  in the high protein and Phenylalanine groups were not different for normal protein group. Intestinal peptide transporter did not seem to be affected by the high protein diet and phenylalanine load with the subjects, duration and doses examined [75].



## 8. STABILITY

Payne and Amyes [76] purified fourteen plasmid-encoded extended-spectrum  $\beta$ -lactamases from *Escherichia coli* transconjugates of original clinical isolates. The  $V_{\max}$ ,  $K_m$  and  $V_{\max}/K_m$  were each determined for cefdinir and other related antibiotics as substrates with eight of these enzymes and with the narrow-spectrum  $\beta$ -lactamase TEM-I. The relative rates of hydrolysis of cefdinir was also determined for the remaining six enzymes. Cefdinir had  $V_{\max}/K_m$  of relative rate of hydrolysis values either equal to or lower than other related antibiotics for the enzymes tested. Cefdinir was more stable to the 15  $\beta$ -lactamases tested than cefixime.

Mimura *et al.* [77] estimated the grinding effect on the solid-state stability of cefdinir by use of microcalorimetry. Ground samples of cefdinir were prepared and microcalorimetry was performed to estimate the effect of grinding on the solid-state stability of cefdinir. High-performed liquid chromatographic analysis was also performed to interpret the microcalorimetric

data. The microcalorimetric study revealed that degradation of solid-state cefdinir of various crystallinities follows zero-order kinetics below 50 °C but not at the accelerated storage temperature of 70 °C. The degradation mechanism was confirmed by HPLC. The degradation rate constants of cefdinir were determined by both microcalorimetry at temperatures below 50 °C and by HPLC analysis at 50 °C. Kinetic parameters evaluated by microcalorimetry revealed that the solid-state stability of cefdinir decreased with decreasing crystallinity. The enthalpy change of cefdinir degradation was  $-97$  Kcal/mol, thereby making possible the prediction of stability of cefdinir of various crystallinities. Microcalorimetry was confirmed to be very useful for studying the effect of grinding on the solid-state stability of cefdinir.

Okamoto *et al.* [78] studied the hydrolytic degradation products of cefdinir in acidic (pH 1), neutral (pH 6), and basic (pH 9) solutions. Seven major degradation products were isolated by preparative and/or HPLC and characterized by ultraviolet, infrared and proton-nuclear magnetic resonance, and mass spectra. To clarify degradation pathways in each pH solution, kinetic and product analyses during hydrolysis of cefdinir were carried out along with the follow-up reaction of representative degradation products. Cefdinir was shown to degrade via two major degradation routes;  $\beta$ -lactam ring-opening and pH-dependent isomerizations (lactonization, epimerization at C-6 or C-7, synanti isomerization of *N*-oxime function).

Okamoto *et al.* [79] reported that the hydrolysis of cefdinir leads to pH-dependent isomerizations and  $\beta$ -lactam ring opening. Lactam ring opened gamma lactones were produced as a mixture of four diastereoisomers based on the lactone methyl, and C-6 isomerizations in acidic to neutral solutions. Cefdinir and its 7-epimer were hydrolyzed to clarify the pathway leading to these lactones and the mechanism of C-6 epimerization with the aid of chiral separation techniques. Chiral separation using a bovine serum albumin column was employed to detect the  $\beta$ -lactam ring opened products of cefdinir and its 7-epimer; the C-6 and C-7 isomerization was observed; however, it was found to be pH-dependent at  $\text{pH} \geq 9$ . Optical activity detection applied to the lactones produced from cefdinir and its 7-epimer demonstrated that the corresponding peaks of these lactones were enantiomeric pairs. In addition, the smallest rate constant at pH 4 was observed for C-6 epimerization of the lactone, and it was found to proceed without deprotonation at C-6 by proton NMR spectrometry. From the results, a plausible mechanism for C-6 epimerization has been proposed. It was confirmed that two degradation pathways were involved during the hydrolysis of cefdinir to the lactone.



## ACKNOWLEDGMENTS

The authors wish to thank Mr. Tanvir A. Butt, secretary of the Department of Pharmaceutical Chemistry, College of Pharmacy, King Saud University, for his secretarial assistance in typing of this profile.

## REFERENCES

- [1] M.J. O'Neil (Ed.), *The Merck Index: An Encyclopedia of Chemical, Drugs and Biologicals*, 14th ed., Merck & Co. Inc, Whitehouse Station, NJ, 2006, Monograph 1920, pp. 314.
- [2] S.C. Sweetman (Ed.), *Martindale: The Complete Drug Reference*, 37th ed., The Pharmaceutical Press, London, 2009, p. 242.
- [3] H.C. Neu, G. Saha, N.X. Chen, Comparative in-vitro activity and  $\beta$ -lactamase stability of FK482 a new oral cephalosporin, *Antimicrob. Agents Chemother.* 33 (1989) 1795–1800.
- [4] R. Wise, J.M. Andrews, D. Thornber, The in-vitro activity of cefdinir (FK482), a new oral cephalosporin, *J. Antimicrob. Chemother.* 28 (1991) 239–249.
- [5] E.J. Perea, M.C.G. Iglesias, Comparative in-vitro activity of cefdinir against multi-resistant *Haemophilus influenza*, *J. Antimicrob. Chemother.* 34 (1994) 161–164.
- [6] A. Marchese, D. Saverino, E.A. Debbia, A. Pesce, G.C. Schito, Antistaphylococcal activity of cefdinir, a new oral third-generation cephalosporin, alone and in combination with other antibiotics, at supra and sub-MIC levels, *J. Antimicrob. Chemother.* 35 (1995) 53–66.
- [7] P.J. Cook, J.M. Andrews, R. Wise, D. Honeybourne, Distribution of cefdinir, a third generation cephalosporin antibiotic, in serum and pulmonary compartments, *J. Antimicrob. Chemother.* 37 (1996) 331–339.
- [8] M. Gonzalez, Z. Rodriguez, B. Tolon, J.C. Rodriguez, H. Velez, B. Valdes, M.A. Lopez, A. Fini, An alternative procedure for preparation of cefdinir, *Farmaco* 58 (2003) 409–418.
- [9] Y. Inamoto, T. Chiba, T. Kamimura, T. Takaya, FK 482, a new orally active cephalosporin, synthesis and biological properties, *J. Antibiot.* 41 (1988) 828–830.
- [10] T. Takaya, H. Takasugi, T. Masugi, H. Yamanaka, K. Kawabata, 7-Substituted-3-vinyl-3-cephem compounds and processes for production of the same, *Chem. Abstr.* 95 (1981)US Pat. 4 559 334. P150687e through ref 1.
- [11] R. Heymes, L. Lutz, 3-Acetoxyethyl-7-(iminoacetamido)-cephalosporanic acid derivatives, *Chem. Abstr.* 87 (1977)US Pat. 4 152 432. P168063t through ref 1.
- [12] H. Kamachi, Y. Narita, T. Okita, Y. Abe, S. Imura, T. Tomatsu, Y. Yamasaki, J. Okumura, T. Naito, T. Oki, H. Kawaguchi, Synthesis and biological activity of a new cephalosporin, BMY-28232 and its prodrug-type esters for oral use, *J. Antibiot.* 41 (1988) 1602–1616.
- [13] T. Takaya, H. Takasugi, T. Murakawa, H. Nakano, Studies on beta-lactam antibiotics. III. Synthesis and enzymatic stability of 3- acyloxymethyl-7 beta-[(Z)-2-(2-amino-4-thiazolyl)-2-(methoxyimino)acetamido]-3-cephem-4-carboxylic acids, *J. Antibiot.* 34 (1981) 1300–1318.
- [14] G.S. Lee, Y.K. Chang, J.P. Chun, J.H. Koh, Process for preparation of cefdinir, EP 0 874 853 B1 (1996).
- [15] Y. Kumar, M. Prasad, A. Prasad, K. Singh, P. Kumar, Process for the preparation of cefdinir, US 0040915 A1 (2006).
- [16] D. Moralikrishna, A. Chetia, V. Pagar, Synthesis of cefdinir from 7-amino-3-vinyl cephem-4-carboxylic acid using N-methyl morpholine as base, *Asian J. Chem.* 21 (2009) 820–822.

- [17] K.V.V.P. Rao, A. Rani, A.V.R. Reddy, C.H. Bharathi, R. Dandala, A. Naidu, Isolation, structural elucidation and characterization of impurities in cefdinir, *J. Pharm. Biomed. Anal.* 43 (2007) 1476–1482.
- [18] K.V.V.P. Rao, R. Dandala, A. Rani, A. Naidu, Synthesis of potential related compounds of cefdinir, *Arkivoc* 15 (2006) 22–27.
- [19] S.K. Singh, Y. Kumar, M. Prasad, N.P. Kumar Cefdinir, PD-134393, CI-983, Fr-80482, FK-482, omnicef, WO 0391261 (2004).
- [20] K. Kawabata, T. Masudi, T. Takaya, H. Taksugi, H. Yamanaka, Synthesis of cefdinir, *Drug Fur.* 13 (1988) 224.
- [21] J. Sakane, Y. Kazuo, Synthesis of cefdinir, Spanish Patent ES 2013828 through US Patent 7105 659B; *Chem. Abstr.* 113 (1993), 23533.
- [22] K.V.V.P. Rao, R. Dandala, M. Sivakumaran, A. Rani, A. Naidu, Novel compounds for the synthesis of cefdinir, *J. Heterocycl. Chem.* 44 (2007) 309–314.
- [23] R. Dandala, V.V.P.R., Korrapati, M. Sivakumaran, Process of preparing cefdinir, US Patent 7,105,659 B2 (2006).
- [24] Japanese Pharmacopoeia. Official Monographs JP XV, pp. 434–437.
- [25] United States Pharmacopoeia, 32—National Formulary 27 page 1826, 1827, 1830.
- [26] P.B. Shah, K. Pundarikakshudu, UV spectroscopic and colorimetric methods for the estimation of cefdinir in capsule dosage forms, *Indian J. Pharm. Sci.* 66 (2004) 665–667.
- [27] D.G. Sankar, M. Sudarshan, M.V. Krishna, P.V.M. Latha, UV spectrophotometric method for determination of cefdinir, *J. Inst. Chem.* 77 (2005) 5–6.
- [28] S.S. Patil, P.V. Kature, Spectrophotometric method for estimation of cefdinir from capsule formulation, *Indian Pharmacist.* 7 (2008) 110–112.
- [29] D.G. Sankar, K.D. Priya, M. Sudarshan, M.L. Surekha, Spectrophotometric determination of cefdinir, *J. Inst. Chem.* 76 (2004) 30–31.
- [30] D.G. Sankar, S.M.L. Gowri, M.V. Krishna, P.V.M. Latha, New spectrophotometric method for the estimation of cefdinir in pure and in pharmaceutical dosage forms, *Int. J. Chem. Sci.* 3 (2005) 499–502.
- [31] B.K. Singh, D.V. Parwate, S. Srivastava, S.K. Shukla, Selective and non-extractive spectrophotometric determination of cefdinir in formulations based on donor-acceptor complex formation, *Quim. Nova* 33 (2010) 1471–1475.
- [32] S.R. Narala, K. Saraswathi, Application of oxidants to the spectrophotometric determination of cephalosporins (cefditoren, pivoxil, and cefdinir) in formulations, *Asian J. Res. Chem.* 4 (2011) 270–271.
- [33] A.A. Gouda, H. Hashem, W. Hassan, Spectrophotometric methods for determination of cefdinir in pharmaceutical formulations via derivatization with 1,2-naphthoquinone-4-sulfonate and 4-chloro-7-nitrobenzo-2-oxa-1,3-diazole, *Drug Test Anal.* 4 (2012) 991–1000.
- [34] A. Suganthi, S. Shrikumar, M.B. Pattesseril, M. Umamaheswari, T.K. Ravi, Spectrophotometric estimation of cefdinir in formulation, *Indian J. Pharm. Sci.* 66 (2004) 689–691.
- [35] R. Jain, K. Radhapyari, N. Jadon, Electrochemical evaluation and determination of cefdinir in dosage form and biological fluid at mercury electrode, *J. Electrochem. Soc.* 154 (2007) F199–F204.
- [36] R. Jain, D. Ashish, M. Ritesh, Voltammetric behavior of cefdinir in solubilized system, *J. Colloid Interface Sci.* 318 (2008) 296–301.
- [37] F. Tao, Z. Yu, X. Han, S. Zheng, S. Dong, Determination of cefdinir by differential pulse voltammetry, *Yaowu Fenxi Zazhi* 28 (2008) 1512–1514.
- [38] S. Dong, Z. Yu, X. Han, T. Huang, J. Zheng, Voltammetric behavior of degradation product and determination of cefdinir, *Chem. Res. Chin. Univ.* 25 (2009) 807–811.
- [39] Y. Okamoto, K. Itoh, Y. Namiki, J. Matsushita, M. Fujioka, T. Yasuda, Method development for the determination of cefdinir and its related substances by high-performance liquid chromatography, *J. Pharm. Biomed. Anal.* 14 (1996) 739–748.

- [40] X.-L. Wang, Determination of cefdinir and its related substances by HPLC, *Zhongguo Xinyao Zazhi* 12 (2003) 114–117.
- [41] Y. Qian, C. Zhao, Y. Yu, Determination of the content of cefdinir capsule by HPLC, *West China J. Pharm. Sci.* 20 (2005) 253–255.
- [42] G.M. Hadad, S. Emara, W.M.M. Mahmoud, Optimization and validation of an LC method for the determination of cefdinir in dosage form and human urine, *Chromatographia* 70 (2009) 1593–1598.
- [43] U.C. Mashelkar, S.D. Renapurkar, A LCMS compatible stability-indicating HPLC assay method for cefdinir, *Int. J. ChemTech. Res.* 2 (2010) 114–121.
- [44] G.M. Shahed, M. Ashik Ullah, A. Al-Maruf, M.U. Ahmed, M.S. Islam, Z. Nahar, A. Hasnat, A simpler-HPLC method for the determination of cefdinir in human serum: validation and application in a pharmacokinetic study with healthy Bangladeshi male volunteers, *Dhaka Univer. J. Pharm. Sci.* 10 (2011) 109–116.
- [45] N. Snali, S. Snali, U. Sizir, M. Gumustas, S.A. Ozkan, Determination of pKa values of cefdinir and cefixime by LC and spectrophotometric methods and their analysis in pharmaceutical dosage forms, *Chromatographia* 73 (2011) 1171–1176.
- [46] J. Li, L. Wang, Z. Chen, R. Xie, Y. Li, T. Hang, G. Fan, Development and validation of a rapid HPLC method for the determination of cefdinir in beagle dog plasma integrated with an automatic on-line solid-phase extraction following protein precipitation in the 96-well plate format, *J. Chromatogr. B* 895–896 (2012) 83–88.
- [47] D.G. Sankar, K.D. Priya, M.V. Krishna, P.V.M. Latha, RP-HPLC method for the estimation of cefdinir in bulk drugs and in dosage forms, *Acta Cienc. Indica Chem.* 30 (2004) 273–276.
- [48] M. Gandhimathi, A. Suganthi, T.K. Ravi, M.B. Pattasseril, RP-HPLC estimation of cefdinir in capsules, *Indian J. Pharm. Sci.* 66 (2004) 248–249.
- [49] T.N. Mehta, G. Subbaiah, K. Pundarikakshudu, Determination of cefdinir by a stability-indicating liquid chromatographic method, *J. AOAC Int.* 88 (2005) 1661–1665.
- [50] G. Zhao, X. Ke, P. Ren, S. Gu, H. Chen, Determination of cefdinir in human plasma by RP-HPLC, *Zhongguo Yaoshi* 11 (2008) 1031–1033.
- [51] P. Hamarpurkar, P. Patil, M. Phale, M. Gandhi, S. Pawar, A developed and validated stability-indicating reverse-phase high-performance liquid chromatographic method for determination of cefdinir in the presence of its degradation products as per international conference on harmonization guidelines, *Pharm. Methods* 2 (2011) 15–20.
- [52] Z. Khan, M.I. Iqbal, K. Khan, A. Javed, L. Khan, Y. Shah Ahmed, F. Nasir, Simultaneous determination of cefdinir and cefixime in human plasma by RP-HPLC/UV detection method: method development, optimization. Validation, and its application to a pharmacokinetic study, *J. Chromatogr. B* 879 (2011) 2423–2429.
- [53] S.R. Narala, K. Saraswathi, RP-HPLC methods for the determination of cephalosporins (cefditoren, pivoxil and cefdinir) in pharmaceutical dosage forms, *J. Pharm. Sci. Res.* 3 (2011) 1002–1004.
- [54] H. Sakamoto, T. Hirose, K. Hatano, Y. Mine, S. Kuwahara, Microbiological assay method for cefdinir, a new oral cephalosporin, in biological fluids, *Chromatography* 37 (1989) 154–164.
- [55] Z. Chen, J. Zhang, J. Yu, G. Cao, X. Wu, Y. Shi, Selective method for the determination of cefdinir in human plasma using liquid chromatography electrospray ionization tandem mass spectrometry, *J. Chromatogr. B Analyt. Technol. Biomed. Life Sci.* 834 (2006) 163–169.
- [56] R.N. Rao, N. Venkateswarlu, R. Narsimha, Determination of antibiotics in aquatic environment by solid-phase extraction followed by liquid chromatography-electrospray ionization mass spectrometry, *J. Chromatogr.* 1187 (2008) 151–164.

- [57] D.R.P. Guay, Pharmacodynamics and pharmacokinetics of cefdinir, an oral extended spectrum cephalosporin, *Pediatr. Infect. Dis. J.* 19 (2000) S141–S146.
- [58] A. Hishida, K. Ohishi, S. Nagashima, M. Kanamaru, M. Obara, A. Kitada, Pharmacokinetic study of an oral cephalosporin, cefdinir, in hemodialysis patients, *Antimicrob. Agents Chemother.* 42 (1998) 1718–1721.
- [59] K.L. Boulware, G.H. McCracker, J. Lozano-Hernandez, F. Ghaffar, Cefdinir pharmacokinetics and tolerability in children receiving 25 mg/kg once daily, *Pediatr. Infect. Dis. J.* 25 (2006) 208–210.
- [60] Y. Tomino, M. Fukui, C. Hamada, S. Inoue, S. Osada, Pharmacokinetics of cefdinir and its transfer to dialysate in patients with chronic renal failure undergoing continuous ambulatory peritoneal dialysis, *Drug Res.* 48 (1998) 862–867.
- [61] P. Ren, G. Zhao, X. Ke, S. Gu, H. Chen, Pharmacokinetics and bioequivalence of cefdinir dispersible tablet in healthy volunteers, *YiYao Dacbao* 28 (2009) 168–170.
- [62] A. Jacolot, M. Tod, O. Petitjean, Pharmacokinetic interaction between cefdinir and two angiotensin-converting enzyme inhibitors in rats, *Antimicrob. Agents Chemother.* 40 (1996) 979–982.
- [63] R. Fujii, H. Yashioka, K. Fujita, H. Sakata, H. Nire, K. Iseki, K. Muro, Y. Takahashi, Y. Wagatsuma, N. Fukushima, et al., Pharmacokinetic and clinical studies of cefdinir in the pediatric field. Pediatric study group of cefdinir, *Jpn. J. Antibiot.* 44 (1991) 1168–1191.
- [64] H. Sakata, H. Hakihashi, K. Fujita, H. Yoshioka, K. Iseki, K. Muro, Y. Takahashi, Clinical and pharmacokinetic evaluation of cefdinir in children, *Jpn. J. Antibiot.* 43 (1990) 1407–1413.
- [65] N. Fukushima, Y. Wagatsuma, A. Takase, A. Ishikawa, S. Takahashi, Pharmacokinetic and clinical studies of cefdinir in pediatric field, *Jpn. J. Antibiot.* 43 (1990) 1783–1788.
- [66] N. Iwai, H. Nakamura, M. Miyazu, Y. Watanabe, Pharmacokinetic, bacteriological and clinical evaluations of cefdinir 10% fine granules in pediatrics, *Jpn. J. Antibiot.* 44 (1991) 1119–1133.
- [67] Y. Toyonaga, K. Hatakeyama, Y. Yamori, N. Sakaguchi, K. Nakano, M. Yamazaki, M. Sugita, M. Hori, Bacteriological, pharmacokinetic and clinical studies of 5% and 10% granules of cefdinir in pediatric field, *Jpn. J. Antibiot.* 45 (1992) 48–73.
- [68] T. Motohiro, S. Handa, S. Yamada, S. Oki, N. Tsumura, Y. Yoshinaga, H. Sasaki, M. Aramaki, K. Oda, A. Kawakami, et al., Pharmacokinetics and clinical effects of cefdinir 10% fine granules in pediatrics, *Jpn. J. Antibiot.* 45 (1992) 74–86.
- [69] K. Sakane, Y. Inamoto, T. Takaya, A new oral cephem, cefdinir: its structure-activity relationships and biological profile, *Jpn. J. Antibiot.* 45 (1992) 909–925.
- [70] T. Haruta, S. Kuroki, K. Okura, N. Yoshida, Y. Kobayashi, Pharmacokinetic, bacteriological and clinical studies on cefdinir fine granules in the field of pediatrics, *Jpn. J. Antibiot.* 44 (1991) 1158–1167.
- [71] S.L. Christopher, R.J. Guttendorf, A.R. Kugler, D.E. Smith, Effects of organic anion, organic cation, and peptide transport inhibitors on cefdinir in the isolated perfused rat kidney, *Antimicrob. Agents Chemother.* 47 (2003) 689–696.
- [72] Y.H. Xiao, L. Gao, Y. Li, Y. Lu, J. Liu, Y. Liu, Comparison of pharmacokinetics/pharmacodynamics of cefdinir, cefpodoxime, proxitel and cefaclor against common bacteria of community acquired infections, *Zhonghua Yi Xue Za Zhi* 84 (2004) 1867–1871.
- [73] S. Nakata, S. Chiba, Pharmacokinetic and clinical studies on cefdinir fine granules in children, *Jpn. J. Antibiot.* 43 (1990) 1789–1795.
- [74] M.M. Paris, K.J. Devcich, Overview of cefdinir: pharmacokinetics, safety, and efficacy in the treatment of uncomplicated skin and skin structure infection, *Cutis* 73 (2004) 14–18.

- [75] T. Fujita, A. Yamazaki, M. Ozaki, M. Majima, Y. Ohtani, Y. Kumagai, Pharmacokinetics of cefdinir in healthy subjects after high protein diet and 1-phenylalanine load, *Clin. Pharmacol. Therapeut.* 77 (2005) P81.
- [76] D.J. Payne, S.G.B. Amyes, Stability of cefdinir (CI-883, FK482) to extended-spectrum plasmid-mediated  $\beta$ -lactamases, *J. Med. Microbiol.* 38 (1993) 114–117.
- [77] H. Mimura, S. Kitamura, Y. Okamoto, T. Yasuda, Estimation of grinding effect on the solid-state stability of cefdinir by use of microcalorimetry, *Drug Stability* 1 (1995) 34–39.
- [78] Y. Okamoto, K. Kiriyaama, Y. Namiki, J. Matsushita, M. Fujioka, T. Yasuda, Degradation kinetics and isomerization of cefdinir, a new oral cephalosporin, in aqueous solution. 1, *J. Pharm. Sci.* 85 (1996) 976–983.
- [79] Y. Okamoto, K. Kiriyaama, Y. Namiki, J. Matsushita, M. Fujioka, T. Yasuda, Degradation kinetics and isomerization of cefdinir, a new oral cephalosporin, in aqueous solution. 2. Hydrolytic degradation pathway and mechanism for beta-lactam ring opened lactones, *J. Pharm. Sci.* 85 (1996) 984–989.



# Curcumin

**Maria L.A.D. Lestari, Gunawan Indrayanto**

Faculty of Pharmacy, Airlangga University, Dharmawangsa Dalam, Surabaya, Indonesia

## Contents

1. General Information	113
1.1 Solubility	114
1.2 Chemical name	114
1.3 Synonym	114
1.4 CAS number	114
1.5 $pK_a$ and coefficient partition	114
1.6 Structural formula	114
1.7 Melting point	116
1.8 Molecular formula and molecular weight	116
2. Stability of Curcumin	116
2.1 Aqueous stability of curcumin	116
2.2 Thermal and photochemical stability of curcumin	117
3. Polymorphism	118
4. Spectroscopy	120
4.1 Ultraviolet/visible and fluorescence	120
4.2 Infrared and Raman Spectroscopy	122
4.3 Mass spectrometry	122
4.4 Nuclear magnetic resonance	131
5. Analysis of Nonbiological Sample	135
5.1 UV fluorometric analysis	135
5.2 Chromatography	138
6. Bioavailability, Metabolite Studies, and Bioanalysis	161
References	198



## 1. GENERAL INFORMATION

Curcumin is one of the main substances found in the rhizome of *Curcuma longa* (L) and other *Curcuma* spp. Commercially curcumin contains about 77% besides two other related compounds, that is, demethoxycurcumin and bis-demethoxycurcumin. These compounds belong to the group of diarylheptanoids. Together, these three compounds are

called curcuminoid. Curcumin itself appears as crystalline compound with a bright orange-yellow color. Curcumin is commonly used as coloring agent as well as food additive. WHO stated the acceptable daily intake of curcumin as food additive in the range of 0–3 mg/kg. Its therapeutic usage has also been investigated and it is known to have potential usage as anticancer [1–3].

### 1.1. Solubility

Curcumin is practically insoluble in water at acidic and neutral pH but soluble in polar and nonpolar organic solvents as well as in alkali or in extremely acidic solvents such as glacial acetic acid [4–6].

### 1.2. Chemical name

[1,7-bis(4-hydroxy-3-methoxyphenyl)-1,6-heptadiene-3,5-dione] [7].

### 1.3. Synonym

Diferuloylmethane [2]

### 1.4. CAS number

458-37-7 [8]

### 1.5. $pK_a$ and coefficient partition

Curcumin is reported to have three different  $pK_a$  values. The first and second values are from the two phenolic OH groups, and the third value is from the enolic proton. In a few publications, only two  $pK_a$  values are reported, but these values are in the range of the three  $pK_a$  values [9–14]. A summary of the  $pK_a$  values found for curcumin, as well as the determination method, is found in Table 3.1.

The octanol–water partition coefficient of curcumin is 3.29 [15].

### 1.6. Structural formula

The chemical structure of curcumin, as well as demethoxycurcumin and bis-demethoxycurcumin, are detailed in Figure 3.1. Curcumin exhibits keto-enol tautomerism dependent on the solution acidity. In acidic and neutral media the keto-form is dominant, while in alkaline media it exists in the enol form. The enol form is stabilized by resonance-assisted hydrogen bonding [16,17].

**Table 3.1**  $pK_a$  values of curcumin

Reported $pK_a$ values	Method	Reference
$pK_{a1}=7.75\text{--}7.80$ $pK_{a2}=8.55$ $pK_{a3}=9.05$	HPLC fluorescence Solvents: KCl/HCl (pH 1–3); $\text{KH}_2\text{PO}_4/\text{NaOH}$ (pH 6–9); $\text{NaHCO}_3/\text{NaOH}$ (pH 9–10). The ionic strength was 0.10–0.15 M	[14]
$pK_{a1}=8.55$ $pK_{a2}=10.41$	UV spectroscopy	[11]
$pK_{a1}=8.10$ $pK_{a2}=10.15$	UV spectroscopy Solvent: pH 6.7, 10.0, 13.0	[13]
$pK_{a1}=8.54$ $pK_{a2}=9.30$ $pK_{a3}=10.69$	Potentiometric titration Solvent: water:MeOH = 1:1	[10]
$pK_{a1}=8.38$ $pK_{a2}=9.88$ $pK_{a3}=10.51$	HCl titration	[9]
$pK_a=8.8\text{--}9.4$	Calculation using Density Functional Theory (DFT) and Time-Dependent Density Functional Theory (TD-DFT)	[12]

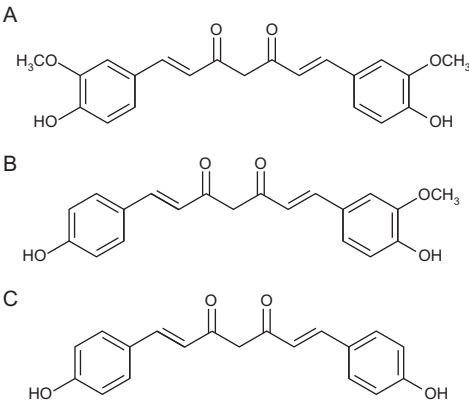


**Figure 3.1** Chemical structure of (A) curcumin, (B) demethoxycurcumin, (C) bis-demethoxycurcumin.



## 1.7. Melting point

The melting point of curcumin is 183 °C [18].

## 1.8. Molecular formula and molecular weight

The molecular formula of curcumin is  $C_{21}H_{20}O_6$ , and its molecular weight is 368.38 Daltons [8].



## 2. STABILITY OF CURCUMIN

### 2.1. Aqueous stability of curcumin

Aqueous media here refers to the acidic or alkaline and biological media. The stability of curcumin is pH dependent, which is proven by change of the color of curcumin solution in various pH values. At  $pH < 1$ , curcumin solutions are red in color due to the presence of the protonated form. At  $pH 1-7$ , curcumin solutions are yellow with the majority of the molecules being in the neutral form. At  $pH$  values higher than 7.5, curcumin solutions exhibit a color change to orange red. Furthermore, for the buffer system being used, curcumin forms complexes with borate, citrate, and phthalate, while being inert toward  $KCl$ ,  $KH_2PO_4$ , and  $NaHCO_3$  [19].

Kinetic degradation of curcumin was investigated in various buffer systems at  $pH 1-11$  at 31.5 °C and in fixed ionic systems. Results showed that the degradation of curcumin followed second-order kinetics. In addition, at  $pH 7.0-7.8$ , different concentrations of phosphate buffer did not show significant change in the rate of the degradation process. In another study [20], degradation of curcumin in 0.1 M buffer solutions of  $pH 3-10$  (using citrate, phosphate, and carbonate buffers) at 37 °C followed apparent first-order reaction kinetics at constant ion strength.

In these studies, three degradation products were found: vanillin, ferulic acid (FA), and feruloyl methane. Vanillin was found to be the major degradation product and the amount increased as the incubation time was extended. It should also be noted that at  $pH 7-10$  and a temperature of 31.5 °C, the primary degradation products of curcumin were FA and feruloylmethane [19].

In biological media such as 0.1 M phosphate buffer or serum-free medium  $pH 7.2$  (both at 37 °C), 90% of curcumin was rapidly degraded within 3 h of incubation. The degradation products were found to be vanillin, FA, and feruloylmethane. This fast degradation is slowed down when the biological media contains fetal calf serum. Similar results were also found

with the use of bovine serum albumin to decrease the degradation of curcumin.

In phosphate buffered saline at pH 7.4, addition of human serum albumin (4% w/v) was found to successfully slow down the degradation of curcumin. In human blood, degradation of curcumin was slower, being less than 20% within 1 h. Furthermore, addition of glutathione (1 mM), *N*-acetyl-L-cysteine (50  $\mu$ M) or ascorbic acid (25  $\mu$ M) into 25  $\mu$ M of curcumin in phosphate buffer (at pH 7.4 and 6.5) was able to prevent the degradation of curcumin. Addition of microsomal protein (0.03 mg protein/mL) and cytosolic fractions of rat liver (0.01 mg/mL) could also inhibit the curcumin degradation [20–23]. Chemical structures of curcumin degradation products are shown in Figure 3.2.

## 2.2. Thermal and photochemical stability of curcumin

Tonnesen *et al.* [24] have reported an intensive study seeking the identification of photodegradation products of curcumin as these were formed in an isopropanol medium. Curcumin was dissolved in isopropanol and exposed to light (wavelengths of 400–510 nm) for 4 h. Degradation products were extracted through preparative TLC and determined using high-resolution mass spectrometry (MS) and nuclear magnetic resonance. The main identified degradation product had the chemical composition of  $C_{12}H_{18}O_6$ , with a mass spectrum exhibiting a molecular ion at  $m/e=366$  (indicating that two hydrogen atoms were removed from its structure). This main product is postulated as being the result of a cyclization process initiated by light irradiation and can be detected after less than 15 min of irradiation. In addition, six minor degradation products were also found and

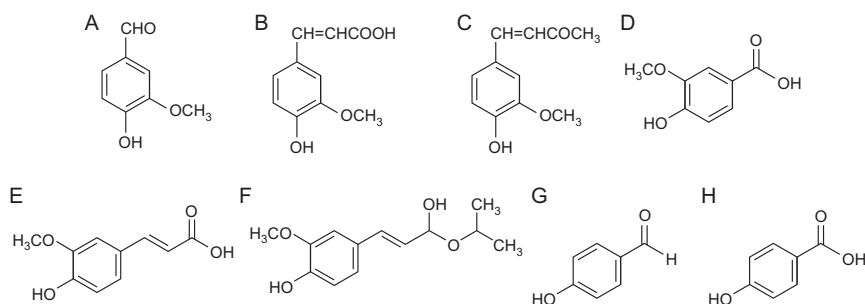


**Figure 3.2** Degradation products of curcumin: (A) vanillin, (B) ferulic acid, (C) feruloyl methanol, (D) vanillic acid, (E) ferulic aldehyde, (F) 4-vinylguaiaicol, (G) *p*-hydroxybenzaldehyde, (H) *p*-hydroxybenzoic acid.

identified as vanillin, vanillic acid (VA), ferulic aldehyde, FA, and 4-vinylguaiaicol. The sixth degradation product could not be identified with available references, but had the empirical formula of  $C_{13}H_8O_4$ .

In another study, exposing methanolic or ethanolic solutions of curcumin for 120 h with sunlight resulted in degradation of curcumin. The degradation products found were vanillin, *p*-hydroxybenzaldehyde, ferulic aldehyde, *p*-hydroxybenzoic acid, VA, and FA. It was also found that curcumin in dried form was more stable against sunlight exposure than in solution [25]. Chemical structures of the degradation products are shown in Figure 3.2.

The stability of curcumin against light was also tested in four different organic solvents: methanol, ethyl acetate, chloroform, and acetonitrile. Wavelengths of the light exposure sources were 400–750 nm and 240–600 nm. In these tested solvents, photodegradation of curcumin apparently followed first-order kinetics, in which the half-life of curcumin in solution followed the order of stability of methanol > ethyl acetate > chloroform > acetonitrile. The cyclization product of curcumin was only detected in methanol and chloroform. However, when the solution of curcumin in each tested solvent was dried as a thin film, its half-life followed second-order kinetics, with the stability series being acetonitrile > chloroform > ethyl acetate > methanol. The use of brown glass or the storage purposes was recommended, since this type of glass only transmits light having wavelengths above 500 nm, for which curcumin has no absorption [24].

Curcumin was found to be stable up to 70 °C when exposed for 10 min. Above this temperature, curcumin starts to decompose, and at 100 °C, its degradation increases as shown by the reduction of its absorbance value [26]. In addition, boiling curcumin for 10 or 20 min contributed to the loss of curcumin to 27% and 32%, respectively. Processing turmeric containing curcumin using a pressure cooker (10 min at 15 psi) resulted in a 53% loss of curcumin [27].



### 3. POLYMORPHISM

Tonnesen *et al.* [28] reported the crystal structure of curcumin which was obtained via a crystallization process from ethanol at 70 °C. Commercially available curcumin was reported to be characterized by the monoclinic space group  $P2_1/n$  (Form-1). Similar findings were

reported later for curcumin obtained from recrystallization with isopropanol. In these reports, no polymorphism of curcumin was found [17].

However, in a recent report by Sanphui *et al.* [29], curcumin obtained from other recrystallization processes was reported to have two other polymorphic forms, termed Form-2 and Form-3. Form-2 was obtained from the crystallization of curcumin from dimethyl sulfoxide and also from a saturated solution of curcumin in ethanol maintained for 2 days in refrigerator at 10 °C. Form-2 was reported to have higher dissolution rate than curcumin Form-1, indicating that Form-2 is metastable with respect to Form-1. Form-2 crystallizes in the orthorhombic space group,  $Pca2_1$ . Form-3 was obtained from a crystallization process with 4,6-dihydroxy-5-nitropyrimidine. Form-3 crystallized in the  $Pbca$  orthorhombic space group. In addition, the amorphous form of curcumin was also reported.

An additional polymorph of curcumin was reported by the slow evaporation crystallization of curcumin from methanol at room temperature. This supposedly new polymorph crystal of curcumin was found to crystallize in the  $Pca2_1$  orthorhombic space group which is identical with the Form-2, previously reported by Sanphui *et al.* [30].

Crystal data for curcumin and two other polymorphs are summarized in Table 3.2, and the X-ray powder diffraction pattern of curcumin is shown in Figure 3.3. Hydrogen bonding and molecular packing of three polymorphs of curcumin are presented in previous publications [29].

**Table 3.2** Crystal data of curcumin

Crystal parameter	Form 1 (commercially curcumin)			Form 2		Form 3 [29]
	[28]	[17]	[29]	[29]	[30]	
Space group	$P2_1/n$	$P2_1/n$	$P2_1/n$	$Pca2_1$	$Pca2_1$	$Pbca$
$a$ (Å)	20.028(3)	12.707(3)	12.5676(11)	35.417(3)	35.5368(8)	12.536(3)
$b$ (Å)	7.073(1)	7.2186(14)	7.0425(6)	7.7792(7)	7.7799(2)	7.9916(17)
$c$ (Å)	12.609(2)	19.880(4)	19.9582(18)	12.6482(11)	12.6796(3)	34.462(7)
$\alpha$	90	90	90	90	90	90
$\beta$	94.94(1)	95.348(4)	94.987(1)	90	90	90
$\gamma$	90	90	90	90	90	90

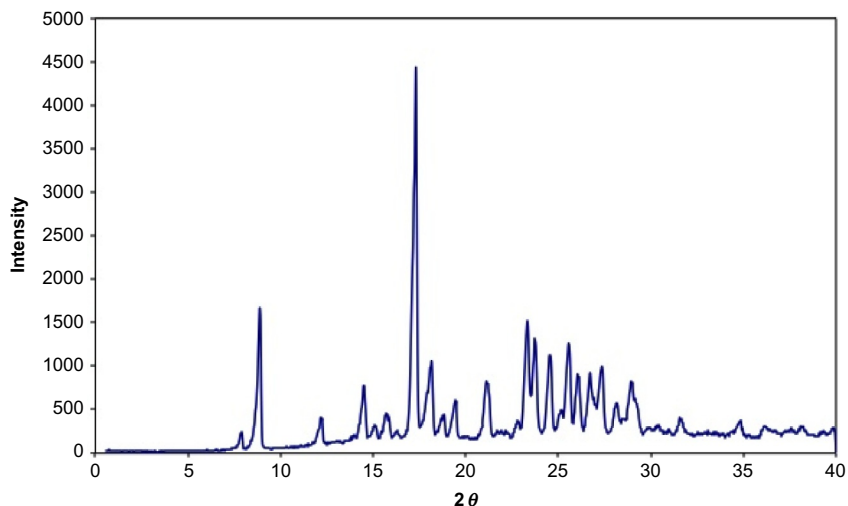


**Figure 3.3** X-ray powder diffraction pattern of commercially curcumin obtained from *Curcuma longa* (turmeric) containing at least 70% of curcumin (Sigma-Aldrich Chemie GmbH, Germany). Scanning was done from  $0.06^\circ$  to  $40^\circ$ ,  $2\theta$  at a step size of  $0.04^\circ$  and step time of 0.5 s.



## 4. SPECTROSCOPY

### 4.1. Ultraviolet/visible and fluorescence

In acetone–bicarbonate buffer (pH 11), curcumin showed an absorption maximum at 520 nm [31]. The absorption band is found to exhibit an asymmetric shape in these nonpolar solvents: chloroform, acetic acid, benzene, toluene, and carbon tetrachloride. This asymmetric shape indicates a difference in the solute–solvent interactions relative to those existing in polar solvents (methanol, acetone, normal amyl methyl ketone, ethanol, tetrahydrofuran, acetyl acetone, and acetic acid). Beer's law was obeyed for curcumin over the concentration range of 0.1–12 ppm or 0.1–15 ppm. Various maximum wavelengths were observed in different solvent systems, ranging from 408 nm (in carbon tetrachloride) to 430 nm (DMSO). On the average, the maximum wavelength was found at 418 nm. The absorption maximum of curcumin in methanol and ethanol was around 420 nm, and the solution exhibited a bright yellow color owing to its  $\pi$ – $\pi^*$  excitation; the  $n$ – $\pi^*$  transition was observed at 426 nm in methanol [32,33].

In more recent investigations, it was found that changing solvent system only slightly affected the absorption spectrum of curcumin. This was observed for the curcumin spectrum in toluene, acetonitrile, and ethanol, which showed that only a small red shift occurred when the solvent system was changed. Changing the solvent from *n*-hexane to methanol only resulted in a small red shift (approximately 0–20 nm). In toluene, as well as in Triton X-100 micelles, the absorption spectrum of curcumin contained some structure. In more polar solvents such as ethanol and acetonitrile, as well as in SDS and DMF, the absorption spectrum of curcumin contains a broad featureless band [34].

On the addition of cyclodextrin, the absorption maximum of curcumin in water (420 nm) was red-shifted to 430 nm; absorption of curcumin–cyclodextrin (10 mM) complex at 430 nm was doubled [13]. Kanhathaisong [35] reported that Cu(II) could decrease the UV absorbance of curcumin in water at 427 nm; with the addition of Cu(II), a new band at 361 nm of Cu(II)–curcumin complex was observed.

While the influence of solvents, water, and pH were minor in UV absorption, the effects have a more pronounced effect on the fluorescence properties. Jasim *et al.* [36] reported the analysis of curcumin in spice and flavors using a fluorometric method. Acetone was used as a solvent, with an excitation wavelength of 424 nm and an emission wavelength of 504 nm. Linearity in fluorescence response was observed up to 0.5 ppm and self-quenching was observed at higher concentrations. Study for the effect of oxygen as well as temperature influence showed that dissolved oxygen and temperature had no effects on the values of  $\lambda_E$  and  $\lambda_F$  (excitation and emission) of curcumin in acetone, but water (more than 0.1%) had a quenching effect. The LOD value obtained was 0.34 ppb with percent recovery of 98.96–100%. In addition, measurements can be conducted at room temperature (20–25 °C) and the fluorescence could last for more than 1 month.

In contrast with UV methods, changing solvent polarity from toluene to alcohol and also SDS micelle resulted in a large spectral shift in fluorescence maximum of curcumin. In the case of protic solvents (such as ethanol), large red shifting indicates that the ketone groups of curcumin molecules are involved in the excited singlet state and that the singlet state must be very polar. In addition, in line with the previous finding, oxygen has a slight effect in the formation of singlet oxygen which correlates to the quenching effect [34].

Besides solvent and water, pH also influences the fluorescence of curcumin. At  $\text{pH} < 1$  and at  $\text{pH} 8.3$ , the fluorescence intensity decreases and this might be due to one or both of these factors: degradation process, considering that curcumin degrades in alkaline media, and changing properties of first-excited singlet state. Detailed investigation of the absorption and fluorescence spectra of curcumin and its derivatives in hexane and methanol have also been done, as summarized in Table 3.3 [4].

## 4.2. Infrared and Raman Spectroscopy

The few reports available for the IR analysis or the Raman spectroscopy of curcumin are summarized in Table 3.4. In general, IR spectra were measured in KBr pellets [37,38] or in Nujol mulls [37]. Kolev *et al.* [39] reported the IR measurement of curcumin spectra in solid state as KBr, CSI, and polyethylene pellets, and also in tetrachloromethane, chloroform, chloroform-D, and acetonitrile solutions.

Sanphui *et al.* [29] reported the IR spectra of two polymorphs as well as the amorphous form of curcumin. The IR spectra of the polymorphs and the amorphous form showed broadening in the  $3400\text{ cm}^{-1}$  O—H functional group region. Raman spectrophotometry was also conducted for these polymorphs. Summary of the IR and Raman spectra for the polymorphs of curcumin is described in Table 3.5. For the Raman spectrophotometric, the excitation wavelength applied was at 647.10 nm with 50 mW laser power [39] while in more recent report, excitation wavelength was at 1064 nm with 100 mW laser power [40].

## 4.3. Mass spectrometry

MS can be used for the qualitative and quantitative analysis of curcumin and its related compounds (demethoxycurcumin and bis-demethoxy curcumin) for both of nonbiological and biological samples. Table 3.6 describes important MS-fragments of the compounds from nonbiological samples using various MS methods. The applications of LC-MS for quantitative purpose of curcumin and its related compounds in biological samples are described in Table 3.12. MALDI-TOF mass spectra of curcumin complexes with Al(III) were reported by Jiang [73].

Kim and Jang [74] identified curcumin ( $m/z$   $\text{M}+\text{H}^+$ : 369.14), demethoxycurcumin ( $m/z$   $\text{M}+\text{H}^+$ : 339.12) and bis-demethoxy curcumin

**Table 3.3** Absorption and fluorescence spectra of curcumin and its derivative

Substitution of curcumin	Chemical name	In hexane			In methanol		
		$\lambda_{\max}^a$	$\varepsilon \times 10^{4b}$	$\lambda_{\max}^c$	$\lambda_{\max}^a$	$\varepsilon \times 10^{4b}$	$\lambda_{\max}^c$
–	Curcumin ([1,7-bis(4-hydroxy-3-methoxyphenyl)-1,6 heptadiene-3,5-dione])	409	4.7	444,469,500 <sup>d</sup>	428	4.8	546
Mono-O-methylated	[1-(4-hydroxy-3-methoxyphenyl)-7-(3,4-dimethoxyphenyl)-1,6 heptadiene-3,5-dione]	409	4.1	444,469,500 <sup>d</sup>	417	3.7	532
Di-O-methylated	[1,7-bis(3,4-dimethoxyphenyl)-1,6 heptadiene-3,5-dione]	413	4.0	448,472,504 <sup>d</sup>	420	4.6	538
Tri (mono-4-C and di-O) methylated	[1,7-bis(3,4-dimethoxyphenyl)-4-methyl-heptadiene-3,5-dione]	358	1.4	452,500 <sup>d</sup>	362	0.9	469.503
Di-O-benzylated	[1,7-bis(4-benzyloxy-3-methoxyphenyl)-1,6 heptadiene-3,5-dione]	346	2.4	367,385,405 <sup>d</sup>	349	2.5	433,464,510 <sup>d</sup>
Tri-(mono-4-C and di-O) methylated	[1,7-bis(4-benzyloxy-3-methoxyphenyl)-4-benzyl-1,6 heptadiene-3,5-dione]	350	1.8	470,505	350	1.6	466,500 <sup>d</sup>
Di-O-acetylated	[1,7-bis(4-acetoxy-3-methoxyphenyl)-1,6 heptadiene-3,5-dione]	395	5.0	433,458	399	5.0	470,500 <sup>d</sup>
Di-O-benzoylated	[1,7-bis(4-benzyloxy-3-methoxyphenyl)-4-1,6 heptadiene-3,5-dione]	400	4.7	437,459,500 <sup>d</sup>	400	4.9	470,500 <sup>d</sup>
Tri-(mono-4-C and di-O)-benzoylated	[1,7-bis(4-benzyloxy-3-methoxyphenyl)-4-benzoyl-1,6 heptadiene-3,5-dione]	366	3.3	461, 500 <sup>d</sup>	367	3.3	467,500

<sup>a</sup>In nm (absorption spectra).<sup>b</sup>M<sup>-1</sup>, cm<sup>-1</sup>.<sup>c</sup>In nm (fluorescence spectra).<sup>d</sup>Shoulder.

Modified from Ref. [4].



**Table 3.4** Important IR and Raman peaks of curcumin

FTIR (wave number $\text{cm}^{-1}$ )	Raman (wave number $\text{cm}^{-1}$ )	Functional group	Extraction and isolation method of curcumin sample	Reference
3427		$\nu$ (OH)	Extraction of curcuminoid: with hexane, followed by defatting process using benzene Isolation: column chromatography with benzene as eluent	[37]
2950–3000		$\nu$ ( $\alpha,\beta$ -unsaturated), aryl C—H		
1287		$\nu$ (CO)		
1207		$\nu$ (CO)		
3523		OH	Extraction of curcuminoid: EtOH, followed by precipitation with petroleum ether Isolation: fractionated column chromatography with $\text{CHCl}_3$ followed by $\text{CHCl}_3/\text{MeOH}$	[38]
1624		Conjugated C=C		
1609		( $\alpha,\beta$ -unsaturated C=O str)		
1510		Aromatic ring str		
1268, 1050		$=\text{C}-\text{O}-\text{CH}_3$		
1140		C—OH		
3508		$\nu$ (OH)	n/a	[39,40]
3293		$\nu$ (OH)		

**Table 3.4** Important IR and Raman peaks of curcumin—cont'd

FTIR (wave number $\text{cm}^{-1}$ )	Raman (wave number $\text{cm}^{-1}$ )	Functional group	Extraction and isolation method of curcumin sample	Reference
1626	1626	$\nu$ (C=C); $\nu$ (C=O)		
1601	1601	$\nu$ (C=C <sub>ring</sub> )		
1508		$\nu$ (C=O)		
	1430	$\sigma$ Phenol C—O		
	1320	$\sigma$ C—CH		
1272		$\sigma$ Enol C—O		
	1249	$\sigma$ Enol C—C		
	1184	$\sigma$ CH <sub>3</sub> , $\sigma$ C—C		
	1152	$\sigma$ C—CH		
1150		$\sigma$ C—CH		
1023		$\sigma$ C—O—C		
	963	$\sigma$ C=O, $\sigma$ C—OH		
959		$\sigma$ Benzoate <i>trans</i> -CH		
	811	$\gamma$ C—CH		
713		$\sigma$ CH (aromatic)		
	572	$\gamma$ C—CH		
3510.9		O—H	n/a	<a href="#">[29]</a>
1627.5		C=O		
1602.6		Aromatic C=C		
1429.0		Phenol C—O		
1281.2		Enol C—O		
	1626.2	C=O		
	1600.4	Aromatic C=C		
	1430.2	Phenol C=O		
	1249.3	Enol C—O		

**Table 3.5** IR and Raman peaks of curcumin polymorphs

FTIR (wave number $\text{cm}^{-1}$ )	Raman (wave number $\text{cm}^{-1}$ )	Functional group	Polymorph
3510.9 1627.5 1602.6 1429.0 1281.2		O—H C=O Aromatic C=C Phenol C—O Enol C—O	Form 1
3401.2 (broad) 3254.1 1651.6 1626.7 1601.4 1588.1 1427.3 1282.6 1263.5		O—H O—H C=O C=O Aromatic C=C Aromatic C=C Phenol C—O Enol C—O Enol C—O	Form 2
3440.9 (broad) 1626.8 1587.3 1416.7 1262.1		O—H C=O Aromatic C=C Phenol C—O Enol C—O	Form 3
3440.6 (broad) 1629.9 1588.4 1428.5 1280.7 1262.8		O—H C=O Aromatic C=C Phenol C—O Enol C—O Enol C—O	Amorphous
	1626.2 1600.4 1430.2 1249.3	C=O Aromatic C=C Phenol C—O Enol C—O	Form 1
	1638.9 1602.3 1591.1 1415.6 1233.1	C=O Aromatic C=C Aromatic C=C Phenol C—O Enol C—O	Form 2
	1637.9 1591.4 1415.2 1234.4	C=O Aromatic C=C Phenol C—O Enol C—O	Form 3
	1630.5 1599.3 1428.8 1243.2	C=O Aromatic C=C Phenol C—O Enol C—O	Amorphous

Modified after Ref. [29].

**Table 3.6** MS data of curcuminoid analysis of nonbiological sample

	Curcumin		Demethoxycurcumin		Bis-demethoxycurcumin			
MS detection method	Elementary composition of ions	<i>m/z</i>	Elementary composition of ions	<i>m/z</i>	Elementary composition of ions	<i>m/z</i>	Sample	Ref.
LC-ESI-MS	[M+H] <sup>+</sup>	369	[M+H] <sup>+</sup>	339	[M+H] <sup>+</sup>	309	Fresh turmeric extract	[41]
	[M+Na] <sup>+</sup>	391	[M+Na] <sup>+</sup>	361	[M+Na] <sup>+</sup>	331		
	[2M+Na] <sup>+</sup>	759	[2M+Na] <sup>+</sup>	699	[2M+Na] <sup>+</sup>	639		
LC-ESI-MS	n/a	367		337		307	Tablet, tea, candy	[42]
LC-ESI-MS/MS	[M-H] <sup>-</sup>	367	[M-H] <sup>-</sup>	337	[M-H] <sup>-</sup>	307	Pure curcuminoids, turmeric fresh rhizome powder	[43]
HPLC-ESI-MS	<i>Positive ion mode</i>		n/a		n/a		Pure and extract of turmeric rhizome	[44]
	MS							
	[M+Na] <sup>-</sup>	391.3						
	[M+H] <sup>+</sup>	369.2						
	MS <sup>2</sup>							
	[M+H-C <sub>7</sub> H <sub>7</sub> O <sub>2</sub> ]	245.1						
	<i>Negative ion mode</i>							
	MS							
	[M-H] <sup>-</sup>	367.1						
	MS <sup>2</sup>							
[M-H-C <sub>9</sub> H <sub>10</sub> O <sub>2</sub> ]	217.0							
LC-ESI-MS	[M-H] <sup>-</sup>	367.1	[M-H] <sup>-</sup>	337.1	[M-H] <sup>-</sup>	307.1	Foodstuff (fish)	[45]

*Continued*

**Table 3.6** MS data of curcuminoid analysis of nonbiological sample—cont'd

MS detection method	Curcumin		Demethoxycurcumin		Bis-demethoxycurcumin		Sample	Ref.
	Elementary composition of ions	<i>m/z</i>	Elementary composition of ions	<i>m/z</i>	Elementary composition of ions	<i>m/z</i>		
HPLC–ESI–MS	$[M-H]^-$	367	$[M-H]^-$	337	$[M-H]^-$	307	Herbal medicine	[46]
EI–MS	$MH^+$	369	$M1H^+$	339	$M2H^+$	309	Crude curcumin sample	[47]
	$[M-C_3H_2O_2]^+$	298	$[M1-C_3H_2O_2]^+$	268				
	$[M-C_9H_9O_2]^+$	191	$[M-C_{11}H_{11}O_3]^+$	177	$[M1-C_{11}H_9O_3]^+$	147		
	$[M1-C_8H_7O]^+$		$[M1-C_{10}H_9O_2]^+$		$[M2-C_{10}H_9O_2]^+$			
	$[M-C_{11}H_{11}O_3]^+$	177	$[M1-C_{11}H_9O_3]^+$	147	n/a	145		
	$[M1-C_{10}H_9O_2]^+$		$[M2-C_{10}H_9O_2]^+$					
					$[M1-C_{13}H_{11}O_4]^+$	107		
	$[M-C_{12}H_{11}O_4]^+$	149	$[M1-C_{13}H_{11}O_4]^+$	107	$[M2-C_{12}H_9O_3]^+$			
	$[M1-C_{11}H_9O_3]^+$		$[M2-C_{12}H_9O_3]^+$					
	$[M-C_{13}H_{11}O_4]^+$	137						
	$[M1-C_{12}H_9O_3]^+$							
MS/MS of ESI–FT–ICR	$MH^+$	369	$M1H^+$	339	$M2H^+$	309		
	$[M-C_{11}H_{11}O_3]^+$	177	$[M-C_{11}H_{11}O_3]^+$	177	$[M1-C_{11}H_9O_3]$	147		
	$[M1-C_{10}H_9O_2]^+$		$[M1-C_{10}H_9O_2]^+$		$[M2-C_{10}H_9O_2]$			
	n/a	145	$[M1-C_{11}H_9O_3]$	147				
			$[M2-C_{10}H_9O_2]$					
			n/a	145				

HPLC–DAD-ESI–MS	Positive ion mode						[44]	
MS								
[M+Na] <sup>−</sup>		391.3						
[M+H] <sup>+</sup>		369.2						
MS <sup>2</sup>								
[M+H−C <sub>7</sub> H <sub>7</sub> O <sub>2</sub> ] <sup>+</sup>		245.1	n/a	n/a	n/a	n/a		
Negative ion mode								
MS								
[M−H] <sup>−</sup>		367.1						
MS <sup>2</sup>								
[M−H−C <sub>9</sub> H <sub>10</sub> O <sub>2</sub> ]		217.0						
UPLC–ESI–MS	Positive ion mode		Positive ion mode		Positive ion mode		Dry ground rhizome, dietary supplement (solid dosage form)	[48]
	[M+H] <sup>+</sup>	369.1	[M+H] <sup>+</sup>	339.1	[M+H] <sup>+</sup>	309.1		
	Negative ion mode	367.1	Negative ion mode		Negative ion mode			
	[M−H] <sup>−</sup>		[M−H] <sup>−</sup>	337.1	[M−H] <sup>−</sup>	307.1		

*Continued*

**Table 3.6** MS data of curcuminoid analysis of nonbiological sample—cont'd

MS detection method	Curcuminoid		Sample	Reference
	Elementary composition of ions	<i>m/z</i>		
PD-MS	MH + <i>a</i>	369	Crude curcumin sample	<a href="#">[47]</a>
	M1H + <i>b</i>	339		
	M2H + <i>c</i>	309		
	[M–C <sub>3</sub> H <sub>2</sub> O <sub>2</sub> ] <sup>+</sup>	298		
	[M1–C <sub>3</sub> H <sub>2</sub> O <sub>2</sub> ] <sup>+</sup>	268		
	[M–C <sub>9</sub> H <sub>9</sub> O <sub>2</sub> ] <sub>+</sub>	219		
	[M1–C <sub>8</sub> H <sub>7</sub> O] <sup>+</sup>			
	[M–C <sub>10</sub> H <sub>9</sub> O <sub>3</sub> ] <sup>+</sup>	191		
	[M1–C <sub>9</sub> H <sub>7</sub> O <sub>2</sub> ] <sup>+</sup>			
	[M–C <sub>11</sub> H <sub>11</sub> O <sub>3</sub> ] <sup>+</sup>	177		
	[M1–C <sub>10</sub> H <sub>9</sub> O <sub>2</sub> ] <sup>+</sup>			
	[M–C <sub>12</sub> H <sub>11</sub> O <sub>4</sub> ] <sup>+</sup>	149		
	[M1–C <sub>11</sub> H <sub>9</sub> O <sub>3</sub> ] <sup>+</sup>			
	[M1–C <sub>11</sub> H <sub>11</sub> O <sub>3</sub> ] <sup>+</sup>	147		
	[M2–C <sub>10</sub> H <sub>9</sub> O <sub>2</sub> ] <sup>+</sup>			
	[M–C <sub>13</sub> H <sub>11</sub> O <sub>4</sub> ] <sup>+</sup>	137		
	[M1–C <sub>12</sub> H <sub>9</sub> O <sub>3</sub> ] <sup>+</sup>			
	[M1–C <sub>13</sub> H <sub>11</sub> O <sub>4</sub> ] <sup>+</sup>	107		
	[M2–C <sub>12</sub> H <sub>9</sub> O <sub>3</sub> ] <sup>+</sup>			

( $m/z$   $M+H^+$ : 309.11) using direct analysis in real time MS. Hiserodt *et al.* [75] optimized two different types of MS, the particle beam EI-mass spectra and thermospray mass spectra. The thermospray LC-MS provided information for molecular weight but with limited fragmentation, while particle beam interface was used to obtain EI-mass spectra of nonvolatile components.

In another study, the fragmentation behavior of curcumin and two other compounds was observed using ion trap LC-MS/MS and confirmed with sustained off-resonance irradiation fragmentation (Fourier Transform Ion Cyclotron Resonance (FTICR) SORI-MS/MS) [43].

#### 4.4. Nuclear magnetic resonance

Roughley *et al.* [76] reported the NMR analysis of curcumin obtained using benzene from the extraction of the *Curcuma longa* dried rhizome. *cis*-Isomers were not detected and NMR spectra indicated that the diketones were in the enolic form. Enolic protons were observed in the [ $^2H_6$ ] solutions at  $-90^\circ C$  but not in the room temperature solutions.

Payton *et al.* [77] described that curcumin existed mostly in mixtures of the keto-enol tautomers in variety of solvents (chloroform, mixture of DMSO and water, buffered aqueous DMSO solutions pH 3–9). HMBC spectra of curcumin (70 mM in DMSO- $d_6$ ) showed a very low concentration (less than 1%) of diketone tautomers; but no C-1 methylene (characteristic of diketone tautomers) was observed in DEPT 135 spectrum. Results of the NMR assay are detailed in Table 3.7.

Gören *et al.* [79] published the use of NMR for the quantitative analysis of curcumin using DMSO- $d_6$  as the solvent and 1,3,5-trimethoxybenzene as the internal standard. Measurement was done with a 600 MHz spectrometer, averaging 64 scans. Quantitative analysis was done based on the peak height calculation. Three reference peaks were observed: 7.29 (d, 2H,  $J=1.8$  Hz, H6 and H06), 6.03 (s, 1H, H-1), and 3.81 (OCH<sub>3</sub>, 6H) in the  $^1H$  NMR spectrum of curcumin in DMSO- $d_6$ . All the proton peaks were well separated at 600 MHz. At 9.62 ppm, a sharp single peak was observed, indicated as the hydroxyl groups of curcumin. However, this peak was not taken into account due to its dependent intensity and chemical shift against sample concentration. The LOD and LOQ were 0.002 and 0.02 mg/mL, respectively, with a recovery of 99–101%.



**Table 3.7** NMR assignment of curcumin

NMR assay	Chemical shift (ppm)	Multiplicity	Assignment	Coupling constant (Hz)	Solvent	Reference
1H	2.42	d	2H; 4,4'-H2	$J=16$	Deuterio-chloroform	[76]
	2.70	d	2H; 6,6'-H2	$J=2$		
	2.84	dd	2H; 10,10'-H2	$J=2, J=8$		
	3.14	d	2H; 9,9'-H2	$J=8$		
	6.09	s	6H; 2 $\times$ OMe			
	6.05	s	1H, C1-H		DMSO- $d_6$	[78]
	6.74	d	2H, 2 $\times$ C3-H	$J=16$		
	6.81	d	2H, 2 $\times$ C9-H	$J=8$		
	7.15	dd	2 $\times$ C10-H	$J_1=8; J_2=2$		
	7.31	s(breit)	2H, C6-H			
	7.54	d	2H, C4-H	$J=16$		
	6.61	d	2H, 2 $\times$ C3-H	$J=16$		
	6.89	d	2H, 2 $\times$ C9-H	$J=8$		
	7.16	d	2H, 2 $\times$ C10-H	$J=8$		
	7.20	s(breit)	2H, C6-H			
	7.62	d	2H, C4-H	$J=16$		
	3.89	s	6H, 2 $\times$ —OCH <sub>3</sub>		Hexadeutero-DMSO	[37]

5.88	s	1H, —C(OH)=CH—, enol form	
6.53	d	2H; 2,6-H	$J=16$
6.87	d	2H; 5',5''-H, aromatic	
7.04	dd	2H; 6',6''-H	$J=2, J=8$
7.07	dd	2H; 6',6''-H	$J=2, J=8$
7.10	d	2H; 2',2''-H aromatic	$J=2$
7.54	d	2H; 1,7-H	$J=16$
9.25		2H, Ar-OH	
9.69	s	3,17-OH	Hexadeutero- DMSO <a href="#">[38]</a>
7.54	d	7,13-H	$J_{7-8}=J_{12-13}=16$
7.32	d	1,15-H	$J_{1-5}=J_{15-19}=2$
7.15	dd	5,19-H	$J_{4-5}=J_{18-19}=8$
6.82	s	4,18-H	$J_{4-5}=J_{18-19}=8$
6.76	d	8,12-H	$J_{7-8}=J_{12-13}=16$
6.06	s	10-H, enol form	
3.83	s	2,16-OCH <sub>3</sub>	

*Continued*

**Table 3.7** NMR assignment of curcumin—cont'd

NMR assay	Chemical shift (ppm)	Multiplicity	Assignment	Coupling constant (Hz)	Solvent	Reference
<sup>13</sup> C	55.7		OCH <sub>3</sub>		DMSO- <i>d</i> <sub>6</sub>	<a href="#">[78]</a>
	101.2		C1			
	111.5		C6			
	115.9		C9			
	121.2		C3			
	123.1		C10			
	126.5		C5			
	140.8		C4			
	148.1		C7			
	149.4		C8			
	183.2		C2			
	183.7, 149.8, 148.5, 141.2, 126.8, 123.6,				Hexadeutero-DMSO	<a href="#">[38]</a>
	121.6, 116.2, 111.8, 101.3, 56.2					



## 5. ANALYSIS OF NONBIOLOGICAL SAMPLE

### 5.1. UV fluorometric analysis

UV spectrophotometric methods for determination of curcumin are summarized in Table 3.8. A derivative method was applied for the analysis of curcumin found in a quaternary mixture with three other colorants. The first derivative ratio spectra gave better recoveries (close to 100%) compared to the first derivative spectrophotometry [80,81]. One important point when applying UV spectrophotometric method for curcumin analysis is the interference of other compounds in curcuminoid, that is, demethoxycurcumin and bis-demethoxycurcumin. In the mixture of EtOH–water (85:15) as solvent, maximum absorbance of curcumin, demethoxycurcumin, and bis-demethoxycurcumin were 429, 424, and 419 nm, respectively [85]. Therefore, the use of pure curcumin standard should be considered.

Jasim *et al.* [36] reported a spectrofluorometric method for the determination of curcumin in spice and flavor samples. Pure acetone was used as the solvent since this solvent gave lowest detection limit and longest duration for the measurement.  $\lambda_{\text{excitation}}$  and  $\lambda_{\text{emission}}$  were 424 and 504 nm, respectively. The limit of detection was 0.34 ppb, with a percent recovery of 98.96–100%. Solutions of curcumin were stable for up to 1 month with storage temperatures of 5–30°C. However, it should also be noted that above concentrations of 0.5 ppm, self-quenching occurred.

Diaz *et al.* [86] reported the spectrofluorometric determination of curcumin in yogurt and mustard using four different methods of spectrofluorometry: normal, synchronous, synchronous first derivative, and synchronous second derivative. The influence of pH was also investigated, for which at  $\text{pH} < 8$ , yellow fluorescence appeared. In basic media, the red solution was not fluorescent. To determine the appropriate solvent to be used, relative fluorescence intensity values were applied. Four organic solvents, which gave large values, were 1,4-dioxane, acetone, ethyl acetate, and acetonitrile (the highest one). Anhydrous acetonitrile was then used as the solvent in this method. The LOD found for direct and synchronous methods was the same (0.08 ng/mL), while the LOD values of synchronous first derivative and second derivative were 0.16 and 0.11 ng/mL, respectively. Sensitivity values for each technique were almost similar to each other. Percent recoveries were  $105.19 \pm 2.09\%$  and  $94.24 \pm 1.24\%$  for yogurt and mustard samples, respectively. The percent recovery for each spectrofluorometric technique was not reported.

**Table 3.8** UV spectrophotometric method for quantitative analysis of curcumin

Sample	Preparation method	Wavelength observation, LOD, LOQ, % recovery	Reference
Colorant in synthetic mixture	Curcumin is buffered at pH 4.8 with acetic acid then extracted with mixture of acetic acid/sodium acetate solution (ionic strength 0.1), 25% EtOH in water (20 mL) and 20 mL methyl-isobutyl ketone (MIBK)	First derivative spectrophotometry, $\Delta\lambda = 4$ nm: LOD: 393.5 nm: 0.291 mg/L 411 nm: 0.510 mg/L 432 nm: 0.451 mg/L LOQ: n/a Rec: 393.5 nm: 63.31–110.32 411 nm: 82.97–95.95 432 nm: 88.48–102.68 First derivative ratio spectra, $\Delta\lambda = 15$ nm: LOD: 388 nm: 0.126 mg/L 411 nm: 0.030 mg/L 456 nm: 0.029 mg/L LOQ: n/a Rec: 388 nm: 88.72–101.27 411 nm: 94.60–104.14 456 nm: 91.46–105.48	[80]
Colorant in synthetic mixture	Curcumin is buffered at pH 4.8 with acetic acid then extracted with mixture of acetic acid/sodium acetate solution (ionic strength 0.1), 25% EtOH in water (20 mL) and 20 mL MIBK	First derivative spectrophotometry, $\Delta\lambda = 8$ nm: LOD: n/a LOQ: n/a Rec: 404 nm: 85–98.6 430 nm: 94.6–120	[81]
Colorant in synthetic mixture	Curcumin is buffered at pH 4.8 with acetic acid then	First derivative ratio spectra, $\Delta\lambda = 16$ nm LOD: n/a	[81]

**Table 3.8** UV spectrophotometric method for quantitative analysis of curcumin—  
cont'd

Sample	Preparation method	Wavelength observation, LOD, LOQ, % recovery	Reference
	extracted with mixture of acetic acid/sodium acetate solution (ionic strength 0.1), 25% EtOH in water (20 mL) and 20 mL MIBK	LOQ: n/a Rec: 412 nm: 95–105.7	
Curry and mustard	Sample was dried at 100 °C for 24 h, powdered, and extracted with ACN	LOD: 0.136 µg/mL LOQ: 0.45 µg/mL Rec: 97.28–101.81 λ: 431 nm	[13]
Curcumin in the presence of β-cyclodextrin ( $7.5 \times 10^{-3}$ mol/L)	Mixture of curcumin in ACN and β-cyclodextrin was diluted to volume with water	LOD: 0.076 µg/mL LOQ: 0.25 µg/mL Rec: n/a λ: 431 nm	[13]
Total curcuminoid content in the dried powder of rhizome	Sample extracted with THF and the supernatant was then diluted with MeOH	LOD: n/a LOQ: n/a Rec: n/a λ: 420 nm	[82]
Rhizome of <i>C. longa</i> in mixture with stem bark of <i>B. aristata</i>	Sample was extracted 3 × with MeOH and added to volume with MeOH	LOD: 0.039 µg/mL LOQ: 0.13 µg/mL Rec: 97.17% λ: 382 nm	[83]
Tablet and bulk drug	Standard and sample dissolved and added to volume with MeOH	LOD: 0.05 µg/mL LOQ: 0.1724 µg/mL Rec: 99.1–101.4	[84]

## 5.2. Chromatography

### 5.2.1 TLC/HPTLC

The use of TLC for qualitative analysis of curcumin is described in the European Pharmacopoeia [87]. In this method, fluorescein and thymol are dissolved in methanol and used as the reference solution. The test solution is also dissolved in methanol. The mobile phase is a mixture of glacial acetic acid and toluene (80:20 v/v). The dry TLC plate is sprayed with 0.4 g/L dichloroquinonechlorimide in 2-propanol. The plate is then exposed to ammonia vapor until the bluish-violet zone (for thymol) and yellow zone in the lower part (for fluorescein) is observed. Two yellowish brown to brown zones between the thymol and fluorescein zone indicate the presence of curcumin and demethoxycurcumin.

For quantitative analysis, both TLC and HPTLC methods have been reported. In the TLC method reported by Pothitirat *et al.* [82], the peaks of curcumin, demethoxycurcumin, and demethoxycurcumin were not well separated, although those three peaks can be distinguished from each other based on their retardation factor ( $R_f$ ). In the HPTLC method, it was found that use of the LiChrosphere HPTLC plate successfully resolved the problem of broadness in the spot. The curcumin peak was also well separated, as shown by its relatively high  $R_f$  apart from the peak of demethoxycurcumin and bis-demethoxycurcumin. However, peaks of demethoxycurcumin and bis-demethoxycurcumin were not completely separated [88]. Good separation for the peaks of curcumin, demethoxycurcumin, and bis-demethoxycurcumin was observed when the silica gel plate was used with a mobile phase consisting of chloroform and methanol. In this method, each peak was completely separated from each other [89–91]. Similar results were also obtained, where the combination of chloroform:MeOH = 19:1 (v/v) gave the best result in the separation of curcuminoid compounds [92]. A summary of the TLC as well as HPTLC methods is provided in Table 3.9.

### 5.2.2 HPLC

An initial HPLC method for the determination of curcumin using HPLC was reported by Asakawa *et al.* [93]. A Nucleosil C18 column was used with a mobile phase consisting of acetonitrile, methanol, and water. However, this method did not successfully separate curcumin from two other compounds in curcuminoid, and a long running time of 40 min was needed.

Later on, Tonnesen *et al.* [7] reported a HPLC method which was able to separate three different components of curcuminoid. Two different

**Table 3.9** HPTLC analysis of curcumin

Compound	Sample	Solvent	Chromatographic condition	LOD, LOQ, % recovery	Reference
Curcumin, demethoxycurcumin, bis-demethoxycurcumin	Rhizome of <i>C. longa</i>	MeOH	Stationary phase: Precoated silica gel aluminum plate 60F <sub>254</sub> Mobile phase: CHCl <sub>3</sub> :benzene: MeOH = 80:15:5 $\lambda$ = 420 nm	LOD: n/a LOQ: n/a Rec: n/a	[82]
Curcumin, demethoxycurcumin, bis-demethoxycurcumin	Rhizome of <i>C. longa</i>	MeOH	Stationary phase: LiChrosphere 60F <sub>254</sub> CHCl <sub>3</sub> :MeOH = 98:2 Temperature: 25 ± 1 °C RH: 35–40% $\lambda$ = 366 nm	LOD: C: 40 ng DC: 40 ng BDC: 20 ng LOQ: C: 100 ng DC: 100 ng BDC: 100 ng Rec: C: 99.79 DC: 96.97 BDC: 99.48	[88]
Curcumin, demethoxycurcumin, bis-demethoxycurcumin	Rhizome of <i>C. longa</i>	MeOH	Stationary phase: HPTLC silica gel 60F <sub>254</sub> CHCl <sub>3</sub> :MeOH = 48:2 Temperature: 25 ± 5 °C RH: 50% $\lambda$ = 425 nm	LOD: n/a LOQ: n/a Rec: C: 97.3 DC: 92.9 BDC: 95.4	[90]

*Continued*



**Table 3.9** HPTLC analysis of curcumin—cont'd

Compound	Sample	Solvent	Chromatographic condition	LOD, LOQ, % recovery	Reference
Curcumin	Rhizome of <i>C. longa</i>	MeOH	Stationary phase: Precoated silica gel aluminum plate 60F <sub>254</sub> Toluene:CHCl <sub>3</sub> :MeOH = 5:4:1 Temperature: 25 ± 2 °C RH: 60 ± 5% $\lambda$ = 430 nm	LOD: 50 ng/spot LOQ: 200 ng/spot Rec: 98.55–100.71	[89]
Curcumin, demethoxycurcumin, bis-demethoxycurcumin	Gel	MeOH	Stationary phase: Precoated silica gel 60F <sub>254</sub> CHCl <sub>3</sub> :MeOH:glacial acetic acid = 7.5:2.0:0.5 Temperature: n/a RH: n/a $\lambda$ = 430 nm	LOD: C: 100 ng/spot DC: 45.0 ng/spot BDC: 52.0 ng/spot LOQ: C: 250 ng/spot DC: 170 ng/spot BDC: 80 ng/spot Rec: C: 100.8 DC: 99.23 BDC: 100.12	[91]

detectors were used based on UV–Vis and on fluorescence. The fluorescence detector showed sensitivity that was 10-fold higher than the UV–Vis detector in detecting three components of curcuminoid (curcumin, demethoxycurcumin, and bis-demethoxycurcumin). Following this result, Tonnesen *et al.* [24] also evaluated the use of different types of stationary phase on the analysis of curcumin. Five different eluents (combination of EtOH–water, MeOH–water, and butanol) as well as eight stationary phases were evaluated. It was found that the 1,3-diketone group in curcuminoids was adsorbed strongly to the silicic acid column, and hence the analysis was not reproducible.

In contrast, the use of amino-bonded stationary phases with spherical particles resulted in good separation of curcumin with other compounds as well as reproducible analysis of curcumin. Poor separation was shown when only pure organic solvent was used as the mobile phase system. Furthermore, the amount of water in the system affected the separation of curcumin and the activity of the stationary phase system. At 10% water content in the mobile phase, loss of curcumin separation was observed, while at 40% water content, separation of curcumin was completely retarded and irreversible deactivation of amino column was observed. In addition, a study conducted by Taylor *et al.* [94] showed that the separation of curcumin on the C18 column was pH independent. Addition of 1% citric acid adjusted to pH 2.8–4.4 was not successfully separating the three compounds of curcuminoid.

In another study, addition of 2% acetic acid into the mobile phase system was successful in separating curcumin and two other compounds on a C18 column [95]. Additionally, the use of trifluoroacetic acid as an ionization suppressant in the mobile phase was found to give good separation and reproducibility of curcumin, demethoxycurcumin, and bis-demethoxycurcumin. This might be due to the highly electronegative fluorine atoms, which caused partial deactivation of the C18 as stationary phase [96].

In general, UV and fluorescence detectors are the common detectors being used for the determination of curcumin and other compounds. However, applications for other detectors were also reported. Smith *et al.* [97] compared the use of a UV detector with an electrochemical detector in order to improve separation of curcumin with other constituents and shorten the analysis time. Washing powdered samples with light petroleum prior to extraction with method reduced the elution time. In addition, phosphate buffer at pH 4.4 also worked to suppress ionization as well as being a

supporting electrolyte for the electrochemical detector. In the optimization of the eluent, acetonitrile gave better resolution of three peaks contained in curcuminoid, while methanol could not resolve these peaks. THF was also a suitable candidate, but was incompatible with the electrochemical detector. Different eluents also changed the elution order due to the methoxy substitution which might alter intermolecular hydrogen bonding. Results of this method comparison showed no significant difference between the use of a UV detector and the use of an electrochemical detector. However, it should also be noted that higher concentrations applied (higher than 41.92 mg/L) will inactivate the surface of the electrode in the electrochemical detector due to the reaction products and result in an irreproducible response.

The use of a mass spectral detector was also reported in a few publications for the purpose of fragmentation and identification of curcuminoid compounds as well as impurities [41,43,44,55,75,98]. In addition, application of MS was also used for the detection of very small amounts or traces of curcuminoid (curcumin, demethoxycurcumin, and bis-demethoxycurcumin) [42].

With respect to the liquid chromatography method, newer methods for curcumin determination using ultra-high performance liquid chromatography with UV–MS detection were reported [48]. The advantage of using this method is a faster analysis time, as well as better resolution compared with conventional HPLC method. In this method, complete separation of curcumin, demethoxycurcumin, and bis-demethoxycurcumin was achieved within 6 min of running time. Summary of the HPLC method for analysis of curcumin in nonbiological samples is detailed in Table 3.10.

### 5.2.3 Capillary electrophoresis

The use of capillary electrophoresis (CE) method for analysis of curcumin has been reported in a few publications using either diode array detector (DAD) or amperometric detector. In addition, micellar electrokinetic chromatography (MEKC) and microemulsion electrokinetic chromatography (MEEKC) method were also reported for separation and detection of curcuminoid compound. Sun *et al.* [107] applied amperometric detection to quantify curcumin in turmeric herbals. Extraction processing was done with solid phase extraction (SPE), where tributyl phosphate resin was the adsorbent. For the extraction process, a maximum 0.3 mL volume of eluate was found to give good recovery (>85%). No correlation was found

**Table 3.10** HPLC analysis of curcumin in nonbiological sample

Compound	Sample	Preparation method	HPLC system	LOD, LOQ, recovery	Reference
Curcuminoid (curcumin, demethoxycurcumin, bis-demethoxycurcumin)	Plant of <i>Curcuma longa</i> L, <i>Curcuma zedoaria</i> , Roscoe	Standard and sample dissolved in MeOH	Column: Nucleosil NH <sub>2</sub> (Chrompack) 5 µm, 250 × 4.6 mm i.d Column temperature: ambient Mobile phase: EtOH, flow rate: 1.2 mL/min Detector: UV 254 nm, Vis 420 nm Fluorescence: emission: 470 nm Excitation: 420 nm	LOD: UV/Vis: all below 20 ng Fluorescence: C: $2 \times 10^{-10}$ g DMC: $1.67 \times 10^{-10}$ g BDMC: $1 \times 10^{-12}$ g LOQ: n/a Rec: n/a	[7]
Curcuminoid (curcumin, demethoxycurcumin, bis-demethoxycurcumin)	Ground dried turmeric	Sample was washed with light petroleum and extracted with MeOH	Column: ODS Hypersil 5 µm, 25 cm × 5 mm i.d Column temperature: n/a Mobile phase: Phosphate buffer 0.05 M (pH 4.4): ACN = 40:60, flow rate: n/a Detector: Coupled UV (254 nm) and electrochemical (+0.8 V vs. Ag–AgCl)	LOD: n/a LOQ: n/a Rec: n/a	[97]

*Continued*

**Table 3.10** HPLC analysis of curcumin in nonbiological sample—cont'd

Compound	Sample	Preparation method	HPLC system	LOD, LOQ, recovery	Reference
Curcuminoid (curcumin, demethoxycurcumin, bis-demethoxycurcumin), ferulic acid, vanillic acid, <i>p</i> -hydroxybenzoic acid, ferulic aldehyde, <i>p</i> -hydroxybenzaldehyde, vanillin Internal standard (IS): nitroaniline	Dried powder or root of <i>Curcuma longa</i>	Standard and sample dissolved in MeOH or EtOH	Column: (1) PartiSphere-5 NH <sub>2</sub> , 25 cm × 4.6 mm i.d (2) Whatman PartiSphere-5 WCX, 11 cm × 4.6 mm i.d—three columns connected in series  Column temperature: n/a Mobile phase: (1) EtOH:water = 96:4, flow rate: 1 mL/min (2) Hexane:EtOH:water = 30:30:0.75, flow rate: 0.4 mL/min  Detector: UV, $\lambda = 280$ nm	LOD: n/a LOQ: n/a Rec: n/a	[25]
Curcuminoid (curcumin, demethoxycurcumin, bis-demethoxycurcumin)	Ethanolic extract of turmeric	Standard: dissolved in EtOH Sample: Ground material was refluxed for 2.5 h with EtOH, filtered and made to volume with EtOH	Column: Styrene-divinylbenzene copolymer 5 $\mu$ m, 15 × 0.49 cm Column temperature: ambient Mobile phase: ACN:water = 55:25, flow rate: 1.0 mL/min Detector: UV, $\lambda = 425$ nm	LOD: 10.2 ng LOQ: n/a Rec: n/a	[94]

Curcuminoid (curcumin, Food colorants demethoxycurcumin, bis- demethoxycurcumin), Annatto (bixin, norbixin)	Standards and sample were dissolved in 50% THF	Column: Zorbax ODS C18, 25 cm × 4.6 mm i.d Column temperature: ambient Mobile phase: Isocratic: Water:THF = 58:42, flow rate: 1.0 mL/min Gradient: Equilibrated with 40% THF then after injection increased to 58% within 10 min and hold for 10 min then decreased to 40% within 2 min. Equilibrated 15 min before next injection. Flow rate: 1.0 mL/min Detector: UV fluorescence C: UV/Vis 428 nm, excitation 433 nm, emission 511 nm D: UV/Vis 424 nm, excitation 428 nm, emission 505 nm BDC: UV/Vis 418 nm, excitation 425 nm, emission 501 nm	LOD: UV/Vis: 2 ng Fluorometric: 0.2 ng LOQ: n/a Rec: n/a	[99]
---	--	---	---	------

*Continued*

**Table 3.10** HPLC analysis of curcumin in nonbiological sample—cont'd

Compound	Sample	Preparation method	HPLC system	LOD, LOQ, recovery	Reference
Curcuminoid (curcumin, demethoxycurcumin, bis-demethoxycurcumin)	Turmeric powder	Standard: dissolved in MeOH Sample: 1.0 g sample powder extracted with 50 mL hexane using Soxhlet extractor for 30 min. The hexane extract was discarded, and the powder was reextracted with 50 mL of methanol for 2 h. 1 mL of this solution was transferred to a 10-mL volumetric flask, and the volume was adjusted to 10 mL with MeOH.	Column: Waters $\mu$ -Bondapak C18, 300 $\times$ 4.6 mm i.d. Column temperature: ambient Mobile phase: A: MeOH B: 2% HAc C: ACN Gradient: 0–15 min: 45–65% of C in B 15–20 min: 65–45% C in B with constant 5% of A Flow rate: 1.0 mL/min Detector: Vis $\lambda$ = 425 nm	LOD: n/a LOQ: 0.05 $\mu$ g Rec: n/a	[95]
Curcuminoid (curcumin, demethoxycurcumin, bis-demethoxycurcumin)	Synthesis results of curcuminoid monoacetate and diacetate	Standard and sample dissolved in MeOH	Column: Discovery <sup>®</sup> HS C18, 3 $\mu$ m, 15 $\times$ 2.1 mm with guard column Discovery <sup>®</sup> HS C18, 3 $\mu$ m, 2 cm $\times$ 2.1 mm Column temperature: 40 °C Mobile phase:	LOD: n/a LOQ: n/a Rec: n/a	[43]

A: buffer 5 mM  
 ammonium formate and  
 0.1% formic acid in  
 redistilled deionized water  
 B: ACN  
 Gradient:  
 0–2 min: 5% B  
 2–57 min: 5–100% B  
 57–60 min: 100% B  
 60–65 min: 100–5% B  
 65–75 min: 5% B  
 Flow rate: 0.25 mL/min  
 Detector: LC–ESI–  
 MS/MS

Curcuminoid (curcumin, Turmeric powder demethoxycurcumin, bis- demethoxycurcumin)	1 g sample powder extracted with 50 mL hexane (50 mL) using a Soxhlet extractor for 1 h. The hexane extract was discarded, and the powder was reextracted with 50 mL methanol for 2 h. One milliliter of this solution was transferred to a 10-mL volumetric flask, and the volume was	Column: Vydac <sup>®</sup> RP-18, 5 µm, 250 mm × 4.6 mm, i.d Column temperature: ambient Mobile phase: ACN:0.1% trifluoroacetic acid (TFA) = 50:50, (adjusted to pH 3.0 with ammonia), flow rate: 1.5 mL/min Detector: Vis λ = 420 nm	LOD: [96] C: 27.99 ng/mL DMC: 31.91 ng/mL BDMC: 21.81 ng/mL LOQ: C: 84.84 ng/mL DMC: 96.72 ng/mL
--	---	---	---

*Continued*



**Table 3.10** HPLC analysis of curcumin in nonbiological sample—cont'd

Compound	Sample	Preparation method	HPLC system	LOD, LOQ, recovery	Reference
		adjusted to 10 mL with MeOH MeOH yielding a volume of 10.0 mL. A 100- $\mu$ L aliquot of this solution was diluted to 10 mL with MeOH and 2.0 mL of this diluted solution was then injected.		BDMC: 66.10 ng/mL Rec: C: 98.4–100.5% DMC: 99.6–101.8% BDMC: 98.4–101%	
Curcuminoid (curcumin, demethoxycurcumin, bis-demethoxycurcumin)	Rhizomes of <i>Curcuma mangga</i> , <i>C. heyneana</i> , and <i>C. aeruginosa</i> (Zingiberaceae), <i>Curcuma soloensis</i>	Standard: dissolved in MeOH Sample: 5 g of grounded sample was extracted with 150 mL pentane using Soxhlet extractor for 2 h. Extract was then dried and extracted with MeOH (150 mL) for 3 h. Methanolic solution was concentrated using rotavapor and redissolved in MeOH yielding a volume of 10.0 mL.	Column: Zorbax Eclipse XDB-C18, 5 $\mu$ m, 250 $\times$ 4.6 mm, i.d Column temperature: 25°C Mobile phase: MeOH: water (containing 0.1% TFA): ACN = 39.5:350:468, w/w/w, flow rate: 0.75 mL/min Detector: Vis $\lambda$ = 425 nm	LOD: C: 0.058 $\mu$ g DMC: 0.048 $\mu$ g BDMC: 0.044 $\mu$ g LOQ: C: 0.58 $\mu$ g DMC: 0.48 $\mu$ g BDMC: 0.44 $\mu$ g Rec: C: 99.9% DMC: 99.8%	[100]

A 100  $\mu$ L aliquot of this solution was diluted to 10 mL with MeOH and 2.0 mL of this diluted solution was then injected.

BDMC:  
100.4%

Curcumin, hyperin, hesperidin, resveratrol, nobiletin, curcumin, emodin, chrysophanol, physcion	Tablet	Standard: dissolved in MeOH Sample: extracted and made to volume with MeOH 70%	Column: ZORBAX Extend C18, 5 $\mu$ m, 250 mm $\times$ 4.6 mm, i.d Column temperature: 25 $^{\circ}$ C A: 0.05% formic acid adjusted to pH 5.0 with triethylamine B: ACN 0 min: B 15% 40 min: B 35% 50 min: B 50% 60 min: B 100% hold for 10 min Flow rate: 0.8 mL/min Detector: UV $\lambda$ = 346 nm HPLC-DAD-ESI-MS Column temperature, mobile phase: same as for UV method. The formate buffer was adjusted to pH 5.0 with ammonia.	UV-Vis HPLC <a href="#">[44]</a> LOD: 0.22 $\mu$ g/mL LOQ: 0.87 $\mu$ g/mL Rec: 99.8%
---	--------	---	---	--

*Continued*

**Table 3.10** HPLC analysis of curcumin in nonbiological sample—cont'd

Compound	Sample	Preparation method	HPLC system	LOD, LOQ, recovery	Reference
Curcumin, sinomenine, paeoniflorin, paeonol	Capsule	Standard and sample were dissolved in EtOH 50%	Column: Phenomenex ODS column, 5 $\mu$ m, 250 mm $\times$ 4.6 mm with security guard cartridge (C18, 4 mm $\times$ 3.0 mm) Column temperature: ambient Mobile phase: A: ACN B: aqueous phase 0.1% phosphoric acid adjusted with TEA to pH 3.5 $\pm$ 0.2 Gradient: 0–25 min: 8–20% A 25–30 min: 20–40% A 30–55 min: 40–70% A 55–60 min: 70–90% A Flow rate: 1.0 mL/min Detector: UV/Vis $\lambda$ = 420 nm	LOD: 0.08 $\mu$ g/mL LOQ: n/a Rec: 95.75%	<a href="#">[101]</a>

Curcumin and its degradation	Curcumin powder, capsule of curcumin powder	<p><i>Acid degradation study</i> 1 mL of 100 µg/mL curcumin in MeOH + 1 mL of 1 N HCl. The flask was sealed and placed at 85 °C for 2 h. Solution was then cooled and neutralized with 1 mL of 1 N NaOH and made up to 10 mL with MeOH, filtered and injected.</p> <p><i>Base degradation study</i> 1 mL of 100 µg/mL curcumin in MeOH + 1 mL of 1 N NaOH. The flask was sealed and placed at 85 °C for 2 h. Solution was then cooled and neutralized with 1 mL of 1 N HCl and made up to 10 mL with MeOH, filtered and injected.</p> <p><i>Oxidative degradation</i> 1 mL of 100 µg/mL</p>	<p>Column: Hi-Q-Sil C18, 10 µm 4.6 mm × 250 mm Column temperature: 25 °C Mobile phase: ACN:buffer sodium acetate 0.04 M (pH 3.0) = 60:40, flow rate: 1.0 mL/min Detector: UV/Vis 425 nm, 280 nm (degradation products)</p>	<p>LOD: 0.06 ± 0.01 µg/mL LOQ: 0.21 ± 0.045 µg/mL Rec: 97.59–103.15%</p>	[102]
------------------------------	---	---	--	--	-------

Continued

**Table 3.10** HPLC analysis of curcumin in nonbiological sample—cont'd

Compound	Sample	Preparation method	HPLC system	LOD, LOQ, recovery	Reference
		<p>curcumin in MeOH + 1 mL of H<sub>2</sub>O<sub>2</sub> (30% v/v). The flask was sealed and placed at 85 °C for 2 h. Volume was made up to 10 mL with MeOH, filtered then injected.</p> <p><i>Thermal degradation</i> 1 mL of 100 µg/mL curcumin in MeOH was transferred to 10 mL amber volumetric flask and added with 2 mL MeOH. The flask was sealed and placed at 85 °C for 2 h. Volume was then made up to 10 mL with MeOH, filtered then injected.</p> <p><i>Photodegradation study</i> 10 mL of 10 µg/mL curcumin in MeOH was sealed in a 10 mL transparent volumetric flask and exposed to direct sunlight for 6 h.</p>			

Curcuminoid (curcumin, demethoxycurcumin, bis-demethoxycurcumin)	Turmeric extract		Column: RP C18 250 × 4 mm i.d Column temperature: n/a Mobile phase: MeOH: IPA:water:acetic acid = 20:4:27:48.5, flow rate 0.5 mL/min Detector: UV–Vis $\lambda$ = 420 nm	LOD: n/a LOQ: n/a Rec: n/a	[103]
Curcuminoid (curcumin, demethoxycurcumin, bis-demethoxycurcumin)	Turmeric extract	Standard: Stock solution was dissolved in ACN then diluted with 50% ACN Sample: dissolved in ACN then diluted and made to volume with 50% ACN	Column: C18, 5 $\mu$ m 150 × 4.6 mm Column temperature: 33 °C Mobile phase: ACN:2% acetic acid = 40:60, flow rate: 2.0 mL/min Detector: UV/Vis $\lambda$ = 425 nm	LOD: 0.90 $\mu$ g/mL LOQ: 2.73 $\mu$ g/mL Rec: 99.16–101.92%	[104]
Curcumin and piperine	Food sample	Standard: standard stock was dissolved in ACN then diluted with mobile phase Sample: extracted with MeOH and aliquot was dried and reconstituted with mobile phase	Column: C18, 5 $\mu$ m 250 × 4.6 mm Column temperature: n/a Mobile phase: 50 mM potassium dihydrogen orthophosphate (pH 3.5): ACN = 40:60, flow rate 0.8 mL/min Detector: UV/Vis $\lambda$ = 424 nm	LOD: 10 ng/mL LOQ: 30 ng/mL Rec: 98.18–110.20%	[105]

*Continued*

**Table 3.10** HPLC analysis of curcumin in nonbiological sample—cont'd

Compound	Sample	Preparation method	HPLC system	LOD, LOQ, recovery	Reference
Curcumin	Nanoparticles of curcumin	Curcumin standard and sample dissolved in dissolution medium: Buffer pH 1.2 containing 50 mL of 0.2 M KCl, 85 mL of 0.2 M HCl, and 65 mL distilled water	Column: LichroCARTPurospher STAR, 5 $\mu$ m 250 $\times$ 4.6 mm i.d Column temperature: 37 °C Mobile phase: Acetic acid:10 mM phosphate buffer (pH 2.5): ACN = 1:50:50, flow rate:0.8 mL/min Detector: UV $\lambda$ = 250 nm	LOD: n/a LOQ: n/a Rec: n/a	[106]
Curcumin, demethoxycurcumin, bis-demethoxycurcumin IS: Naphtalene-d <sub>8</sub> (98 + atom %D), 4-fluoro-4'-hydroxybenzophenone (97%)	Powdered turmeric	Standard, IS, and sample for non LC–MS: dissolved with MeOH Sample for LC–MS: 150 mg sample + 5 mL water was vortexed and centrifuged. Water decanted and replaced with 10 mL MeOH and vortexed. 1 mL aliquot of this extract was diluted	Column: Supelcosil LC-18, 5 $\mu$ m 250 $\times$ 4.6 mm i.d Mobile phase: UV A: 1% citric acid (pH 3.0) B: ACN Gradient: 50% B at initial, hold for 10 min, increased to 80% B within 30 min and hold for 10 min. LC–ESI–MS	LOD: n/a LOQ: n/a Rec: n/a	[75]

		quantitatively with 1.0 mL 4-fluoro-4'- hydroxybenzophenone in MeOH.	A: 50 mM NH <sub>4</sub> OAc–5% HOAc B: ACN Gradient: 50% B at initial, hold for 10 min, increased to 80% B within 30 min and hold for 10 min. Detector: UV, LC–ESI–MS		
Curcuminoids and sesquiterpenoids (curcumin, demethoxycurcumin, bis-demethoxycurcumin, ar-turmerone and curlone)	Turmeric extract	Standard: dissolved in MeOH Sample: 1 g powdered extract refluxed with 20 mL MeOH for 1 h then filtered and injected to HPLC system	Column: Waters Symmetry C18, 5 µm, 20 × 3.9 mm with guard column (C18, 5 µm, 15 × 2.1 mm) Column temperature: 48 °C Mobile phase: A: water containing 0.25% HOAc B: ACN Gradient: 0–17 min: 40–60% B 17–32 min: 60–100% B 32–38 min: 100% B 38–40 min: 100–40% B Flow rate: 0.2 mL/min HPLC–UV: Curcumin: 260 nm, 425 nm Ar-Turmelone and Curlone: 238 nm ESI–MS	LOD: n/a LOQ: n/a Rec: n/a	[41]

*Continued*



**Table 3.10** HPLC analysis of curcumin in nonbiological sample—cont'd

Compound	Sample	Preparation method	HPLC system	LOD, LOQ, recovery	Reference
Curcumin, demethoxycurcumin, bis-demethoxycurcumin	Tablet, tea, candy	Standard: dissolved in MeOH Sample: extracted and made to volume with MeOH for low curcuminoid content; pretreatment with SPE column BOND ELUT C8 500 mg/3 mL. Sample added with 3 mL water and eluted with SPE column which was preconditioned with 3.0 mL MeOH, continued with 3.0 mL distilled water. Sample eluted was then washed with 3.0 mL water and 5.0 mL MeOH, dried under N <sub>2</sub> at 40°C. Residue was then dissolved with MeOH.	Column: Senshu Pak Pegasil ODS, 5 µm 150 × 2.0 mm Column temperature: n/a Mobile phase: A: 0.01% acetic acid in water B: ACN Gradient: 0 min at 45% B 0–15 min: increased linearly 45–95% B and hold at 95% B. Flow rate: 0.2 mL/min Detector: LC–ESI–MS SIM mode: <i>m/z</i> 307, 337, 367	LOD: 1.0 ng/mL LOQ: n/a Rec: 92.9–94.6%	[42]

Curcumin, demethoxycurcumin, bis-demethoxycurcumin (purification of curcuminoid compounds)	Turmeric powder	Standard: stock dissolved in MeOH and diluted with 50% MeOH HSCC of samples: 25 mg sample dissolved in each fraction of mixture of <i>n</i> -hexane/ CHCl <sub>3</sub> /MeOH/ water = 5/10/7.5/2.5 v/ v. Supernatant was assayed using FIA for separation of curcuminoid and identified further with LC/MS/MS method.	Column: TSK-GEL ODS 80 Ts Column temperature: 40 °C Mobile phase: FIA: 0.1% formic acid in water:0.1% formic acid in ACN = 50:50, flow rate 1.0 mL/min LC/MS/MS: A: 0.1% formic acid in water B: 0.1% formic acid in ACN 0 min: 50% B 15 min: 50% B 15.1 min: 98% B 20 min: 98% B 20.1 min: 50% B Flow rate 1.0 mL/min Detector: FIA: 405 nm LC/MS/MS with ESI at negative ionization mode	LOD: n/a LOQ: n/a Rec: n/a	[98]
---	-----------------	--	---	----------------------------------	------

*Continued*

**Table 3.10** HPLC analysis of curcumin in nonbiological sample—cont'd

Compound	Sample	Preparation method	HPLC system	LOD, LOQ, recovery	Reference
Curcumin	Turmeric rhizome	Standard dissolved with acetone Sample was extracted and made to volume with acetone	Column: C18, 250 × 4.6 mm Column temperature: n/a Mobile phase: THF: water containing 1% citric acid adjusted to pH 3 with concentrated KOH = 40:60, flow rate 1.0 mL/min Detector: UV-Vis $\lambda = 420$ nm	LOD: n/a LOQ: n/a Rec: n/a	[92]
Curcumin, demethoxycurcumin, bis-demethoxycurcumin, ar-turmerone	Rhizome of <i>C. longa</i> , supplement capsule	Standard dissolved in MeOH Sample: 25–50 mg rhizome or 500 mg capsule content + 2.5 mL MeOH, sonicated for 30 min and centrifuged. Supernatant was then withdrawn. This process was repeated thrice.	Column: UPLC™ BEH Shield RP18 column (50 mm × 2.1 mm i.d, 1.7 $\mu$ m) equipped with LC-18 guard column (Vanguard 2.1 × 5.5 mm, Waters, USA) Column temperature: 40 °C sample temperature 25 °C Mobile phase: A: 0.05% formic acid in	LOD: C, DC, BDC: 0.01 $\mu$ g/mL LOQ: C, DC, BDC: 0.03 $\mu$ g/mL Rec: n/r	[48]

water  
B: 0.05% formic acid in  
ACN  
Gradient: 0 min: 55%  
A within 5 min: 20%  
A separation followed by  
1 min washing with 100%  
B and reequilibrated for  
2.5 min  
Flow rate: 0.25 mL/min  
Strong needle wash: 95/5  
ACN/water  
Weak needle wash: 10/90  
ACN/water  
Detector:  
Curcuminoid: 420 nm  
Ar-turmerone: 240 nm  
Analysis of effluent with  
ESI:  
SIR (Selected Ion  
Recording) mode:  
 $[M - H]^-$   
C: 367  
DC: 337  
BDC: 307

---

between the pH of the eluate and the percent recovery. The only consideration is that higher pH is associated with concentrated NaOH, which led to the large background noise during detection at 1.20 V.

In another publication, Lechtenberg *et al.* [108] reported the use of a DAD for both qualitative and quantitative analysis of curcumin, demethoxycurcumin, and bis-demethoxycurcumin in rhizome and curry powder. In their method, a combination of phosphate,  $\beta$ -cyclodextrin ( $\beta$ -CD) hydrate and sodium hydroxide was applied to obtain an optimal analysis. In the optimization process, it was observed that increasing concentration of phosphate improved the separation of curcuminoid compounds, but prolonged the time of analysis. From the use of three different cyclodextrins,  $\beta$ -CD hydrate gave better separation with short migration time ( $<6$  min), and at a concentration of 14 mM, optimum separation was achieved. Due to its similar chromophore with the curcuminoid compounds, 3,4-dimethoxy-*trans*-cinnamic acid was chosen as the internal standard. Standard and sample solutions were found to be stable for at least 2 h. Addition of methyl- $\beta$ -CD (100 mg in water/MeOH, 1:1 v/v) to the standard/sample solution was needed to maintain stability in methanolic solution.

Marakova *et al.* [109] optimized the combination of complexing buffer, carrier anion, counter-ion, and pH of the buffer to determine curcuminoid compounds. Compared to the previous CE-DAD method, the use of (3-cyclohexylamino)-1-propanesulfonic acid (CAPS) gave better results compared to the use of phosphate as the carrier electrolyte. In addition, more effective resolution was achieved with the HP- $\beta$ -CD compared to native  $\beta$ -CD or ionizable TMA- $\beta$ -CD. Furthermore, higher HP- $\beta$ -CD levels were able to reduce adsorption of curcuminoid onto the capillary wall and also maintained stability of curcuminoid in the alkaline separation environment. In term of pH, higher pH values were preferred due to their ability to facilitate ionization of curcuminoid, thus increasing separation efficiency and resolution, as well as shortening analysis time. In addition, coating the fused-silica capillary tube with hydroxyethylcellulose (molecular weight 30,000) could replace the need to rinse the capillary in order to suppress electro-osmotic flow. Connection with the DAD also enabled a spectral purity check of the sample.

For the MEKC method, Watanabe *et al.* [110] reported the successful separation of three components of curcuminoid using a butyl acrylate-butyl methacrylate-methacrylic acid copolymer sodium salt solution containing 50% dimethyl sulfoxide as the running buffer. As comparison, a HPLC

method was also used and it was found that analysis with MEKC was faster than when using HPLC. In the earlier development, 25 mM SDS solution in 30 mM borate buffer at pH 8.0 was applied, but could not separate curcuminoid component.

As an alternative to the CE method, Nhujak *et al.* [111] investigated the application of MEEKC to analyze curcuminoid compounds. In MEEKC, a microemulsion is used as the carrier electrolyte. This microemulsion consists of oil droplets stabilized in aqueous solution by a surfactant to stabilize and to give negative charge to the microemulsion. The principle of separation is based on partitioning of the analyte between an aqueous phase and a pseudo-stationary phase of oil droplets. Since curcumin is unstable in basic media, an acidic buffer was preferred. The organic cosolvent in the separation process is needed to partition the analytes in the organic-aqueous phase. In this research, three organic cosolvents were investigated, acetonitrile, methanol, ethanol, and isopropanol at concentrations of 0–30%. Based on the results obtained, the use of isopropanol at 25% yielded good separation of the curcuminoid compounds. In the selection of appropriate alcohols, it was observed that higher number of carbon atoms in the aliphatic chain resulted in greater retention factor of analytes. The influence of temperature was also studied, since increasing temperature will reduce the viscosity of the micelle and enhance faster migration. However, above 25 °C, Joule heating caused decreasing efficiency ( $N$ ) or increasing in thermal dispersion ( $H_t$ ) as well as slight decrease in  $\alpha$ . As a result, the resolution of the compounds became worse. Therefore, the temperature used for the analysis process was set at 25 °C.

A summary of the CE as well as MEKC and MEEKC methods is detailed in Table 3.11.



## **6. BIOAVAILABILITY, METABOLITE STUDIES, AND BIOANALYSIS**

Most studies on curcuminoid compounds have been performed on animals (mice, rats, or dogs), and only few publications have reported studies on humans. Clinical studies showed that curcumin is safe for humans even at high doses, but unfortunately its bioavailability is very low that its therapeutic use is limited [72]. A high rate of curcumin conjugation via glucoronidation and sulfation might explain why the concentration of free curcumin is very low in blood [58]. Preclinic studies reported that due to

**Table 3.11** CE method for analysis of curcumin

Analyte(s)	Sample	Standard and sample preparation	Analytical condition	LOD, LOQ, and recovery	Reference
Curcuminoid (curcumin, demethoxycurcumin, bis- demethoxycurcumin)	Dried turmeric	Sample: Sample was extracted through sonication with EtOH 99.5%, solvent was evaporated and diluted to volume with EtOH 99.5%	Capillary type: n/a (36 cm × 50 µm i.d) Running solution: 1% butyl acrylate–butyl methacrylate–methacrylic acid solution in 30 mM borate buffer contains 50% DMSO at pH 8.0 Applied voltage: 18 kV Temperature: 20 °C Detection: 425 nm	LOD: 0.1 µg/mL LOQ: n/r Rec: n/r	[110]
Curcumin	Turmeric	Standard: Stock solution of 1 mM curcumin in 0.01 M NaOH, and $5 \times 10^{-5}$ mol/L curcumin in light petroleum Sample: Extraction was done with light petroleum, then subjected to SPE containing tributyl phosphate (TBP) resin SPE activation: 2 mL 0.01 M NaOH followed by	Capillary type: Uncoated fused-silica capillaries (32 cm, 25 µm inner diameter, 360 µm outer diameter) Pretreatment: Washed overnight with 0.1 M NaOH Between runs: @90 s: double-distilled water, 0.1 M NaOH, double-distilled water; 180 s	LOD: $3 \times 10^{-8}$ mol/L LOQ: n/r Rec: 85%	[107]

		double-distilled water until eluent became neutral. Extracted curcumin in light petroleum was passed through SPE, being adsorbed for seconds then eluted with diluted NaOH (pH 9.5). Eluent was then collected, analyzed directly to the CE.	buffer solution Running solution: 15 mM phosphate buffer (pH 9.7) Temperature: n/a Detector: amperometric Separation voltage: 16 kV Injection: 6 s at 9 kV Detection: 1.2 V	
Curcuminoid (curcumin, demethoxycurcumin, bis- demethoxycurcumin) Internal standard (IS): dimethoxy- <i>trans</i> - cinnamic acid	<i>C. xanthorrhizae</i> rhizome, <i>C. longae</i> rhizome, curry powder	Standard: Calibration standard was extracted from 2.2 g <i>C. longae</i> rhizome using MeOH as solvent and isolated using TLC preparative method IS: dissolved in ACN: water=8:2 Sample: Dry plant material was suspended in ACN: water=8:2 (v/v), mixed with ultraturrax at 25,000 rpm, then filtered and analyzed	Capillary type: Uncoated fused-silica capillaries (370 mm × 50 µm i.d) Running solution: 20 mM phosphate, 14 mM β-CD hydrate and 50 mM sodium hydroxide (pH 12.1) Applied voltage: 20 kV Temperature: 27 °C Detection: 258 nm (with internal standard) and 470 nm for curcuminoid	LOD: C, DC, [108] BDC: 0.01 mg/L LOQ: n/r Rec: C: 98% DC: n/r BDC: n/r

Continued



**Table 3.11** CE method for analysis of curcumin—cont'd

Analyte(s)	Sample	Standard and sample preparation	Analytical condition	LOD, LOQ, and recovery	Reference
Curcuminoid (curcumin, demethoxycurcumin, bis- demethoxycurcumin) IS: 2,4-dinitrophenyl phthalimide	Turmeric	Standard: Stock solution in EtOH, diluted with microemulsion without phosphate buffer and organic cosolvent Sample: Extracted with EtOH, centrifuged, then supernatant diluted with microemulsion component	Capillary type: Uncoated fused-silica capillary (40.2 cm × 50 μm i.d) Capillary treatment: Pretreatment: @5 min: EtOH, 0.1 M NaOH, water; 15 min microemulsion buffer After consecutive analysis: @2 min: EtOH, 0.1 M NaOH, water; 3 min microemulsion buffer After daily analysis: @5 min: EtOH, water; then @10 min 0.1 M NaOH, water Microemulsion: 50 mM phosphate buffer pH 2.5, 1.1% (v/v) <i>n</i> -octane, 180 mM SDS (surfactant), 890 mM 1-butanol	LOD C: 5.5 ± 0.1 ppm DC: 4.7 ± 0.1 ppm BDC: 5.7 ± 0.1 ppm LOQ: C: 13.3 ± 0.1 ppm D: 10.6 ± 0.1 ppm BDC: 10.7 ± 0.1 ppm Rec: C: 95.0 ± 1.2% DC: 98.6 ± 1.4% BDC: 96.8 ± 1.9%	[111]

(cosurfactant), 25%  
(v/v) 2-propanol  
(organic cosolvent)  
Applied voltage:  
–15 kV  
Temperature: 25 °C  
Detection: 214 nm,  
425 nm

Curcuminoid (curcumin, demethoxycurcumin, bis- demethoxycurcumin)	Commercial plant extract, capsules	Standard: Curcumin substance dissolved in MeOH and isolated for the C, DC, BDC using TLC preparative method to obtain stock solution of C, DC, BDC. Each of this compound was then dissolved in EtOH: water = 1:1 Sample: EtOH:water = 1:1	Capillary type: Fused silica capillary tube (160 mm × 300 µm i.d) coated with hydroxyethylcellulose (HEC) 30000 Running solution: 50 mM (3- cyclohexylamino)-1- propanesulfonic acid (CAPS) adjusted to pH 10.2 with 2-aminoethanol, 100 mg/mL HP-β-CD and 2 g/L HEC Applied voltage: 6 kV Temperature: n/a Detection: 480 nm	LOD C: 1.59 µg/mL DC: 1.37 µg/ mL BDC: 1.86 µg/ mL LOQ C: 5.30 µg/mL DC: 4.57 µg/ mL BDC: 6.20 µg/ mL Rec: C: 94.5–96.7% DC: 96.8–98.9% BDC: 97.8–98.3%	[109]
---	---------------------------------------	--	--	--	-------

C, curcumin; DC, demethoxycurcumin; BDC, bis-demethoxycurcumin.

its extensive metabolism, the concentrations of curcumin in plasma and target tissue were very low [57].

Yang *et al.* [55] reported that the oral bioavailability of curcumin in rats was below 1%. Various methods have been devised to enhance the bioavailability of curcumin. Complexes of curcumin with phospholipids showed higher serum concentrations relative to those of pure curcumin. This complex also showed better antioxidant activity and hepato-protective activity [53,54]. Polymeric micellar formulation of curcumin increased the half-life in rats [56]. Curcumin complexed in liposomes increased the absolute bioavailability in rats to 2.7% [61]. Complexation with piperine, an inhibitor of UDP-glucuronosyl transferase, could increase plasma concentrations of curcumin, but unfortunately piperin is toxic in experimental animals [59]. However, in human study, the presence of piperin did increase the bioavailability of curcumin [60].

Kakkar *et al.* [64] showed that administration of curcumin-loaded solid lipid nanoparticles significantly improved the bioavailability of curcumin in rats. In tumor tissue, this solid lipid formulation could improve concentration of curcumin [66]. Curcumin-loaded PLG nanoparticles increased the absorption of curcumin in rats, resulting in an oral bioavailability that was 22 times higher than for conventional curcumin [67]. The oral bioavailability of curcumin in rats was improved 1.45-fold by administration of amorphous curcumin [69]. The curcuminoids curcumin, desmethoxy curcumin (DeMC), and bis-desmethoxy curcumin (BDeMC) were found to be metabolized by rats into tetrahydrocurcumin (THC), hexahydrocurcumin (HHC), curcumin glucuronide (COG), and curcumin sulfate (CS) [57]. Li *et al.* [66] reported that curcuminoids were mainly found as glucuronides in mice plasma, while in mice tumor tissues, they were found in their free forms.

It was reported that after oral consumption of 10–12 g curcumin in a single dose by humans, COG and CS were found in plasma [58]. Chen *et al.* [68] reported that after ingestion of curcumin by healthy subjects, COG could be detected in plasma, but not curcumin itself. After consuming breads containing free curcumin, encapsulated curcumin and curcumin plus piperine, quercetin, and genistein, many metabolites were detected in human plasma, urine, or fecal samples. The metabolites were DeMC, BDeMC, COG, HHC, HHC glucuronide, chlorogenic acid, FA, VA, 3,4-dihydroxyphenylacetic acid, 4-hydroxyphenylacetic acid, and 3-(4-hydroxyphenyl)propionic acid [72]. Curcumin metabolites HHC, THC, and CS had very low activity for inhibition of phorbol ester-induced

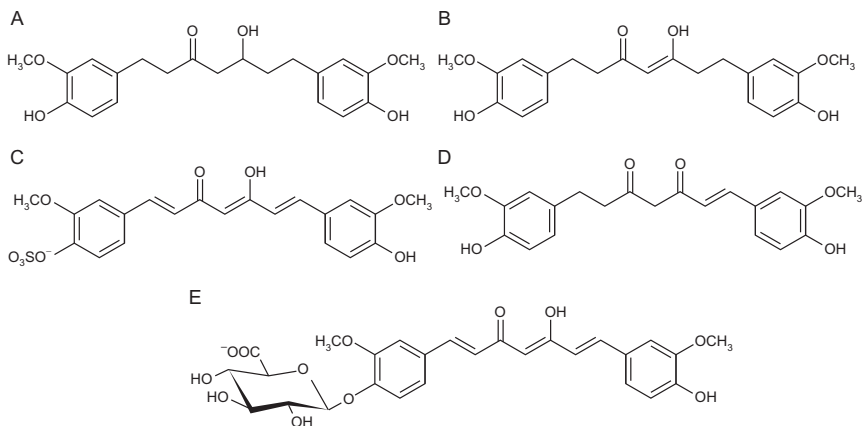


**Figure 3.4** Chemical structure of curcumin metabolites: (A) hexahydrocurcumin (HHC), (B) tetrahydrocurcumin (THC), (C) curcumin sulfate (CS), (D) dihydrocurcumin (DHC), (E) curcumin glucuronide (COG).

prostaglandin E2 production in human colonic epithelial cells compared to the parent compound curcumin [58].

Hassaninasab *et al.* [112] reported the existence of a curcumin-converting microorganism that is able to convert curcumin into dihydrocurcumin and THC by a two-step reduction process. The enzyme responsible for this transformation is NADPH-dependent curcumin/tetrahydrocurcumin reductase (CurA). The gene (*curA*) encoding the enzyme CurA was also identified, and the chemical structures of the metabolites are presented in Figure 3.4.

Most of the reported methods of analysis in biological fluids used an HPLC system equipped with UV/Vis, fluorescence, or mass spectral detectors. A summary of these reports is presented in Table 3.12.

Gupta *et al.* [113] described a spectrofluorometric method (excitation 232 nm, emission at 614 nm) for the determination of curcumin in goat and rat serum. The binding of curcumin with soy protein isolate in water was quantified by fluorescence spectrophotometry [114], where the complex was reconstituted in water, simulated gastric fluids, or simulated intestinal fluids.

Chen *et al.* [115] reported the determination of curcumin in human urine by using a resonance light scattering (RLS) technique. Curcumin samples were added in the form of a CuSO<sub>4</sub> (0.01 M) solution and Britton–Robinson buffer solution. RLS spectra were obtained by a synchronous

**Table 3.12** Summary of bioanalysis's method of curcumin, related compounds, and its metabolites

Analytes (samples)	Chromatography conditions	Biological sample/matrices	Internal standard (IS)	Preparation of standard, sample extraction	Validation data of recovery/accuracy/bias, precision, others results	Reference
Curcumin	Column (HPLC-UV): Symmetry Shield C18, Waters, USA (3.9 × 150 mm; 5 µm); guard column: C18, Alltech Associates, USA (30 × 4.6 mm) Mobile phase: ACN: MeOH:H <sub>2</sub> O:acetic acid (41:23:36:1, v/v/v/v) Detection: UV 262 nm	Pooled human plasma and urine	β-17-Estradiol	Standard: Curcumin was dissolved in MeOH (200 µg/mL); working solution was prepared by mixed 0.5 mL of this solutions with 9.5 mL mobile phase; calibration curve was prepared by adding this working solutions into plasma/urine. IS was prepared in MeOH (250 µg/mL) Extraction:  – 200 µL sample + 80 µL deionized water then vortex-mixed for 20 s, then 40 µL IS solution was added, vortex-mixed again for 20 s.	Average recovery: 96–112% RSD interday assay: Plasma: 6.2–12.7% Urine: 2.3–12.2%	[49]

- Add 500  $\mu\text{L}$  extracted solution (EtOAc: MeOH = 95:5), then vortex-mixed 30 s, centrifuged 5 min (13,500 rpm).
- 420  $\mu\text{L}$  of organic layer was removed, evaporated, then dissolved in 200  $\mu\text{L}$  mobile phase, injected to HPLC (20  $\mu\text{L}$ ).

Curcumin	<p>Column (HPLC-UV): Symmetry shield C18, Waters, USA (<math>3.9 \times 150</math> mm; 5 <math>\mu\text{m}</math>); guard column: C18, Pnenomenex, USA (<math>3.0 \times 4</math> mm)</p> <p>Mobile phase: 0.1% citric acid pH 3.0 (adjusted by 45% KOH): tetrahydrofuran (50/50, v/v)</p> <p>Detection: UV 280 nm</p>	Pig plasma	$\beta$ -Estradiol	<p>Extraction by EtOAc (25–250 ng/mL in plasma):</p> <ul style="list-style-type: none"> <li>– 1 mL blank plasma + 20 <math>\mu\text{L}</math> methanolic (range concentrations: 1.25–12.5 <math>\mu\text{L}/\text{mL}</math>) + 100 <math>\mu\text{L}</math> citrate buffer pH 3.0 + 2 mL EtOAc, then samples were shaken,</li> </ul>	<p>Rec: 66–78% Intra- and interday precision: &lt;15%</p>	<a href="#">[50]</a>
----------	--	------------	--------------------	---	---	----------------------

*Continued*

**Table 3.12** Summary of bioanalysis's method of curcumin, related compounds, and its metabolites—cont'd

Analytes (samples)	Chromatography conditions	Biological sample/ matrices	Internal standard (IS)	Preparation of standard, sample extraction	Validation data of recovery/accuracy/ bias, precision, others results	Reference
				centrifuged $1200 \times g$ (10 min). – 1.65 mL EtOAc was removed, evaporated, then dissolved in 100 $\mu\text{L}$ MeOH, 50 $\mu\text{L}$ was injected.		
				Extraction with $\text{CHCl}_3$ (5–25 ng/mL in plasma): 2 mL blank plasma + 40 $\mu\text{L}$ methanolic (range concentrations: 0.25–1.25 $\mu\text{L}/\text{mL}$ ) + 300 $\mu\text{L}$ citrate buffer pH 3.0 + 2 mL $\text{CHCl}_3$ , then samples were shaken, centrifuged $1200 \times g$ (10 min):		

- 1.7 mL was removed, evaporated, then dissolved in 75  $\mu\text{L}$  MeOH, 50  $\mu\text{L}$  was injected.

Extraction with  $\text{CHCl}_3$   
(2.5–50 ng/mL in plasma):  
2 mL blank plasma + 20  $\mu\text{L}$  methanolic (range concentrations: 0.25–5  $\mu\text{L}/\text{mL}$ ) + 20  $\mu\text{L}$  IS in MeOH (20  $\mu\text{L}/\text{mL}$ ) + 2 mL  $\text{CHCl}_3$ , then samples were shaken, centrifuged  $1200 \times g$  (10 min):

- Organic layer was removed, evaporated, then dissolved in 75  $\mu\text{L}$  MeOH, 50  $\mu\text{L}$  was injected.



**Table 3.12** Summary of bioanalysis's method of curcumin, related compounds, and its metabolites—cont'd

Analytes (samples)	Chromatography conditions	Biological sample/ matrices	Internal standard (IS)	Preparation of standard, sample extraction	Validation data of recovery/accuracy/ bias, precision, others results	Reference
Tetra-hydrocurcumin (THC)	Column (HPLC-UV): Symmetry Shield C18, Waters, USA (3.9 × 150 mm; 5 µm); guard column: C18, Alltech Prevail Amide, USA (30 × 4.6 mm) Mobile phase: Reagent A: ACN Reagent B: 0.1% ammonium sulfate (pH 7.8) (adjusted by 1 M KOH) Reagent C: ACN: deionized water: MeOH:acetic acid (41:35:23:1, v/v/v/v) Gradient: Reagent B: 6 min Reagent C: 10 min then wash with Reagent A 8 min. Detection: UV 280 nm	Pooled-human plasma and urine	β-17-Estradiol	Standard: 5.0 mg of THC in MeOH (5 mL); working standards were prepared (1, 10, and 100 µg/mL) Samples: Extracting solvent: EtOAc: MeOH (95:5, v/v) 200 µL sample + 1.1 mL deionized water then vortex-mixed for 20 s, then 60 µL IS solution (20 µg/mL) was added, vortex-mixed again  – Add 700 µL extracted solvent, then vortex-mixed, centrifuged 5 min (11,500 rpm). – organic layer was removed, evaporated, then dissolved in 120 µL Reagent C, injected to HPLC (100 µL).	Rec: Plasma: 98–100% Urine: 101–201.7% Precision: <8.6%	<a href="#">[51]</a>

Curcumin	<p>Column (HPLC-UV): LiChrosphere C18 (200 × 4.6 mm; 5 μm)</p> <p>Mobile phase: ACN: 5% citric acid (52:48)</p> <p>Detection: UV 425 nm</p>	Dog plasma	Berberine	<p>Standard solution: Curcumin (0.1–6.4 μg/mL) and IS (25 μg/mL) were dissolved in MeOH; calibration was made by addition of standard in blank plasma</p> <p>Sample:</p> <ul style="list-style-type: none"> <li>– 1 mL plasma + 20 μL IS then vortex-mixed for 10 s.</li> <li>– After vortex-mixing 100 μL 1 M HCl was added, mixed, then + 5 mL EtOAc, vortex-mixed 5 min, centrifuged 1500 × g for 10 min.</li> <li>– 4 mL of organic layer was taken, evaporated, then residue was dissolved in mobile phase (100 μL), vortex-mixed, centrifuged then 40 μL was injected into HPLC.</li> </ul>	<p>Rec.: 98.7–10 5%</p> <p>RSD precision: Intraday: 3.1–7.3% Interday: 5.7–6.2%</p>	[52]
----------	---	------------	-----------	---	---	------

**Table 3.12** Summary of bioanalysis's method of curcumin, related compounds, and its metabolites—cont'd

Analytes (samples)	Chromatography conditions	Biological sample/ matrices	Internal standard (IS)	Preparation of standard, sample extraction	Validation data of recovery/accuracy/ bias, precision, others results	Reference
Curcumin, tetra-hydro-curcumin (THC); (curcumin administrated as curcumin and curcumin–phospholipid complex)	Column (LC–MS/ MS): C18 Phenomenex Luna (250 × 4.6 mm) Mobile phase: ACN:0.05% acetic acid in water (70:30) Detection: MRM (positive ion mode) Curcumin: <i>m/z</i> 369.3–285.1 THC: <i>m/z</i> 373.2–137.1 IS: <i>m/z</i> 240.2–148.1	Rat plasma	Salbutamol	Standards: Curcumin, THC, and IS were dissolved in MeOH (50 µg/mL); calibration standards, QC samples were prepared by spiking stock solutions into blank plasma Samples: – 0.1 mL aliquot plasma + 50 µL phosphate buffer (pH 6.86, 0.1 M) + 1000 U β-glucuronidase, incubated 1 h at 37 °C. – Then 50 µL mobile phase containing 1 µg/mL IS, vortex-mixed 30 s, then add 1 mL EtOAc,	Bias: Curcumin: Intraday: –2.01% to –6.00% Interday: –2.67% to –9.52% THC: Intraday: +1.30% to +4.32% Interday: –5.05% to +1.48% RSD precision: Curcumin: Intraday: 2.56% to –13.52% Interday: 3.77–12% THC: Intraday: 6.36–13.75% Interday: 3.91–12.47%	[53]

- vortex-mixed again for 1 min, and ultrasonicated for 15 min, centrifuged 6 min ( $15,000 \times g$ ).
- The organic layer was taken, evaporated, then dissolved in 100  $\mu\text{L}$  mobile phase, 10  $\mu\text{L}$  was injected into HPLC.

Curcumin (administrated as phospholipid complex)	Column (HPLC-UV/ Vis): Waters $\mu$ -Bondapak C18 ( $300 \times 4.6$ mm) Mobile phase: MeOH:2% acetic acid: ACN (5:30:65) Detection: UV 425 nm	Rat plasma n/r	Standard: Curcumin was dissolved in MeOH (0.1 ppm) Samples:	Rec.: 82.70–84.29% RSD precision: Intraday: 2.78–3.56% Interday: 2.12–3.24%	<a href="#">[54]</a>
			<ul style="list-style-type: none"> <li>– 1 mL serum + 5 mL MeOH, shaken vigorously 25–30 min (<math>75\text{--}80^\circ\text{C}</math>), then diluted with MeOH (10 mL).</li> <li>– Centrifugation 10 min (5000 rpm), 20 was injected into HPLC.</li> </ul>		

**Table 3.12** Summary of bioanalysis's method of curcumin, related compounds, and its metabolites—cont'd

Analytes (samples)	Chromatography conditions	Biological sample/matrices	Internal standard (IS)	Preparation of standard, sample extraction	Validation data of recovery/accuracy/ bias, precision, others results	Reference
Curcumin, dimethoxy-curcumin (DC)	Column (LC–MS/MS): Zorbax Extend-C18 (150 × 4.6 mm; 5 μm). Mobile phase: ACN: 1 mM HCOOH (70:30, v/v) Detection: MRM (negative ion mode) Curcumin: <i>m/z</i> 367–217 DC: <i>m/z</i> 337–217	Rat plasma	Honokiol	Standard: Curcuminoids and IS were dissolved in MeOH (1 mg/mL) Samples: – 150 μL blood samples were centrifuged (3000 × g, 5 min). – 50 μL plasma + IS Solution (0.1 μg/mL), vortex-mixed and centrifuged. – 20 μL was injected.	Bias: Curcumin: Intraday: 5% to +12% Interday: 0.6–8% DC: Intraday: –0.4% to +12% Interday: 0.8–16% RSD precision: Intraday: 1% to +18% Interday: 0.5–19% DC: Intraday: 0.6–18% Interday: 0.3–17%	[55]
Curcumin (curcumin administrated as solubilized curcumin and its micellar formulations)	Column (HPLC–UV/Vis): Waters μ-Bondapak™ C18 (300 × 3.9 mm) Mobile phase: ACN:1% citric acid (w/v) pH 3 (adjusted by	Rat plasma	4-Hydroxy-benzophenone	Standard: Curcumin and IS were dissolved in MeOH (1 mg/mL); calibrations were prepared by adding stock solutions into blank plasma	Rec: 94.9–97.1% RSD precision: Intraday: 2.03–2.6% Interday: 4.43–12.7%	[56]

concentrated NaOH)  
(55:45, v/v)  
Detection: UV/Vis:  
428 and 300 nm

Samples:

- 100 µL  
plasma + 50 µL IS,  
mixed then 250 µL  
ACN was added,  
vortex-mixed,  
centrifuged  
14,000 × g for 5 min,  
100 µL supernatant  
was injected.

Curcumin and its  
metabolites in rats

Column (HPLC-UV,  
quantitative): Atlantis  
dC18 (150 × 4.6 mm,  
3 µm), guard column  
(20 × 3 mm, 3 µm)  
Mobile phase:  
A: 10 mM ammonium  
acetate pH 4.5 B:  
ACN: Gradient: initial  
95% A, progressing to  
55% A (20 min) and 5%  
A (33 min)  
Detection: UV 280 nm  
Column (LC-MS/MS,  
identification

Rat      n/r  
plasma,  
intestinal  
mucosa,  
and liver

Curcumin and its  
metabolites were  
extracted using SPE  
(1 mL Oasis HLB  
cartridge, Waters).  
Plasma:

- 1 mL plasma was  
loaded
- SPE was washed with  
MeOH:H<sub>2</sub>O:glacial  
acetic acid (25:25:1)  
and eluted with 1 mL  
MeOH containing  
2% glacial acetic acid.

Quantitative validation [57]  
data: n/r  
Curcumin,  
desmethoxy curcumin,  
bis-desmethoxy  
curcumin, tetra-  
hydrocurcumin, hexa  
hydrocurcumin,  
curcumin glucoronide,  
and curcumin sulfate  
were detected in  
plasma, intestinal  
mucosa, and liver

*Continued*

**Table 3.12** Summary of bioanalysis's method of curcumin, related compounds, and its metabolites—cont'd

Analytes (samples)	Chromatography conditions	Biological sample/ matrices	Internal standard (IS)	Preparation of standard, sample extraction	Validation data of recovery/accuracy/ bias, precision, others results	Reference
	metabolite): Conditions same as quantitative except A consisted of 5 mM ammonium acetate pH 4.5 Metabolites were detected using MRM			Mucosa and liver:  – Suspended and homogenized using KCl then extracted with acetone:formic acid (9:1), then centrifuged; supernatant was taken and evaporated to dryness under nitrogen.		
Curcumin, COG, CS	Column (HPLC-UV/ Vis): $\mu$ -Bondapack C18 (250 $\times$ 4.6 mm, 10 $\mu$ m) Mobile phase: A: 0.1% acetic acid: MeOH:H <sub>2</sub> O (0.1:65:35) B: MeOH, gradient	Human plasma	$\beta$ -17-Estradiol acetate	Extraction curcumin:  – 200 $\mu$ L plasma + 80 $\mu$ L water + 20 $\mu$ L IS vortex-mixed. – The solution was extracted thrice using	Rec: Curcumin at 1 $\mu$ g/mL was 95.14% (RSD = 2.75)	[58]

elution 100% A to  
100% B in 15 min  
Detection: Vis 420 nm

by vortexing using  
1 mL mixture of  
EtOAc:MeOH  
(95:5) for 3 min.

- Sample was centrifuged 3000 rpm (15 min, 4 °C), organic layer was collected, evaporated to dryness then dissolved in 100  $\mu$ L MeOH.

Hydrolysis of curcumin  
conjugates:

- Same as above, samples were then mixed with  $\beta$ -glucuronidase (50  $\mu$ L, 446 U, in 0.1 M phosphate buffer pH 6.8) and sulfatase (45  $\mu$ L, 52 U, in Na acetate buffer pH 5), then incubated for 3.5 h.
- Samples were extracted as described above.



**Table 3.12** Summary of bioanalysis's method of curcumin, related compounds, and its metabolites—cont'd

Analytes (samples)	Chromatography conditions	Biological sample/matrices	Internal standard (IS)	Preparation of standard, sample extraction	Validation data of recovery/accuracy/bias, precision, others results	Reference
Curcumin	Column (HPLC-UV/Vis): C18 ODS Phenomenex (250 × 4.6 mm, 5 μm) Mobile phase: MeOH Detection: UV 420 nm	Human plasma	n/a	Extraction:  – 5 mL blood was centrifuged 10 min (2000 × g). – 2.5 g plasma was extracted thrice using EtOAc (3, 2, 2 mL). – Pooled extract was evaporated to dryness under N <sub>2</sub> , then residue was dissolved in 2 mL MeOH by vortexing.	Validation data: n/r	[59]
Curcumin, piperin	Column (HPLC-UV/Vis): Chromolith® Speed ROD RP-18 (50 × 4/6 mm) Mobile phase: ACN: MeOH: TFA:H <sub>2</sub> O	Human plasma	β-17-Estradiol acetate	Standards: Stock solutions were prepared by dissolving each of the analytes in MeOH (1 mg/mL); calibration standards, QC samples were prepared by spiking stock solutions	Accuracy: Intraday: Curcumin: 94.5 ± 2.0% Piperin: 98.0 ± 4.8% Interday: Curcumin: 94.0 ± 2.5%	[60]

(17.6:35.3:0.1:47,  
v/v/v/v)  
Detection:  
Curcumin: 415 nm  
Piperin: 335 nm  
IS: 280 nm

into blank plasma  
Samples:

- 100  $\mu$ L IS  
(1500 ng/mL) +  
0.5 mL distilled  
water + 100  $\mu$ L  
phosphate buffer  
pH 3.4 + 6 mL  
extraction solvent  
(EtOAc:  
propanol = 9:1, v/v)  
were added to  
0.5 mL of samples,  
then vortex-mixed,  
then shaken well in a  
rotating mixer for  
15 min, centrifuged  
15 min ( $100 \times g$ ).
- The upper organic  
layer was taken,  
evaporated then  
dissolved in 100  $\mu$ L  
MeOH, and 40  $\mu$ L  
was injected.

Piperin:  $97.2 \pm 5$  1%  
RSD precision:  
Intraday:  
Curcumin:  $5.7 \pm 2.1\%$   
Piperin:  $5.4 \pm 2.7\%$   
Interday:  
Curcumin:  $5.9 \pm 2.7\%$   
Piperin:  $6.1 \pm 3.0\%$

---

*Continued*

**Table 3.12** Summary of bioanalysis's method of curcumin, related compounds, and its metabolites—cont'd

Analytes (samples)	Chromatography conditions	Biological sample/matrices	Internal standard (IS)	Preparation of standard, sample extraction	Validation data of recovery/accuracy/bias, precision, others results	Reference
Curcumin (administrated as curcumin liposome)	Column (HPLC-PDA): Diamonsil C18 (100 × 4.6 mm, 5 μm) Mobile phase: ACN: 5% acetic acid (75:25, v/v) Detection: UV 420 nm	Rat plasma	Emodin	Standards: Curcumin and IS were dissolve in ACN, at concentrations 0.5 and 1.5 mg/mL, respectively. Calibration standards and QC samples were prepared by spiking appropriate solutions into blank plasma Samples:  – Samples were prepared in 96-well format plate (1 mL, Variant, USA). – 90 μL rat blank plasma + 10 μL standard working solutions, 100 μL aliquot plasma samples and QC	Accuracy and (RSD precision) Intraday: 94.15–106.23% (1.74–7.51%) Interday: 100.92–107.05% (3.37–9.24%)	[61]

samples were pipetted into 96-well plates.

- Then add 100  $\mu\text{L}$  ACN containing IS (0.15  $\mu\text{g}/\text{mL}$ ), capped, vortex-mixed then centrifuged  $2500 \times g$  15 min.
- 350  $\mu\text{L}$  supernatant was transferred to the 96-well plates, 50  $\mu\text{L}$  was injected into HPLC.

Curcumin, tetrahydrocurcumin (THC), 1,7-bis(3,4, dimethoxyphenyl)-4,4-dimethyl-1,6 heptadiene-3,5 dione (TMC), 1,7-bis(3,4, dimethoxyphenyl)-4-cyclohexyl-1,6 heptadiene-3,5 dione (DMCHC)	Column (LC–MS/MS): Beta basic C8 ( $50 \times 2.1 \text{ mm}$ , $5 \mu\text{m}$ ) with guard column Beta basic C8 javelin ( $10 \times 2.1 \text{ mm}$ , $2 \mu\text{m}$ ) Mobile phase: 50% ACN containing 0.1% formic acid Detection by SRM: Curcumin: $m/z$	Mouse plasma, cell medium	Hesperitin	Standards: Standard solutions of curcumin. THC, TMC, DMCHC, and IS were prepared in ACN; standard solution in the range of 10–10,000 $\text{ng}/\text{mL}$ were prepared by dilutions. Calibration standards and QC	Accuracy (RSD) Intraday: Curcumin: 99.7 (6.22)–103.1 (14.01)% THC: 90.3 (5.64)–109.9 (5.92)% TMC: 86.2 (9.23)–99.5 (7.87)% DMCHC: 97.9 (9.35)–101.2 (5.96)%.	<a href="#">[62]</a>
--	--	---------------------------	------------	---	---	----------------------

Continued

**Table 3.12** Summary of bioanalysis's method of curcumin, related compounds, and its metabolites—cont'd

Analytes (samples)	Chromatography conditions	Biological sample/matrices	Internal standard (IS)	Preparation of standard, sample extraction	Validation data of recovery/accuracy/bias, precision, others results	Reference
	369–177 THC: $m/z$ 373–137 TMC: $m/z$ 425–191 DMCHC: $m/z$ 465–191 IS: $m/z$ 303–153			<p>samples were prepared by spiking the solutions into mouse plasma or cell medium</p> <p>Samples:</p> <ul style="list-style-type: none"> <li>– 200 <math>\mu</math>L RPMI cell medium, or 100 <math>\mu</math>L plasma that contained IS (1000 ng/mL) were extracted with 1 mL EtOAc for 60 min mechanical shaking.</li> <li>– After extraction, samples were centrifuged 2 min (11,000 <math>\times g</math>), and place on dry ice for 1 min.</li> <li>– Supernatant of EtOAc were</li> </ul>	<p>Interday:</p> <p>Curcumin:</p> <p>92.7 (7.61)–98.5 (5.02)%</p> <p>THC: 89.9 (5.36)–105.5 (7.51)%</p> <p>TMC: 88.5 (15.10)–100.1 (3.99)%</p> <p>DMCHC: 95.64 (9.25)–100.5 (5.78)%</p>	

evaporated to dryness  
under nitrogen,  
reconstituted in  
100  $\mu$ L ACN 50%,  
and centrifuged  
2 min (11,000  $\times$  g);  
20  $\mu$ L supernatant  
was used for analysis.

Curcumin	Column (LC–MS/ MS): Supelco Discovery C18 (50 $\times$ 4.6 mm; 5 $\mu$ m) Mobile phase: 0.01 M ammonium acetate pH 5.5:ACN (10:90) Detection: MRM (negative ion mode): Curcumin: $m/z$ 367–217 IS: $m/z$ 283–268	Rat plasma	Biochanin	Standard:  – Primary stock solutions were prepared by dissolving 5 mg in 0.2 mL DMSO and appropriate dilutions were made with MeOH. Calibration standards and QC samples were prepared by spiking working solutions into control pooled rat plasma.	Accuracy (RSD precision): 96.33–107.67% (0.71–5.97%)	[63]
----------	---	------------	-----------	--	---	------

*Continued*

**Table 3.12** Summary of bioanalysis's method of curcumin, related compounds, and its metabolites—cont'd

Analytes (samples)	Chromatography conditions	Biological sample/ matrices	Internal standard (IS)	Preparation of standard, sample extraction	Validation data of recovery/accuracy/ bias, precision, others results	Reference
				<p>Samples:</p> <ul style="list-style-type: none"><li>– 100 µL plasma + 10 µL IS solution (MeOH, 1 µg/mL), mixed for 15 s.</li><li>– Add 2 mL mixture of CH<sub>2</sub>Cl<sub>2</sub>:EtOA (1:1, v/v) then vortex-mixed 3 min, centrifuged 5 min (2000 × g).</li><li>– 1.6 mL organic layer was removed, evaporated, then dissolved in 200 µL mobile phase, 10 µL was injected into LC.</li></ul>		

Curcumin (administrated as free curcumin and as solid lipid nanoparticle)	Column (LC–MS/ MS): Chromolith™ (50 × 4.6 mm, 5 µm) Mobile phase: ACN:10 mM ammonium acetate buffer (80:20, v/v) Detection: MRM (negative): Curcumin: <i>m/z</i> 367–217 IS: <i>m/z</i> 307–229	Rat plasma Nimesulide	Standard: Curcumin and IS were dissolved in MeOH (100 µg/mL); calibration standard and QC were prepared by spiking the appropriate working solutions into plasma Samples:  – 100 µL rat plasma + 10 µL IS solution + 200 µL β-glucoronidase, incubate 37 °C for 1 h. – Curcumin was extracted by using 2 mL diethyl ether by vortexing (1 min) then cold centrifuged (4 °C, 5 min, 5000 rpm). – Supernatant was evaporated to dryness in nitrogen (50 °C) and residue was dissolved in mobile phase.	Accuracy (RSD precision): Intraday: 102.43–105. 67% (2–3.55%) Interday: 105.7–108.5% (2.05–3.55%)	[64]
--	--	-----------------------	--	---	------



**Table 3.12** Summary of bioanalysis's method of curcumin, related compounds, and its metabolites—cont'd

Analytes (samples)	Chromatography conditions	Biological sample/matrices	Internal standard (IS)	Preparation of standard, sample extraction	Validation data of recovery/accuracy/bias, precision, others results	Reference
Curcumin, curcumin di-decanoate (CurDD)	Column (HPLC-UV/Vis): C18 Phenomenex <sup>®</sup> (250 × 4.6 mm, 5 μm) Mobile phase: Gradient elution ACN:THF: H <sub>2</sub> O with 0.1% formic acid (0–8 min: 35:20:45, 8–13 min: 35:20:45–50:40:10, and 13–21 min: 50:40:10) Detection: Vis 425 nm	Rat plasma	Emodin	Standard: Stock solutions of curcumin CurDD and IS were prepared in ACN. Working solutions of curcumin and IS were prepared by dilution with MeOH, while for CurDD, ACN was used. Calibration standard and QC were prepared by spiking the appropriate working solutions into plasma Samples (prepared in low temperature 0–8 °C)  – 50 μL plasma + 10 μL IS (so	Bias: Curcumin: –2.77% to +3.15% CurDD: –6.07% to +8.88% RSD Precision Intraday: Curcumin: 5.71–11.5% CurDD: 1.64–9.06% Interday Curcumin: 7.24–11.4% CurDD: 3.77–18.7%	[65]

- the concentrations of IS was 500 ng/mL).
- After vortex-mixing for 10 s, then 50  $\mu$ L of 10% sodium dodecyl sulfate was added, vortex-mixed for 15 s.
  - Add 600  $\mu$ L of EtOA, vortex-mixed 90 s then centrifuged 5 min (12,000 rpm).
  - Supernatant was taken, evaporated, the residue was dissolved in 80% ACN, 50  $\mu$ L was injected.

Curcumin, demethoxycurcumin (DMC), bis-demethoxycurcumin (BDMC) (administrated as curcuminoid nano particle formulation)	Column (LC–MS/MS): Metabolite identification: YMC Pack ODS A C18 (250 $\times$ 4.6 mm, 5 $\mu$ m); guard column: Agilent Zorbax Sb C18 (12.5 $\times$ 4.6 mm, 5 $\mu$ m) Mobile phase: Solvent	Mice tumor	Honokiol	Standards: Stock solutions were prepared by dissolving each analyte and IS in MeOH (500 $\mu$ g/mL); working solutions were prepared by mixing each of the stock solutions	Bias (RSD precision) Intrabatch: Curcumin: –1% to +5.5% (5.5–11.2%) DMC: –11.7% to –14.3% (4.6–7.5%) BDMC: –11.9% to –14.0% (3.3–4.8%) Interbatch:	66
--	--	------------	----------	--	--	----

*Continued*

**Table 3.12** Summary of bioanalysis's method of curcumin, related compounds, and its metabolites—cont'd

Analytes (samples)	Chromatography conditions	Biological sample/ matrices	Internal standard (IS)	Preparation of standard, sample extraction	Validation data of recovery/accuracy/ bias, precision, others results	Reference
	<p>A: ACN, solvent B: 0.1% aqueous formic acid; gradient elution: 0 min: (A:B):5:95,v/v, 30 min linear gradient to 45:55, 50 min: 95:5, 55 min 95:5</p> <p>Quantitative: Agilent Zorbax SB C8 (150 × 4.6 mm, 5 μm); guard column: Agilent Zorbax Sb C18 (12.5 × 4.6 mm, 5 μm)</p> <p>Mobile phase: 0 min: (A:B): 50:50, 6 min: 85:15, 7 min: 95:5, 8 min: 95:5</p> <p>Detection: (–) <i>m/z</i>: Curcumin (367.3–149.2) DMC (337.1–119.2) BDMC (307.2–119.1) IS (265.2–224.1)</p>			<p>Calibration standards and QC samples were prepared by spiking the appropriate working solutions into the tumor homogenate</p> <p>Samples:</p> <ul style="list-style-type: none"> <li>– 330 μL aliquot of tumor homogenate + 20 μL IS (10 μg/mL) vortex-mixed 30 s, then extracted with 1400 μL ACN, then vortex-mixing 1 min followed by ultrasonification 30 s.</li> <li>– After centrifugation for 10 min (9500 × <i>g</i>), organic layer was taken, evaporated under nitrogen, and the</li> </ul>	<p>Curcumin: –5.2% to +5.1% (11.1–13.4%)</p> <p>DMC: –10.9% to –13.2% (3.8–6.6%)</p> <p>BDMC: –12.8% to –14.1% (3.6–6.5%)</p>	

residue was dissolved  
in 200  $\mu\text{L}$  MeOH  
(vortex-mixing  
1 min,  
ultrasonification  
30 s), 5  $\mu\text{L}$  was  
injected.

Curcumin (administrated as curcumin-loaded PLGA nano particle)	Column (HPLC- PDA): Eclipse XDB Agilent C18 (150 $\times$ 4.6 mm; 5 $\mu\text{m}$ ) Mobile phase: ACN: 10 mM monosodium phosphate pH 3.5, adjusted by $\text{H}_3\text{PO}_3$ (40:60, v/v): Detection: 425 nm	Rat plasma, fecal, and urine	2-(4'- hydroxy-benzene- azo) benzoic acid	Standard: Stock solution: Curcumin was dissolved in ACN (500 $\mu\text{g}/\text{mL}$ ); working solutions were prepared by dilution of stock solution with 50% ACN; IS was dissolved in ACN (1.5 $\mu\text{g}/\text{mL}$ ) Calibration standards and QC samples were prepared by spiking appropriate solutions into blank plasma/ urine/fecal supernatant Samples: Plasma: 50 $\mu\text{L}$ plasma + 100 $\mu\text{L}$ IS solution, vortex-mixed then centrifuged 15 min (12,000 $\times g$ );	Accuracy, precision intra- and interday are within 15%	[67]
---	--	---------------------------------------	---	--	--	------

*Continued*

**Table 3.12** Summary of bioanalysis's method of curcumin, related compounds, and its metabolites—cont'd

Analytes (samples)	Chromatography conditions	Biological sample/ matrices	Internal standard (IS)	Preparation of standard, sample extraction	Validation data of recovery/accuracy/ bias, precision, others results	Reference
				20 µL was injected Fecal: 50 µL fecal supernatant + 100 µL IS solution, vortex-mixed then centrifuged 15 min (12,000 × g); 20 µL was injected Urine: 50 µL urine supernatant was extracted with 1 mL EtOAc by vortex-mixed, then centrifuged 5 min (8000 rpm), after drying with vacuum centrifugation, the residue was dissolved 100 µL 50% IS solution, then 20 µL was injected		
Curcumin, Curcumin-O-glucoronide (COG)	Column (LC-MS/MS): Beta Basic C8 (50 × 2.1 mm; 2 µm), guard column: Beta C8 (10 × 2.1 mm; 2 µm)	Human plasma	Hesperitin	Samples extraction:  – 10 µL standard solutions of curcumin and COG	Accuracy (% RSD) Intraday: Curcumin: 91.3–112% (3.45–8.32%) COG: 82.7–102%	[68]

Mobile phase: ACN:  
H<sub>2</sub> containing 0.1%  
formic acid (50:50, v/v)  
Detection MRM:  
Curcumin: *m/z*  
369–177  
COG: *m/z* 545–369  
IS: *m/z* 303–177

(20–20,000 ng/mL), (3.12–9.73%)  
IS (10 µg/mL) were Interday:  
added to 100 µL Curcumin: 99.5–101%  
human plasma; (5.18–12.7%)  
calibrations curve COG: 105–109%  
containing curcumin (6.08–11.3%)  
and COG

(2–2000 ng/mL)  
while QC samples  
containing  
2–500 ng/mL.

- The mixture was vortex-mixed and diluted with 0.15 M phosphate saline buffer (900 µL) then extracted with EtOAc, after the organic layer was taken and evaporated, residue was dissolve in 100 µL mobile phase.
- After centrifuged for 2 min (12,000 × *g*), 25 µL of supernatant was injected.

**Table 3.12** Summary of bioanalysis's method of curcumin, related compounds, and its metabolites—cont'd

Analytes (samples)	Chromatography conditions	Biological sample/ matrices	Internal standard (IS)	Preparation of standard, sample extraction	Validation data of recovery/accuracy/ bias, precision, others results	Reference
Curcumin (administrated as amorphous curcumin)	Column (HPLC-Fluorescent): LiChrosphere C18 (200 × 4.6, μm) Mobile phase: 1% (w/v) citric acid mono hydrate pH 3: ACN: THF (48:32:20) Detection: Fluorescent detector: $\lambda_{\text{ex}}/\lambda_{\text{em}}$ 420/530 nm	Rat plasma	Rhoda-mine 6G	Standard: n/r Plasma was extracted with ACN	n/r	[69]
Curcumin	Column (HPLC-UV/Vis): Shim-Pack CLC C18 (250 × 4.6 mm; 5 μm) Mobile phase: THF:0.1% citric acid pH 3 (60:40) Detection: n/r	Human serum	n/r	Standard: n/r Extraction method was performed using dispersive liquid-liquid microextraction in a cold column trapping (CCT-DLLME)	n/r	[70]
Curcumin (administrated as free	Column (HPLC-UV/Vis): Hypersil ODS C18 (150 × 4.6 mm,	Mice blood and	n/r	Standard: n/r Stomach tissue:	n/r	[71]

curcumin and nanoencapsulation)	5 µm) Mobile phase: MeOH:3.6% aqueous acetic acid (73:27, v/v) Detection: UV 425 nm	stomach tissue		<ul style="list-style-type: none"> <li>– The freeze-dried tissue (10–20 mg) was shaken with 2 mL EtOAc overnight, centrifuge <math>8000 \times g</math> (10 min), filtered and dried under N<sub>2</sub>, dissolved in 1 mL MeOH, then injected (20 µL).</li> </ul> <p>Blood:</p> <ul style="list-style-type: none"> <li>– 200 µL plasma + 500 µL EtOAc vortex-mixed for 60 s and sonicated for 60 s, filtered and dried under N<sub>2</sub>, dissolved in 1 mL MeOH, then injected (20 µL).</li> </ul>		
Curcumin and metabolites, and 13 other compounds (administrated as	Column (LC–MS/MS): Phenomenex 3 µ C18(2) 100 nA (50 × 2 mm)	Human blood, urine, and feces	n/a	Quantitative measurements of curcumin metabolites were performed using	Intra- and interday accuracy and precision < 15%	[72]

*Continued*



**Table 3.12** Summary of bioanalysis's method of curcumin, related compounds, and its metabolites—cont'd

Analytes (samples)	Chromatography conditions	Biological sample/ matrices	Internal standard (IS)	Preparation of standard, sample extraction	Validation data of recovery/accuracy/ bias, precision, others results	Reference
enriched bread; in microencapsulated curcumin)	<p>Mobile phase: A = H<sub>2</sub>O:ACN:formic acid (94.9:5:0.1, v/v) B = ACN:formic acid (99.9:0.1, v/v); linear gradient:0–1 min: 4–40% B; 1–3 min: 40–100% B; 3–5 min: 100% B; 6–10 min: 4% B</p> <p>Detection: MRM (negative ion mode): <i>m/z</i>Curcumin: 367 &gt; 217 DeMC:337 &gt; 217 BDeMC: 307 &gt; 217 COG: 543 &gt; 367 Curcumin sulfate: 447 &gt; 367 THCG: 547 &gt; 135 Hexa hydrocurcumin (HHC): 373 &gt; 179 HHCG: 549 &gt; 373</p>			<p>calibration curve of curcumin</p> <ul style="list-style-type: none"> <li>– Blood samples centrifuged 4000 rpm (10 min, 4 °C).</li> <li>– Urine samples were treated with 0.005% butylated hydroxyl toluene (BHT).</li> <li>– Feces was diluted 1:10 (w/v) PBS 10 mM, containing 0.005% BHT, vortex-mixed and centrifuged 4000 rpm (15 min, 4 °C).</li> <li>– Serum, urine and fecal supernatant were stored at –40 °C before analysis.</li> </ul>		

- 1 mL serum, 3 mL urine and fecal were extracted with 6 and 9 mL EtOAc, respectively.
- Supernatant were dried under N<sub>2</sub>, residue was dissolved in 50 µL (MeOH: H<sub>2</sub>O = 70:30), 20 µL was injected into HPLC.

---

n/r: not reported; n/a: not available.

Desmethoxycurcumin = demethoxycurcumin; Bis-desmethoxycurcumin = bis-demethoxycurcumin.

scanning of excitation and emission from 300 to 700 nm; the analytical wavelength for measurements was 538.5 nm. Recoveries were 97.3–104.5% (RSD = 1.3–2.45).

Detection and quantification of curcumin in mouse lung cell cultures by matrix-assisted laser desorption ionization time mass spectrometry (MALDI-TOFMS) was described by May *et al.* [116]. Matrices were prepared using  $\alpha$ -cyano-4-hydroxycinnamic acid (CHCA), trihydroxyacetophenone, and dihydroxybenzoic acid, and it was shown that CHCA was the superior matrix. MALDI analysis showed that cells take up 7–12% available curcumin.

## REFERENCES

- [1] Evaluation of certain food additives and contaminants: sixty-first report of the Joint FAO/WHO Expert Committee on Food Additives, Rome, Italy, 2003.
- [2] B.B. Aggarwal, A. Kumar, A.C. Bharti, Anticancer potential of curcumin: preclinical and clinical studies, *Anticancer Res* 23 (2003) 363–398.
- [3] R.A. Sharma, A.J. Gescher, W.P. Steward, Curcumin: the story so far, *Eur. J. Cancer* 41 (2005) 1955–1968.
- [4] P.-H. Bong, Spectral and photophysical behaviors of curcumin and curcuminoids, *Bull. Korean Chem. Soc.* 21 (1) (2000) 81–86.
- [5] H.H. Tonnesen, Chemistry of curcumin and curcuminoids, in: C.-T. Ho, C.Y. Lee, M.-T. Huang (Eds.), *Phenolic Compounds in Food and Their Effects on Health I: Analysis, Occurrence, and Chemistry*, American Chemical Society, Washington, DC, , 1992, pp. 143–154.
- [6] H.H. Tonnesen, M. Masson, T. Loftsson, Studies of curcumin and curcuminoids. XXVII. Cyclodextrin complexation: solubility, chemical and photochemical stability, *Int. J. Pharm.* 244 (2002) 127–135.
- [7] H.H. Tonnesen, J. Karlsen, High-performance liquid chromatography of curcumin and related compounds, *J. Chromatogr.* 259 (1983) 367–371.
- [8] Curcumin. [http://pubchem.ncbi.nlm.nih.gov/summary/summary.cgi?cid=969516&loc=ec\\_rcs](http://pubchem.ncbi.nlm.nih.gov/summary/summary.cgi?cid=969516&loc=ec_rcs) (accessed 03 March 2013).
- [9] M. Bernabé-Pineda, M.T. Ramirez-Silva, M. Romero-Romo, E. González-Vergara, A. Rojas-Hernández, Determination of acidity constants of curcumin in aqueous solution and apparent rate constant of its decomposition, *Spectrochim. Acta A* 60 (2004) 1091–1097.
- [10] M. Borsari, E. Ferrari, R. Grandi, M. Saladini, Curcuminoids as potential new iron-chelating agents: spectroscopic, polarographic and potentiometric study on their Fe(III) complexing ability, *Inorg. Chim. Acta* 328 (2002) 61–68.
- [11] S.V. Jovanovic, S. Steenken, C.W. Boone, M.G. Simic, H-atom transfer is a preferred antioxidant mechanism of curcumin, *J. Am. Chem. Soc.* 121 (1999) 9677–9681.
- [12] L. Shen, H.-F. Ji, Theoretical study on physicochemical properties of curcumin, *Spectrochim. Acta A* 67 (2007) 619–623.
- [13] B. Tang, L. Ma, H.-Y. Wang, G.-Y. Zhang, Study on the supramolecular interaction of curcumin and  $\beta$ -cyclodextrin by spectrophotometry and its analytical application, *J. Agric. Food Chem.* 50 (2002) 1355–1361.
- [14] H.H. Tonnesen, J. Karlsen, Studies on curcumin and curcuminoids VI. Kinetics of curcumin degradation in aqueous solution, *Z. Lebensm. Unters. Forsch.* 180 (1985) 402–404.

- [15] T.M. DiMauro, U.S. Patent US 2009/0326275A1, 31 December 2009.
- [16] P. Anand, A.B. Kunnumakkara, R.A. Newman, B.B. Aggarwal, Bioavailability of curcumin: problems and promises, *Mol. Pharm.* 4 (6) (2007) 807–818.
- [17] S.P. Parimita, Y.V. Ramshankar, S. Suresh, T.N.G. Rowa, Redetermination of curcumin: (1E,4Z,6E)- 5-hydroxy-1,7-bis(4-hydroxy-3-methoxy- phenyl)hepta-1,4,6-trien-3-one, *Acta Cryst. E63* (2007) 860–862.
- [18] Curcumin. <http://www.chemspider.com/Chemical-Structure.839564.html> (accessed 03 March 2013).
- [19] H.H. Tonnesen, J. Karlsen, Studies on curcumin and curcuminoids V. Alkaline degradation of curcumin, *Z. Lebensm. Unters. Forsch.* 180 (1985) 132–134.
- [20] Y.-J. Wang, M.-H. Pan, A.-L. Cheng, L.-I. Lin, Y.-S. Ho, C.-Y. Hsieh, J.-K. Lin, Stability of curcumin in buffer solutions and characterization of its degradation products, *J. Pharm. Biomed. Anal.* 15 (1997) 1867–1876.
- [21] Z. Ma, A. Haddadi, O. Molavi, A. Lavasanifar, R. Lai, J. Samuel, Micelles of poly(ethylene oxide)-b-poly( $\epsilon$ -caprolactone) as vehicles for the solubilization, stabilization, and controlled delivery of curcumin, *J. Biomed. Mater. Res. A* 86A (2) (2008) 300–310.
- [22] S.P. Mitra, Binding and stability of curcumin in presence of bovine serum albumin, *J. Surface Sci. Technol.* 23 (3–4) (2007) 91–110.
- [23] S. Oetari, M. Sudibyo, J.N. Commandeur, R. Samhoedi, N.P. Vermeulen, Effects of curcumin on cytochrome P450 and glutathione s-transferase activities in rat liver, *Biochem. Pharmacol.* 51 (1996) 39–45.
- [24] H.H. Tonnesen, J. Karlsen, G.B.v. Henegouwen, Studies on curcumin and curcuminoids VIII. Photochemical stability of curcumin, *Z. Lebensm. Unters. Forsch.* 183 (1986) 116–122.
- [25] A. Khurana, C.-T. Ho, High performance liquid chromatographic analysis of curcuminoids and their photo-oxidative decomposition compounds in *Curcuma longa* L, *J. Liq. Chromatogr.* 11 (11) (1988) 2295–2304.
- [26] Y. Wang, Z. Lu, F. Lv, X. Bie, Study on microencapsulation of curcumin pigments by spray drying, *Eur. Food Res. Technol.* 229 (2009) 391–396.
- [27] D. Suresh, H. Manjunatha, K. Srinivasan, Effect of heat processing of spices on the concentrations of their bioactive principles: turmeric (*Curcuma longa*), red pepper (*Capsicum annuum*) and black pepper (*Piper nigrum*), *J. Food Compos. Anal.* 20 (2007) 346–351.
- [28] H.H. Tonnesen, J. Karlsen, A. Mostad, Structural studies of curcuminoids. I. The crystal structure of curcumin, *Acta Chem. Scand. B* 36 (1982) 475–479.
- [29] P. Sanphui, N.R. Goud, U.B.R. Khandavilli, S. Bhanothb, A. Nangia, New polymorphs of curcumin, *Chem. Commun.* 47 (2011) 5013–5015.
- [30] A.R. Parameswari, B. Devipriya, S.J. Jennieffer, P.T. Muthiah, P. Kumaradhas, Low temperature crystal structure of 5-hydroxy-1,7-bis- (4-hydroxy-3-methoxy-phenyl)-hepta-1,6-dien-3-one, *J. Chem. Crystallogr.* 42 (2012) 227–231.
- [31] F. Jasim, F. Ali, A novel method for the spectrophotometric determination of curcumin and its application to curcumin spices, *Microchem. J.* 38 (1988) 106–110.
- [32] F. Jasim, F. Ali, Measurements of some spectrophotometric parameters of curcumin in 12 polar and nonpolar organic solvents, *Microchem. J.* 39 (1989) 156–159.
- [33] J. Ramya, Surface Functionalization of Nanoparticles and Their Biological Applications, University of Pune, Pune, India, 2011. <http://hdl.handle.net/10603/2446>.
- [34] C.F. Chignell, P. Bilskj, K.J. Reszka, A.G. Motten, R.H. Sik, T.A. Dahl, Spectral and photochemical properties of curcumin, *Photochem. Photobiol.* 59 (3) (1994) 295–302.
- [35] S. Kanhathaisong, S. Rattanaphani, V. Rattanaphani, T. Manyum, A Spectroscopic investigation of the complex of turmeric dye with Copper (II) in aqueous solution, *Suranaree J. Sci. Technol.* 18 (2) (2011) 159–165.

- [36] F. Jasim, F. Ali, A novel and rapid method for the spectrofluorometric determination of curcumin in curcumin spices and flavors, *Microchem. J.* 46 (1992) 209–214.
- [37] H. Chowdhury, S. Walia, V.S. Saxena, Isolation, characterization and insect growth inhibitory activity of major turmeric constituents and their derivatives against *Schistocerca gregaria* (Forsk) and *Dysdercus koenigii* (Walk), *Pest Manag. Sci.* 56 (2000) 1086–1092.
- [38] W. Chearwae, C.-P. Wu, H.-Y. Chu, T.R. Lee, S.V. Ambudkar, P. Limtrakul, Curcuminoids purified from turmeric powder modulate the function of human multidrug resistance protein 1 (ABCC1), *Cancer Chemother. Pharmacol.* 57 (2006) 376–388.
- [39] T.M. Kolev, E.A. Velcheva, B.A. Stamboliyska, M. Spitteler, DFT and experimental studies of the structure and vibrational spectra of curcumin, *Int. J. Quantum Chem.* 102 (2005) 1069–1079.
- [40] P.R.K. Mohan, G. Sreelakshmi, C.V. Muralaeeharan, R. Joseph, Water soluble complexes of curcumin with cyclodextrins: characterization by FT-Raman spectroscopy, *Vib. Spectrosc.* 62 (2012) 77–84.
- [41] X.-G. He, L.-Z. Lin, L.-Z. Lian, M. Lindenmaier, Liquid chromatography–electrospray mass spectrometric analysis of curcuminoids and sesquiterpenoids in turmeric (*Curcuma longa*), *J. Chromatogr. A* 818 (1998) 127–132.
- [42] K. Inoue, S. Hamasaki, Y. Yoshimura, M. Yamada, M. Nakamura, Y. Ito, H. Nakazawa, Validation of LC/electrospray-MS for determination of major curcuminoids in foods, *J. Liq. Chromatogr. Rel. Technol.* 26 (1) (2003) 53–62.
- [43] H. Jiang, A. Somogyi, N.E. Jacobsen, B.N. Timmermann, D.R. Gang, Analysis of curcuminoids by positive and negative electrospray ionization and tandem mass spectrometry, *Rapid Commun. Mass Spectrom.* 20 (2006) 1001–1012.
- [44] R. Liu, J. Zhang, M. Liang, W. Zhang, S. Yan, M. Lin, Simultaneous analysis of eight bioactive compounds in Danning tablet by HPLC-ESI-MS and HPLC-UV, *J. Pharm. Biomed. Anal.* 43 (2007) 1007–1012.
- [45] M.J. Scotter, Synthesis and chemical characterisation of curcuminoid colouring principles for their potential use as HPLC standards for the determination of curcumin colour in foods, *LWT Food Sci. Technol.* 42 (2009) 1345–1351.
- [46] R. Li, C. Xiang, M. Ye, H.-F. Li, X. Zhang, D.-A. Guo, Qualitative and quantitative analysis of curcuminoids in herbal medicines derived from *Curcuma* species, *Food Chem.* 126 (2011) 1890–1895.
- [47] R.V. Coorey, P. Hakansson, Application of mass spectrometry to characterize the components present in a curcumin sample, *Sri Lankan J. Phys.* 4 (2003) 11–20.
- [48] B. Avula, Y.-H. Wang, I.A. Khan, Quantitative determination of curcuminoids from the roots of *Curcuma longa*, *Curcuma* species and dietary supplements using an UPLC-UV-MS method, *J. Chrom. Separ. Tech.* 3 (1) (2012).
- [49] D.D. Heath, M.A. Pruitt, D.E. Brenner, C.L. Rock, Curcumin in plasma and urine: quantitation by high-performance liquid chromatography, *J. Chromatogr. B* 783 (2003) 287–295.
- [50] Y. Pak, R. Patek, M. Mayersohn, Sensitive and rapid isocratic liquid chromatography method for the quantitation of curcumin in plasma, *J. Chromatogr. B* 2 (2003) 339–346.
- [51] D.D. Heath, M.A. Pruitt, D.E. Brenner, A.N. Begum, S.A. Frautschy, C.L. Rock, Tetrahydrocurcumin in plasma and urine: quantitation by high performance liquid chromatography, *J. Chromatogr. B* 824 (2005) 206–212.
- [52] K. Hao, X.P. Zhao, X.Q. Liu, G.J. Wang, LC determination of curcumin in dog plasma for a pharmacokinetic study, *Chromatographia* 64 (2006) 531–535.
- [53] A. Liu, H. Lou, L. Zhao, P. Fan, Validated LC/MS/MS assay for curcumin and tetrahydrocurcumin in rat plasma and application to pharmacokinetic study of phospholipid complex of curcumin, *J. Pharm. Biomed. Anal.* 40 (2006) 720–727.

- [54] K. Maiti, K. Mukherjee, A. Gantait, B.P. Saha, P.K. Mukherjee, Curcumin-phospholipid complex: preparation, therapeutic evaluation and pharmacokinetic study in rats, *Int. J. Pharm.* 330 (2007) 155–163.
- [55] K.-Y. Yang, L.-C. Lin, T.-Y. Tseng, S.-C. Wang, T.-H. Tsai, Oral bioavailability of curcumin in rat and the herbal analysis from *Curcuma longa* by LC–MS/MS, *J. Chromatogr. B* 853 (2007) 183–189.
- [56] Z. Ma, A. Shayeganpour, D.R. Brocks, A. Lavasanifar, J. Samuel, High-performance liquid chromatography analysis of curcumin in rat plasma: application to pharmacokinetics of polymeric micellar formulation of curcumin, *Biomed. Chromatogr.* 21 (2007) 546–552.
- [57] T.H. Marczylo, R.D. Verschoyle, D.N. Cooke, P. Morazzoni, W.P. Steward, A.J. Gescher, Comparison of systemic availability of curcumin with that of curcumin formulated with phosphatidylcholine, *Cancer Chemother. Pharmacol.* 60 (2007) 171–177.
- [58] S.K. Vareed, M. Kakarala, M.T. Ruffin, J.A. Crowell, D.P. Normolle, Z. Djuric, D.E. Brenner, Pharmacokinetics of curcumin conjugate metabolites in healthy human subjects, *Cancer Epidemiol. Biomarkers Prev.* 17 (2008) 1411–1417.
- [59] B. Antony, B. Merina, V.S. Iyer, N. Yudi, K. Lennertz, S. Loyal, A pilot cross-over study to evaluate human bioavailability of BCM-95R CG (Biocurmax™), a novel bioenhanced preparation of curcumin, *Indian J. Pharm. Sci.* 70 (4) (2008) 445–449.
- [60] P. Sethi, V.K. Dua, S. Mohanty, S.K. Mishra, R. Jain, G. Edwards, Development and validation of a reversed phase HPLC method for simultaneous determination of curcumin and piperine in human plasma for application in clinical pharmacological studies, *J. Liq. Chrom. Rel. Technol.* 32 (2009) 2961–2974.
- [61] J. Li, Y. Jiang, J. Wen, G. Fan, Y. Wu, C. Zhang, A rapid and simple HPLC method for the determination of curcumin in rat plasma: assay development, validation and application to a pharmacokinetic study of curcumin liposome, *Biomed. Chromatogr.* 23 (2009) 1201–1207.
- [62] U.V.R.V. Saradhi, Y. Ling, J. Wang, M. Chiu, E.B. Schwartz, J.R. Fuchs, K.K. Chan, Z. Liu, A liquid chromatography–tandem mass spectrometric method for quantification of curcuminoids in cell medium and mouse plasma, *J. Chromatogr. B* 878 (2010) 3045–3051.
- [63] S.P. Singh, W. Wahajuddin, G.K. Jain, Determination of curcumin in rat plasma by liquid–liquid extraction using LC–MS/MS with Electrospray Ionization: assay development, validation and application to a pharmacokinetic study, *J. Bioanal. Biomed.* 2 (4) (2010) 79–84.
- [64] V. Kakkar, S. Singh, D. Singla, S. Sahwney, A.S. Chauhan, G. Singh, I.P. Kaur, Pharmacokinetic applicability of a validated liquid chromatography tandem mass spectroscopy method for orally administered curcumin loaded solid lipid nanoparticles to rats, *J. Chromatogr. B* 878 (2010) 3427–3431.
- [65] Y.-R. Han, J.-J. Zhu, Y.-R. Wang, X.-S. Wang, Y.-H. Liao, A simple RP-HPLC method for the simultaneous determination of curcumin and its prodrug, curcumin didecanoate, in rat plasma and the application to pharmacokinetic study, *Biomed. Chromatogr.* 25 (2011) 1144–1149.
- [66] R. Li, X. Qiao, Q. Li, R. He, M. Ye, C. Xiang, X. Lin, D. Guo, Metabolic and pharmacokinetic studies of curcumin, demethoxycurcumin and bisdemethoxycurcumin in mice tumor after intragastric administration of nanoparticle formulations by liquid chromatography coupled with tandem mass spectrometry, *J. Chromatogr. B* 879 (2011) 2751–2758.
- [67] Y.-M. Tsai, W.-C. Jan, C.-F. Chien, W.-C. Lee, L.-C. Lin, T.-H. Tsai, Optimised nano-formulation on the bioavailability of hydrophobic polyphenol, curcumin, in freely-moving rats, *Food Chem.* 127 (2011) 918–925.

- [68] W. Chen, P. Fan-Havard, L.D. Yee, Y. Cao, G.D. Stoner, K.K. Chan, Z. Liu, A liquid chromatography–tandem mass spectrometric method for quantification of curcumin–O–glucuronide and curcumin in human plasma, *J. Chromatogr. B* 900 (2012) 89–93.
- [69] Y.B. Pawar, G. Shete, D. Popat, A.K. Bansal, Phase behavior and oral bioavailability of amorphous Curcumin, *Eur. J. Pharm. Sci.* 47 (2012) 56–64.
- [70] M. Safdarian, P. Hashemi, M. Naderlou, In-line cold column trapping of organic phase in dispersive liquid–liquid microextraction: enrichment and determination of curcumin in human serum, *J. Chromatogr. A* 1244 (2012) 14–19.
- [71] N. Suwannateep, W. Banlunara, S.P. Wanichwecharungruang, K. Chiablaem, K. Lirdprapamongkol, J. Svasti, Mucoadhesive curcumin nanospheres: biological activity, adhesion to stomach mucosa and release of curcumin into the circulation, *J. Control. Release* 151 (2011) 176–182.
- [72] P. Vitaglione, R.B. Lumaga, R. Ferracane, I. Radetsky, I. Mennella, R. Schettino, S. Koder, E. Shimoni, V. Fogliano, Curcumin bioavailability from enriched bread: the effect of microencapsulated ingredients, *J. Agric. Food Chem.* 60 (2012) 3357–3366.
- [73] T. Jiang, L. Wang, S. Zhang, P.-C. Sun, C.-F. Ding, Y.-Q. Chu, P. Zhou, Interaction of curcumin with Al(III) and its complex structures based on experiments and theoretical calculations, *J. Mol. Struct.* 1004 (2011) 163–173.
- [74] H.J. Kim, Y.P. Jang, Direct analysis of curcumin in turmeric by DART-MS, *Phytochem. Anal.* 20 (2009) 372–377.
- [75] R. Hiserodt, T.G. Hartman, C.-T. Ho, R.T. Rosen, Characterization of powdered turmeric by liquid chromatography mass spectrometry and gas chromatography-mass spectrometry, *J. Chromatogr.* 740 (1996) 51–63.
- [76] P.J. Roughley, D.A. Whiting, Experiments in the biosynthesis of curcumin, *J. Chem. Soc. Perkin Trans. 1* (1973) 2379–2388.
- [77] F. Payton, P. Sandusky, W.L. Alworth, NMR Study of the solution structure of curcumin, *J. Nat. Prod.* 70 (2) (2007) 143–146.
- [78] B. Unterhalt, Curcuma und seine Verwendung im Speisesenf, *Z. Lebensm. Unters. Forsch.* 170 (1980) 425–428.
- [79] A.C. Gören, S. Çikrikçi, M. Çergel, G. Bilsel, Rapid quantitation of curcumin in turmeric via NMR and LC–tandem mass spectrometry, *Food Chem.* 113 (2009) 1239–1242.
- [80] J.J.B. Nevado, C.G. Cabanillas, A.M.C. Salcedo, Simultaneous determination of carminic acid, riboflavine, curcumin and erythrosine by derivative spectrophotometry and ratio spectra derivative, *Talanta* 41 (5) (1994) 789–797.
- [81] J.J.B. Nevado, J.R. Flores, M.J.V. Llerena, Simultaneous determination of tartrazine, riboflavine, curcumin and erythrosine by derivative spectrophotometry, *Fresenius J. Anal. Chem.* 350 (1994) 610–613.
- [82] W. Pothitirat, W. Gritsanapan, Quantitative analysis of curcumin, demethoxycurcumin and bisdemethoxycurcumin in the crude curcuminoid extract from *Curcuma longa* in Thailand by TLC–densitometry, *J. Pharm. Sci.* 32 (1–2) (2005) 23–30, Mahidol University.
- [83] K. Pundarikakshudu, H.N. Dave, Simultaneous determination of curcumin and berberine in their pure form and from the combined extracts of *Curcuma longa* and *Berberis aristata*, *Int. J. Appl. Sci. Eng.* 8 (1) (2010) 19–26.
- [84] K. Sharma, S.S. Agrawal, M. Gupta, Development and validation of UV spectrophotometric method for the estimation of curcumin in bulk drug and pharmaceutical dosage forms, *Int. J. Drug Dev. Res.* 4 (2) (2012) 375–380.
- [85] L. Peret-Almeida, A.P.F. Cherubino, R.J. Alves, L. Dufosse, M.B.A. Gloria, Separation and determination of the physico-chemical characteristics of curcumin, demethoxycurcumin and bisdemethoxycurcumin, *Food Res. Int.* 38 (2005) 1039–1044.

- [86] A.N. Diaz, M.C.R. Peinado, Fluorometric determination of curcumin in yogurt and mustard, *J. Agric. Food Chem.* 40 (1992) 56–59.
- [87] Turmeric, Javanese, *Curcuma xanthorrhizae* rhizoma, European Pharmacopoeia 5th ed., European Directorate for the Quality of Medicines (EDQM), Strasbourg, France, 2004, 2645.
- [88] V. Pathania, A.P. Gupta, B. Singh, Improved HPTLC method for determination of curcuminoids from *Curcuma longa*, *J. Liq. Chromatogr. Rel. Technol.* 29 (2006) 877–887.
- [89] K. Ashraf, M. Mujeeb, A. Ahmad, M. Amir, M.N. Mallick, D. Sharma, Validated HPTLC analysis method for quantification of variability in content of curcumin in *Curcuma longa* L (turmeric) collected from different geographical region of India, *Asian Pac. J. Trop. Biomed.* 2 (2) (2012) S584–S588.
- [90] M. Paramasivam, M.W. Aktar, R. Poi, H. Banerjee, A. Bandyopadhyay, Occurrence of curcuminoids in *Curcuma longa*: a quality standardization by HPTLC, *Bangladesh J. Pharmacol.* 3 (2008) 55–58.
- [91] S. Sheikh, S. Asghar, S. Ahmad, Development of HPTLC method and its validation for the estimation of curcuminoids from polyherbal mouth ulcer gel formulation, *IOSR J. Pharm.* 3 (1) (2013) 29–34.
- [92] S. Revathy, S. Elumalai, M. Benny, B. Antony, Isolation, purification and identification of curcuminoids from turmeric (*Curcuma longa* L.) by column chromatography, *J. Exp. Sci.* 2 (7) (2011) 21–25.
- [93] N. Asakawa, M. Tsuno, T. Hattori, M. Ueyama, A. Shinoda, Y. Miyake, K. Kagei, Determination of curcumin content of turmeric by high performance liquid chromatography, *Yakugaku Zasshi* 101 (4) (1981) 374–377.
- [94] S.J. Taylor, I.J. McDowell, Determination of the curcuminoid pigments in Turmeric (*Curcuma domestica* Val) by reversed-phase high-performance liquid chromatography, *Chromatographia* 34 (1/2) (1992) 73–77.
- [95] G.K. Jayaprakasha, L.J.M. Rao, K.K. Sakariah, Improved HPLC method for the determination of curcumin, demethoxycurcumin, and bisdemethoxycurcumin, *J. Agric. Food Chem.* 50 (2002) 3668–3672.
- [96] B.-K. Jadhav, K.-R. Mahadik, A.-R. Paradkar, Development and validation of improved reversed phase-HPLC method for simultaneous determination of curcumin, demethoxycurcumin and bis-demethoxycurcumin, *Chromatographia* 65 (2007) 483–488.
- [97] R.M. Smith, B.A. Witowska, Comparison of detectors for the determination of curcumin in turmeric by high-performance liquid chromatography, *Analyst* 109 (1984) 259–261.
- [98] K. Inoue, C. Nomura, S. Ito, A. Nagatsu, T. Hino, H. Oka, Purification of curcumin, demethoxycurcumin, and bisdemethoxycurcumin by high-speed countercurrent chromatography, *J. Agric. Food Chem.* 56 (2008) 9328–9336.
- [99] R.L. Rouseff, High performance liquid chromatographic separation and spectral characterization of the pigments in turmeric and annatto, *J. Food Sci.* 53 (6) (1988) 1823–1826.
- [100] R. Bos, T. Windono, H.J. Woerdenbag, Y.L. Boersma, A. Koulman, O. Kayser, HPLC-photodiode array detection analysis of curcuminoids in curcuma species indigenous to Indonesia, *Phytochem. Anal.* 18 (2007) 118–122.
- [101] Y. Xie, Z.-H. Jiang, H. Zhoua, X. Cai, Y.-F. Wong, Z.-Q. Liu, Z.-X. Bian, H.-X. Xu, L. Liu, Combinative method using HPLC quantitative and qualitative analyses for quality consistency assessment of a herbal medicinal preparation, *J. Pharm. Biomed. Anal.* 43 (2007) 204–212.
- [102] P.P. Dandekar, V.B. Patravale, Development and validation of a stability-indicating LC method for curcumin, *Chromatographia* 69 (2009) 871–877.



- [103] C.E. Green, S.L. Hibbert, Y.A. Bailey-Shaw, L.A.D. Williams, S. Mitchell, E. Garraway, Extraction, processing, and storage effects on curcuminoids and oleoresin yields from *Curcuma longa* L. grown in Jamaica, *J. Agric. Food Chem.* 56 (2008) 3664–3670.
- [104] W. Wicitnithad, N. Jongaroonngamsang, S. Pummangura, P. Rojsitthisak, A Simple isocratic HPLC method for the simultaneous determination of curcuminoids in commercial Turmeric extracts, *Phytochem. Anal.* 20 (2009) 314–319.
- [105] K.V. Nagappan, S.N. Meyyanathan, R.B. Raja, E. Kannan, A liquid chromatography method for the simultaneous determination of curcumin and piperine in food products using Diode Array Detection, *Asian J. Res. Chem.* 2 (2) (2009) 115–118.
- [106] F.-L. Yen, T.-H. Wu, C.-W. Tzeng, L.-T. Lin, C.-C. Lin, Curcumin nanoparticles improve the physicochemical properties of curcumin and effectively enhance its antioxidant and antihepatoma activities, *J. Agric. Food Chem.* 58 (2010) 7376–7382.
- [107] X. Sun, C. Gao, W. Cao, X. Yang, E. Wang, Capillary electrophoresis with amperometric detection of curcumin in Chinese herbal medicine pretreated by solid-phase extraction, *J. Chromatogr. A* 962 (2002) 117–125.
- [108] M. Lechtenberg, B. Quandt, A. Nahrstedt, Quantitative determination of curcuminoids in curcuma rhizomes and rapid differentiation of *Curcuma domestica* Val. and *Curcuma xanthorrhiza* Roxb. by capillary electrophoresis, *Phytochem. Anal.* 15 (2004) 152–158.
- [109] K. Maráková, P. Mikuš, J. Piešťanský, E. Havránek, Determination of curcuminoids in substances and dosage forms by cyclodextrin-mediated capillary electrophoresis with diode array detection, *Chem. Pap.* 65 (4) (2011) 398–405.
- [110] T. Watanabe, T.K. Mazumder, A. Yamamoto, S. Nagai, S. Terabe, Separation and determination of curcuminoids in turmeric samples by micellar electrokinetic chromatography with a high molecular mass surfactant, *Nippon Shokuhin Kagaku Kogaku Kaishi* 47 (10) (2000) 780–786.
- [111] T. Nhujak, W. Saisuwan, M. Srisa-art, A. Petsom, Microemulsion electrokinetic chromatography for separation and analysis of curcuminoids in turmeric samples, *J. Sep. Sci.* 29 (2006) 666–676.
- [112] A. Hassaninasab, Y. Hashimoto, K. Tomita-Yokotani, M. Kobayashi, Discovery of the curcumin metabolic pathway involving a unique enzyme in an intestinal microorganism, *Proc. Natl. Acad. Sci. U.S.A.* 108 (2010) 6615–6620. <http://www.pnas.org/content/early/2011/04/04/1016217108.full.pdf>.
- [113] N.K. Gupta, A. Nahata, V.K. Dixit, Development of a spectrofluorometric method for the determination of curcumin, *Asian J. Tradit. Med.* 5 (1) (2010) 12–18.
- [114] A. Tapal, P.K. Tikku, Complexation of curcumin with soy protein isolate and its implications on solubility and stability of curcumin, *Food Chem.* 130 (2012) 960–965.
- [115] Z. Chen, L. Zhu, T. Song, J. Chen, Z. Guo, A novel curcumin assay with the metal ion Cu (II) as a simple probe by resonance light scattering technique, *Spectrochim. Acta A* 72 (2009) 518–522.
- [116] L.A. May, E. Tourkina, S.R. Hoffman, T.A. Dix, Detection and quantitation of curcumin in mouse lung cell cultures by matrix-assisted laser desorption ionization time of flight mass spectrometry, *Anal. Biochem.* 337 (2005) 62–69.



# Dasatinib

Hesham M. Korashy<sup>\*</sup>, A.F.M. Motiur Rahman<sup>†</sup>,  
Mohammed Gabr Kassem<sup>†</sup>

<sup>\*</sup>Department of Pharmacology and Toxicology, College of Pharmacy, King Saud University, Riyadh, Saudi Arabia

<sup>†</sup>Department of Pharmaceutical Chemistry, College of Pharmacy, King Saud University, Riyadh, Saudi Arabia

## Contents

1. Introduction	205
1.1 Nomenclature	206
1.2 Formula	206
1.3 Elemental analysis	207
1.4 Physical properties	207
1.5 Uses and applications	207
2. Methods of Preparation	207
3. Physical Properties	214
3.1 Spectroscopy	214
3.2 Mass spectrum	218
4. Methods of Analysis	220
4.1 Chromatographic methods	220
4.2 Colorimetric methods	228
4.3 UV spectrophotometric methods	229
5. Pharmacology	229
5.1 Pharmacokinetics	229
5.2 Pharmacodynamics	231
5.3 Toxicities	231
Acknowledgment	232
References	232



## 1. INTRODUCTION

Tyrosine kinase inhibitors (TKIs) are a class of small molecule drugs that block the intracellular signals which drive proliferation in many malignant cells by specifically inhibiting the kinase function of individual intracellular pathways involved in receptor-mediated growth signaling [1]. Dasatinib (BMS-354825, Sprycel<sup>TM</sup>), is a thiazole-based ATP-competitive,

dual Src/Abl kinase inhibitor [2], approved for the treatment of imatinib-resistant and imatinib-intolerant patients across all phases of chronic myelogenous leukemia (CML) [3].

## 1.1. Nomenclature

### 1.1.1 Systematical chemical names

*N*-(2-chloro-6-methylphenyl)-2-((6-(4-(2-hydroxyethyl)piperazin-1-yl)-2-methylpyrimidin-4-yl)amino)thiazole-5-carboxamide [4,5]

*N*-(2-chloro-6-methylphenyl)-2-[[6-[4-(2-hydroxyethyl)-1-piperazinyl]-2-methyl-4-pyrimidinyl]amino]-1,3-thiazole-5-carboxamide [6,7]

*N*-(2-chloro-6-methylphenyl)-2-({6-[4-(2-hydroxyethyl)piperazin-1-yl]-2-methylpyrimidin-4-yl}amino)-1,3-thiazole-5-carboxamide [8]

### 1.1.2 Nonproprietary names

Dasatinib

Synonyms: BMS-354825 [9–11]

### 1.1.3 Proprietary names

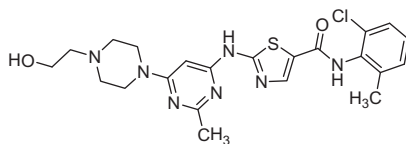
Sprycel [9–11]

## 1.2. Formula

### 1.2.1 Empirical formula, molecular weight, obtained mass and CAS number

Chemical formula:  $C_{22}H_{26}ClN_7O_2S$ , molecular weight: 488.0055, exact mass: 487.1557, monoisotopic mass: 487.155721508,  $m/z$ : 487.7  $[M+H]^+$  (obtained),  $m/z$ : 488.1635  $[M+H]^+$  [6], CAS no. 302962-49-8 [6,9–12]

### 1.2.2 Structural formula



Dasatinib

### 1.2.3 SMILES

CC1=NC(NC2=NC=C(S2)C(=O)NC2=C(C)C=CC=C2Cl)=CC(=N1)N1CCN(CCO)CC1 [13]

### 1.2.4 InChI

1S/C22H26ClN7O2S/c1-14-4-3-5-16(23)20(14)28-21(32)17-13-24-22(33-17)27-18-12-19(26-15(2)25-18)30-8-6-29(7-9-30)10-11-31/h3-5,12-13,31H,6-11H2,1-2H3,(H,28,32)(H,24,25,26,27) [13]

## 1.3. Elemental analysis

Elemental analysis: C, 54.15%; H, 5.37%; Cl, 7.26%; N, 20.09%; O, 6.56%; S, 6.57% (calculated); C, 53.90%; H, 5.30%; N, 20.07% [3]; C, 54.17%; H, 5.38%; N, 20.09% [14].

## 1.4. Physical properties

### 1.4.1 Appearance

White powder

### 1.4.2 Solubility

Water solubility: 0.0128 mg/mL

### 1.4.3 Melting point

285 °C, 280–286 °C [9], 279–280 °C [6], 285.25–286.28 °C [4]

### 1.4.4 Dissociation constant

pK<sub>a</sub>: 10.28 [9]

### 1.4.5 Partition coefficient

(*P* is the partition coefficient of the molecule in the water–octanol system)  
log *P*: 1.8 [9]

## 1.5. Uses and applications

Dasatinib, as protein TKI, works by blocking the action of an abnormal protein that signals cancer cells to multiply. This helps to stop the spread of cancer cells [15].



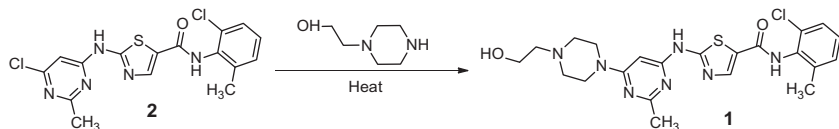
## 2. METHODS OF PREPARATION

In most of the reports [2,4,6,16,17], synthesis of dasatinib (**1**) involves the reaction of *N*-(2-chloro-6-methylphenyl)-2-(6-chloro-2-methylpyrimidin-4-ylamino)-1,3-thiazole-5-carboxamide **2** with 1-(2-hydroxyethyl) piperazine by heating the mixture at 80 °C refluxing in

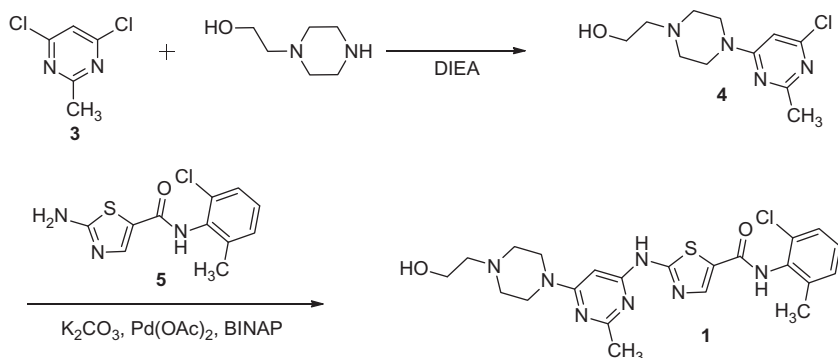
dioxane or in presence of base, most likely *N,N*-Diisopropylethylamine (DIEA) in *tert*-butanol at 118 °C (Scheme 4.1).

The detailed synthetic procedures have been illustrated below for the synthesis of dasatinib. In 2006 [16], McIntyre *et al.* reported that the reaction of 4,6-dichloro-2-methylpyrimidine **3** with 1-(2-hydroxyethyl) piperazine in the presence of DIEA in  $\text{CH}_2\text{Cl}_2$  afforded the pyrimidine derivative **4**, which was then condensed with the aminothiazole derivative **5** in the presence of  $\text{K}_2\text{CO}_3$ ,  $\text{Pd}(\text{OAc})_2$ , and 2,2'-bis(diphenylphosphino)-1,1'-binaphthyl (BINAP) in toluene at 100 °C to obtain dasatinib (Scheme 4.2).

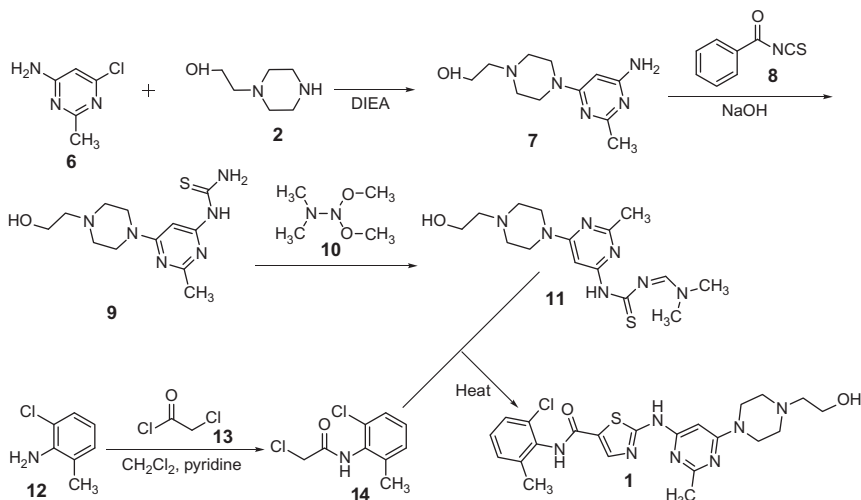
Later, they claimed other procedures [16,18] for the synthesis of dasatinib **1**. Treatment of 4-amino-6-chloro-2-methylpyrimidine **6** with 1-(2-hydroxyethyl) piperazine in the presence of DIEA in  $\text{CH}_2\text{Cl}_2$  affords the pyrimidine derivative **7**, which after reaction with benzoyl isothiocyanate **8** in  $\text{CHCl}_3$  followed by hydrolysis with aqueous NaOH in MeOH provided the thiourea intermediate **9**. Condensation of compound **9** with *N,N*-dimethylformamide dimethyl acetal **10** in EtOH at 73 °C yields compound **11**, which was finally reacted with 2-chloro-*N*-(2-chloro-6-methylphenyl) acetamide **14** (prepared by acylation of the aniline derivative **12** with chloroacetyl chloride **13** in the presence of *N*-Methylmorpholine in acetone) in refluxing MeOH to give dasatinib **1** (Scheme 4.3).



**Scheme 4.1** Synthesis of dasatinib (**1**) from carboxamide (**2**).



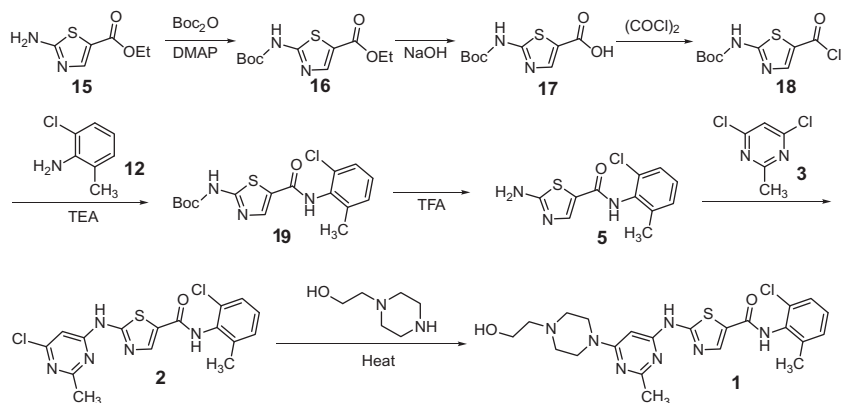
**Scheme 4.2** Synthesis of dasatinib (**1**) from 4,6-dichloro-2-methylpyrimidine (**3**) [4,16].



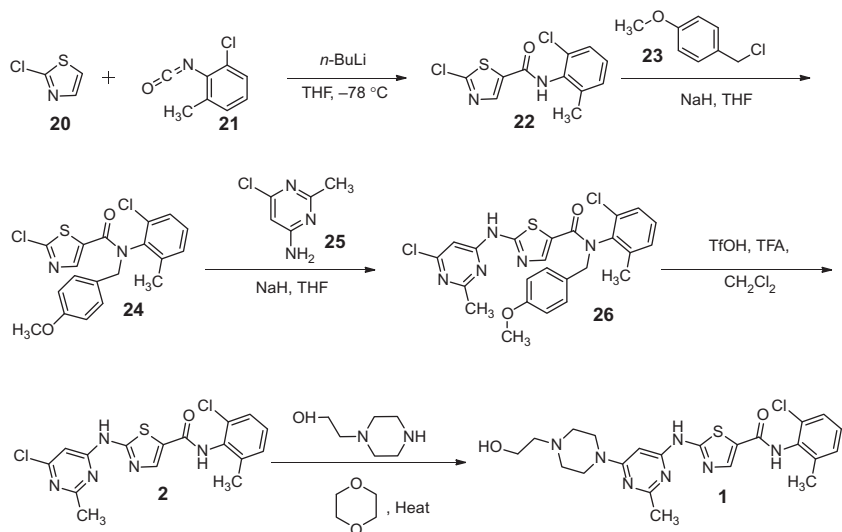
**Scheme 4.3** Synthesis of dasatinib **1** from 4-amino-6-chloro-2-methylpyrimidine **6** [16,18].

Intermediate **2** can be synthesized by several different procedures [14,16,17,19,20]; protection of ethyl 2-aminothiazole-5-carboxylate **15** with Boc<sub>2</sub>O and DMAP in THF gives compound **16**, which was hydrolyzed with NaOH in THF/MeOH to yield the corresponding carboxylic acid derivative **17**. Reaction of compound **17** with oxalyl chloride in THF affords the acyl chloride **18**, which was condensed with 2-chloro-6-methylaniline **12** in the presence of TEA in CH<sub>2</sub>Cl<sub>2</sub> to give **19**. Deprotection of compound **19** by TFA gives the 2-aminothiazole derivative **5**, which was finally reacted with 4,6-dichloro-2-methylpyrimidine **3** with strong base NaH in THF to give intermediate **2**. This intermediate **2** was then reacted with 1-(2-hydroxyethyl)piperazine and dasatinib **1** was obtained (Scheme 4.4).

Reaction of 2-chlorothiazole **20** with 2-chloro-6-methylphenylisocyanate **21** in presence of *n*-butyl lithium in THF at  $-78^{\circ}\text{C}$  produces 2-chloro-*N*-(2-chloro-6-methylphenyl)thiazole-5-carboxamide **22**, which was then N-protected with 4-methoxybenzyl chloride **23** using base (NaH) in THF to yield compound **24**. Reaction of **24** with 4-amino-6-chloro-2-methylpyrimidine **25** in presence of NaH in THF affords the adduct **26**, which was then deprotected using TfOH/TFA in CH<sub>2</sub>Cl<sub>2</sub> to obtain intermediate **2**. This intermediate **2** reacted with 1-(2-hydroxyethyl)piperazine in dioxane and gave dasatinib **1** (Scheme 4.5) [2,6,16].

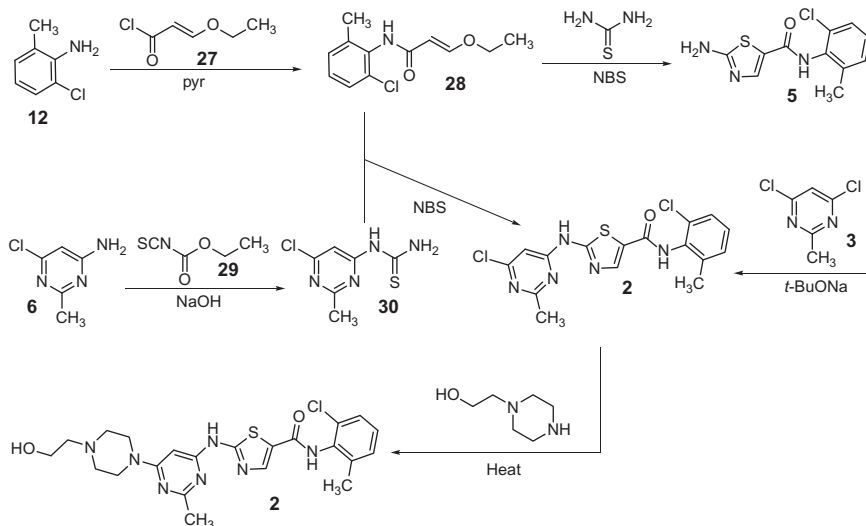


**Scheme 4.4** Synthesis of dasatinib **1** from ethyl 2-aminothiazole-5-carboxylate **15** [14,16,17,19,20].



**Scheme 4.5** Synthesis of dasatinib **1** from 2-chlorothiazole **20** [2,6,16].

Condensation of 2-chloro-6-methylaniline **12** with 2-ethoxyacryloyl chloride **27** in pyridine/THF gave the corresponding acrylamide derivative **28**, which was cyclized with thiourea in presence of *N*-bromosuccinimide (NBS) in hot dioxane to yield 2-amino-*N*-(2-chloro-6-methylphenyl)thiazole-5-carboxamide **5**. Compound **5** was then condensed with 4,6-dichloro-2-methylpyrimidine **3** in presence of base (*t*-BuONa) in THF to obtain intermediate **2**. On the other hand, reaction of 4,6-dichloro-2-methylpyrimidine **3** with ethyl isothiocyanatoformate **29** in



**Scheme 4.6** Synthesis of dasatinib **1** from 2-chloro-6-methylaniline **12** [4,16].

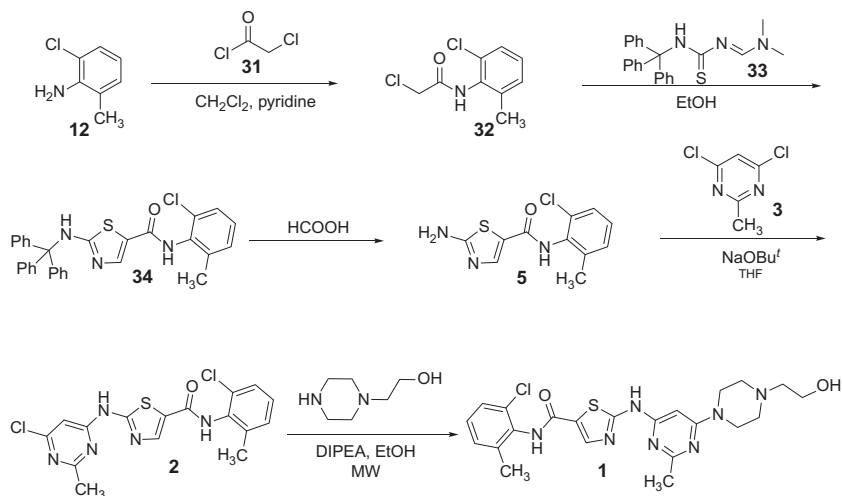
THF at refluxing followed by hydrolysis in 1 M NaOH at 50 °C yields the thiourea derivative **30**; later, compound **30** was finally cyclized with the acrylamide **28** in presence of NBS in THF/H<sub>2</sub>O to give the same intermediate **2** [2,5,10]. This intermediate **2** later reacted with 1-(2-hydroxyethyl)piperazine and gave dasatinib **1** (Scheme 4.6).

Reaction of 2-chloro-6-methylaniline **12** with chloroacetyl chloride **31** in pyridine/CH<sub>2</sub>Cl<sub>2</sub> gave compound **32**, which was reacted with thiourea derivative **33** in ethanol to yield triphenyl methyl protected 2-amino-*N*-(2-chloro-6-methylphenyl)thiazole-5-carboxamide **34** followed by deprotection using formic acid to obtain **5**. Compound **5** was then condensed with 4,6-dichloro-2-methylpyrimidine **3** in presence of base (*t*-BuONa) in THF to obtain intermediate **2**. This intermediate **2** later reacted with 1-(2-hydroxyethyl)piperazine and gave dasatinib **1** (Scheme 4.7) [21].

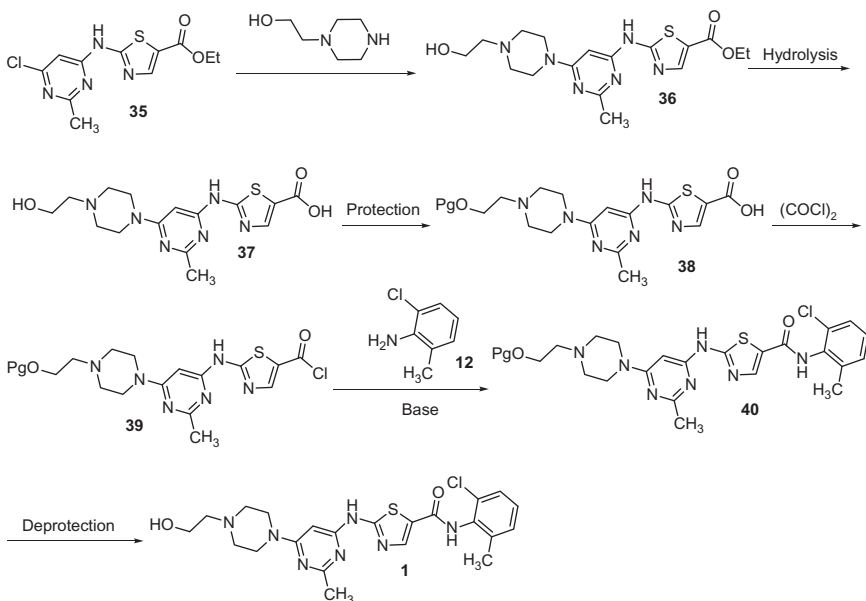
Reaction of 2-(4-chloro-2-methyl-6-pyrimidinylamino)thiazole-5-ethylcarboxylate **35** with 1-(2-hydroxyethyl)piperazine gave compound **36**, which was then hydrolyzed to get acid **37** followed by protection of **37** to obtain **38**. The acid **38** was converted to its corresponding acid chloride **39**, subsequently reacted with compound **12** to obtain hydroxy-protected dasatinib **40**. Deprotection of hydroxy group **40** gave dasatinib **1** (Scheme 4.8) [20].

Reaction of **3** with 1-(2-hydroxyethyl)piperazine gave compound **4**, which after protection gave **41**, which was reacted with 2-amino-



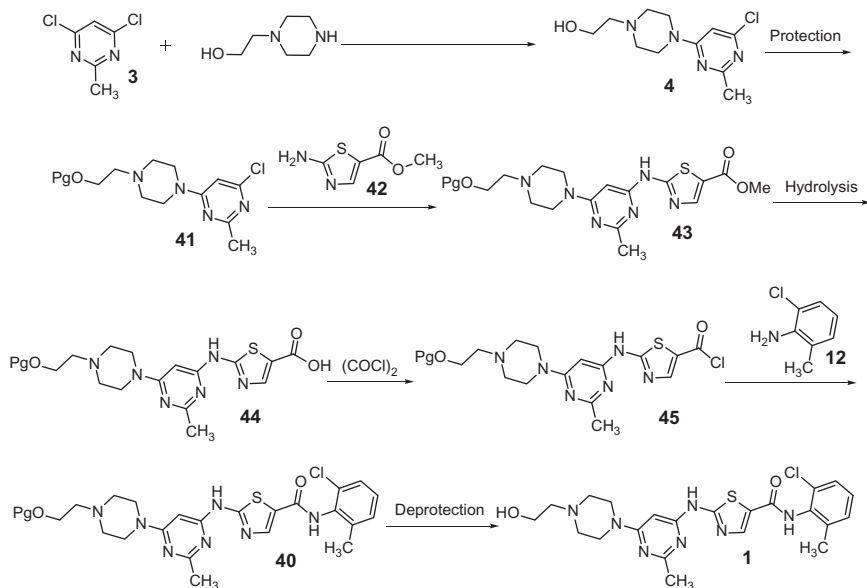


**Scheme 4.7** Synthesis of dasatinib **1** from 2-chloro-6-methylaniline **12** [21].

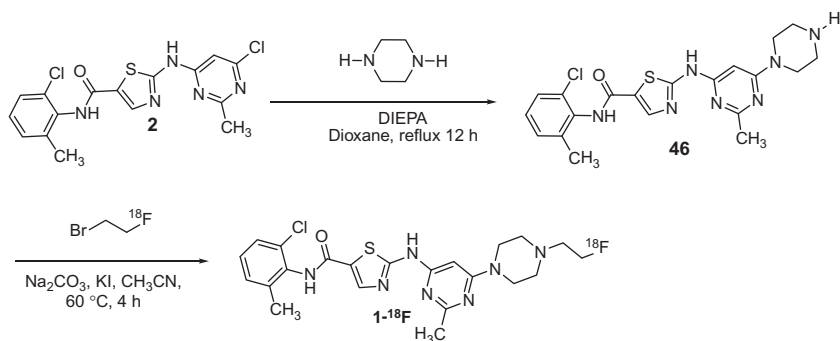


**Scheme 4.8** Synthesis of dasatinib **1** from carboxylate **35** [20].

5-methylcarboxylate **42** to obtain **43**. Compound **43** was hydrolyzed, followed by acid chloride formation for the reaction with compound **12** to obtain protected dasatinib **40**, which was then deprotected to get dasatinib **1** (Scheme 4.9) [21].



**Scheme 4.9** Synthesis of dasatinib **1** from 4,6-dichloro-2-methylpyrimidine **3** [21].



**Scheme 4.10** Synthesis of fluorine-18 derivative of dasatinib **1** [22].

Darren R. Veach *et al.* [22] synthesized the <sup>18</sup>F derivative of dasatinib from the intermediate **2**. Intermediate **2** was reacted with piperazine in the presence of DIEPA in dioxane to give *N*-(2-chloro-6-methylphenyl)-2-(2-methyl-6-(piperazin-1-yl)pyrimidin-4-ylamino)thiazole-5-carboxamide (**46**), which was then reacted with 1-bromo-2-fluoro (<sup>18</sup>F) ethane to give <sup>18</sup>F derivative of dasatinib **1-<sup>18</sup>F** (Scheme 4.10).



### 3. PHYSICAL PROPERTIES

#### 3.1. Spectroscopy

##### 3.1.1 Ultraviolet spectroscopy

The ultraviolet/visible (UV/VIS) absorption spectrum of dasatinib was recorded for selecting the proper maximum absorption peak ( $\lambda_{\max}$ ). Using a UV/VIS spectrometer (Varian Cary 50 Conc UV/VIS spectrophotometer), the absorption spectrum of dasatinib in ethanol was scanned from 200 to 400 nm. As shown in Figure 4.1, the  $\lambda_{\max}$  of dasatinib is located at 321 nm.

##### 3.1.2 Vibrational spectroscopy

###### 3.1.2.1 IR spectroscopy of dasatinib

The infrared absorption spectrum of dasatinib was obtained in a KBr pellet, using a Shimadzu infrared spectrophotometer. The IR spectrum is shown in Figure 4.2. The principal peaks were observed at 3418, 3200, 2946, 2815, 1620, 1582, 1513, 1456, 1391, 1294, 1216, 1194, 1004, 862, 814, 773, and 591  $\text{cm}^{-1}$ . Assignments for the major infrared absorption band are provided in Table 4.1.

##### 3.1.3 Nuclear magnetic resonance spectrometry

$^1\text{H}$  and  $^{13}\text{C}$  NMR spectra of dasatinib (shown in Figures 4.3 and 4.4, respectively) were obtained using a Bruker 500 MHz NMR spectrometer.

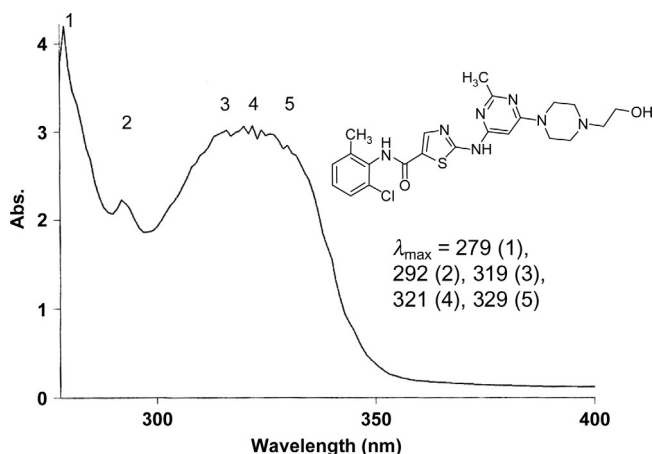


Figure 4.1 UV spectrum of dasatinib ( $1 \times 10^{-4}$  M solution in ethanol).

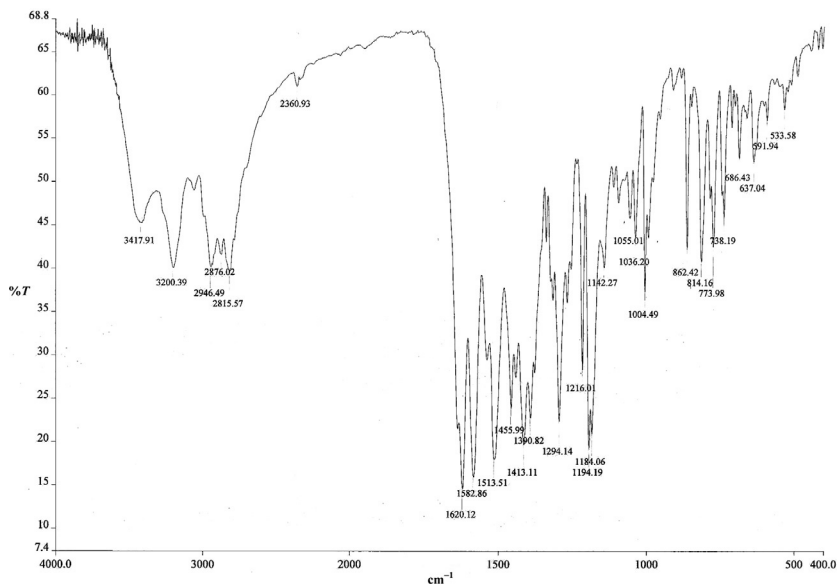


Figure 4.2 Infrared spectrum of dasatinib in KBr plate.

Table 4.1 Infrared spectroscopic data for dasatinib in KBr plate

Entry	Bond	Absorption peaks ( $\lambda_{\max}$ ) ( $\text{cm}^{-1}$ )	Appearance
1	C—Cl	773, 591	Strong
2	C—O	1110	Strong
3	—C—H, HC=CH (aryl)	1582, 1513, 1456, 1391	Strong
4	C=O	1620	Strong
5	CH <sub>2</sub> , C—H (alkyl)	2946	Strong
6	O—H	3200	Broad
7	N—H	3418	Broad

Chemical shifts were expressed in parts per million (ppm) (Table 4.2) with respect to the tetramethylsilane signal for  $^1\text{H}$  and  $^{13}\text{C}$  NMR.

### 3.1.3.1 $^1\text{H}$ NMR spectrum

$^1\text{H}$ -NMR (DMSO- $d_6$ , 500 MHz):  $\delta$  11.47 (s, 1H, NH), 9.88 (s, 1H, NH), 8.23 (s, 1H), 7.40 (d,  $J=6.5$  Hz, 1H, HAr), 7.29 (d,  $J=6.0$  Hz, 1H, HAr), 7.27 (t,  $J=7.5$  Hz, 1H, HAr), 6.06 (s, 1H), 4.45–4.36 (m, 1H), 3.52 (s, 4H),

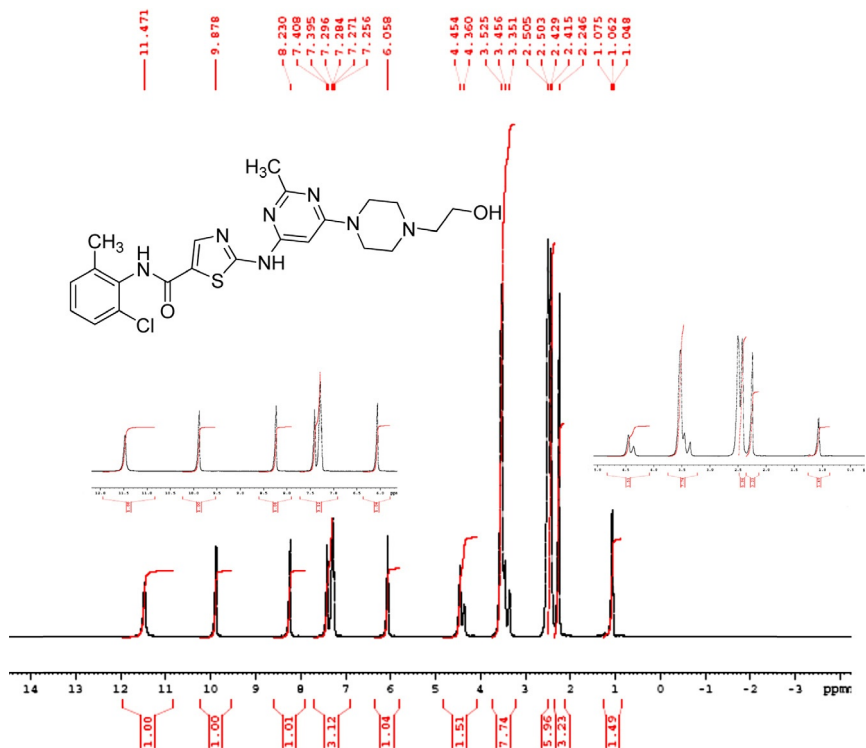


Figure 4.3 <sup>1</sup>H NMR spectra of dasatinib in DMSO-d<sub>6</sub>.

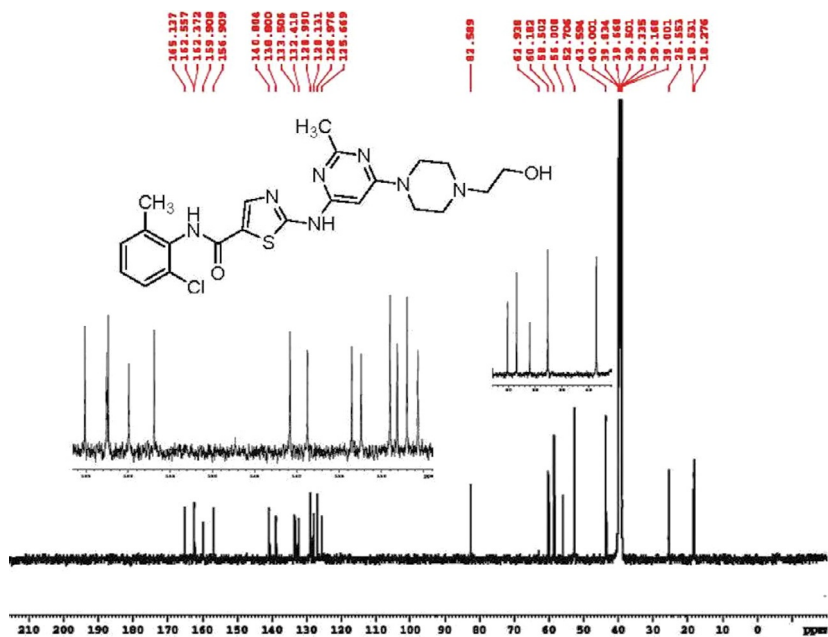


Figure 4.4 <sup>13</sup>C NMR spectrum of dasatinib in DMSO-d<sub>6</sub>.

**Table 4.2** Comparative study of  $^1\text{H}$  NMR spectra for dasatinib ( $\text{DMSO}-d_6$ ) with literature [6,14]

Entry	Chemical shift (500 MHz, $\text{DMSO}-d_6$ )	Chemical shift [14] (500 MHz, $\text{DMSO}-d_6$ )	Chemical shift [6] (400 MHz, $\text{DMSO}-d_6$ )
1	11.47 (s, 1H, NH)	11.48 (s, 1H) ( $\text{D}_2\text{O}$ exchangeable)	11.67 (br s, 1H)
2	—	—	10.50 (br s, 1H)
3	9.88 (s, 1H, NH)	9.88 (s, 1H) ( $\text{D}_2\text{O}$ exchangeable)	9.96 (s, 1H)
4	8.23 (s, 1H)	8.23 (s, 1H)	8.27 (s, 1H)
5	7.40 (d, $J=6.5$ Hz, 1H, HAr)	7.25–7.30 (m, 3H)	7.40 (d, $J=7.7$ Hz, 1H)
6	7.29 (d, $J=6.0$ Hz, 1H, HAr)		7.28 (dd, $J=6.6, 6.7$ Hz, 1H)
7	7.27 (t, $J=7.5$ Hz, 1H, HAr)		7.25 (d, $J=7.7$ Hz, 1H)
8	6.06 (s, 1H)	6.05 (s, 1H)	6.17 (s, 1H)
9	4.45–4.30 (m, 1H)	4.46 (s, 1H)	4.33 (d, $J=12.6$ Hz, 2H)
10	3.52 (s, 4H)	3.52–3.56 (q, 6H)	3.79 (dd, $J=5.0, 5.5$ Hz, 2H)
11	3.45–3.35 (m, 1H)	—	3.60 (d, $J=11.6$ Hz, 2H)
12	2.50 (s, 3H)	2.49–2.51 (m, 4H)	3.38 (dd, $J=12.1, 12.6$ Hz, 2H)
13	2.50 (m, 2H)		3.22–3.19 (m, 2H)
14	2.42 (s, 4H)	2.41–2.45 (s, 5H)	3.13–3.07 (m, 2H)
15	2.25 (s, 3H)	2.24 (s, 3H)	2.45 (s, 3H)
16	1.06 (t, $J=6.5$ Hz, 1H, —OH)		2.24 (s, 3H)

3.45–3.35 (m, 1H), 2.50 (s, 3H), 2.50 (m, 2H), 2.42 (s, 4H), 2.25 (s, 3H), and 1.06 (t,  $J=6.5$  Hz, 1H, —OH) ppm.

### 3.1.3.2 $^{13}\text{C}$ NMR spectrum

$^{13}\text{C}$  NMR ( $\text{DMSO}-d_6$ , 125 MHz):  $\delta$  165.14, 162.56, 162.37, 159.91, 156.91, 140.80, 138.80, 133.51, 132.42, 128.99, 128.13, 126.98, 125.67, 82.59, 60.18, 58.50, 56.01, 52.71, 43.60, 25.55, and 18.28 ppm.

$^{13}\text{C}$  NMR (DMSO- $d_6$ , 125 MHz):  $\delta$  165.7, 162.8, 162.1, 160.4, 157.5, 141.2, 139.4, 133.8, 133.0, 129.6, 128.8, 127.6, 126.5, 84.0, 58.1, 55.2, 51.1 (2), 41.2 (2), 25.7, 18.8 [3].

$^{13}\text{C}$  NMR (DMSO- $d_6$ , 125 MHz):  $\delta$  (ppm) 18.756, 26.034, 44.098, 53.186, 58.997, 60.658, 83.098, 126.157, 127.458, 128.612, 129.474, 132.910, 134.002, 139.285, 141.286, 157.410, 160.393, 162.964, 165.629 [9].

### 3.2. Mass spectrum

The mass spectral studies of dasatinib were carried out with an Agilent 6320 Ion Trap LC/MS system by infusion of 2  $\mu\text{g}$  of dasatinib solution in acetonitrile:H $_2\text{O}$  (1:1) without a column. Source parameters were as follows: temperature was 350  $^\circ\text{C}$ , gas flow was 12 L/min, and nebulizer was 60 psi. Figure 4.5 shows the mass spectrum for the parent compound ( $m/z=487.3$ ), and Figures 4.6 and 4.7 show the detailed mass fragmentation

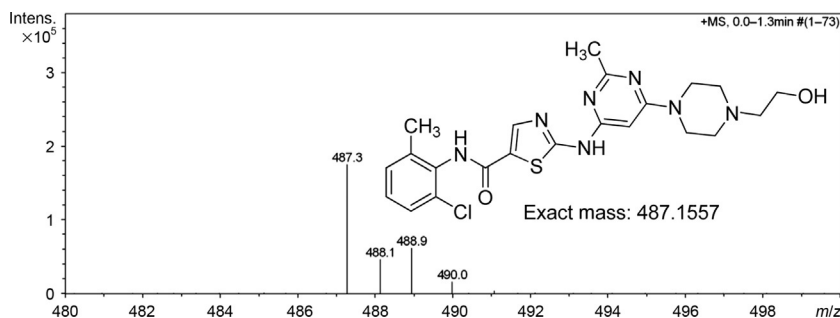


Figure 4.5 Dasatinib shows  $m/z=487.3$  [ $\text{M}(^{35}\text{Cl}) + \text{H}$ ] $^+$  molecular ion peak in positive mode.

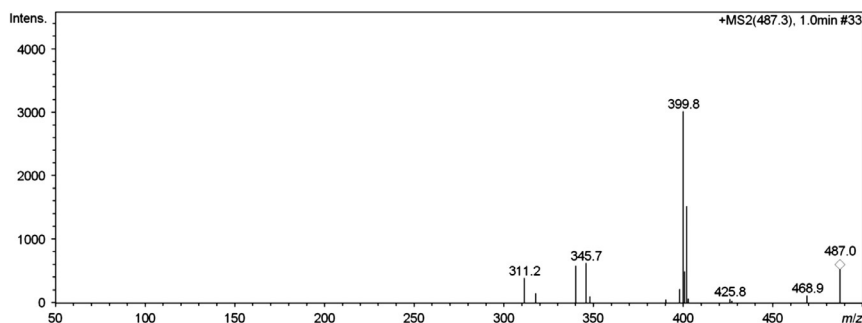
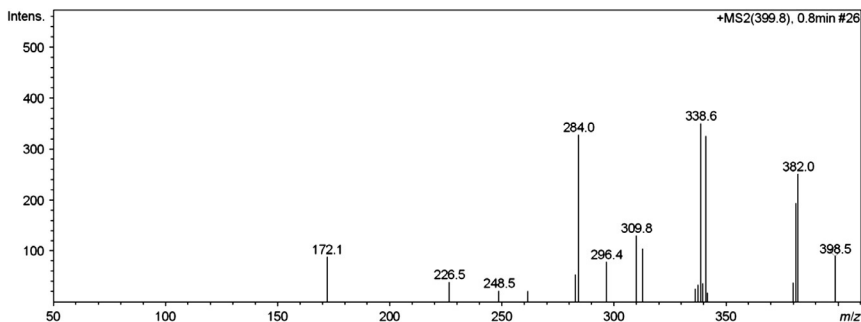
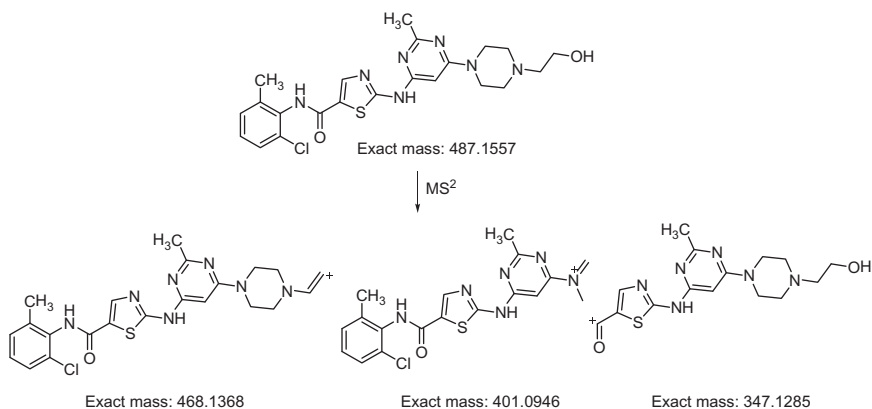


Figure 4.6 MS/MS spectrum of the  $m/z=487.3$  dasatinib fragment in the positive mode.



**Figure 4.7** MS/MS/MS spectrum of the dasatinib  $m/z=399.8$  fragment in the positive mode.



**Scheme 4.11** Possible MS/MS fragments of dasatinib for the  $m/z=487.3$  fragment.

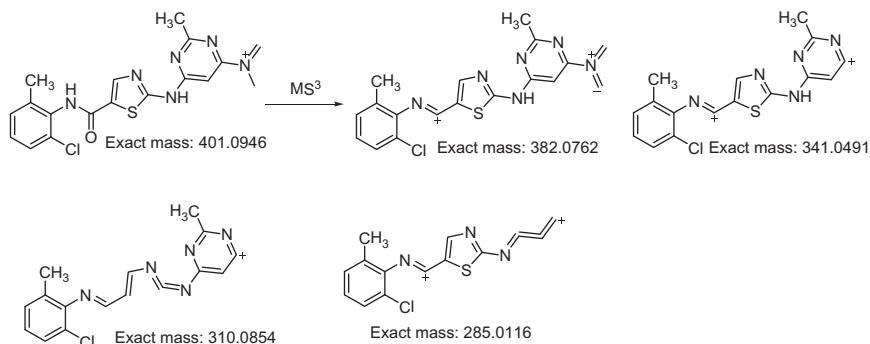
pattern interpretation of the drug substance. The reported  $m/z$  for dasatinib ( $C_{22}H_{26}ClN_7O_2S$ ) was ESI ( $M+1$ ): 490.27 [5], 488.1635 [ $M+H$ ]<sup>+</sup> [6], and the obtained  $m/z$  487.3 [ $M(^{35}Cl)+H$ ]<sup>+</sup>, the reported  $m/z$  488.9 is [ $M(^{37}Cl)+H$ ]<sup>+</sup>, while the calculated exact mass is 487.1557.

### 3.2.1 Fragmentation pattern of dasatinib

The MS/MS scan of the molecular ion peak of dasatinib shows three fragments at  $m/z$  468.9, 399.8, and 345.7 (Figure 4.6; Scheme 4.11).

The MS/MS/MS scan of the  $m/z=399.8$  fragment of dasatinib (Figure 4.7) yielded a number of peaks, including  $m/z=382.0$ , 338.6, 309.8, 296.4, 284.0, 248.5, 226.5, and 172.1. Fragments are shown in Scheme 4.12.





**Scheme 4.12** Possible fragments for the MS/MS/MS of dasatinib.



## 4. METHODS OF ANALYSIS

### 4.1. Chromatographic methods

#### 4.1.1 High-performance liquid chromatography/mass spectrometry

In recent years, numerous laboratories have reported the use of high-throughput bioanalytical procedures for the single and simultaneous quantification of plasma concentrations of antileukemia drugs [23–36]. High-performance liquid chromatography (HPLC) methods for the pharmacokinetics (PK) of imatinib have been well investigated [2,37–49]. Measurement of TKIs plasma concentrations, in fact, is a reliable tool to perform therapeutic drug monitoring (TDM); however, only the drugs fraction reaching the intracellular compartment is expected to exert action. Then a convenient correlation should be done, also, between clinical outcome and intracellular drug levels reached in treated patients. As variability in drug PK and inadequate patient compliance, also poor penetration of drugs into body compartments, particularly in leukocytes or peripheral blood mononuclear cell (PBMC), may contribute to the occurrence of subtherapeutic drug level, leading to loss of treatment efficacy. The mechanisms by which TKI drugs accumulate within cells remain generally unknown and very few data are published to date [2,50–52]. D'Avolio *et al.* [53] have described a new method using HPLC coupled with electrospray mass spectrometry for the quantification of PBMC concentration of TKIs imatinib, dasatinib, and nilotinib. A simple PBMC isolation and extraction procedure was applied on 10–14 mL of blood aliquots. Chromatographic separation of drugs and Internal Standard (quinoxaline) was achieved with a gradient (acetonitrile and water + formic acid 0.05%) on a C18 reverse-phase analytical

column with 25 min of analytical run, at a flow rate of 0.25 mL/min. Mean intra- and interday precision for all compounds were 8.76% and 12.20%, mean accuracy was  $-3.86\%$ , and extraction recovery ranged within 79% and 91%. Calibration curves ranged from 50.0 to 0.25 ng. The limit of quantification was set at 0.25 ng for all the analyzed drugs. This method allows a specific, sensitive, and reliable simultaneous intracellular determination of the three TKIs imatinib, dasatinib, and nilotinib in a single chromatographic run, useful for drugs estimation in PBMC of patients affected by CML.

#### 4.1.2 LC/MS/MS methods for simultaneous quantification of dasatinib and its metabolites

Furlong *et al.* [54] reported the development, validation, and successful application of the first liquid chromatography–tandem mass spectrometry method (LC/MS/MS) assay capable of quantifying dasatinib and two pharmacologically active metabolites M4 and M5 (Figures 4.8 and 4.9). Validation of the LC/MS/MS method was carried out in accordance with the FDA Guidance for Industry—Bioanalytical Method Validation [55] and Bristol–Myers Squibb Standard Operating Procedures. Accuracy, precision, and sensitivity were established in three core analytical runs for dasatinib and M5; a fourth analytical run was included for M4 due to insufficient M4 dilution quality control (QC) samples (3/6) passing for accuracy in one of the

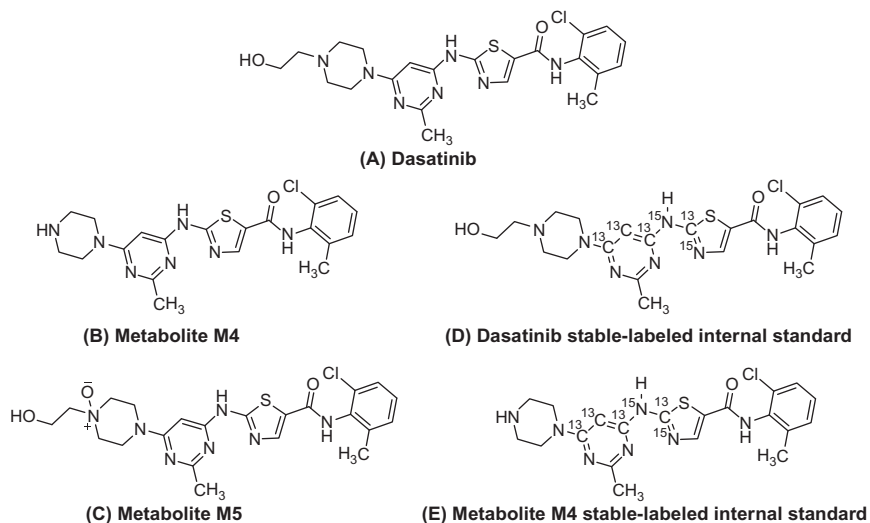


**Figure 4.8** Chemical structures of analytes and internal standards. The stable-labeled internal standard for dasatinib was used to quantify dasatinib and M5 [54].

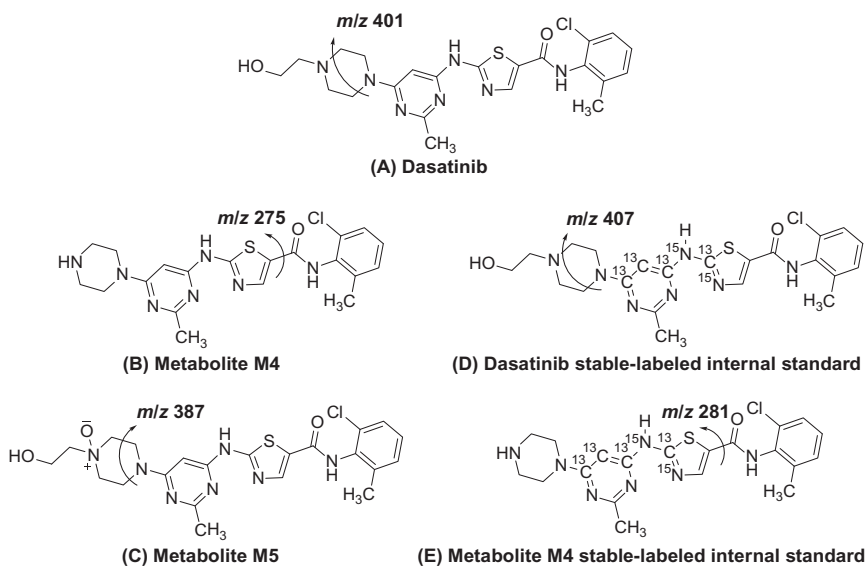


**Figure 4.9** Arrows indicate the proposed fragmentation pathways leading to the product ions monitored in the assay for dasatinib and its metabolites as well as stable-labeled internal standard [54].

three core analytical runs. The lower limit of quantitation was evaluated by spiking the three analytes into six unique human plasma lots at 1.00 ng/mL followed by extraction and quantification. Specificity was assessed for potential matrix interferences in six lots of blank human plasma by extraction and inspection of the resulting chromatograms for interfering peaks at the retention times of the three analytes and internal standards. Specificity was similarly assessed for potential internal standard-derived interferences using six lots of internal standard-spiked blank plasma. The recovery of dasatinib, M4, M5, and the internal standards from human plasma during extraction was determined at 50 and 800 ng/mL by comparing the response ratios in human plasma samples spiked with the analytes prior to extraction with those spiked postextraction. The matrix effect was determined at concentrations of 50 and 800 ng/mL for dasatinib, M4, M5, and the internal standards by dividing the analyte peak area responses in human plasma spiked postextraction by the analyte responses spiked in reconstitution solution. Capability of dilution was evaluated using QC samples that were prepared at a concentration of 5000 ng/mL and subsequently diluted 10-fold with blank human plasma prior to analysis.

#### 4.1.3 LC/MS/MS methods for metabolic stability study of dasatinib

Kamath *et al.* [37] described a metabolic stability study for dasatinib, in which metabolic stability of dasatinib was measured after incubation with liver microsomes (either NADPH- or UDPGA-fortified) and isolated hepatocytes obtained from mouse, rat, dog, monkey, and human. In all cases, substrate depletion over time was measured and appropriate scaling factors were used to predict *in vivo* clearance. PKs of dasatinib were determined in mice, rats, dogs, and monkeys after administration of single intravenous or oral doses. In addition, the routes of excretion were investigated after administration of dasatinib to bile duct cannulated rats. Absorption and first-pass metabolism were evaluated as possible reasons for the incomplete oral bioavailability using various *in vitro* and *in vivo* models like Caco-2 cells, P-glycoprotein (P-gp) knockout mice, and intraportal dosing in rats. Samples from all the PK studies and samples from the protein binding and blood cell partitioning studies were analyzed by the following LC/MS/MS method. Plasma or serum samples were treated with two volumes of acetonitrile containing 200 ng/mL of the internal standard (IS, BMS proprietary compound). After centrifugation to remove precipitated proteins, a 10  $\mu$ L portion of the clear supernatant was analyzed by LC/MS/MS. Bile, urine, and gastrointestinal tract (GIT) samples were first diluted 1:10 in the corresponding blank plasma, followed by the plasma sample extraction procedure. The HPLC system consisted of two Shimadzu LC10AD pumps, a HTS PAL autosampler, and a Hewlett Packard Series 1100 column compartment. The column used was a YMC C18-AQ, 2 mm  $\times$  50 mm, 3- $\mu$ m particle size, maintained at 60  $^{\circ}$ C with a flow rate of 0.3 mL/min. The mobile phase consisted of 0.1% formic acid in water (A) and 0.1% formic acid in acetonitrile (B). Initial mobile phase composition was 85% solvent A and 15% solvent B. After sample injection, the mobile phase was changed using a linear gradient to 5% solvent A and 95% solvent B over 1 min and held at that composition for an additional 1 min. The mobile phase was then returned to initial conditions and the column reequilibrated for 1.0 min. The total analysis time was 3 min. The HPLC was interfaced to either a Micromass Quattro Micro triple quadrupole mass spectrometer equipped with an electrospray interface or a Sciex API 3000 triple quadrupole mass spectrometer with a turbo ionspray interface. On Micromass Quattro Micro UHP, nitrogen was used as the nebulizing and desolvation gas at flow rates of 100 L/h for nebulization and 1000 L/h for desolvation. The desolvation temperature was 300  $^{\circ}$ C and the source temperature was 150  $^{\circ}$ C. Data acquisition employed selected reaction

monitoring (SRM). Positively charged ion representing the  $[M+H]^+$  for dasatinib and the IS were selected in MS2 scan and collisionally dissociated with argon at a pressure of  $2 \times 10^{-3}$  Torr to form specific product ions which were subsequently monitored by MS<sup>2</sup>. All dwell times were 100 ms. The SRM transitions monitored were  $m/z$  488  $\rightarrow$  01 for dasatinib and  $m/z$  459  $\rightarrow$  338 for the IS. Cone voltage was optimized at 45 V for dasatinib and 30 V for the IS, while the collision energy was 30 eV for dasatinib and 20 eV for the IS. The retention times for dasatinib and the IS were approximately 1.0 and 1.2 min, respectively. The Sciex API 3000 triple quadrupole mass spectrometer used the turbo ionspray interface with an ionspray voltage of 4500 V. Gas 1 and gas 2 were set at 8 and 800, respectively. The turbo ionspray temperature was set at 400 °C. The declustering potential was 41 V for dasatinib and 61 V for the IS. The focusing potential was 170 V for dasatinib and 100 V for the IS. The collision energy was 41 and 29 eV for dasatinib and the IS, respectively. The nitrogen collision gas setting was 6. The standard curves ranged from 1 to 20,000 nM. The standards were analyzed in duplicate. QC samples at concentrations of 80, 800, and 8000 nM were analyzed in duplicate with the analytical set. Predicted concentrations of more than 80% of the QCs were within 20% of nominal concentrations, indicating acceptable assay performance. Liver microsomal samples for determination of metabolic stability were analyzed using a high-throughput LC/MS assay. Samples from the Caco-2 permeability and glucuronidation studies were analyzed by HPLC–UV. The HPLC system consisted of the 2690 Waters separation module and a Waters 996 photodiode array detector.

#### **4.1.4 LC/MS/MS methods for simultaneous quantification of dasatinib and other TKIs in human plasma**

Several validated LC/MS/MS methods have been described to support simultaneous quantification of dasatinib and other TKIs in human plasma [24,26,51,56,57]. Bouchet *et al.* [24] described an UPLC/MS/MS method with SPE, adapted to routine application, allowing rapid, specific, and sensitive determination of the nine TKIs. Under the described chromatographic conditions, all compounds were separated in 3 min, retention time for each analyte being between 0.76 and 2.51 min. Calibration curves ranged from 10 to 5000 ng/mL for imatinib, its metabolite, nilotinib, lapatinib, erlotinib, and sorafenib, and from 0.1 to 200 ng/mL for dasatinib, axitinib, gefitinib, and sunitinib. Peaks of each compound (retention time from 0.76 to 2.51 min) were adequately separated. The mean relative extraction recovery

was in the range of 90.3–106.5%, thanks to the use of stable isotopes as internal standard. There was no significant ion suppression observed at the respective TKI retention times. SPE was chosen because it allows the use of a single protocol to quantify several TKIs that have a wide range of chemical properties:  $pK_a$  values from 5 to 10, and  $\log D$  values from 0 to 4.35 at pH 7 or  $-3.75$  to  $3.9$  at pH 2 (benchmarked using Marvin 5.0.0 software, [www.chemaxon.com](http://www.chemaxon.com)). This could not be done with liquid/liquid extraction because of the different  $pK_a$  values and thus the need of different steps or buffers to extract all analytes. The second reason for choosing SPE concerns the matrix effect because it is considered as the “Achilles’ heel” of mass spectrometry, Taylor reporting that protein precipitation using an organic solvent or dilute and shoot are the dirtiest sample preparation techniques and thus produces the most matrix effects compared to solid phase extraction [58].

SPE coupled to UPLC/MS/MS remains the most effective sample preparation to reduce matrix effect and specifically ion suppression [59]. Furthermore, the recent marketing of the SPE-plates (such as MCX used here) makes the method presented herein ready-to-use for robotic automation. This is less time-consuming and more compatible than SPE-cartridges that often require an evaporation step or protein precipitation that must be followed by centrifugation. By combining SPE and UPLC/MS/MS, this method allowed great sensitivity, which is of particular importance for drugs such as dasatinib and axitinib. These molecules have a short half-life (3–6 h) and thus the trough concentration is low. EPARs data show that mean trough concentration is of 1 ng/mL.

A HPLC method coupled with electrospray mass spectrometry was described for the quantification of plasma concentration of imatinib, dasatinib, and nilotinib [26]. A simple protein precipitation extraction procedure was applied on 250  $\mu$ L of plasma aliquots. Chromatographic separation of drugs and IS (quinoxaline) was achieved with a gradient (acetonitrile and water + formic acid 0.05%) on a C18 reverse-phase analytical column with 20 min of analytical run, at a flow rate of 1 mL/min. Mean intra- and interday precision for all compounds were 4.3% and 11.4%; mean accuracy was 1.5%; extraction recovery ranged within 95% and 114%. Calibration curves ranged from 10,000 to 62.5 ng/mL. The limit of quantification was set at 78.1 ng/mL for imatinib and at 62.5 ng/mL for dasatinib and nilotinib. This novel developed methodology allows a specific, sensitive, and reliable simultaneous determination of the three TKIs imatinib, dasatinib, and nilotinib in a single chromatographic run, useful for drugs estimation in plasma of patients affected by CML.

Roche *et al.* [51] have developed an assay for the determination of cellular levels of lapatinib and dasatinib based on LLE coupled to LC/MS/MS. This method had been applied to cancer cell line models and used to examine potential mechanisms of PK resistance in cancer cell models. There are significant differences in the overall cellular uptake of lapatinib and dasatinib; the biological implications of this difference is unclear but clearly this has the potential to impact efficacy. Cellular samples were extracted with a *tert*-butyl methyl ether:acetonitrile (3:1, v/v):1 M ammonium formate pH 3.5 (8:1, v/v) mixture. Separation was achieved on a Hyperclone BDS C18 (150 mm  $\times$  2.0 mm, 3  $\mu$ m) column with isocratic elution using a mobile phase of acetonitrile–10 mM ammonium formate, pH 4 (54:46, v/v), at a flow rate of 0.2 mL/min.

The TKIs were quantified using a triple quadrupole mass spectrometer which was operated in multireaction-monitoring mode employing positive electrospray ionization. The limits of detection and quantification for lapatinib was determined to be 15 and 31 pg on column, respectively, whereas for dasatinib was 3 and 15 pg on column, respectively.

Haouala *et al.* [56] described a sensitive LC/MS/MS method for the simultaneous analysis in a small volume of plasma of the six major TKIs currently used: imatinib, nilotinib, dasatinib, sunitinib, sorafenib, and lapatinib. This assay is notably applied for plasma levels monitoring of TKIs in some specific clinical situations (toxicity, questionable compliance, managing drug interactions, and less than optimal clinical response) where information on drug plasma exposure may be useful for optimizing patient treatment management. They developed a LC/MS/MS method requiring 100  $\mu$ L of plasma for the simultaneous determination of the six major TKIs currently in use. Plasma is purified by protein precipitation and the supernatant is diluted in ammonium formate 20 mM (pH 4.0) 1:2. Reverse-phase chromatographic separation of TKIs is obtained using a gradient elution of 20 mM ammonium formate (pH 2.2) and acetonitrile containing 1% formic acid, followed by rinsing and reequilibration to the initial solvent composition up to 20 min. Analyte quantification, using matrix-matched calibration samples, is performed by electrospray ionization–triple quadrupole mass spectrometry by selected reaction-monitoring detection using the positive mode. The method was validated according to FDA recommendations, including assessment of extraction yield, matrix effects variability (<9.6%), overall process efficiency (87.1–104.2%), as well as TKIs short- and long-term stability in plasma. The method is precise (interday CV%: 1.3–9.4%), accurate (−9.2 to +9.9%), and sensitive (lower limits of

quantification comprised between 1 and 10 ng/mL). This is the first broad-range LC/MS/MS assay covering the major currently in-use TKIs. It is an improvement over previous methods in terms of convenience (a single extraction procedure for six major TKIs, reducing significantly the analytical time), sensitivity, selectivity, and throughput. It may contribute to filling the current knowledge gaps in the PKs/pharmacodynamics relationships of the latest TKIs developed after imatinib and better define their therapeutic ranges in different patient populations in order to evaluate whether a systematic TDM-guided dose adjustment of these anticancer drugs could contribute to minimize the risk of major adverse reactions and to increase the probability of efficient, long-lasting, therapeutic response.

Hydrophilic interaction liquid chromatography (HILIC) interfaced with atmospheric pressure ionization (API) sources and MS/MS were developed by Hsieh *et al.* [57] for the simultaneous determination of dasatinib, imatinib, and nilotinib in mouse plasma samples. The retention profiles of all analytes on several silica stationary phases under HILIC conditions were explored. The influences of experimental factors such as the compositions of mobile phases on the chromatographic performance and the ionization efficiency of all analytes in positive ion mode were investigated. The applicability of the proposed HILIC/MS/MS approach following a protein precipitation procedure for the quantitative determination of dasatinib, imatinib, and nilotinib at low nanomole levels was examined with respect to assay specificity and linearity. The analytical results obtained by various HILIC/MS/MS approaches were found to be in good agreement with those obtained by reversed-phase liquid chromatography/MS/MS methods in terms of assay sample throughputs, sensitivity, and accuracy. Furthermore, the potential of matrix ionization suppression on the proposed HILIC/MS/MS systems was investigated using the postcolumn infusion technique.

#### **4.1.5 LC/MS/MS methods for pharmacokinetic study of dasatinib**

A detailed PK study was conducted in mice to derive the PK variables using LC/MS/MS method [60]. Following single i.v. administration of 5 mg/kg dasatinib, plasma samples were collected at different time points and deproteinized with acetonitrile; the supernatant was analyzed by HPLC/MS. The HPLC column used was a C18-ODS3 column (2 mm × 50 mm, 3 µm particles) at 60 °C with a flow rate of 0.5 mL/min, whereas the mobile phase consisted of 5 mmol/L ammonium formate (pH 3.75) (A) and acetonitrile (B). The initial mobile phase composition was 87.5% A/12.5% B. After sample injection, the mobile phase was changed to 37.5% A/62.5%



B over 2 min and was held at that composition for 1.5 min. The HPLC was interfaced to a Finnigan LCQ Advantage ion-trap mass spectrometer operated in the positive ion electrospray and full tandem mass spectrometry mode. The limit of quantitation for the purpose of this assay was 1 ng/mL.

#### **4.1.6 High-performance liquid chromatography/ultraviolet detection**

##### **4.1.6.1 Stability indicating HPTLC and LC determination of dasatinib in pharmaceutical dosage form [61]**

Two sensitive and reproducible methods are described by Mhaske *et al.* [61] for the quantitative determination of dasatinib in the presence of its degradation products. The first method was based on high-performance thin layer chromatography (HPTLC) followed by densitometric measurements of their spots at 280 nm. The separation was on HPTLC aluminum sheets of silica gel 60 F254 using toluene:chloroform (7.0:3.0, v/v). This system was found to give compact spots for dasatinib after development (R<sub>F</sub> value of  $0.23 \pm 0.02$ ). The second method was based on HPLC of the drug from its degradation products on reversed phase, Perfect Sil column [C18 (5  $\mu$ m, 25 cm  $\times$  4.6 mm, i.d.)] at ambient temperature using mobile phase consisting of methanol:20 mM ammonium acetate with acetic acid (45:55, v/v), pH 3.0, and retention time ( $t_R = 8.23 \pm 0.02$  min). Both separation methods were validated as per the ICH guidelines. No chromatographic interference from the tablet excipients was found. Dasatinib was subjected to acid–alkali hydrolysis, oxidation, dry heat, wet heat, and photodegradation. The drug was susceptible to acid–alkali hydrolysis and oxidation. The drug was found to be stable in neutral, wet heat, dry heat, and photodegradation conditions. As the proposed analytical methods could effectively separate the drug from its degradation products, they can be employed as stability indicating.

## **4.2. Colorimetric methods**

A colorimetric method for the routine estimation of dasatinib has been developed by Vadia *et al.* [62]. The method is based on the formation of a blue-colored complex by dasatinib in presence of Folin–Ciocalteu reagent and NaOH. The developed colored complex showed  $\lambda_{\max}$  at 745 nm. Beer's law in the concentration range of 10–80  $\mu$ g/mL. Results of analysis were authenticated statistically as well as by recovery studies, which gave mean recovery between 99% and 100%. The method was successful in determining dasatinib in physical mixture and in tablet formulation, with an average recovery of 99% and 100%, respectively. The proposed method

could find application to product development scientists in ongoing research as well provide an additional tool for routine analysis of dasatinib in academia and QC laboratory.

### 4.3. UV spectrophotometric methods

UV spectrophotometric method has been developed by Sankar *et al.* [63] for the quantitative estimation of dasatinib in pure form as well as in pharmaceutical formulations. The drug exhibits absorption maximum at 330 nm in 0.1 N HCl and obeys Beer's law in the concentration range of 2–10  $\mu\text{g/mL}$ . The method was extended to pharmaceutical preparations and there is no interference from any common pharmaceutical additives.



## 5. PHARMACOLOGY

### 5.1. Pharmacokinetics

#### 5.1.1 Absorption

A phase 1 trial study on 29 patients with advanced solid tumors receiving oral dasatinib (20 mg/d) for two days showed a  $C_{\text{max}}$  of 14 ng/mL with area under the curve (AUC) of approximately 71 ng h/mL [64]. Dasatinib is rapidly absorbed after oral administration of 1.25, 2.5, or 5 mg/kg with a  $T_{\text{max}}$  of 1 h for all three oral doses, whereas the  $C_{\text{max}}$  and the  $(\text{AUC})_{0-24}$  seemed dose dependent [60]. Oral bioavailability of dasatinib ranged from 14% in mouse to 34% in the dog [37]. Upon oral administration, solubility of dasatinib is dependent on pH; therefore, antacids, histamine  $H_2$ -receptor antagonists, or proton pump inhibitors such as famotidine or omeprazole should be avoided. If antacid therapy is needed, it should be given at least 2 h before or 2 h after the dose of dasatinib [65]. In this regard, famotidine, a  $H_2$ -receptor antagonists, reduced dasatinib exposure by 61% [66]. In addition, it has been reported that oral administration of dasatinib with high-fat containing meal increased the AUC by approximately 14%, which was not clinically relevant. The maximum concentration of dasatinib is reached between 0.5 and 6 h.

#### 5.1.2 Distribution

Dasatinib extensively binds to human plasma proteins *in vitro* by approximately 96%. In leukemic patient, the calculated apparent volume of distribution for dasatinib was 2502 L, implying that dasatinib is extensively distributed in the extravascular space and tissues [37]. The elimination half-life of dasatinib was approximately 3–5 h [37]. Although the brain

penetration of dasatinib is poor, with a CSF: plasma ratios ranging from 0.05 to 0.28, dasatinib appears to be more potent against CNS tumors than imatinib. This could be a result of a much greater potency of dasatinib and the large fraction of unbound drug [67].

### 5.1.3 Metabolism

*In vitro* studies demonstrate that multiple cytochrome P450 (CYP) isoforms (e.g., CYP1A1, 1B1, and 3A4) are involved in metabolizing dasatinib [68]. Dasatinib is metabolized in humans markedly by CYP3A4 to active metabolites that represent around 5% of the parent compound, which is unlikely to play a major role in the anticancer effect of dasatinib (Figures 4.8 and 4.9) [69]. Thus, coadministration of dasatinib with enzyme inducers (carbamazepine, dexamethasone, phenobarbital, phenytoin, and rifampicin) or inhibitors (ketoconazole, macrolide antibacterials, HIV-protease inhibitors, and nefazodone) may reduce or increase blood concentrations of dasatinib, respectively. For example, it has been reported that coingestion of ketoconazole with dasatinib resulted in a fivefold increase in dasatinib concentration in healthy volunteers, whereas rifampicin decreased dasatinib exposure by 82% [70]. On the other hand, flavin-containing monooxygenase 3 and phase II drug-metabolizing enzymes, such as UDP glucuronosyltransferase, are also involved in metabolizing dasatinib [71]. Furthermore, *in vitro* studies have demonstrated that dasatinib is a substrate of transporters, such as ATP-Binding Cassette (ABC)B1 and ABCG2, but unlike nilotinib, not a potent inhibitor of these transporters [72,73], in that, inhibition of ABCB1 transporter by nilotinib increased the intracellular concentration of dasatinib in CML cells [72]. In Caco-2 cells, the efflux ratio of dasatinib was approximately twofold, indicating that it may be a substrate for an intestinal efflux transporter [37]. However, studies on P-gp knockout mice showed no difference in the amount of dasatinib remaining unabsorbed in the GIT as compared to wild-type mice, suggesting that P-gp may not be responsible for poor bioavailability of dasatinib [37].

### 5.1.4 Excretion

Dasatinib is mainly eliminated via the feces (85%), of which relatively small amount of dasatinib is excreted unchanged as intact drug (19%) [70,74]. Urinary excretion of dasatinib represents only 4%, of which <1% as unchanged dasatinib. Dasatinib exhibited a biexponential and high clearance exceeding the hepatic blood flow [60]. Although there are no data on the excretion of

dasatinib into human milk, the manufacturer recommends that women who are taking dasatinib do not breast-feed.

## 5.2. Pharmacodynamics

Dasatinib, a second-generation TKI, has been shown to be effective as an anticancer drug in the treatment of patients with CML or Philadelphia chromosome-positive (Ph+) acute lymphoblastic leukemia who are resistant or intolerant to imatinib. Dasatinib inhibits several multiple tyrosine kinases, including BCR-ABL and SRC family kinases, which are indicated for the treatment of adults with newly diagnosed chronic phase of CML. Dasatinib exerts its anticancer effect through inhibiting several oncogenic tyrosine kinases such as BCR-ABL, expressed by Ph+ stem cells, and is directly involved in the pathogenesis of CML. Importantly, the ability of dasatinib to inhibit 18 of the 19 BCR-ABL mutants that are resistant to imatinib makes dasatinib more potent against BCR-ABL than imatinib *in vitro* [75,76]. In this regard, dasatinib that is reported as being approximately 325-fold more active than imatinib in inhibiting wild-type ABL kinase *in vitro* is active against a wide variety of imatinib-resistant BCR-ABL mutants. However, the primary mechanism of resistance to dasatinib is believed to be attributed to resistance of dasatinib to The T315I, a novel BCR-ABL mutant clone [77,78]. *Four-week treatment with dasatinib has been shown to reduce BCR-ABL transcript by approximately 32% using real-time polymerase chain reaction* [79]. Dasatinib is also effective against multiple myeloma cell lines *in vitro*, at clinically achievable concentrations, through increased caspase-8 and caspase-12 activation and sensitized primary multiple myeloma cells to other agents that activate caspase-9, such as dexamethasone and bortezomib [80]. Furthermore, dasatinib inhibited the viability of both non-small cell lung cancer and head and neck squamous cell cancer cell lines *in vitro* through apoptosis-dependent mechanism [81].

## 5.3. Toxicities

Most of the adverse effects associated with dasatinib therapy are mild to moderate in severity and are usually reversible and manageable with appropriate intervention. Examples of these common side effects include cardiac failure, hypertension, and coronary artery disease [10]. Dasatinib has the potential to prolong the QT interval and thus should be given with caution to patients with hypokalemia or hypomagnesemia. Pleural effusion is another common side effect associated with dasatinib; however, it can be

effectively managed with prompt delivery of supportive care and dose modification. Dasatinib also causes thrombocytopenia and bleeding, which may be additive with antiplatelet and anticoagulant drugs [16].

## ACKNOWLEDGMENT

This work was supported by the College of Pharmacy Research Center, King Saud University.

## REFERENCES

- [1] S.R. Hubbard, J.H. Till, Protein tyrosine kinase structure and function, *Annu. Rev. Biochem.* 69 (2000) 373–398.
- [2] L.J. Lombardo, F.Y. Lee, P. Chen, D. Norris, J.C. Barrish, K. Behnia, S. Castaneda, L.A. Cornelius, J. Das, A.M. Doweyko, C. Fairchild, J.T. Hunt, I. Inigo, K. Johnston, A. Kamath, D. Kan, H. Klei, P. Marathe, S. Pang, R. Peterson, S. Pitt, G.L. Schieven, R.J. Schmidt, J. Tokarski, M.L. Wen, J. Wityak, R.M. Borzilleri, Discovery of N-(2-chloro-6-methyl-phenyl)-2-(6-(4-(2-hydroxyethyl)-piperazin-1-yl)-2-methylpyrimidin-4-ylamino)thiazole-5-carboxamide (BMS-354825), a dual Src/Abl kinase inhibitor with potent antitumor activity in preclinical assays, *J. Med. Chem.* 47 (2004) 6658–6661.
- [3] P. Ramirez, J.F. DiPersio, Therapy options in imatinib failures, *Oncologist* 13 (2008) 424–434.
- [4] B.C. Chen, R. Droghini, J. Lajeunesse, J. D. DiMarco, M. Galella, R. Chindambaram, Process for preparing 2-aminothiazole-5-aromatic carboxamides as kinase inhibitors, US patent 2006004067, 2006.
- [5] Chemical Structure name was obtained from ChemBioDraw, ChemBioDraw Ultra 12.0. software.
- [6] J. Das, P. Chen, D. Norris, R. Padmanabha, J. Lin, R.V. Moquin, Z. Shen, L.S. Cook, A.M. Doweyko, S. Pitt, S. Pang, D.R. Shen, Q. Fang, H.F. de Fex, K.W. McIntyre, D.J. Shuster, K.M. Gillooly, K. Behnia, G.L. Schieven, J. Wityak, J.C. Barrish, 2-aminothiazole as a novel kinase inhibitor template. Structure-activity relationship studies toward the discovery of N-(2-chloro-6-methylphenyl)-2-[[6-[4-(2-hydroxyethyl)-1-piperazinyl]-2-methyl-4-pyrimidinyl]amino]-1,3-thiazole-5-carboxamide (dasatinib, BMS-354825) as a potent pan-Src kinase inhibitor, *J. Med. Chem.* 49 (2006) 6819–6832.
- [7] P.V. Spirin, D. Baskaran, N.N. Orlova, A.V. Rulina, N.A. Nikitenko, E.L. Chernolovskaya, M.A. Zenkova, V.V. Vlassov, P.M. Rubtsov, P.M. Chumakov, C. Stocking, V.S. Prassolov, Downregulation of activated leukemic oncogenes AML1-ETO and RUNX1(K83N) expression with RNA-interference, *Mol. Biol. (Mosk.)* 44 (2010) 876–888.
- [8] A.V. Rulina, P.V. Spirin, V.S. Prassolov, Activated leukemic oncogenes AML1-ETO and c-kit: role in development of acute myeloid leukemia and current approaches for their inhibition, *Biochemistry (Mosc.)* 75 (2010) 1650–1666.
- [9] Drug bank accession number is DB01254. <http://www.drugbank.ca>.
- [10] S. Sweetman, Martindale: The Complete Drug Reference, 36 ed., Pharmaceutical press, London, 2009, 709.
- [11] Maryadele J. O'Neil, Patricia E. Heckelman, Cherie B. Koch, Kristin J. Roman, Catherine M. Kenny, Maryann R. D'Arecca (Eds.), In: The Merck Index, an Encyclopedia of Chemicals, Drugs and Biologicals, vol. 14, Merck & Co., Inc., Whitehouse Station, NJ, USA, 2006, p. 2829.
- [12] Chemical Abstracts Service (CAS) registry no. 302962-49-8. <http://www.cas.org>.

- [13] Chemspider ID: 2323020. <http://www.chemspider.com>.
- [14] R. Yan, Yang, Hao, Hou, Wen, Xu, Yongxiang synthesis process of dasatinib and intermediate, WO/2011/095126 A (2011).
- [15] P. Imming, C. Sinning, A. Meyre, Drugs, their targets and the nature and number of drug targets, *Nat. Rev. Drug Discov.* 5 (2006) 821–834.
- [16] J. McIntyre, J. Castanner, M. Bayes, Dasatinib, *Drugs Fut.* 31 (2006) 291.
- [17] J. Das, R. Radmanabha, P. Chen, D.J. Norris, A.M.P. Doweyko, J.L. Barrish, J. Wityak, Cyclic protein tyrosine kinase inhibitors, US patent US6596746, 2003.
- [18] B.C. Chen, R. Zhao, B. Wang, Process for preparing 2-aminothiazole-5-carboxamides as kinase inhibitors, US patent US 2005176965, 2005.
- [19] J. Das, R. Radmanabha, P. Chen, D.J. Norris, A.M.P. Doweyko, J.L. Barrish, J. Wityak, Cyclic protein tyrosine kinase inhibitors, Chinese patent CN1348370A, 2002.
- [20] G.M. Peter, *Green's Protective Groups in Organic Synthesis*, Fourth ed., John Wiley & Sons, Inc., NJ, USA, 2007, pp. 16–366.
- [21] J.C. Li, B.C. Chen, D. Smith, J.H. Sun, Process for preparing N-(2-chloro-6-methylphenyl)-2-[6-[4-(2-hydroxyethyl)piperazin-1-yl]-2-methylpyrimidin-4-ylamino]thiazole-5-carboxamide and related metabolites thereof, US patent WO 2007106879 A2, 2007.
- [22] D.R. Veach, M. Namavari, N. Pillarsetty, E.B. Santos, T. Beresten-Kochetkov, C. Lambek, B.J. Punzalan, C. Antczak, P.M. Smith-Jones, H. Djaballah, B. Clarkson, S.M. Larson, Synthesis and biological evaluation of a fluorine-18 derivative of dasatinib, *J. Med. Chem.* 50 (2007) 5853–5857.
- [23] A. Awidi, I.I. Salem, N. Najib, R. Mefleh, B. Tarawneh, Determination of imatinib plasma levels in patients with chronic myeloid leukemia by high performance liquid chromatography-ultraviolet detection and liquid chromatography-tandem mass spectrometry: methods' comparison, *Leuk. Res.* 34 (2010) 714–717.
- [24] S. Bouchet, E. Chauzit, D. Ducint, N. Castaing, M. Canal-Raffin, N. Moore, K. Titier, M. Molimard, Simultaneous determination of nine tyrosine kinase inhibitors by 96-well solid-phase extraction and ultra performance LC/MS-MS, *Clin. Chim. Acta* 412 (2011) 1060–1067.
- [25] A. Davies, A.K. Hayes, K. Knight, S.J. Watmough, M. Pirmohamed, R.E. Clark, Simultaneous determination of nilotinib, imatinib and its main metabolite (CGP-74588) in human plasma by ultra-violet high performance liquid chromatography, *Leuk. Res.* 34 (2010) 702–707.
- [26] S. De Francia, A. D'Avolio, F. De Martino, E. Pirro, L. Baietto, M. Siccardi, M. Simiele, S. Racca, G. Saglio, F. Di Carlo, G. Di Perri, New HPLC-MS method for the simultaneous quantification of the antileukemia drugs imatinib, dasatinib, and nilotinib in human plasma, *J. Chromatogr. B Analyt. Technol. Biomed. Life Sci.* 877 (2009) 1721–1726.
- [27] J. Klawitter, Y.L. Zhang, N. Anderson, N.J. Serkova, U. Christians, Development and validation of a sensitive assay for the quantification of imatinib using LC/LC-MS/MS in human whole blood and cell culture, *Biomed. Chromatogr.* 23 (2009) 1251–1258.
- [28] K. Micova, D. Friedecky, E. Faber, A. Polynkova, T. Adam, Flow injection analysis vs. ultra high performance liquid chromatography coupled with tandem mass spectrometry for determination of imatinib in human plasma, *Clin. Chim. Acta* 411 (2010) 1957–1962.
- [29] M. Miura, N. Takahashi, K. Sawada, High-performance liquid chromatography with solid-phase extraction for the quantitative determination of nilotinib in human plasma, *Biomed. Chromatogr.* 24 (2010) 789–793.
- [30] M. Miura, N. Takahashi, K. Sawada, Quantitative determination of imatinib in human plasma with high-performance liquid chromatography and ultraviolet detection, *J. Chromatogr. Sci.* 49 (2011) 412–415.

- [31] R.L. Oostendorp, J.H. Beijnen, J.H. Schellens, O. Telling, Determination of imatinib mesylate and its main metabolite (CGP74588) in human plasma and murine specimens by ion-pairing reversed-phase high-performance liquid chromatography, *Biomed. Chromatogr.* 21 (2007) 747–754.
- [32] R.A. Parise, M.J. Egorin, S.M. Christner, D.D. Shah, W. Zhou, J.H. Beumer, A high-performance liquid chromatography-mass spectrometry assay for quantitation of the tyrosine kinase inhibitor nilotinib in human plasma and serum, *J. Chromatogr. B Analyt. Technol. Biomed. Life Sci.* 877 (2009) 1894–1900.
- [33] S. Pursche, O.G. Ottmann, G. Ehninger, E. Schleyer, High-performance liquid chromatography method with ultraviolet detection for the quantification of the BCR-ABL inhibitor nilotinib (AMN107) in plasma, urine, culture medium and cell preparations, *J. Chromatogr. B Analyt. Technol. Biomed. Life Sci.* 852 (2007) 208–216.
- [34] O. Roth, O. Spreux-Varoquaux, S. Bouchet, P. Rousselot, S. Castaigne, S. Rigau, V. Raggueneau, P. Therond, P. Devillier, M. Molimard, B. Maneglier, Imatinib assay by HPLC with photodiode-array UV detection in plasma from patients with chronic myeloid leukemia: comparison with LC-MS/MS, *Clin. Chim. Acta* 411 (2010) 140–146.
- [35] K. Titier, S. Picard, D. Ducint, E. Teilhet, N. Moore, P. Berthaud, F.X. Mahon, M. Molimard, Quantification of imatinib in human plasma by high-performance liquid chromatography-tandem mass spectrometry, *Ther. Drug Monit.* 27 (2005) 634–640.
- [36] M. Yuki, Y. Yamakawa, T. Uchida, T. Nambu, T. Kawaguchi, A. Hamada, H. Saito, High-performance liquid chromatographic assay for the determination of nilotinib in human plasma, *Biol. Pharm. Bull.* 34 (2011) 1126–1128.
- [37] A.V. Kamath, J. Wang, F.Y. Lee, P.H. Marathe, Preclinical pharmacokinetics and in vitro metabolism of dasatinib (BMS-354825): a potent oral multi-targeted kinase inhibitor against SRC and BCR-ABL, *Cancer Chemother. Pharmacol.* 61 (2008) 365–376.
- [38] M.C. Frame, Src in cancer: deregulation and consequences for cell behaviour, *Biochim. Biophys. Acta* 1602 (2002) 114–130.
- [39] M. Steinberg, Dasatinib: a tyrosine kinase inhibitor for the treatment of chronic myelogenous leukemia and philadelphia chromosome-positive acute lymphoblastic leukemia, *Clin. Ther.* 29 (2007) 2289–2308.
- [40] H. Kantarjian, F. Giles, L. Wunderle, K. Bhalha, S. O'Brien, B. Wassmann, C. Tanaka, P. Manley, P. Rae, W. Mietlowski, K. Bochinski, A. Hochhaus, J.D. Griffin, D. Hoelzer, M. Albitar, M. Dugan, J. Cortes, L. Alland, O.G. Ottmann, Nilotinib in imatinib-resistant CML and Philadelphia chromosome-positive ALL, *N. Engl. J. Med.* 354 (2006) 2542–2551.
- [41] E. Weisberg, P.W. Manley, W. Breitenstein, J. Bruggen, S.W. Cowan-Jacob, A. Ray, B. Huntly, D. Fabbro, G. Fendrich, E. Hall-Meyers, A.L. Kung, J. Mestan, G.Q. Daley, L. Callahan, L. Catley, C. Cavazza, M. Azam, D. Neuberger, R.D. Wright, D.G. Gilliland, J.D. Griffin, Characterization of AMN107, a selective inhibitor of native and mutant Bcr-Abl, *Cancer Cell* 7 (2005) 129–141.
- [42] M.M. Oken, R.H. Creech, D.C. Tormey, J. Horton, T.E. Davis, E.T. McFadden, P.P. Carbone, Toxicity and response criteria of the Eastern Cooperative Oncology Group, *Am. J. Clin. Oncol.* 5 (1982) 649–655.
- [43] A. D'Avolio, M. Simiele, S. De Francia, A. Ariaudo, L. Baietto, J. Cusato, C. Fava, G. Saglio, F. Di Carlo, G. Di Perri, HPLC-MS method for the simultaneous quantification of the antileukemia drugs imatinib, dasatinib and nilotinib in human peripheral blood mononuclear cell (PBMC), *J. Pharm. Biomed. Anal.* 59 (2010) 109–116.
- [44] G. Saglio, D.W. Kim, S. Issaragrisil, P. le Coutre, G. Etienne, C. Lobo, R. Pasquini, R.E. Clark, A. Hochhaus, T.P. Hughes, N. Gallagher, A. Hoenekopp, M. Dong,

- A. Haque, R.A. Larson, H.M. Kantarjian, Nilotinib versus imatinib for newly diagnosed chronic myeloid leukemia, *N. Engl. J. Med.* 362 (2010) 2251–2259.
- [45] M. Baccarani, G. Saglio, J. Goldman, A. Hochhaus, B. Simonsson, F. Appelbaum, J. Apperley, F. Cervantes, J. Cortes, M. Deininger, A. Gratwohl, F. Guilhot, M. Horowitz, T. Hughes, H. Kantarjian, R. Larson, D. Niederwieser, R. Silver, R. Hehlmann, Evolving concepts in the management of chronic myeloid leukemia: recommendations from an expert panel on behalf of the European LeukemiaNet, *Blood* 108 (2006) 1809–1820.
- [46] N. Singh, L. Kumar, R. Meena, T. Velpandian, Drug monitoring of imatinib levels in patients undergoing therapy for chronic myeloid leukaemia: comparing plasma levels of responders and non-responders, *Eur. J. Clin. Pharmacol.* 65 (2009) 545–549.
- [47] E. Faber, D. Friedecky, K. Micova, M. Divoka, B. Katrincsakova, S. Rozmanova, M. Jarosova, K. Indrak, T. Adam, Imatinib dose escalation in two patients with chronic myeloid leukemia, with low trough imatinib plasma levels measured at various intervals from the beginning of therapy and with suboptimal treatment response, leads to the achievement of higher plasma levels and major molecular response, *Int. J. Hematol.* 91 (2010) 897–902.
- [48] B. Peng, M. Hayes, D. Resta, A. Racine-Poon, B.J. Druker, M. Talpaz, C.L. Sawyers, M. Rosamilia, J. Ford, P. Lloyd, R. Capdeville, Pharmacokinetics and pharmacodynamics of imatinib in a phase I trial with chronic myeloid leukemia patients, *J. Clin. Oncol.* 22 (2004) 935–942.
- [49] S. Picard, K. Titier, G. Etienne, E. Teilhet, D. Ducint, M.A. Bernard, R. Lassalle, G. Marit, J. Reiffers, B. Begaud, N. Moore, M. Molimard, F.X. Mahon, Trough imatinib plasma levels are associated with both cytogenetic and molecular responses to standard-dose imatinib in chronic myeloid leukemia, *Blood* 109 (2007) 3496–3499.
- [50] M. Holdhoff, J.G. Supko, G.L. Gallia, C.L. Hann, D. Bonekamp, X. Ye, B. Cao, A. Olivi, S.A. Grossman, Intratumoral concentrations of imatinib after oral administration in patients with glioblastoma multiforme, *J. Neurooncol.* 97 (2010) 241–245.
- [51] S. Roche, G. McMahon, M. Clynes, R. O'Connor, Development of a high-performance liquid chromatographic-mass spectrometric method for the determination of cellular levels of the tyrosine kinase inhibitors lapatinib and dasatinib, *J. Chromatogr. B Analyt. Technol. Biomed. Life Sci.* 877 (2009) 3982–3990.
- [52] T. Nambu, A. Hamada, R. Nakashima, M. Yuki, T. Kawaguchi, H. Mitsuya, H. Saito, Association of SLC01B3 polymorphism with intracellular accumulation of imatinib in leukocytes in patients with chronic myeloid leukemia, *Biol. Pharm. Bull.* 34 (2011) 114–119.
- [53] M. D'Antonio, V. Pendino, S. Sinha, F.D. Ciccarelli, Network of Cancer Genes (NCG 3.0): integration and analysis of genetic and network properties of cancer genes, *Nucleic Acids Res.* 40 (2012) D978–D983.
- [54] M.T. Furlong, S. Agrawal, D. Hawthorne, M. Lago, S. Unger, L. Krueger, B. Stouffer, A validated LC-MS/MS assay for the simultaneous determination of the anti-leukemic agent dasatinib and two pharmacologically active metabolites in human plasma: application to a clinical pharmacokinetic study, *J. Pharm. Biomed. Anal.* 58 (2012) 130–135.
- [55] FDA, Guidance for Industry, Bioanalytical Method Validation, 2001.
- [56] A. Haouala, B. Zanolari, B. Rochat, M. Montemurro, K. Zaman, M.A. Duchosal, H.B. Ris, S. Leyvraz, N. Widmer, L.A. Decosterd, Therapeutic Drug Monitoring of the new targeted anticancer agents imatinib, nilotinib, dasatinib, sunitinib, sorafenib and lapatinib by LC tandem mass spectrometry, *J. Chromatogr. B Analyt. Technol. Biomed. Life Sci.* 877 (2009) 1982–1996.
- [57] Y. Hsieh, G. Galviz, Q. Zhou, C. Duncan, Hydrophilic interaction liquid chromatography/tandem mass spectrometry for the simultaneous determination of dasatinib,



- imatinib and nilotinib in mouse plasma, *Rapid Commun. Mass Spectrom.* 23 (2009) 1364–1370.
- [58] P.J. Taylor, Matrix effects: the Achilles heel of quantitative high-performance liquid chromatography-electrospray-tandem mass spectrometry, *Clin. Biochem.* 38 (2005) 328–334.
- [59] E. Chambers, D.M. Wagrowski-Diehl, Z. Lu, J.R. Mazzeo, Systematic and comprehensive strategy for reducing matrix effects in LC/MS/MS analyses, *J. Chromatogr. B Analyt. Technol. Biomed. Life Sci.* 852 (2007) 22–34.
- [60] F.R. Luo, Z. Yang, A. Camuso, R. Smykla, K. McGlinchey, K. Fager, C. Flefle, S. Castaneda, I. Inigo, D. Kan, M.L. Wen, R. Kramer, A. Blackwood-Chirchir, F.Y. Lee, Dasatinib (BMS-354825) pharmacokinetics and pharmacodynamic biomarkers in animal models predict optimal clinical exposure, *Clin. Cancer Res.* 12 (2006) 7180–7186.
- [61] D.V. Mhaske, S.R. Dhaneshwar, Stability indicating HPTLC and LC determination of dasatinib in pharmaceutical dosage form, *Chromatographia* 66 (2007) 95–102.
- [62] N. Vadia, S. Rajput, Study on formulation variables of methotrexate loaded mesoporous MCM-41 nanoparticles for dissolution enhancement, *Eur. J. Pharm. Sci.* 45 (2012) 8–18.
- [63] D.G. Sankar, A. Rajeswari, A.N. Babu, M.V. Krishna, UV-spectrophotometric determination of dasatinib in pharmaceutical dosage forms, *Asian J. Chem.* 21 (2009) 5777–5779.
- [64] F.M. Johnson, S. Agrawal, H. Burris, L. Rosen, N. Dhillon, D. Hong, A. Blackwood-Chirchir, F.R. Luo, O. Sy, S. Kaul, A.A. Chiappori, Phase 1 pharmacokinetic and drug-interaction study of dasatinib in patients with advanced solid tumors, *Cancer* 116 (2010) 1582–1591.
- [65] T. Eley, F.R. Luo, S. Agrawal, A. Sanil, J. Manning, T. Li, A. Blackwood-Chirchir, R. Bertz, Phase I study of the effect of gastric acid pH modulators on the bioavailability of oral dasatinib in healthy subjects, *J. Clin. Pharmacol.* 49 (2009) 700–709.
- [66] M. Brave, V. Goodman, E. Kaminskas, A. Farrell, W. Timmer, S. Pope, R. Harapanhalli, H. Saber, D. Morse, J. Bullock, A. Men, C. Noory, R. Ramchandani, L. Kenna, B. Booth, J. Gobburu, X. Jiang, R. Sridhara, R. Justice, R. Pazdur, Sprycel for chronic myeloid leukemia and Philadelphia chromosome-positive acute lymphoblastic leukemia resistant to or intolerant of imatinib mesylate, *Clin. Cancer Res.* 14 (2008) 352–359.
- [67] K. Porkka, P. Koskenvesa, T. Lundan, J. Rimpilainen, S. Mustjoki, R. Smykla, R. Wild, R. Luo, M. Aman, B. Brethon, L. Eccersley, H. Hjorth-Hansen, M. Hoglund, H. Klamova, H. Knutsen, S. Parikh, E. Raffoux, F. Gruber, F. Brito-Babapulle, H. Dombret, R.F. Duarte, E. Elonen, R. Paquette, C.M. Zwaan, F.Y. Lee, Dasatinib crosses the blood-brain barrier and is an efficient therapy for central nervous system Philadelphia chromosome-positive leukemia, *Blood* 112 (2008) 1005–1012.
- [68] L. Wang, L.J. Christopher, D. Cui, W. Li, R. Iyer, W.G. Humphreys, D. Zhang, Identification of the human enzymes involved in the oxidative metabolism of dasatinib: an effective approach for determining metabolite formation kinetics, *Drug Metab. Dispos.* 36 (2008) 1828–1839.
- [69] X. Li, Y. He, C.H. Ruiz, M. Koenig, M.D. Cameron, T. Vojtkovsky, Characterization of dasatinib and its structural analogs as CYP3A4 mechanism-based inactivators and the proposed bioactivation pathways, *Drug Metab. Dispos.* 37 (2009) 1242–1250.
- [70] L.J. Christopher, D. Cui, C. Wu, R. Luo, J.A. Manning, S.J. Bonacorsi, M. Lago, A. Allentoff, F.Y. Lee, B. McCann, S. Galbraith, D.P. Reitberg, K. He, A. Barros Jr., A. Blackwood-Chirchir, W.G. Humphreys, R.A. Iyer, Metabolism

- and disposition of dasatinib after oral administration to humans, *Drug Metab. Dispos.* 36 (2008) 1357–1364.
- [71] G. Dai, M. Pfister, A. Blackwood-Chirchir, A. Roy, Importance of characterizing determinants of variability in exposure: application to dasatinib in subjects with chronic myeloid leukemia, *J. Clin. Pharmacol.* 48 (2008) 1254–1269.
- [72] D.K. Hiwase, D. White, S. Zrim, V. Saunders, J.V. Melo, T.P. Hughes, Nilotinib-mediated inhibition of ABCB1 increases intracellular concentration of dasatinib in CML cells: implications for combination TKI therapy, *Leukemia* 24 (2010) 658–660.
- [73] D.K. Hiwase, V. Saunders, D. Hewett, A. Frede, S. Zrim, P. Dang, L. Eadie, L.B. To, J. Melo, S. Kumar, T.P. Hughes, D.L. White, Dasatinib cellular uptake and efflux in chronic myeloid leukemia cells: therapeutic implications, *Clin. Cancer Res.* 14 (2008) 3881–3888.
- [74] L.J. Christopher, D. Cui, W. Li, A. Barros Jr., V.K. Arora, H. Zhang, L. Wang, D. Zhang, J.A. Manning, K. He, A.M. Fletcher, M. Ogan, M. Lago, S.J. Bonacorsi, W.G. Humphreys, R.A. Iyer, Biotransformation of [<sup>14</sup>C]dasatinib: in vitro studies in rat, monkey, and human and disposition after administration to rats and monkeys, *Drug Metab. Dispos.* 36 (2008) 1341–1356.
- [75] M. Copland, A. Hamilton, L.J. Elrick, J.W. Baird, E.K. Allan, N. Jordanides, M. Barow, J.C. Mountford, T.L. Holyoake, Dasatinib (BMS-354825) targets an earlier progenitor population than imatinib in primary CML but does not eliminate the quiescent fraction, *Blood* 107 (2006) 4532–4539.
- [76] N.P. Shah, F.Y. Lee, R. Luo, Y. Jiang, M. Donker, C. Akin, Dasatinib (BMS-354825) inhibits KITD816V, an imatinib-resistant activating mutation that triggers neoplastic growth in most patients with systemic mastocytosis, *Blood* 108 (2006) 286–291.
- [77] T. O'Hare, C.A. Eide, J.W. Tyner, A.S. Corbin, M.J. Wong, S. Buchanan, K. Holme, K.A. Jessen, C. Tang, H.A. Lewis, R.D. Romero, S.K. Burley, M.W. Deininger, SGX393 inhibits the CML mutant Bcr-AblT315I and preempts in vitro resistance when combined with nilotinib or dasatinib, *Proc. Natl. Acad. Sci. U.S.A.* 105 (2008) 5507–5512.
- [78] A. Quintas-Cardama, J.E. Cortes, S. O'Brien, F. Ravandi, G. Borthakur, D. Liu, E. Bleickardt, T.T. Chen, H.M. Kantarjian, Dasatinib early intervention after cytogenetic or hematologic resistance to imatinib in patients with chronic myeloid leukemia, *Cancer* 115 (2009) 2912–2921.
- [79] A. Hochhaus, Management of Bcr-Abl-positive leukemias with dasatinib, *Expert Rev. Anticancer Ther.* 7 (2007) 1529–1536.
- [80] A.M. Coluccia, T. Cirulli, P. Neri, D. Mangieri, M.C. Colanardi, A. Gnoni, N. Di Renzo, F. Dammacco, P. Tassone, D. Ribatti, C. Gambacorti-Passerini, A. Vacca, Validation of PDGFRbeta and c-Src tyrosine kinases as tumor/vessel targets in patients with multiple myeloma: preclinical efficacy of the novel, orally available inhibitor dasatinib, *Blood* 112 (2008) 1346–1356.
- [81] A.A. Miller, H. Pang, L. Hodgson, N. Ramnath, G.A. Otterson, M.J. Kelley, R.A. Kratzke, E.E. Vokes, A phase II study of dasatinib in patients with chemosensitive relapsed small cell lung cancer (Cancer and Leukemia Group B 30602), *J. Thorac. Oncol.* 5 (2010) 380–384.



# Gefitinib

**A.F.M. Motiur Rahman<sup>\*</sup>, Hesham M. Korashy<sup>†</sup>,  
Mohammed Gabr Kassem<sup>\*</sup>**

<sup>\*</sup>Department of Pharmaceutical Chemistry, College of Pharmacy, King Saud University, Riyadh, Saudi Arabia

<sup>†</sup>Department of Pharmacology and Toxicology, College of Pharmacy, King Saud University, Riyadh, Saudi Arabia

## Contents

1. Introduction	239
1.1 Nomenclature	240
1.2 Formulae	240
1.3 Elemental analysis	241
1.4 Physical properties	241
1.5 Uses and applications	242
2. Methods of Preparation	242
3. Physical Properties	247
3.1 Spectroscopy	247
3.2 Mass spectrum	251
3.3 X-Ray powder diffraction pattern	253
4. Methods of Analysis	253
4.1 Chromatographic methods	253
5. Pharmacology	259
5.1 Pharmacokinetics	260
5.2 Toxicities	261
Acknowledgment	261
References	262



## 1. INTRODUCTION

The epidermal growth factor receptor (EGFR) protein tyrosine kinase is one of the important kinases that play a fundamental role in signal transduction pathways [1]. Many human cancers overexpress EGFR and the related human epidermal growth factor receptor (HER-2). Compounds, such as gefitinib (Iressa<sup>®</sup>), that inhibit the kinase activity of EGFR and

HER-2 after binding of their cognate ligand, have been used as new therapeutic antitumor agents [2,3].

Gefitinib, a potent and selective ATP-competitive inhibitor of EGFR and HER-2 kinases, is the first EGFR-targeting agent launched as an anti-cancer drug in Japan, Australia, and the United States for the treatment of chemoresistant non-small cell lung cancer (NSCLC) patients [4,5]. In pre-clinical studies, gefitinib has demonstrated antitumor activity against a variety of human cancer cell lines expressing EGFR, including lung, ovarian, breast, and colon [6–8]. In human xenograft models, gefitinib (ZD1839) in combination with standard cytotoxic agents resulted in both delayed tumor growth and tumor regression, leading to enhanced survival [9]. Gefitinib is indicated as monotherapy for the treatment of patients with locally advanced or metastatic NSCLC after failure of both platinum-based and docetaxel chemotherapies.

## 1.1. Nomenclature

### 1.1.1 Systematical chemical names

- *N*-(3-chloro-4-fluorophenyl)-7-methoxy-6-(3-morpholin-4-ylpropoxy)quinazolin-4-amine [10].
- *N*-(3-chloro-4-fluorophenyl)-7-methoxy-6-[3-(morpholin-4-yl)propoxy]quinazolin-4-amine [11,12].
- 4-(3'-Chloro-4'-fluoroanilino)-7-methoxy-6-(3-morpholinopropoxy)quinazoline [13–15].
- 4-Quinazolinamine, *N*-(3-chloro-4-fluorophenyl)-7-methoxy-6-(3-(4-morpholin)propoxy) [16].

### 1.1.2 Nonproprietary names

Gefitinib [14–16]

Synonyms: ZD-1839, ZD1839 [14–16]

### 1.1.3 Proprietary names

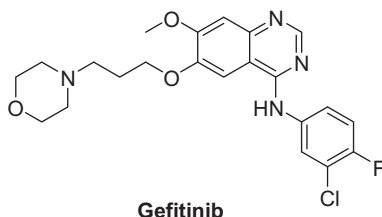
Iressa® [14–16]

## 1.2. Formulae

### 1.2.1 Empirical formula, molecular weight, and CAS number

Gefitinib:  $C_{22}H_{24}ClFN_4O_3$ , average: 446.902, monoisotopic: 446.152096566, CAS number: 184475-35-2 [10,11].

### 1.2.2 Structural formula



### 1.2.3 SMILES

COC1=CC2=C(C=C1OCCCN1CCOCC1)C(NC1=CC(Cl)=C(F)C=C1)=NC=N2 [11,17].

### 1.2.4 InChI

1S/C22H24ClFN4O3/c1-29-20-13-19-16(12-21(20)31-8-2-5-28-6-9-30-10-7-28)22(26-14-25-19)27-15-3-4-18(24)17(23)11-15/h3-4,11-14H,2,5-10H2,1H3,(H,25,26,27) [11].

## 1.3. Elemental analysis

C, 59.13%; H, 5.41%; N, 12.54% [calculated].

Found: C, 59.17%; H, 5.21%; N, 12.33% [13].

## 1.4. Physical properties

### 1.4.1 Appearance

White powder [11,14,16]

### 1.4.2 Solubility

Gefitinib can be defined as sparingly soluble at pH 1, but is practically insoluble above pH 7, with the solubility dropping sharply between pH 4 and pH 6. In nonaqueous solvents, gefitinib is freely soluble in glacial acetic acid and dimethyl sulfoxide, soluble in pyridine, sparingly soluble in tetrahydrofuran, and slightly soluble in methanol, ethanol (99.5%), ethyl acetate, and propan-2-ol and acetonitrile [16].

### 1.4.3 Melting point

174–175 °C [18], 119–120 °C [12], 193–195 °C [13].

### 1.4.4 Stability

#### 1.4.4.1 Storage and stability

Gefitinib is provided as a solid product and shipped at room temperature. Store at  $-20^{\circ}\text{C}$ . Solid product is stable 1 year at  $-20^{\circ}\text{C}$  when properly stored. Upon resuspension, gefitinib should be aliquoted and stored at  $-20^{\circ}\text{C}$ , and one must avoid repeated freeze–thaw cycles. Resuspended product is stable for 3 months at  $-20^{\circ}\text{C}$  when properly stored.

#### 1.4.4.2 Description

Gefitinib is a selective inhibitor of EGFR, a growth factor that plays a pivotal role in the control of cell growth, apoptosis, and angiogenesis. EGFR activation stimulates many complex intracellular signaling pathways, primarily the mitogen-activated protein kinases/extracellular signal-regulated kinases and PI3K/AKT pathways [18,19]. Following EGFR activation, Src tyrosine kinases and signal transducer and activator of transcription downstream signaling have also been well documented. Recent studies demonstrated that gefitinib can inhibit nucleotide oligomerization domain protein 2 (NOD2)-induced cytokine release and nuclear factor kappa B (NF- $\kappa$ B) activation by inhibiting receptor-interacting protein 2 tyrosine phosphorylation which is critical for activation of NOD2 downstream signaling pathways [20].

### 1.4.5 Dissociation constant

$pK_a$  values: 5.4 and 7.2 [16]

### 1.4.6 Partition coefficient

( $P$  is the partition coefficient of the molecule in the water–octanol system)  
 $\log P$ : 3.2 [11].

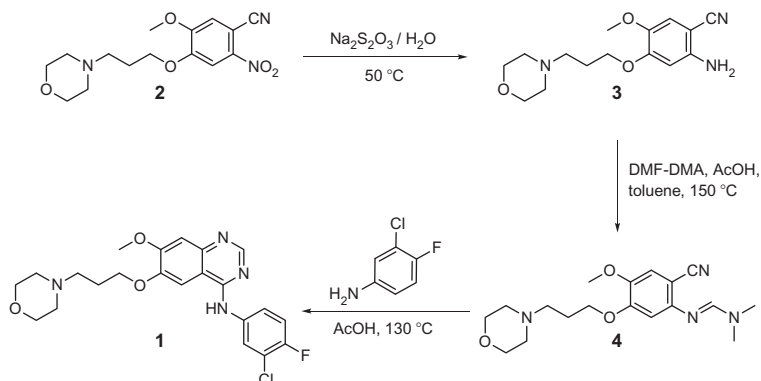
## 1.5. Uses and applications

Gefitinib (originally coded ZD1839) is a drug used in the treatment of certain types of cancer. Acting in a similar manner to erlotinib (Tarceva<sup>®</sup>), gefitinib selectively targets the mutant proteins in malignant cells. It is marketed by AstraZeneca under the trade name Iressa [11].



## 2. METHODS OF PREPARATION

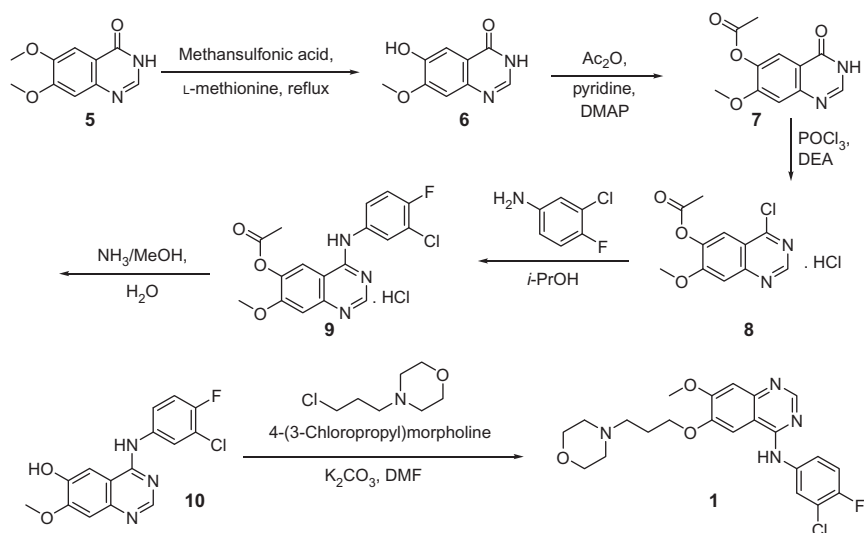
Synthesis of gefitinib (**1**) (Scheme 5.1) has been accomplished starting from key intermediate **3** [13]. Reduction of the nitro group of compound **3** was carried out in aqueous medium using sodium dithionite at  $50^{\circ}\text{C}$  to



**Scheme 5.1** Synthesis of gefitinib (1) [13].

obtain compound 4 in 95% yield. Compound 4 was treated with dimethylformamide–dimethylacetal in toluene to produce *N,N*-dimethyl formamidine derivative 5. To the formamidine 5 formed without further purification was added acetic acid and 3-chloro-4-fluoroaniline, and the mixture was heated to  $130^\circ\text{C}$  to produce crude material 1, which was further purified by recrystallization to give pure material in 70% yield.

The synthesis of gefitinib (3, Scheme 5.2) also was achieved by Venkateshappa Chandregowda in 2006 [13] starting with regioselective



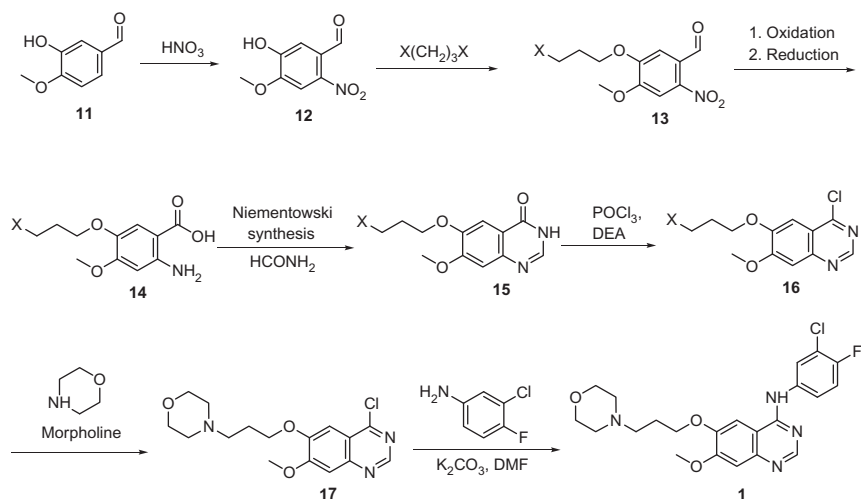
**Scheme 5.2** Synthesis of gefitinib (1) [21–23].

demethylation of 6,7-dimethoxy-3H-quinazolin-4-one followed by O-protection in 33% overall yields.

Rao *et al.* in 2010 as well as Tung in 2011 synthesized gefitinib (**1**, Scheme 5.3) [22–24] from isovanillin with previously described modified method [21].

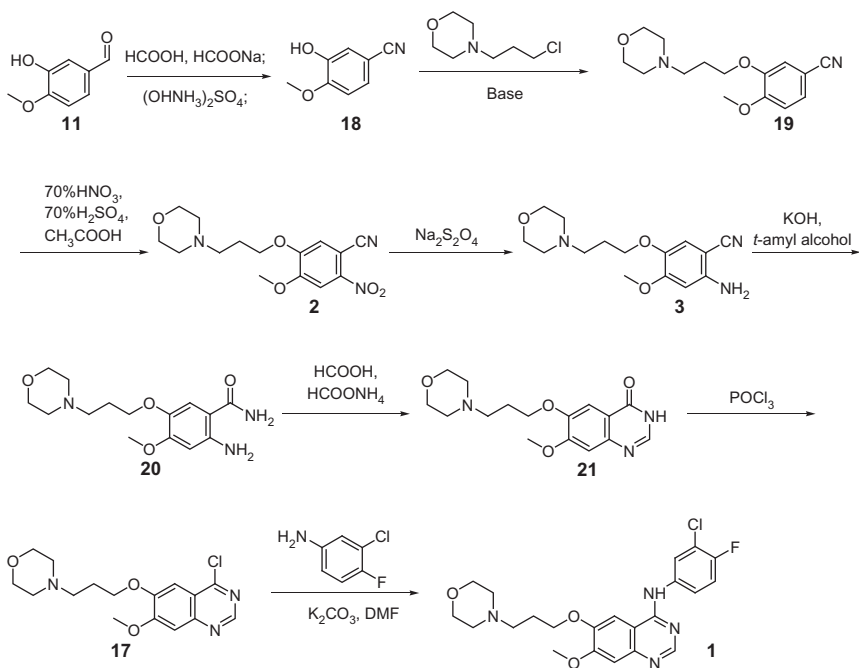
Gilday *et al.* [25] have designed a novel method (Scheme 5.4) for synthesizing gefitinib starting from the conversion of 3-hydroxy-4-methoxybenzaldehyde (**11**) into the corresponding nitrile, followed by alkylation, nitration, reduction, nitrile hydrolysis, cyclization, chlorination, and then the reaction of the chloride with 3-chloro-4-fluoroaniline to afford gefitinib in eight steps overall. Wang *et al.* have used this route to produce the target compound in radiolabeled form in 11% overall yield [26].

Novel synthesis of gefitinib (Scheme 5.5) was established from methyl 3-hydroxy-4-methoxybenzoate (**22**). This compound was alkylated with 1-bromo-3-chloropropane to afford the intermediate **23** in 94.7% yield [12]. Nitration of **23** with nitric acid in acetic acid gave compound **24**, which was reduced by powdered iron in acetic acid to give compound **25** in satisfactory yield (77%). Catalytic hydrogenation using Raney/Ni or 5% Pd/C gave incomplete conversions even after long reaction times. Cyclization of **25** with formamidine acetate and chlorination with thionyl chloride affords compound **27**. The final product was obtained after two reactions with different amines.

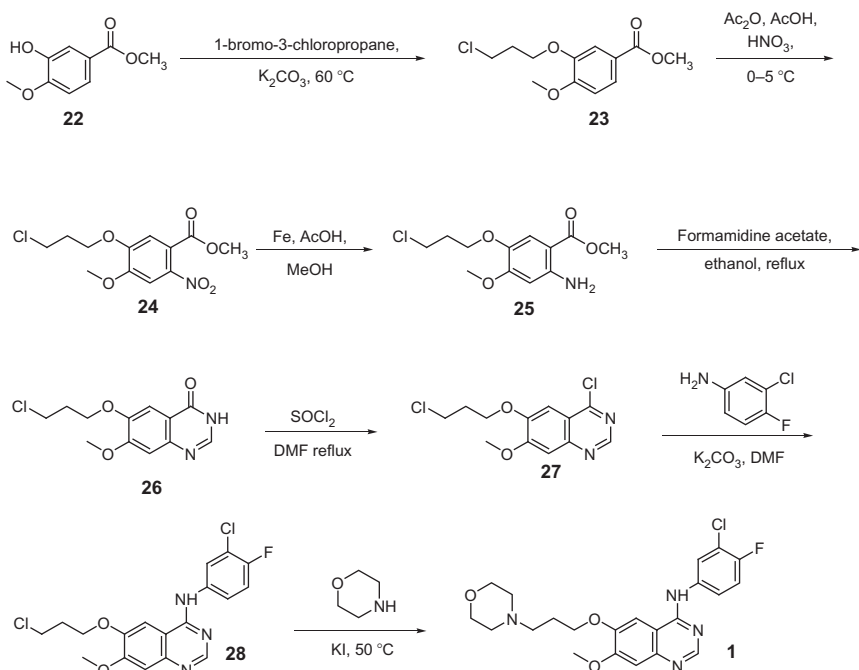


Scheme 5.3 Synthesis of gefitinib (**1**) [22].





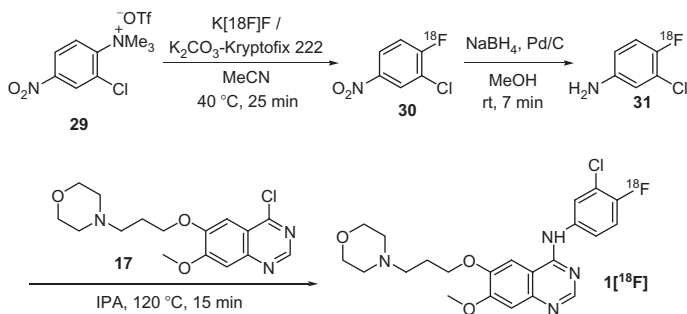
Scheme 5.4 Synthesis of gefitinib (**1**) [26].



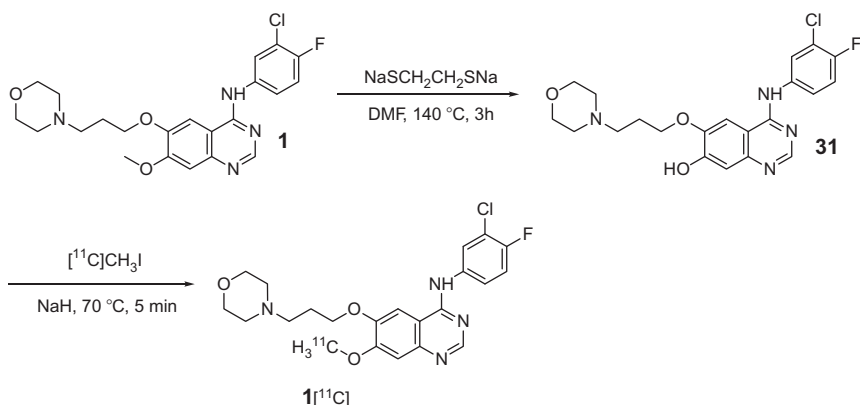
Scheme 5.5 Synthesis of gefitinib (**1**) [12].

$^{18}\text{F}$ -gefitinib was prepared in a three-step reaction sequence as depicted in Scheme 5.6 [27]. Fluorination of 3-chloro-4-trimethyl ammonium-nitrobenzene triflate provided 3-chloro-4- $^{18}\text{F}$ fluoro-nitrobenzene, which was reduced to 3-chloro-4- $^{18}\text{F}$  fluoroaniline, and coupled to the quinazoline precursor to yield  $^{18}\text{F}$  gefitinib.

Deprotection of methyl group of gefitinib done for the radiosynthesis of  $^{11}\text{C}$  gefitinib obtained **31**. The radiosynthesis was carried out using an automated synthesis system for  $^{11}\text{C}$ -labeled radiopharmaceuticals.  $^{11}\text{C}$  Methylation of **31** with  $^{11}\text{C}$ - $\text{CH}_3\text{I}$  was performed in the presence of NaH at 70 °C for 5 min. After the reaction, purification, and formulation,  $^{11}\text{C}$ -gefitinib was obtained with radioactivity incorporation yields of 41–62% (Scheme 5.7) [28].



Scheme 5.6 Synthesis of  $^{18}\text{F}$ -gefitinib (**1**) [27].



Scheme 5.7 Synthesis of **1**  $^{11}\text{C}$  gefitinib ( $^{11}\text{C}$ Iressa) [28].



## 3. PHYSICAL PROPERTIES

### 3.1. Spectroscopy

#### 3.1.1 Ultraviolet spectroscopy

Gefitinib ultraviolet/visible (UV/VIS)-absorption spectrum was recorded for selecting the proper maximum absorption peak ( $\lambda_{\max}$ ). The absorption spectrum of gefitinib in ethanol was scanned from 200 to 400 nm, using UV/VIS spectrometer (Varian Cary 50 Conc UV/VIS spectrophotometer). As shown in [Figure 5.1](#), the  $\lambda_{\max}$  of gefitinib is located at 331 nm.

#### 3.1.2 Vibrational spectroscopy

##### 3.1.2.1 IR Spectroscopy of gefitinib

The infrared absorption spectrum of gefitinib was obtained in a KBr pellet, using a Shimadzu infrared spectrophotometer. The IR spectrum is shown in [Figure 5.2](#). The principal peaks were observed at 3400, 2956, 2808, 1625, 1578, 1532, 1500, 1472, 1429, 1398, 1227, 1219, 1110, 1028, 847, and 542  $\text{cm}^{-1}$ . Assignments for the major infrared absorption band are provided in [Table 5.1](#).

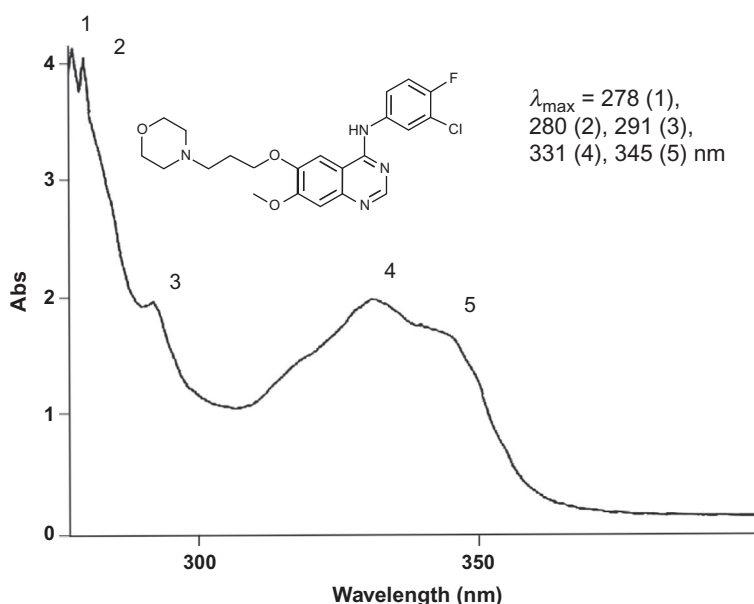
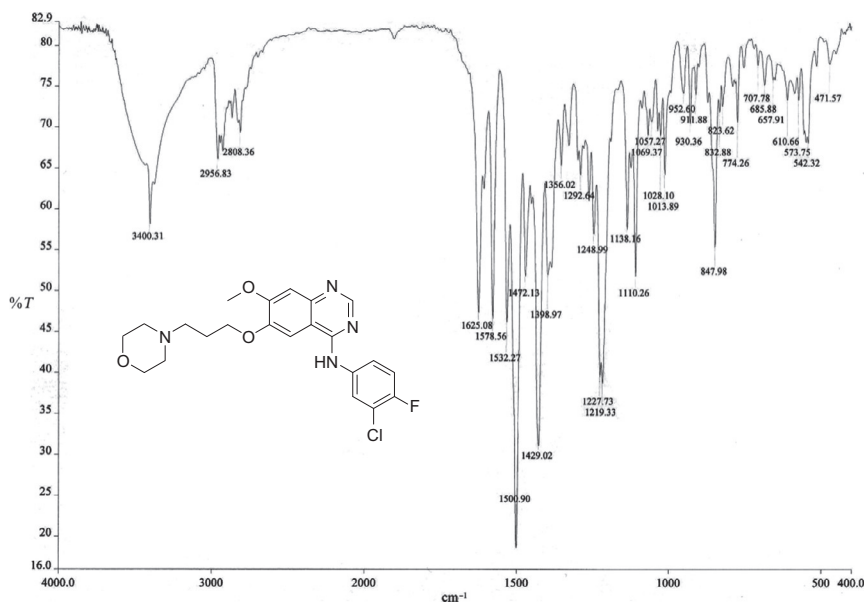


Figure 5.1 UV spectra of gefitinib ( $1 \times 10^{-4}$  M solution in ethanol).



**Figure 5.2** Infrared spectroscopy (IR) spectra of gefitinib in KBr plate.

**Table 5.1** Infrared spectroscopic data for gefitinib in KBr plate

Entry	Bond	Absorption peaks ( $\lambda_{\max}$ ) ( $\text{cm}^{-1}$ )	Appearance
1	C—F	1028	Strong
2	C=C, C=N	1625	Strong
2	C—O	1110	Strong
3	CH <sub>2</sub> , C—H (alkyl)	2956	Strong
4	HC=CH (aryl)	1500	Strong
5	N—H	3400	Broad

### 3.1.3 Nuclear magnetic resonance spectrometry

<sup>1</sup>H and <sup>13</sup>C nuclear magnetic resonance (NMR) spectra of gefitinib were registered with a Bruker 500 MHz Nuclear Magnetic Spectrometer. Chemical shifts were expressed in parts per million (ppm) (Table 5.2) with respect to the tetramethylsilane signal for <sup>1</sup>H and <sup>13</sup>C NMR (Figures 5.3 and 5.4, respectively).

#### 3.1.3.1 <sup>1</sup>H NMR spectrum

<sup>1</sup>H-NMR (DMSO-*d*<sub>6</sub>, 500 MHz):  $\delta$  9.54 (s, 1H, HAr), 8.50 (s, 1H, HAr), 8.13 (s, 1H, HAr), 7.80 (d, *J* = 5.5 Hz, 2H, HAr), 7.45–7.42 (m, 1H, HAr),

**Table 5.2** Comparative study of  $^1\text{H}$  spectra for gefitinib with literature

Entry	Chemical shift <sup>a</sup> (gefitinib) (500 MHz, $\text{DMSO}-d_6$ )	Chemical shift <sup>b</sup> (200 MHz, $\text{DMSO}-d_6$ )	Chemical shift <sup>c</sup> (200 MHz, $\text{CDCl}_3$ )
1	9.54 (s, 1H, HAr)	9.51 (s, 1H, HAr)	8.66 (s, 1H)
2	8.50 (s, 1H, HAr)	8.48 (s, 1H, HAr)	7.84–7.88 (m, 1H)
3	8.13 (s, 1H, HAr)	8.08–8.13 (m, 1H, HAr)	7.50–7.58 (m, 1H)
4	7.80 (d, $J=5.5$ Hz, 2H, HAr)	7.45–7.82 (m, 2H, HAr)	7.34 (br s, 1H, exchangeable with $\text{D}_2\text{O}$ )
5	7.45–7.42 (m, 1H, HAr)	7.35–7.45 (m, 1H, HAr)	7.26 (s, 1H)
6	7.19 (s, 1H, HAr)	7.16 (s, 1H, HAr)	7.16 (t, $J=8.8$ Hz, 1H)
7	4.18 (d, $J=5.5$ Hz, 2H, $\text{ArOCH}_2$ )	4.12–4.18 (m, 2H, $\text{ArOCH}_2$ )	7.09 (s, 1H)
8	3.94 (s, 3H, $\text{OCH}_3$ )	3.92 (s, 3H, $\text{OCH}_3$ )	4.17 (t, $J=6.5$ Hz, 2H)
9	3.59 (s, 4H, $\text{O}(\text{CH}_2)_2$ )	3.54–3.59 (m, 4H, $\text{O}(\text{CH}_2)_2$ )	3.98 (s, 3H)
10	3.40 (s, 1H, NH)	–	3.74 (dd, $J=4.5$ and 4.4 Hz, 4H)
11	2.50–2.40 (m, 6H, $\text{N}(\text{CH}_2)_3$ )	2.34–2.51 (m, 6H, $\text{N}(\text{CH}_3)_3$ )	2.46–2.59 (m, 6H)
12	2.00 (m, 2H, $\text{CH}_2\text{CH}_2\text{CH}_2$ )	1.93–2.00 (m, 2H, $\text{CH}_2\text{CH}_2\text{CH}_2$ )	2.11 (m, 2H)

<sup>a</sup> $^1\text{H}$  NMR was taken in  $\text{DMSO}-d_6$ .<sup>b</sup>Ref. [21].<sup>c</sup>Ref. [13].

7.19 (s, 1H, HAr.), 4.18 (d,  $J=5.5$  Hz, 2H,  $\text{ArOCH}_2$ ), 3.94 (s, 3H,  $\text{OCH}_3$ ), 3.59 (s, 4H,  $\text{O}(\text{CH}_2)_2$ ), 3.40 (s, 1H, NH), 2.50–2.40 (m, 6H,  $\text{N}(\text{CH}_2)_3$ ), and 2.00 (m, 2H,  $\text{CH}_2\text{CH}_2\text{CH}_2$ ) ppm.

### 3.1.3.2 $^{13}\text{C}$ NMR spectrum

Unreported  $^{13}\text{C}$  NMR data of gefitinib are given below:  $^{13}\text{C}$ -NMR ( $\text{DMSO}-d_6$ , 125 MHz):  $\delta$  155.97, 154.48, 153.10 ( $^2J_{\text{C-F}}=241.25$  Hz), 152.56, 148.32, 146.75, 136.80, 123.44, 122.27 ( $^4J_{\text{C-F}}=6.38$  Hz), 118.72 ( $^3J_{\text{C-F}}=18.25$  Hz), 116.45 ( $^3J_{\text{C-F}}=21.25$  Hz), 108.75, 107.26, 102.49, 67.11, 66.15, 55.83, 54.93, 53.41, and 25.85 ppm.

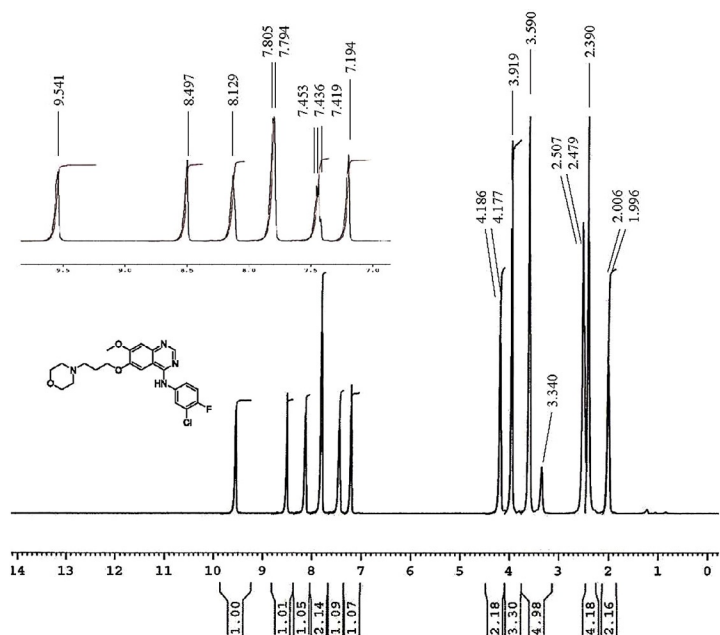


Figure 5.3 <sup>1</sup>H NMR spectra of gefitinib in DMSO-*d*<sub>6</sub>.

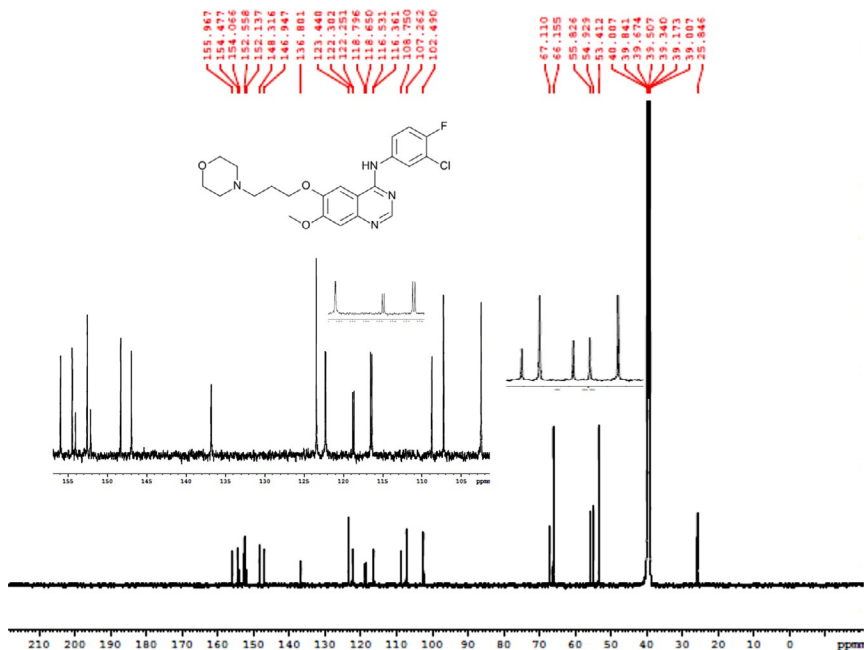


Figure 5.4 <sup>13</sup>C NMR Spectra of gefitinib in DMSO-*d*<sub>6</sub>.

## 3.2. Mass spectrum

Mass spectra of gefitinib was carried out with Agilent 6320 Ion Trap LC/MS system by infusion of 2  $\mu\text{g}$  of gefitinib solution in acetonitrile:H<sub>2</sub>O (1:1) without a column. Smart fragmentor and automatic optimization were done to obtain the spectra and make fragmentation. Source parameters were as follows: temperature was 350 °C, gas flow was 12 L/min, and nebulizer was 60 psi. Figure 5.5 shows the mass spectrum for the parent compound ( $m/z=447.0$ ), Figures 5.6 and 5.7 show the detail mass fragmentation pattern interpretation of the drug substance. The reported  $m/z$  was 446 (M)<sup>+</sup> [13].

### 3.2.1 Fragmentation pattern of gefitinib

The MS–MS scan of the molecular ion peak gives four fragments, at  $m/z$  428.3, 348.2, 310.2, and 127.4 (Figure 5.6).

The MS–MS–MS scan of the  $m/z=428.3$  fragment yielded a number of peaks, including  $m/z$  410.8, 396.1, 381.7, 353.4, 327.9, 280.5, 245.4, 213.7, 166.4, and 146.2. The major fragments are shown in Figure 5.7.

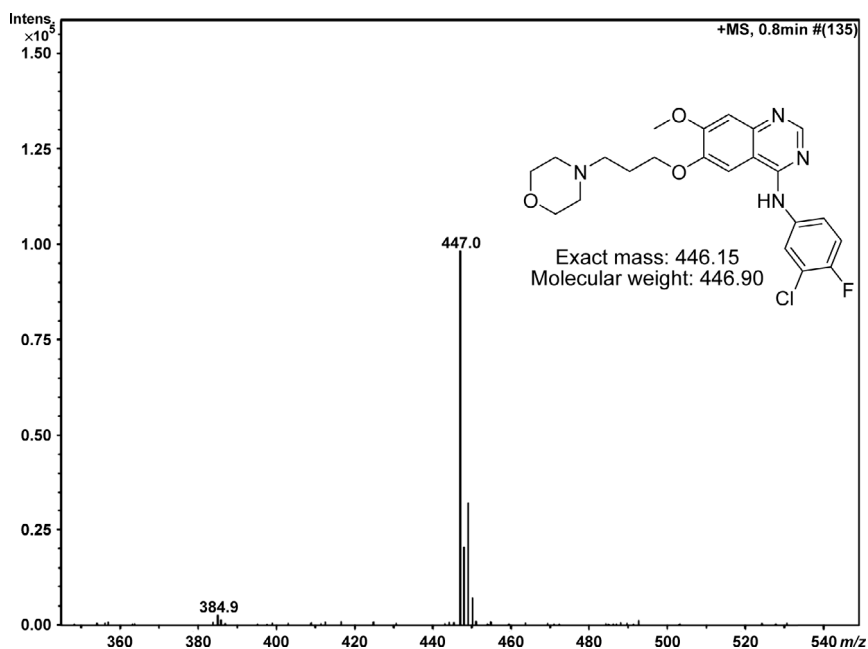


Figure 5.5 Gefitinib shows a  $m/z=447.0$  molecular ion peak in positive mode.

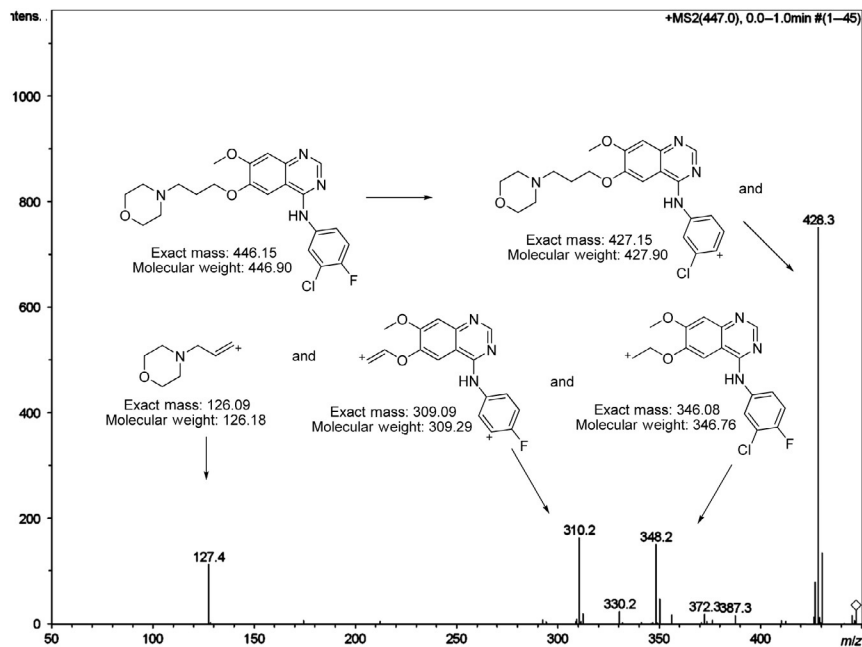


Figure 5.6 MS-MS spectra for the  $m/z=447.0$  fragment in positive mode.

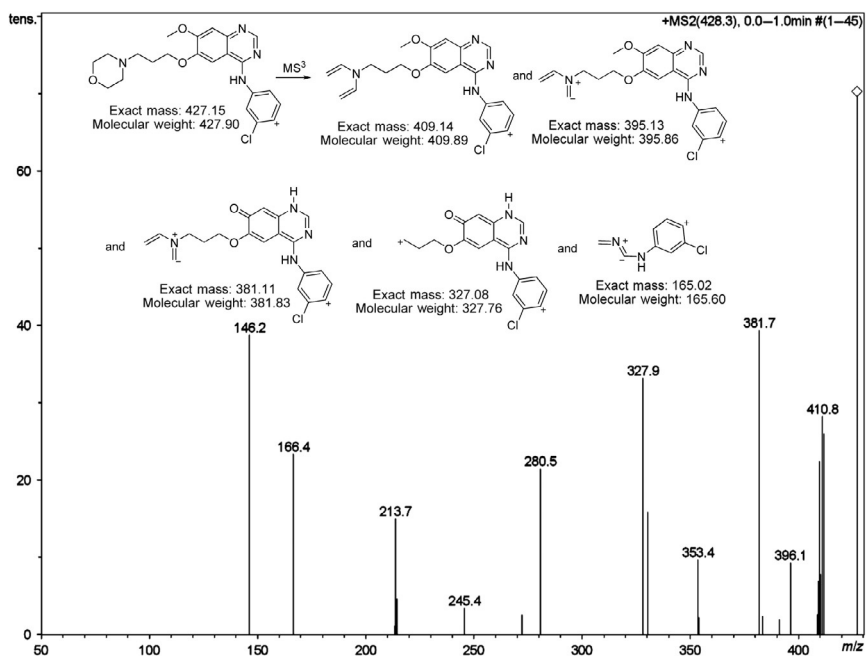


Figure 5.7 MS-MS-MS spectrum for the  $m/z=428.3$  fragment in positive mode.



**Table 5.3** Crystal and experimental data [29]

---

Formula: C <sub>22</sub> H <sub>24</sub> ClNFN <sub>4</sub> O <sub>3</sub>
Formula weight: 446.91
Crystal system: triclinic
Space group: <i>P</i> 1 <i>Z</i> =2
<i>a</i> =8.928 (1) Å; $\alpha$ =97.12 (1)°
<i>b</i> =9.717 (2) Å; $\beta$ =93.31 (1)°
<i>c</i> =12.604 (2) Å; $\gamma$ =101.47 (1)°
<i>V</i> =1059.6 (3) Å <sup>3</sup> [30]
<i>D<sub>x</sub></i> =1.401 g/cm <sup>3</sup> [30]
No. of reflections ( <i>I</i> >2.00 $\sigma$ ( <i>I</i> ))=2766
$\theta_{\text{max}}$ =68.25° with   Cu <i>K<sub>α</sub></i>
<i>R</i> ( <i>I</i> >2.00 $\sigma$ ( <i>I</i> ))=0.053
( $\Delta/\sigma$ ) <sub>max</sub> =0.000
( $\Delta/\sigma$ ) <sub>max</sub> =0.33 eÅ [30]
( $\Delta/\sigma$ ) <sub>min</sub> =−0.29 eÅ [30]
Measurement: Rigaku RAXIS-RAPID
Program system: CrystalStructure 3.5.1 [31]
Structure determination : SIR92 [30]
Refinement: full-matrix

---

### 3.3. X-Ray powder diffraction pattern

Gefitinib crystallizes in the triclinic *P*1 space group, with cell dimension of *a*=8.928 (1), *b*=9.717 (2), *c*=12.604 (2) Å,  $\alpha$ =97.12 (1), and  $\beta$ =93.31 (1), and  $\gamma$ =101.47 (1)°. The final *R* value is 0.053 (Table 5.3). The quinazoline and benzene rings are nearly coplanar [29].



## 4. METHODS OF ANALYSIS

### 4.1. Chromatographic methods

#### 4.1.1 High-performance liquid chromatography/mass spectrometry [7,31–34]

Several high-performance liquid chromatography/mass spectrometry (LC/MS/MS) methods have been reported to determine gefitinib, either as a single drug or in combination with other tyrosine kinase inhibitors (TKIs) and/or its metabolite *o*-desmethyl gefitinib in plasma [31,35–39]. Table 5.4 outlines recent methods published for the analysis of gefitinib LC/MS/MS. Honeywell *et al.* [32] have reported the use of LC/MS/MS techniques for the analysis of gefitinib. Utilizing a simple protein precipitation with acetonitrile, a 20  $\mu$ L sample volume of biological matrixes can be

**Table 5.4** Comparison of LC–MS/MS methods for gefitinib biological matrices

Biological matrix	Sample clean up	Run time	Sensitivity (LOQ)	%Recovery	Ref.
Cell culture	Protein precipitation	5 min	11.2 nM	86–107%	[32]
Human plasma, mouse plasma, and tissues	Protein precipitation	3 min	1 ng/mL (human), 5 ng/mL (mouse)	81–103%	[34]
Plasma	LLE	–	0.1 ng/mL	–	[33]
Human plasma	LLE	5 min	0.5 ng/mL	111–124%	[35]
Human plasma	–	3 min	5 ng/mL for both gefitinib and O-desmethyl gefitinib	89.7–104.7% for gefitinib and 100.4–106.0% for O-desmethyl gefitinib	[36]
Human plasma	LLE	–	5 ng/mL	90–110%	[37]
Human plasma	Solid phase extraction (SPE)	0.8 min	0.46 ng/mL	90.3–106.5%	[39]
Human plasma	LLE	–	0.30 ng/mL	91.0–97.7%	[38]

extracted at 4 °C with minimal effort. After centrifugation, the sample extract is introduced directly onto the LC/MS/MS system without further clean-up and assayed across a linear range of 1–4000 ng/mL. Chromatography was performed using a Dionex Ultimate 3000 with a Phenomenex prodigy ODS3 (2.0 mm × 100 mm, 3 µm) column and eluted at 200 µL/min with a tertiary mobile phase consisting of 20 mM ammonium acetate:acetonitrile:methanol (2.5:6.7:8.3%). Injection volumes varied from 0.1 to 1 µL depending on the concentration of the drug observed. Samples were observed to be stable for a maximum of 48 h after extraction when kept at 4 °C. Detection was performed using a turbo-spray ionization source and mass spectrometric positive multireaction-monitoring mode (+MRM) for gefitinib (447.1 *m/z*; 127.9 *m/z*), erlotinib (393.9 *m/z*; 278.2 *m/z*), sunitinib

(399.1  $m/z$ ; 283.1  $m/z$ ), and sorafenib (465.0  $m/z$ ; 251.9  $m/z$ ) at an ion voltage of +3500 V. The accuracy, precision, and limit of quantification (LOQ) from cell culture medium were as follows: gefitinib:  $100.2 \pm 3.8\%$ , 11.2 nM; erlotinib:  $101.6 \pm 3.7\%$ , 12.7 nM; sunitinib:  $100.8 \pm 4.3\%$ , 12.6 nM; sorafenib:  $93.9 \pm 3.0\%$ , 10.8 nM, respectively. This was reproducible for plasma, whole blood, and serum. The method was observed to be linear between the LOQ and 4000 ng/mL for each analyte. Effectiveness of the method is illustrated with the analysis of samples from a cellular accumulation investigation and from determination of steady-state concentrations in clinically treated patients.

Zhao *et al.* [34] described a rapid and sensitive analytical method for the determination of gefitinib concentrations in human plasma and mouse plasma and tissue based on LC/MS/MS with electrospray positive ionization after a single protein precipitation with acetonitrile. Sample preparation involved a single protein precipitation step by the addition of 0.1 mL of plasma or a 200 mg/mL tissue homogenate diluted 1/10 in human plasma with 0.3 mL acetonitrile. Separation of the compounds of interest, including the internal standard (d8)-gefitinib, was achieved on a Waters X-Terra™ C18 (50 mm  $\times$  2.1 mm i.d., 3.5  $\mu$ m) analytical column using a mobile phase consisting of acetonitrile–water (70:30, v/v) containing 0.1% formic acid and isocratic flow at 0.15 mL/min for 3 min. The analytes were monitored by tandem mass spectrometry with electrospray positive ionization. Linear calibration curves were generated over the range of 1–1000 ng/mL for the human plasma samples and 5–1000 ng/mL for mouse plasma and tissue samples with values for the coefficient of determination of greater than 0.99. The values for both within- and between-day precision and accuracy were well within the generally accepted criteria for analytical methods (less than 15%). This method was subsequently used to measure concentrations of gefitinib in mice following administration of a single dose of 150 mg/kg I.P. and in cancer patients receiving an oral daily dose of 250 mg.

The development of an on-column focusing gradient capillary LC method coupled to tandem mass spectrometry (quadrupole–linear ion trap) for the quantitative determination of gefitinib in blood plasma was described by Guetens *et al.* [33]. Plasma samples (0.2 mL) were extracted with methyl *tert*-butyl ether. The analytes of interest, ZD1839 and the internal standard [(2)H8]ZD1839 (ZD1839-d8) were eluted on a 50 mm  $\times$  1 mm, 5  $\mu$ m particle size, capillary ODS Hypersil column using an aqueous ammonium acetate gradient at 40  $\mu$ L/min. Mass spectrometric detection was performed by a Q-Trap tandem mass spectrometer with electrospray positive ionization

and monitored in the multiple reaction monitoring transitions  $447 > 128$  and  $455 > 136$ , respectively. The LOQ of ZD1839 was 0.1 ng/mL. The method proved to be robust, allowing quantification of ZD1839 with sufficient precision, accuracy, and sensitivity.

Jones *et al.* [35] described a method for the quantitative determination of gefitinib concentrations in treated healthy volunteers and patients with cancer that has been developed and validated. Plasma samples (0.5 mL) were extracted, at basic pH, with methyl-*t*-butyl ether using deuterated gefitinib as an internal standard. The extracts were chromatographed on an Inertsil ODS3 column eluted with acetonitrile/ammonium acetate and gefitinib and the internal standard quantified by mass spectrometric detection. The method was validated with respect to linearity, selectivity, precision, accuracy, LOQ, recovery, and stability. The precision and accuracy of the assay were good, and the LOQ was 0.5 ng/mL. The assay has been successfully applied to a number of clinical and pharmacokinetic studies and been shown to be robust and reliable during routine use.

A LC/MS/MS method was developed and validated by Wang *et al.* [36] for the simultaneous quantification of gefitinib and its predominant metabolite, *O*-desmethyl gefitinib, in human plasma. Chromatographic separation of analytes was achieved on an Alltima C18 analytical HPLC column (150 mm  $\times$  2.1 mm, 5  $\mu$ m) using an isocratic elution mode with a mobile phase comprised acetonitrile and 0.1% formic acid in water (30:70, v/v). The flow rate was 300  $\mu$ L/min. The chromatographic run time was 3 min. The column effluents were detected by API 4000 triple quadrupole mass spectrometer using electrospray ionization (ESI) in positive mode. Linearity was demonstrated in the range of 5–1000 ng/mL for gefitinib and 5–500 ng/mL for *O*-desmethyl gefitinib. The intra- and interday precisions for gefitinib and *O*-desmethyl gefitinib were  $\leq 10.8\%$  and the accuracies ranged from 89.7% to 104.7% for gefitinib and 100.4% to 106.0% for *O*-desmethyl gefitinib. This method was used as a bioanalytical tool in a phase I clinical trial to investigate the possible effect of hydroxychloroquine on the pharmacokinetics of gefitinib. The results of this study enabled clinicians to ascertain the safety of the combination therapy of hydroxychloroquine and gefitinib in patients with advanced (Stage IIIB–IV) NSCLC.

A quantitative LC/MS/MS method was developed and validated for the tyrosine kinase inhibitors erlotinib, gefitinib, and imatinib in human plasma by Chahbouni *et al.* [37]. Pretreatment of the samples was achieved by using liquid–liquid extraction using d8 imatinib as internal standard. Separation was performed on a Waters Alliance 2795 LC system using an XBridge

RP18 column. The mass spectrometer micromass was equipped with an ESI probe, operating in the positive mode. The calibration curves in plasma were linear for erlotinib, gefitinib, and imatinib over the concentration range of 5–3000, 5–3000, and 5–5000 ng/mL, respectively. The intra- and interday accuracy ranged from 90% to 110% and the intra- and interday precision of the method was within 5%. The reported method provided the necessary linearity, precision, and accuracy to determine tyrosine kinase inhibitors in clinical research and for therapeutic drug monitoring.

A highly sensitive liquid chromatography electrospray tandem mass spectrometry (LC–ESI–MS/MS) method had been developed by Feng Bai *et al.* [38] for the measurement of gefitinib (ZD1839) in human plasma. The method was validated over a linear range of 0.5–1000 ng/mL, using deuterated gefitinib (d8-ZD1839) as the internal standard. Compounds were extracted from 500  $\mu$ L of sodium heparin plasma by 6.0 mL butyl methyl ether liquid–liquid extraction. The dried residue was reconstituted with 250  $\mu$ L of 20% acetonitrile with 1.0% formic acid and 30  $\mu$ L injected onto the LC–ESI–MS/MS system. Chromatographic separation was achieved on a Phenomenex<sup>®</sup> Synergi 4  $\mu$  MAX-RP 80 Å C<sub>12</sub> column (75  $\times$  2.0 mm<sup>2</sup>) with an isocratic mobile phase of acetonitrile–1.0% formic acid (30:70, v/v). The analytes were detected with a PE Sciex API 365 triple quadrupole mass spectrometer using turbo ionspray<sup>®</sup> source with positive ionization. Ions monitored in the MRM mode were  $m/z$  447.2 (precursor ion) to  $m/z$  127.8 (product ion) for gefitinib and  $m/z$  455.2 (precursor ion) to  $m/z$  136.0 (product ion) for d8-ZD1839. The lower limit of quantitation of gefitinib was 0.30 ng/mL ( $S/N \geq 10$ ), and results from a 5-day validation study demonstrated acceptable within-day and between-day precision (CV % values  $\leq 6.0\%$  and  $\leq 5.2\%$ , respectively) and accuracy (range 91.0–97.7%). This method is now used to analyze plasma samples from pediatric pharmacokinetic studies of ZD1839, and the wide linear range (approximately 4 log units) of this method provides a distinct advantage, as shown by the results of a representative patient.

#### 4.1.2 Ultra-performance liquid chromatography/mass spectrometry

Bouchet *et al.* [39] described an UPLC–MS/MS method with SPE, adapted to routine application, allowing rapid, specific, and sensitive determination of the nine tyrosine kinase inhibitors. Under the described chromatographic conditions, all compounds were separated in 3 min, retention time for each analyte being between 0.76 and 2.51 min. Calibration curves ranged from 10 to 5000 ng/mL for imatinib, its metabolite, nilotinib, lapatinib, erlotinib

and sorafenib and from 0.1 to 200 ng/mL for dasatinib, axitinib, gefitinib and sunitinib. Peaks of each compound (retention time from 0.76 to 2.51 min) were adequately separated. The mean relative extraction recovery was in the range of 90.3–106.5%. There was no significant ion suppression observed at the respective TKI retention times. SPE was chosen because it allows the use of a single protocol to quantify several TKIs that have a wide range of chemical properties:  $pK_a$  values from 5 to 10, and  $\log D$  values from 0 to 4.35 at pH 7 or  $-3.75$  to  $3.9$  at pH 2 (benchmarked using Marvin 5.0.0 software, [www.chemaxon.com](http://www.chemaxon.com)). This could not be done with liquid-liquid extraction because of the different  $pK_a$  values and thus the need of different steps or buffers to extract all analytes. The second reason for choosing SPE concerns the matrix effect because it is considered as the “Achilles’ heel” of the mass spectrometry, Taylor reporting “that protein precipitation using an organic solvent or dilute and shoot are the dirtiest sample preparation techniques and thus produce the most matrix effects compared to solid phase extraction” [40].

SPE coupled to UPLC/MS–MS remains the most effective sample preparation to reduce matrix effect and specifically ion suppression [41]. Furthermore, the recent marketing of the SPE-plates (such as MCX used here) makes the method presented herein ready-to use for robotic automation. This is less time-consuming and more compatible than SPE-cartridges that often require an evaporation step, or protein precipitation that must be followed by centrifugation. By combining SPE and UPLC/MS–MS, this method allowed great sensitivity, which is of particular importance for drugs such as dasatinib and axitinib. These molecules have a short half-life (3–6 h) and thus the trough concentration is low. EPARs data show that mean trough concentration is of 1 ng/mL.

#### **4.1.3 High-performance liquid chromatography/ultraviolet detection [42–44]**

Most of the analytical methods for assessing gefitinib, in bulk as well as in pharmaceutical dosage forms, are based on HPLC methodology. These methods enable analysis of gefitinib, either as a single compound or in combination with its degradation products. In the method developed by Satyanarayana and Murali [42], an Inertsil ODS C-18, 5  $\mu$ m column having  $250 \times 4.6$  mm internal diameter in isocratic mode with mobile phase containing acetonitrile:methanol:tetrahydrofuran in the ratio of 20:70:10 (v/v/v) was used. The flow rate was 1.0 mL/min and effluents were monitored at 251 nm. The retention time for gefitinib was 4.28 min.

The method was validated for linearity, accuracy, precision, specificity, limit of detection, LOQ, and robustness. Limit of detection and LOQ were found to be 0.09 and 0.29 ppm, respectively, and recovery of gefitinib from tablet formulation was found to be 99.16%.

In another method for the estimation of gefitinib in tablet dosage form has been developed by Kumar *et al.* [43]. A Hypersil BDS RP C18,  $250 \times 4.6$  mm, 5  $\mu$ m particle size, with mobile phase consisting of 0.02 M dipotassium hydrogen orthophosphate and methanol in the ratio of 10:90 v/v was used. The flow rate was 1.0 mL/min and the effluents were monitored at 246 nm. The retention time was 3.7 min. The detector response was linear in the concentration of 25–300 g/mL. The respective linear regression equation being  $Y = 94342.26x + 77672.7$ . The limit of detection and LOQ was 0.125 and 0.15  $\mu$ g/mL respectively. The percentage recovery of gefitinib was 99.5%.

A degradation pathway for gefitinib is established as per ICH recommendations by validation and stability indicating reverse-phase liquid chromatographic method, which was developed by Madireddy Venkataramanna *et al.* [44], gefitinib is subjected to stress conditions of acid, base, oxidation, thermal, and photolysis. Significant degradation is observed in acid and base stress conditions. Two impurities are studied, among which one impurity is found to be the prominent degradant. The stress samples are assayed against a qualified reference standard, and the mass balance is found close to 99.5%. Efficient chromatographic separation is achieved on a Agilent make XDB-C18,  $50 \times 4.6$  mm with 1.8  $\mu$ m particles stationary phase with simple mobile phase combination delivered in gradient mode, and quantification is carried at 250 nm at a flow rate of 0.5 mL/min. In the developed RPLC method, the resolution between gefitinib and the potential impurities is found to be greater than 5.0. Regression analysis shows an  $r$  value (correlation coefficient) of greater than 0.998 for gefitinib and the two potential impurities. This method is capable to detect the impurities of gefitinib at a level of 0.01% with respect to test concentration of 0.5 mg/mL for a 4- $\mu$ L injection volume.



## 5. PHARMACOLOGY

Gefitinib is a small-molecule (446.9 Da) chemotherapeutic agent that specifically inhibits EGFR-tyrosine kinase for the treatment of NSCLC [45]. Gefitinib competitively and reversibly binds to the ATP-binding sites of EGFR, causing downregulation of EGFR phosphorylation and subsequent downstream signaling molecules [45,46]. This in turn strongly increases

the intracellular concentrations of coadministered drug molecules that are transporter substrates. In addition, gefitinib improves progression-free survival (PFS) versus a platinum doublet regime in patients harboring EGFR mutations. Although gefitinib is yet to be proven to be effective in other types of cancer, several studies showed a potential for gefitinib use in the treatment of EGFR overexpressed-type of cancer [46]. In randomized, large-scale, double-blinded study comparing gefitinib versus carboplatin/paclitaxel for treatment of advanced NSCLC showed that progression-free survival was significantly longer for gefitinib than other chemotherapies in patients with EGFR mutation positive tumors [45].

## 5.1. Pharmacokinetics

### 5.1.1 Absorption

Gefitinib is usually administered as a once-daily oral tablet. After oral administration, gefitinib is absorbed slowly with a bioavailability of approximately 60% in human [47]. However, this bioavailability is not altered dramatically by food or any other gastrointestinal factors [48].

### 5.1.2 Distribution

The relationship between the pharmacokinetics and long-term antitumor activity of gefitinib in patients with EGFR mutation-positive lung adenocarcinoma has been reported. In that, lung cancer patients on gefitinib who showed partial response exhibited a lower  $C_{\max}$  (278 ng/mL) than that of patients with stable disease 588 ng/mL [49]. Conversely, a significant negative correlation was found between the area under the plasma concentration–time curve (AUC)<sub>0–24</sub> of gefitinib and longer survival [49]. After oral administration, gefitinib is widely distributed throughout the body. Following IV dosing (5 mg/kg) of gefitinib, a plasma elimination half-life of 7–14 h was reported in rats and dogs using HPLC–MS assay, with an apparent volume of distribution of 1400 L [50]. Gefitinib is highly bound to human plasma albumin and  $\alpha$ 1-acid glycoprotein by 90%. In human, the maximum elimination half-life reaches 48 h and the steady state plasma concentrations are achieved within 10 days. Following administration of [<sup>14</sup>C]-gefitinib, concentrations of radioactivity in plasma exceeded gefitinib throughout the profile, indicating the presence of circulating metabolites [51]. In comparison with erlotinib, gefitinib has a longer elimination half-life and a larger tissue distribution [52].



### 5.1.3 Metabolism

Gefitinib is metabolized extensively in the liver by cytochrome P450 enzymes, primarily by CYP3A4 and to a lesser extent by CYP3A5 and CYP2D6 [53]. Five metabolites were identified in human plasma, among which only O-desmethyl gefitinib has a similar EGFR–TK activity to gefitinib [51]. Gefitinib has also been implicated as an inhibitor of CYP2C19 and CYP2D6 activity, but weak inhibitor of CYP2C9, CYP3A4, and CYP1A2. Therefore, gefitinib may inhibit the metabolism of coadministered drugs that are substrates of CYP2C19 and CYP2D6. At the highest concentration studied (5000 ng/mL), gefitinib inhibited CYP2C19 by 24% and CYP2D6 by 43% [53]. After administration of gefitinib 5 mg/kg to rats and dogs, five metabolites were detected, but at levels much lower than the parent drug [50]. In clinical studies, coadministration of gefitinib and rifampicin reduced gefitinib maximum concentration and AUC by approximately 65% and 83%, respectively.

### 5.1.4 Excretion

In human, gefitinib is mainly eliminated hepatically, with total plasma clearance of 595 mL/min after intravenous administration, in which the excretion is predominantly via the feces (86%) [47]. However in rats and dogs, the plasma clearance was reported approximately 25 and 16 mL/min/kg for both male rats and dogs, respectively [50].

## 5.2. Toxicities

In phase I clinical trials, gefitinib was found to be well tolerated, with clinical efficacy observed well below the maximum tolerated dose. Most of the adverse effects associated with gefitinib therapy are mild to moderate in severity and are usually reversible and manageable with appropriate intervention. Examples of these common side effects include diarrhea, dry skin, acneiform rash, and nausea and vomiting [54]. Rare cases (about 1%) of interstitial lung disease such as pneumonia or inflammation were also reported. Serious side effects have been reported with the use of gefitinib including: allergic reactions, difficulty of breathing, swelling of the lips, tongue, and elevated liver enzymes [55].

## ACKNOWLEDGMENT

This work was supported by the College of Pharmacy Research Center, King Saud University.

## REFERENCES

- [1] J. Schlessinger, Cell signaling by receptor tyrosine kinases, *Cell* 103 (2000) 211–225.
- [2] J. Baselga, Targeting tyrosine kinases in cancer: the second wave, *Science* 312 (2006) 1175–1178.
- [3] S. Kamath, J.K. Buolamwini, Targeting EGFR and HER-2 receptor tyrosine kinases for cancer drug discovery and development, *Med. Res. Rev.* 26 (2006) 569–594.
- [4] K. Grosios, P. Traxler, Q. Zhou, Tyrosine kinases targets in drug discovery, *Drugs Fut.* 28 (2003) 679–697.
- [5] A.J. Barker, K.H. Gibson, W. Grundy, A.A. Godfrey, J.J. Barlow, M.P. Healy, J.R. Woodburn, S.E. Ashton, B.J. Curry, L. Scarlett, L. Henthorn, L. Richards, Studies leading to the identification of ZD1839 (IRESSA): an orally active, selective epidermal growth factor receptor tyrosine kinase inhibitor targeted to the treatment of cancer, *Bioorg. Med. Chem. Lett.* 11 (2001) 1911–1914.
- [6] F. Ciardiello, R. Caputo, R. Bianco, V. Damiano, G. Pomato, S. De Placido, A.R. Bianco, G. Tortora, Antitumor effect and potentiation of cytotoxic drugs activity in human cancer cells by ZD-1839 (Iressa), an epidermal growth factor receptor-selective tyrosine kinase inhibitor, *Clin. Cancer Res.* 6 (2000) 2053–2063.
- [7] J.R. Woodburn, A.J. Barker, K.H. Gibson, S.E. Ashton, A.E. Wakeling, B.J. Curry, L. Scarlett, L.R. Henthorn, ZD1839, an epidermal growth factor tyrosine kinase inhibitor selected for clinical development, *Proc. Am. Assoc. Cancer Res.* 38 (1997) 633–634.
- [8] F.M. Sirotnak, M.F. Zakowski, V.A. Miller, H.I. Scher, M.G. Kris, Efficacy of cytotoxic agents against human tumor xenografts is markedly enhanced by coadministration of ZD1839 (Iressa), an inhibitor of EGFR tyrosine kinase, *Clin. Cancer Res.* 6 (2000) 4885–4892.
- [9] J. Albanell, F. Rojo, J. Baselga, Pharmacodynamic studies with the epidermal growth factor receptor tyrosine kinase inhibitor ZD1839, *Semin. Oncol.* 28 (2001) 56–66.
- [10] IUPAC. <http://en.wikipedia.org/wiki/Gefitinib>.
- [11] D. Bank. <http://drugbank.ca/drugs/DB00317>.
- [12] M.D. Li, Y.G. Zheng, M. Ji, Synthesis of gefitinib from methyl 3-hydroxy-4-methoxybenzoate, *Molecules* 12 (2007) 673–678.
- [13] V. Chandregowda, G.V. Rao, G.C. Reddy, Convergent approach for commercial synthesis of gefitinib and erlotinib, *Org. Process Res. Dev.* 11 (2007) 83–816.
- [14] S. Sweetman (Ed.), *Martindale: The Complete Drug Reference*, 36th ed., Pharmaceutical press, London, 2009, p. 709.
- [15] T.M. Index, *An Encyclopedia of Chemicals, Drugs, and Biologicals*, 14th ed., Merck & Co., Inc., Whitehouse Station, NJ, USA, 2006, p. 754.
- [16] Drug-Bank, Gefitinib. [http://www.drugbank.ca/system/fda\\_labels/DB00317.pdf?1265922813](http://www.drugbank.ca/system/fda_labels/DB00317.pdf?1265922813); 2012.
- [17] ChemSpider. <http://www.chemspider.com/Search.aspx?q=gefitinib>.
- [18] K. Okamoto, I. Okamoto, W. Okamoto, K. Tanaka, K. Takezawa, K. Kuwata, H. Yamaguchi, K. Nishio, K. Nakagawa, Role of survivin in EGFR inhibitor-induced apoptosis in non-small cell lung cancers positive for EGFR mutations, *Cancer Res.* 70 (2010) 10402–10410.
- [19] D.L. Wheeler, E.F. Dunn, P.M. Harari, Understanding resistance to EGFR inhibitors-impact on future treatment strategies, *Nat. Rev. Clin. Oncol.* 7 (2010) 493–507.
- [20] J.T. Tigno-Aranjuez, J.M. Asara, D.W. Abbott, Inhibition of RIP2's tyrosine kinase activity limits NOD2-driven cytokine responses, *Genes Dev.* 24 (2010) 2666–2677.
- [21] P. Knesl, D. Roseling, U. Jordis, Improved synthesis of substituted 6,7-dihydroxy-4-quinazolineamines: tandutinib, erlotinib and gefitinib, *Molecules* 11 (2006) 286–297.

- [22] D.R. Rao, R.N. Khakan, S.L. Pathi, US Patent 0137586, 2010.
- [23] H.K. Gibson, Quinazoline derivatives, US Patent 5770599, 1998.
- [24] R. Tung, US Patent 0059046, 2011.
- [25] J.P. Gilday, M. David, Process for the preparation of 4-(3'-chloro-4'-fluoroanilino)-7-methoxy-6-(3-morpholinopropoxy)quinazoline, WO2004024703, 2006.
- [26] J.Q. Wang, M. Gao, K.D. Miller, G.W. Sledge, Q.H. Zheng, Synthesis of [<sup>11</sup>C]Iressa as a new potential PET cancer imaging agent for epidermal growth factor receptor tyrosine kinase, *Bioorg. Med. Chem. Lett.* 16 (2006) 4102–4106.
- [27] T. Lappchen, M.L. Vlaming, E. Custers, J. Lub, C.F. Sio, J. DeGroot, O.C. Steinbach, Automated synthesis of [<sup>18</sup>F]gefitinib on a modular system, *Appl. Radiat. Is.* 70 (2012) 205–209.
- [28] M.R. Zhang, K. Kumata, A. Hatori, N. Takai, J. Toyohara, T. Yamasaki, K. Yamamoto, J. Yui, K. Kawamura, S. Koike, K. Ando, K. Suzuki, [<sup>11</sup>C]Gefitinib ([<sup>11</sup>C]Iressa): radiosynthesis, in vitro uptake, and in vivo imaging of intact murine fibrosarcoma, *Mol. Imaging Biol.* 12 (2010) 181–191.
- [29] R. Tanaka, M. Haramura, A. Tanaka, N. Hirayama, Structure of gefitinib, *Analyt. Sci.* 20 (2004) x173–x174.
- [30] A. Altomare, G. Cascarano, C. Giacovazzo, A. Guagliardi, M. Burla, G. Polodori, M. Camalli, SIR92, *J. Appl. Cryst.* 1194 (1994) 435.
- [31] R.A. Rigaku, Crystal Structure, Crystal Structure Analysis Package, version 3.5.1 2000–2003.
- [32] R. Honeywell, K. Yarzadah, E. Giovannetti, N. Losekoot, E.F. Smit, M. Walraven, J.S. Lind, C. Tibaldi, H.M. Verheul, G.J. Peters, Simple and selective method for the determination of various tyrosine kinase inhibitors used in the clinical setting by liquid chromatography tandem mass spectrometry, *J. Chromatogr. B Analyt. Technol. Biomed. Life Sci.* 878 (2010) 1059–1068.
- [33] G. Guetens, H. Prenen, G. De Boeck, W. Van Dongen, E. Esmans, F. Lemiere, A.T. van Oosterom, P. Schoffski, E.A. de Bruijn, Sensitive and specific quantification of the anticancer agent ZD1839 (Gefitinib) in plasma by on-column focusing capillary liquid chromatography–tandem mass spectrometry, *J. Chromatogr. A* 1082 (2005) 2–5.
- [34] M. Zhao, C. Hartke, A. Jimeno, J. Li, P. He, Y. Zabelina, M. Hidalgo, S.D. Baker, Specific method for determination of gefitinib in human plasma, mouse plasma and tissues using high performance liquid chromatography coupled to tandem mass spectrometry, *J. Chromatogr. B Analyt. Technol. Biomed. Life Sci.* 819 (2005) 73–80.
- [35] H.K. Jones, L.E. Stafford, H.C. Swaisland, R. Payne, A sensitive assay for ZD1839 (Iressa) in human plasma by liquid-liquid extraction and high performance liquid chromatography with mass spectrometric detection: validation and use in Phase I clinical trials, *J. Pharm. Biomed. Anal.* 29 (2002) 221–228.
- [36] L.Z. Wang, M.Y. Lim, T.M. Chin, W.L. Thuya, P.L. Nye, A. Wong, S.Y. Chan, B.C. Goh, P.C. Ho, Rapid determination of gefitinib and its main metabolite, O-desmethyl gefitinib in human plasma using liquid chromatography–tandem mass spectrometry, *J. Chromatogr. B Analyt. Technol. Biomed. Life Sci.* 879 (2011) 2155–2161.
- [37] A. Chahbouni, J.C. den Burger, R.M. Vos, A. Sinjewel, A.J. Wilhelm, Simultaneous quantification of erlotinib, gefitinib, and imatinib in human plasma by liquid chromatography tandem mass spectrometry, *Ther. Drug Monit.* 31 (2009) 683–687.
- [38] F. Feng Bai, L.C. Iaconoa, B. Johnstona, C.F. Stewart, Determination of gefitinib in plasma by liquid chromatography with a C<sub>12</sub> column and electrospray tandem mass spectrometry detection, *J. Liq. Chrom. Relat. Tech.* 27 (2004) 2743–2758.
- [39] S. Bouchet, E. Chauzit, D. Ducint, N. Castaing, M. Canal-Raffin, N. Moore, K. Titier, M. Molimard, Simultaneous determination of nine tyrosine kinase inhibitors by 96-well solid-phase extraction and ultra performance LC/MS-MS, *Clin. Chim. Acta* 412 (2011) 1060–1067.

- [40] P.J. Taylor, Matrix effects: the Achilles heel of quantitative high-performance liquid chromatography-electrospray-tandem mass spectrometry, *Clin. Biochem.* 38 (2005) 328–334.
- [41] E. Chambers, D.M. Wagrowski-Diehl, Z. Lu, J.R. Mazzeo, Systematic and comprehensive strategy for reducing matrix effects in LC/MS/MS analyses, *J. Chromatogr. B Analyt. Technol. Biomed. Life Sci.* 852 (2007) 22–34.
- [42] P. Satyanarayana, M. Murali, Development and validation of LC method for the estimation of gefitinib in pharmaceutical dosage form, *IJRPC* 1 (2011) 338–341.
- [43] V.K. Kumar, N.A. Raju, S. Begum, J.S. Rao, T. Satyanarayana, The estimation of aprepitant in capsules dosage forms by RP-HPLC, *Res. J. Pharm. Technol.* 2 (2009) 412–414.
- [44] M. Venkataramanna, I.V. Somaraju, K.S. Babu, Identification of degradant impurity in gefitinib by using validated RRLC method, *Am. J. Anal. Chem.* 2 (2011) 75–83.
- [45] M. Joshi, A. Ayoola, C.P. Belani, Small-cell lung cancer: an update on targeted therapies, *Adv. Exp. Med. Biol.* 779 (2013) 385–404.
- [46] H.Y. Lu, X.J. Wang, W.M. Mao, Targeted therapies in small cell lung cancer, *Oncol. Lett.* 5 (2013) 3–11.
- [47] H.C. Swaisland, R.P. Smith, A. Laight, D.J. Kerr, M. Ranson, C.H. Wilder-Smith, T. Duvauchelle, Single-dose clinical pharmacokinetic studies of gefitinib, *Clin. Pharmacokinet.* 44 (2005) 1165–1177.
- [48] E. Bergman, P. Forsell, E.M. Persson, L. Knutson, P. Dickinson, R. Smith, H. Swaisland, M.R. Farmer, M.V. Cantarini, H. Lennernas, Pharmacokinetics of gefitinib in humans: the influence of gastrointestinal factors, *Int. J. Pharmaceut.* 341 (2007) 134–142.
- [49] S. Hirano, K. Sano, Y. Takeda, S. Ishii, G. Naka, M. Iikura, S. Izumi, M. Hojo, H. Sugiyama, N. Kobayashi, K. Kudo, The pharmacokinetics and long-term therapeutic effects of gefitinib in patients with lung adenocarcinoma harboring the epidermal growth factor receptor (EGFR) mutation, *Gan To Kagaku Ryoho* 39 (2012) 1501–1506.
- [50] D. McKillop, E.A. Partridge, M. Hutchison, S.A. Rhead, A.C. Parry, J. Bardsley, H.M. Woodman, H.C. Swaisland, Pharmacokinetics of gefitinib, an epidermal growth factor receptor tyrosine kinase inhibitor, in rat and dog, *Xenobiotica* 34 (2004) 901–915.
- [51] D. McKillop, A.D. McCormick, G.S. Miles, P.J. Phillips, K.J. Pickup, N. Bushby, M. Hutchison, In vitro metabolism of gefitinib in human liver microsomes, *Xenobiotica* 34 (2004) 983–1000.
- [52] D. Leveque, Pharmacokinetics of gefitinib and erlotinib, *Lancet Oncol.* 12 (2011) 1093.
- [53] M. Scheffler, P. Di Gion, O. Doroshenko, J. Wolf, U. Fuhr, Clinical pharmacokinetics of tyrosine kinase inhibitors: focus on 4-anilinoquinazolines, *Clin. Pharmacokinet.* 50 (2011) 371–403.
- [54] X. Li, T.M. Kamenecka, M.D. Cameron, Bioactivation of the epidermal growth factor receptor inhibitor gefitinib: implications for pulmonary and hepatic toxicities, *Chem. Res. Toxicol.* 22 (2009) 1736–1742.
- [55] R. Kumasaka, N. Nakamura, K. Shirato, H. Osawa, S. Takanashi, Y. Hasegawa, H. Yamabe, M. Nakamura, M. Tamura, K. Okumura, Side effects of therapy: case 1. Nephrotic syndrome associated with gefitinib therapy, *J. Clin. Oncol.* 22 (2004) 2504–2505.



# Imatinib Mesylate

**Badraddin M.H. Al-Hadiya<sup>\*</sup>, Ahmed H.H. Bakheit<sup>\*</sup>,  
Ahmed A. Abd-Elgalil<sup>†</sup>**

<sup>\*</sup>Department of Pharmaceutical Chemistry, College of Pharmacy, King Saud University, Riyadh, Saudi Arabia

<sup>†</sup>Research Center, College of Pharmacy, King Saud University, Riyadh, Saudi Arabia

## Contents

1. Background	266
2. Description	266
2.1 Nomenclature	266
2.2 Formulae	267
2.3 Elemental analysis	267
2.4 Appearance	267
3. Methods of Preparation of Imatinib	267
4. Physical Characteristics	270
4.1 Optical activity	270
4.2 Ionization constant	270
4.3 Solubility characteristics	271
4.4 Particle morphology	271
4.5 Crystallographic properties	271
4.6 Hygroscopicity	272
4.7 Thermal methods of analysis	272
4.8 Spectroscopy	275
4.9 Mass spectrometry	277
5. Methods of Analysis	279
5.1 Compendial methods of analysis	279
5.2 Electrochemical methods of analysis	282
5.3 Spectroscopic methods of analysis	283
5.4 Chromatographic methods of analysis	286
5.5 Determination in body fluids and tissues	288
6. Stability	288
7. Clinical Applications	291
7.1 Pharmacodynamics (an overview)	291
7.2 Mechanism of action	291
7.3 Clinical uses	291
7.4 Mechanisms of drug resistance	292
7.5 Pharmacokinetics	293
7.6 Toxicity	294
References	294



## 1. BACKGROUND

Imatinib was developed in the late 1990s by biochemist Nicholas Lydon, a former researcher for Novartis, and oncologist Brian Druker of Oregon Health & Science University. Other major contributions to imatinib development were made by Carlo Gambacorti-Passerini, a physician scientist and hematologist at University of Milano–Bicocca, Italy, John Goldman at Hammersmith Hospital in London, UK, and later on by Charles Sawyers of Memorial Sloan Kettering Cancer Center. Druker led the clinical trials confirming its efficacy in myelogenous leukemia (CML) [1].

Imatinib was developed by rational drug design. After the Philadelphia chromosome mutation and hyperactive bcr–abl protein were discovered, the investigators screened chemical libraries to find a drug that would inhibit that protein. With high-throughput screening, they identified 2-phenylaminopyrimidine. This lead compound was then tested and modified by the introduction of methyl and benzamide groups to give it enhanced binding properties, resulting in imatinib [2].

Gleevec received FDA approval in May 2001. Druker, Lydon, and Sawyers received the Lasker-DeBakey Clinical Medical Research Award in 2009 for “converting a fatal cancer into a manageable chronic condition.” Gleevec also holds the record for the drug with the fastest approval time by the FDA. Novartis filed international patent applications, was the manufacturer of the drug and marketed it under the name Gleevec.



## 2. DESCRIPTION

### 2.1. Nomenclature

#### 2.1.1 Systematic chemical names

$\alpha$ -(4-Methyl-1-piperazinyl)-3'-{[4-(3-pyridyl)-2-pyrimidinyl]amino}-*p*-tolu-*p*-toluidide methanesulfonate [3].

*N*-(4-methyl-3-{[4-(pyridin-3-yl) pyrimidin-2-yl] amino} phenyl) 4-[(4-methylpiperazin-1-yl)methyl]benzamide [4].

4-(4-Methylpiperazin-1-ylmethyl)-*N*-[4-methyl-3-[[4-(pyridin-3-yl) pyrimidin-2-yl]amino]phenyl]benzamide [5].

#### 2.1.2 Nonproprietary names

*Generic:* Imatinib (Imatinib Mesylate) [5].

Synonyms: CGP-57-148B; Imatinib, Mesilated; Imatinib Mesylate (USAN); Imatinibi Mesilas; Mesilatode imatinib; STI571; Imatinib Methanesulfonate [3].

### 2.1.3 Proprietary names

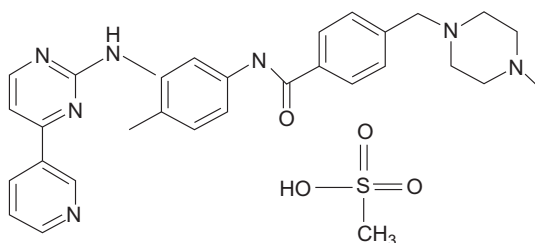
GLEEVEC, Glivec [5,6].

## 2.2. Formulae [5,6]

### 2.2.1 Empirical formula, molecular weight, and CAS number

	Empirical formula	M. weight	CAS number
Imatinib	$C_{13}H_8Cl_2N_2O_4$	493.6027	152459-95-5
Imatinib mesylate	$C_{29}H_{31}N_7O \cdot CH_4O_3S$	589.7	220127-57-1

### 2.2.2 Structural formula



### 2.3. Elemental analysis

C: 61.05%, H: 05.94%, N: 16.62%, O: 10.85%, S: 05.43%.

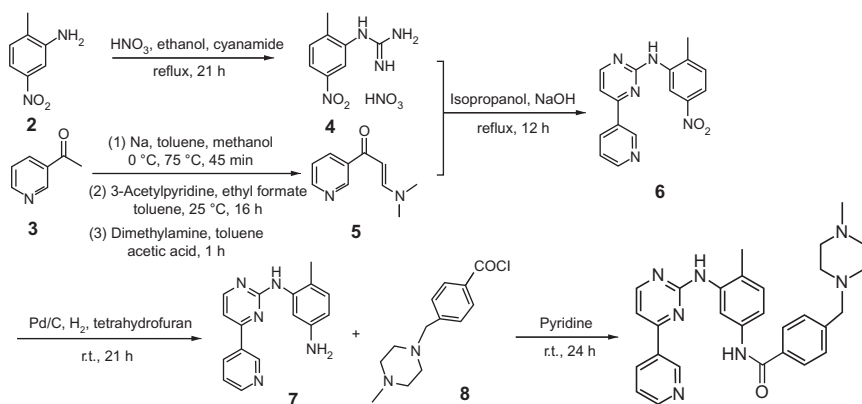
### 2.4. Appearance

White-to-off-white, odorless, crystalline powder [7,8].



## 3. METHODS OF PREPARATION OF IMATINIB

Imatinib was first synthesized by Zimmermann in 1993 (Scheme 6.1) [9]. Accordingly, 2-methyl-5-nitro-aniline (**2**) was reacted with cyanamide and nitric acid in ethanol as solvent at reflux temperatures to give [N-(2-methyl-5-nitro-phenyl) carbamimidoyl] ammonium nitrate (**4**). Condensation of **4** with 3-dimethylamino-1-(3-pyridyl)-2-propen-1-one

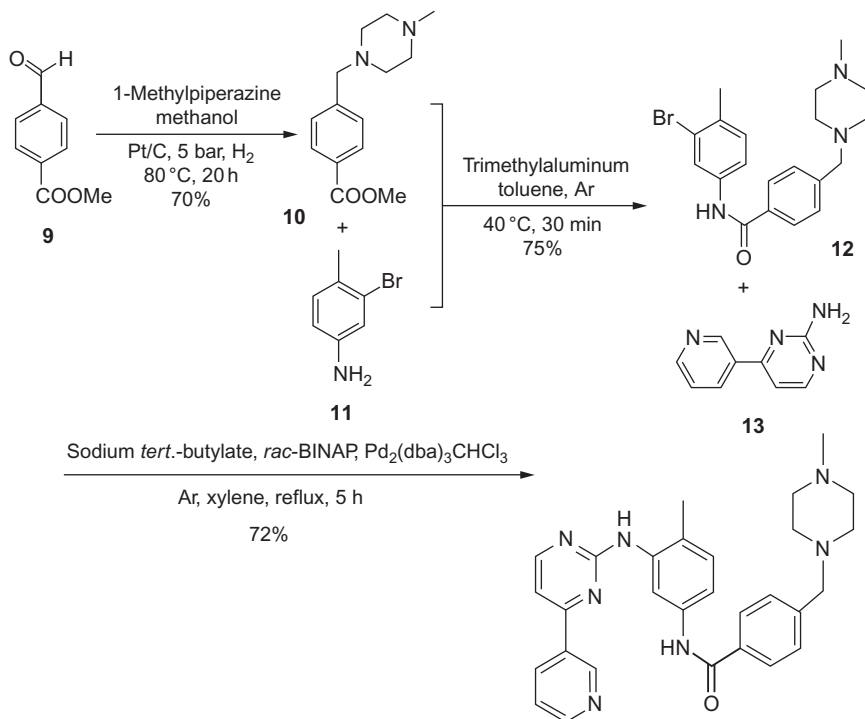


**Scheme 6.1** Zimmermann's route for the preparation of imatinib base.

(5) in presence of sodium hydroxide as base in isopropanol as solvent at elevated temperature resulted into *N*-(2-methyl-5-nitro-phenyl)-4-(3-pyridyl)pyrimidin-2-amine (6). Compound (6) was then hydrogenated in presence of 10% palladium on carbon catalyst in ethyl acetate as solvent at ambient temperature resulted in 4-methyl-*N*-3-[4-(3-pyridyl)pyrimidin-2-yl]benzene-1,3-diamine (7). The final step involves condensation of (7) with 4-(4-methylpiperazinomethyl)-benzoyl chloride (8) in pyridine at base and solvent at ambient temperature to afford 4-[(4-methylpiperazin-1-yl)methyl]-*N*-[4-methyl-3-[[4-(3-pyridyl)pyrimidin-2-yl]amino]phenyl]benzamide (1), also called imatinib.

Loiseleur *et al.* [10] described a process for the preparation of imatinib base (Scheme 6.2), in which compound (10) was prepared by the reductive amination of aldehyde 4-acetyl-benzoic acid methyl ester (9) using Pt/C-catalyzed hydrogenation. Compound (10) reacts with 3-bromo-4-methyl-phenylamine (11) in presence of trimethylaluminum, toluene, and argon at 40 °C for 30 min; the result is *N*-(3-bromo-4-methyl-phenyl)-4-(4-methylpiperazin-1-ylmethyl)-benzamide (12). The final step involves condensation of 12 with 4-pyridin-3-ylpyrimidin-2-ylamine (13) in presence of Pd<sub>2</sub>(dba)<sub>3</sub>CHCl<sub>3</sub>-catalyzed C–N coupling reaction with the use of organophosphorus reagent rac-BINAP as ligand to give 4-[(4-methylpiperazin-1-yl)methyl]-*N*-[4-methyl-3-[[4-(3-pyridyl)pyrimidin-2-yl]amino]phenyl]benzamide or imatinib (1). Subsequently, Kompella *et al.* [11] and Szakacs *et al.* [12] also, respectively, provided an improved process based on Loiseleur's method. However, the

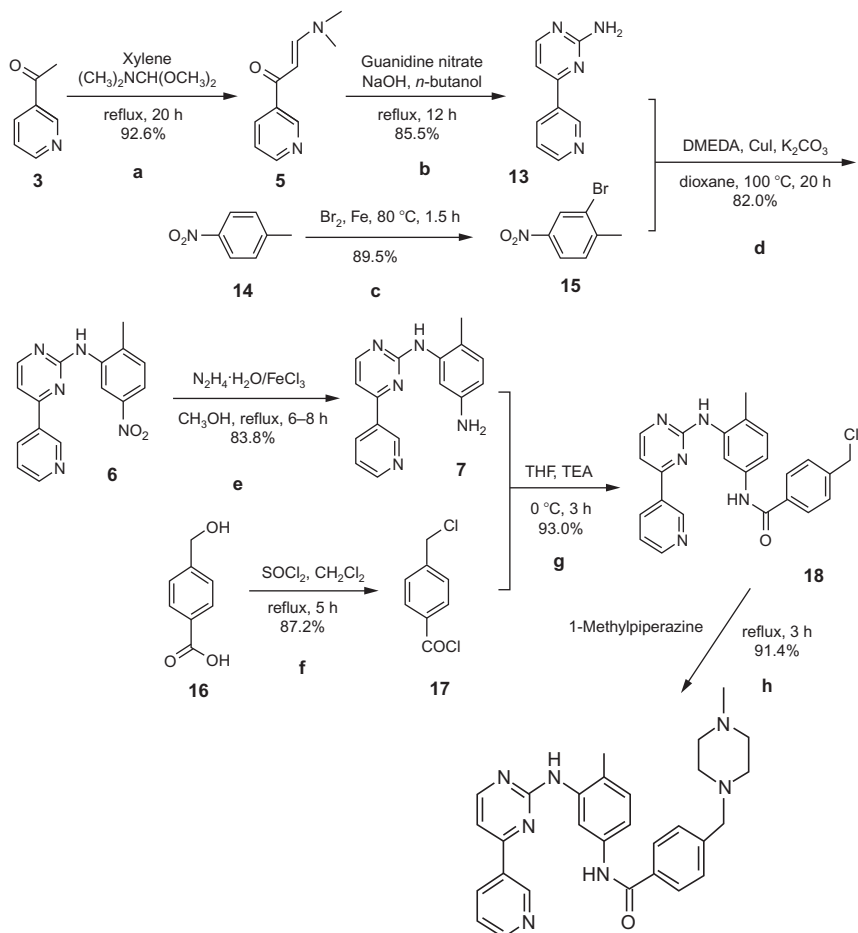




**Scheme 6.2** Loiseleur's route for the preparation of imatinib base.

insufficiencies of these approaches are (i) the use of a toxic, hazardous reagent cyanamide and (ii) using high-cost palladium as catalyst for C–N coupling reaction. Therefore, these approaches cannot be used in large-scale industrial applications.

An improved method [13] for the preparation of imatinib is described in Scheme 6.3. In this protocol, the reaction of enaminone (5) with guanidine nitrate gave pyrimidinyl amine (13), and the coupling reaction of 2-bromo-1-methyl-4-nitrobenzene (15) with compound (13) was processed in the presence of CuI and *N,N'*-dimethylethylenediamine (DMEDA) ligand to give the key intermediate (6) in 82% yield. Intermediate (6) was reduced by  $\text{N}_2\text{H}_4\cdot\text{H}_2\text{O}/\text{FeCl}_3/\text{C}$  system in water solvent. Sequentially, compound (7) was acylated with the corresponding acid chlorides to give the amide (18). The aminating reaction of benzyl chloride on the amide (18) molecule with 1-methylpiperazine finally yielded imatinib base.



**Scheme 6.3** Schematic synthetic procedure of imatinib and its analogues.



## 4. PHYSICAL CHARACTERISTICS

### 4.1. Optical activity

Imatinib mesylate does not have chiral centers, and it is not optically active.

### 4.2. Ionization constant

$\text{p}K_a = 13.45$  (imatinib mesylate).

### 4.3. Solubility characteristics

Imatinib-free base is practically insoluble in water (0.001 g/100 mL) [3]. However, the mesylate salt is very soluble in water at pH values <5.5, but is poorly soluble or insoluble at neutral and alkaline pH. The compound is freely soluble to very slightly soluble in DMSO, methanol, and ethanol, but is insoluble in *n*-octanol, acetone, and acetonitrile [7,14].

### 4.4. Particle morphology

Sandhu *et al.* [15] used chitosan and HPMC K100 as release-retarding agents to formulate sustained release microspheres of imatinib mesylate. They used scanning electron microscopy (SEM) and optical microscopy to image the shape and surface morphology of imatinib mesylate microspheres, and a representative SEM photomicrograph is shown in Figure 6.1. The obtained microcapsules are round to sphere in shape.

Jenkins and Liversidge [16] directed the invention to nanoparticulate compositions of imatinib mesylate, or a salt or derivative thereof, having improved pharmacokinetic profiles and reduced fed–fasted variability. They found that the nanoparticulate imatinib mesylate particles of composition have an effective average particle size of less than about 2000 nm and are useful in the treatment of chronic myeloid leukemia, gastrointestinal stromal tumors, and related diseases.

### 4.5. Crystallographic properties

#### 4.5.1 X-ray powder diffraction pattern

The X-ray powder diffraction pattern of imatinib mesylate has been measured using a Bruker AXS D8 advance X-ray powder diffractometer having

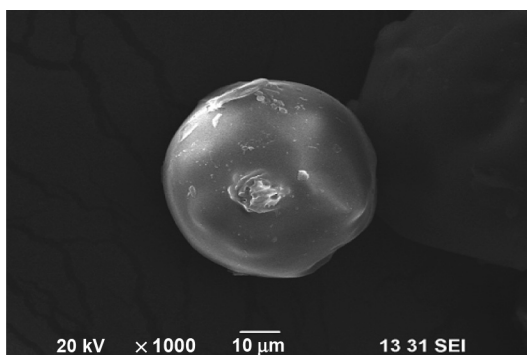


**Figure 6.1** Scanning electron microscope of optimized formulation.

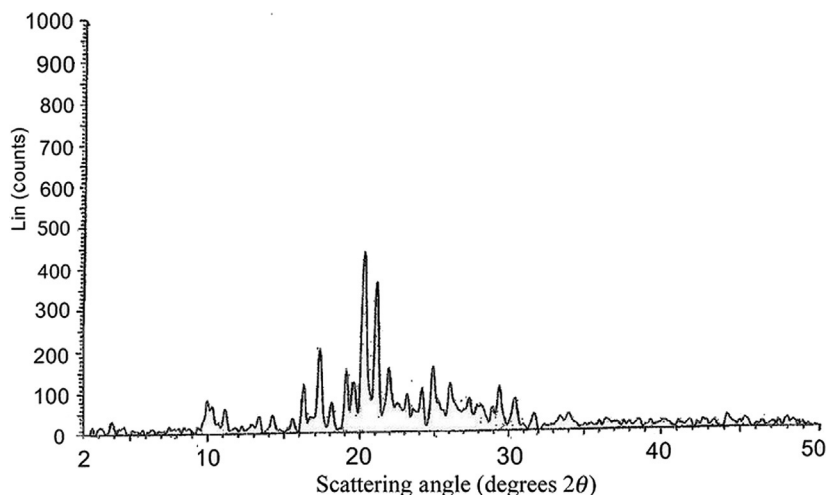


**Figure 6.2** X-ray powder diffraction pattern of imatinib mesylate.

a copper  $K\alpha$  radiation. The pattern obtained is shown in [Figure 6.2](#), and the data of scattering angle (degrees  $2\theta$ ) and the relative intensities ( $I/I_{\max}$ ) were displayed in [Table 6.1](#) [17,18].

## 4.6. Hygroscopicity

The compound is nonhygroscopic [19].

## 4.7. Thermal methods of analysis

### 4.7.1 Melting behavior

The melting range of imatinib mesylate is from 225.41 to 226 °C [20].

### 4.7.2 Differential scanning calorimetry

The differential scanning calorimetry (DSC) thermogram of imatinib was obtained using a DSC 822e Mettler Toledo scanning calorimeter. The curve shown in [Figure 6.3](#) was collected from 20 to 250 °C using a heating rate of 10 °C/min under nitrogen atmosphere. It was found that the compound melted at 226 °C.

### 4.7.3 Thermogravimetric analysis

See [Figure 6.4](#) [54].

**Table 6.1** An  $\alpha_2$  crystalline form of imatinib mesylate which has the XRPD characteristics given below

Angle ( $2\theta$ )	<i>D</i> value (Å)	Intensity (%)
4.841	18.24057	33.6
10.410	8.49070	100.0
11.194	7.89775	14.2
11.856	7.45827	19.9
12.881	6.86709	6.8
13.819	6.40328	12.9
14.860	5.95663	67.
16.439	5.38788	32.4
17.049	5.19665	5.6
17.623	5.02870	58.6
18.052	4.9100	61.6
18.567	4.77491	98.8
19.032	4.65925	70.2
19.772	4.48657	15.3
21.236	4.18055	60.8
21.582	4.11431	59.4
22.594	3.93217	19.7
23.137	3.84112	21.8
23.696	3.75172	25.0
24.851	3.57993	58.6
26.250	3.39226	9.1
27.341	3.25932	18.7
28.475	3.13204	42.4
31.896	2.80347	9.0
32.533	2.75005	6.6
43.447	2.08117	6.4

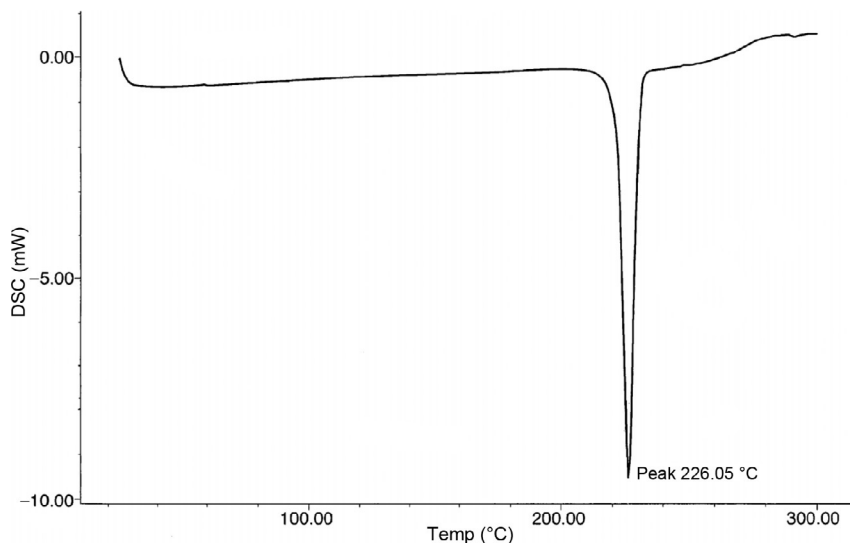


Figure 6.3 Differential scanning calorimetry (DSC) thermogram of imatinib.

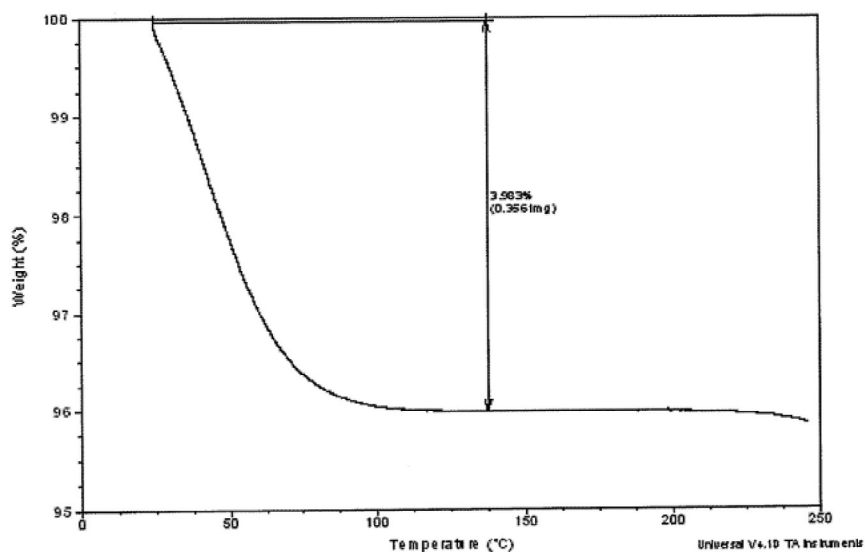


Figure 6.4 TGA curve of amorphous imatinib mesylate.

#### 4.7.4 Boiling point, enthalpy of vapor, flash point, and vapor pressure

The calculated value of the boiling point of imatinib mesylate under a pressure of 760 mmHg was 754.9 °C. The calculated value of enthalpy of vapor was 115.42 kJ/mol. The calculated value of flash point was found to be 410.3 °C, and the vapor pressure was calculated to be  $6.03 \times 10^{-24}$  mmHg at 25 °C [21,22].

## 4.8. Spectroscopy

### 4.8.1 UV/vis spectroscopy

The UV absorption spectra of imatinib mesylate in different solvent systems, buffer phases (pH 1–13), are shown in Figure 6.5. The figures were recorded using a V-570 double beam UV–vis spectrophotometer (Jasco, Japan) in 10 mm matched quartz cells. Data acquisition and analysis were performed using Spectramanager<sup>®</sup> workstation (Jasco, Japan). Absorption spectra were recorded from 190 to 800 nm at a speed of 400 nm/min with 0.2 nm data interval, using medium response and 1 nm bandwidth. The formulation matrix has shown a UV absorbance spectrum with minimum change at

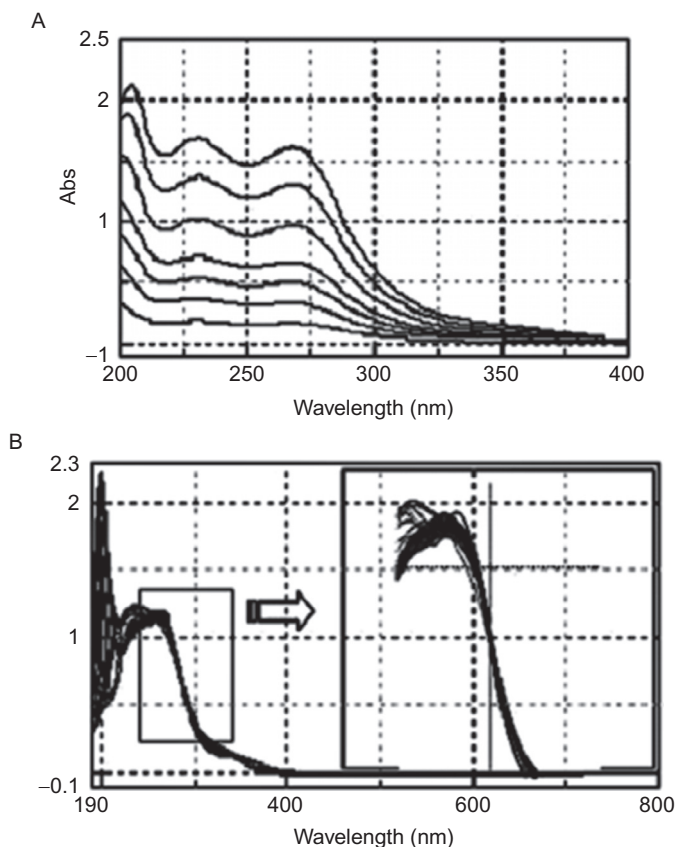


**Figure 6.5** (A) UV–visible absorption spectrum of imatinib mesylate (A) in 50:50 v/v methanol:phosphate buffer solution (PBS) (1–25 µg/mL) and (B) in buffer and unbuffered media (pH 1–13).

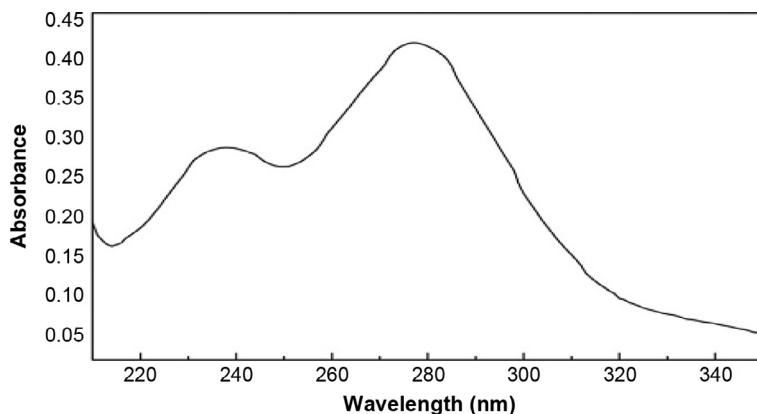


**Figure 6.6** UV-vis absorption spectrum of ImM ( $\beta$ -form).

285 nm (Figure 6.5A and B) [23]. The UV spectrum of imatinib mesylate in distilled water showed  $\lambda_{\text{max}}$  at 256 nm [24].

The UV-vis absorption spectrum of ImM ( $\beta$ -form) recorded in methanol solvent is presented in Figure 6.6. There are no changes observed in the spectra of both the forms in the solution. It shows two strong transitions at 238 and 277 nm. The solvent effect has been calculated using TD-DFT method [25,26] and IEF-PCM model [27–29] employing 6–31G basis. The computed results state that the first excited state originates from the HOMO (highest occupied molecular orbital) to LUMO (lowest unoccupied molecular orbital) transition that corresponds to the  $\lambda_{\text{max}}$  absorption band in the UV-vis spectrum [30].

#### 4.8.2 Vibrational spectroscopy

The infrared absorption spectrum of imatinib was recorded neat as a thin film (in KBr pellet) on a Perkin-Elmer Spectrum One FTIR spectrometer using Universal ATR sampling accessories. The spectrum was shown in Figure 6.7. The principal peaks were noted at 1038, 1260, 1280, 1308, 1441, 1499, 1579, 1639, and 3275  $\text{cm}^{-1}$ . The broad band at 3275  $\text{cm}^{-1}$  is due to the N–H stretching vibration absorption for open-chain amides in the imatinib solid state [31].

#### 4.8.3 Nuclear magnetic resonance spectrometry

##### 4.8.3.1 $^1\text{H}$ NMR spectrum

The  $^1\text{H}$  NMR (nuclear magnetic resonance) spectra of imatinib were recorded on a Bruker Avance DRX-600 or DPX-400 spectrometer with



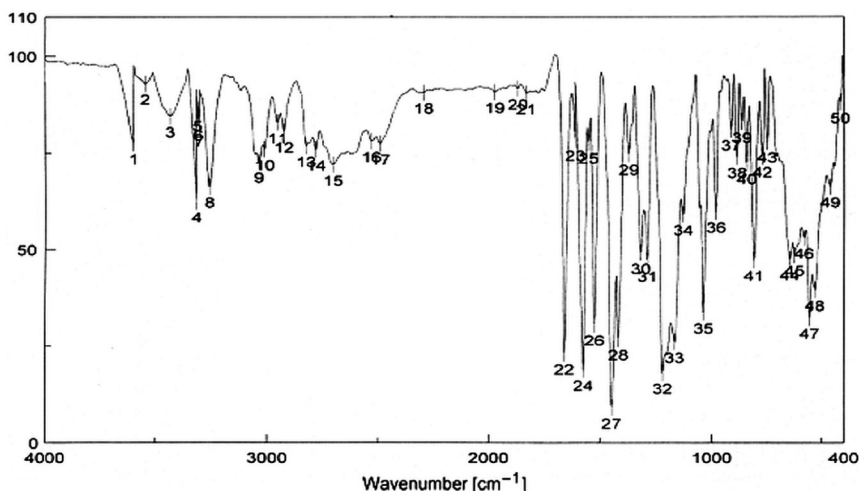


**Figure 6.7** Infrared absorption spectrum of imatinib.

residual  $\delta_{\text{H}}$  ( $d_6$ -DMSO, 600 MHz) as the internal reference (DMSO  $\delta_{\text{H}} = 2.50$  ppm). COSY and HMQC experiments were used to aid in the assignment of signals in the  $^1\text{H}$  and  $^{13}\text{C}$  NMR spectra.

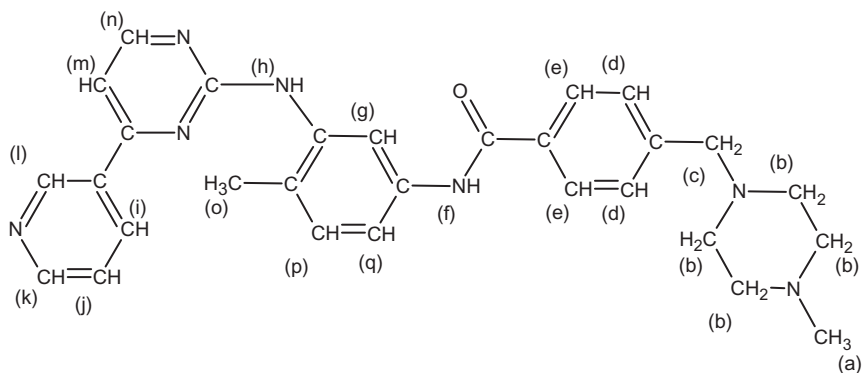
The chemical shift of the proton (Table 6.2) is highly dependent upon temperature and as the spectrum was run at 100 °C, the resonance of imatinib might occur almost anywhere over the usual 1000 Hz range ( $\sim 11.4$  ppm) [32] (Figure 6.8).

#### 4.8.3.2 $^{13}\text{C}$ NMR spectrum

$^{13}\text{C}$  NMR spectra were obtained using the same spectrometers with the central peak of  $\text{CDCl}_3$  as the internal reference ( $\text{CDCl}_3$   $\delta_{\text{C}} = 77.2$  ppm, 150 MHz). DEPT 135 experiments were used to aid in the assignment of signals in the  $^{13}\text{C}$  NMR spectra (Table 6.3; Figure 6.9).

### 4.9. Mass spectrometry

The mass spectrum of imatinib was obtained utilizing an Agilent HP1100 (Agilent Technologies, Palo Alto, USA) mass spectrometer using electrospray ionization (ESI) sources of the TSQ-MS or the LTQ-MS, respectively, monitored by the Xcalibur software (Thermo Corporation, San Jose, USA), also using an AEI single focusing mass spectrometer model MS12 with VG micromass 2S8, using an ion source temperature of 100–300 °C, an electron energy of 70 eV, and with a trap current of 100  $\mu\text{A}$ .

**Table 6.2** Assignments for the resonance bands observed in the  $^1\text{H}$  NMR spectrum of imatinib

Chemical shift (ppm)	Number of protons	Multiplicity and coupling constant (J)	Assignment
2.13	3	Singlet	H <sub>a</sub>
2.2	3	Singlet	H <sub>o</sub>
2.2–2.5	8	Multiple (2.7 Hz)	H <sub>b</sub>
3.51	2	Singlet	H <sub>c</sub>
7.18	1	Doublet of doublets (8.3 Hz)	H <sub>p</sub>
7.40–7.42	3	Multiple	H <sub>m</sub> , H <sub>d</sub>
7.46	1	Doublet of doublets (8.3 and 1.5 Hz)	H <sub>q</sub>
7.5	1	Doublet of doublets (7.9 and 4.8 Hz)	H <sub>j</sub>
7.89	2	Doublet (8.1 Hz)	H <sub>e</sub>
8.06	1	Doublet (1.5 Hz)	H <sub>g</sub>
8.46	1	Doublet of doublets of doublets (7.9, 1.5, and 1.2 Hz)	H <sub>i</sub>
8.49	1	Doublet (5.1 Hz)	H <sub>n</sub>
8.66	1	Doublet of doublets (4.8 and 1.2 Hz)	H <sub>k</sub>
8.95	1	Singlet	H <sub>h</sub>
9.26	1	Doublet (1.5 Hz)	H <sub>l</sub>
10.14	1	Singlet	H <sub>f</sub>

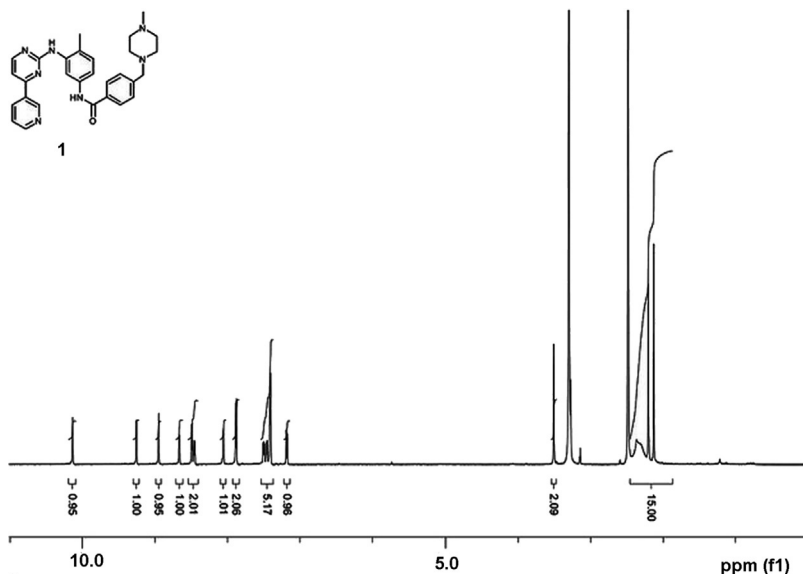


Figure 6.8 Full  $^1\text{H}$  NMR spectrum of imatinib in  $d_6$ -DMSO.

Product ion spectra of imatinib with the TSQ-MS and the LTQ-MS are shown in Figures 6.10 and 6.11, respectively. The major peaks in the spectrum occur at  $m/z$  394, 379, 377, 351, 290, 264, 247, and 222. The base peak appeared at  $m/z$  = 394. The first steps of imatinib fragmentation are drawn in Figure 6.4 and are single-bond cleavages. But only one major fragment at  $m/z$  394, which corresponds to the neutral loss of methylpiperazine, is observed [33].

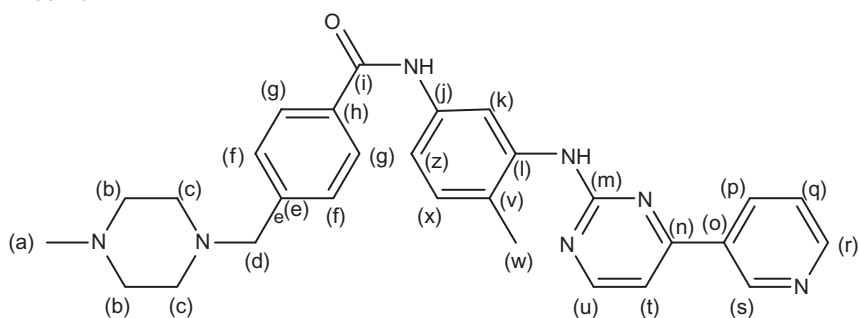
Proposed structures of fragment ions formed by collision-induced dissociation of the imatinib ion,  $[\text{M} + \text{H}]^+$  at  $m/z$  494, with ESIC-TSQ-MS<sup>2</sup> and ESIC-TQ-MS<sup>2-3</sup> product scan acquisitions were given in the Figure 6.13A–C. Fragment ions of imatinib- $d_8$  ( $d_8$ ,  $m/z$  502) are also given where necessary.

## 5. METHODS OF ANALYSIS

### 5.1. Compendial methods of analysis

#### 5.1.1 Identification [8]

Imatinib mesylate was determined by infrared absorption spectrophotometry. The spectrum was compared with that of imatinib mesylate RS, or with a qualified reference spectrum of imatinib mesylate.

**Table 6.3** Assignments for the resonance bands observed in the  $^{13}\text{C}$  NMR spectrum of imatinib

Chemical shift (ppm)	Assignment	Chemical shift (ppm)	Assignment
17.65	$\text{C}_x$	132.66	$\text{C}_h$
45.98	$\text{C}_a$	133.88	$\text{C}_o$
53.1	$\text{C}_c$	134.92	$\text{C}_p$
55.07	$\text{C}_b$	136.6	$\text{C}_j$
62.49	$\text{C}_d$	137.77	$\text{C}_e$
108.32	$\text{C}_k$	142.52	$\text{C}_l$
113.19	$\text{C}_t$	148.48	$\text{C}_r$
115.35	$\text{C}_z$	151.44	$\text{C}_s$
123.71	$\text{C}_q$	158.99	$\text{C}_u$
124.23	$\text{C}_v$	160.57	$\text{C}_n$
127	$\text{C}_g$	162.72	$\text{C}_i$
129.28	$\text{C}_f$	165.42	$\text{C}_m$
130.75	$\text{C}_x$		

### 5.1.2 Other tests

#### 5.1.2.1 Water [8]

Not more than 1.0%, determined on 1.0 g.

#### 5.1.2.2 Sulfated ash

Not more than 0.2% [8].

#### 5.1.2.3 Heavy metals [8]

1.0 g complies with limit test for heavy metal, method B (20 ppm).

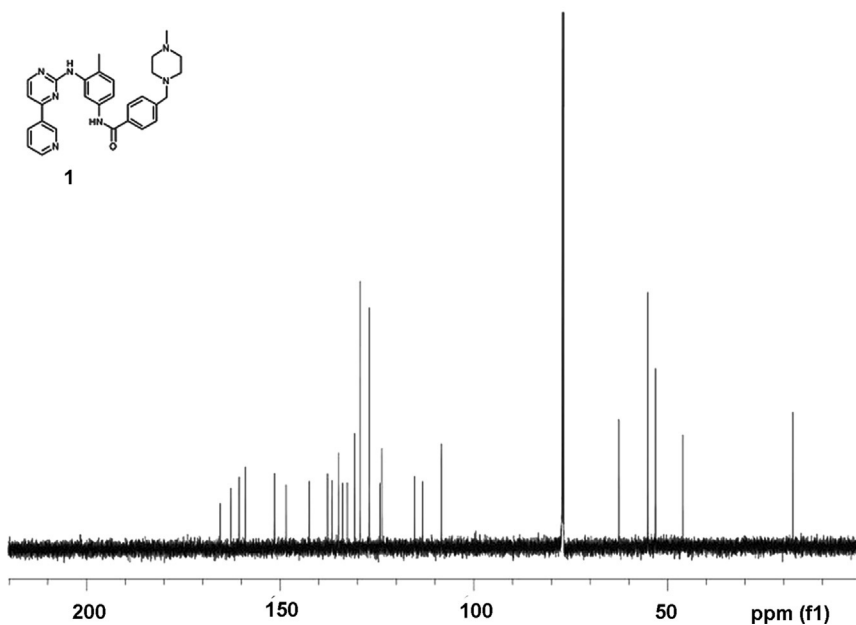


Figure 6.9 Full  $^{13}\text{C}$  NMR spectrum of imatinib in  $\text{CDCl}_3$ .

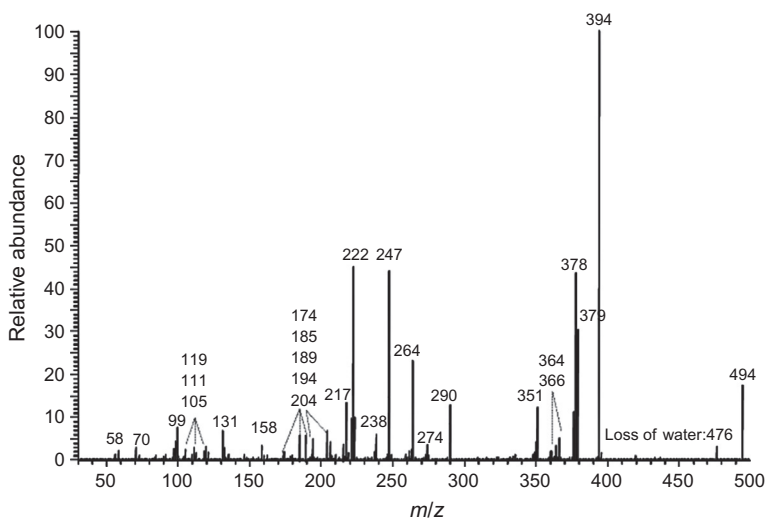
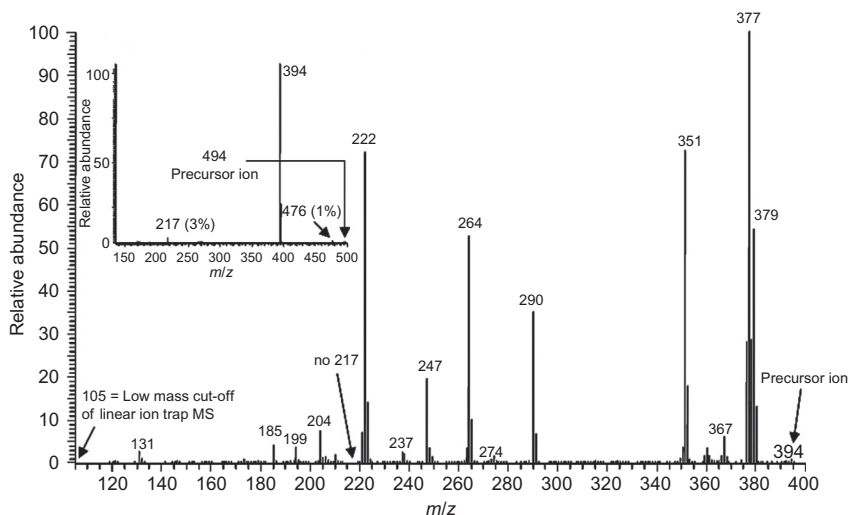


Figure 6.10 MS product ion spectrum of  $[\text{M}+\text{H}]^+$  imatinib ion ( $m/z$  494) with  $\text{ESI}^+$ -TSQ-MS (triple stage quadrupole MS).



**Figure 6.11** MS/MS (A, insert) and MS<sup>3</sup> (B) product ion spectra of [M + H]<sup>+</sup> imatinib ion:  $m/z$  494 → product ions and  $m/z$  494 → 394 → productions, respectively, on the ESIC-LTQ-MS (linear ion trap MS). MS<sup>2</sup> product ion at  $m/z$  394 is the base peak and corresponds to imatinib with the loss of methylpiperazine (100 amu). A product ion with the methylpiperazine ring is observed at  $m/z$  217 (A) (see also Figure 6.12).

### 5.1.3 Assay method [8]

Determined by liquid chromatography by comparing the test solution with the reference solution under the following chromatographic system conditions:

- A stainless steel column 25 cm × 4.6 mm, packed with octadecylsilane bonded to porous silica (5 μm),
- Mobile phase: a mixture of 40 volumes of 1% w/v solution of ammonium acetate and 60 volumes of acetonitrile,
- Flow rate: 0.7 mL/min,
- Spectrophotometer set at 254 nm,
- Injection volume: 20 μL.

## 5.2. Electrochemical methods of analysis

### 5.2.1 Voltammetry

A simple, rapid voltammetric method for the quantitative determination of imatinib was described by Hammam *et al.* on the basis of square-wave voltammetric technique [34]. A well-defined irreversible oxidation peak

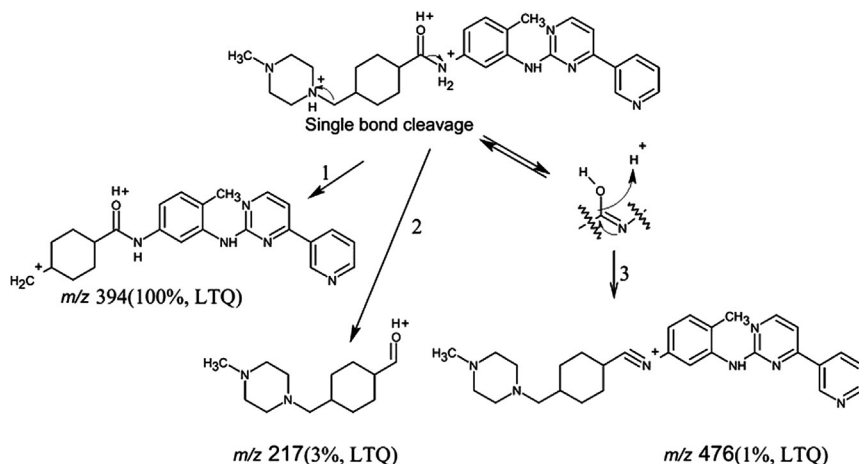


**Figure 6.12** First step of imatinib fragmentation. Proposed mechanism and MS fragment structures of imatinib obtained in LTQ-MS spectra. Single-bond cleavage with charge migration is drawn and is dependent on the initial HC positions in the imatinib structure.

current was obtained at 1.00 V. The detection limit was found to be  $6.2 \times 10^{-5}$  M for albendazole.

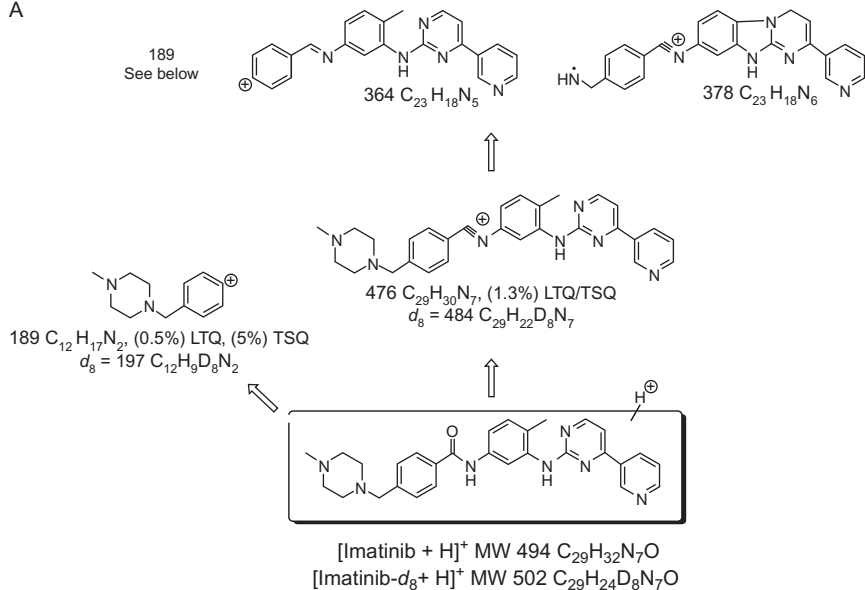
The voltammetric behavior of imatinib and its main metabolite (*N*-demethylated piperazine derivative) was studied employing square-wave techniques [35]. The method was rapid and sensitive, with limits of detection for square wave and stripping square wave were  $5.55 \times 10^{-9}$  and  $5.19 \times 10^{-9}$  M, respectively, and also it is clinically applicable to real patients. The voltammograms and cyclic voltammograms were obtained with models 384B and 264A polarographic analyzers, and analyzer/stripping voltammeter combined with mercury drop electrodes using Ag/AgCl reference electrodes.

### 5.3. Spectroscopic methods of analysis

#### 5.3.1 Spectrophotometry

Bende *et al.* [23] developed a new, simple and sensitive UV-spectrophotometric method for the determination of imatinib mesylate in bulk and pharmaceutical formulations (tablets and nanoparticles). The method has demonstrated excellent linearity over the range of 2.5–25  $\mu\text{g/mL}$ .

A



B

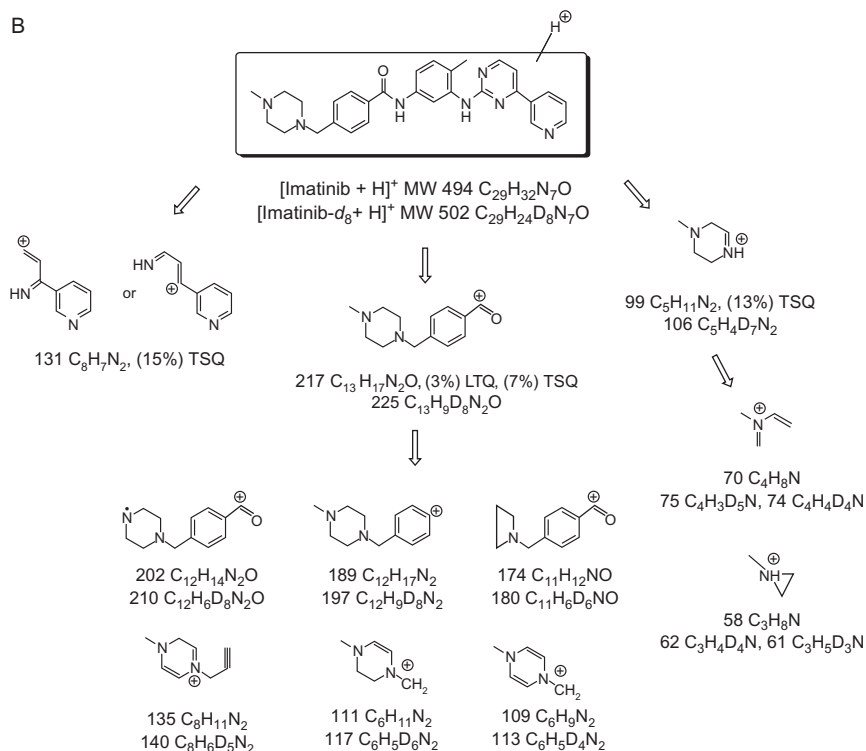
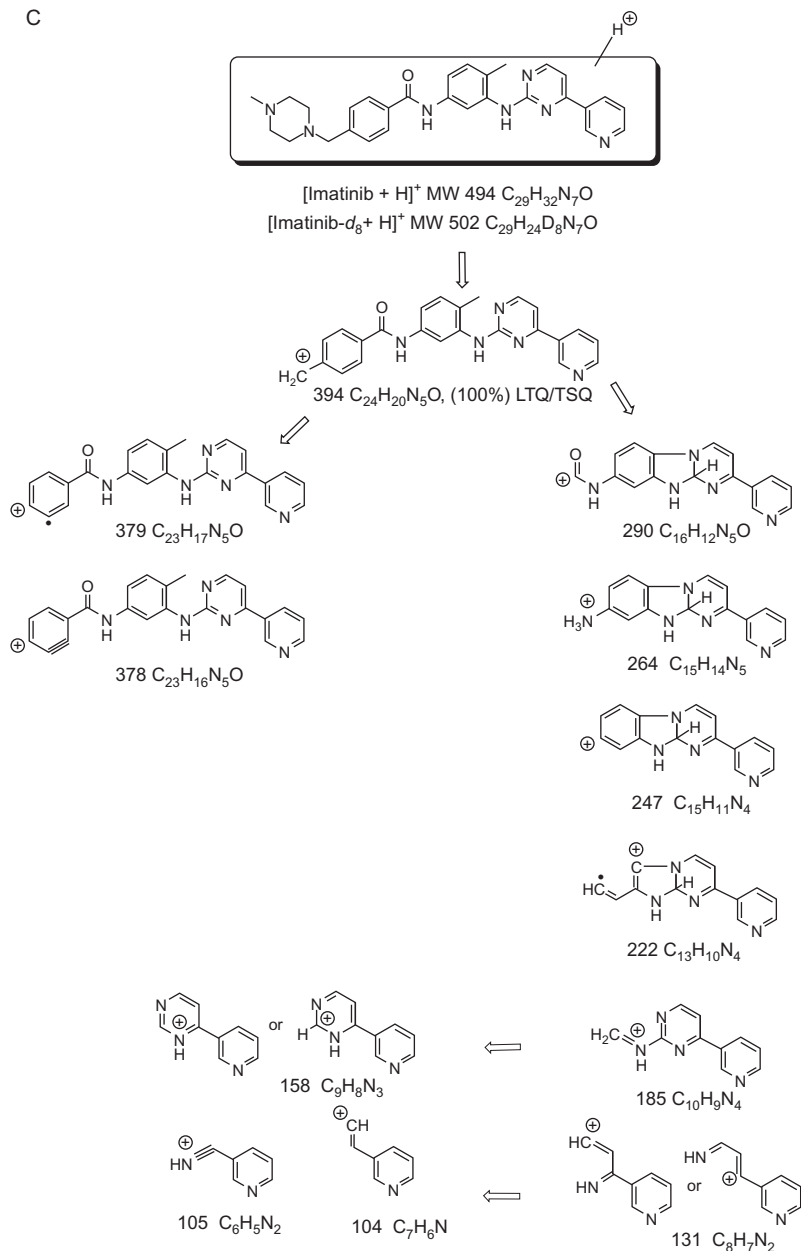


Figure 6.13—cont'd



C



**Figure 6.13** Proposed structures of fragment ions formed by collision-induced dissociation of the imatinib ion,  $[\text{M} + \text{H}]^+$  at  $m/z$  502, with ESIC-TSQ-MS and ESIC-TQ-MS product scan acquisitions.

## 5.4. Chromatographic methods of analysis

### 5.4.1 Electrophoresis

A validated, new, simple and fast electrophoretic method for imatinib determination in human plasma was reported by Ajimura *et al.* [36]. The analysis was performed using a 50 mmol/L sodium phosphate buffer pH 2.5, as BGE; hydrodynamic injection time of 20 s (50 mbar); voltage of 30 kV; capillary temperature of 35 °C; and detection at 200 nm. The method was linear from 0.125 to 5.00 mg/mL. Furthermore, the application of the method was performed in the analysis of plasma samples from CML patients undergoing treatment with imatinib.

Analyses were performed on an Agilent Technologies CE system (Waldbronn, Germany) model G1600A consisting of an analyzer, an automatic sampler, and a diode array detector operating at 200 nm. Agilent ChemStation Software was used for data acquisition. A fused-silica uncoated capillary (Agilent Technologies, Waldbronn, Germany) of 50 mm i.d., 46.5 cm total length, and 38.0 cm effective length was used (Figure 6.14).

A capillary zone electrophoretic method was investigated for the determination of Gleevec and its main metabolite (*N*-demethylated piperazine derivative) in human urine using a fused-silica capillary (75  $\mu$ m i.d., 360 cm total length, 10 cm effective length). The separation was performed with a hydrodynamic injection time of 10 s (0.5 p.s.i.), a voltage of  $-25$  kV, a capillary temperature of 25 °C, and a 100 mM phosphoric acid adjusted to pH 2 with the addition of triethanolamine. Under these conditions, the

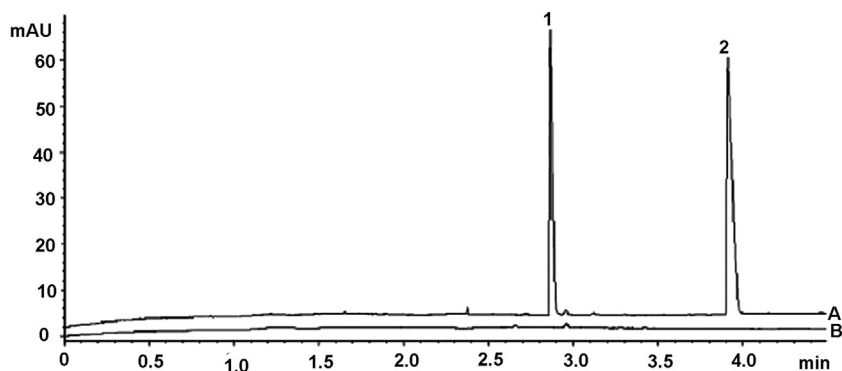


**Figure 6.14** Electropherograms of human plasma spiked with 1.00 mg/mL of IMAT and 1.25 mg/mL of LID (IS) (A) and human blank plasma (B). (1) IMAT and (2) LID (IS). Electrophoretic conditions: uncoated fused-silica capillary, 46.5 cm total length, 38.0 cm effective length, 50 mm i.d., 30 kV of voltage, 351 °C capillary temperature, detection at 200 nm, hydrodynamic injection at a pressure of 50 mbar for 20 s.

analysis takes about 5 min. A linear response over the 0.4–30.0 mg/L concentration range was investigated for two compounds. A dilution of the sample was the only step necessary before the electrophoresis analysis. Detection limits of 0.1 mg/L for Gleevec and its metabolite ( $S/N=3$ ) were obtained. The developed method is easy, rapid, and sensitive and has been applied to determine Gleevec and its main metabolite in clinical urine samples [37].

#### 5.4.2 Thin layer chromatography

A simple, selective, precise and stability-indicating high-performance thin layer chromatographic method of analysis of imatinib mesylate both as a bulk drug and in formulations was reported by Vadera *et al.* [38]. The method employed high-performance thin layer chromatography (HPTLC) aluminum plates precoated with silica gel 60F-254 as the stationary phase. The solvent system consisted of chloroform/methanol (6:4, v/v). The system was found to give compact spot for imatinib mesylate ( $R_f$  value of  $0.53 \pm 0.02$ ). Densitometric analysis of imatinib mesylate was carried out in the absorbance mode at 276 nm. The linear regression analysis data for the calibration plots showed good linear relationship with  $r^2 = 0.9966 \pm 0.0013$  with respect to peak area in the concentration range 100–1000 ng per spot. The slope and intercept were  $164.85 \pm 0.72$  and  $1168.3 \pm 8.26$  with respect to peak area. The method was validated for precision, recovery, and robustness. The limits of detection and quantitation were 10 and 30 ng per spot, respectively. Imatinib mesylate was subjected to acid and alkali hydrolysis, oxidation, and thermal degradation. The drug undergoes degradation under acidic, basic, oxidation, and heat conditions. This indicates that the drug is susceptible to acid, base hydrolysis, oxidation, and heat. Statistical analysis proves that the method is repeatable, selective, and accurate for the estimation of said drug. The proposed developed HPTLC method can be applied for identification and quantitative determination of imatinib mesylate in bulk drug and dosage forms [38] (Figure 6.15).

#### 5.4.3 High-performance liquid chromatography

Several high-performance liquid chromatography (HPLC) procedures for the determination of imatinib and its *N*-[4-methyl-3-(4-pyridin-3-yl-pyrimidin-2-ylamino)-phenyl]-4-piperazin-1-ylmethyl-benzamide (*N*-demethyl-imatinib or *N*-desmethyl-imatinib [35], *N*-demethyl-metabolite [33]) have been reported in the literature. For the simultaneous quantification of imatinib and its *N*-desmethyl-metabolite, in human or monkey plasma, methods using liquid chromatography coupled with

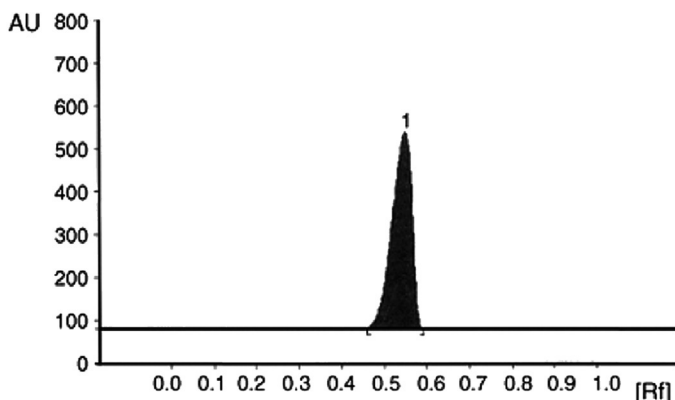


**Figure 6.15** HPTLC chromatogram of imatinib.

tandem mass spectrometry were worked out [32,39]. Rapid and sensitive HPLC methods were developed to estimate imatinib in human plasma using UV detectors [40]. Ivanovic *et al.* [41] have reported the HPLC method for simultaneous determination of imatinib and its main metabolite *N*-desmethyl-imatinib in pharmaceutical dosage forms (Table 6.4).

### 5.5. Determination in body fluids and tissues

Imatinib concentration was measured in plasma, liver, brain, spleen, and kidney by an optimized HPLC method for quantification in tissues [46]. Imatinib tissue concentrations were six- to eightfold higher than plasma, except brain, where the ratio decreased from 0.24 to 0.08 suggesting limited brain penetration, likely due to blood–brain barrier efflux transporters. The extensive distribution supports the expansion of therapeutic applications [46].



## 6. STABILITY

A literature survey revealed few stability-indicating analytical methods for the quantification of imatinib based on HPLC [47], reverse phase (RP) ultra-performance liquid chromatography [48], and HPTLC [38]. There have been some RP-HPLC methods for the estimation of imatinib and its impurities in Glivec capsules [41,49].

Preliminary investigations have established the main degradation pathways, namely, oxidation to *N*-oxide under oxidative stress conditions. Degradation was not observed after storage at high temperatures (100 °C).

**Table 6.4** HPLC methods for the analysis of imatinib mesylate

Material	Column	Mobile phase (flow rate)	Detector	References
Human plasma	Nucleosil 100-5m C18 AB column	50% Methanol and water containing both 0.05% ammonium acetate	UV-diode array detection	[42]
Bulk and in pharmaceutical formulations	Develosil column C18 (150 × 4.6 mm i.d., 5 µm particle size) column	NaH <sub>2</sub> PO <sub>4</sub> , pH adjusted to 8.0 with triethylamine: methanol: acetonitrile in the ratio of 55:27:18 (% v/v/v)	At 240 nm	[43]
Human plasma	CAPCELL PAK C18 MGII column (250 × 4.6 mm)	(0.5% KH <sub>2</sub> PO <sub>4</sub> (pH 3.5): acetonitrile: methanol) (55:25:20,v/v/v)	At 265 nm	[44]
Tablet dosage form	Hypersil BDS C18 column (length: 250 mm, diameter: 4.6 mm, particle size: 5 µm)	(Ammonium phosphate buffer: acetonitrile) (40:60 v/v)	At 250 nm	[45]

Stability study was carried out for the formulation by exposing it to different temperatures, 0 °C, ambient temperature, and 40 °C for 3 months. The sample was analyzed for drug content at the regular intervals. No remarkable change was found in the drug content of formulation. This indicates that the drug was stable at the above optimized formulation [15].

Stability studies have been performed under The International Conference on Harmonization of Technical Requirements for Registration of Pharmaceuticals for Human Use (ICH Q1A) conditions and other experimental conditions have been reported. No apparent change of the drug substance quality was observed in these studies. A retest period of 2 years at 25 °C is proposed when the substance is stored in tight packing protected from light.

Szczepek *et al.* [50] studied the decomposition of imatinib mesylate (ImM) under hydrolytic (neutral, acidic, alkaline), oxidative, and photolytic conditions. They were found that the imatinib mesylate is effectively

photostable and stable under neutral conditions. The main degradation products under acidic and alkaline conditions are compounds: 4-methyl-*N*-[[4-pyridin-3-yl-pyrimidin-2-yl]-benzene-1,3-diamine (**2**) and 4-(4-methylpiperazin-1-ylmethyl)-benzoic acid (**3**). The main degradation products under oxidation conditions, that is, 4-[[4-methyl-4-oxido-piperazin-1-yl]-methyl]-*N*-[4-methyl-3-(4-pyridin-3-yl-pyrimidin-2-ylamino)-phenyl]-enzamide (**6**), 4-[[4-methyl-1-oxido-piperazin-1-yl]-methyl]-*N*-[4-methyl-3-(4-pyridin-3-yl-pyrimidin-2-ylamino)-phenyl]-benzamide (**7**), and 4-[[4-methyl-1,4-dioxido-piperazin-1-yl]-methyl]-*N*-[4-methyl-3-(4-pyridin-3-yl-pyrimidin-2-ylamino)-phenyl]-enzamide (**8**), were isolated from the reaction mixtures and identified by the HPLC,  $^1\text{H}$  NMR, and MS techniques (Figures 6.16 and 6.17).

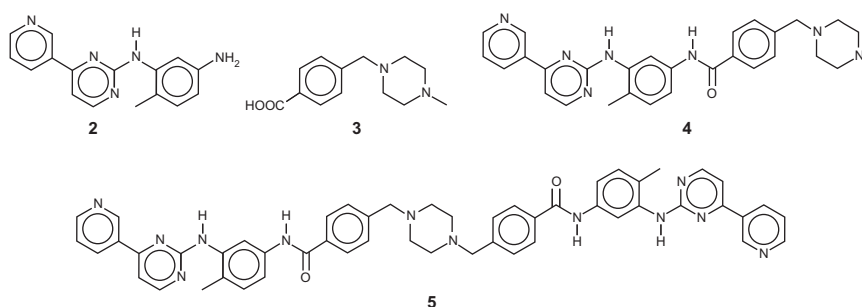


**Figure 6.16** Structure of compound 2,3-*N*-desmethyl metabolite (main metabolite, CGP-74588) **4** and expected impurity **5**.

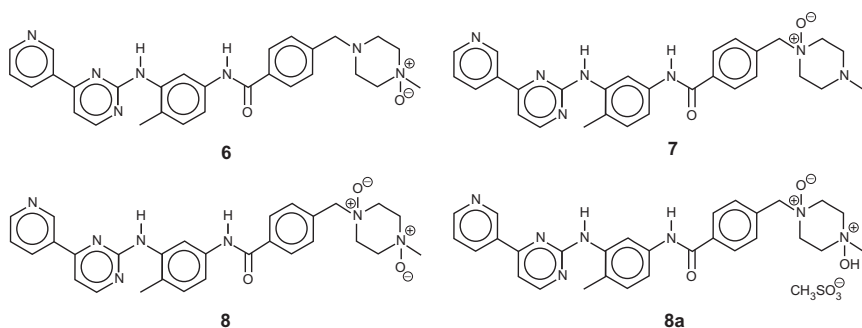


**Figure 6.17** Structure of degradation products obtained under oxidation conditions (compounds **6**, **7**, **8**, and **8a**).



## 7. CLINICAL APPLICATIONS

### 7.1. Pharmacodynamics (an overview)

Imatinib was identified through high-throughput screening against the Breakpoint cluster region–Abelson proto-oncogene kinase (BCR–ABL) kinase, then it considered as a potent and selective inhibitor of the protein tyrosine kinase Bcr–Abl, platelet-derived growth factor receptors (PDGFR $\alpha$  and PDGFR $\beta$ ), and KIT. The lead compound of this series, a 2-phenylaminopyrimidine, had low potency and poor specificity, inhibiting both serine/threonine and tyrosine kinases. The addition of a 3'-pyridyl group at the 3' position of the pyrimidine enhanced its potency. Imatinib mesylate was the first molecularly targeted protein kinase inhibitor to receive FDA approval. It targets the BCR–ABL tyrosine kinase, which underlies CML. A single molecular event, in this case the 9:22 translocation, leads to expression of the ABL fused to BCR, yielding a constitutively activated protein kinase, BCR–ABL, and then the malignant phenotype.

Imatinib clinical and molecular remissions were found in more than 90% of CML patients in the chronic phase of disease. Imatinib effectively treats other tumors that carry related tyrosine kinase mutations, including GI stromal tumors (driven by protein encoded by kit gene (c-KIT) mutation), and hypereosinophilia syndrome, chronic myelomonocytic leukemia, and dermatofibrosarcoma protuberans (all driven by mutations that activate the PDGFR) [51].

### 7.2. Mechanism of action

Crystallographic and mutagenesis studies indicate that imatinib binds to a segment of the kinase domain that fixes the enzyme in a closed or non-functional state, in which the protein is unable to bind its substrate/phosphate donor, adenosine triphosphate {(IC<sub>50</sub>) = 100 nM} [51].

### 7.3. Clinical uses

These protein tyrosine kinase inhibitors have efficacy in diseases in which the ABL, kit, or PDGFR have dominant roles in driving the proliferation of the tumor, reflecting the presence of a mutation that results in constitutive activation of the kinase, either by fusion with another protein or via point mutations. Thus, imatinib shows remarkable therapeutic benefits in patients with:

- Chronic-phase CML (BCR–ABL)
- Gastrointestinal Stromal Tumor GIST (kit mutation positive)
- Chronic myelomonocytic leukemia (EVT6-PDGFR translocation)
- Hypereosinophilia syndrome (FIP1L1–PDGFR)
- Dermatofibrosarcoma protuberans (constitutive production of the ligand for PDGFR).

The currently recommended dose of imatinib is 400–600 mg/day.

#### 7.4. Mechanisms of drug resistance

Resistance to the tyrosine kinase inhibitors arises from point mutations in three separate segments of the kinase domain. The contact points between imatinib and the enzyme become sites of mutations in drug-resistant leukemic cells; these mutations prevent tight binding of the drug and lock the enzyme in its open configuration, in which it has access to substrate. Most such mutations hold the enzyme in its open and enzymatically active confirmation. The most common resistance mutations affect amino acids 255 and 315, both of which serve as contact points for imatinib; these mutations confer high-level resistance to imatinib is unaffected by mutation at 255 but is ineffective in the presence of mutation at 315.

Other mutations affect the phosphate-binding region and the “activation loop” of the domain with varying degrees of associated resistance. Some mutations, such as at amino acids 351 and 355, confer low levels of resistance to imatinib. This finding may explain the clinical response of some resistant patients to dose escalation of imatinib. Molecular studies of circulating tumor cells have detected resistance-mediating kinase mutations prior to initiation of therapy, particularly in patients with Ph+ acute lymphoblastic leukemia or CML in blastic crisis. This finding strongly supports the hypothesis that drug-resistant cells arise through spontaneous mutation and expand under the selective pressure of drug exposure. Mutations may become detectable in the peripheral blood of patients receiving imatinib in the accelerated phase and in the late (> 4 years from diagnosis) chronic phase of CML, heralding the onset of drug resistance. Mechanisms other than BCR–ABL kinase mutation play a minor role in resistance to imatinib. Amplification of the wild-type kinase gene, leading to overexpression of the enzyme, has been identified in tumor samples from patients resistant to treatment. The multidrug resistant gene, which codes for a drug efflux protein, confers resistance experimentally but has not been implicated in clinical resistance.



Finally, Philadelphia chromosome-negative clones lacking the BCR–ABL translocation and displaying the karyotype of myelodysplastic cells may emerge in patients receiving imatinib for CML and may progress to myelodysplasia and to acute myelocytic leukemia. Their origin is unclear [51].

## 7.5. Pharmacokinetics

Imatinib is well absorbed after oral administration and reaches maximal plasma concentrations within 2–4 h. The elimination  $t_{1/2}$  of imatinib and that of its major active metabolite, the *N*-desmethyl derivative, are ~18 and 40 h, respectively. Mean imatinib area under the curve (AUC) increases proportionally with increasing dose in the range 25–1000 mg. Food does not change the pharmacokinetic profile of imatinib. Doses more than 300 mg/day achieve trough levels of 1  $\mu$ M, which correspond to *in vitro* levels required to kill BCR–ABL-expressing cells. Inhibition of the BCR–ABL tyrosine kinase in white blood cells from patients with CML reaches a maximum in the dose range of 250–750 mg/day. Nonrandomized studies suggest that response may be restored in a minority of resistant patients with doses of 600 or 800 mg/day, as opposed to the standard 400 mg/day. In the treatment of GIST, higher doses (600 mg/day) may improve response rates [51].

Imatinib is approximately 95% bound to human plasma proteins, mainly albumin and  $\alpha$ 1-acid glycoprotein. The drug is eliminated predominantly via the bile in the form of metabolites, one of which (CGP 74588) shows comparable pharmacological activity to the parent drug. The fecal to urinary excretion ratio is approximately 5:1 [52].

Imatinib is metabolized mainly by the cytochrome P450 (CYP) 3A4 or CYP3A5; enzymes CYPs 1A2, 2D6, 2C9, and 2C19 play minor roles in its metabolism. Accordingly, imatinib can competitively inhibit the metabolism of drugs that are CYP3A4 or CYP3A5 substrates. Interactions may occur between imatinib and inhibitors or inducers of these enzymes, leading to changes in the plasma concentration of imatinib as well as coadministered drugs [52]. As examples of such interactions, single dose of ketoconazole, an inhibitor of CYP3A4, increases the maximal imatinib concentration in plasma and its plasma AUC by 26% and 40%, respectively. Coadministration of imatinib and rifampin, an inducer of CYP3A4, lowers the plasma imatinib AUC by 70%. Likewise, imatinib, as a competitive

CYP3A4 substrate, inhibits the metabolism of simvastatin and increases its plasma AUC by 3.5-fold [51].

Hepatic and renal dysfunction, and the presence of liver metastases may result in more variable and increased exposure to the drug, although typically not necessitating dosage adjustment. Age (range 18–70 years), race, sex, and bodyweight do not appreciably impact the pharmacokinetics of imatinib [52].

## 7.6. Toxicity

Imatinib causes GI distress (diarrhea, nausea, and vomiting), but these symptoms usually are easily controlled; also the drug promotes fluid retention, which may lead to dependent edema and periorbital swelling. Significant myelosuppression occurs infrequently but may require transfusion support, dose reduction, or discontinuation of the drug. Drug intake can be associated with hepatotoxicity. Most nonhematological adverse reactions are self-limited and respond to dose adjustments. After the adverse reactions, such as edema, myelosuppression, or GI symptoms, have resolved, the drug may be reinitiated and titrated back to effective doses [53].

## REFERENCES

- [1] C. Gambacorti-Passerini, Part I: milestones in personalised medicine—imatinib, *Lancet Oncol.* 9 (6) (2008) 600.
- [2] B.J. Druker, N.B. Lydon, Lessons learned from the development of an ab1 tyrosine kinase inhibitor for chronic myelogenous leukemia, *J. Clin. Investig.* 105 (1) (2000) 3–8.
- [3] S.C. Sweetman (Ed.), *Martindale: The Complete Drug Reference*, 36th ed., Pharmaceutical Press, USA, 2009, p. 733, Frpharms.
- [4] <http://www.Drugbank.Ca/Drugs/Db00619>.
- [5] <http://En.Wikipedia.Org/Wiki/Imatinib>.
- [6] J.B. Zimmermann, E.H. Mett, T. Meyer, N.B. Lydon, Traxler, *Bioorg. Med. Chem. Lett.* 6 (1996) 1221–1226.
- [7] <http://www.Seqchem.Com/SafetySheet.Php?Sqindex=Srp00530i>.
- [8] Indian Pharmacopoeia, Controller of publications, New Delhi, 2010, p. 1484.
- [9] N.R. Sandhu, S.K. Loganathan, S.P. Sengodan, Design and evaluation of imatinib mesylate microspheres using chitosan and hpmc k100, *Int. J. Pharm. Technol.* (2012) Available Online through Research Article [www.ijptonline.com](http://www.ijptonline.com) (0975–766X).
- [10] O. Loiseleur, D. Kaufmann, S. Abel, H.M. Buerger, M. Meisenbach, B. Schmitz, G.W. O. Sedelmeier, Patent 03/066,613, 2003.
- [11] A. Kompella, R. Bhujanga, C. Venkaiah, Process for the preparation of the anticancer drug imatinib and its analogues, WO Patent 108,699, 2004.
- [12] Z. Szakács, S. Béni, Z. Varga, L. Örfi, G. Kéri, B. Noszál, Acid-base profiling of imatinib (gleevec) and its fragments, *J. Med. Chem.* 48 (1) (2005) 249–255.
- [13] A. Huang, L. Xing, L. Zelikovitch, J. Kaspi, U.S. Patent 2,006,149,061, 2006.
- [14] <http://www.Lclabs.Com/Prodfile/G-K/I-5508.Php4>.

- [15] N.R. Sandhu, S.K. Loganathan, S.P. Sengodan, Design and evaluation of imatinib mesylate microspheres using chitosan and hpmc k100, *Int. J. Pharm. Technol.* (2012). Available online through research article, [www.ijptonline.com](http://www.ijptonline.com) (0975-766X).
- [16] S. Jenkins, G. Liversidge, Nanoparticulate imatinib mesylate formulations, WO Patent 2,006,133,046, 2006.
- [17] R.B. Parthasaradhi, R.K. Rathnakar, R.R. Raji, R.D. Muralidhara, R.K.S. Chander, Polymorphs of imatinib mesylate, U.S. Patent 7,300,938, 2007, Google Patents.
- [18] K. Amala, T.S. Rao, S. Rachakonda, N.V. Chowdary, K. Podili, Polymorphic form of imatinib mesylate and a process for its preparation, U.S. Patent 8,048,883, 2011.
- [19] M. Veverka, P. Šimon, J. Gallovič, V. Jorík, E. Veverková, T. Dubaj, Imatinib mesylate cocrystals: synthesis, screening, and preliminary characterization, *Monatshefte für Chemie-Chemical Monthly* 143 (10) (2012) 1405–1415.
- [20] M. Łaszcz, B. Kosmacińska, K. Korczak, B. Śmigielska, M. Glice, W. Maruszak, A. Groman, H. Beczkowicz, Ł. Żelazko, Tudy on compatibility of imatinib mesylate with pharmaceutical excipients, *J. Therm. Anal. Calorim.* 88 (2) (2007) 305–310.
- [21] <http://www.Lookchem.Com/Imatinib-Mesylate/>.
- [22] <http://www.Guidechem.Com/Dictionary/220127-57-1.html>.
- [23] G. Bende, S. Kollipara, V. Sekar, R. Saha, UV-spectrophotometric determination of imatinib mesylate and its application in solubility studies, *Pharmazie* 63 (9) (2008) 641–645.
- [24] J. Kumar Raja, V.D. Sundar, A.R. Magesh, S. Nandhakumar, M.D. Dhanaraju, Validated spectrophotometric estimation of imatinib mesylate in pure and tablet dosage form, *Int. J. Pharm. Technol.* 2 (3) (2010) 490–495.
- [25] M.E. Casida, K.C. Casida, D.R. Salahub, Excited-state potential energy curves from time-dependent density-functional theory: a cross section of formaldehyde's 1A1 manifold, *Int. J. Quant. Chem.* 70 (4–5) (1998) 933–941.
- [26] R.E. Stratmann, G.E. Scuseria, M.J. Frisch, An efficient implementation of time-dependent density-functional theory for the calculation of excitation energies of large molecules, *J. Chem. Phys.* 109 (1998) 8218.
- [27] E. Cancès, B. Mennucci, J. Tomasi, A new integral equation formalism for the polarizable continuum model: theoretical background and applications to isotropic and anisotropic dielectrics, *J. Chem. Phys.* 107 (1997) 3032.
- [28] M. Cossi, G. Scalmani, N. Rega, V. Barone, New developments in the polarizable continuum model for quantum mechanical and classical calculations on molecules in solution, *J. Chem. Phys.* 117 (2002) 43.
- [29] B. Mennucci, J. Tomasi, Continuum solvation models: a new approach to the problem of solute's charge distribution and cavity boundaries, *J. Chem. Phys.* 106 (1997) 5151.
- [30] A. Srivastava, B. Joshi, P. Tandon, A. Ayala, A. Bansal, D. Grillo, Study of polymorphism in imatinib mesylate: a quantum chemical approach using electronic and vibrational spectra, *Spectrochim. Acta A Mol. Biomol. Spectrosc.* 103 (2013) 325–332.
- [31] Y.F. Liu, C.L. Wang, Y.J. Bai, N. Han, J.P. Jiao, X.L. Qi, A facile total synthesis of imatinib base and its analogues, *Org. Process Res. Dev.* 12 (3) (2008) 490–495.
- [32] M.D. Hopkin, I.R. Baxendale, S.V. Ley, A flow-based synthesis of Imatinib: the API of Gleevec, *Chem. Comm.* 46 (14) (2010) 2450–2452.
- [33] M. Marull, B. Rochat, Fragmentation study of imatinib and characterization of new imatinib metabolites by liquid chromatography–triple-quadrupole and linear ion trap mass spectrometers, *J. Mass Spectrom.* 41 (3) (2006) 390–404.
- [34] E. Hammam, H. El-Desoky, A. Tawfik, M. Ghoneim, Voltammetric behavior and quantification of the anti-leukemia drug imatinib in bulk form, pharmaceutical formulation, and human serum at a mercury electrode, *Can. J. Chem.* 82 (7) (2004) 1203–1209.

- [35] H.P. Gschwind, U. Pfaar, F. Waldmeier, M. Zollinger, C. Sayer, P. Zbinden, M. Hayes, R. Pokorný, M. Seiberling, M. Ben-Am, Metabolism and disposition of imatinib mesylate in healthy volunteers, *Drug Metab. Dispos.* 33 (10) (2005) 1503–1512.
- [36] T.O. Ajimura, K.B. Borges, A.F. Ferreira, F.A. De Castro, C.M. De Gaitani, Capillary electrophoresis method for plasmatic determination of imatinib mesylate in chronic myeloid leukemia patients, *Electrophoresis* 32 (14) (2011) 1885–1892.
- [37] J. Rodríguez Flores, J. Berzas, G. Castaneda, N. Rodríguez, Direct and fast capillary zone electrophoretic method for the determination of Gleevec and its main metabolite in human urine, *J. Chromatogr. B* 794 (2) (2003) 381–388.
- [38] N. Vadera, G. Subramanian, P. Musmade, Stability-indicating HPTLC determination of imatinib mesylate in bulk drug and pharmaceutical dosage form, *J. Pharm. Biomed. Anal.* 43 (2) (2007) 722–726.
- [39] R. Bakhtiar, J. Lohne, L. Ramos, L. Khemani, M. Hayes, F. Tse, High-throughput quantification of the anti-leukemia drug STI571 (Gleevec™) and its main metabolite (CGP 74588) in human plasma using liquid chromatography–tandem mass spectrometry, *J. Chromatogr. B* 768 (2) (2002) 325–340.
- [40] T. Velpandian, R. Mathur, N.K. Agarwal, B. Arora, L. Kumar, S.K. Gupta, Development and validation of a simple liquid chromatographic method with ultraviolet detection for the determination of imatinib in biological samples, *J. Chromatogr. B* 804 (2) (2004) 431–434.
- [41] D. Ivanovic, M. Medenica, B. Jancic, A. Malenovic, Reversed-phase liquid chromatography analysis of imatinib mesylate and impurity product in Glivec capsules, *J. Chromatogr. B* 800 (1) (2004) 253–258.
- [42] N. Widmer, A. Béguin, B. Rochat, T. Buclin, T. Kovacsics, M. Duchosal, S. Leyvraz, A. Rosselet, J. Biollaz, L. Decosterd, Determination of imatinib (Gleevec) in human plasma by solid-phase extraction–liquid chromatography–ultraviolet absorbance detection, *J. Chromatogr. B* 803 (2) (2004) 285–292.
- [43] E.R.G. Satyanarayana, P. Jitendra Kumar, K. Hanumantha Rao, B. Sridhar, P. Nagaraju, Development and Validation of New Reversed Phase High Performance Liquid Chromatography Method for the Estimation of Imatinib in Bulk and Pharmaceutical Dosage Forms, *Int. J. Res. Pharm. Biomed. Sci.* 1 (1) (2010) 6–9.
- [44] M. Miura, N. Takahashi, K.I. Sawada, Quantitative determination of imatinib in human plasma with high-performance liquid chromatography and ultraviolet detection, *J. Chromatogr. Sci.* 49 (5) (2011) 412–415.
- [45] Kuna, Arun Kumar, Kuna Jagadeesh Kumar, RP-HPLC method development and validation of imatinib mesylate in tablet dosage form, *Int. J. Pharm. Pharm. Sci.* 3 (0975–1491) (2011) 162–165.
- [46] M. Teoh, P. Narayanan, K. Moo, S. Radhakrishnan, R. Pillappan, N. Bukhari, I. Segarra, HPLC determination of imatinib in plasma and tissues after multiple oral dose administration to mice, *Pak. J. Pharm. Sci.* 23 (1) (2010) 35–41.
- [47] G. Bende, S. Kollipara, V. Kolachina, R. Saha, Development and validation of an stability indicating RP-LC method for determination of imatinib mesylate, *Chromatographia* 66 (11) (2007) 859–866.
- [48] A. Nageswari, K. Mukkanti, Stability-indicating UPLC method for determination of imatinib mesylate and their degradation products in active pharmaceutical ingredient and pharmaceutical dosage forms, *J. Pharm. Biomed. Anal.* 66 (2012) 109–115.
- [49] M. Medenica, B. Jancic, D. Ivanovic, A. Malenovic, Experimental design in reversed-phase high-performance liquid chromatographic analysis of imatinib mesylate and its impurity, *J. Chromatogr. A* 1031 (1) (2004) 243–248.

- [50] W. Szczepek, B. Kosmacińska, A. Bielejewska, W. Łuniewski, M. Skarżyński, D. Rozmarynowska, Identification of imatinib mesylate degradation products obtained under stress conditions, *J. Pharm. Biomed. Anal.* 43 (5) (2007) 1682–1691.
- [51] W.A. Catterall, K. Mackie, Goodman and Gilman's The Pharmacological Basis of Therapeutics, Local Anesthetics (L.L. Brunton, B.A. Chabner, B.C. Knollmann, Eds.), 2011, pp. 1732–1734.
- [52] B. Peng, P. Lloyd, H. Schran, Clinical pharmacokinetics of imatinib, *Clin. Pharmacokinet.* 44 (9) (2005) 879–894.
- [53] T.B. Sneed, H.M. Kantarjian, M. Talpaz, S. O'Brien, M.B. Rios, B.N. Bekele, X. Zhou, D. Resta, W. Wierda, S. Faderl, F. Giles, J.E. Cortes, The significance of myelosuppression during therapy with imatinib mesylate in patients with chronic myelogenous leukemia in chronic phase, *Cancer* 100 (1) (2004) 116–121.
- [54] A. Weisman, S. Krlovnos, E. Danon, I. Adin, C. Iustain, Stable amorphous imatinib mesylate and production process therefor, US 2008/0234286 A1, 2008.



# Moxifloxacin Hydrochloride

**Mahmoud M.H. Al Omari<sup>\*</sup>, Deema S. Jaafari<sup>\*</sup>, Khaldoun A. Al-Sou'od<sup>†</sup>,  
Adnan A. Badwan<sup>\*</sup>**

<sup>\*</sup>The Jordanian Pharmaceutical Manufacturing Co., PO Box 94, Naor, Jordan

<sup>†</sup>Department of Chemistry, Al al-Bayt University, Mafraq, Jordan

## Contents

1. Description	300
1.1 Nomenclature	300
1.2 Formulae	301
1.3 Elemental analysis	301
1.4 Appearance	302
2. Methods of Preparation	302
2.1 Method I	302
2.2 Method II	303
2.3 Method III	304
2.4 Method IV	305
2.5 Method V	307
2.6 Method VI	309
2.7 Method VII	309
2.8 Method VIII	309
2.9 Method IX	309
2.10 Method X	310
2.11 Method XI	311
2.12 Method XII	312
2.13 Method XIII	313
3. Physical Characteristics	316
3.1 Ionization constants	316
3.2 Solubility characteristics	316
3.3 Partition coefficients	318
3.4 Optical activity	318
3.5 Polymorphism	319
3.6 Particle morphology	325
3.7 Hygroscopicity	325
3.8 X-ray powder diffraction pattern	327
3.9 Thermal analysis	329
3.10 Spectroscopy	332
3.11 Mass spectrometry	340

4. Methods of Analysis	345
4.1 Compendial methods	345
4.2 Titrimetric methods	375
4.3 Electrochemical methods	375
4.4 Spectroscopic methods	377
4.5 Chromatographic methods	383
4.6 Biological methods	396
5. Stability	398
5.1 Solid-state stability	398
5.2 Solution-phase stability	404
5.3 Stability in biological fluids	412
5.4 Interaction with metals	414
6. Pharmacology	415
6.1 Uses, applications, and pertinent history	415
6.2 Absorption	416
6.3 Distribution	417
6.4 Metabolism	418
6.5 Elimination	418
6.6 Pharmacological Effects	419
References	420



## 1. DESCRIPTION

### 1.1. Nomenclature

#### 1.1.1 Systematic chemical names

1-Cyclopropyl-6-fluoro-8-methoxy-7-[(4a*S*,7a*S*)-octahydro-6*H*-pyrrolo[3,4-*b*]pyridin-6-yl]-4-oxo-1,4-dihydroquinoline-3-carboxylic acid hydrochloride [1].

1-Cyclopropyl-6-fluoro-1,4-dihydro-8-methoxy-7-[(4a*S*,7a*S*)-octahydro-6*H*-pyrrolo[3,4-*b*]pyridin-6-yl]-4-oxo-3-quinolinecarboxylic monohydrochloride [2].

(4a*S*-cis)-1-cyclopropyl-6-fluoro-1,4-dihydro-8-methoxy-7-[-octahydro-6*H*-pyrrolo [3,4-*b*] pyridin-6-yl]-4-oxo-3-quinolinecarboxylic monohydrochloride [2].

1-cyclopropyl-7-[(*S*,*S*)-2,8-diazabicyclo[4.3.0]non-8-yl]-6-fluoro-8-methoxy-1,4-dihydro-4-oxo-3-quinolinecarboxylic acid hydrochloride [3].

7-[(4a*S*,7a*S*)-octahydro-1*H*-pyrrolo[3,4-*b*]pyridin-6-yl]-1-cyclopropyl-6-fluoro-8-methoxy-4-oxo-1,4-dihydroquinoline-3-carboxylic acid [4].

### 1.1.2 Nonproprietary names [5]

Recommended international nonproprietary name (INN): Moxifloxacin.

Compendial name (USAN): Moxifloxacin hydrochloride.

Synonyms: BAY 12-8039.

### 1.1.3 Proprietary names

Actimax<sup>®</sup> (Sankyo), Actira<sup>®</sup> (Bayer), Avelox<sup>®</sup> (Bayer), Moxeza<sup>®</sup> (Alcon), Octegra<sup>®</sup> (Bayer), Proflox<sup>®</sup> (Esteve), Vigamox<sup>®</sup> (Alcon) [4–6].

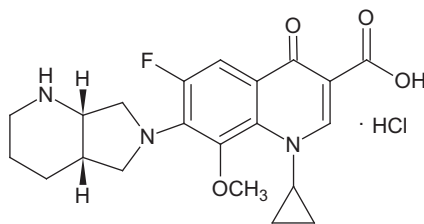
## 1.2. Formulae

### 1.2.1 Empirical formula, molecular weight, CAS number [2,5]

Moxifloxacin	C <sub>21</sub> H <sub>24</sub> FN <sub>3</sub> O <sub>4</sub>	401.4	[151 09609-2]
Moxifloxacin HCl	C <sub>21</sub> H <sub>25</sub> ClFN <sub>3</sub> O <sub>4</sub>	437.9	[186826-86-8]

### 1.2.2 Structural formula

Moxifloxacin HCl differs from other quinolones in that it has a methoxy function at the 8-position, and an *S,S* configured diazabicyclononyl ring moiety at the 7-position [3].



## 1.3. Elemental analysis

The experimental values of moxifloxacin elemental analysis (C, H, N) agree well with the theoretical values (Table 7.1) [7]. However, the experimental values corresponding to the hydrate form of moxifloxacin HCl [8] differ to some extent from the theoretical values due to a variation in water content.



**Table 7.1** The theoretical elemental compositions of moxifloxacin, anhydrous, and monohydrate forms of moxifloxacin HCl

Compound	Molecular formula	%					
		C	H	Cl	F	N	O
Moxifloxacin	$C_{21}H_{24}FN_3O_4$	62.83 (62.78)	6.03 (5.98)	–	4.73	10.47 (10.46)	16.00
Moxifloxacin HCl (anhydrous)	$C_{21}H_{25}ClFN_3O_4$	57.60	5.75	8.10	4.34	9.60	14.61
Moxifloxacin HCl (hydrate)	$C_{21}H_{25}ClFN_3O_4 \cdot H_2O$	55.33 (55.84)	5.97 (5.76)	7.78	4.17	9.22 (9.29)	17.55

Values between brackets represent the experimental data.

## 1.4. Appearance

Light yellow or yellow powder or crystals, slightly hygroscopic [1].

Slightly yellow to yellow powder or crystals [9].

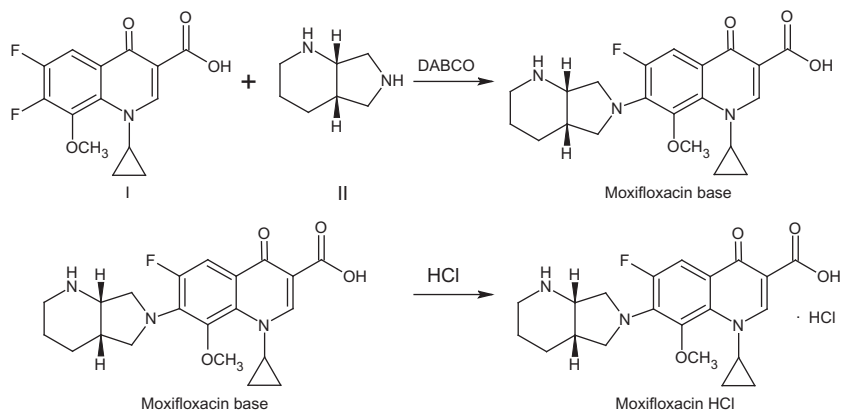


## 2. METHODS OF PREPARATION

### 2.1. Method I [10–12]

1-Cyclopropyl-6,7-difluoro-8-methoxy-1,4-dihydro-4-oxo-3-quinoline-carboxylic acid (**I**) is condensed with *cis* [S,S]-2,8-diazabicyclo[4.3.0]nonane (**II**) under reflux in a mixture of acetonitrile and dimethylformamide in the presence of 1,4-diazabicyclo [2.2.2]octane (DABCO) as a catalyst to get moxifloxacin base. The later compound is dissolved in HCl solution by means of heat, then concentrated, cooled, and precipitated by ethanol to give moxifloxacin HCl (Scheme 7.1). For further purification, it is dissolved in hot water, HCl is added, cooled and the crystalline product is filtered, washed well with ethanol, and then dried.

To prepare compound (**I**), 3,4,6-trifluoro-5-methoxybenzoyl chloride (**1**) is reacted with diethyl malonate (**2**) in a mixture of absolute ethanol and toluene in the presence of magnesium ethoxide as a base to give diethyl (3,4,6-trifluoro-5-methoxybenzoyl)-malonate as a crude product, followed by partial hydrolysis and decarboxylation with aqueous *p*-toluenesulphonic acid to give ethyl (3,4,6-trifluoro-5-methoxybenzoyl)-acetate (**3**). The later compound is heated under reflux with triethyl orthoformate in acetic anhydride to produce ethyl 2-(3,4,6-trifluoro-5-methoxybenzoyl)-3-ethoxy-acrylate (**4**) as an oil, which is further condensed with cyclopropylamine



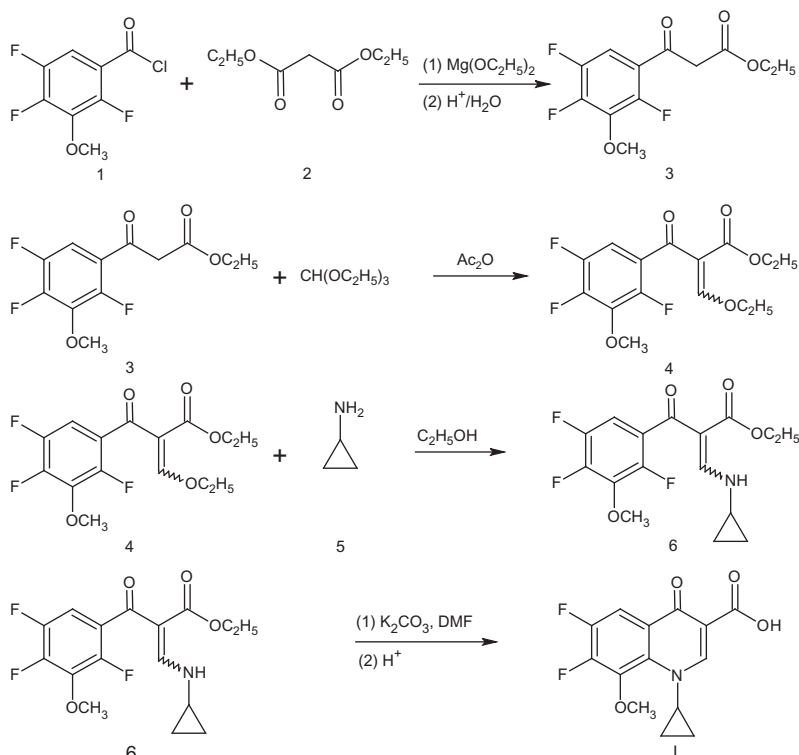
**Scheme 7.1** Preparation of moxifloxacin HCl.

(**5**) in ethanol to produce ethyl 2-(3,4,6-trifluoro-5-methoxybenzoyl)-3-cyclopropylamino-acrylate (**6**). The later is refluxed in DMF in the presence of potassium carbonate, followed by hydrolysis in acidic media to produce ethyl 1-cyclopropyl-6,7-difluoro-8-methoxy-1,4-dihydro-4-oxo-3-quinolinecarboxylate (**I**) (Scheme 7.2).

Compound (**II**) is prepared by reacting *N*-benzylmaleinimide (**1**) with 2-propenal-dimethylhydrazone (**2**) in acetonitrile to produce 1,4-dihydropyridine-2,3-dicarboxylic acid *N*-benzylimide (**3**), followed by hydrogenation in tetrahydrofuran over palladium on active charcoal to produce crude hexahydropyridine-2,3,-dicarboxylic acid *N*-benzylimide (**4**). Further hydrogenation of compound (**4**) by lithium aluminum hydride in absolute tetrahydrofuran produces *cis* 8-benzyl-2,8-diazabicyclo[4.3.0]nonane (**5**) as a racemic mixture. L-(+)- and D-(−)-tartaric acids were used to separate the enantiomers in DMF by crystallization, recrystallization, and base libration to produce enantiomerically pure [S,S]-8-benzyl-2,8-diazabicyclo[4.3.0]nonane (**6**). Finally, [S,S]-8-benzyl-2,8-diazabicyclo[4.3.0]nonane is hydrogenated over palladium on active charcoal in methanol to produce compound (**II**) (Scheme 7.3).

## 2.2. Method II [13]

The preparation of [S,S]-8-benzyl-2,8-diazabicyclo[4.3.0]nonane (**6**) in Scheme 7.3 as a pure enantiomer was reported. A mixture of [S,S]-8-benzyl-2,8-diazabicyclo[4.3.0]nonane and [R,R]-8-benzyl-2,8-diazabicyclo[4.3.0]nonane is converted to tartarate salt by reacting with L-(+)-tartaric acid in a solvent mixture of alcohol and water, followed by reaction with

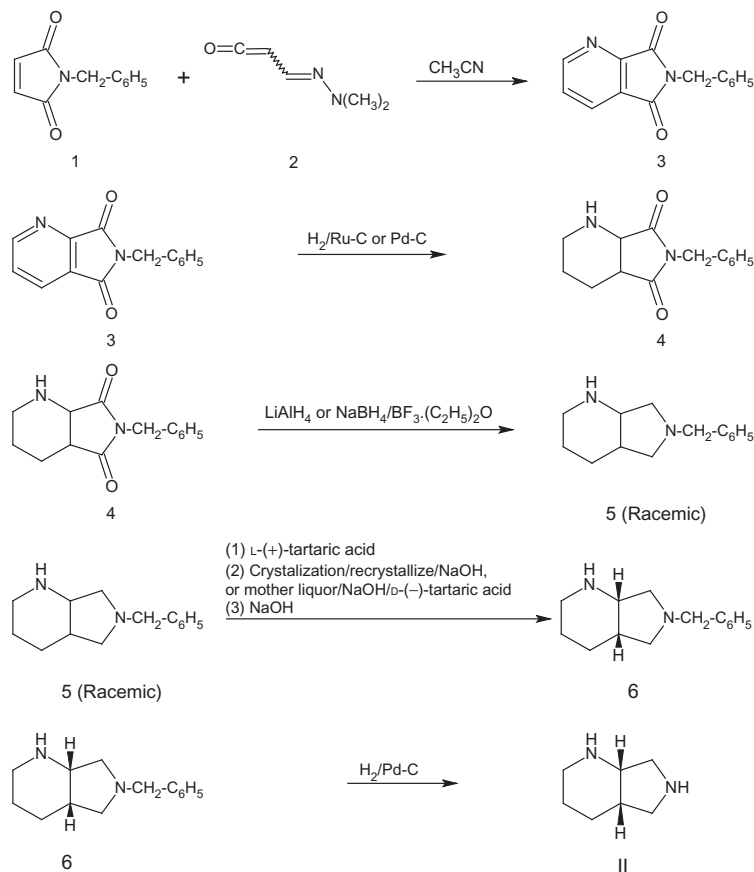


**Scheme 7.2** Preparation of 1-cyclopropyl-6,7-difluoro-8-methoxy-1,4-dihydro-4-oxo-3-quinolinecarboxylic acid (**I**).

a base to produce [S,S]-8-benzyl-2,8-diazabicyclo[4.3.0]nonane. The obtained compound is useful to prepare [S,S]-2,8-diazabicyclo[4.3.0]nonane (**II**), which is used for preparing moxifloxacin.

### 2.3. Method III [14]

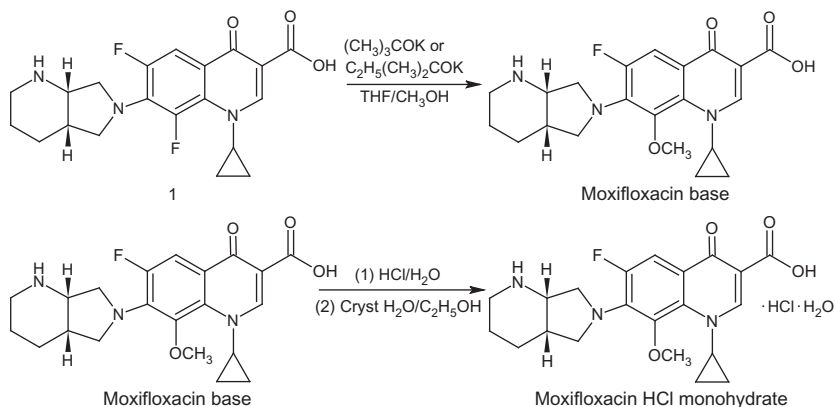
1-Cyclopropyl-7-([S,S]-2,8-diazabicyclo[4.3.0]non-8-yl)-6,8-difluoro-1,4-dihydro-4-oxo-3-quinolinecarboxylic acid (**1**), prepared using the procedure reported earlier [10,11], is reacted with 1 equiv of potassium tert-butoxide (or tert-amylate) in a mixture of THF and methanol. The moxifloxacin HCl is precipitated by adding the reaction solution to a mixture of water and HCl and concurrently by seeding with crystals of moxifloxacin (Bayer 12-8039). For purification, ethanol and water mixture is used for crystallization leading to moxifloxacin HCl monohydrate (Scheme 7.4).



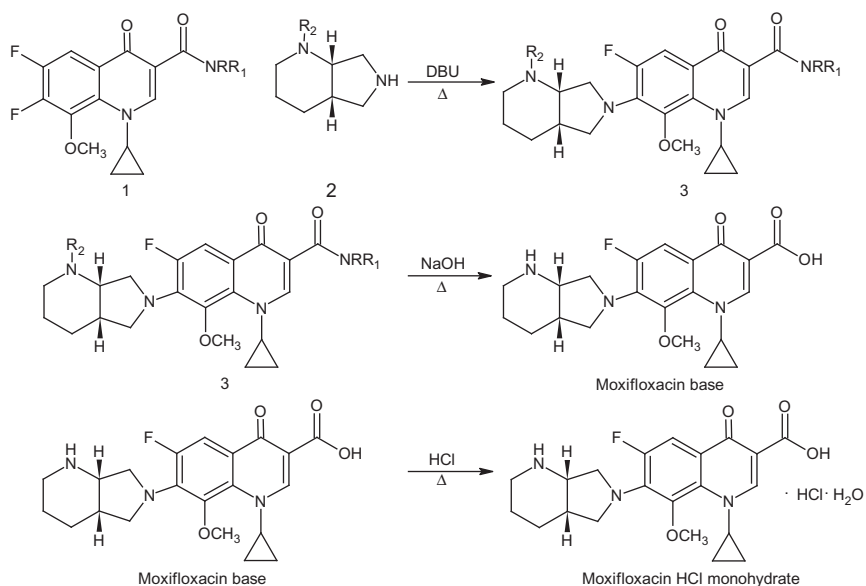
**Scheme 7.3** Preparation of cis [5,5]-2,8-diazabicyclo[4.3.0]nonane (II).

## 2.4. Method IV [15]

This preparation deals with a condensation of a novel quinoline carboxamide with an N-substituted diazabicyclononane. A mixture of 1-cyclopropyl-6,7-difluoro-1,4-dihydro-8-methoxy-4-oxoquinoline-3-carboxamide or its N,N-dialkyl derivatives (**1**) is condensed with cis [S,S]-2,8-diazabicyclo[4.3.0]nonane or its N-substituted derivatives (**2**) in acetonitrile in the presence of diazabicyclo[5.4.0]undec-7-ene (DBU) to produce the amide compound (**3**), followed by hydrolysis in a mixture of water, NaOH, and ethylene glycol to produce moxifloxacin base. The HCl salt of moxifloxacin as monohydrate is prepared in a mixture of water and methanol by adjusting the pH of solution to 1.6 using HCl (Scheme 7.5).

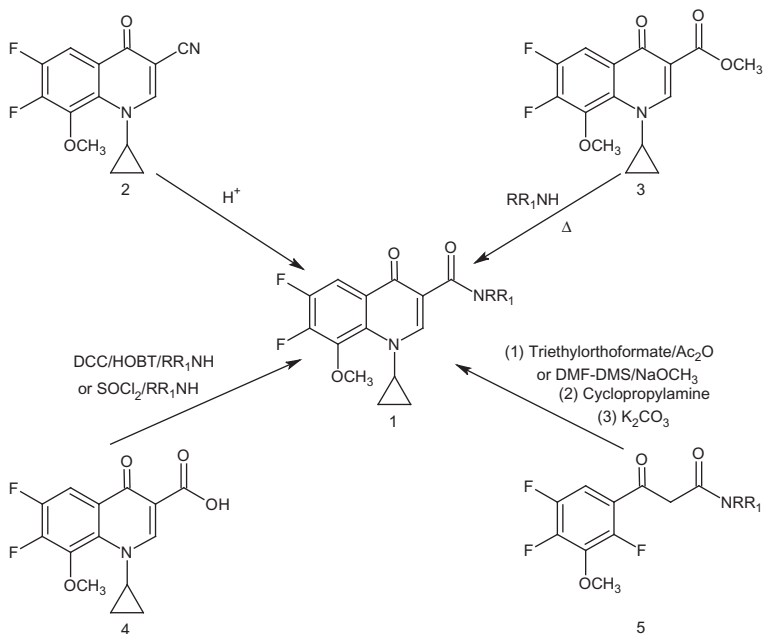


**Scheme 7.4** Preparation of moxifloxacin HCl monohydrate.

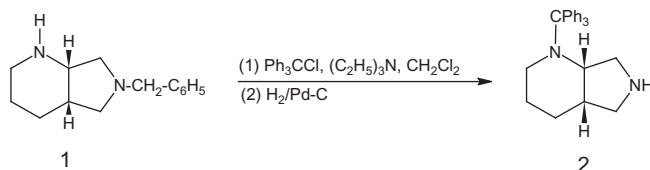


**Scheme 7.5** Preparation of moxifloxacin HCl monohydrate. Where R and R<sub>1</sub> are hydrogen or selected from C<sub>1</sub> to C<sub>5</sub> linear or branches chain alkyl group, R<sub>2</sub> is hydrogen, trityl, silyl, or COOR<sub>3</sub> group, where R<sub>3</sub> is phenyl, ethyl, or butyl analogs.

The quinoline carboxamide (1) in [Scheme 7.5](#) can be prepared by the conventional methods as illustrated in [Scheme 7.6](#). While, the N-substituted diazabicyclononane (2), can be prepared by the reaction of [S,S]-2-benzyl-2,8-diazabicyclo-[4.3.0]nonane (1) with, for example, trityl chloride (R<sub>2</sub> = Ph<sub>3</sub>C) in dichloromethane and triethylamine, followed by hydrogenation with Pd/C in 2-butanol ([Scheme 7.7](#)).



**Scheme 7.6** Preparation of quinoline carboxamide (**1**).

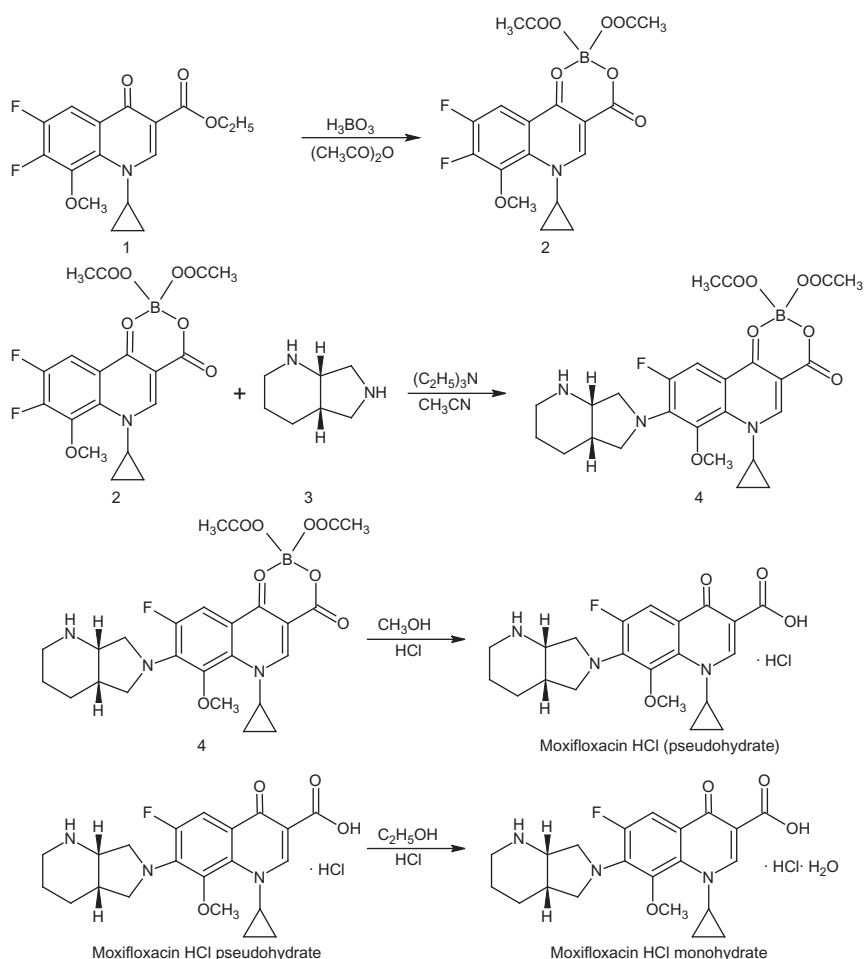


**Scheme 7.7** Preparation of N-substituted diazabicyclononane (**2**).

## 2.5. Method V [16]

In this preparation, a novel intermediate, [4a*S*-cis]-(1-cyclopropyl-7-(2,8-diazabicyclo[4.3.0]non-8-yl)-6-fluoro-8-methoxy-4-oxo-1,4-dihydro-3-quinoline carboxylic acid- $O^3, O^4$ )bis(acyloxy-*O*)borate, is used. Ethyl-1-cyclopropyl-6,7-difluoro-8-methoxy-4-oxo-1,4-dihydro-3-quinoline carboxylate (**1**) is reacted with boron acetate (prepared from boric acid and acetic anhydride) to produce (1-cyclopropyl-6,7-difluoro-8-methoxy-4-oxo-1,4-dihydro-3-quinolinecarboxylic acid- $O^3, O^4$ )bis(acyloxy-*O*)borate (**2**). The boron acetate complex (**2**) is condensed with [*S,S*]-2,8-diazabicyclo

[4.3.0]nonane (**3**) in acetonitrile in the presence of triethylamine as a catalyst to produce [4a*S*-cis]-(1-cyclopropyl-7-(2,8-diazabicyclo [4.3.0]non-8-yl)-6-fluoro-8-methoxy-4-oxo-1,4-dihydro-3-quinoline carboxylic acid- $O^3, O^4$ )bis(acyloxy- $O$ )borate (**4**). The intermediate (**4**) is reacted with HCl (pH  $\sim$  0.5) in ethanol to produce moxifloxacin HCl pseudohydrate with water content of 0.64%. The pseudohydrate form is recrystallized from a mixture of ethanol and HCl to produce moxifloxacin HCl monohydrate (Scheme 7.8).



**Scheme 7.8** Preparation of moxifloxacin HCl monohydrate.

## 2.6. Method VI [17]

The same procedure of Method V is followed herein, but using propionic anhydride instead of acetic anhydride to form the chelating agent and without using any basic catalyst to obtain the boron complex. Moreover, *n*-butanol and methanol are used instead of acetonitrile and ethanol in the condensation and salt formation steps, respectively. Using such modifications, the industrial processing to produce moxifloxacin HCl becomes simple, safe, and cost effective with high product yield and quality.

## 2.7. Method VII [18]

1-cyclopropyl-6,7-difluoro-8-methoxy-4-quinolone-3-carboxylic acid difluoro borate complex (1) is condensed with [S,S]-2,8-diazabicyclo[4.3.0]nonane derivative (2) in organic solvent (methanol, ethanol, isopropanol, ethylether and/or acetonitrile) in the presence of triethylamine to obtain quinolone carboxylic acid complex (3), followed by refluxing in organic solvent to obtain quinolone carboxylic acid derivative (4) and finally by salification in HCl solution to obtain moxifloxacin HCl. Such method has advantages of good reaction selectivity, simple process, mild conditions, and suitability for industrial production (Scheme 7.9).

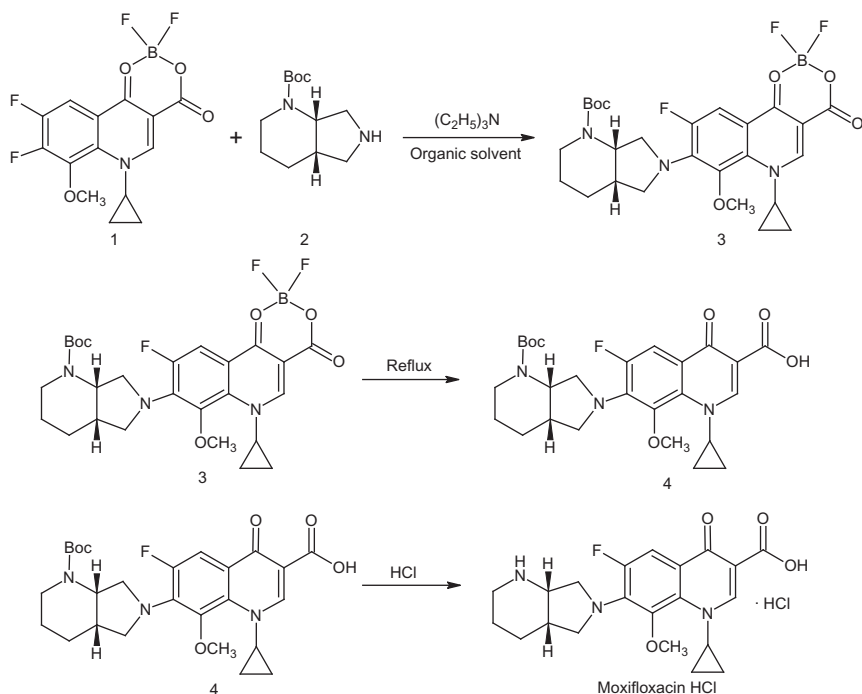
## 2.8. Method VIII [19]

This method is similar to Method V, but using the free acid of ethyl-1-cyclopropyl-6,7-difluoro-8-methoxy-4-oxo-1,4-dihydro-3-quinoline carboxylate (1). The main advantages of this method are demonstrated by its mild condition, simple operation, simple posttreatment, high yield, and its suitability for commercial production.

## 2.9. Method IX [20]

The reaction of ethyl 1-cyclopropyl-6,7-difluoro-8-methoxy-4-oxo-1,4-dihydro-3-quinolinecarboxylate ester (1) with the chelating agent  $B(OCOCF_3)_3$  (prepared from reaction of boric anhydride with trifluoroacetic anhydride) to produce the boron trifluoroacetate complex (2), followed by condensation with [S,S]-2,8-diazabicyclo[4.3.0]nonane (3) to produce the boron trifluoroacetate complex (4), then hydrolysis in the presence of a base, and finally the addition of an acid to give moxifloxacin base (Scheme 7.10). The main advantages of this method





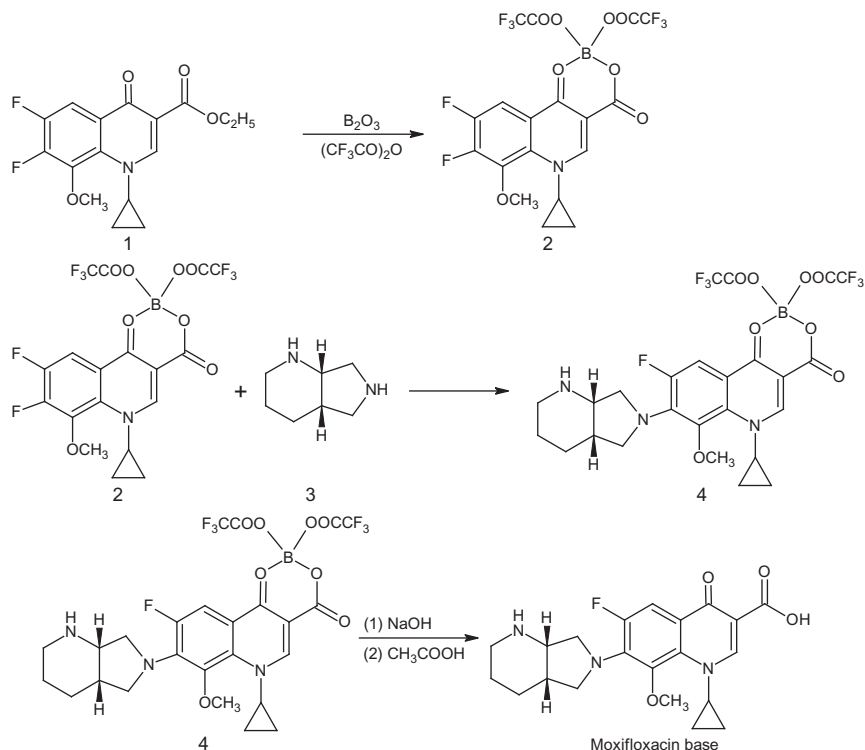
**Scheme 7.9** Preparation of moxifloxacin HCl. Where Boc is ter-butoxycarbonyl group.

are demonstrated by its simple procedures, high product yield and purity, low cost, high selectivity, and mild reaction conditions.

## 2.10. Method X [21]

1-Cyclopropyl-6,7-difluoro-1,4-dihydro-8-methoxy-4-oxo-3-quinolinic acid (**1**), is reacted with magnesium methoxide in DMF to produce the magnesium complex (**2**). The complex is condensed with [S,S]-2,8-diazabicyclo[4.3.0]nonane (**2**) in the presence of tetrabutylammonium chloride (TBAC) to produce the magnesium complex (**4**), followed by reaction with HCl to produce moxifloxacin HCl (Scheme 7.11). An additional procedure was further reported using magnesium hydroxide and *N*-methyl pyrrolidone (NMP) instead of magnesium methoxide and DMF, respectively.

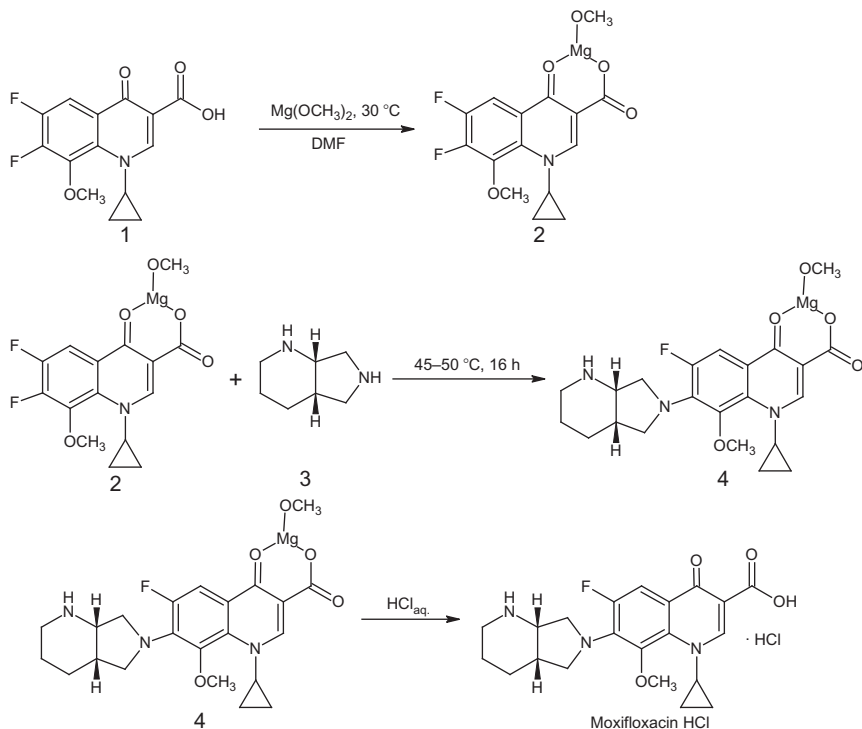
The proposed process offers a more region-selective reaction with magnesium salt, thereby contamination is avoided by positional isomer, resulting in high yields without using toxic reactants such as  $\text{BF}_3$ .



**Scheme 7.10** Preparation of moxifloxacin.

## 2.11. Method XI [22]

This method provides a stereoselective preparation of *cis* [*S,S*]-2,8 diazabicyclo[4.3.0]nonane (**II**) in [Scheme 7.1](#) using enzymic resolution as a key step, which can then be used to prepare moxifloxacin. Pyridine-2,3-dicarboxylic acid (**1**) is converted to its methyl ester, that is, dimethyl-pyridine-2,3-dicarboxylate (**2**), by  $HCl$  in anhydrous methanol. The obtained methyl ester is hydrogenated with  $Pd/C$  (anhydrous) to produce compound (**3**), followed by reaction with acetic anhydride in toluene in the presence of triethylamine, and dimethylaminopyridine (DMAP), followed by methyl tert-butyl ether (MTBE) used as a crystallization solvent to obtain compound (**4**) as a white crystal with a *trans* diastereoisomer of about 0.02% as a contaminant. Compound (**4**), is treated with CALB-T2-150 Chiralvision, batch 48107227 (enzyme CAL-B covalently immobilized on polyacrylic matrix beads) in phosphate buffer at pH 6, followed by extraction with ethylacetate to obtain the diester (2*S*,3*R*

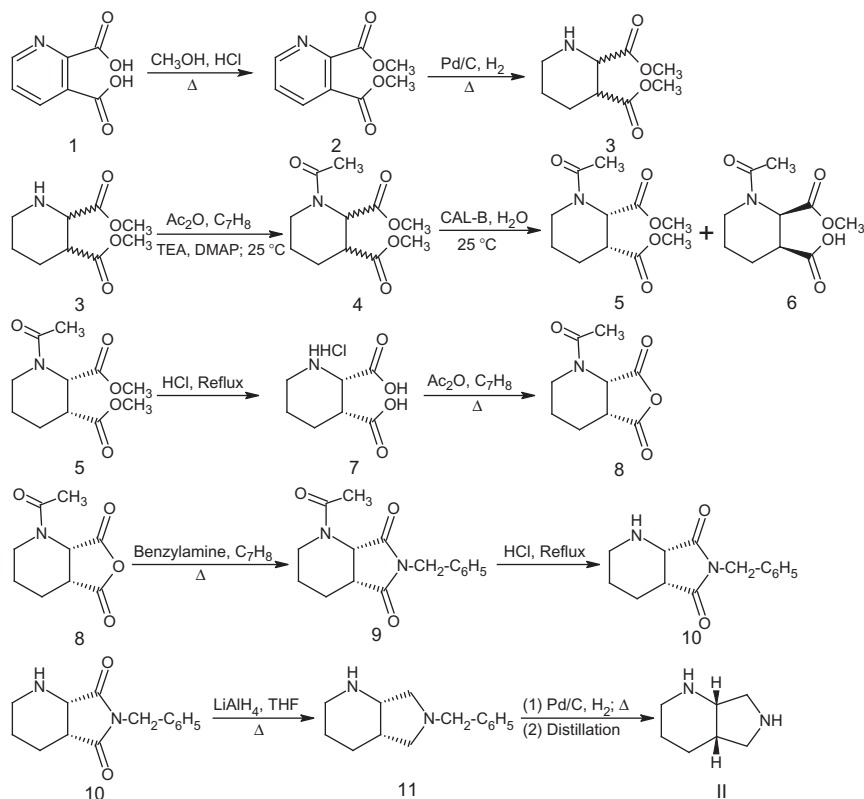


**Scheme 7.11** Preparation of moxifloxacin HCl.

enantiomer, compound (5), in the organic phase, while the monoacid (2*R*,3*S* enantiomer, compound (6), remains in the aqueous phase. Compound (5) is refluxed in HCl solution to produce compound (7), which is then reacted with acetic anhydride to produce compound (8). The obtained compound (8) is reacted with benzylamine to produce the desired product (9) as oil. The later compound (9) is heated in HCl solution to produce compound (10). Compound (10) is hydrogenated with  $\text{LiAlH}_4$  in THF to produce compound (11). Furthermore compound (11) is hydrogenated with Pd/C in methanol to produce compound (II) (Scheme 7.12). To prepare moxifloxacin HCl, compound (II) is condensed with the particular fluoroquinolone using the same procedures of Methods I and III [10–12,14].

## 2.12. Method XII [23]

This method provides a stereoselective preparation of cis [*S,S*]-2,8 diazabicyclo [4.3.0]nonane (II) in Scheme 7.1 by the highly efficient racemisation process, which then can be used to prepare moxifloxacin. [1*R*,6*S*]-8-benzyl-7,

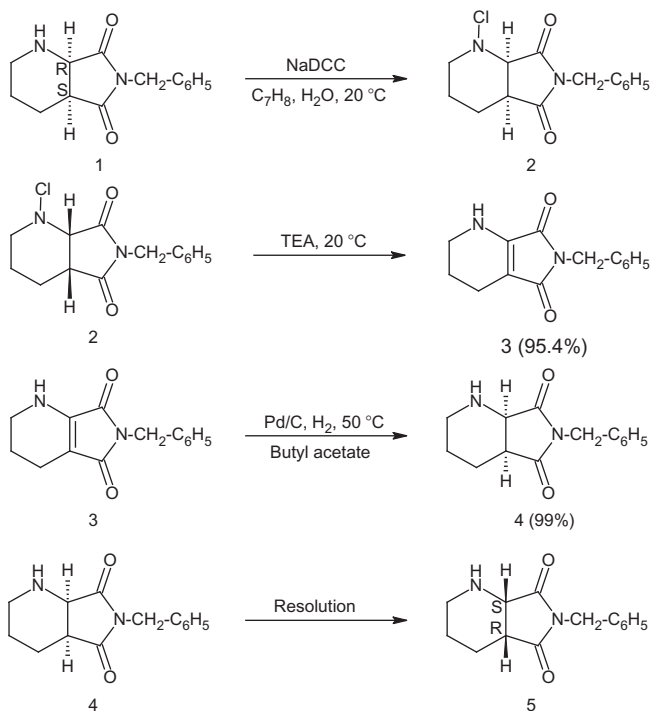


**Scheme 7.12** Preparation of *cis* [S,S]-2,8-diazabicyclo[4.3.0]nonane (**II**).

9-dioxo-2,8-diazabicyclo[4.3.0]nonane (**1**) is N-chlorinated by sodium dichloroisocyanurate (NaDCC), dehydrochlorinated by triethylamine (TEA), followed by hydrogenation to produce *rac*-*cis*-8-benzyl-7,9-dioxo-2,8-diazabicyclo[4.3.0]nonane intermediate (**4**) (Scheme 7.13). The resulting *trans*-free *cis* racemate is recycled into the resolution process to yield [1*S*,6*R*]-8-benzyl-7,9-dioxo-2,8-diazabicyclo [4.3.0]nonane (**5**).

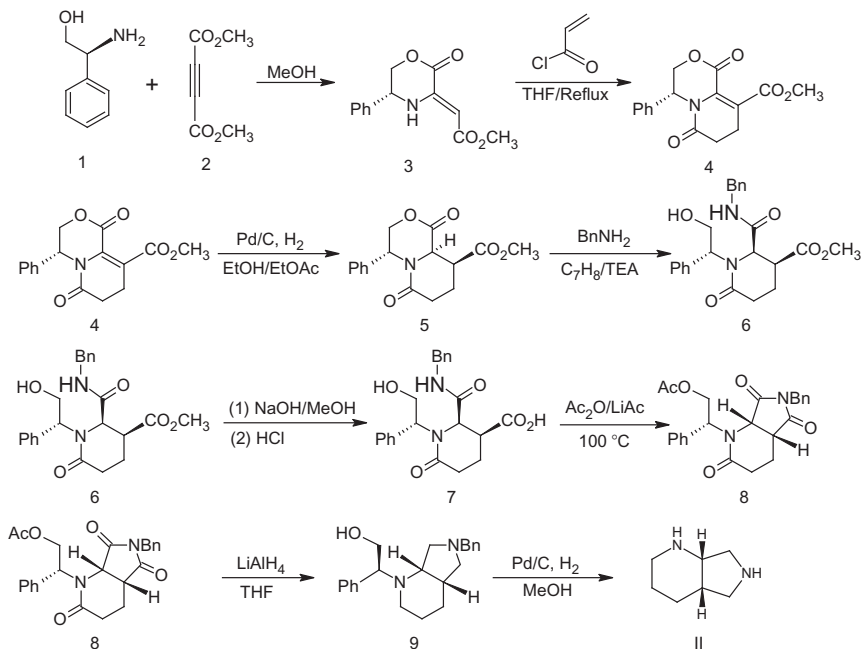
## 2.13. Method XIII [24]

This method provides an enantioselective preparation of *cis* [S,S]-2,8-diazabicyclo[4.3.0]nonane (**II**) in Scheme 7.1 by using [R]-2-amino-2-phenyl-ethanol (**1**) as a chiral starting material, which can be then used to prepare moxifloxacin. [R]-2-amino-2-phenyl-ethanol (**1**) by subsequent reaction with dimethyl acetylene dicarboxylate (**2**) in methanol to



**Scheme 7.13** Preparation of [15,6R]-8-benzyl-7,9-dioxo-2,8-diazabicyclo[4.3.0] nonane.

produce [R]-3-methoxycarbonylmethylene-5-phenyl-3,4,5,6-tetrahydro-2H-1,4-oxazin-2-one (**3**), followed by reaction with acryloyl chloride in THF to give [4S]-1,6-dioxo-4-phenyl-1,3,4,6,7,8-hexahydropyrido-[2,1-c][1,4]oxazine-9-carboxylic acid methyl ester (**4**). The later lactam (**4**) is hydrogenated with Pd/C in a mixture of ethanol and ethylacetate (10:1) to give [4S-4 $\alpha$ ,9 $\alpha$ ,9 $\alpha\alpha$ ]-1,6-dioxo-4-phenyloctahydropyrido [2,1-c][1,4] oxazine-9-carboxylic acid methyl ester (**5**). Amidation of compound (**5**) with benzyl amine in toluene produces [2R,3S]-methyl-2-(benzylcarbamoyl)-1-([R]-2-hydroxy-1-phenylethyl)-6-oxopiperidine-3-carboxylate (**6**), which is then hydrolyzed by NaOH in methanol, and then acidified with HCl to produce compound (**7**). The later compound is reacted with acetic anhydride in the presence of lithium acetate to produce [R]-2-([4aR,7aS]-6-benzyl-2,5,7-trioxooctahydro-1H-pyrrolo[3,4-b] pyridin-1-yl)-2-phenylethyl acetate (**8**), followed by hydrogenation with lithium aluminum hydride in THF to produce compound (**9**). Further hydrogenation with PD/C in methanol is carried out to yield cis [S,S]-2,8-diazabicyclo[4.3.0]nonane (**II**) (Scheme 7.14).



**Scheme 7.14** Preparation of cis [5,5]-2,8-diazabicyclo[4.3.0]nonane (II). Where BnNH<sub>2</sub>: benzyl amine.

The effect of different parameters on the yield and purity of moxifloxacin HCl prepared based on Method I (Scheme 7.1) was examined [25]. The reaction pathway through the nucleophilic substitution was identified using the Dynochem software. The effect of base used, concentration of reactants, and time of reaction on the yield and impurities formation was investigated. It was found that using diisopropylethylamine instead of pyridine as a base in acetonitrile offers the best yield (80%) with minimum amount of impurities formed by demethylation of compound (I) and moxifloxacin.

Various sulphonamide derivatives of moxifloxacin linked at the secondary alkyl amine were prepared by reacting moxifloxacin with chloro derivative of various sulphonamides in pyridine or triethylamine [26]. The prepared compounds were found to exhibit moderate to good antibacterial activity with no toxicity at the oral dose of 2000 mg/kg. Furthermore, the compounds showed higher *in vitro* and *in vivo* efficiency against various gram-positive strains, which are recognized as the challenging microbes against various leading antibiotics.

### 3. PHYSICAL CHARACTERISTICS

#### 3.1. Ionization constants

Moxifloxacin is an amphoteric compound, which contains a secondary alkyl amine, two tertiary arylamines, and a carboxylic acid (Figure 7.1).

The ionization constants ( $pK_{a1}$  and  $pK_{a2}$ ) were measured by means of potentiometry and spectrophotometry [27]. The obtained two  $pK_a$  values were 6.25 and 9.29 for carboxylic acid and secondary amine, respectively. The low acidic character of moxifloxacin was explained by the formation of intramolecular hydrogen bond between the carboxyl and keto groups in the quinoline ring. Nearly similar values ( $pK_{a1} = 6.4$  and  $pK_{a2} = 9.5$ ) were also reported [28].

#### 3.2. Solubility characteristics

Moxifloxacin HCl is soluble in 0.1 N NaOH; sparingly soluble in water and in methanol; slightly soluble in 0.1 N HCl, in dimethylformamide, and in alcohol; practically insoluble in methylene chloride, in acetone, in ethyl acetate, and in toluene; in addition it is insoluble in tert-butyl methyl ether and *n*-heptane [1,9].

As shown in Figure 7.2, moxifloxacin HCl exhibits high solubility in water in comparison with the other organic solvents. The foregoing was attributed to the ionization of this compound in water leading to the formation of ionic species ( $\text{MoxifloxacinH}^+$  and  $\text{Cl}^-$ ), thus promoting enhancement in solubility [29]. Furthermore, moxifloxacin HCl's solubility is solvent polarity and temperature dependent (i.e., solubility increases with polarity and temperature).

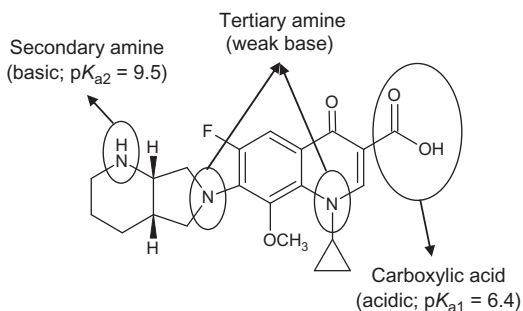


**Figure 7.1** The chemical structure of moxifloxacin showing the various functional groups with their ionization constants ( $pK_a$ s).

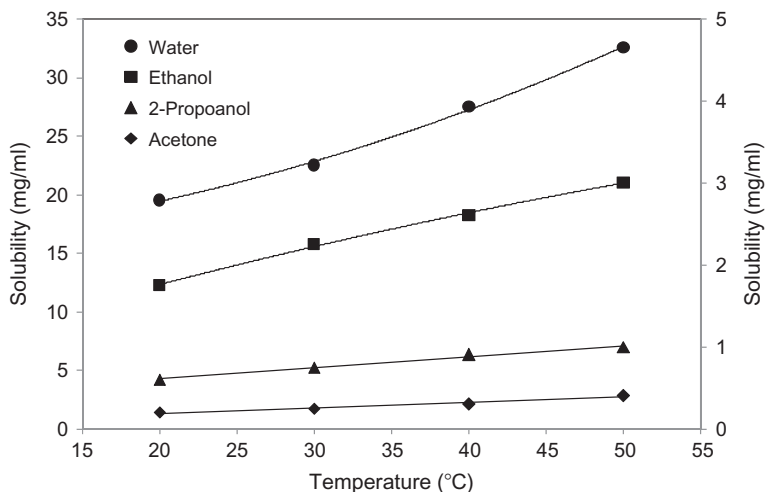


**Figure 7.2** The solubility of moxifloxacin HCl in water and different organic solvents as a function of temperature, left y-axis corresponds to water.

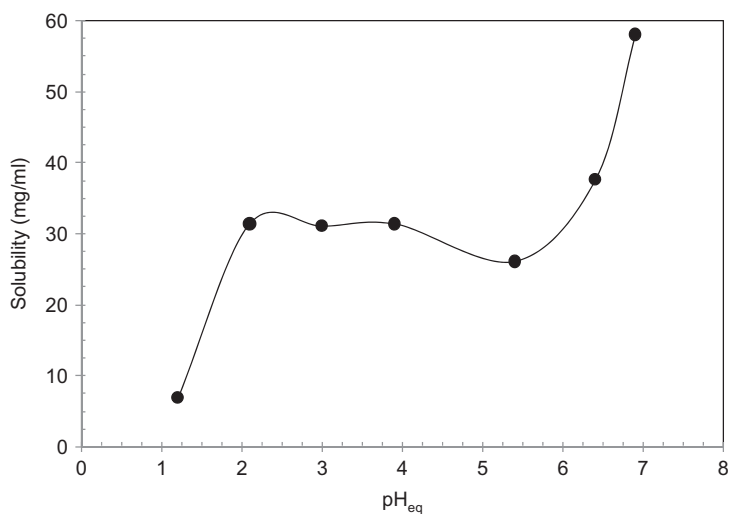


**Figure 7.3** The pH solubility of moxifloxacin HCl in 0.05 M phosphate buffer at 30 °C (pH 1.2 corresponds to 0.1 N HCl solution).

On the other hand, the solubility of moxifloxacin HCl is pH dependent (Figure 7.3), it increases with pH (above 6) due to the ionization of the carboxylate group ( $pK_{a1}=6.4$ ). The significant reduction in the solubility below pH 2 is due to the common-ion effect by chloride ions [30].



According to the WHO, EMA, and USFDA guidelines [31–33], moxifloxacin HCl can be considered as a highly soluble drug based on the Biopharmaceutics Classification System (BCS). The drug exhibits a dose/solubility (D/S) of <250 ml over the pH range 1.2–6.8 (Table 7.2).

### 3.3. Partition coefficients

The apparent partition coefficients of moxifloxacin ( $\log P_{app}$ ) in 1-octanol/buffer systems were measured at different pH values (5.9–8.7) and at room temperature using the shake-flask technique [27]. Results are summarized in Table 7.3.

The true partition coefficient ( $\log P$ ) value was calculated using the apparent partition coefficients and the micro-ionization constants and was found to have a value of 0.832. According to this finding and the high absolute bioavailability (well absorbed from the gastrointestinal tract with approximately 90%) [3], moxifloxacin HCl can be considered a highly permeable drug [27,32,33].

Based upon the high drug solubility and high permeability, moxifloxacin HCl can be classified as BCS Class I drug [32,33].

### 3.4. Optical activity

Moxifloxacin HCl has two chiral centers, located at the diazabicyclononyl moiety, leading to possible formation of four different isomers (Figure 7.4) [34].

**Table 7.2** The pH solubility (S) data of moxifloxacin HCl and the calculated dose/solubility (D/S)

pH <sub>eq</sub>	S (mg/ml)	D/S (ml)
1.2	6.8	59
2.1	31.3	13
3.0	31.0	13
3.9	31.3	13
5.4	26.0	15
6.4	37.6	11
6.9	58.0	7

The highest single dose (D) is 400 mg.

**Table 7.3** The apparent partition coefficient ( $\log P_{\text{app}}$ ) values of moxifloxacin at different pH values at room temperature

pH	$\log P_{\text{app}}$
5.9	-0.689
6.4	-0.508
7.4	-0.280
8.0	-0.237
8.7	-0.352
9.3	-0.550

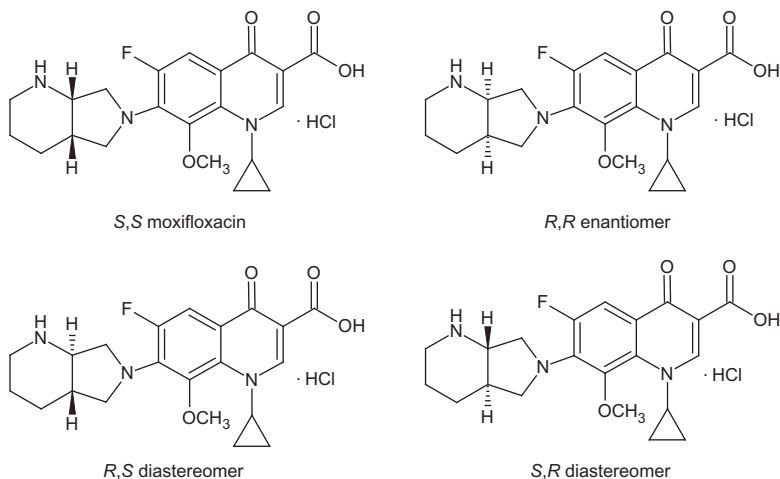


**Figure 7.4** The chemical structures of *S,S*-moxifloxacin HCl and its potential isomers.

The specific optical rotation range required by official compendia is between  $-125^\circ$  and  $-138^\circ$  at  $20^\circ\text{C}$ , determined in a 10-mg/ml solution of water and acetonitrile (1:1) mixture [1,2].

### 3.5. Polymorphism

Moxifloxacin HCl exists in different forms as shown in Table 7.4. The anhydrous form can be converted to the monohydrate when exposed to water, a mixture of water, and ethanol [35] or a controlled humidification environment at 60% or 80% RH [36].

The amorphous form can be prepared by dissolving crystalline moxifloxacin HCl in a solvent (e.g., methanol) and then spray dried [37].

**Table 7.4** The list of different forms of moxifloxacin HCl with their preparations and methods of characterization

Form	Preparation	Characterization	Reference
Form I (anhydrous crystalline form of moxifloxacin base)	Moxifloxacin hydrochloride or/and its hydrates are suspended in a suitable polar solvent, the pH is adjusted to 7–8 with NaOH or NH <sub>4</sub> OH at 25–30 °C, the reaction mixture is extracted with suitable chloro or ester solvents, the solvent is completely distilled under reduced pressure at below 60 °C, the reaction mixture is cooled to 25–35 °C, the crude is treated with a suitable organic solvent like keto solvent, the product is isolated by filtration and optionally washed with water, and then dried to get the form	XRPD, FT-IR, DSC, microscope	[15]
Form I (anhydrous crystalline)	The anhydrous form is the only crystal modification known in the prior art [10–12]	XRPD, DSC, TGA, <sup>13</sup> C NMR, Raman, FT-IR, microscope	[35]
Form II (monohydrate crystalline)	The anhydrous form is suspended and stirred in aqueous media until hydration or dissolved in ethanol either with or without water and distilled off and dried under humid condition to get prism and needle crystals		
Hydrated crystalline	Crystalline anhydrous or monohydrate forms of moxifloxacin HCl, or mixtures is placed into a controlled humidification environment at 60% or 80% RH and 30 °C for 18 and 16 h, respectively	XRPD	[36]
Amorphous	Crystalline moxifloxacin HCl is dissolved in a solvent (e.g., methanol), subjected to spray drying and further dried	XRPD, FT-IR	[37]

Form A (crystalline)	Moxifloxacin is suspended in organic solvents (e.g., methanol), treated with dry hydrogen chloride, dried under control conditions to get the crystalline Form A of moxifloxacin HCl with moisture content below 2%	XRPD, FT-IR, DSC	<a href="#">[38]</a>
Form X (anhydrous crystalline)	Moxifloxacin HCl is azeotropically refluxed in hydrocarbon solvents, cooled, filtered, and dried	XRPD	<a href="#">[39]</a>
Form Y (anhydrous crystalline)	Moxifloxacin is dissolved in alcoholic solvents by heat and adjusting the pH to 7.5–8.5 using with aqueous alkaline solution. The pH is adjusted to below 0.5 with aqueous HCl at <15 °C and the reaction mass is maintained for 30–60 min at <15 °C, followed by drying		
Form III (anhydrous crystalline)	Moxifloxacin HCl is azeotropically refluxed in lower branched or chained acid esters or an aliphatic hydrocarbon solvent or aromatic hydrocarbons. The reaction mixture is cooled with stirring till the solid mass crystallizes, followed by drying	XRPD, <sup>13</sup> C NMR, FT-IR, TGA, DSC	<a href="#">[40]</a>
New crystalline form	Moxifloxacin HCl is dissolved in a mixture of methanol/water by heating at the reflux temperature; acetone is added and the solution is heated at 40–45 °C, cooled to 15–25 °C, filtered, and dried	XRPD, FT-IR	<a href="#">[41]</a>

*Continued*

**Table 7.4** The list of different forms of moxifloxacin HCl with their preparations and methods of characterization—cont'd

Form	Preparation	Characterization	Reference
Crystalline form of moxifloxacin base	Moxifloxacin or its HCl salt is suspended in water and pH was adjusted to >11 with NaOH. The basified solution is washed with toluene and then pH adjusted to 8.0–8.2 with HCl. The reaction mixture is extracted with methylene chloride and the organic layer is dried under reduced pressure. The solid thus obtained is recrystallized from acetonitrile	XRPD, <sup>13</sup> C NMR, FT-IR, TGA, DSC	[42]
Form A (hydrated crystalline)	Moxifloxacin HCl (anhydrous or monohydrate) is suspended in a solvent selected from alcohols and polyols or mixtures, in which the resulting mixture has an overall water content of between 0.01% and 2.5% by weight, refluxed, cooled, and then the form is isolated	XRPD, <sup>13</sup> C NMR, FT-IR, TGA, DSC	[43]
Form B (anhydrous crystalline)	The same procedure of Form A, but the isolated form is reslurried at reflux in a solvent selected from alcohols and polyols or mixtures, in which the resulting mixture has an overall water content of between 0.01% and 2.5% by weight and then the form is isolated		
Form IV (anhydrous crystalline)	Moxifloxacin base is dissolved (or its HCl salt is suspended) in an organic solvent, cooled, saturated with HCl (not required in case of the HCl salt), maintained for 2 h, the solvent is removed under vacuum and the residue is resuspended in the same solvent, cooled to a temperature to 0 and 10 °C for 1–3 h, the formed crystals are separated by filtration, wash and dry the obtained product until a constant weight	XRPD, <sup>13</sup> C NMR, FT-IR	[44]

Form $\alpha$ 1 (hydrated crystalline)	Moxifloxacin HCl is suspended in a mixture of water and 37% HCl, dissolved by heating at 100 °C, cooled to 20 °C and the attained solid material was filtered, washed with water, and dried under reduced pressure at 95 °C to afford the form having a water content of 3.64%	XRPD, DSC	[45]
Form $\alpha$ 2 (hydrated crystalline)	Moxifloxacin HCl is suspended in <i>N</i> -methyl-2-pyrrolidinone and water, heated to 130 °C, cooled to 20 °C. The obtained solid is filtered, washed with acetone, and dried under reduced pressure at 60 °C to afford the form having a water content of 4.02%		
Form IV (monohydrate crystalline)	Moxifloxacin HCl is suspended in methanol and water and the pH is adjusted to 1.0–2.0 with concentrated HCl at 25 °C, and cooled to 5 °C. The solid obtained is collected by filtration and the solid is dried at 60–65 °C	XRPD	[46]
Form $\beta$ (monohydrate crystalline)	Moxifloxacin base is suspended in methanol and water. HCl and EDTA are added, heated to 34–38 °C for 1 h, cooled to 0–5 °C for 1 h, filtered, and washed with chilled methanol. The solid again is heated in methanol and water to 55 °C to get a clear solution, cooled slowly to 40–45 °C (20–25 °C for Form $\gamma$ ) and HCl is added (not required for Form $\gamma$ ), cooled slowly to 0–5 °C and maintained for 1 h, filtered, washed with chilled methanol, and water thrice (only methanol for Form $\gamma$ ) and dried at 50–55 °C for 2 h (80–85 °C for 12 h for Form $\gamma$ ), sieved, and dried further under vacuum at 45–55 °C for 30 h (80–85 °C for 36 h for Form $\gamma$ )	XRPD, DSC	[47]
Form $\gamma$ (anhydrous crystalline)			

Continued

**Table 7.4** The list of different forms of moxifloxacin HCl with their preparations and methods of characterization—cont'd

Form	Preparation	Characterization	Reference
Form F (anhydrous crystalline)	Moxifloxacin HCl is suspended in water and ethanol, heated at 75–85 °C under stirring, filtered, and washed with ethanol. Ethanol is added dropwise at 70–80 °C to the solid, cooled slowly to 20–30 °C, and crystallized for 120 min, filtered and washed with absolute ethanol. Absolute ethanol and HCl are added to the wet crystal, stirred at 40–50 °C for 1.5–2 h, cooled to 10–20 °C, stirred for 2–3 h, washed with absolute ethanol, and dried under vacuum to water content $\leq 1.0\%$	XRPD, FT-IR, DSC, TGA	[48]
Hydrate crystalline	Anhydrous moxifloxacin or/and moxifloxacin hydrate is dissolved in organic solvent–water mixture by heat at 50–150 °C, the pH is adjusted with HCl to pH 1–2, stirred for 5–60 min, and cooled for crystallization. The organic solvent is one or more of acetone, dioxane, and ethyl acetate	XRPD	[49]
Form C (crystalline)	Moxifloxacin HCl is stirred with methanol and triethyl amine at 25–30 °C. The reaction mass is concentrated partially. Further methanol is added and the pH is adjusted to 1.0–2.0 using HCl gas dissolved in methanol at 20–25 °C. The content is cooled to 0–5 °C and maintained at 0–5 °C for 2 h. The resulting solid is filtered, washed with chilled methanol, and dried under vacuum at 80–90 °C	XRPD, FT-IR, DSC, Raman	[50]

Different forms of moxifloxacin HCl hydrate and its anhydrous form can be obtained from different aqueous and organic solvents under controlled experimental conditions (Table 7.4). They are characterized by distinctive X-ray powder diffraction (XRPD) patterns,  $^{13}\text{C}$ -nuclear magnetic resonance ( $^{13}\text{C}$  NMR), differential scanning calorimetry (DSC), Fourier transform infrared (FT-IR), Raman spectroscopy, thermal gravimetric analysis (TGA), and microscope.

### 3.6. Particle morphology

Moxifloxacin HCl monohydrate may exist in different shapes depending upon the solvent used for crystallization. The prism shape (Figure 7.5A) is obtained when the anhydrous form is treated with a solvent mixture containing water at a percentage content of 10% maximum to obtain the monohydrate form, while the needle shape (Figure 7.5B) is obtained when the water content exceeds 10%. Drying is carried out under a relative humidity (RH) of not less than 30% to avoid the formation of the anhydrous form [35]. The oval shape (Figure 7.5C) is obtained when moxifloxacin HCl is recrystallized from a mixture of alcohol and chloro solvent [15].

### 3.7. Hygroscopicity

Anhydrous moxifloxacin HCl is hygroscopic and absorbs water under adverse storage conditions and handling [35].

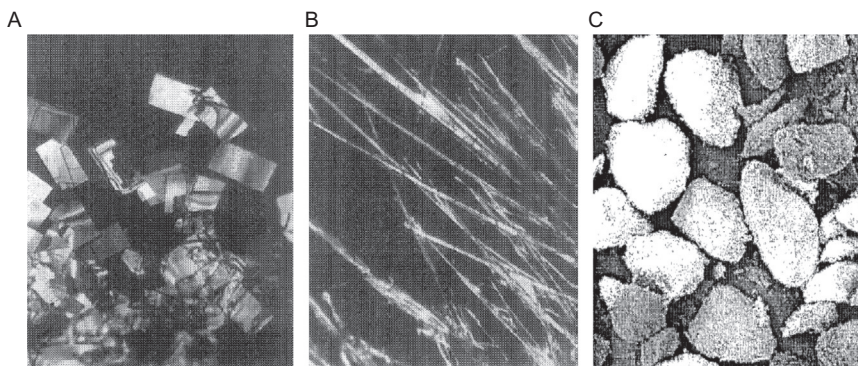


**Figure 7.5** The photographs of microscopic moxifloxacin HCl monohydrate (A) prism, (B) needle, and (C) oval shapes.



The extent of water uptake by anhydrous form of moxifloxacin HCl was studied [30]. Samples obtained from a particular supplier were incubated at different storage conditions of heat and humidity (25 °C/25% RH, 25 °C/52% RH, 25 °C/95% RH and 40 °C/75% RH) for different periods of time and then tested using Mettler DSC-25 instrument with a heating rate of 10 °C/min. The DSC thermograms show that the endotherm peaks corresponding to the unbounded water appear below 80 °C when the sample is exposed to a RH above 25% (Figure 7.6c and d). The presence of broad endotherm peak in the range of 60–100 °C at 40 °C/75% RH (Figure 7.6e) indicates that the bounded water starts to form beside the unbounded water. However, the DSC thermogram of the Ph. Euro reference material of the monohydrate form (Figure 7.6f) shows a broad endotherm peak corresponding to bounded water centered at about 110 °C similar to that of Bayer Form II [35]. All the samples tested show almost the same endotherm melting peak at about 252 °C.

The effect of different environmental conditions on the extent of water uptake by hydrate form was also investigated [30]. Moxifloxacin HCl monohydrate obtained from a particular supplier was incubated in an open container at 25 °C/60% RH, 30 °C/65% RH, and 40 °C/75% RH for different periods of time and its water content was measured.

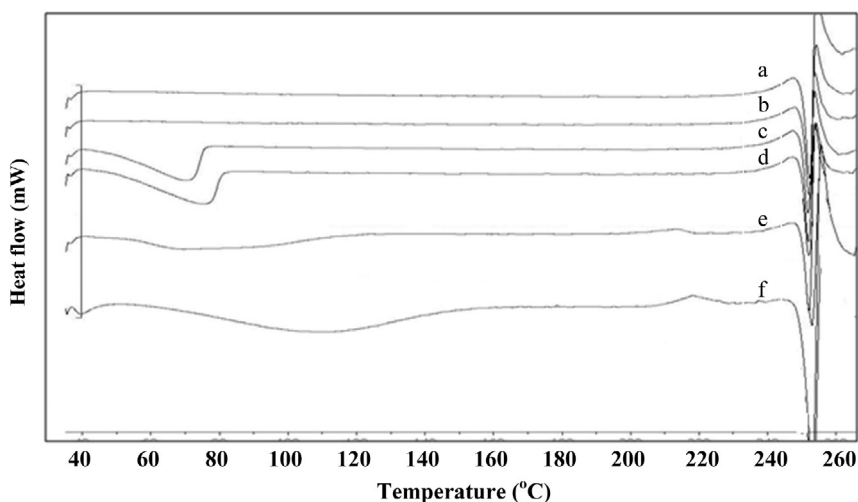


**Figure 7.6** The DSC thermograms of anhydrous moxifloxacin HCl after incubation at (a) initial, (b) 25 °C/25% RH/12 h, (c) 25 °C/52% RH/1 h, (d) 25 °C/95% RH/1 h, (e) 40 °C/75% RH/3 weeks, and (f) Ph. Euro. RS.

The maximum water uptake ( $<0.1\%$ ) was attained after 3 days of incubation at  $40\text{ }^{\circ}\text{C}/75\%$  RH.

### 3.8. X-ray powder diffraction pattern

The XRPD of anhydrous moxifloxacin HCl (Form I) and its monohydrate form (Form II) were recorded with a STOE transmission powder diffractometer and are shown in Figure 7.7 [35]. The crystallographic data

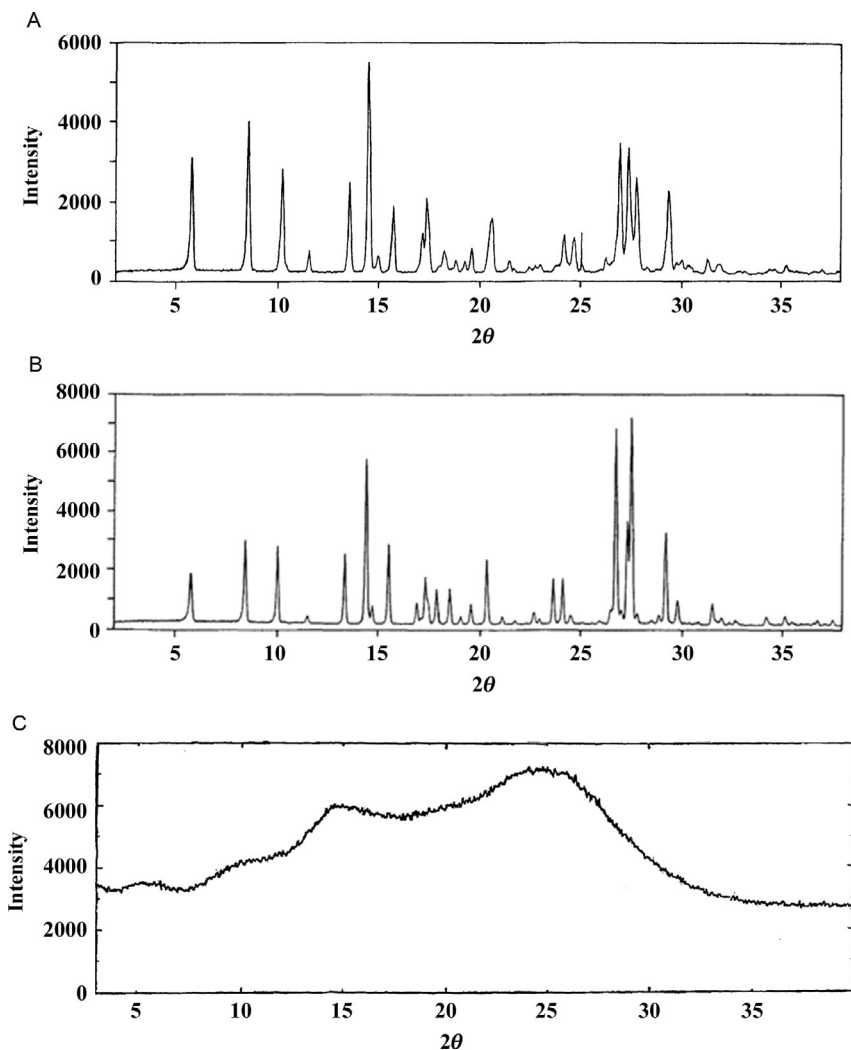


**Figure 7.7** The XRPD patterns of (A) anhydrous moxifloxacin HCl (Form I), (B) moxifloxacin HCl monohydrate (Form II), and (C) amorphous moxifloxacin HCl.

**Table 7.5** The crystallographic results from the X-ray powder diffraction patterns of anhydrous moxifloxacin HCl (Form I) and moxifloxacin HCl monohydrate (Form II)

Anhydrous moxifloxacin HCl (Form I)			Moxifloxacin HCl monohydrate (Form II)		
Scattering angle (degrees $2\theta$ )	$d$ -Spacing (Å)	Relative intensity (%)	Scattering angle (degrees $2\theta$ )	$d$ -Spacing (Å)	Relative intensity (%)
5.8	15.2373	53.8	5.8	15.2373	23.5
8.6	10.2816	71.2	8.5	10.4023	39.2
10.3	8.5881	50.0	10.1	8.7577	37.3
11.6	7.6284	9.6	13.4	6.6075	33.3
13.6	6.5108	42.3	14.5	6.1086	80.4
14.5	6.1086	100.0	14.8	5.9855	7.8
15.0	5.9061	7.7	15.6	5.6803	39.2
15.8	5.6088	32.7	17.0	5.2155	9.8
17.3	5.1257	17.3	17.4	5.0965	21.6
17.5	5.0676	34.6	17.5	5.0676	9.8
18.3	4.8478	9.6	17.9	4.9552	15.7
18.9	4.6953	5.8	18.6	4.7703	15.7
19.3	4.5988	5.8	19.6	4.5291	9.8
19.6	4.5291	11.5	20.4	4.3533	31.4
20.6	4.3115	25.0	17.4	5.0965	21.6
21.5	4.1330	3.8	22.7	3.9171	3.9
24.2	3.6776	17.3	23.0	3.8667	2.0
24.7	3.6043	15.4	23.6	3.7698	21.6
25.0	3.5617	19.2	24.1	3.6927	21.6
26.3	3.3886	5.8	24.5	3.6333	3.9
27.0	3.3023	61.5	26.5	3.3634	7.8
27.4	3.2550	59.6	26.7	3.3387	94.1
27.8	3.2090	44.2	27.0	3.3023	5.9
29.4	3.0379	38.5	27.3	3.2667	49.0
29.7	3.0079	3.8	27.5	3.2434	100.0
30.0	2.9785	5.8	27.8	3.2090	3.9

**Table 7.5** The crystallographic results from the X-ray powder diffraction patterns of anhydrous moxifloxacin HCl (Form I) and moxifloxacin HCl monohydrate (Form II)—cont'd

Anhydrous moxifloxacin HCl (Form I)			Moxifloxacin HCl monohydrate (Form II)		
Scattering angle (degrees 2θ)	d-Spacing (Å)	Relative intensity (%)	Scattering angle (degrees 2θ)	d-Spacing (Å)	Relative intensity (%)
30.3	2.9497	3.8	22.7	3.9171	3.9
31.3	2.8577	7.7	28.9	3.0893	3.9
31.8	2.8139	5.8	29.2	3.0583	45.1
			29.7	3.0079	11.8
			31.4	2.8488	9.8
			28.9	3.0893	3.9
			34.2	2.6217	3.9
			35.1	2.5566	3.9

generated from the XRPD patterns of both forms are listed in [Table 7.5](#). The interplaner *d*-spacing is calculated from Bragg equation ( $2d\sin \theta = n\lambda$ ), where  $\lambda$  (=1.5418 Å) is the wavelength of the X-ray (Cu K $\alpha$  radiator). In this study, the monohydrate form (Form II) is characterized with a band at  $2\theta = 26.7$  ([Figure 7.7B](#)).

The XRPD pattern of the amorphous form of moxifloxacin HCl prepared by spray drying technique is shown in [Figure 7.7C](#) [37]. The plain halo shape of the pattern proves the amorphous nature when the drug is spray dried.

In addition to these three forms and as mentioned previously in [Section 3.5](#), there are other crystalline forms of anhydrous and hydrate moxifloxacin HCl that can be clearly characterized using this technique.

### 3.9. Thermal analysis

#### 3.9.1 Melting behavior

The melting point was measured using the Büchi B-450 device by the capillary technique [51]. Results, as shown in [Table 7.6](#), indicate that the melting point of moxifloxacin HCl monohydrate increases with the heating rate. The significant difference between data of Merck Index [52] with the aforementioned results and the DSC data ([Table 7.7](#)) cannot be justified

<b>Table 7.6</b> The melting point of moxifloxacin and moxifloxacin HCl			
<b>Compound</b>	<b>Melting point (°C)</b>	<b>Heating rate (K min<sup>-1</sup>)</b>	<b>Reference</b>
Moxifloxacin HCl	238–242	NA	[4]
Moxifloxacin HCl monohydrate	242.0–247.4	3	[51]
	248.0–252.0	5	
	255.1–258.2	10	
Moxifloxacin	203–208 (decomp.)	NA	[52]
Moxifloxacin HCl	324–325 (decomp.)	NA	

NA, not available.

on the basis of differences in experimental conditions (e.g., heating rate) and in the purities of the tested samples, unlike to what was claimed [51].

### 3.9.2 Differential scanning calorimetry

The DSC thermograms of the anhydrous form of moxifloxacin HCl (Form I) and its monohydrate form (Form II) were recorded using the Perkin-Elmer DSC-7 thermoanalyser [35]. Figure 7.8 shows that both forms have an endotherm melting peak at about 255 °C. The broadness of the endotherm peak, centered at approximately 110 °C, for the monohydrate form is due to the rearrangement of the crystal lattice, the dissociation of moxifloxacin HCl and water, and the enthalpy of vaporization of the release of water of crystallization [35].

Different forms of anhydrous and hydrate moxifloxacin HCl were thoroughly investigated by the DSC technique and the summary data are listed in Table 7.7.

Regardless of the form type, the results in Table 7.7 show that the melting points of the free base of moxifloxacin and its hydrochloride salt are in the range of 210–218 and 242–255 °C, respectively. It should be noted that a salt usually exhibits a higher melting point than the free base. Furthermore, the results indicate that there are two types of water, unbounded and bounded water molecules, which are demonstrated by the two endotherm peaks at 65–75 and 100–110 °C, respectively.

It is worth mentioning that the endotherm peaks of the different forms are almost the same (e.g., Form II, Form  $\alpha$ 2, and Form  $\beta$ ). Consequently, the other supportive techniques such as XRPD and FT-IR are of significant importance to prove the existence of different forms (Table 7.4). However, there is lack of information on experimental conditions (atmosphere, heating rate) and on the purity of the tested forms. These parameters have to be considered for comparison purposes.

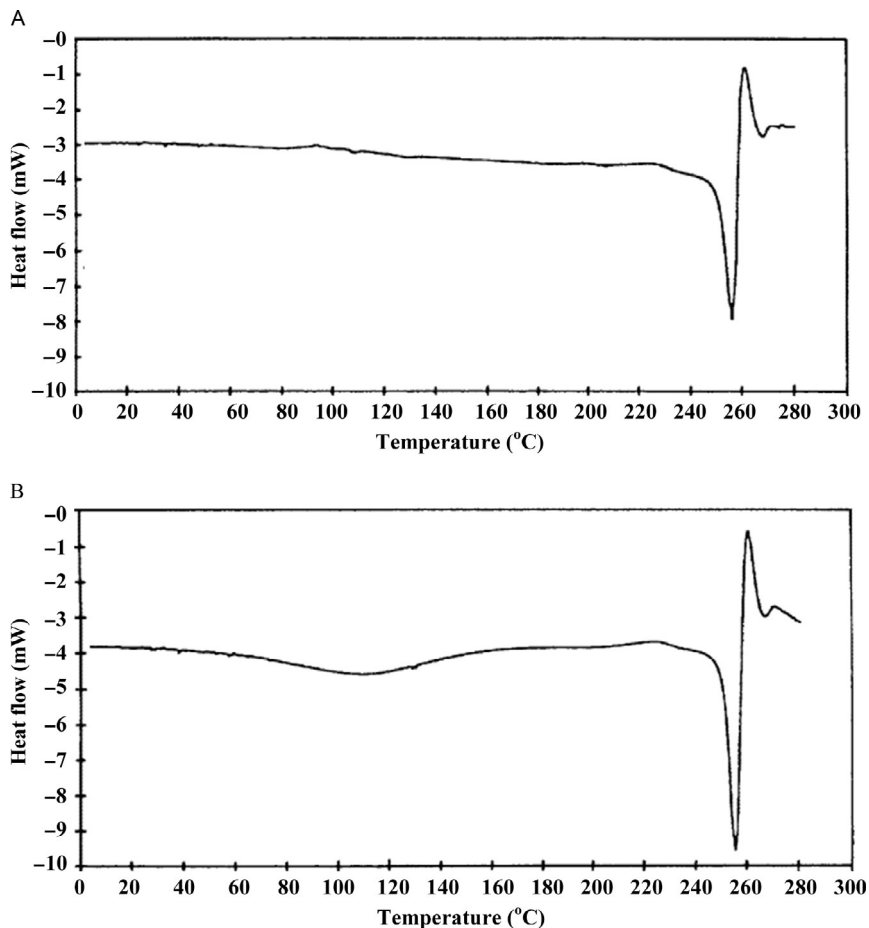


**Figure 7.8** The DSC thermograms of (A) anhydrous moxifloxacin HCl (Form I) and (B) moxifloxacin HCl monohydrate (Form II).

### 3.9.3 Thermogravimetric analysis

The TGA thermograms of the anhydrous form of moxifloxacin HCl (Form I) and its monohydrate form (Form II) were recorded using the Perkin-Elmer DSC-7 thermoanalyser [35]. Form I exhibits no loss in weight until heated beyond the temperature of its thermal decomposition (Figure 7.9A), whereas Form II shows a weight loss in two steps. The first step begins gradually to reach complete loss of 1 mol equiv of water (3.9% w/w) at around 150 °C. The second loss was recorded above 250 °C and it corresponds to thermal decomposition (Figure 7.9B). The obtained value of water loss is in good agreement with the theoretical loss and the transition temperatures of the DSC data.

**Table 7.7** The DSC data of different forms of moxifloxacin HCl

Form	Endotherm melting peak (°C)	Reference
Form I (anhydrous of moxifloxacin base)	~211	[15]
Form I (anhydrous)	~255	[35]
Form II (monohydrate)	~255	
	~110 (loss of water)	
Form A	~242	[38]
	~65 (loss of water)	
Form III (anhydrous)	~246	[40]
Crystalline form of moxifloxacin base	~210–218	[42]
	~150–165 (weak peak)	
Form A (hydrated)	~244	[43]
	~73 (loss of water)	
Form B (anhydrous)	~244	
Form $\alpha 1$ (hydrated)	~250	[45]
	~75 (loss of water)	
Form $\alpha 2$ (hydrated)	~253	
	~100 (loss of water)	
Form $\beta$ (monohydrate)	~252	[47]
	~100 (loss of water)	
Form $\gamma$ (anhydrous)	~254	
Form F (anhydrous)	~243	[48]
Form C (anhydrous)	~253	[50]

### 3.10. Spectroscopy

#### 3.10.1 UV/VIS spectroscopy

The UV/VIS absorption spectra of moxifloxacin HCl monohydrate in different solvents were recorded using the Beckman Coulter DU-650 spectrophotometer [30]. Figure 7.10 shows the UV/VIS absorption spectrum of moxifloxacin HCl monohydrate (0.0043 mg/ml as anhydrous) in methanol. The two maxima, recorded at 232 and 295 nm, are apparently due to the  $\pi \rightarrow \pi^*$  electronic transitions in the aromatic ring. The longest wavelength

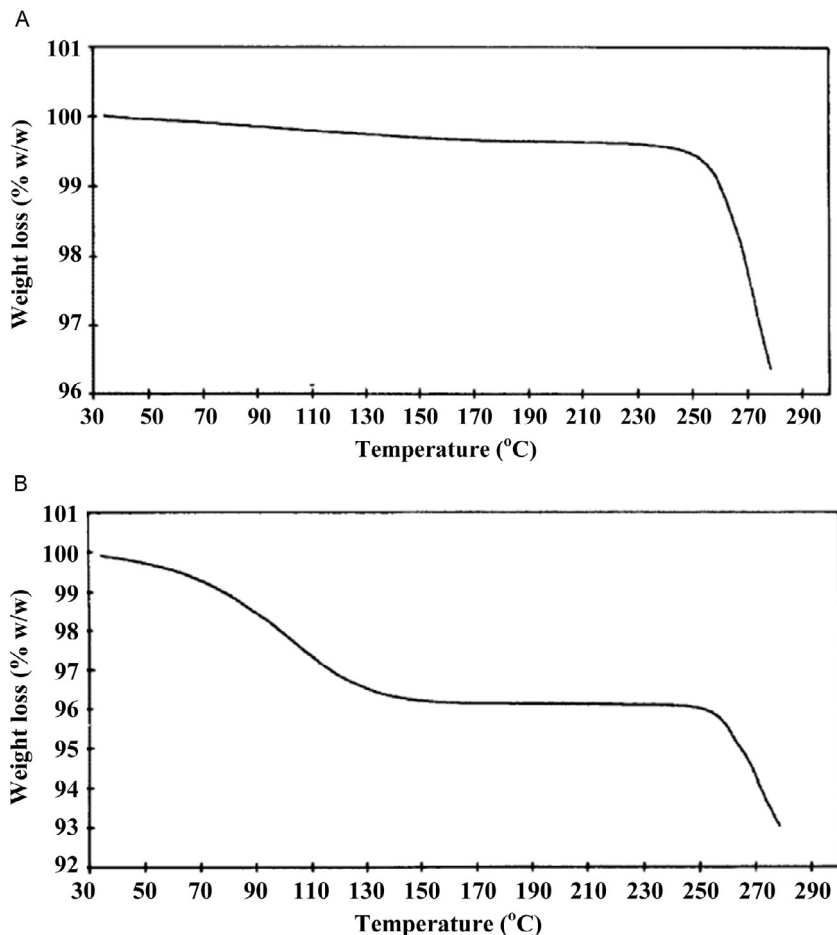


**Figure 7.9** The TGA thermograms of (A) anhydrous moxifloxacin HCl (Form I) and (B) moxifloxacin HCl monohydrate (Form II).

maximum, recorded between 320 and 380 nm, is due to an  $n \rightarrow \pi^*$  electronic transition [53].

The UV/VIS absorption summary data including solvent type,  $\lambda_{\text{max}}$ , and the intensity of absorption (A [1%, 1 cm]) are listed in Table 7.8.

### 3.10.2 Vibrational spectroscopy

#### 3.10.2.1 FT-IR spectroscopy

The FT-IR absorption spectrum of moxifloxacin HCl from Sigma was recorded using the JASCO FTIR 460 PLUS (KBr disc) in the range of 4000–400  $\text{cm}^{-1}$  [7]. The FT-IR spectrum is shown in Figure 7.11 and its corresponding assignments are given in Table 7.9. As mentioned in



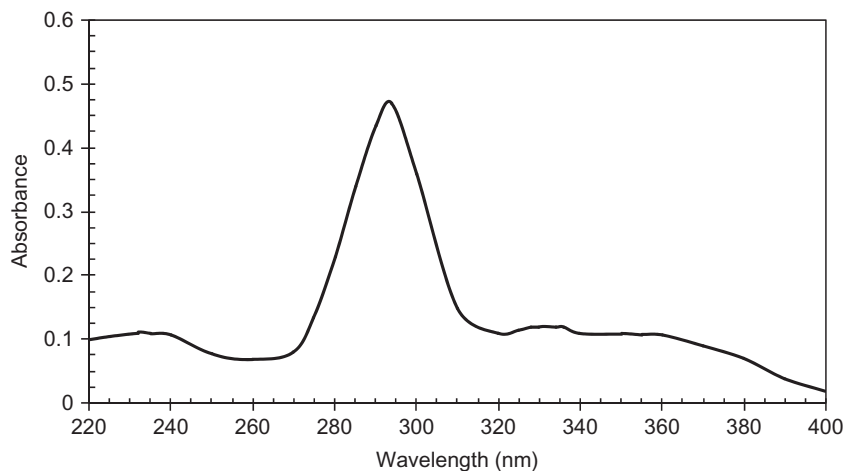


**Figure 7.10** The UV/VIS absorption spectrum of moxifloxacin HCl (0.0043 mg/ml as anhydrous) in methanol.

**Table 7.8** The UV/VIS absorption data of moxifloxacin HCl in different solvents

Solvent	$\lambda_{\max}$ (nm)	$A$ (1%, 1 cm) (gm/100 ml) $^{-1}$ cm $^{-1}$
Methanol	232	255
	295	1100
	334	280
	358	250
	358	250
Water	245	300
	288	995
	338	385
0.1 N HCl	217	340
	295	1050
	335	260
	360	235
0.1 N NaOH	242	305
	291	1055
	339	335
	355	285

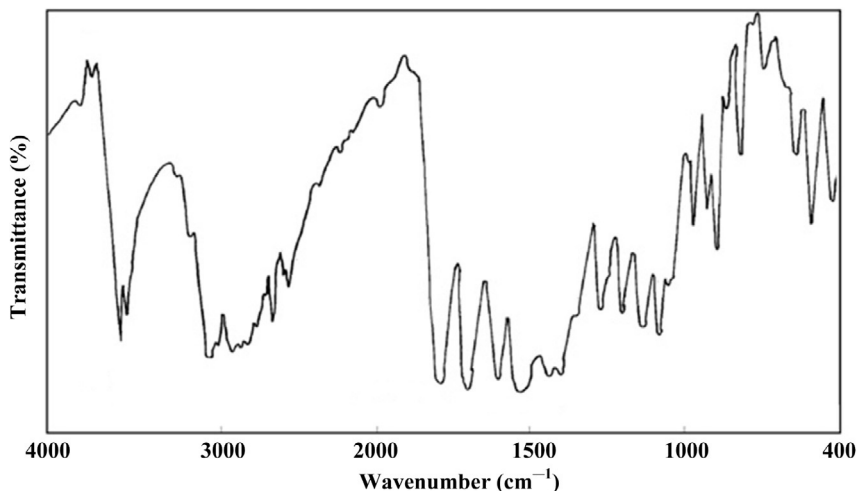


**Figure 7.11** The FT-IR absorption spectrum of moxifloxacin HCl monohydrate (KBr disc).

**Table 7.9** The assignments of the FT-IR absorption bands of moxifloxacin HCl monohydrate

Wavenumber (cm <sup>-1</sup> )	Assignment
3530–3472	$\nu(\text{O—H})$ ; H <sub>2</sub> O; COOH
3156–3056	$\nu(\text{C—H})$ ; aromatic
2976–2800	$\nu(\text{C—H})$ ; aliphatic
2733–2422	$\nu(-\text{NH}_2^+)$
1709	$\nu(\text{C=O})$ ; COOH
1620–1520	$\nu(\text{C=O})$ ; phenyl breathing
1454–1358	$-\text{CH}$ ; deformations of CH <sub>2</sub>
1323–1256	$\delta_{\text{b}}(-\text{CH}_2)$
1184	$\nu(\text{C—O})$
1166	$\nu(\text{C—N})$
1111	$\nu(\text{C—C})$
1049	$\delta_{\text{r}}(-\text{CH}_2)$
991–802	$-\text{CH}$ -bend; phenyl
772–721	$\delta_{\text{b}}(\text{COO}^-)$
691–424	Ring deformation

$\nu$ , stretching;  $\delta_{\text{b}}$ , bending.

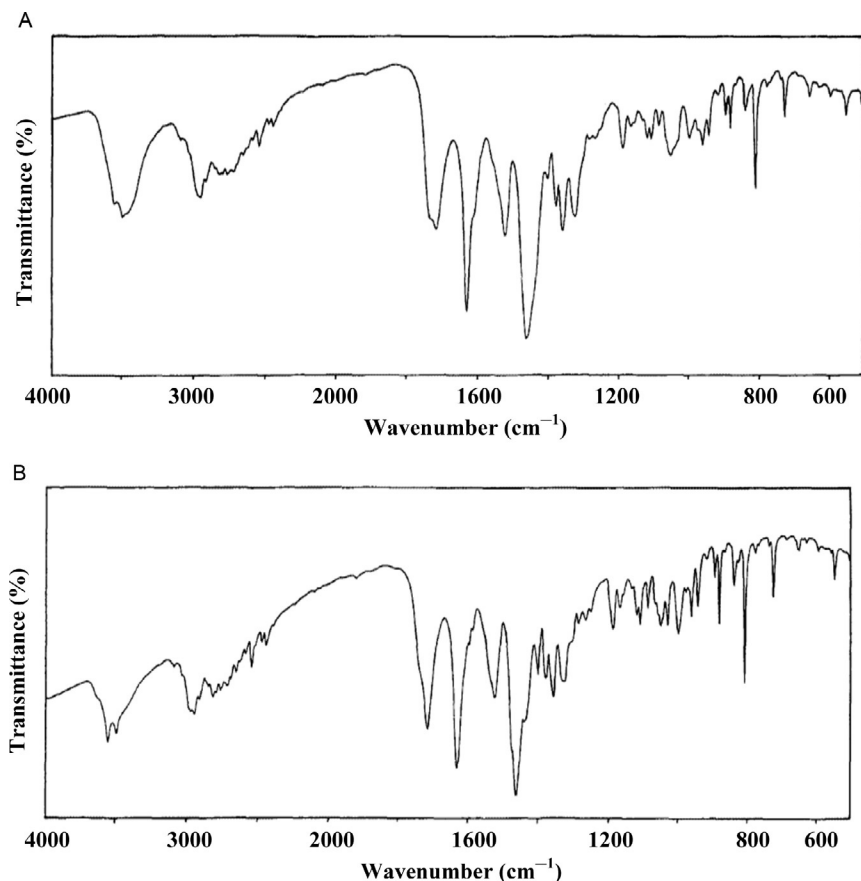


**Figure 7.12** The FT-IR absorption spectrum of (A) anhydrous (Form I) and (B) monohydrate (Form II) of moxifloxacin HCl (KBr disc).

**Section 3.5**, FT-IR technique can be used to distinguish between different forms of anhydrous and hydrate moxifloxacin HCl. For example, moxifloxacin HCl monohydrate (Form II) has characteristic IR bands in the region of  $3600\text{--}3100\text{ cm}^{-1}$  (OH valency vibrations) corresponding to water of crystallization ([Figure 7.12](#)). Such bands are already absent in the anhydrous moxifloxacin HCl (Form I) [35]. Furthermore, moxifloxacin HCl monohydrate (Form II) differs from Form I in the other frequency ranges proving different arrangement of the molecules in the crystal lattices of the two forms.

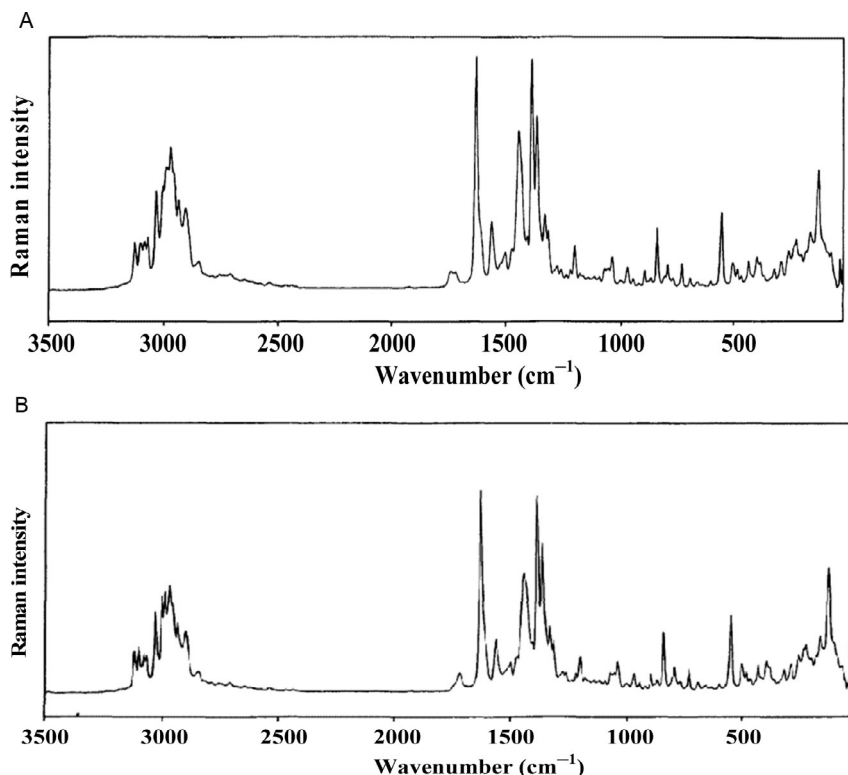


**Figure 7.13** The Raman absorption spectrum of (A) anhydrous (Form I) and (B) monohydrate (Form II) of moxifloxacin HCl.

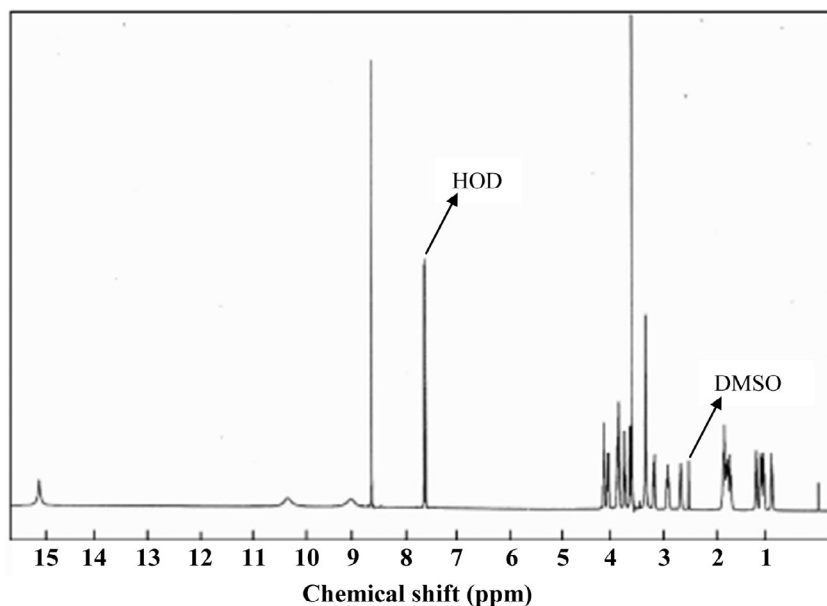
### 3.10.2.2 Raman spectroscopy

The Raman absorption spectra of anhydrous moxifloxacin HCl (Form I) and moxifloxacin HCl monohydrate (Form II) were recorded using the BRUKER Fourier-IR spectrometer IFS 88 [35]. The Raman spectra of the aforementioned drug forms are shown in Figure 7.13 and the assignments of part of distinctive Raman bands are given in Table 7.10. As shown in Figure 7.13, the differences in the spectra of the two forms are minimal in the range 3200–2800 cm<sup>-1</sup>. The fact that the spectra of the different forms of moxifloxacin HCl obtained by different workers are almost similar [35,50,53], therefore this technique was not widely used to distinguish between the different forms.

**Table 7.10** The assignments of some of the Raman absorption bands of moxifloxacin HCl monohydrate

Wavenumber ( $\text{cm}^{-1}$ )	Assignment
3150–3050	$\nu(\text{O—H, N—H})$
3120	$\nu(=\text{C—H})$
3000–2800	$\nu(\text{C—H})$
1711	$\nu(\text{C=O})$
1619	$\nu(\text{C=C})$
1433	$\delta_{\text{b}}(\text{CH}_2)$
1376–1352	$\nu(\text{Quinolone ring})$

$\nu$ , stretching;  $\delta_{\text{b}}$ , bending.

**Figure 7.14** The  $^1\text{H}$  NMR spectrum of moxifloxacin HCl in  $\text{DMSO-d}_6$ .

### 3.10.3 Nuclear magnetic resonance spectrometry

#### 3.10.3.1 $^1\text{H}$ NMR spectrum

The  $^1\text{H}$  NMR spectrum of moxifloxacin HCl (water content 2–2.5%) was obtained using the BRUKER-AV-500 spectrometer [54]. The sample was dissolved in  $\text{DMSO-d}_6$  and all resonance bands were referenced to the tetramethylsilane (TMS) internal standard. The  $^1\text{H}$  NMR and COSY  $^1\text{H}$  NMR spectra of moxifloxacin HCl are shown in Figures 7.14 and 7.15,

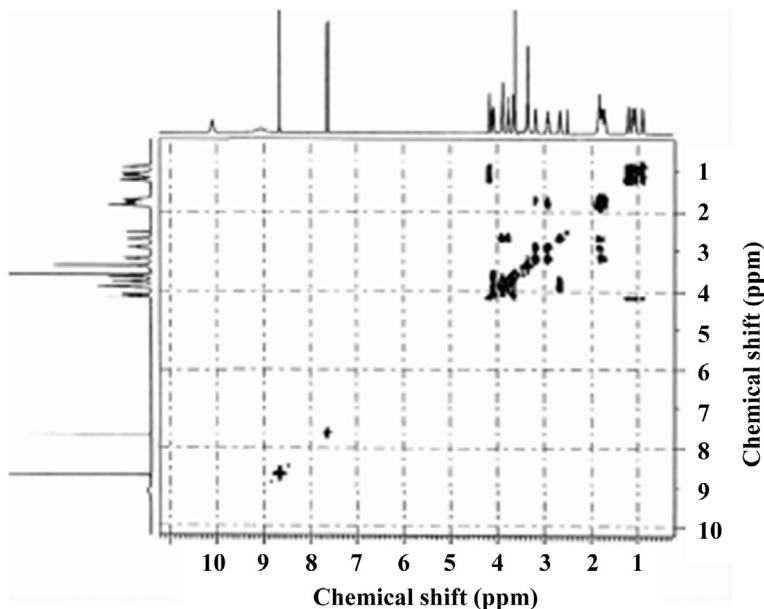


**Figure 7.15** The COSY <sup>1</sup>H NMR spectrum of moxifloxacin HCl in DMSO-d<sub>6</sub>.

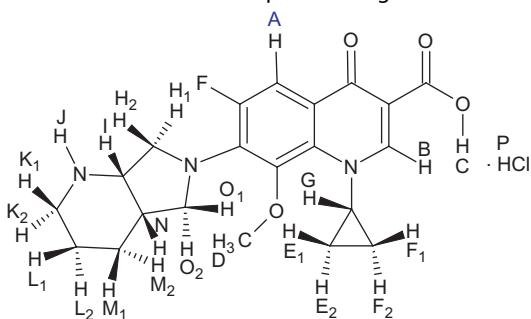
respectively. In [Figure 7.14](#), the presence of broad signals at 15.09, 10.26, and 9.03 ppm is due to the exchangeable (O–H and N–H) protons. The assignments of the resonance bands are given in [Table 7.11](#).

### 3.10.3.2 <sup>13</sup>C NMR spectrum

The <sup>13</sup>C NMR spectrum of moxifloxacin HCl (water content 2–2.5%) was obtained using the BRUKER-AV-500 spectrometer [\[54\]](#). The sample was dissolved in DMSO-d<sub>6</sub> and all resonance bands were referenced to the tetramethylsilane (TMS) internal standard. The <sup>13</sup>C NMR, DEPT, HMQC, and HMBC spectrum of moxifloxacin HCl are shown in [Figures 7.16–7.19](#). Their corresponding assignments are given in [Table 7.12](#).

### 3.10.3.3 Solid <sup>13</sup>C NMR spectrum

The solid <sup>13</sup>C NMR spectra of anhydrous moxifloxacin HCl (Form I) and moxifloxacin HCl monohydrate (Form II) were recorded using the BRUKER SML300 spectrometer [\[35\]](#). The solid <sup>13</sup>C NMR spectra are shown in [Figure 7.20](#) and the assignments of the solid <sup>13</sup>C NMR bands are given in [Table 7.13](#). The <sup>13</sup>C NMR spectra show the significant difference between the two forms due to the presence of a sharp peak at 168.1 ppm for the monohydrate form (Form II) in the range 180–160 ppm ([Figure 7.20](#)). Such difference in the spectra may be attributed to existing inter-hydrogen bonding between water and the carboxylic group.

**Table 7.11** The  $^1\text{H}$  NMR spectral assignments for moxifloxacin HCl

Chemical shift (ppm)	Number of proton	Multiplicity	Assignment	$^1\text{H}$ - $^1\text{H}$ COSY
15.11	1 <sup>a</sup>	s	C	/
10.28	1 <sup>a</sup>	s, br	P	/
9.07	1 <sup>a</sup>	s, br	J	/
8.65	1	s	B	/
7.63	1	d	A	/
4.16	1	m	G	GE, GF
4.08, 3.65	2	dd	H <sub>1</sub> , H <sub>2</sub>	H <sub>1</sub> I, H <sub>2</sub> I
3.91, 3.76	2	m	O	O <sub>1</sub> N, O <sub>2</sub> N
3.88	1	m	I	IH, IN
3.61	3	s	D	/
3.18, 2.92	2	m	K <sub>1</sub> , K <sub>2</sub>	K <sub>1</sub> L, K <sub>2</sub> L
2.67	1	m	N	NI
1.84, 1.70	2	m	M <sub>1</sub> , M <sub>2</sub>	M <sub>1</sub> N, M <sub>2</sub> N
1.75–1.80	2	m	L <sub>1</sub> , L <sub>2</sub>	L <sub>1</sub> K, L <sub>2</sub> K
1.02–1.14	2	m	F <sub>1</sub> , F <sub>2</sub>	F <sub>1</sub> G, F <sub>2</sub> G
0.89, 1.21	2	m	E <sub>1</sub> , E <sub>2</sub>	E <sub>1</sub> G, E <sub>2</sub> GE <sub>1</sub> G, E <sub>2</sub> G

<sup>a</sup>Disappear by increase of water content.

d, doublet; s, singlet; m, multiplet; dd, doublet doublet; br, broad.

### 3.11. Mass spectrometry

The mass spectra of moxifloxacin HCl monohydrate was carried out using the quadrupole ion trap mass spectrometry (QITM) [55] and Fourier transform ion cyclotron resonance mass spectrometry (FTICRMS) [56]

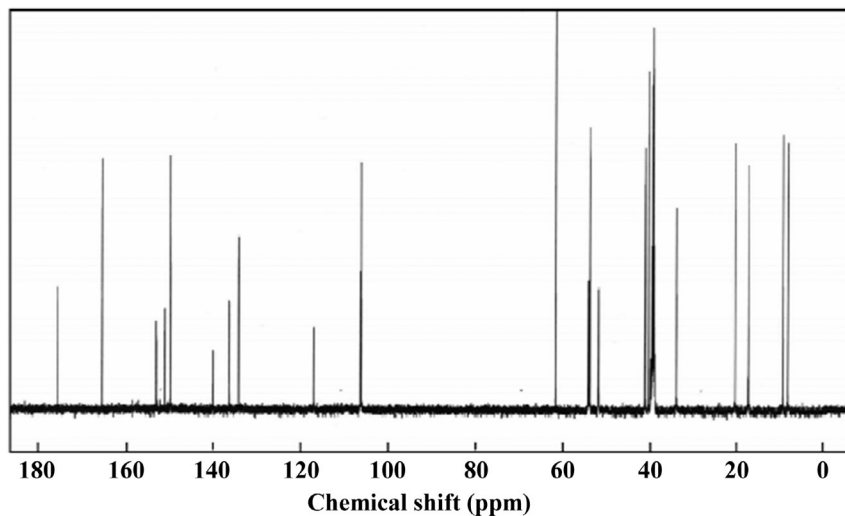


Figure 7.16 The  $^{13}\text{C}$  NMR spectrum of moxifloxacin HCl in  $\text{DMSO-d}_6$ .

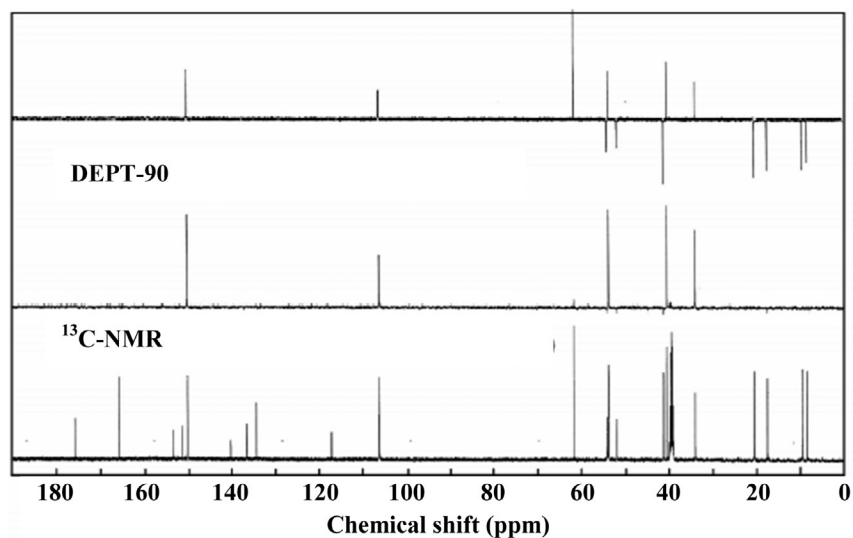


Figure 7.17 The DEPT spectrum of moxifloxacin HCl in  $\text{DMSO-d}_6$ .

analysers, both equipped with an electrospray ionization (ESI) source. Figure 7.21 shows the full mass fragmentation pattern and Table 7.14 shows its corresponding mass fragments.

It was suggested that the fragment ions at  $m/z$  181 and 169 are formed by cleavage of a benzene ring attributed to the stability of the product ions,



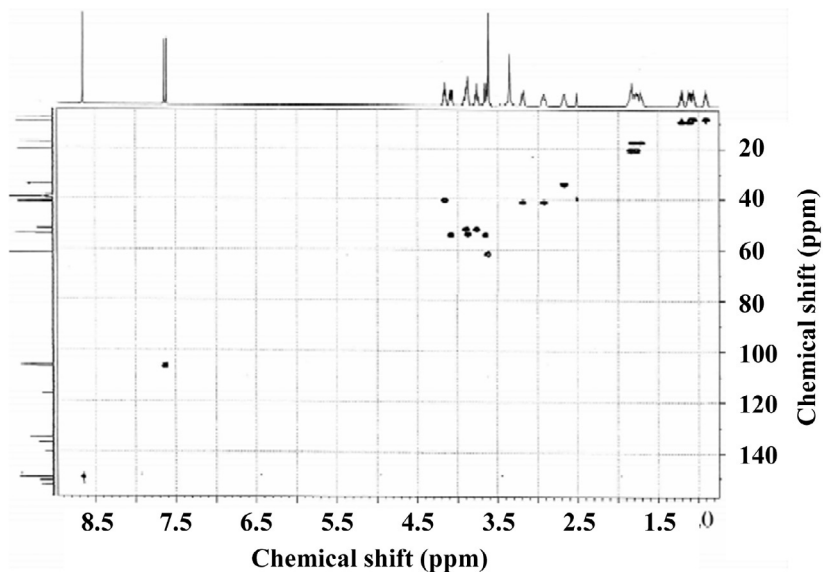


Figure 7.18 The HMQC spectrum of moxifloxacin HCl in DMSO-d<sub>6</sub>.

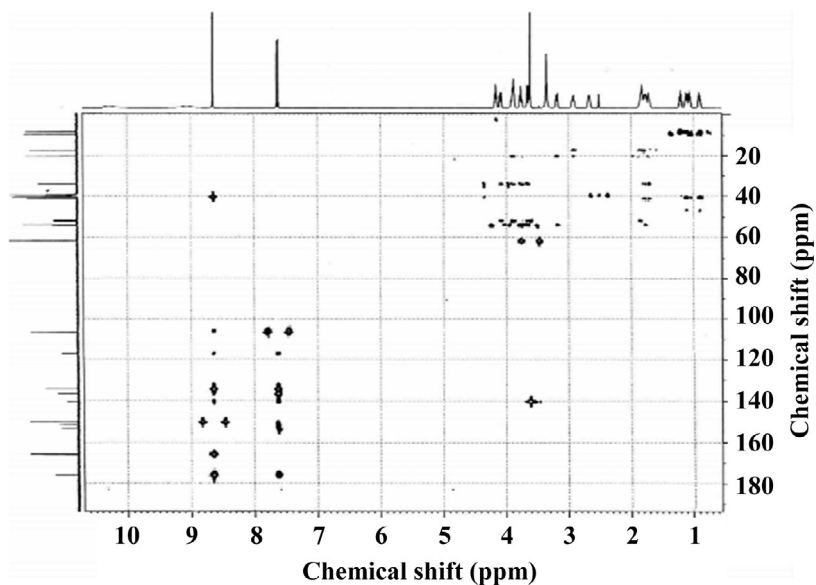
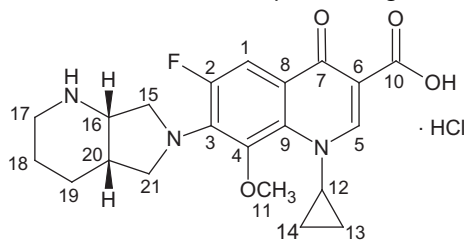
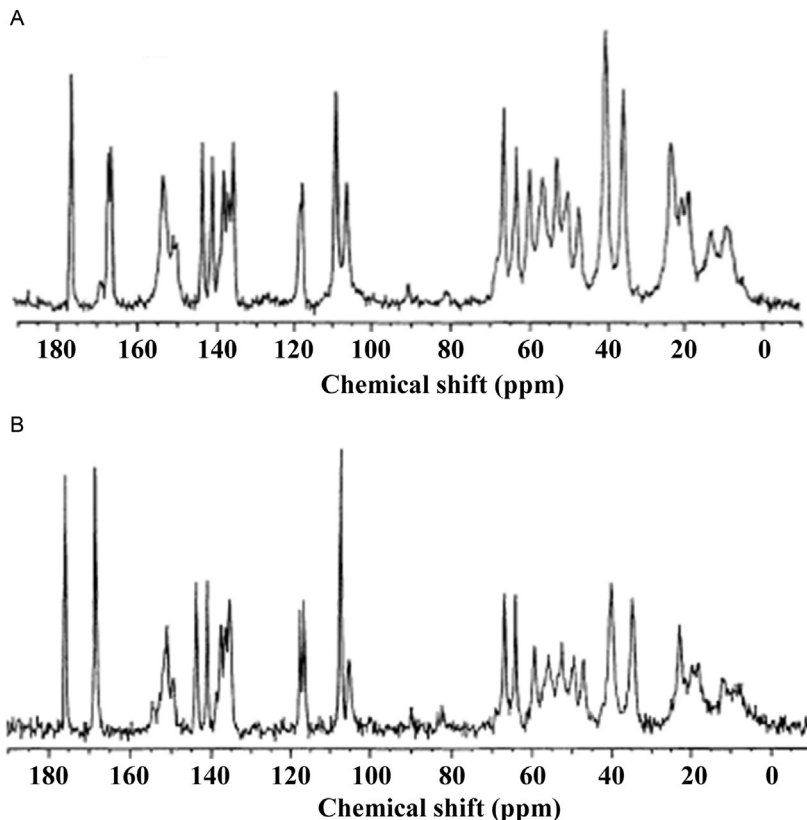


Figure 7.19 The HMBC spectrum of moxifloxacin HCl in DMSO-d<sub>6</sub>.

**Table 7.12** The  $^{13}\text{C}$  NMR spectral assignments for moxifloxacin HCl

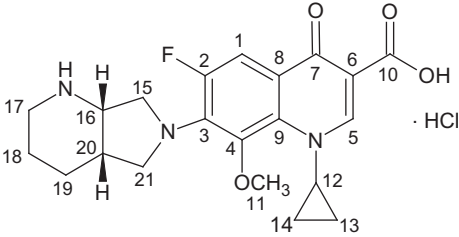
Chemical shift (ppm)	Assignment	HMQC	HMBC
175.85	7	/	7-C A, 7-C B
165.71	10	/	/
153.41, 151.42	2	/	2-C A
150.13	5	B	/
140.33	4	/	4-C A, 4-C B, 4-C D
136.56	3	/	3-C A
134.39	9	/	9-C A, 9-C B
117.22	8	/	8-C A, 8-C B
106.49	1	A	1-C B
106.32	6	/	6-C B
61.83	11	D	/
54.24	15	H <sub>1</sub> , H <sub>2</sub>	15-C I
53.93	16	I	16-C H, 16-C K, 16-C L, 16-C O
51.97	21	O <sub>1</sub> , O <sub>2</sub>	21-C H, 21-C L, 21-C M
41.32	17	K <sub>1</sub> , K <sub>2</sub>	17-C L
40.52	12	G	12-C E, 12-C F, 12-C B
34.51	20	N	20-C H, 20-C L, 20-C O
20.51	19	M <sub>1</sub> , M <sub>2</sub>	19-C K, 19-C I
17.48	18	L <sub>1</sub> , L <sub>2</sub>	18-C M, 18-C K
9.45	13	E <sub>1</sub> , E <sub>2</sub>	13-C G, 13-C F
9.33	14	F <sub>1</sub> , F <sub>2</sub>	14-CE, 14-C G



**Figure 7.20** The solid  $^{13}\text{C}$  NMR spectrum of moxifloxacin (A) anhydrous (Form I) and (B) monohydrate (Form II) of moxifloxacin HCl.

while the fragment ion at  $m/z$  145 is probably formed by the migration of a fluorine atom to nitrogen followed by cleavage of the N—C bond. The driving force for such migration appears to be due to the loss of a stable neutral molecule with a triple bond in the aromatic ring (substituted benzyne). The mechanism involving loss of benzyne is expected to be initiated with the abstraction of orthohydrogen to the fluorine by the nitrogen atom [55]. Furthermore, fragment ion at  $m/z$  364 is formed by loss of HF leading to the formation of the four-membered ring azetidine [56].

**Table 7.13** The solid <sup>13</sup>C NMR spectral assignments for moxifloxacin HCl monohydrate



Chemical shift (ppm)	Assignment
175.5	7
168.1	10
150.9, 149.3	2, 5
143.5, 140.8	4
137.4, 136.1, 135.2	3, 9
117.4	8
107.1, 105.0	1, 6
67–64	11
60–45	15, 16, 21
40.2	12, 17
34.9	20
22.9, 19.8, 18.2	18, 19
12.1, 9.0	13, 14

## 4. METHODS OF ANALYSIS

### 4.1. Compendial methods

#### 4.1.1 Moxifloxacin HCl drug substance

Moxifloxacin HCl is a drug substance listed in the European pharmacopeia (Ph. Euro.) [1], United States pharmacopeia-national formulary (USP-NF) [2] and United States pharmacopeia-medicines compendium (USP-MC) [57]. Table 7.15 shows its summary of specifications and methods of analysis.

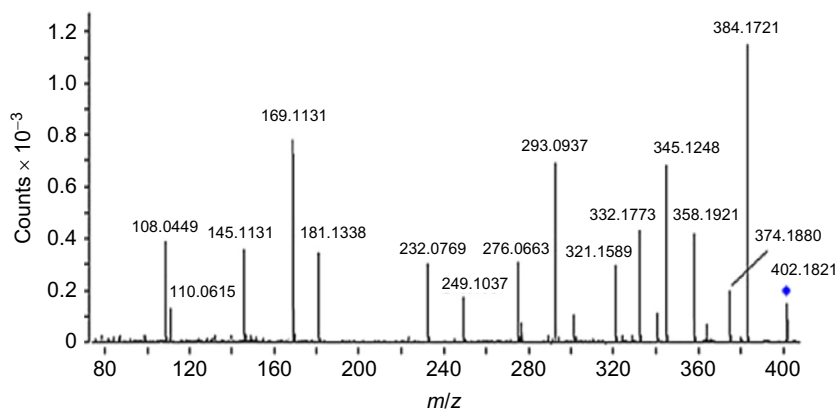


**Figure 7.21** The mass spectrum of moxifloxacin HCl monohydrate.

In addition to the mentioned “Reference Procedure” (Table 7.15), the USP-MC monograph includes the criteria-based procedures necessary to demonstrate that an “Acceptable Procedure” is equivalent to the “Reference Procedure” based upon “Performance-Based Monograph” concept. The procedure should be validated as described in the USP-MC general chapter “Assessing Validation Parameters for Reference and Acceptable Procedures <10>” and should meet the requirements of precision, accuracy, specificity, and range criteria. This approach is applied for all the USP-MC monographs of moxifloxacin HCl and its different pharmaceutical preparation (ophthalmic, solution, injection, and tablets) mentioned below.

In addition to the specifications mentioned in Table 7.15, the Ph. Euro states that production method of moxifloxacin HCl is validated to demonstrate the satisfactory enantiomeric purity of the final product.

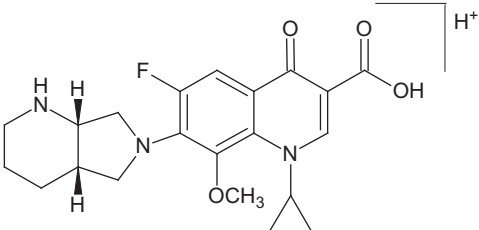
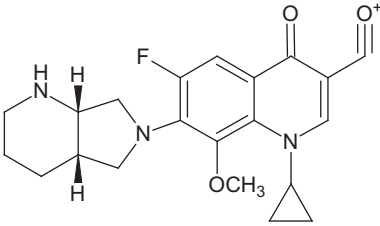
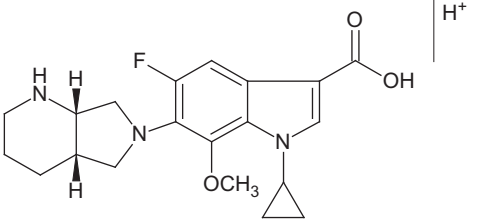
#### **4.1.2 Moxifloxacin HCl ophthalmic solution**

Moxifloxacin HCl ophthalmic solution is listed in the USP-NF [58] and the USP-MC [59]. Table 7.16 shows a summary of its specifications and methods of analysis.

#### **4.1.3 Moxifloxacin injection**

Moxifloxacin injection is listed the USP-MC [60]. Table 7.17 shows a summary of its specifications and methods of analysis.

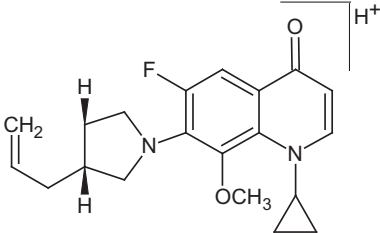
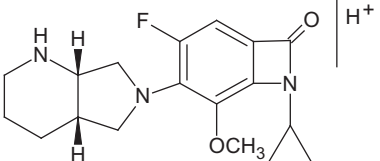
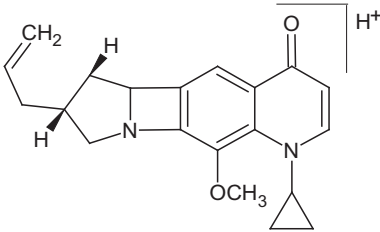
**Table 7.14** The mass spectral fragmentation for moxifloxacin HCl monohydrate

Fragment			
<i>m/z</i>	Relative abundance (%)	Formula	Structure
402.18	11.4	$[\text{C}_{21}\text{H}_{25}\text{FN}_3\text{O}_4]^+$	
384.17	100.0	$[\text{C}_{21}\text{H}_{25}\text{FN}_3\text{O}_4]^+ - [\text{H}_2\text{O}]$	
374.19	17.7	$[\text{C}_{21}\text{H}_{25}\text{FN}_3\text{O}_4]^+ - [\text{CO}]$	

*Continued*

**Table 7.14** The mass spectral fragmentation for moxifloxacin HCl monohydrate—cont'd

<i>m/z</i>	Relative abundance (%)	Fragment	
		Formula	Structure
364.16	6.3	$[\text{C}_{21}\text{H}_{25}\text{FN}_3\text{O}_4]^+ - [\text{H}_2\text{O} + \text{HF}]$	
358.19	36.7	$[\text{C}_{21}\text{H}_{25}\text{FN}_3\text{O}_4]^+ - [\text{CO}_2]$	
345.12	59.5	$[\text{C}_{21}\text{H}_{25}\text{FN}_3\text{O}_4]^+ - [\text{C}_3\text{H}_7\text{N}]$	

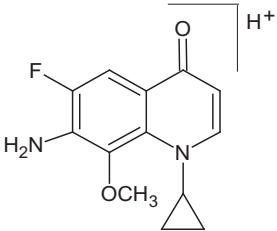
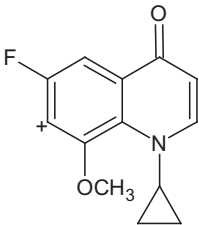
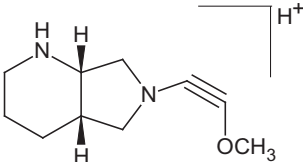
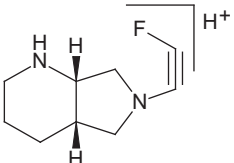
341.17	10.1	$[\text{C}_{21}\text{H}_{25}\text{FN}_3\text{O}_4]^+ - [\text{CO}_2 + \text{NH}_3]$	
332.17	38.0	$[\text{C}_{21}\text{H}_{25}\text{FN}_3\text{O}_4]^+ - [\text{CO}_2 + \text{C}_2\text{H}_2]$ $[\text{C}_{21}\text{H}_{25}\text{FN}_3\text{O}_4]^+ - [\text{C}_3\text{H}_2\text{O}_2]$	
321.16	26.6	$[\text{C}_{21}\text{H}_{25}\text{FN}_3\text{O}_4]^+ - [\text{CO}_2 + \text{NH}_3 + \text{HF}]$	

*Continued*



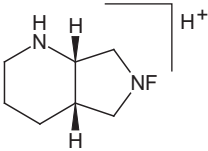
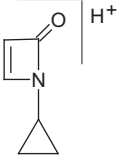
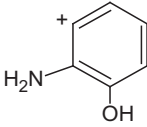
**Table 7.14** The mass spectral fragmentation for moxifloxacin HCl monohydrate—cont'd

		Fragment	
<i>m/z</i>	Relative abundance (%)	Formula	Structure
301.14	10.1	$[\text{C}_{21}\text{H}_{25}\text{FN}_3\text{O}_4]^+ - [\text{CO}_2 + \text{C}_3\text{H}_7\text{N}]$	
293.09	60.8	$[\text{C}_{21}\text{H}_{25}\text{FN}_3\text{O}_4]^+ - [\text{C}_3\text{H}_7\text{N} + \text{C}_4\text{H}_4]$	
276.07	27.8	$[\text{C}_{21}\text{H}_{25}\text{FN}_3\text{O}_4]^+ - [\text{C}_7\text{H}_{14}\text{N}_2]$	

249.10	15.2	$[\text{C}_{21}\text{H}_{25}\text{FN}_3\text{O}_4]^+ - [\text{CO}_2 + \text{C}_3\text{H}_7\text{N} - \text{C}_4\text{H}_4]$	
232.08	26.6	$[\text{C}_{21}\text{H}_{25}\text{FN}_3\text{O}_4]^+ - [\text{CO}_2 + \text{C}_3\text{H}_7\text{N} - \text{C}_4\text{H}_4 - \text{NH}_3]$	
181.13	24.0	$[\text{C}_{10}\text{H}_{17}\text{N}_2\text{O}]^+$	
169.11	68.4	$[\text{C}_9\text{H}_{14}\text{FN}_2]^+$	

*Continued*

**Table 7.14** The mass spectral fragmentation for moxifloxacin HCl monohydrate—cont'd

Fragment			
<i>m/z</i>	Relative abundance (%)	Formula	Structure
145.11	31.6	$[\text{C}_7\text{H}_{14}\text{FN}_2]^+$	
110.06	11.4	$[\text{C}_6\text{H}_8\text{NO}]^+$	
108.04	34.2	$[\text{C}_6\text{H}_6\text{NO}]^+$	

**Table 7.15** The summary of the compendial methods of moxifloxacin HCl

Test	Eur. Ph.	USP-NF	USP-MC
Definition	1-Cyclopropyl-6-fluoro-8-methoxy-7-[(4a <i>S</i> ,7a <i>S</i> )-octahydro-6 <i>H</i> -pyrrolo[3,4- <i>b</i> ]pyridine-6-yl]-4-oxo-1,4-dihydroquinoline-3-carboxylic acid hydrochloride	(4a <i>S</i> -cis)-1-cyclopropyl-6-fluoro-1,4-dihydro-8-methoxy-7-(octahydro-6 <i>H</i> -pyrrolo [3,4- <i>b</i> ]pyridin-6-yl)-4-oxo-3-quinolinecarboxylic acid, monohydrochloride	
	Moxifloxacin HCl contains NLT 98.0% and NMT 102.0% of moxifloxacin HCl (C <sub>21</sub> H <sub>24</sub> FN <sub>3</sub> O <sub>4</sub> ·HCl), calculated on the anhydrous basis.		
Characters	Light yellow or yellow powder or crystals, slightly hygroscopic. Sparingly soluble in water, slightly soluble in ethanol (96%), practically insoluble in acetone	Slightly yellow to yellow powder or crystals. Soluble in 0.1 N NaOH, sparingly soluble in water, and in methanol; slightly soluble in 0.1 N HCl, in dimethylformamide, and in alcohol; practically insoluble in methylene chloride, in acetone, in ethyl acetate, and in toluene; insoluble in tert-butyl methyl ether and <i>n</i> -heptane	Slightly yellow to yellow, crystalline powder
Identification A	Specific optical rotation (see Test below)	IR. Absorption <197K>	

*Continued*

**Table 7.15** The summary of the compendial methods of moxifloxacin HCl—cont'd

Test	Eur. Ph.	USP-NF	USP-MC
Identification B	IR absorption spectrophotometry (2.2.24)	The RT of the major peak in the chromatogram of the assay preparation corresponds to that in the chromatogram of the standard preparation, as obtained in the assay	Identification tests—general, chloride <191>
Identification C	To 10 mg/ml in H <sub>2</sub> O, add 1 ml of dilute HNO <sub>3</sub> , mix, stand for 5 min and filter. The filtrate gives reaction (a) of chlorides (2.3.1)	To a solution (1 in 160), add diluted HNO <sub>3</sub> , and filter. The filtrate meets the requirements of the tests for Chloride <191>	—
Appearance of solution	Not more opalescent than RS II (2.2.1) and not more intensely colored than RS GY2 (2.2.2, Method II). If intended for use in the manufacture of parenteral preparations, the solution is clear (2.2.1) and not more intensely colored than RS GY2 (2.2.2, Method II). 50 mg/ml in dilute NaOH solution	—	—
pH	3.9–4.6, 2 mg/ml in CO <sub>2</sub> -free H <sub>2</sub> O [(2.2.3) and <791>]		—

Specific optical rotation	– 125 to –138 (anhydrous substance), 10 mg/ml in CAN:H <sub>2</sub> O (1:1 v/v) [(2.2.7) and <781S>]		
Related substance/related compounds/organic impurities (protect solutions from light) [(2.2.29) and <621>]			
Diluent	0.50 g of TBAHSO <sub>4</sub> and 1.0 g KH <sub>2</sub> PO <sub>4</sub> in about 500 ml of H <sub>2</sub> O. Add 2 ml of H <sub>3</sub> PO <sub>4</sub> and 50 mg of anhydrous Na <sub>2</sub> SO <sub>3</sub> , then dilute to 1000.0 ml with H <sub>2</sub> O	0.50 g of TBAHSO <sub>4</sub> and 1.0 g KH <sub>2</sub> PO <sub>4</sub> in H <sub>2</sub> O, add 2 ml of H <sub>3</sub> PO <sub>4</sub> and 20 mg of anhydrous Na <sub>2</sub> SO <sub>3</sub> , then dilute to 1000.0 ml with H <sub>2</sub> O	MeOH
Mobile phase (v/v)	MeOH:A solution containing 0.5 g/l TBAHSO <sub>4</sub> , 1.0 g/l KH <sub>2</sub> PO <sub>4</sub> and 3.4 g/l H <sub>3</sub> PO <sub>4</sub> (28:72)	MeOH:A solution containing 0.5 g/l TBAHSO <sub>4</sub> , 1.0 g/l KH <sub>2</sub> PO <sub>4</sub> and 2 ml/l H <sub>3</sub> PO <sub>4</sub> (7:18)	MeOH: A solution A: 0.1% DEA in H <sub>2</sub> O, pH of 2.3 with TFA (40:60).
Test solution (a)	1.0 mg/ml in diluent	0.1 mg/ml in diluents, prepare from stock solution (5 mg/ml)	1.0 mg/ml in MeOH
Test solution (b)	0.1 mg/ml in diluent, prepare from test solution (a)	–	0.1 mg/ml in MeOH, prepare from test solution (a)
Reference solution	–	0.1 mg/ml moxifloxacin HCl in diluent	0.1 mg/ml of moxifloxacin HCl in MeOH
Reference solution (a)	0.1 mg/ml moxifloxacin HCl in diluent	0.002 mg/ml moxifloxacin HCl in diluent	1 µg/ml each of moxifloxacin HCl, impurities A, B, C, D, and E in MeOH

*Continued*

**Table 7.15** The summary of the compendial methods of moxifloxacin HCl—cont'd

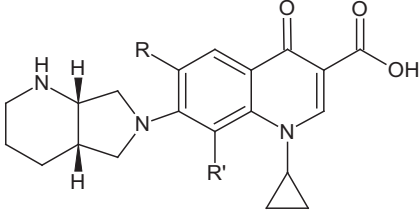
Test	Eur. Ph.	USP-NF	USP-MC
Reference solution (b)	1 mg/ml moxifloxacin for peak identification CRS (containing impurities A, B, C, D, and E) in diluent	0.1 mg/ml and 0.001 mg/ml of moxifloxacin HCl and impurity A in diluent, respectively	1 µg/ml of moxifloxacin HCl and impurity A in MeOH
Reference solution (c)	0.001 mg/ml in diluent, prepare from test solution (b)	0.05 µg/ml [ <i>Note:</i> Store the solution under refrigeration and protected from light], prepare from reference solution (a).	—
Column	End-capped phenylsilyl silica gel for chromatography R (5 µm, 250 × 4.6 mm)	Packing L11 (5 mm, 250 × 4.0 mm)	Packing L11 (5 µm, 150 × 4.6 mm)
Detection	UV: 293 nm		200–700 nm [calculations should be made at an isobestic point of moxifloxacin and impurity spectra or at 293 nm if an isobestic point is not available] MS source: ES scan (+ and –), source temperature: 90 °C, desolvation temperature: 400 °C
Injection (µl)	10	25	10
Flow rate (ml/min.)	1.3	0.9	1.0

Temperature (°C)	45		Oven: 40, autosampler: 5
Run time	2.5 × the RT of moxifloxacin	2 × the RT of moxifloxacin	–
Identification of impurities (rRT)	Reference to moxifloxacin <sup>a</sup> Impurity A: about 1.1 Impurity B about 1.3 Impurity C about 1.4 Impurity D about 1.6 Impurity E about 1.7	Reference to moxifloxacin Impurity A: about 1.15 Impurity B about 1.32 Impurity C about 1.48 Impurity D about 1.71 Impurity E about 1.83	–
System suitability	Resolution: ≥ 1.5 between moxifloxacin and impurity A; The chromatogram obtained is similar to the chromatogram supplied with moxifloxacin for peak identification CRS, use reference solution (b)	Resolution: ≥ 1.5 between moxifloxacin and impurity A, use reference solution (b) Column efficiency: 4000 theoretical plates Tailing factor: ≤ 2.0 Relative standard deviation: ≤ 2.0%, use reference solution (a) Signal-to-noise ratio: ≥ 10, use reference solution (c)	Resolution: ≥ 1.5 between moxifloxacin and impurity A, use reference solution (b) Relative standard deviation: ≤ 1.0%, use reference solution
Limits	Correction factors: for the calculation of content, multiply the peak areas of the following impurities by the corresponding correction factor: impurity B = 1.4; impurity E = 3.5.	Correction factors: for the calculation of content, multiply the peak areas of the following impurities by the corresponding correction factor: impurity B = 0.71; impurity E = 0.29.	Any individual impurity: ≤ 0.1% Total: ≤ 2.0%

*Continued*



**Table 7.15** The summary of the compendial methods of moxifloxacin HCl—cont'd

Test	Eur. Ph.	USP-NF	USP-MC
	Impurities A, B, C, D, E: $\leq 0.1\%$ (each) Unspecified impurities: $\leq 0.10\%$ Total: $\leq 0.3\%$ Disregard limit: $\leq 0.05\%$	Impurities A, B, C, D, E: $\leq 0.1\%$ (each) Unspecified impurities: $\leq 0.1\%$ Total: $\leq 0.5\%$	
Assay	As described in the test for related substances with the following modification: Injection: Test solution (b) and reference solution (a).	As described in the test for related substances with the following modification: Injection: Test solution (a) and reference solution	As described in the test for related substances with the following modification: Injection: Test solution (a) and reference solution, detector: at 293 nm To confirm the absence of co-eluting known and unknown impurity, substitute the Detector under related substances
List of impurities	Specified impurities: A, B, C, D, E. Impurity A (6,8-difluoro): $R = R' = F$ Impurity B (6,8-dimethoxy): $R = R' = OCH_3$ Impurity C (8-ethoxy): $R = F$ , $R' = OC_2H_5$		

	Impurity D (6-methoxy-8-fluoro): R = OCH <sub>3</sub> , R' = F Impurity E (8-hydroxy): R = F, R' = OH		
Water	≤4.5%, use 0.200 g [(2.5.12) and <921 >], method Ia		
Anhydrous: ≤0.5%. Monohydrate: ≤4.0% [<921 >, method I]			
Sulfated ash	≤0.1%, use 1.0 g in a platinum crucible [(2.4.14) and <281 >]		
Sulfate	—	A 0.6-g portion shows no more sulfate than corresponds to 0.25 ml of 0.020 N sulfuric acid (0.04%) [<221 >]	—
Elemental impurities	—	—	Proceed as directed in the general chapter.[< 232 >]
Residual solvents	—	—	Proceed as directed in the general chapter [< 467 >]
Microbial enumeration tests and Tests for specified microorganisms	—	The total aerobic microbial count: ≤1000 cfu/g The total combined molds and yeasts count: ≤100 cfu/g [<61 > and < 62 >]	—

*Continued*

**Table 7.15** The summary of the compendial methods of moxifloxacin HCl—cont'd

Test	Eur. Ph.	USP-NF	USP-MC
Storage	In an airtight container, protected from light	In tight, light-resistant containers. Store at room temperature	—
Labeling	The label states, where applicable, that the substance is suitable for use in the manufacture of parenteral preparations	—	—

<sup>a</sup>Use the chromatogram supplied with moxifloxacin for peak identification CRS and the chromatogram obtained with reference solution (b) to identify the peaks due to impurities A, B, C, D, and E.

ACN, acetonitrile; TBA, tetrabutylammonium; RT, retention time; rRT, relative retention time; DEA, diethylamine; TFA, trifluoroacetic acid.

**Table 7.16** The summary of the compendial methods of moxifloxacin HCl ophthalmic solution

Test	USP-NF	USP-MC
Definition	Moxifloxacin ophthalmic solution is a sterile, self-preserved aqueous solution of Moxifloxacin HCl. It contains NLT 90.0% and NMT 110.0% of the labeled amount of moxifloxacin ( $C_{21}H_{24}FN_3O_4$ )	Moxifloxacin ophthalmic solution contains an amount of moxifloxacin HCl equivalent to NLT 95.0% and NMT 105.0% of the labeled amount of moxifloxacin ( $C_{21}H_{24}FN_3O_4$ )
Identification	The retention time of the major peak in the chromatogram of the assay preparation corresponds to that in the chromatogram of the standard preparation, as obtained in the Assay	The response of moxifloxacin from the sample solution corresponds to that of the standard solution, as obtained in the assay
Uniformity of dosage units	—	Meets the requirements [ $<905>$ ]
Sterility	It meets the requirements when tested as directed for Membrane Filtration under Test for Sterility of the product to be examined [ $<71>$ ]	
pH	6.3–7.3 [ $<791>$ ]	—
Osmolality	260–320 mOsmol/kg [ $<785>$ ]	—
Related compounds/Organic impurities [ $<621>$ ]		
Test 1: Early-eluting related compounds (relative retention time less than 1.8) [protect solutions from light. Analyze the Test solution immediately after preparation]		—
Buffer solution/Blank solution	0.5 g of TBAHSO <sub>4</sub> and 1.0 g of KH <sub>2</sub> PO <sub>4</sub> in 1000 ml of H <sub>2</sub> O, add 2 ml of H <sub>3</sub> PO <sub>4</sub>	—

*Continued*

**Table 7.16** The summary of the compendial methods of moxifloxacin HCl ophthalmic solution—cont'd

Test	USP-NF					USP-MC
Mobile phase (v/v)/Flow rate (ml/min)	Time (min)	Flow rate (ml/min)	Buffer solution	MeOH	Elution	MeOH: A solution A: 0.1% DEA in H <sub>2</sub> O, pH of 2.3 with TFA (40:60)/1.0
	0–30	0.5	69	31	Isocratic	
	30–31	0.5	69 → 60	31 → 40	Linear gradient	
	31–36	0.9	60	40	Isocratic	
	31–36	0.9	60	40	Isocratic	
	36–37	0.9	60 → 69	40 → 31	Linear gradient	
	37–42	0.5	69	31	Equilibration	
Resolution solution	0.1 mg/ml moxifloxacin HCl and 0.001 mg/ml impurity A in buffer solution					1 µg/ml each of moxifloxacin HCl and impurity A in MeOH
Reference solution	0.002 mg/ml moxifloxacin HCl in buffer solution					1 µg/ml each of moxifloxacin HCl, impurity A, impurity B, impurity C, impurity D, and impurity E in MeOH
Sensitivity solution	0.05 µg/ml moxifloxacin HCl, prepared from reference solution [store under refrigeration and protected from light]					–
Test solution	A volume of solution equivalent to 0.1 mg/ml moxifloxacin in buffer solution					A volume of solution equivalent to 1 mg/ml moxifloxacin in MeOH
Column	Packing L11 (5 µm, 250 × 4.0 mm)					Packing L11 (5 µm, 150 × 4.6 mm)

Detection	UV: 293 nm				200–700 nm [calculations should be made at an isobestic point of moxifloxacin and impurity spectra or at 293 nm if an isobestic point is not available] MS source: ES scan (+ and –), source temperature: 90 °C, desolvation temperature: 400 °C
Temperature (°C)	45				Column oven: 40, autosampler: 5
System suitability	Resolution: $\geq 2.0$ between moxifloxacin and impurity A, use resolution solution Column efficiency: 4000 theoretical plates Tailing factor: $\leq 2.0$ Relative standard deviation: $\leq 2.0\%$ , use reference solution Signal-to-noise ratio: $\geq 10$ , use sensitivity solution				Resolution: $\geq 1.5$ between moxifloxacin and impurity A, use resolution solution Relative standard deviation: $\leq 1.0\%$ , use reference solution
Limits	Related compound	F	rRT	Limit (%)	Any individual impurity: $\leq 0.20\%$
	Specified unknown impurity #1	1.0	0.3	0.2	
	Decarboxy	0.13	0.4	0.3	
	Specified unknown impurity #2	1.0	0.9	0.3	
	Any specified and identified impurity	1.0	–	1.0	
	Other single impurities	1.0	–	0.1	
	Impurity A <sup>a</sup>		1.1	–	
	8-Hydroxy (impurity E) <sup>b</sup>	–	–	–	

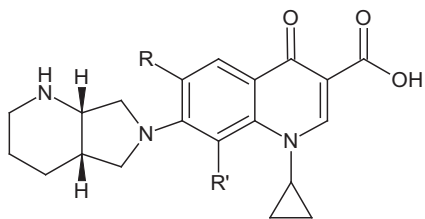
*Continued*

**Table 7.16** The summary of the compendial methods of moxifloxacin HCl ophthalmic solution—cont'd

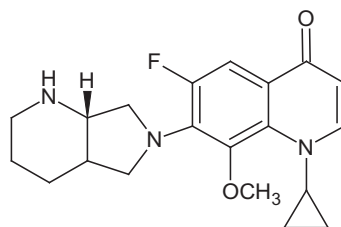
Test	USP-NF	USP-MC
Related compounds [ $<621>$ ]		—
Test 2: Late-eluting related compounds (relative retention time equal to more than 1.8) [protect solutions from light. Analyze the Test solution immediately after preparation]		—
Buffer solution/Black solution	0.5 g of TBAHSO <sub>4</sub> and 1.0 g of KH <sub>2</sub> PO <sub>4</sub> in 1000 ml of H <sub>2</sub> O, add 2 ml of H <sub>3</sub> PO <sub>4</sub>	—
Mobile phase (v/v)	MeOH:Buffer solution (40:60)	—
Reference solution	0.002 mg/ml moxifloxacin HCl in buffer solution	—
Sensitivity solution	0.05 µg/ml moxifloxacin HCl, prepared from reference solution [ <i>Note</i> : Store the sensitivity solution under refrigeration and protected from light]	—
Test solution	0.1 mg/ml moxifloxacin in buffer solution	—
Column	Packing L11 (5 µm, 250 × 4.0 mm)	—
Temperature (°C)	45	—
Detection (nm)	UV: 293	—
Flow rate (ml/min)	0.9	—
Injection volume (µl)	25	—
System suitability	Column efficiency: 2000 theoretical plates Tailing factor: $\leq 2.0$ Signal-to-noise ratio: $\geq 10$ , use sensitivity solution	—

Limits	Related compound	F	rRT	Limit (%)	–	–
	8-Hydroxy	0.29	1.8	0.2		–
	Specified unknown impurity #3	1.0	3.4	0.2		–
	Specified impurity #4	0.42	3.9	0.2		–
	Other single impurities	1.0	–	0.1		–
	Total impurities (Test 1 and Test 2)	–	–	1.5		–

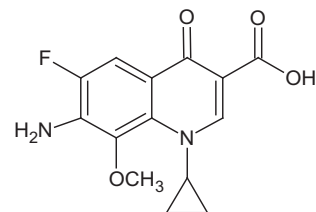
#### List of impurities



Specified impurities: A, B, C, D, E.  
 Impurity A: R = R' = F  
 Impurity B: R = R' = OCH<sub>3</sub>  
 Impurity C: R = F, R' = OC<sub>2</sub>H<sub>5</sub>  
 Impurity D: R = OCH<sub>3</sub>, R' = F  
 Impurity E (8-hydroxy): R = F, R' = OH



1-Cyclopropyl-6-fluoro-8-methoxy-7-[(4aS,7aS)-octahydro-pyrrolo[3,4-b]pyridin-6-yl]-1H-quinolin-4-one (decarboxy)



7-Amino-1-cyclopropyl-6-fluoro-8-methoxy-4-oxo-1,4-dihydroquinoline-3-carboxylic acid (specified impurity #4)

Continued



**Table 7.16** The summary of the compendial methods of moxifloxacin HCl ophthalmic solution—cont'd

Test	USP-NF					USP-MC
Elemental impurities	–					Proceed as directed in the chapter [ $<232>$ ]
Residual solvents	–					Proceed as directed in the chapter [ $<467>$ ]
Assay [ $<621>$ ]						
Buffer solution/Blank solution	0.5 g of TBAHSO <sub>4</sub> and 1.0 g of KH <sub>2</sub> PO <sub>4</sub> in 1000 ml of H <sub>2</sub> O, add 2 ml of H <sub>3</sub> PO <sub>4</sub>					–
Mobile phase (v/v)/Flow rate (ml/min)	Time (min)	Flow rate (ml/min)	Buffer solution	MeOH	Elution	
	0–30	0.5	69	31	Isocratic	
	30–31	0.5	69 → 60	31 → 40	Linear gradient	
	31–36	0.9	60	40	Isocratic	
	36–37	0.9	60 → 69	40 → 31	Linear gradient	
	37–42	0.5	69	31	Equilibration	
Resolution solution	0.1 mg/ml moxifloxacin HCl and 0.001 mg/ml impurity A in buffer solution					1 µg/ml each of moxifloxacin HCl and impurity A in MeOH
Reference solution	0.1 mg/ml moxifloxacin HCl in buffer solution					0.1 mg/ml moxifloxacin HCl in MeOH
Test solution	0.1 mg/ml moxifloxacin in buffer solution, prepare from test solution obtained from organic impurities test					0.1 mg/ml moxifloxacin in MeOH, prepare from test solution obtained from organic impurities test

Column	Packing L11 (5 µm, 250 × 4.0 mm)	Packing L11 (5 µm, 150 × 4.6 mm)
Temperature (°C)	45	Column oven: 40 °C, autosampler: 5 °C
Detection (nm)	UV: 293	UV: 293 [to confirm the absence of co-eluting known and unknown impurity peaks, substitute the detector from the test for organic impurities].
Injection volume (µl)	25	10
System suitability	Resolution: $\geq 2.0$ between moxifloxacin and impurity A, use resolution solution Column efficiency: 4000 theoretical plates Tailing factor: $\leq 2.0$ Relative standard deviation: $\leq 2.0\%$ , use reference solution	Resolution: $\geq 1.5$ between moxifloxacin and impurity A, use resolution solution Relative standard deviation: $\leq 1.0\%$ , use reference solution
Limits	90.0–110.0% (as moxifloxacin)	95.0–105.0% (as moxifloxacin)
Storage	Preserve in tight containers. Store between 2 and 25 °C	–

<sup>a</sup>Disregard this peak because this is a process impurity controlled for the drug substance.

<sup>b</sup>disregard this peak because it is quantitated using Test 2.

TBA, tetrabutylammonium; DEA, diethylamine; TFA, trifluoroacetic acid; F, correction factor; rRT, relative retention time.

**Table 7.17** The summary of the compendial methods of moxifloxacin injection  
**Test** **USP-MC**

Definition	Moxifloxacin injection contains an amount of moxifloxacin HCl equivalent to NLT 95.0% and NMT 105.0% of the labeled amount of moxifloxacin ( $C_{21}H_{24}FN_3O_4$ ).
Identification	The response of moxifloxacin from the sample solution corresponds to that of the standard solution, as obtained in the assay
Uniformity of dosage units	Meets the requirements [ $<905>$ ]
Bacterial endotoxins	Proceed as directed in the chapter [ $<85>$ ]
Sterility	Proceed as directed in the chapter [ $<71>$ ]
Organic impurities (protect solutions from light)	[ $<621>$ ]
Mobile phase (v/v)	MeOH: A solution A: 0.1% DEA in $H_2O$ , pH of 2.3 with TFA (40:60).
Resolution solution	1 $\mu\text{g/ml}$ each of moxifloxacin HCl and impurity A in MeOH
Reference solution	1 $\mu\text{g/ml}$ each of moxifloxacin HCl, impurity A, impurity B, impurity C, impurity D, and impurity E in MeOH
Sensitivity solution	—
Test solution	A volume of injection equivalent to 1 mg/ml moxifloxacin in MeOH
Column	Packing L11 (5 $\mu\text{m}$ , $150 \times 4.6$ mm)
Detection	200–700 nm [calculations should be made at an isobestic point of moxifloxacin and impurity spectra or at 293 nm if an isobestic point is not available]. MS source: ES scan (+ and –), source temperature: 90 °C, desolvation temperature: 400 °C
Temperature (°C)	Column oven: 40, autosampler: 5
flow rate (ml/min)	1.0
System suitability	Resolution: $\geq 1.5$ between moxifloxacin and impurity A, use resolution solution Relative standard deviation: $\leq 1.0\%$ , use reference solution



**Table 7.17** The summary of the compendial methods of moxifloxacin injection—cont'd

Test	USP-MC
Injection volume (μl)	10
System suitability	Resolution: $\geq 1.5$ between moxifloxacin and impurity A, use resolution solution Relative standard deviation: $\leq 1.0\%$ , use reference solution
Limits	95.0–105.0% (as moxifloxacin)

DEA, diethylamine; TFA, trifluoroacetic acid.

**Table 7.18** The summary of the compendial methods of moxifloxacin tablets (Reference Procedures)

Test	USP-MC
Definition	Moxifloxacin tablets contain an amount of moxifloxacin HCl equivalent to NLT 95.0% and NMT 105.0% of the labeled amount of moxifloxacin ( $C_{21}H_{24}FN_3O_4$ ).
Identification	The response of moxifloxacin from the sample solution corresponds to that of the standard solution, as obtained in the assay
Uniformity of dosage units	Meets the requirements [ $<905>$ ]
Water	$\leq 6.0\%$ [ $<921>$ , method I]
Organic impurities (protect solution from light)	[ $<621>$ ]
Mobile phase (v/v)	MeOH: A solution A: 0.1% DEA in $H_2O$ , pH of 2.3 with TFA (40:60).
Resolution solution	1 μg/ml each of moxifloxacin HCl and impurity A in MeOH
Reference solution	1 μg/ml each of moxifloxacin HCl, impurity A, impurity B, impurity C, impurity D, and impurity E in MeOH
Sensitivity solution	—
Test solution	A portion of powdered tablets equivalent to 1 mg/ml moxifloxacin in MeOH. Sonicate for 15 min, cool, and filter
Column	Packing L11 (5 μm, 150 × 4.6 mm)
Detection	200–700 nm (calculations should be made at an isobestic point of moxifloxacin and impurity spectra or at 293 nm if an isobestic point is not available) MS source: ES scan (+ and –), source temperature: 90 °C, desolvation temperature: 400 °C



**Table 7.18** The summary of the compendial methods of moxifloxacin tablets (Reference Procedures)—cont'd

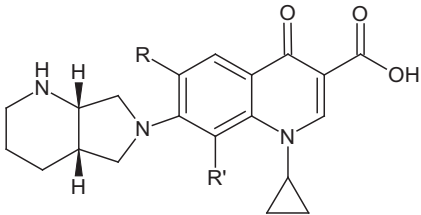
Test	USP-MC
Temperature (°C)	Column oven: 40 °C, autosampler: 5 °C
Flow rate (ml/min)	1.0
Detection (nm)	UV: 293 [to confirm the absence of co-eluting known and unknown impurity peaks, substitute the detector from the test for Organic Impurities].
Injection volume (μl)	10
System suitability	Resolution: $\geq 1.5$ between moxifloxacin and impurity A, use resolution solution Relative standard deviation: $\leq 1.0\%$ , use reference solution
Limits	95.0–105.0% (as moxifloxacin)
Dissolution [ $<711>$ ]	See USP-MC general chapter [Assessing Drug Product Performance Quality $<12>$ ]

DEA, diethylamine; TFA, trifluoroacetic acid.

**Table 7.19** The summary of the compendial methods of moxifloxacin tablets (Acceptable Procedures)

Test	USP-MC
Organic impurities (protect solutions from light) [ $<621>$ ]	
Diluent	0.5 g/l of TBAHSO <sub>4</sub> and 1.0 g/l KH <sub>2</sub> PO <sub>4</sub> in 0.3 M H <sub>3</sub> PO <sub>4</sub>
Mobile phase (v/v)	MeOH: A solution containing 0.5 g/l TBAHSO <sub>4</sub> , 1.0 g/l KH <sub>2</sub> PO <sub>4</sub> and 3.4 g/l H <sub>3</sub> PO <sub>4</sub> (7:18)
Resolution solution	1 μg/ml each of moxifloxacin HCl and impurity A in diluent
Reference solution	2.2 μg/ml moxifloxacin HCl in diluent
Test solution	A portion of powdered tablets equivalent to 1 mg/ml moxifloxacin in diluent. Sonicate for 15 min, cool, and filter
Column	Packing L11 (5 μm, 250 × 4.6 mm)
Detection	UV: 293 nm
Temperature (°C)	45

**Table 7.19** The summary of the compendial methods of moxifloxacin tablets (Acceptable Procedures)—cont'd

Test	USP-MC		
flow rate (ml/min)	1.5		
Injection volume (μl)	10		
Run time (min)	2 × the retention time of moxifloxacin		
System suitability	Resolution: ≥ 1.2 between moxifloxacin and impurity A, use resolution solution Tailing factor: ≤ 2.0, use reference solution Relative standard deviation: ≤ 5.0%, use reference solution		
Identification of impurities	<i>Compound name</i>	<i>rRT</i>	<i>F</i>
	Moxifloxacin	1.0	—
	impurity A	1.1	1.0
	Impurity B	1.4	0.71
	Impurity C	1.5	1.0
	Impurity D	1.5	1.0
	Impurity E	1.8	0.29
Limits	Any individual impurity: ≤ 0.2%		
List of impurities	<p>Specified impurities: A, B, C, D, E. Impurity A (6,8-difluoro): R = R' = F Impurity B (6,8-dimethoxy): R = R' = OCH<sub>3</sub> Impurity C (8-ethoxy): R = F, R' = OC<sub>2</sub>H<sub>5</sub> Impurity D (6-methoxy-8-fluoro): R = OCH<sub>3</sub>, R' = F Impurity E (8-hydroxy): R = F, R' = OH</p> 		
Assay (protect solutions from light) [ $<621>$ ]			
Diluent	0.5 g/l of TBAHSO <sub>4</sub> and 1.0 g/l KH <sub>2</sub> PO <sub>4</sub> in 0.3 M H <sub>3</sub> PO <sub>4</sub>		

Continued



**Table 7.19** The summary of the compendial methods of moxifloxacin tablets (Acceptable Procedures)—cont'd

Test	USP-MC
Mobile phase (v/v)	MeOH: A solution containing 0.5 g/l TBAHSO <sub>4</sub> , 1.0 g/l KH <sub>2</sub> PO <sub>4</sub> and 3.4 g/l H <sub>3</sub> PO <sub>4</sub> (7:18)
Reference solution	0.1 mg/ml moxifloxacin HCl in diluent
Test solution	0.1 mg/ml in diluent, prepare from the test solution obtained from organic impurities test
Column	Packing L11 (5 µm, 250 × 4.6 mm)
Detection	UV: 293 nm
Temperature (°C)	45
flow rate (ml/min)	1.3
Injection volume (µl)	10
Run time (min)	1.5 × the retention time of moxifloxacin
System suitability	Tailing factor: ≤ 2.0, use reference solution Relative standard deviation: ≤ 2.0%, use reference solution
Limits	95.0–105.0% (as moxifloxacin)
Dissolution <711>	
Medium	0.1 N HCl; 900 ml Time: 45 min.
Dissolution apparatus	2, 50 rpm
Reference stock solution	0.5 mg/ml of moxifloxacin HCl in MeOH
Reference solution	Dilute the standard stock solution with medium to obtain a final concentration of about (L/100,000) mg/ml, where L is the label claim in mg/tablet
Test solution	Pass a portion of the solution through a suitable filter. Dilute with medium, if necessary, to obtain a final concentration similar to that of the standard solution
Analysis	By UV spectroscopy at 293 nm, pathlength: 1 cm, blank: medium
Tolerance	≥ 75% (Q)

#### 4.1.4 Moxifloxacin tablets

Moxifloxacin tablets are listed in the USP-MC [61]. Tables 7.18 and 7.19 demonstrate a summary of its specifications and methods of analysis using the “Reference Procedures” and “Acceptable Procedures”, respectively.

Table 7.19 shows detailed description of procedures that may be used for the evaluation of the material under test. These procedures meet the requirements of the “Performance-Based Monograph” mentioned earlier (Section 4.1.1). Validation data were provided to demonstrate the acceptability, and therefore equivalence, of these procedures and the “Reference Procedures”.

Users must demonstrate that the procedure will give acceptable results on their drug substance before using “Acceptable Procedures”. This is carried out by meeting the requirements of the criteria-based procedures presented in the “Performance-Based Monograph” (Section 4.1.1).

### 4.2. Titrimetric methods

#### 4.2.1 Aqueous titration

About 400 mg of moxifloxacin HCl, accurately weighed, are dissolved in 50 ml of water. The sample is potentiometrically titrated with 0.1 N NaOH VS. Each ml of 0.1 N NaOH is equivalent to 40.14 mg of  $C_{21}H_{24}FN_3O_4$  [30].

#### 4.2.2 Nonaqueous titration

About 400 mg of moxifloxacin HCl, accurately weighed, are dissolved in 50 ml of anhydrous glacial acetic acid. 10 ml of 6% mercuric acetate solution (in acetic acid) is added. The sample is potentiometrically titrated with 0.1 N perchloric acid VS. Each ml of 0.1 N perchloric acid is equivalent to 40.14 mg of  $C_{21}H_{24}FN_3O_4$  [30].

### 4.3. Electrochemical methods

#### 4.3.1 Voltammetry

Cyclic voltammetry study was carried out using a glassy carbon electrode to understand the electrochemical behavior of moxifloxacin [62]. Britton–Robinson buffer (acetic acid–boric acid–phosphoric acid), acetate buffer, and phosphate buffer were tested as supporting electrolytes. Britton–Robinson buffer gave well-defined voltammogram with high sensitivity. The highest peak current was obtained with 0.04 M Britton–Robinson buffer at pH 6.0. Using such method, moxifloxacin was tested by differential pulse voltammetry, Osteryoung square-wave voltammetry, and high-performance liquid chromatography. The proposed methods were found to be of high precision and accuracy, showing recoveries in the range of

97.5–101.3% (RSDs: 0.64–1.03%) and 97.5–100.3% (RSDs: 0.62–0.87%) for spiked human plasma and tablets analysis, respectively.

Interaction of moxifloxacin with Cu (II) ion was studied using a hanging mercury drop electrode [63]. A well-defined reduction peak at  $-0.21$  V versus Ag/AgCl in  $0.04$  M phosphate buffer at pH 8.0 was observed for the complex moxifloxacin–Cu (II) using square-wave voltammetry. The proposed method showed good sensitivity with detection and quantitation limits of  $3.60 \times 10^{-8}$  M and  $1.20 \times 10^{-7}$  M, respectively. The assay result of Avelox<sup>®</sup> tablets (102.08%) with RSD of 1.00% ( $n=5$ ) proves the accuracy and precision of the proposed method.

Adsorptive voltammetric behavior of moxifloxacin was investigated [64]. In a supporting electrolyte of  $0.25$  M phosphate buffer at pH 6.38, a reduction peak of moxifloxacin with a potential of  $-1.24$  V versus Ag/AgCl. Adsorptive characteristics are observed by linear sweep voltammetry at mercury electrode. The adsorbed species are most probably the neutral molecules of moxifloxacin. The saturated adsorption amount of  $4.31 \times 10^{-11}$  mol cm<sup>-2</sup> and an area occupied by each molecule of  $2.12$  nm<sup>2</sup> at mercury electrode for moxifloxacin are obtained. On the surface of the hanging mercury drop electrode, the adsorption obeys Langmuir adsorption isotherm. Base upon this investigation, a method for the assay of moxifloxacin is proposed by adsorptive stripping voltammetry. The detection limit of the method is  $2.0 \times 10^{-8}$  M under the optimized conditions.

A highly sensitive electroanalytical method for the determination of moxifloxacin HCl using differential pulse voltammetry was further investigated [65]. The electrochemical behavior of moxifloxacin HCl was investigated in Britton–Robinson buffer at the pH range of 2.0–11.0 using chloranil modified carbon paste electrode. The anodic peak currents increased linearly with concentration in the range of  $4.0 \times 10^{-7}$  to  $3.6 \times 10^{-6}$  M. Limits of detection and quantification were  $6.74 \times 10^{-8}$  and  $2.25 \times 10^{-7}$  M, respectively. The relative standard deviation was found to lie in the following range: 0.57–0.97%. Moreover, the percentage recovery was found to lie in the following range: 99.28–100.60%. The method was successfully applied to the determination of moxifloxacin HCl in tablets without previous separation.

#### 4.3.2 Polarography

Differential pulse polarographic (DPP) method for moxifloxacin HCl determination was developed and validated [66]. This method was applied for the determination of trace amounts of moxifloxacin in pharmaceuticals, serum, and urine. Moxifloxacin showed a well-defined irreversible cathodic peak at

−1.61 V versus a saturated calomel electrode in Britton–Robinson buffer (pH 10). In this method, the current was characterized as being diffusion-controlled process whereby the diffusion current constant was  $1.48 \pm 0.12$  and the current versus concentration plot was rectilinear over the range from  $5 \times 10^{-7}$  to  $1 \times 10^{-4}$  M ( $r = 0.995$ ,  $n = 10$ ).

Polarographic reduction of Co (II) in the presence of moxifloxacin using DDP was also studied [67]. The investigation revealed the presence of an additional adsorption peak corresponding to the reduction of Co (II)–moxifloxacin complex on the mercury drop electrode at −1.17 V. The new peak is applicable to Co (II) determination with linearity proportional to the Co (II) concentration in the range of  $4.93 \times 10^{-7}$ – $6.90 \times 10^{-5}$  M attributed to adsorption-controlled process with an irreversible reduction. Without using moxifloxacin, the polarographic determination of  $2.50 \times 10^{-6}$  M Co (II) is impossible under the aforementioned conditions due to the very poor sensitivity at −1.38 V. The proposed method showed good precision and accuracy with a relative standard deviation of 3.01% and a relative error of 6.40% for the determination of  $2.50 \times 10^{-6}$  M Co (II) in the presence of  $5.0 \times 10^{-6}$  M of Zn (II), Ni (II), and Cd (II). The accuracy of the method was also checked by the determination of Co(II) spiked to tap water and certified sea water, the percentage recoveries were 97.5% and 96.7%, respectively ( $n = 4$  at 95% confidence interval).

Electrochemical behavior of moxifloxacin HCl was studied in aqueous medium using direct current polarography and cyclic voltammetry [68]. In this method, moxifloxacin exhibits single well-defined cathodic peak in all buffers; for example, acetate buffer, phosphate buffer, and Britton–Robinson buffer. The characteristics of the resulted peak were examined at different concentrations, pH, and scan rates. This behavior is suggested to be attributed to the reduction of the C=O double bond of the reactant species in acidic and basic media. The experimental result shows that the reduction is irreversible and diffusion controlled.

## 4.4. Spectroscopic methods

### 4.4.1 Spectrophotometry

Direct measurements of moxifloxacin as a bulk material and in its different pharmaceutical formulations by UV/visible spectrophotometric methods were reported (Table 7.20). The determination is based on the use of different absorption modes including zero, first- and second-derivatives methods, and of aqueous media of different pHs in most studies.

It was reported that the presence of Al (III) can enhance the appearance of UV characteristic of moxifloxacin [86]. The reaction conditions of

**Table 7.20** The UV/visible parameters of the methods used for the determination of moxifloxacin

Material	Mode	$\lambda$ (nm)	Solvent	Reference
Tablets and bulk material in the presence of its acid degrades (decarboxylated)	First derivative	280.4 303.4	0.3 N HCl	[69]
Human plasma	Second derivative Peak to peak amplitude in a wavelength range 335–345	Peak to peak amplitude in a $\lambda$ range 335–345	Citrate-PO <sub>4</sub> buffer (pH 7.2) and SDS (12.0 mN)	[70]
Bulk material, tablets, i.v. infusions, eye drops, and polymeric nanoparticles	Zero order	296 289	0.1 N HCl PO <sub>4</sub> buffer (pH 7.4)	[71]
Tablets	Zero order	296	0.1 N HCl	[72]
Bulk material and tablets	Zero order	295	0.1 N HCl	[73]
Tablets	Zero order	295	H <sub>2</sub> O	[74]
Bulk material and tablets	Zero order	294.4	0.01 N HCl	[75]
Bulk material and ophthalmic solution	AUC zero order AUC first derivative	279.0–296.4 289.4–305.6	H <sub>2</sub> O	[76]
Bulk material, tablets, and eye drops	Zero order First derivative First derivative	293 282 (max.) 302 (min.)	H <sub>2</sub> O	[77]
Tablets (combination with cefixime)	Zero order (simultaneous equation) Zero order (ratio-Q analysis)	286 and 295 279 and 295	0.1 N HCl	[78]
Eye drops (combination with bromefenac Na)	Zero order (simultaneous equation)	265 and 294 276.66 and 301.71	Methanolic 0.1 N HCl	[79]

**Table 7.20** The UV/visible parameters of the methods used for the determination of moxifloxacin—cont'd

Material	Mode	$\lambda$ (nm)	Solvent	Reference
	Zero order (ratio-Q analysis) First derivative	293.22 and 301.71		
Eye drops (combination with bromefenac Na)	Zero order (simultaneous equation)	268 and 289	H <sub>2</sub> O	[80]
Pharmaceutical formulations	First derivative First derivative	283 (max.) 304 (min.)	H <sub>3</sub> PO <sub>4</sub>	[81]
Ophthalmic solution (combination with dexamethasone Na PO <sub>4</sub> )	First derivative Second derivative	243.30 and 261.90 266 and 241	H <sub>2</sub> O	[82]
Eye drops (combination with prednisolone acetate)	First derivative (ratio-Q analysis)	247 and 288	H <sub>2</sub> O/MeOH	[83]
Tablets (combination with cefixime)	Zero order First derivative (ratio-Q analysis)	287.0 and 317.9 269.6 and 359.3	H <sub>2</sub> O	[84]
Tablets (combination with cefixime)	Zero order (ratio-Q analysis)	275 and 295	0.1 N HCl	[85]

AUC, area under curve; SDS, sodium dodecyl sulfate.

Al (III)-moxifloxacin system were investigated in detail. The linear range was 1.82–15.68  $\mu\text{g/ml}$  and the regression equation was  $A = 0.02573 + 0.1060C$  ( $\mu\text{g/ml}$ ) ( $r = 0.9991$ ). The average recovery of moxifloxacin was 97.70% with RSD of 2.68%. The proposed method is simple, accurate, rapid, and can be used to determine moxifloxacin in tablet.

Moreover the effect of different surfactants on the UV intensity of Al (III)-moxifloxacin system was studied. It was found that Cetyltrimethylammonium bromide can increase the UV intensity of the system. The proposed method is simple, rapid, and sensitive in the determination of moxifloxacin in tablets [87].

#### 4.4.2 Colorimetry

Three different methods (A–C) were used for the determination of moxifloxacin in tablets based upon the formation of its complexes with alkaloidal

precipitants [88]. Aqueous iodine, ammonium molybdate, or phosphomolybdic acid were used as precipitants in methods A, B, and C, respectively. Then color was developed with either unreacted precipitant of the filtrate (in  $I_2$ ) or released precipitant from the molecular complex (in ammonium molybdate or phosphomolybdic acid) with chromogenic reagent such as *p*-*N*-methyl amino phenol sulfate-sulphanilic acid (for  $I_2$ ), potassium thiocyanate (for ammonium molybdate), cobalt nitrate-disodium salt of ethylene diamine tetra acetic acid complex (for phosphomolybdic acid). The  $\lambda_{\max}$  for methods A, B, and C were 520, 480, and 840 nm, respectively.

The accurate, rapid, and simple colorimetric method was developed for the determination of moxifloxacin and other fluoroquinolones in tablets [89]. The proposed methods depend upon the reaction of ammonium reineckate (ammonium tetrathiocyanotodiamminochromate (III) monohydrate) with the drug to form stable precipitate of ion-pair complexes, which was dissolved in acetone. The pink colored complex was determined calorimetrically at  $\lambda_{\max}$  of 525 nm.

A simple and sensitive visible spectrophotometric method based upon the formation of yellow colored complex of moxifloxacin with sodium nitroprusside and hydroxylamine hydrochloride in alkaline medium was reported [90]. The quantitative measurements were made at  $\lambda_{\max} = 361$  nm. Such method was adopted successfully to determine moxifloxacin in tablets.

Two simple spectrophotometric methods were developed and validated for the determination of moxifloxacin HCl in pure form and in tablets [91]. Method A is a kinetic method based upon the oxidation of moxifloxacin HCl by Fe (III) ions in the presence of 1,10 *o*-phenanthroline, while method B is based on the ability of moxifloxacin to reduce Fe (III) to Fe (II), which is rapidly converted to the corresponding stable colored complex when reacted with 2,2' bipyridyl. The absorbance of the tris complex formed in both methods A and B was measured at  $\lambda_{\max}$  of 510 and 520 nm, respectively.

The reaction between moxifloxacin HCl and Fe (III) in slightly acidic medium was used to determine moxifloxacin HCl as a bulk material or in blood samples. The reaction gives brown color complex with  $\lambda_{\max}$  of 407 nm [92].

#### 4.4.3 Fluorimetry

Determination of moxifloxacin by fluorimetric technique was reported by different workers (Table 7.21). The methods were based on the use of fluorescence enhancer (e.g., sodium dodecyl sulfate), Eu (III) with sodium dodecyl benzene sulfonate as enhancer or derivative formation with 4-chloro-7-nitrobenzofurazan. The extent of the linear range and detection

**Table 7.21** The fluorimetric parameters of the method used for the determination of moxifloxacin

Material	Fluorescence agent	Solvent	$\lambda_{\text{exc}}$ (nm)	$\lambda_{\text{em}}$ (nm)	Range (ng/ml)	DL (ng/ml)	Reference
Tablets	None	PO <sub>4</sub> buffer (pH 8.3)	287	465	30–300	10	[93]
Human serum and urine	SDS enhancer	AC buffer (pH 4.0)	294	503	30–300	15	
Tablets	NBD-Cl	EAC	464	537	33.5–1000	10	[94]
Tablets, i.v. infusions, eye drops, human urine, and plasma	SDS enhancer	H <sub>2</sub> O	294	494	1–320	0.5	[95]
Tablets, human serum and urine	Eu (III) with SDBS	Tri-HCl buffer (pH 9.2)	373	614	0.02–7.3	0.003	[96]

DL, detection limit; SDS, sodium dodecyl sulfate; NBD-Cl, 4-chloro-7-nitrobenzofurazan; SDBS, sodium dodecyl benzene sulfonate; AC, acetate; EAC, ethylacetate.

limit depends upon the fluorescence probe formed, pH of solution, and solvent type. The use of Eu (III) with sodium dodecyl benzene sulfonate as fluorescence enhancer gave the highest sensitivity in comparison with the other methods (Table 7.21).

It was found that the presence of Y (III) enhances intensity of fluorescence of moxifloxacin [97]. As a result, a novel method for the determination of moxifloxacin in urine was developed. The linearity range and detection limit were reported to lie within 4.0–400 and 0.34 ng/ml, respectively.

In a Britton–Robinson buffer medium of pH 6.50, an indirect method for the determination of moxifloxacin in tablets by the fluorescence quenching of rhodamine B-acridine system in the presence of sodium dodecyl sulfate was proposed [98]. The method was found to be linear in the range of 1.00–10.0 µg/ml with a detection limit of 0.039 µg/ml. Furthermore, it was found that the effective energy transfer could occur between congo red and calcein in the Britton–Robinson buffer (pH 6), which quenched the fluorescence of calcein. The fluorescence of calcein



reappeared with the addition of moxifloxacin. Therefore, a novel fluorescence method was developed for indirect determination of moxifloxacin in tablets and urine [99].

#### **4.4.4 Chemiluminometry**

Determination of moxifloxacin in tablets by a flow injection method including chemiluminescence detection was reported [100]. The proposed method is based on the luminescent properties of the system Ce (IV)–sulphite–moxifloxacin and the addition of Eu (III), a trivalent lanthanide ion, as emission sensitizer. The effect of acidity of Eu (III) and Ce (IV) solutions, concentration of Ce (IV) and sulfate, and the flow rate on the chemiluminescence emission were considered to attain the optimal experiment variables. The linearity range and detection limit are 0.2–2.0 and 0.035 µg/ml, respectively.

A batch type chemiluminescence method was used to determine moxifloxacin [101]. The method is based on the enhancement of chemiluminescence emission of tris(2,2-bipyridyl) Ru (II)–Ce(IV) system. Under the optimum experimental conditions, the linear range and detection limit are 0.4–40.0 and 0.12 µg/ml, respectively. The same tris(2,2-bipyridyl) ruthenium(II)–Ce(IV) system was studied by flow injection method [102]. The concentration of moxifloxacin was held in the range of 0.04–40.0 µg/ml with a detection limit of 0.012 µg/ml. The influence of potential interfering substances was also studied. The proposed method was successfully applied for the determination of moxifloxacin in pharmaceutical preparations.

#### **4.4.5 Atomic absorption spectroscopy**

Direct and indirect atomic absorption spectroscopic methods for the determination of moxifloxacin as a bulk material and in its tablets were reported [91]. The method is based on the formation of ion–pair associated between moxifloxacin and Bi (III) tetraiodide in acidic medium to form orange–red ion–pair associate. This associate can be quantitatively determined by two different procedures. The formed precipitate is either filtered off and the residual unreacted metal complex in the filtrate is determined through its Bi content using indirect atomic absorption spectrometric method, or the decomposed by HCl, and the Bi content is determined by direct atomic absorption spectrometric. The proposed indirect and direct methods are linear in the range of 16–72 and 16–96 µg/ml, respectively with a limit of detection of 1.4 µg/ml. The proposed methods were successfully

applied to determine the drug in its pharmaceutical formulations without interference from the common excipients.

## 4.5. Chromatographic methods

### 4.5.1 High performance thin layer chromatography

Different HPTLC methods were reported for the determination of moxifloxacin as a bulk material in the presence of its degradates and in different dosage forms (Table 7.22). The detection of moxifloxacin was estimated at the wavelength range of 260–298 nm by densitometry using silica gel G60F254 as a stationary phase and using different basic mixtures as mobile phases.

**Table 7.22** The HPTLC parameters of the method used for the determination of moxifloxacin

Material	Mobile phase (v/v)	$\lambda$ (nm)	Linearity range ( $\mu\text{g}/\text{spot}$ )	DL ( $\mu\text{g}/\text{spot}$ )	Reference
Tablets and bulk material in the presence of its acid degradates (decarboxylated)	0.3 M $\text{NH}_4\text{AC}$ :25% $\text{NH}_3$ : <i>n</i> -PrOH (1:1:8)	290	0.1–1.4	–	[69]
Tablets	<i>n</i> -BuOH:MeOH: $\text{NH}_3$ (4:4:2)	295	0.400–1.0	0.01	[103]
Polymeric nanoparticles and bulk material in the presence of its degradates	<i>n</i> -PrOH: EtOH:6 M $\text{NH}_3$ (4:1:2)	298	0.1–0.8	0.004	[104]
Tablets	MC:MeOH: 25% $\text{NH}_3$ :ACN (10:10:5:10)	292	0.009–0.054	–	[105]
Tablets and bulk material in the presence of its acid degradates	MC:EtOH: toluene: <i>n</i> -BuOH: 25% $\text{NH}_3$ : $\text{H}_2\text{O}$ (6:6:2:3:1.8:0.3)	294	0.06–1.5	0.012	[106]
Eye drops with bromfenac sodium	MC:ACN: MeOH: $\text{NH}_3$ (2.5:2.5:2.0:1.0)	260	0.6–4.2	–	[107]

Stationary phase used: Precoated silica gel G60F254. DL, detection limit; AC, acetate; MC, methylene chloride; ACN, acetonitrile.

#### 4.5.2 High performance liquid chromatography

Various HPLC methods were reported for the determination of moxifloxacin as a bulk material, in pharmaceutical formulations and in biological fluids. HPLC systems with ultraviolet, fluorimetric, or mass spectrometric detection were applied for the determination of moxifloxacin. These HPLC methods with their full parameters and applications are listed in Table 7.23.

Different fluoroquinolones (ciprofloxacin, enoxacin, gatifloxacin, levofloxacin, lomefloxacin, moxifloxacin, norfloxacin, pazufloxacin, and tosufoxacina) were determined by HPLC/fluorescent detection. The method was claimed to be useful for PK/PD analysis [157].

The effect of different parameters (methanol content in mobile phase, pH and buffer concentration, column types) on the chromatographic behavior of levofloxacin, ciprofloxacin and moxifloxacin was investigated [158]. As a result, a simple and rapid HPLC method/UV detection at 293 nm was developed for the separation of the three drugs. BDS Hypersil<sup>®</sup> C<sub>18</sub> (100 × 4.6 mm, 2.4 μm) column was used with an isocratic mobile phase consisting of MeOH/0.025 M phosphate buffer 28/72 (v/v) at pH 3 and flow rate 1 ml min<sup>-1</sup>.

An HPLC method with UV detection at 290 nm was developed to determine moxifloxacin in human's serum, urine, and displacement liquid with pulse high volume hemofiltration (PHVHF) [159]. Yilite Hypersil ODS-BP column (5 μm, 150 × 4.6 mm) was used with a flow rate of 1.0 ml/min. The method is linear in the range of 0.1–10.0 μg/ml with recovery values of 98.7–101.0% (serum), 85.7–95.7% (displacement liquid), and 97.4–101.7% (urine).

Photostability of moxifloxacin was monitored after UV-A irradiation in solution and solid phase without and with presence of Cu (II), Zn (II), Al (III), and Fe (III) by TLC-densitometric and LC-MS/MS methods [160].

#### 4.5.3 Ultra performance liquid chromatography

Recently, a novel approach in chromatographic separation technology was developed and is currently known as the ultra-performance liquid chromatography (UPLC). Columns packed with sub-2 μ particles are used, which enable elution of sample components in much narrower, more concentrated bands, resulting in better chromatographic resolution, increased peak capacity, and reduced chromatographic runs. Different UPLC methods were reported to determine the moxifloxacin in tablets, environmental samples, aquatic products and in pharmacokinetic analysis (Table 7.24).

**Table 7.23** The HPLC parameters of the method used for the determination of moxifloxacin

Material	Stationary phase	Mobile phase (v/v)	Detection	Flow rate (ml/min)	Linearity range (µg/ml)	Reference
Metabolites identification	Kromasil C <sub>18</sub> column (5 µm, 100 × 4.6 mm)	(A) 0.1% HCOOH and (B) ACN (50:50)	MS	0.5	–	[55]
Bulk material, identification of impurities	Zorbax XDB-C <sub>18</sub> (5 µm, 250 × 4.6 mm)	Gradient system: (A) 0.2% HCOOH and (B) MeOH	UV: 293 FTICRMS	1.0	–	[56]
Spiked human plasma and tablets	Supelcosil C <sub>18</sub> (5 µm, 150 × 4.6 mm)	EtOH:ACN (50:50)	UV: 270	1.0	1.6–20.0	[62]
Moxifloxacin in the presence of its acid degrades (separation)	Waters XBridge C <sub>18</sub>	Gradient system: (A) ACN-0.01% HCOOH and (B) H <sub>2</sub> O-0.01% HCOOH	MS	0.06	–	[106]
Eye drops with bromfenac sodium	ACE C <sub>18</sub> (5 µm, 150 × 4.6 mm)	0.01 M PO <sub>4</sub> buffer, pH 7.0: ACN (72:28)	UV: 265	1.0	10.0–100.0	[107]
Human plasma, saliva, and urine	Nucleosil 100 C <sub>18</sub> (5 µm, 250 × 4.6 mm)	Gradient system: (A) 0.01 M TBASO <sub>4</sub> and 0.05 M NaH <sub>2</sub> PO <sub>4</sub> , pH 3.0 and (B) ACN	Fluorescence: $\lambda_{\text{ex}} = 296$ , $\lambda_{\text{em}} = 504$	1.1	0.0025–1.0 (urine) 0.005–1.5 (plasma) 0.01–1.0 (saliva)	[108]
Spiked serum	Spherisorb S5 C <sub>8</sub> (5 µm, 100 × 4.6 mm)	0.16% H <sub>3</sub> PO <sub>4</sub> , pH 3 by TBAOH:ACN (95:5)	Fluorescence: $\lambda_{\text{ex}} = 290$ , $\lambda_{\text{em}} = 500$	1.5	0.5–4.0	[109]

*Continued*

**Table 7.23** The HPLC parameters of the method used for the determination of moxifloxacin—cont'd

Material	Stationary phase	Mobile phase (v/v)	Detection	Flow rate (ml/min)	Linearity range (µg/ml)	Reference
Human plasma	Nucleosil 100 C <sub>18</sub> (5 µm, 250 × 4.6 mm)	Gradient system: (A) 0.01 M TBAHSO <sub>4</sub> , pH 2.0 and (B) CAN	Fluorescence: $\lambda_{\text{ex}} = 296$ , $\lambda_{\text{em}} = 504$	—	0.0025–5.0	<a href="#">[110]</a>
	Purospher C <sub>18</sub> e (5 µm, 125 × 4 mm)	Gradient system: (A) 0.01 M NH <sub>4</sub> AC, pH 2.0 and (B) CAN	MS	—		
Human and other mammalian species	Nucleosil C <sub>18</sub> (5 µm, 250 × 4.6 mm)	Gradient system: (A) 1% TBAHSO <sub>4</sub> and (B) ACN	Fluorescence: $\lambda_{\text{ex}} = 296$ , $\lambda_{\text{em}} = 504$	1.0	0.005–1.0	<a href="#">[111]</a>
Plasma and lung tissue	Supelcosil ABZ + Plus (5 µm, 15 × 4.6 mm)	ACN: 0.01 M KH <sub>2</sub> PO <sub>4</sub> buffer (18:82), pH 4 by H <sub>3</sub> PO <sub>4</sub>	UV: 296	1.25	0.025–3.2 (plasma) 0.25–16.0 (lung tissue)	<a href="#">[112]</a>
Mueller-Hinton Broth growth media	Supelcosil ABZ + Plus (5 µm, 150 × 4.6 mm)	Switching system: (A) 0.01 M K <sub>2</sub> HPO <sub>4</sub> , pH 5.4 with H <sub>3</sub> PO <sub>4</sub> : MeOH (97:3) and (B) 0.01 M KH <sub>2</sub> PO <sub>4</sub> , pH 2.5 by H <sub>3</sub> PO <sub>4</sub> containing 0.02 M TBABr:ACN (85:15)	Fluorescence: $\lambda_{\text{ex}} = 296$ , $\lambda_{\text{em}} = 550$	1.0 (A) 1.25 (B)	0.05–3.2	<a href="#">[113]</a>

Human plasma	BDS Hypersil C <sub>18</sub> (5 mm, 100 × 4.6 mm)	0.15 HCOOH:ACN (60:40)	MS	1.0	0.001–1.0	[114]
Pharmaceutical preparations	Inertsil C <sub>18</sub> -2 (5 µm, 250 × 4.6 mm)	1% TEA, pH 4.5 by H <sub>3</sub> PO <sub>4</sub> :ACN (84:16)	UV: 296	1.0	0.4–3.0	[115]
Human plasma with levofloxacin and gatifloxacin	Supelcosil ABZ + Plus (5 µm, 150 × 4.6 mm)	Switching system: (A) 0.01 M K <sub>2</sub> HPO <sub>4</sub> , pH 5.4 by H <sub>3</sub> PO <sub>4</sub> :ACN (98:2) and (B) 0.01 M KH <sub>2</sub> PO <sub>4</sub> , pH 2.5 containing 0.002 M TBABr:ACN (88:12)	Fluorescence: $\lambda_{\text{ex}} = 296$ , $\lambda_{\text{em}} = 504$	1.0 (A) 1.2 (B)	0.125–4.0	[116]
5%LHB CAMHB (cation- adjusted Mueller-Hinton Broth with 5% lysed horse blood)	Alltech Nucleosil 100 C <sub>18</sub>	PO <sub>4</sub> buffer (TEA: H <sub>3</sub> PO <sub>4</sub> :H <sub>2</sub> O) (0.37:0.30:99.3): MeOH:ACN (66.8:15.1:18.1)	Fluorescence: $\lambda_{\text{ex}} = 295$ , $\lambda_{\text{em}} = 418$	1.3	1.0–50.0	[117]
Impurities of moxifloxacin (identification)	ACE 5 C <sub>18</sub> (5 µm, 250 × 4.0 mm)	Gradient system: (A) H <sub>3</sub> PO <sub>4</sub> :TFA:H <sub>2</sub> O (10:1:989), pH 2.2 by TEA:MeOH (85:15) and (B) MeOH:H <sub>2</sub> O (80:20)	UV: 295	1.0	–	[118]

*Continued*

**Table 7.23** The HPLC parameters of the method used for the determination of moxifloxacin—cont'd

Material	Stationary phase	Mobile phase (v/v)	Detection	Flow rate (ml/min)	Linearity range (µg/ml)	Reference
Human urine with cefepime, garenoxacin, and levofloxacin	LiChrospher 100 C <sub>18</sub> (5 µm, 250 × 4.0 mm)	Gradient system: (A), ACN and (B) 0.1 M PO <sub>4</sub> buffer, pH 3.0 and (C) 0.01 M <i>n</i> -octylamine, pH 3.0 by H <sub>3</sub> PO <sub>4</sub>	UV: 294	1.0	4.0–80.0	[119]
Tablets	Shim-pack CLC-C <sub>18</sub> (5 µm, 250 × 4.6 mm)	(A) 0.17% H <sub>3</sub> PO <sub>4</sub> with 0.05 M TMAOH and ACN (95:5) and (B) MeOH (55:45), pH 3.0	UV: 294	1.0	12.0–42.0	[120]
Residues in food and other matrices with other fluoroquinolones	YMC-Pack Pro C <sub>18</sub> (3 µm, 250 × 4.6 mm)	Gradient system: (A) 0.05 M HCOOH, (B) MeOH, and (C) H <sub>2</sub> O	Fluorescence: $\lambda_{\text{ex}} = 290$ , $\lambda_{\text{em}} = 500$ MS	0.8 0.2	0.0025–2.0	[121]
Human plasma	Supelco LC-Hisep shielded hydrophobic phase	ACN:0.25 M Na <sub>3</sub> PO <sub>4</sub> (pH 3) (5:95)	Fluorescence: $\lambda_{\text{ex}} = 290$ , $\lambda_{\text{em}} = 500$	1.0	0.003–1.3	[122]
Human plasma with levofloxacin	Nucleosil 100-5C <sub>18</sub> Nautilus (5 µm, 125 × 4 mm)	Gradient system: (A): ACN:0.01 M NaH <sub>2</sub> PO <sub>4</sub> , pH 2.7 (3:97) and (B) ACN:0.01 M NaH <sub>2</sub> PO <sub>4</sub> , pH 2.7 (50:50)	Fluorescence: $\lambda_{\text{ex}} = 295$ , $\lambda_{\text{em}} = 440$	1.5	0.2–7.0	[123]

Human plasma and tonsillar tissue	Nucleosil 100 C <sub>18</sub> (5 μm, 250 × 4.6 mm)	Gradient system: (A) 0.1% TBASO <sub>4</sub> , pH 3.0 and (B) TBASO <sub>4</sub> :ACN (50:50)	Fluorescence: 1.0 λ <sub>ex</sub> = 296, λ <sub>em</sub> = 504	0.005–1.5	[124]	
Human and rabbit aqueous and vitreous humor with ofloxacin	Waters AccQ Tag amino acid analysis (4 μm, 150 × 3.9 mm)	Gradient system: (A) ACN:MeOH:0.05 M TBACl:TFA, pH 3.0 (37.5:12.5:949:1) and (B) ACN: MeOH:0.05 M TBACl: TFA, pH 3.0 (75:25:899:1)	Fluorescence: 1.0 λ <sub>ex</sub> = 290, λ <sub>em</sub> = 500	0.01–100.0	[125]	
Nasal drops with ephedrine HCl	Shim-pack VP-C <sub>18</sub> (5 μm, 150 × 4.6 mm)	PO <sub>4</sub> buffer soln. (0.02 M NaH <sub>2</sub> PO <sub>4</sub> and 0.3% TEA, pH to 3.0 by H <sub>3</sub> PO <sub>4</sub> ):MeOH (60:40)	UV: 214	1.0	0.1–0.8	[126]
Human serum	Gemini C <sub>18</sub>	MeOH:H <sub>2</sub> O:TEA (112.5:208.9:0.06)	UV: 289	1.0	0.3–10.0	[127]
Human plasma, its derivate with 4-chloro-7-nitrobenzodioxazole	Phenomenex C <sub>18</sub> (5 μm, 250 × 4.6 mm)	ACN:0.01 M H <sub>3</sub> PO <sub>4</sub> , pH 2.5 (80:20)	Fluorescence: 1.2 λ <sub>ex</sub> = 464, λ <sub>em</sub> = 537	0.015–2.7	[128]	
Human plasma with gatifloxacin and sparfloxacin	Kromasil C <sub>18</sub>	PO <sub>4</sub> buffer, pH 2.5: ACN (80:20)	–	1.0	1.0–10.0	[129]

*Continued*



**Table 7.23** The HPLC parameters of the method used for the determination of moxifloxacin—cont'd

Material	Stationary phase	Mobile phase (v/v)	Detection	Flow rate (ml/min)	Linearity range (µg/ml)	Reference
Bulk material, Identification of impurities	Shiseido capcell MG C <sub>18</sub> (5 µm, 250 × 4.6 mm) Sumipax C <sub>18</sub> A-212 (5 µm, 150 × 6 mm) Alltech Alltima C <sub>18</sub> (5 µm, 250 × 4.6 mm)	1% TEA, pH 2.5 with H <sub>3</sub> PO <sub>4</sub> :MeOH (70:30) PO <sub>4</sub> buffer (1 g of KH <sub>2</sub> PO <sub>4</sub> and 10 mmol TBASO <sub>4</sub> in 1000 ml of H <sub>2</sub> O, pH 2.5 with H <sub>3</sub> PO <sub>4</sub> ):ACN (85:15) ACN:H <sub>2</sub> O (50:50)	PDA: 200–500 MS	1.0 0.6	–	[130]
Aquatic environment	Nertsil ODS-3VC <sub>18</sub> (5 µm, 250 × 4.6 mm)	Gradient system: (A) 0.1% TFA and (B) ACN	PDA: 280 MS	1.0	0.001–5.0	[131]
Impurities of moxifloxacin in tablets and i.v. infusion and its degrades	Waters XTerra C <sub>18</sub> (5 µm, 50 × 4.6 mm)	2% TEA, pH 6.0 by H <sub>3</sub> PO <sub>4</sub> :ACN (90:10)	UV: 290	1.5	0.2–2.0	[132]
Human plasma with ofloxacin and ciprofloxacin	Waters XBridge C <sub>18</sub> (3.5 µm, 150 × 2.1 mm)	Gradient system: (A) ACN:MeOH:0.025 M TBACl:TFA (75:25:899:1) and (B) same with (150:50:799:1), pH 3.5	Fluorescence: λ <sub>ex</sub> = 290, λ <sub>em</sub> = 500	0.25	0.02–7.5	[133]

Extemporaneously prepared moxifloxacin oral suspension	Spherisorb phenyl (5 $\mu\text{m}$ , 150 $\times$ 4.6 mm)	PO <sub>4</sub> buffer (0.094 M KH <sub>2</sub> PO <sub>4</sub> ):ACN:MeOH (80:15:5) with 3 ml/l TFA	UV: 296	1.0	-	[134]
Human plasma	Cloversil-C <sub>18</sub> (5 $\mu\text{m}$ , 150 $\times$ 3.0 mm)	ACN:0.05% TFA (25:75)	MS	-	0.0005–0.1	[135]
Ear drops with dexamethasone acetate	Shim-pack VP-C <sub>18</sub> (5 $\mu\text{m}$ , 150 $\times$ 4.6 mm)	PO <sub>4</sub> buffer (0.02 M NaH <sub>2</sub> PO <sub>4</sub> and 0.3% TEA):MeOH (40:60), pH 3.0 by H <sub>3</sub> PO <sub>4</sub>	UV: 241	1.0	0.3–2.4	[136]
Human plasma	Lichrospher 100 C <sub>18</sub> e (5 mm, 150 $\times$ 4.6 mm)	0.05 M PO <sub>4</sub> buffer, pH 2.6 with 1 N HCl: ACN (80:20)	Fluorescence: $\lambda_{\text{ex}} = 290$ , $\lambda_{\text{em}} = 460$	1.5	0.125–10.0	[137]
Bulk material, tablets, human serum, and in presence of metals	Merck Purospher Star C <sub>18</sub> (5 $\mu\text{m}$ , 250 $\times$ 4.6 mm) and Supelco Discovery C <sub>18</sub> (5 $\mu\text{m}$ , 250 $\times$ 4.6 mm)	MeOH:ACN:H <sub>2</sub> O (85:5:10), pH 2.75 by H <sub>3</sub> PO <sub>4</sub>	UV: 290	1.0	0.39–25.0	[138]
Human plasma, plasma ultrafiltrate, and cerebrospinal fluid	Thermo Electron HyPurity C <sub>18</sub> (5 $\mu\text{m}$ , 50 $\times$ 2.1 mm)	(A) 1% NH <sub>4</sub> AC, 0.0035% acetic acid, and 0.002% TFA anhydride (B) H <sub>2</sub> O and (C) ACN	MS	0.3	0.05–5.0	[139]

*Continued*

**Table 7.23** The HPLC parameters of the method used for the determination of moxifloxacin—cont'd

Material	Stationary phase	Mobile phase (v/v)	Detection	Flow rate (ml/min)	Linearity range (µg/ml)	Reference
Tablets	Luna C <sub>18</sub> (5 µm, 250 × 4.6 mm)	PO <sub>4</sub> buffer (0.2% H <sub>3</sub> PO <sub>4</sub> , pH 2.5 by TEA):MeOH (55:45)	UV: 293	1.0	20.0–60.0	[140]
Human plasma	Kromasil C <sub>8</sub> (5 µm, 250 × 4.6 mm)	ACN:MeOH:0.02 M KH <sub>2</sub> PO <sub>4</sub> buffer (containing 1% TEA, pH 3.0 with H <sub>3</sub> PO <sub>4</sub> ) (15:20:65)	UV: 296	1.0	0.05–5.0	[141]
Ocular tissue with gatifloxacin	LiChrospher C <sub>18</sub> (5 µm, 125 × 4 mm)	20% ACN, in 0.1% TFA (pH 3.0) with 30 mM TBACl	UV: 295 Fluorescence: λ <sub>ex</sub> = 345, λ <sub>em</sub> = 470	0.5	0.01–10.0	[142]
Tablets, bioequivalence and stability	Shim-Pak ODS (5 µm, 250 × 4.6 mm)	MeO:H <sub>2</sub> O:ACN (45:30:25)	UV: 295	1.0	0.02–100	[143]
Rat plasma	Zorbax Edipse XDB C <sub>8</sub> (5 µm, 150 × 4.6 mm)	H <sub>2</sub> O:0.1% TFA:ACN (40:35:25)	UV: 296	1.0	0.05–10.0	[144]
Human saliva	Lichrospher 100 C <sub>18</sub> e (5 mm, 150 × 4.6 mm)	0.05 M PO <sub>4</sub> buffer, pH 2.6 with 1 N HCl: ACN (80:20)	Fluorescence: λ <sub>ex</sub> = 290, λ <sub>em</sub> = 460	1.5	0.25–10.0	[145]

Eye drops	Grace C <sub>18</sub> (5 µm, 250 × 4.6 mm)	0.01 M PO <sub>4</sub> buffer: MeOH (60:40, pH 4.4 with H <sub>3</sub> PO <sub>4</sub> )	UV: 294	1.0	10.0–100.0	[146]
Bulk material with cimetidine, famotidine and ranitidine, and tablets	Purospher STAR C <sub>18</sub> (5 µm, 250 × 4.6 mm)	MeOH:H <sub>2</sub> O:ACN (60:45:5, pH 2.7 with H <sub>3</sub> PO <sub>4</sub> )	UV: 236, 270, 310	1.0	0.078–5.0	[147]
Human plasma	Diamonsil C <sub>18</sub> (5 µm, 150 × 4.6 mm)	ACN:H <sub>2</sub> O (containing 0.04 M H <sub>3</sub> PO <sub>4</sub> and 0.4% TEA)	UV: 290	1.0	0.05–5.0	[148]
Aqueous, photolysis	Luna C <sub>18</sub> (3 µm, 150 × 3.0 mm)	ACN:H <sub>2</sub> O (0.1% HCOOH) (14:86)	UV: 296	–	–	[149]
Bulk material, R-isomer determination	Daicel Chiralpack (5 µm, 250 × 4.6 mm)	<i>n</i> -hexane:iso-PrOH: DEA:acetic acid (85:15:0.2:0.1)	UV: 293	1.0	0.54–5.4	[150]
Cheap plasma after i.v. administration	Supelco C <sub>18</sub> (5 µm, 150 × 4.6 mm)	1% TBAHSO <sub>4</sub> :ACN (80:20)	Fluorescence: λ <sub>ex</sub> = 296, λ <sub>em</sub> = 504	1.0	0.025–20.0	[151]
Untreated river water under natural sunlight	Supelco Ascentis RPAmide (5 µm, 250 × 4.6 mm)	25 mM H <sub>3</sub> PO <sub>4</sub> :ACN (80:20)	Fluorescence: λ <sub>ex</sub> = 290, λ <sub>em</sub> = 500	1.0	–	[152]
Aqueous with artificial light source, photolysis monitor	Waters Symmetry (5 µm, 150 × 4.6 mm)	H <sub>2</sub> O (pH 2.5 with 37% HCl):ACN (85:15)	UV: 275	1.2	–	
Aqueous with artificial light source, photoproducts identification	Luna C <sub>18</sub> (5 µm, 150 × 4.6 mm)	H <sub>2</sub> O (HCOOH 0.5%): ACN (85:15)	MS	1.0	–	

*Continued*

**Table 7.23** The HPLC parameters of the method used for the determination of moxifloxacin—cont'd

Material	Stationary phase	Mobile phase (v/v)	Detection	Flow rate (ml/min)	Linearity range (µg/ml)	Reference
Bulk material with ornidazole	Phenomenex C <sub>18</sub> (5 µm, 250 × 4.6 mm)	PO <sub>4</sub> buffer:ACN, pH 4.3 with H <sub>3</sub> PO <sub>4</sub> (68:32)	UV: 294	1.5	10.0–50.0	[153]
Tablets with cefixime	Phenomix C <sub>18</sub> (5 µm, 250 × 4.6 mm)	ACN:0.08 M KH <sub>2</sub> PO <sub>4</sub> , pH 8 with NaOH (40:60)	UV: 290	1.0	20.0–80.0	[154]
Mouse plasma and brain tissue	Lichrospher C <sub>18</sub> (5 µm, 250 × 4.6 mm)	ACN:MeOH:citrate buffer (0.025 M citric acid, 0.010 M SDS and 0.01 M TBABr in 500 ml H <sub>2</sub> O; pH 3.5 with 0.1 M NaOH) (40:3:57)	Fluorescence: $\lambda_{\text{ex}} = 290$ , $\lambda_{\text{em}} = 550$	1.0	0.005–0.25 (plasma) 0.1–2.5 µg/g (tissue)	[155]
Eye drops with ketorelac tromethamine	BDS Hypersil C <sub>8</sub> (5 µm, 250 × 4.6 mm)	MeOH: PO <sub>4</sub> buffer (2.72 g of KH <sub>2</sub> PO <sub>4</sub> in 1000 ml H <sub>2</sub> O, 1 ml TEA, pH 3.0 with H <sub>3</sub> PO <sub>4</sub> ) (55:45)	UV: 243	0.7	20.0–140.0	[156]

TBA, tetrabutylammonium; ACN, acetonitrile; TMA, tetramethylammonium; TFA, trifluoroacetic acid, AC, acetate, TEA, triethylamine, DEA, diethylamine, SDS, sodium dodecyl sulfate; PDA, photo diode array.

**Table 7.24** The UPLC parameters of the method used for the determination of moxifloxacin

Material	Stationary phase	Mobile phase (v/v)	Detection	Flow rate (ml/min)	Linearity range (µg/ml)	Reference
Surface and wastewater screening with other antibiotics	Acquity BEH C <sub>18</sub> (1.7 µm, 50 × 2.1 mm)	Gradient system: (A) H <sub>2</sub> O with 0.01% HCOOH and (B) MeOH.	QTOF-MS	0.3	0.001–2.5	[161]
Rabbit aqueous humor	Acquity BEH C <sub>18</sub> (1.7 µm, 50 × 2.1 mm)	Gradient system: (A) 0.1% TFA and (B) ACN	UV: 296	0.4	0.01–1.0	[162]
Tablets	HSS C <sub>18</sub> (1.8 µm, 100 × 2.1 mm)	0.34% KH <sub>2</sub> PO <sub>4</sub> , pH 1.8 with H <sub>3</sub> PO <sub>4</sub> :MeOH:ACN (60:20:20),	UV: 296	0.3	40.0–160.0	[163]
Aquatic products with gatifloxacin and levofloxacin	Acquity BEH C <sub>18</sub> (1.7 µm, 50 × 2.1 mm)	Gradient system: (A) ACN and (B) 0.005 M NH <sub>4</sub> AC	MS	–	Within 0.1	[164]
Rabbit aqueous humor	Acquity BEH C <sub>18</sub> (1.7 µm, 50 × 2.1 mm)	0.1% HCOOH	QTOF-MS	0.25	0.0001–0.2	[165]

MS, mass spectroscopy; ACN, acetonitrile; TFA, trifluoroacetic acid; AC, acetate.

#### 4.5.4 Capillary electrophoresis

A capillary electrophoresis method with laser-induced fluorescence was developed to determine moxifloxacin in human plasma and microdialysate [166]. The separation was carried out at 20 °C in a 50  $\mu\text{m} \times 27$  cm fused-silica capillary with applied voltages of 18 and 20 kV for microdialysate and plasma, respectively. The electrophoresis buffers were 0.06 M  $\text{H}_3\text{PO}_4$  at a pH 2.2 and 0.08 M  $\text{H}_3\text{PO}_4$  at a pH of 2.0 (triethylamine was used to adjust the pH) for plasma and microdialysate, respectively. The fluorescence detector was set at an excitation wavelength of 325 nm and an emission wavelength of 520 nm. The method is linear in a concentration range of 0.0025–5.0 for plasma and 0.005–5.0  $\mu\text{g}/\text{ml}$  for microdialysate. The quantitation limit is 0.0025 for plasma and 0.005  $\mu\text{g}/\text{ml}$  for microdialysate.

Determination of the enantiomeric purity of moxifloxacin as a bulk material and in the ophthalmic/otic drug product was carried out by a capillary electrophoresis technique connected to a UV detector set at 295 nm [34]. The separation of moxifloxacin (*S,S* enantiomer) from its potential enantiomers (*R,R* enantiomer, *R,S* diastereomer, and *S,R* diastereomer) was carried out at 20 °C in a 50  $\mu\text{m} \times 40$  cm fused-silica capillary with an applied voltage of 13 kV using a 0.0125-M triethylamine-phosphate buffer (pH 2.5) containing 5% highly sulfated gamma-cyclodextrin and 6% acetonitrile. The linearity range and quantitation limit for all potential impurities are 0.05–5.0 and 0.055  $\mu\text{g}/\text{ml}$ , respectively.

Determination of moxifloxacin, rifloxacin, and enoxacin in chicken tissue using a capillary electrophoresis-potential gradient detection method was reported [167]. The separation was carried out in a 75  $\mu\text{m} \times 16$  cm fused-silica capillary with an applied voltage of 6 kV using a 0.05-M acetic acid and 0.006 M KOH at pH 3.7. The linearity range and quantitation limit for moxifloxacin are 0.2–2 and 0.079  $\mu\text{g}/\text{g}$ , respectively.

Determination of moxifloxacin, rifloxacin, ciprofloxacin, enrofloxacin, and gatifloxacin in chicken tissue by capillary electrophoresis with contactless conductivity detection technique was reported [168]. The separation was carried out in a fused-silica capillary 50  $\mu\text{m} \times 42$  cm with an applied voltage of 13 kV using a buffer composed of 0.01 M tartaric acid, 0.014 M sodium acetate and 15% (v/v) methanol at pH 3.8. The linearity range and detection limit for moxifloxacin are 2.0–40 and 0.33  $\mu\text{g}/\text{ml}$ , respectively.

#### 4.6. Biological methods

Determination of moxifloxacin in human body fluids by a conventional cup-plate agar diffusion method with *Bacillus subtilis* as indicator organism

was reported [108,169]. The method was used as a reference to a proposed HPLC method with fluorescence detection. The excellent correlation between results of both methods (slope 1.05) was found. The linearity range and quantitation limit are 0.06–2.0 (urine and plasma) and 0.06 µg/ml, respectively.

*In vitro* activity of moxifloxacin against *Legionella* species and the effect of medium on susceptibility test results were investigated using an ager dilution method with buffered charcoal yeast extract agar containing  $\alpha$ -ketoglutarate [170]. A spore suspension of *Bacillus subtilis* was used as the indicator organism and the medium was Iso-Sensitest agar. The study revealed that charcoal has inhibitory effect on the test media, as a result the MIC was corrected to the charcoal-bound fraction of the drug.

*Escherichia coli* (NCTC 10418) was used as indicator organism in studying *in vitro* pharmacodynamic activity of moxifloxacin for *Staphylococcus aureus* and Streptococci of Lancefield Group A and G [171]. The method showed a detection limit of 0.03 µg/ml. Results of this study revealed that moxifloxacin has significant bactericidal action against *Staphylococcus aureus* with MICs  $\leq 0.14$  mg/l but may be less bactericidal against  $\beta$ -haemolytic streptococci.

A disk diffusion microbioassay with *Bacillus subtilis* (ATCC 6633) was used to evaluate the bactericidal effectiveness and the pharmacodynamic profile of moxifloxacin in cerebrospinal fluid (CSF) and to compare the bactericidal activity with that of ceftriaxone and meropenem therapy [172]. Calibration curves were constructed using concentration ranges of 0.2–10 and 0.1–6 µg/ml for plasma and CSF samples, respectively. The detection limit was 0.2 for plasma and 0.1 µg/ml for CSF specimens.

A parallel-line bioassay was used to investigate the antimicrobial activity of moxifloxacin photodegradation products [173]. A continuous flow photochemical reaction unit (Beam-Boost) was used to partially photodegrade the drug (30–83%, as confirmed by HPLC). These results were compared by parallel-line bioassays using *Escherichia coli*, *Enterobacter cloacae*, and *Klebsiella oxytoca*. The estimated relative potencies (ERP; the ratio of the matched control solution concentration to that of the irradiated solution concentration) for irradiated versus control solutions showed no significant difference after 30% or 54% photodegradation with any of the indicator organisms, nor after 83% photodegradation with *Escherichia coli* and *Klebsiella oxytoca*. The ERPs were significantly different for 83% photodegradation using *Enterobacter cloacae*.

Bioassay was used in studying the activities of mutant prevention concentration-targeted moxifloxacin and levofloxacin against *Streptococcus*



*pneumoniae* in an *in vitro* pharmacodynamic model [174]. The concentration of moxifloxacin and levofloxacin were determined using tryptic soy agar supplemented with 5% sheep blood as the medium and *Klebsiella pneumoniae* (ATCC 33495) as the indicator organism. The detection limit was 0.31 µg/ml.

Bioassay was used for evaluation using moxifloxacin in pleural empyema, a serious complication of pneumonia, therapy [175]. Moxifloxacin concentrations in serum and pleural fluid were measured microbiologically using *Bacillus subtilis* (ATCC 6633) on trypticase soy agar pH 9.0. Concentration range and the detection limit were 0.15–20.0 and 0.15 µg/ml, respectively.



## 5. STABILITY

### 5.1. Solid-state stability

Forced degradation of moxifloxacin HCl in solid state was investigated by using densitometric TLC method [104]. It was found that heating moxifloxacin HCl at 100 °C for 8 h leads to a decrease in percentage recovery to 91% with the detection of three degradates.

Stability of moxifloxacin HCl in its tablet dosage form after incubation at 40 °C/75% RH and 50 °C/75% RH for 6 months was investigated using HPLC/UV detection [143]. The stability data for two products (Avelox<sup>®</sup> and Staxin<sup>®</sup>) proved that the drug is stable without any significant decrease in percentage assay after 6 months of incubation (percentage assay range: 99.8–100.0% at 40 °C/75% RH).

Forced degradation of moxifloxacin HCl in the solid state was monitored by HPLC/UV detection [146]. It was found that the drug is stable when exposed to daylight and to thermal stress at 60 °C for 30 days.

Following the photodegradation by UPLC/MS detection, moxifloxacin HCl in its solid state was found to be not stable when exposed to a UV lamp (365 nm) in a watch glass for 48 h as one photodegrade was detected [165].

The effect of heat, humidity, and light on the racemization of moxifloxacin HCl in its solid state was studied by capillary electrophoresis [34]. Stress degradation studies were carried out at 40 °C/75% RH, 60 °C for 12 weeks, and in a stability light chamber (provides ICH-required illumination levels with 4-week exposure) at 25 °C/40% RH. Results revealed that racemization was not a significant degradation pathway of the drug under the investigated conditions.

The effect of heat, humidity, and light on the stability of moxifloxacin HCl in its pure solid state was investigated by HPLC/UV detection

[176]. No any degradation products were observed when it was subjected to thermal degradation at 100 °C and to photodegradation according to option 2 of Q1B of the ICH guidelines for 5 and 11 days, respectively. The accelerated (40 °C/75% RH) and long-term (30 °C/65% RH) stability testing was conducted for 6 and 12 months, respectively. Results indicated that moxifloxacin HCl was stable under long-term and accelerated storage conditions with percentage assay ranging from 99.7% to 100.1% and total impurities of <0.1%.

Compatibility of moxifloxacin HCl with some directly compressible diluents in 1:1 (w/w) ratio mixtures was investigated by DSC [177]. Data was supported by isothermal stability studies (IST) carried out at 30 °C and at 50 °C for the period of 6 months. Stability of the drug in solution state in the presence of diluents and the influence of pH were also investigated by UV spectrophotometric method. DSC results revealed incompatibility of drug with sorbitol powder (Neosorb), dextrose anhydrous, and mannitol (Pearlitol) on the basis of enthalpy loss and absence of melting endotherm of the drug. Compatibility was predicted with microcrystalline cellulose (PH101 and PH102), dibasic calcium phosphate dehydrate (Emcompress), dibasic calcium phosphate anhydrous (Anhydrous Emcompress), partially pregelatinized maize starch (Lycatab), lactose monohydrate (Lactochem fine powder) and lactose monohydrate (Lactopress spray dried) on the basis of DSC analysis. Results of stability study in liquid state indicate that there was no significant adsorption, absorption, or degradation of the drug in presence of the aforementioned diluents. For the case of emcompress and anhydrous emcompress diluents, which are alkaline, there was a change in pH from 1.4 to 3.6, which might be one of the probable cause for the apparent discoloration of powder mixtures of moxifloxacin HCl with these diluents.

Different formulations of moxifloxacin HCl control ocular inserts were prepared by an aqueous dispersion of drug, sodium alginate, polyvinyl alcohol, and dibutyl phthalate by the film casting method. The effect of cross linking with  $\text{CaCl}_2$  and different grades of Eudragit polymer were also investigated [178]. The polymers used were Eudragit S-100, Eudragit RL-100, Eudragit RS-100, Eudragit E-100, and Eudragit L-100. Stability studies were carried out on ocular insert formulations packed in Al foils at 40 °C/75% RH and at room temperature for 6 months. The stability study revealed that formulations containing  $\text{CaCl}_2$  and Eudragit RL-100 have the lowest degradation and maximum shelf life.

Chemical and physical stability of moxifloxacin HCl against form transformation was investigated by HPLC and XRPD techniques [30]. Stability

of moxifloxacin HCl in the presence of different pharmaceutical excipients in tables at 40 °C/75% RH for 3 months was studied. The tablets were prepared by roll compaction using different formulation excipients and stored in close containers (Table 7.25). Tablets during stability were tested according to moxifloxacin tablets monograph in USP-MC (Section 4.1.4; Table 7.19). The obtained stability data as shown in Table 7.26 indicate that moxifloxacin HCl is highly stable when compressed in the presence of different excipients where the assay and organic impurities results are within the acceptable limits. As shown in Figure 7.22, both reference product (Avelox<sup>®</sup>) and formula 4 (F-4) initially have almost the same dissolution profile, while the other formulas (F-1, F-2, and F-3) show slow release in comparison with Avelox<sup>®</sup>. Moreover, Avelox<sup>®</sup> and F-4 did not show any significant decrease in their dissolution profiles upon storage at 40 °C/75% RH for 3 months. It is worth mentioning that the Avelox<sup>®</sup> tablets have the same composition of formula 1 (F-1) but using most probably form II of moxifloxacin HCl and using a wet granulation technique in processing [179].

**Table 7.25** The list of different tablet formulations of moxifloxacin HCl

Item	Formula			
	F-1	F-2	F-3	F-4
Form	Form Z (anhydrous form obtained from drug supplier)			
Excipients	Microcrystalline cellulose			
	Magnesium stearate			
	Lactose·H <sub>2</sub> O	Spray dried mannitol	Spray dried mannitol	Spray dried mannitol
	Croscarmellose sodium	Croscarmellose Sodium	Croscarmellose Sodium	Sodium starch glycolate
			Compretol 888 ATO	Compretol 888 ATO
				Colloidal anhydrous silica
Granulation	Dry (roll compaction)			
Storage	40 °C/75% RH in Al/Al			

Compretol 888 ATO: Glyceryl behenate.

**Table 7.26** The stability data for different tablet formulations of moxifloxacin HCl at 40 °C/75% RH in close container

Formula	Assay				Organic impurities			
	95.0–105.0%				Any individual ≤0.2%			
	Month				Month			
	0	1	2	3	0	1	2	3
F-1	101.9	101.8	101.7	—	0.03	0.02	0.02	—
F-2	102.9	103.7	103.5	—	0.03	0.02	0.02	—
F-3	102.2	102.9	103.4	—	0.03	0.02	0.02	—
F-4	102.9	99.3	100.1	101.3	0.02	0.02	0.04	0.04

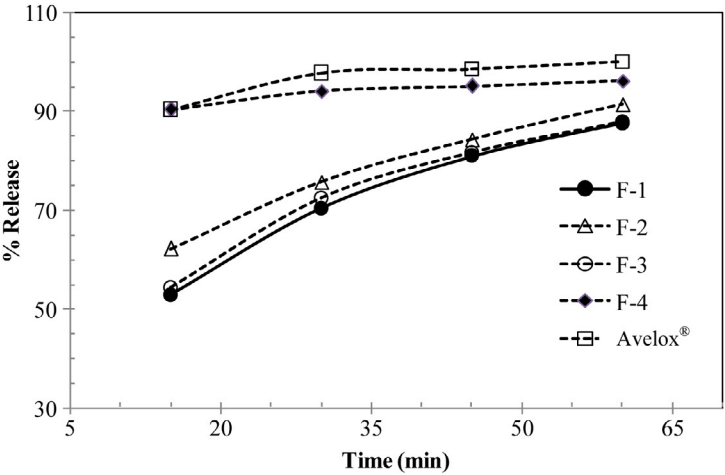


**Figure 7.22** Comparative dissolution profiles for different formulations with Avelox® tablets (Bayer product).

By monitoring form transformation of moxifloxacin HCl using XRPD, it was found that Form W (hydrate form obtained from drug supplier) converts to Form II (Bayer hydrate form) by time after incubation at 40 °C/75% RH in open container (Figure 7.23). The intensities of the bands at  $2\theta=7.3$  and  $17.4$  corresponding to Form W (Figure 7.23B) decrease dramatically after 2 months of incubation, the intensities of the two bands at around  $2\theta=27$  and  $28$  were enhanced (Figure 7.23D). However, Form W was found to be stable without any significant transformation when protected from humidity.

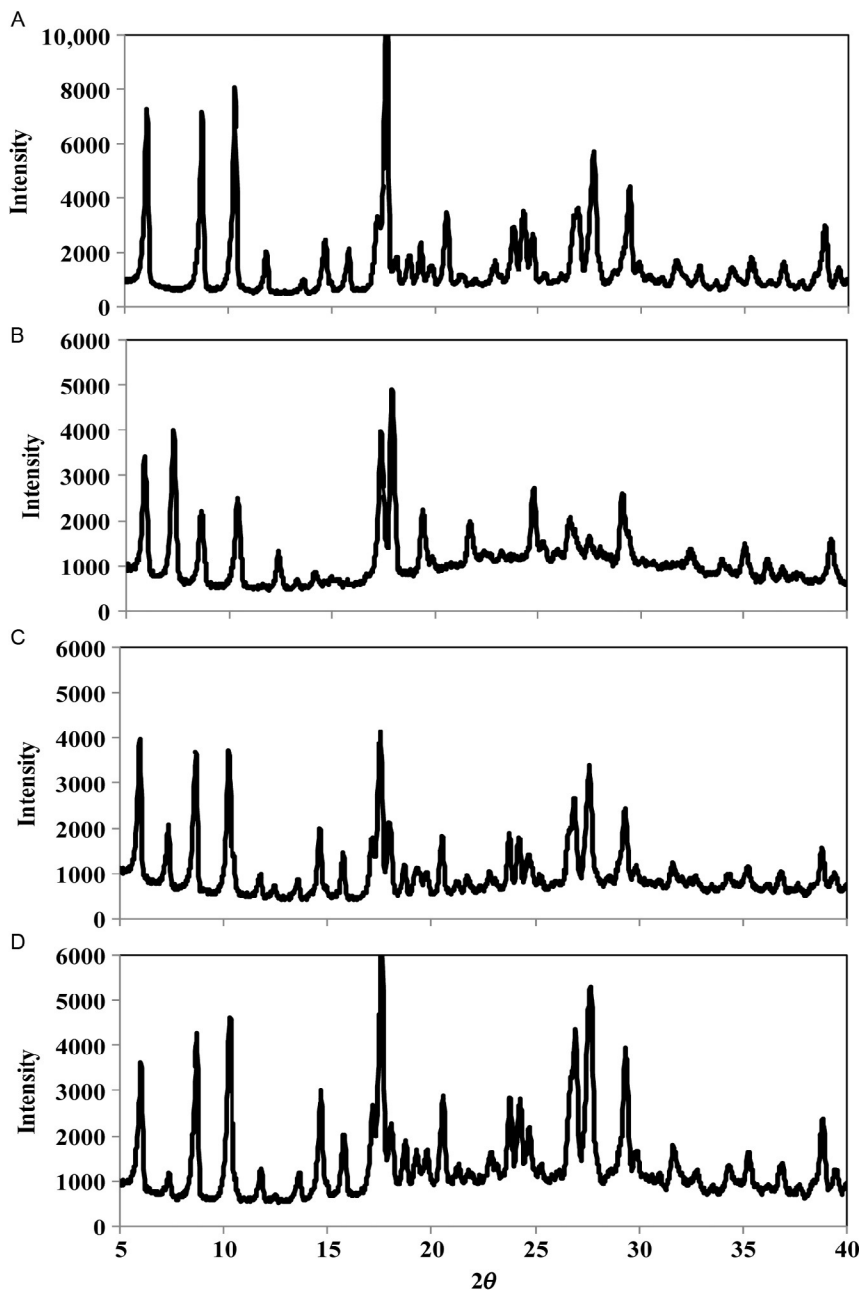


**Figure 7.23** XRPD of moxifloxacin HCl (A) Form II, (B) Form W, and (C) and (D) Form W incubated at 40 °C/75% RH for 1 and 2 months, respectively, in open container. Form II (Bayer hydrate form prepared by recrystallization from water/ethanol system).

In tablet formulations, it was noticed that the types of moxifloxacin HCl form can be easily distinguished by XRPD [30]. For example, Forms Z and W have a distinguishable band at  $2\theta = 7.3$ , while it is absent in Form II (Bayer form) (Figure 7.24). Forms Z and W were found to be stable without any significant form transformations when protected from humidity.

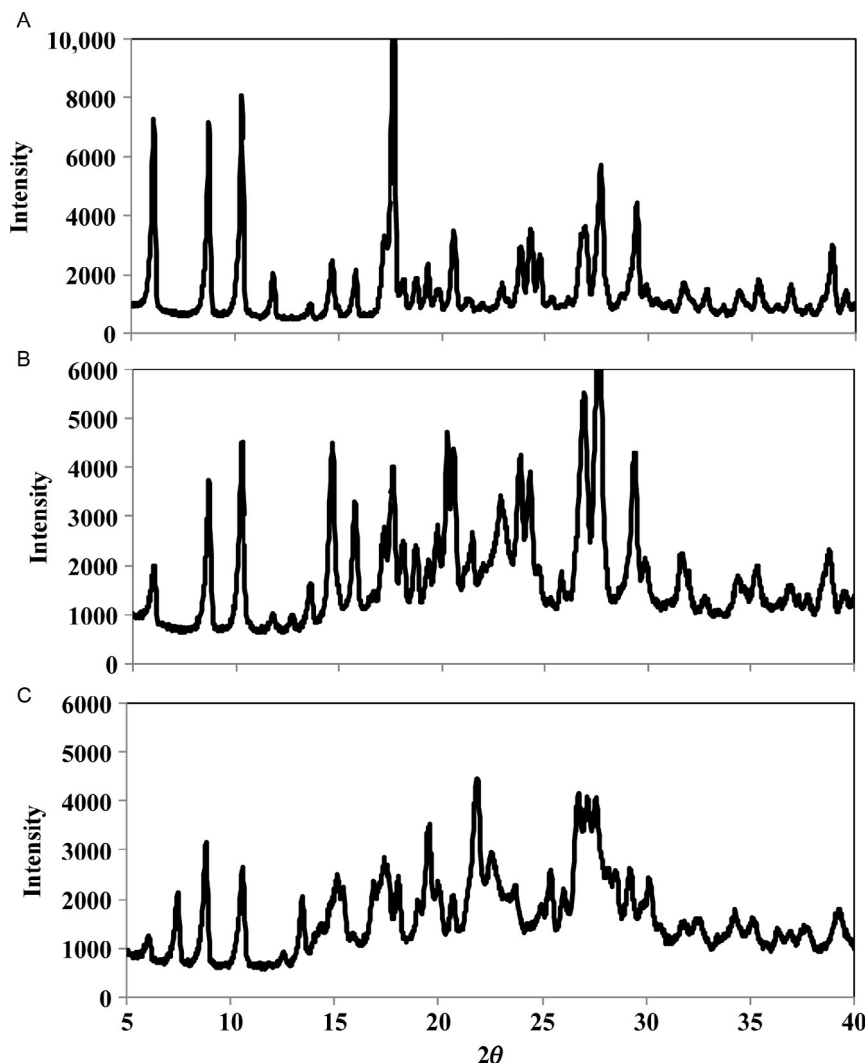


**Figure 7.24** XRPD of (A) moxifloxacin HCl Form II (Bayer form), (B) Avelox® tablets, and (C) formula 4 (F-4) after grinding. Form II (Bayer hydrate form prepared by recrystallization from water/ethanol system).

**Table 7.27** The list of different tablet formulations of moxifloxacin HCl

Item	Avelox <sup>®</sup>	Formula 5 (F-5)
Form	Form II (Bayer form)	
Excipients (core)	Microcrystalline cellulose	
	Magnesium stearate	
	Lactose·H <sub>2</sub> O	Spray dried mannitol
	Croscarmellose sodium	Sodium starch glycolate
		Colloidal anhydrous silica
Coat	Hypromellose, polyethylene glycol, titanium dioxide, red iron oxide	Hypromellose, polyethylene glycol, titanium dioxide, lactose H <sub>2</sub> O, triacetin, red Iron oxide, FD&C Blue #2 aluminum lake, black Iron oxide
Granulation	Wet	Dry (roll compaction)
Package	Al/Al, PP/Al	Al/Al, PVDC/Al
Storage	40 °C/75% RH	

PP, polypropylene; PVDC, polyvinylidene chloride.

Furthermore, stability of moxifloxacin HCl in tables was investigated [30]. Two different formulations (Table 7.27) with different excipients, manufacturing processes, and packaging materials were included in this investigation.

As shown in Table 7.28, the drug is highly stable regardless the type of excipients, manufacturing process, and packaging materials.

## 5.2. Solution-phase stability

As a member of fluorinated quinolones, moxifloxacin HCl was expected to decompose into its decarboxylated degrade when refluxed in acidic solution (2 N HCl) away from light [69]. Subsequently, measurement of moxifloxacin HCl in the presence of such degrade was achieved by densitometric TLC and spectrophotometric methods.

Stability of moxifloxacin HCl in solution was studied using densitometric TLC [104]. The drug was found to be unstable under acidic (1 N HCl), basic (1 N NaOH) and oxidation (30% H<sub>2</sub>O<sub>2</sub>) stress conditions at 80 °C for 3 h. The drug recoveries were 36.91%, 63.42%, and 79.19%, respectively. On the other hand, methanolic solution of moxifloxacin HCl did not show

**Table 7.28** The stability data for different tablet formulations of moxifloxacin HCl at 40 °C/75% RH packed in different packaging materials

Product	Assay			Organic impurities		
	95.0–105.0%			Any individual ≤0.2%		
	Month			Month		
	0	3	6	0	3	6
Avelox <sup>®</sup> (Al/Al)	103.0	—	98.1	0.02	—	0.04
Avelox <sup>®</sup> (PP/Al)	101.0	—	101.3	0.00	—	0.00
F-5 (Al/Al)	98.8	98.7	99.0	0.00	0.01	0.01
F-5 (PVDC/Al)	98.8	100.8	101.2	0.00	0.00	0.02

F, formula; PP, polypropylene, PVDC, polyvinylidene chloride.

any significant decrease in its potency (% recovery 99.18%) when exposed to the same stress condition. The photostability in methanol showed that the drug is less stable to daylight exposure (% recovery 86.76%) than UV (254 nm) irradiation (% recovery of 95.32%).

The effect of pH on the stability of moxifloxacin HCl in 0.05 M buffer solutions was studied at 50 and 80 °C for 1 and 3 days, respectively [30]. The samples and buffer solutions were prepared following the same procedure reported earlier [104]. Analysis was carried out using the HPLC method with UV detection [2]. From Figure 7.25, it can be concluded that the drug is relatively stable under the investigated conditions. It is worth mentioning that precipitates were formed in samples prepared in phthalate buffers (pH 2.2–5.0), which is most probable due to the formation of moxifloxacin phthalate salt with limited solubility (low Ksp). This finding is in contradiction with that reported [104]. The later showed that moxifloxacin HCl is extremely degraded at 40 °C over the pH range of 1.2–10.8, where the half-life time ( $t_{1/2}$ ) is ranging from 8.3 to 15.6 h depending on the pH value.

The effect of different metal ions on the stability of moxifloxacin HCl in acidic media was investigated using different techniques including TLC/densitometry, HPLC/UV, HPLC/MS, and <sup>1</sup>H NMR [106]. The stability studies in acidic condition (1.3 N HCl) were carried out in the absence and presence of Cu (II), Zn (II), Fe (III), and Al (III) ions at 90 and 110 °C for 72 h away from light. After 72 h of heating at 90 °C, the decomposition of the drug in the absence of metal ions did not exceed 10%. On the other hand, the decomposition was higher in the presence of metal ions (Cu (II) 41.92%, Fe (III) 13.61%, Zn (II) 12.8%, and Al (III) 11.25%). At



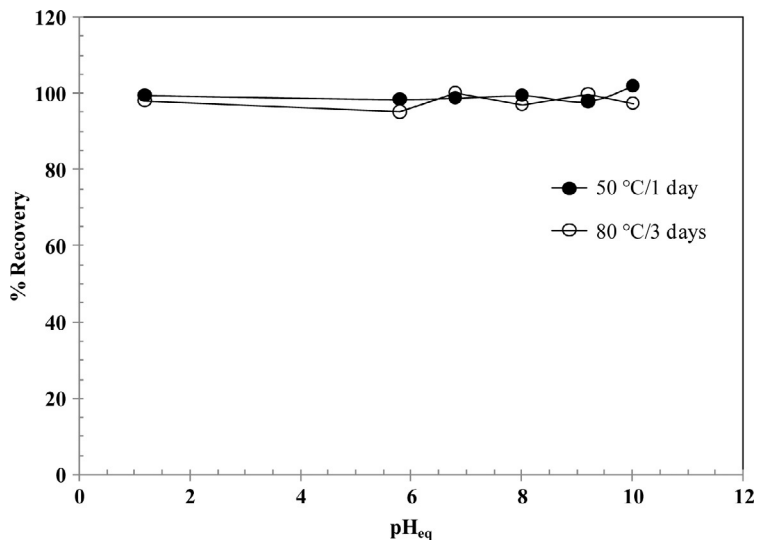


**Figure 7.25** pH stability profile of moxifloxacin HCl at 50 and 80 °C for 1 and 3 days, respectively.

110 °C, the decomposition was found to be faster and followed the order at 48 h: Cu (II) (79.35%) > Fe (III) (63.97%) > Al (III) (62.42%) > Zn (II) (58.62%) > Drug alone (52.04%). Moxifloxacin HCl was found to undergo thermal degradation through the loss of the functional carboxyl (decarboxylation) and hydrolysis of 2,8-diazabicyclo[4.3.0]non-8-yl groups (Figure 7.26).

Stability of moxifloxacin HCl in solution was investigated by HPLC/fluorescence detection [108]. It was found that the drug in organic solvent stored at room temperature and at 37 °C for 22 days is stable when protected from light (brown glass or in dark). The obtained percentage recoveries were 97.1% and 99.3%, respectively. For the case of exposure to daylight in a white glass at room temperature, the drug showed a significant decrease in percentage recovery to 39.8%.

Photodegradation of moxifloxacin HCl in water by sunlight was monitored by HPLC/MS detection as a function of time [121]. Samples were kept under environmental conditions (open air, protected from rain). After 136 h, the drug content decreased by at least 50% of the initial concentration. Moxifloxacin *N*-oxide, formed by photooxidation of the alicyclic ring, was detected by MS analysis.

The degradation of moxifloxacin was studied by HPLC/UV detection under different stress conditions (0.1 N HCl, water, and 0.1 N NaOH) at

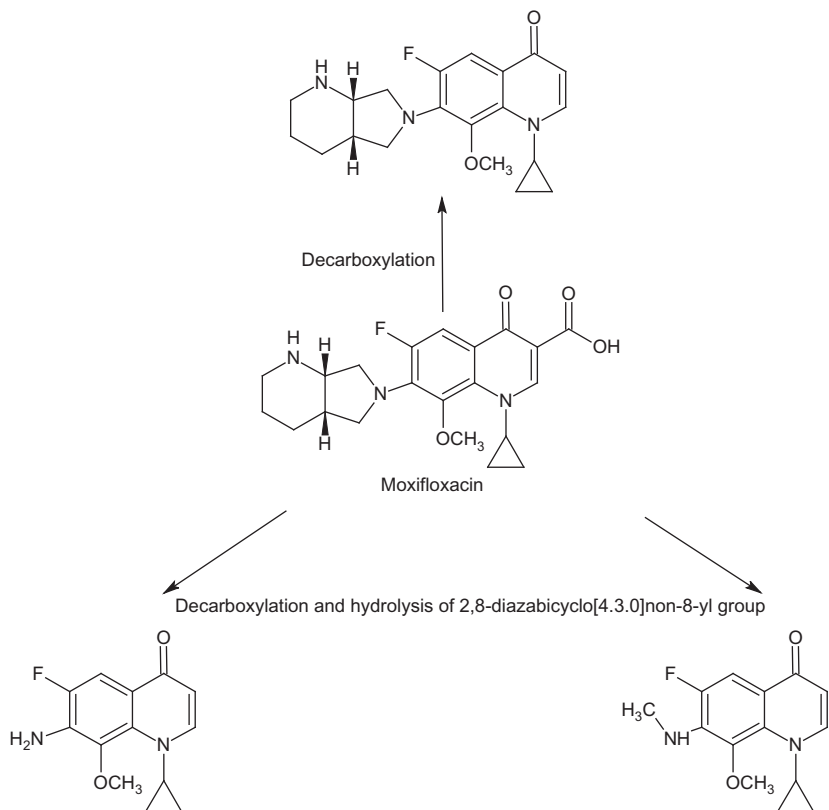


**Figure 7.26** Acid degradation pathways of moxifloxacin HCl at 110 °C in the presence of Cu (II) ions.

50 °C for 3 h. Oxidation stress was performed in 3% H<sub>2</sub>O<sub>2</sub> solution for 6 h at room temperature, while photolytic stress was carried out inside a light chamber equipped with lamp bank with two Osram UV lamps. A total of 840 Wh/m<sup>2</sup> irradiation units for 3 h were used [132]. Two degradation products were detected in acid and basic hydrolysis with a total percentage of about 0.3%. No degradates were apparent under photolytic or oxidative conditions.

Short-term stability of extemporaneously compounded suspensions of moxifloxacin 20 mg/ml in a 1:1 mixture of Ora-Plus and Ora-Sweet or Ora-Sweet SF prepared from the commercially available tablets (Avelox<sup>®</sup>) was studied using HPLC/UV detection at room temperature [134]. Results indicate that the suspensions are stable for at least 90 days when stored in 2-oz amber plastic bottles at room temperature. To prove

the suitability of the HPLC method as a stability indicating technique, decomposition of the drug was forced by standing different prepared suspensions in direct sunlight for 90 days after adding 3%  $\text{H}_2\text{O}_2$ , adjusting the pH to 12 with 1 N NaOH or to 2 with 1 N HCl. Then all solutions were heated to 60 °C for 2 h. About 35% degradation of the drug was measured in the acidic solution and about 20% with  $\text{H}_2\text{O}_2$ ; however, no appreciable change was recorded in basic media.

Forced degradation of moxifloxacin in solution was monitored by HPLC/UV detection [146]. Keeping the drug in mobile phase (phosphate buffer and methanol (60:40 v/v) of pH 4.4) at room temperature for 30 h did not affect its stability. The drug was found to be stable under acidic (0.1 N HCl/6 h), neutral (water/6 h) and oxidation (3%  $\text{H}_2\text{O}_2$ /2 h) stress conditions at 80 °C. The drug was degraded up to 70% in 0.1 N NaOH after heating at 80 °C for 6 h showing one major degradation product.

UV-A and UV-C induced photolysis and  $\text{TiO}_2$ -P25 mediated heterogeneous photocatalysis were investigated as advanced oxidation technologies for the removal of fluoroquinolones in aqueous solution [149]. The photolytic and  $\text{TiO}_2$  mediated heterogeneous photocatalytic degradation of the drug are measured at pHs 3, 7, and 10, under UV-A and UV-C irradiation at different intervals of time using HPLC/UV detection. Results revealed that the photolysis and photocatalysis with  $\text{TiO}_2$ -P25 techniques are both capable of degrading the drug in an aqueous solution with the most promising results obtained with heterogeneous photocatalysis under UV-C irradiation at pH 7.

Photolytic and photocatalysis with  $\text{TiO}_2$  of fluoroquinolones in untreated river water (pH 7.7) under natural sunlight were investigated [152]. The photodegradation rate is  $5 \times$  faster in the presence of  $\text{TiO}_2$  suspension as indicated by HPLC/fluorescence detection. To identify the photoproducts, the aqueous solution (deionized water) of the drug in the absence and presence of  $\text{TiO}_2$  was exposed to low pressure mercury arcs with emission maximum centered at 310 nm. The irradiated samples were immediately analyzed by HPLC/UV prior HPLC/ESI-MS/MS analysis. As shown in Figure 7.27, photodegradation behavior patterns pass through (i) photosubstitution of fluorine on carbon 6 of the aromatic moiety by a hydroxyl group, (ii) reductive dehalogenation, and (iii) bimolecular reactions where the excited state of the drug or of some impurity attacks the drug causing electron or hydrogen transfer from the electron-rich moiety present, viz. the amino side-chain. The photolysis of moxifloxacin in aqueous solution gave six products resulting from OH/F substitution ( $\text{M3}_{\text{WT}}$  and  $\text{M1}_{\text{WT}}$ ,

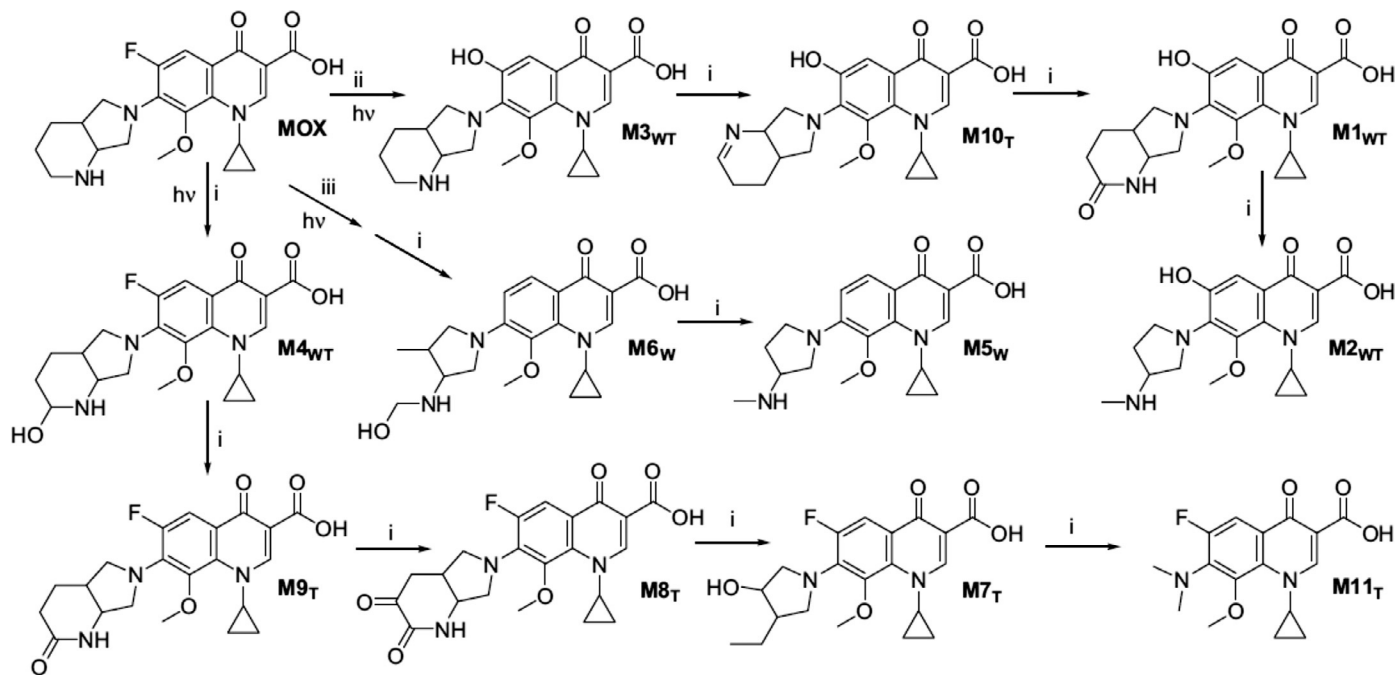


Figure 7.27 Degradation pathways and by products in the photolysis (W) and photocatalysis (T) of moxifloxacin HCl.

M2<sub>WT</sub> by further oxidation), reductive dehalogenation combined with side-chain oxidation (M6<sub>W</sub> and M5<sub>W</sub>) and side-chain oxidation (M4<sub>WT</sub>) in roughly equivalent amounts. On the other hand, photocatalysis gave tiny amounts of M3<sub>WT</sub> and its degradation products (M10<sub>T</sub>, M2<sub>WT</sub>, and M1<sub>WT</sub>) while the main products resulted from primary oxidative degradation of the amine side-chain M4<sub>WT</sub> (along with M9<sub>T</sub>, M8<sub>T</sub>, M7<sub>T</sub>, and M11<sub>T</sub>).

Forced degradation of moxifloxacin with cefixime in solution was monitored by HPLC/UV detection [154]. Keeping the drug in mixture of phosphate buffer and acetonitrile (60:40 v/v) of pH 8.0 at room temperature for 24 h and in 1 N NaOH for 1 h did not affect its stability, while it was degraded in acidic (2 M HCl/1 h) and by oxidation (6% H<sub>2</sub>O<sub>2</sub>/1 h) at 80 °C.

Forced degradation of moxifloxacin with ketorolac tromethamine in solution was monitored by HPLC/UV detection [156]. Keeping the drug in methanol and phosphate buffer (55:45 v/v) of pH 3.0 at different temperature (25 °C/19 h, 40 °C/1 h, and 160 °C on a hot plate/1 h) did not affect its stability. While exposing this solution to sunlight for 1 h showed a significant decrease in the content of the drug (% recovery of 84.2%). The drug was found to be stable in 1 N and 5 N NaOH, 1 N and 5 N HCl and by oxidation (6% H<sub>2</sub>O<sub>2</sub>) at 40 °C for 1 h (% recoveries were >99%). However, exposing these solutions to more stress condition by heating at 160 °C on a hot plate for 1 h affected the stability of the drug (% recoveries were 84.4%, 91.6%, and 94.6% for 5 N HCl, 6% H<sub>2</sub>O<sub>2</sub>, and 5 N NaOH, respectively).

Photodegradation of moxifloxacin by UV-A irradiation in solutions and solid phase in the presence and absence of Cu (II), Zn (II), Al (III), and Fe (III) was investigated [160]. It was found that presence of a metal ion enhanced the photodegradation of the drug in solutions, and the influence of Cu (II) and Fe (III) ions was higher than that of Zn (II) and Al (III) ions as measured by TLC/densitometry. On the other hand, all metal ions decreased the photodegradation in solid phase; however, the influence of Al (III) and Zn (II) ions was weaker than that of Cu (II) and Fe (III) ions. Moxifloxacin HCl was found to undergo photodegradation through the oxidation and hydrolysis of 2,8-diazabicyclo[4.3.0]non-8-yl group (Figure 7.28).

From the forced degradation study by UPLC/MS detection, moxifloxacin was found to be not stable under oxidative (6% H<sub>2</sub>O<sub>2</sub>), alkaline (0.02 N NaOH), and acidic (2 N HCl) stress conditions at 60 °C for 48 h. Various unknown degradates were detected in the investigated solutions [165].

Racemization of moxifloxacin in solution under acidic, neutral, basic, and oxidizing conditions was investigated by capillary electrophoresis [34]. Samples were prepared in citrate buffer (pH 4.0); phosphate buffer (pH 7.0),

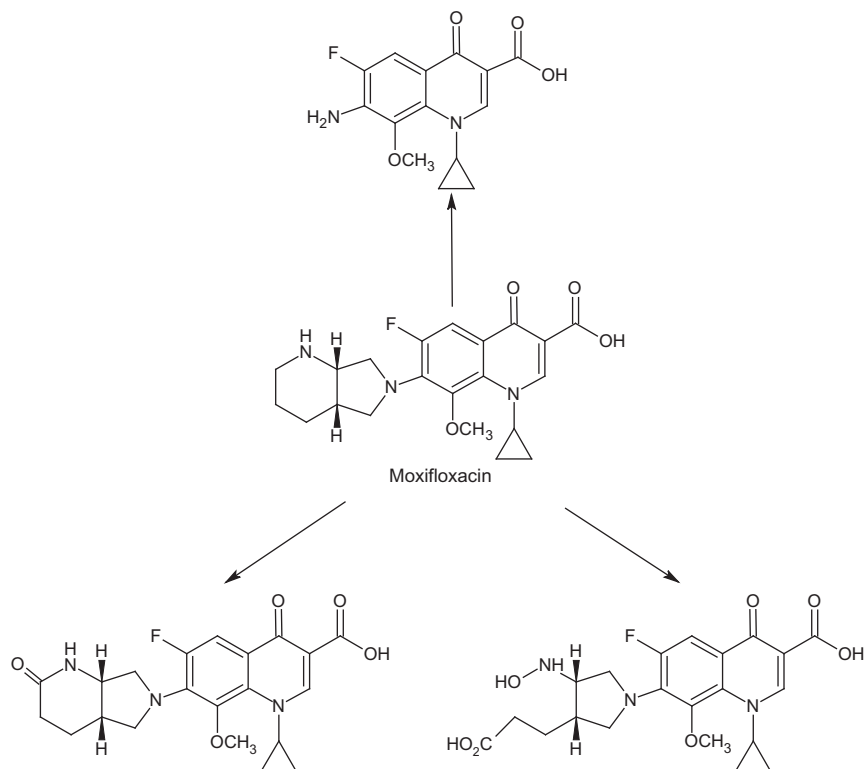


**Figure 7.28** Photodegradation pathways of moxifloxacin HCl after UV-A irradiation.

borate buffer (pH 9.0) and in water (unbuffered) sparged with  $O_2$  for 20 min and stored at 50 °C for 12 weeks. The unbuffered sample in water was stored in a stability light chamber at 25 °C/40% RH for 12 weeks. Results revealed that racemization was not a significant degradation pathway of the drug substance in solution.

Moreover, moxifloxacin HCl in aqueous solution showed instability when exposed to 245 nm UV lamp [173]. The extent of photodegradation (30%, 54%, or 83%) was achieved using various flow rate and retention coil lengths of the photochemical reaction unit and monitoring by HPLC/fluorescence detection.

Forced degradation of moxifloxacin in 0.5 N HCl and 0.5 N NaOH at 70 °C for 5 days and in 3%  $H_2O_2$  at ambient temperature for 3 days was studied by HPLC/UV detection [176]. Significant degradation was observed by oxidative stress (83.4%) and by basic (94.6%) conditions; no degradation was observed under acidic (99.2%) condition.

The stability of moxifloxacin injection (2%) in dialysis peritoneal solution bags at two glucose concentrations (Dianeal PD1 1.36%<sup>®</sup> and Dianeal PD1 3.86%<sup>®</sup>) at 4, 25, and 37 °C was investigated by HPLC/fluorescence detection [180]. In Dianeal PD1 1.36%<sup>®</sup> solution, the drug concentration remained  $\geq 90\%$  of the initial concentration for 14, 7, and 3 days at 4, 25, and 37 °C, respectively. In Dianeal PD1 3.86%<sup>®</sup>, the drug concentrations remained  $\geq 90\%$  for 14, 3 days, 12 h at 4, 25, and 37 °C, respectively. In addition, the drug did not show any precipitation (i.e., chelating with Ca and Mg cations) suggesting that moxifloxacin does not produce complexes with the metals. Accordingly, moxifloxacin injected into PD bags shows sufficient stability and may be used for treating peritonitis in PD patients.

### 5.3. Stability in biological fluids

Stability of moxifloxacin HCl in human body fluids was investigated by HPLC/fluorescence detection [108]. For short-term stability, it was found that moxifloxacin HCl in whole blood and plasma is stable when kept at room temperature away from daylight (brown glass) for 4 and 75 h with percentage recoveries of 100.0% and 98.0%, respectively. For plasma sample kept in a white glass, there was a significant decrease in moxifloxacin HCl content when exposed to daylight (% recovery = 90%). Long-term stability at -20 °C over 12 months did not show any significant loss in moxifloxacin HCl content, where percentage recoveries were in the range of 96–104% regardless the type of container material used (glass, polystyrene, or polypropylene). The stability study covered up to five freeze-thaw cycles.

Moxifloxacin HCl was found to be stable in human plasma when stored at -20 °C for 2 months and at room temperature for 24 h using HPLC/fluorescence detection technique [128]. The freeze-thaw stability was assessed in the moxifloxacin HCl spiked plasma samples storage at -20 °C for 2 months. In the short-term stability study, moxifloxacin-4-chloro-7-nitrobenzodioxazole derivative was stable for 1 week at 4 °C and at room temperature for 24 h. In the long-term stability study, the plasma samples spiked with moxifloxacin HCl were stored for 2 months at -20 °C and after three freeze-thaw cycles.

Short-term stability of moxifloxacin HCl in plasma was studied by HPLC/fluorescence detection under two experimental conditions: after storage in autosampler (20 °C) for 15 h and after three freeze-thaw cycles [133]. Results revealed that moxifloxacin HCl at a concentration level of 1.5 µg/ml, is stable and consequently, extracted samples could be left in

the autosampler (at 20 °C) for 15 h prior to analysis. In three freeze-thaw cycles, moxifloxacin HCl was stable in plasma, indicating no significant substance loss during repeated thawing and freezing at the low (0.06 µg/ml) and the middle (1.20 µg/ml) concentration. However, QC samples at the high (7.20 µg/ml) concentration level showed a statistically significant difference in mean after three freeze-thaw cycles for moxifloxacin HCl, but it lies within 15% of its respective nominal value, complying with the internationally accepted criteria. Thus it may be considered stable in plasma at the high concentration level after three freeze-thaw cycles.

Stability study of moxifloxacin HCl in plasma and CSF was investigated by HPLC/MS detection [139]. All stability tests were performed at low (0.5 µg/ml) and high (4.9 µg/ml) concentration levels. Stability is defined as a change in concentration and should be  $\leq 15\%$ . After three freeze-thaw cycles, the stability of moxifloxacin HCl was not affected. Storage in the refrigerator for 120 h, storage at refrigerator (4 °C), at room temperature, and after sample preparation in the autosampler (20 °C) did not affect the stability either (low or high). Exposure to light had no significant effect on stability of moxifloxacin HCl for 120 h.

Stability of moxifloxacin HCl in plasma under different conditions was evaluated at three concentration levels (0.1, 1.6, and 5.0 µg/ml) by HPLC/UV detection [141]. Freeze-thaw stability was determined by following three freeze-thaw cycles from  $-20$  °C to room temperature for every 24 h. The long-term and short-term stability of plasma samples were evaluated at  $-20$  °C for 1, 2, 4, 12 weeks and at room temperature for 2, 4, 8, 12 h, respectively. The stability of extracted plasma samples was evaluated by keeping samples at room temperature for 2, 4, 6, 12 h. Regardless the level of concentration, moxifloxacin in human plasma sample was stable during the storage, freeze-thaw cycles, processing and analysis (% recovery range: 96.6–102.1%).

Long-term stability of moxifloxacin HCl at  $-20$  °C,  $-80$  °C, three freeze-thaw cycles, and 18 h in the autosampler at three levels of concentrations (20, 125, and 225 mg/ml for plasma, 0.2, 1.25, and 2.25 mg/mg for cerebral tissue) was studied by HPLC/fluorescence detection [155]. The drug was found stable over three freeze-thaw cycles (CV  $< 11\%$  for plasma and  $< 10\%$  for brain, and recovery ranged from 99% to 103% for plasma and from 100% to 105% for brain). It also remained stable 18 h after sample treatment (CV  $< 5\%$ , recovery between 98–105% for plasma and 99–106% for brain).

As determined by UPLC/UV detection, moxifloxacin was found to be stable in aqueous humor at 20 °C for at least 24 h and at 4 °C for 2 days with



average recovery of 95.7% and 97.6%, respectively [162]. The freeze-thaw data indicated that three cycles can be tolerated without losses greater than 10%.

Stability of moxifloxacin in aqueous humor at 4 °C, room temperature, and after freeze-thaw cycles was determined by UPLC/MS detection [165]. The drug was found to be stable at the temperature used in the stability studies. The average recovery was 96.5%, 97.2%, and 93.9% at room temperature, 4 °C and freeze-thaw at a concentration level of 10 ng/ml, respectively.

From the above stability studies, it can be summarized that moxifloxacin HCl is relatively stable drug in solid state and in solution under moderate conditions of heat. In solution, moxifloxacin HCl is liable to degrade upon exposure to high temperature (above 80 °C), to light or to oxidizing agent.

It is worth mentioning that the differences in stability behavior of moxifloxacin HCl (e.g., extent, pathway) in these studies may be attributed to the differences in the experimental conditions (e.g., drug and reagent concentrations, temperature, exposure time, light source, etc.).

## 5.4. Interaction with metals

Fluoroquinolones containing pyridine and carboxylate oxygen atoms are liable to form complexes with metal ions. Such complexes formation was suggested to play an important role in the biological activities. For examples, the complexes formed between moxifloxacin and different metal ions (V (IV), Zr (IV), and U (VI)) showed good antibacterial effect to some bacterial strains as compared to the free drug [7]. Mg (II) was shown to modulate the quinolone-DNA binding through the formation of a ternary complex involving the drug, the metal ion, and the DNA [181].

It was reported that the simultaneous presence of antacid containing Mg (II) and Al (III) has noticeable effect on the dissolution rate of moxifloxacin tablets [182].

Complexation of Gd (III) with moxifloxacin in solution was fully investigated by [183]. The effect of moxifloxacin, and for comparison purpose, diethylene triamine pentaacetic acid (DTPA) on Gd (III) plasma speciation was evaluated by computer simulation. The study revealed that the stable tris complex  $\text{Gd}(\text{HMOXI})_3$  formed between Gd (III) ion and moxifloxacin is stable enough to exhaust the normal gadolinium concentration in plasma upon oral intake of one 400 mg dose of moxifloxacin, at low Gd (III) concentration ( $10^{-6}$ – $10^{-5}$  mM). However, at higher Gd (III) concentrations,

moxifloxacin is not competitive chelator with regard to MRI agents (such as DTPA).

It was reported that the complex formation between Mg (II) and moxifloxacin intermediate prevents the formation of isomer impurity in moxifloxacin preparation [21]. This facilitates the nucleophilic substitution of fluoride in position 7 rather than the substitution of the fluoride in position 6 (Scheme 7.11).

Interaction of some metal ions with moxifloxacin is widely used for analysis of pharmaceutical and biological samples [63,67,86,87,91,92,96,97,100]. These studies are fully discussed earlier in method of analysis section.

Some ternary complexes consisting of moxifloxacin, 1,10-phenanthroline, and metal ion (Co (II), Ni (II), or Cu (II)) were prepared and characterized [184]. These prepared ternary complexes were found to have appreciable antimicrobial activity against different bacterial and fungal species.



## **6. PHARMACOLOGY**

### **6.1. Uses, applications, and pertinent history**

#### **6.1.1 Systemic use**

Moxifloxacin HCl is a fluoroquinolone antibacterial indicated for treating infections in adults caused by designated, susceptible bacteria. It was initially approved in a tablet form by the EMA in June 1999 [185] and by the USFDA in December 1999 [186].

Moxifloxacin HCl tablets and intravenous are indicated in patients aged 18 years and older for the treatment of the following bacterial infections if they are caused by bacteria susceptible to moxifloxacin:

- Acute bacterial sinusitis
- Acute exacerbations of chronic bronchitis.
- Community-acquired pneumonia [187,188].
- Uncomplicated and complicated skin and skin structure infections.
- Complicated intraabdominal infections, including polymicrobial infections such as abscess. [188].

The intravenous administration is recommended when it offers a route of administration advantageous to the patient (e.g., severe infection or the patient cannot tolerate the oral dosage form) [3,188].

Moxifloxacin HCl tablets are also indicated for the treatment of mild to moderate pelvic inflammatory disease (i.e., infections of the female upper

genital tract, including salpingitis and endometritis), without an associated tubo-ovarian or pelvic abscess. It should be given in combination with another appropriate antibacterial agent (e.g., a cephalosporin) due to increasing moxifloxacin resistance of *Neisseria gonorrhoeae*, unless moxifloxacin-resistant *Neisseria gonorrhoeae* can be excluded [187].

### 6.1.2 Topical use

Moxifloxacin HCl ophthalmic solution was approved by the FDA in April 2003 for the treatment of bacterial conjunctivitis caused by designated susceptible organisms [189]. Susceptible organisms include *Corynebacterium* species, *Micrococcus luteus*, *Staphylococcus aureus*, *Staphylococcus epidermidis*, *Staphylococcus haemolyticus*, *Staphylococcus hominis*, *Staphylococcus warneri*, *Streptococcus pneumoniae*, *Streptococcus viridans* group, *Acinetobacter lwoffii*, *Haemophilus influenzae*, *Haemophilus parainfluenzae*, *Chlamydia trachomatis* [190].

## 6.2. Absorption

### 6.2.1 Oral

Moxifloxacin is readily absorbed from the gastrointestinal tract after oral administration. It is not subject to significant presystemic biotransformation (“first-pass” effect). In consequence, the absolute bioavailability is almost complete ( $\approx 90\%$ ) [191].

Peak plasma concentrations ( $C_{\max}$ ) and area under the plasma concentration–time curve (AUC) increased linearly with dose after administration of single oral moxifloxacin doses of 50–800 mg. After the recommended dose of 400 mg, a mean  $C_{\max}$  of 2.5 mg/l was reached in 1.5 h ( $t_{\max}$ ) and AUC was 26.9 mg/l h [192].

Moxifloxacin has no clinically relevant interactions with food [191]. Concomitant intake of dairy products slightly delayed the rate, but not the extent, of absorption of the drug [192]. Changes in gastric pH by pretreatment with ranitidine had no influence on absorption. In common with the fluoroquinolones, moxifloxacin is likely to form nonabsorbable complexes in the presence of multivalent cations. Accordingly, its absorption is impaired by the concomitant administration of Maalox<sup>®</sup> and iron supplements [191].

Moxifloxacin pharmacokinetics are linear and dose-proportional with repeated oral doses of up to 600 mg once daily over 10 days. Plasma concentrations rose readily after oral doses, achieving and maintaining appropriately high levels over 24 h. Stable steady-state conditions are reached within 2–3 days with no indication of clinically relevant accumulation [193].

Repeated administration of moxifloxacin 400 mg/day orally for 10 days to healthy volunteers ( $n=10$ ) resulted in a  $C_{\max}$  of 4.52 mg/l [192]. The area accumulation ratios ( $AUC_{24, \text{ day 10}}/AUC_{\infty, \text{ day 1}}$ ) of 100–131% and 120% after repeated doses of 400 and 600 mg once daily, and 95% and 107% after repeated doses of 100 and 200 mg twice daily indicate absence of clinically relevant accumulation [193].

### 6.2.2 Intravenous

Moxifloxacin pharmacokinetics are linear and dose-proportional in the range of 100–400 mg single dose [193]. Intravenous administration of moxifloxacin 400 mg produced a  $C_{\max}$  of 3.62 mg/l and AUC of 34.6 mg h/l [192].

### 6.2.3 Topical

Following the administration of bilateral topical ocular doses of moxifloxacin 0.5% ophthalmic solution 3  $\times$  a day in healthy subjects, mean steady-state  $C_{\max}$  (2.7 ng/ml) and estimated daily exposure AUC (45 ng h/ml) values were 1600 and 1000  $\times$  lower than the respective values reported after therapeutic 400 mg doses of moxifloxacin [190].

Conjunctival tissue levels of moxifloxacin rose to peak levels within 15–30 min after topical administration of moxifloxacin 0.5% ophthalmic solution. Conjunctival tissues  $C_{\max}$  was 24.1 mg/g. The  $AUC_{0-3}$  was 27.1 (mg h)/g [194].

## 6.3. Distribution

Moxifloxacin is approximately 30–50% bound to serum proteins, independent of drug concentration. The volume of distribution ranges from 1.7 to 2.7 l/kg. It is widely distributed throughout the body, with tissue concentrations often exceeding plasma concentrations. The rates of elimination of moxifloxacin from tissues generally parallel the elimination from plasma [188]. Moxifloxacin reaches higher concentrations in saliva, capillary blood [195], skin blister fluid, epithelial lining fluid, bronchial biopsies, and maxillary sinus mucosa than in plasma. Similar results were noted in anterior ethmoid mucosa and nasal polyp tissue [192]. Free drug concentrations in subcutaneous tissue and skeletal muscle are comparable to those of the unbound drug in plasma. Very high concentrations are achieved in the alveolar macrophages and bronchial mucosa [195]. Moxifloxacin was also detected in nasal and bronchial secretions and abdominal tissues and fluids following oral or intravenous administration of 400 mg [188]. The

high volume of distribution, low protein binding, and rapid early distribution phase into target tissues are indicative of optimal distribution properties allowing for effective treatment of the indicated infections [195]. In animal studies, orally administered moxifloxacin penetrated across the placental barrier and into breast milk in rats, and achieved good penetration into CSF in rabbits, particularly in those with experimental meningitis [192].

## 6.4. Metabolism

Moxifloxacin does not appear to be metabolized by the cytochrome P-450 pathway. It is metabolized to inactive metabolites via conjugation to a sulfo- (M1) and a glucuronide (M2) derivative in principal (Figure 7.29) [55,192,196,197].

## 6.5. Elimination

Up to 96% and 98%, respectively, of the oral and intravenous dose of moxifloxacin was recovered as either parent compound ( $\approx 45\%$ ), metabolite M1 ( $\approx 38\%$ ), or metabolite M2 ( $\approx 14\%$ ). About 20% of the administered dose is recovered unchanged in urine. Urinary excretion is independent of the dose and route of administration. Renal clearance is lower than

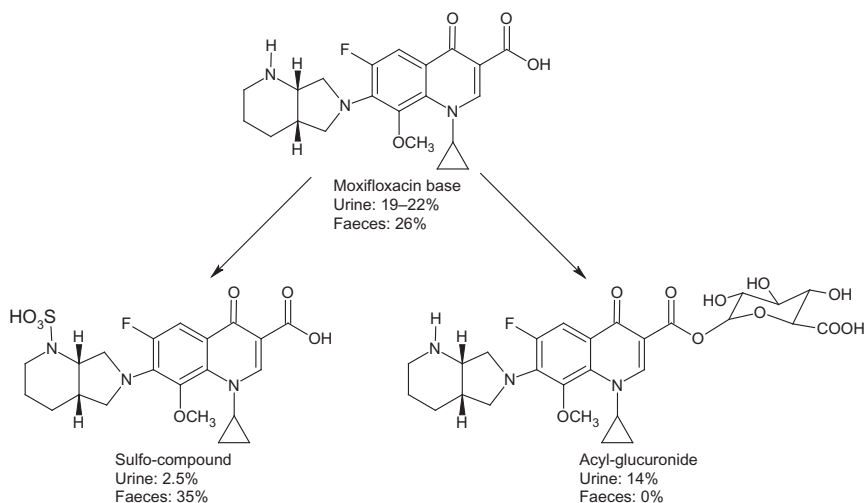


**Figure 7.29** The metabolic pattern of the main metabolites of moxifloxacin with their recovery in humans.

creatinine clearance suggesting tubular reabsorption. Of the administered dose, about 25% is excreted unchanged via feces and up to 50% is recovered indirectly via conjugates excreted in urine and feces. In rats, 68% of a radiolabeled intravenous dose of moxifloxacin was excreted in the bile. Excessive accumulation of moxifloxacin is unlikely in the event of impaired renal or hepatic function since its elimination (biotransformation and excretion) pathways are balanced. They do not rely exclusively on either renal or hepatic function [196].

The reported mean plasma elimination half-life ( $t_{1/2\beta}$ ) of oral moxifloxacin 50–800 mg ranges from 8 to 16 h. Plasma clearance ranges from 9 to 15 l/h and occurs primarily by nonrenal mechanisms, with renal clearance being approximately 1.3–3 l/h [197].

The plasma half-life of moxifloxacin was estimated to be 13 h following the administration of bilateral topical ocular doses of 0.5% moxifloxacin ophthalmic solution 3 × a day in healthy subjects [190].

## 6.6. Pharmacological Effects

Moxifloxacin is a fluorinated 4-quinolone. In common with quinolone antibiotics, the bactericidal action of moxifloxacin results from inhibition of the topoisomerase II (DNA gyrase) and topoisomerase IV required for bacterial DNA replication, transcription, repair, and recombination. Topoisomerase IV is the primary activity inhibited for many gram-positive bacteria whereas DNA gyrase is the primary quinolone target in many gram-negative microbes. The C<sub>8</sub> methoxy group in moxifloxacin markedly reduces the propensity for drug resistance [188,198].

Moxifloxacin was shown to be active against most isolates of the following bacteria, both *in vitro* and in clinical infections:

- Gram-positive bacteria: *Enterococcus faecalis*, *Staphylococcus aureus*, *Streptococcus anginosus*, *Streptococcus constellatus*, *Streptococcus pneumoniae* (including multidrug resistant isolates [MDRSP]) and *Streptococcus pyogenes*.
- Gram-negative bacteria: *Enterobacter cloacae*, *Escherichia coli*, *Haemophilus influenza*, *Haemophilus parainfluenzae*, *Klebsiella pneumonia*, *Moraxella catarrhalis*, and *Proteus mirabilis*.
- Anaerobic bacteria: *Bacteroides fragilis*, *Bacteroides thetaiotaomicron*, *Clostridium perfringens*, and *Peptostreptococcus species*.
- Other microorganisms: *Chlamydomphila pneumoniae* and *Mycoplasma pneumonia* [188].

## REFERENCES

- [1] European Pharmacopeia, seventh ed., Council of Europe, Strasbourg, Moxifloxacin Hydrochloride Monograph, 2011, pp. 2531–2532.
- [2] United States Pharmacopeia 35/National Formulary 30 (USP 35/NF 29), Moxifloxacin Hydrochloride Monograph, vol. 3, USP Convention. INC, Maryland, 2012, pp. 3959–3960.
- [3] Avelox<sup>®</sup> Product Monograph, Bayer Site, <http://www.bayer.ca/files/AVELOX-PM-ENG-20JAN2012-150618.pdf>, accessed date March 2013.
- [4] Drug Bank Site, Moxifloxacin Monograph, <http://www.drugbank.ca/drugs/DB00218>, accessed date March 2013.
- [5] Food and Drugs Administration (FDA) Site, Vigamox: Chemistry Review, [http://www.accessdata.fda.gov/drugsatfda\\_docs/nda/2003/21-598\\_Vigamox\\_chemr.PDF](http://www.accessdata.fda.gov/drugsatfda_docs/nda/2003/21-598_Vigamox_chemr.PDF), accessed date March 2013.
- [6] Moxifloxacin Monograph, Tuberculosis 88 (2008) 127–131.
- [7] S.A. Sadeek, W.H. El-Shwiniy, W.A. Zordok, E. Kotb, Spectroscopic studies, thermal analyses and biological evaluation of new V(IV), Zr(IV) and U(VI) moxifloxacin complexes, *J. Mol. Struct.* 1006 (2011) 192–209.
- [8] BDG Synthesis Site, Moxifloxacin HCl Analysis Data Sheet, [http://www.bdg.co.nz/coa/coa\\_110255\\_10180.1\\_20100520\\_V1\\_Moxifloxacin\\_HCl.pdf](http://www.bdg.co.nz/coa/coa_110255_10180.1_20100520_V1_Moxifloxacin_HCl.pdf), accessed date March 2013.
- [9] United States Pharmacopeia 35/National Formulary 30 (USP 35/NF 30), Description and Solubility Chapter, vol. 1, USP Convention, INC, Maryland, 2012, p. 1131.
- [10] U. Petersen, T. Schenke, A. Krebs, K. Grohe, M. Schriewer, I. Haller, K.G. Metzger, R. Endermann, H.-J. Zeiler, 7-(4-Oxa or 4-thia-2,7-diazabicyclo[3.3.0]oct-2-en-3-yl)-3-quinolone-and-naphthyridone-carboxylic acid derivatives as antibacterial agents and feed additives, United States Patent US5059597, 1991.
- [11] U. Petersen, A. Krebs, T. Schenke, T. Philipps, K. Grohe, K.-D. Bremm, R. Endermann, K.-G. Metzger, I. Haller, Quinolone- and naphthyridone carboxylic acid derivatives as antibacterial agents, European Patent EP0550903, 1992.
- [12] U. Petersen, W. Schröck, D. Häbich, A. Krebs, T. Schenke, T. Philipps, K. Grohe, R. Endermann, K.-D. Bremm, K.-G. Metzger, Quinolonecarboxylic acids, United States Patent US5480879, 1996.
- [13] P. Fey, Method for producing (S, S)-benzyl-2,8-diazabicyclo[4.3.0]nonane, United States Patent US6235908, 2001.
- [14] R. Gehring, K. Mohrs, W. Heilmann, H. Diehl, Method for producing 8-methoxy-quinolinecarboxylic acids, United States Patent US7115744, 2006.
- [15] M.S. Reddy, C. Nagaraju, S.T. Rajan, A.K. Ramprasad, R. Satyanarayana, Novel process for the preparation of moxifloxacin hydrochloride and a novel polymorph of moxifloxacin, World Intellectual Property Organization Patent WO2008059521, 2008.
- [16] C. Satyanarayana, G.S. Ramanjaneyulu, V.U. Rao, D.V.L. Narasimharao, Quinoline carboxylic acid-O, O-bis-acyloxy borate and process of making, United States Patent US20090259041, 2009.
- [17] D.R. Rao, R.N. Kankan, S.L. Pathi, R. Puppala, M. Gangrade, S. Kanathala, Process for the synthesis of moxifloxacin hydrochloride, United States Patent US20100152229, 2010.
- [18] Q. Jun, W. Guangtu, S. Hao, Method for synthesis of high-effective broad-spectrum antimicrobial moxifloxacin hydrochloride, Chinese Patent CN101817820, 2010.
- [19] Z. Faxiang, Z. Ying, Process for preparation of moxifloxacin hydrochloride, Chinese Patent CN102276603, 2011.
- [20] H. Huabin, Y. Jianbo, L. Yi, J. Chengjun, Process for preparation of moxifloxacin, Chinese Patent CN102351858, 2012.
- [21] A. Castellin, P. Padovan, L. Jiageng, Y. Zhou, L. Feng, Process for preparing moxifloxacin and salts thereof, United States Patent US8207339, 2012.

- [22] R. Motterle, G. Arvotti, E. Bergantino, A. Castellin, S. Fogal, M. Galvagni, Synthesis of (4a*S*,7a*S*)-octahydro-1*H*-pyrrolo[3,4-*b*]pyridine, United States Patent US20110137036, 2011.
- [23] M. Pallavicini, C. Bolchi, L. Fumagalli, O. Piccolo, E. Valoti, Highly efficient racemisation of a key intermediate of the antibiotic moxifloxacin, *Tetrahedron: Asymmetry* 22 (2011) 379–380.
- [24] G.X. Li, L. Wu, Q.Q. Fu, Z. Tang, X.M. Zhang, First way of enantioselective synthesis of moxifloxacin intermediate, *Sci. Chin. Chem.* 56 (2013) 307–311.
- [25] P.G. Reddy, P. Keerthi, N. Gudimalla, S. Mohanty, R. Bandichhor, Reaction kinetics of nucleophilic substitution in the synthesis of moxifloxacin, *Chem. Biol. Interface.* 2 (2012) 303–313.
- [26] K.B. Deepika, E.S. Priya, K. Murali, N.R. Kumar, Synthesis of various sulphonamide-linked fluoroquinolones as antibacterial agents, *Asian J. Chem.* 22 (2010) 4363–4370.
- [27] M.-H. Langlois, M. Montagut, J.-P. Dubost, J. Grellet, M.-C. Saux, Protonation equilibrium and lipophilicity of moxifloxacin, *J. Pharm. Biomed. Anal.* 37 (2005) 389–393.
- [28] C.M. Cárceles, L. Villamayor, E. Escudero, P. Marín, E. Fernández-Varón, Pharmacokinetics and milk penetration of moxifloxacin after intramuscular administration to lactating goats, *Vet. J.* 173 (2007) 452–455.
- [29] F. Varanda, M.J.P. de Melo, A.I. Caço, R. Dohrn, F.A. Makrydaki, E. Voutsas, D. Tassios, I.M. Marrucho, Solubility of antibiotics in different solvents. 1. hydrochloride forms of tetracycline, moxifloxacin, and ciprofloxacin, *Ind. Eng. Chem. Res.* 45 (2006) 6368–6374.
- [30] A.A. Badwan, The Jordanian Pharmaceutical Manufacturing Co. Personal communication.
- [31] WHO Technical Report Series, No 937, 40th report, annex 8, Who expert committee on specifications for pharmaceutical preparations, 2006, [http://whqlibdoc.who.int/trs/who\\_trs\\_937\\_eng.pdf](http://whqlibdoc.who.int/trs/who_trs_937_eng.pdf), accessed date March 2013.
- [32] EMA Guideline on the Investigation of Bioequivalence, 2010, [http://www.emea.europa.eu/docs/en\\_GB/document\\_library/Scientific\\_guideline/2010/01/WC500070039.pdf](http://www.emea.europa.eu/docs/en_GB/document_library/Scientific_guideline/2010/01/WC500070039.pdf), accessed date March 2013.
- [33] USFDA Guidance for Waiver of in vivo bioavailability and bioequivalence studies for immediate-release solid oral dosage forms based on a Biopharmaceutics Classification System, 2000, <http://www.fda.gov/downloads/Drugs/GuidanceComplianceRegulatoryInformation/Guidances/UCM070246.pdf>, accessed date March 2013.
- [34] L.A. Cruz, R. Hall, Enantiomeric purity assay of moxifloxacin hydrochloride by capillary electrophoresis, *J. Pharm. Biomed. Anal.* 38 (2005) 8–13.
- [35] A. Grunenberg, P. Bosché, Crystal modification of CDCH, a process for its preparation and pharmaceutical formulations comprising this modification, United States Patent US5849752, 1998.
- [36] A. Becker, Novel hydrate form, United States Patent US20110224249, 2011.
- [37] S. Biswas, P. Bose, Y. Kumar, Amorphous moxifloxacin hydrochloride, United States Patent US20060252789, 2006.
- [38] R. Dandala, J. Mitra, A.K. Gupta, S. Meenakshisunderam, New crystalline form of moxifloxacin hydrochloride and process for its preparation, World Intellectual Property Organization Patent WO2006134491, 2006.
- [39] M.S. Reddy, C. Nagaraju, S.T. Rajan, A.K. Ramprasda, Novel crystalline forms of moxifloxacin hydrochloride and process for preparation thereof, World Intellectual Property Organization Patent WO2007010555, 2007.
- [40] M.S. Reddy, S. Eswaraiah, V.V.N.K.V.P. Raju, R.R. Kumar, N. Srinivasreddy, V. Ravindra, Crystalline form III of anhydrous moxifloxacin hydrochloride and a process for preparation thereof, United States Patent US7230006, 2007.



- [41] F.P. Nicolau, J.V. Prieto, Crystalline form of moxifloxacin hydrochloride, World Intellectual Property Organization Patent WO2008028959, 2008.
- [42] F.P. Nicolau, J.V. Prieto, Crystalline form of moxifloxacin base, World Intellectual Property Organization Patent WO2008095964, 2008.
- [43] S. Turchetta, V. Aromatario, Polymorphs of 1-cyclopropyl-7-([S, S]-2,8-diazadicyclo [4.3.0]non-8-Yl)-6-fluoro-1,4-dihydro-8-methoxy-4-oxo-3-quinoline carboxylic acid hydrochloride and methods for the preparation thereof, European Patent EP1685130, 2008.
- [44] F.P. Nicolau, J.V. Prieto, Novel crystalline form (form IV) of moxifloxacin hydrochloride anhydrate, Spanish Patent ES2316270, 2009.
- [45] G. Ventimiglia, D. Magrone, G. Castaldi, Polymorphic forms of moxifloxacin hydrochloride and processes for preparation thereof, European Patent EP2083010, 2009.
- [46] B.P. Reddy, K.R. Reddy, R.R. Reddy, D.M. Reddy, M.M. Reddy, D.B. Reddy, Novel polymorph of moxifloxacin hydrochloride, United States Patent US20110212990, 2011.
- [47] A. Ramakrishnana, S. Pamujula, Crystal modification of moxifloxacin hydrochloride, World Intellectual Property Organization Patent WO2011121596, 2011.
- [48] F. Zhang, Y. Zhang, New anhydrous moxifloxacin hydrochloride crystal F and preparation method thereof, Chinese Patent CN102321083, 2012.
- [49] Y. Zhang, J. Zou, Y. Liu, Y. Yang, W. Wang, Moxifloxacin hydrochloride monohydrate crystal form and preparation method thereof, Chinese Patent CN102344447, 2012.
- [50] D.R. Rao, R.N. Kankan, S.L. Pathi, R. Puppala, M. Gangrade, S. Kanathala, Process for the synthesis of moxifloxacin hydrochloride, United States patent US8198451, 2012.
- [51] V.L. Dorofeev, A.P. Arzamastsev, O.M. Veselova, Melting point determination for the analysis of drugs of the fluoroquinolone group, *Pharm. Chem. J.* 38 (2004) 333–335.
- [52] The Merck Index: An Encyclopedia of Chemical Drugs and Biologicals, 13th ed., Merck Research Labs., Whitehouse Station, 2001.
- [53] U. Neugebauer, A. Szeghalmi, M. Schmitt, W. Kiefer, J. Popp, U. Holzgrabe, Vibrational spectroscopic characterization of fluoroquinolones, *Spectrochim. Acta A Mol. Biomol. Spectrosc.* 61 (2005) 1505–1517.
- [54] M.-G. Zhang, Z.-J. Xia, L. Jiang, B. Wang, M.-L. Wang, L.-J. Zang, Z.-X. Chen, Spectra and structure data analysis of moxifloxacin hydrochloride, *Anal. Test. Technol. Instrum.* 18 (2012) 85–91.
- [55] B. Raju, M. Ramesh, R.M. Borkar, R. Srinivas, R. Padiya, S.K. Banerjee, *In vivo* metabolic investigation of moxifloxacin using liquid chromatography/electrospray ionization tandem mass spectrometry in combination with online hydrogen/deuterium exchange experiments, *Rapid Commun. Mass Spectrom.* 26 (2012) 1817–1831.
- [56] C.S. Wu, Z.X. Jia, B.M. Ning, J.L. Zhang, S. Wu, Separation and identification of moxifloxacin impurities in drug substance by high-performance liquid chromatography coupled with ultraviolet detection and Fourier transform ion cyclotron resonance mass spectrometry, *Chin. Chem. Lett.* 23 (2012) 1185–1188.
- [57] United States Pharmacopeia-Medicines Compendium (USP-MC), Moxifloxacin Hydrochloride Monograph, 2012, <https://www.usp-mc.org/monographs/moxifloxacin-hydrochloride-1-0>, accessed date March 2013.
- [58] United States Pharmacopeia 35/National Formulary 30 (USP 35/NF 29), Moxifloxacin Ophthalmic Solution Monograph, vol. 3, USP Convention, INC, Maryland, 2012, pp. 3960–3962.

- [59] United States Pharmacopeia-Medicines Compendium (USP-MC), Moxifloxacin Ophthalmic Solution Monograph, 2012, <https://www.usp-mc.org/monographs/moxifloxacin-ophthalmic-solution-1-0>, accessed date March 2013.
- [60] United States Pharmacopeia-Medicines Compendium (USP-MC), Moxifloxacin Injection Monograph, 2012, <https://www.usp-mc.org/monographs/moxifloxacin-injection-1-0>, accessed date March 2013.
- [61] United States Pharmacopeia-Medicines Compendium (USP-MC), Moxifloxacin Tablets Monograph, 2012, <https://www.usp-mc.org/monographs/moxifloxacin-tablets-1-0>, accessed date March 2013.
- [62] E. Erk, Voltammetric behaviour and determination of moxifloxacin in pharmaceutical products and human plasma, *Anal. Bioanal. Chem.* 378 (2004) 1351–1356.
- [63] M.A.G. Trindade, P.A.C. Cunha, T.A. de Araújo, G.M. da Silva, V.S. Ferreira, Interaction study of moxifloxacin with Cu(II) ion using square-wave voltammetry and its application in the determination in tablets, *Lectica Quim.* 31 (2006) 31–38.
- [64] B.-L. Zhu, J.-L. Wang, J.-H. Gao, Adsorptive voltammetric behavior of moxifloxacin hydrochloride and its application, *J. Southwest Univ. Natl. (Nat. Sci. Ed.)* (2008) 317–322, [http://en.cnki.com.cn/Article\\_en/CJFDTOTAL-XNMZ200802026.htm](http://en.cnki.com.cn/Article_en/CJFDTOTAL-XNMZ200802026.htm), accessed date March 2013.
- [65] A.K. Attia, M.A. El-Shal, Electrochemical determination of antibacterial drug moxifloxacin hydrochloride using chloranil modified carbon paste electrode, *Anal. Bioanal. Electrochem.* 4 (2012) 213–224.
- [66] R. İnam, H. Mercan, E. Yılmaz, B. Uslu, Differential pulse polarographic determination of moxifloxacin hydrochloride in pharmaceuticals and biological fluids, *Anal. Lett.* 40 (2007) 529–546.
- [67] R. İnam, H. Mercan, E. Yılmaz, B. Uslu, Differential pulse polarographic determination of Co(II) using moxifloxacin, *J. Anal. Chem.* 62 (2007) 592–598.
- [68] R. Sharda, Pandey, Electrochemical behaviour of fourth-generation fluoroquinolone antibacterial drug moxifloxacin by DC polarography and cyclic voltammetry, *Int. J. Pharm. Pharm. Sci.* 4 (2012) 349–355.
- [69] M.Y. Salem, N.M. El-Guindi, H.K. Mikael, L.E.-S. Abd-El-Fattah, Stability indicating methods for the determination of some fluoroquinolones in the presence of their decarboxylated degradates, *Chem. Pharm. Bull.* 54 (2006) 1625–1632.
- [70] C. Andrija, J. Ratomir, J. Ljubinka, J.-S. Milena, D. Predrag, Determination of moxifloxacin in human plasma by derivative UV spectrophotometry in a micellar medium, *Can. J. Anal. Sci. Spectros.* 52 (2007) 343–350.
- [71] S.K. Motwani, S. Chopra, F.J. Ahmad, R.K. Khar, Validated spectrophotometric methods for the estimation of moxifloxacin in bulk and pharmaceutical formulations, *Spectrochim. Acta A Mol. Biomol. Spectrosc.* 68 (2007) 250–256.
- [72] M.-Q. Du, D. Li, Y. Yang, Determination of moxifloxacin chloride tablets by ultraviolet spectrophotometry, *Chin. J. Mod. Drug Appl.* 2 (2008) 6–7, [http://en.cnki.com.cn/Article\\_en/CJFDTotal-ZWYY200802003.htm](http://en.cnki.com.cn/Article_en/CJFDTotal-ZWYY200802003.htm), accessed date March 2013.
- [73] M. Misra, A.K. Misra, P. Zope, G.M. Panpalia, A.K. Dorle, Simple and validated UV-spectroscopic method for estimation of moxifloxacin HCl in Bulk and formulation, *J. Global Pharm. Technol.* 2 (2010) 21–27.
- [74] D. Vandana, A.K. Chaudhary, A novel and validated UV-spectrophotometric method for estimation of moxifloxacin hydrochloride in tablets, *Afr. J. Pharm. Sci. Pharm.* 1 (2010) 50–56.
- [75] S.K. Sahu, M.A. Azam, D. Sahu, M. Banarjee, Spectrophotometric estimation of moxifloxacin in bulk and its pharmaceutical formulations, *Pharmacology (online)* 2 (2010) 491–502.

- [76] D.M. Dhumal, A.A. Shirkhedkar, S.J. Surana, Quantitative determination of moxifloxacin hydrochloride in bulk and ophthalmic solution by UV-spectrophotometry and first order derivative using area under curve, *Der Pharmacia Lettre* 3 (2011) 453–456.
- [77] K.N. Tarkase, S.S. Admane, N.G. Sonkhede, S.R. Shejwal, Development and validation of UV-spectrophotometric methods for determination of moxifloxacin HCl in bulk and pharmaceutical formulations, *Der Pharma Chemica*. 4 (2012) 1180–1185.
- [78] R.K. Patel, R.R. Parmar, V.M. Patel, D.A. Shah, Method development and validation of cefixime and moxifloxacin in pharmaceutical dosage form By UV spectrophotometric method, *Int. J. Pharm. Res. Bio-Sci.* 2 (2012) 81–93.
- [79] P.J. Vyas, J.B. Dave, C.N. Patel, Simultaneous estimation of moxifloxacin HCl and bromfenac sodium in eye drops by spectrophotometric methods, *Int. J. Pharm. Sci. Res.* 3 (2012) 2137–2142.
- [80] A.N. Parmar, R.R. Parmar, V.M. Patel, D.A. Shah, The simultaneous estimation of moxifloxacin hydrochloride and bromfenac sodium in eye drops by UV, *J. Pharm. Sci. Biosci. Res.* 2 (2012) 36–39.
- [81] V.A. Sindhuja, M.M. Annapurna, Derivative spectrophotometric method for the determination of moxifloxacin in pharmaceutical formulations, 3rd Congr. on Bio-availability and bioequivalence, 2012, <http://www.omicsonline.org/0975-0851/0975-0851-S1.11-044.pdf>, accessed date March 2013.
- [82] J. Bhalani, K. Vadalia, Z.R. Dedania, Validated first and second order derivative UV spectrophotometric methods for simultaneous estimation of moxifloxacin hydrochloride and dexamethasone sodium phosphate in ophthalmic dosage form, *Invent. Rapid Pharm. Anal. Qual. Assur.* (2012), <http://inventi.in/Article/ppaqa/424/12.aspx>, accessed date March 2013.
- [83] R. Patel, S.K. Shrivastava, P. Bhandari, A. Patidar, Simultaneous estimation of moxifloxacin HCl and prednisolone acetate from eye drop formulation by Q analysis method, *Int. J. Pharm. Res. Dev.* 4 (2012) 118–122.
- [84] M.V. Attimarad, B.E. Al-Dhubiab, I.A. Alhaider, A.B. Nair, H.N. Sree, A.K. Mueen, Simultaneous determination of moxifloxacin and cefixime by first and ratio first derivative ultraviolet spectrophotometry, *Chem. Cent. J.* 6 (2012) 105, <http://journal.chemistrycentral.com/content/pdf/1752-153X-6-105.pdf>, accessed date March 2013.
- [85] C.K. Shah, D. Umalkar, K.S. Rajesh, Simultaneous spectrophotometric determination of cefixime and moxifloxacin in bulk drug and drug formulation by absorption ratio method, *Global Res. J. Pharm. Sci.* 1 (2012) 19–22.
- [86] H.-M. Zhu, H.-P. Xi, W.-Q. Gong, UV characteristic of  $\text{Al}^{(3+)}$ -moxifloxacin and determination of moxifloxacin tablets, *Chin. J. Health Lab. Technol.* (2009), [http://en.cnki.com.cn/Article\\_en/CJFDTOTAL-ZWJZ200909015.htm](http://en.cnki.com.cn/Article_en/CJFDTOTAL-ZWJZ200909015.htm), accessed date March 2013.
- [87] H. Xi, H. Xie, W. Gong, Ultraviolet characteristic of CTMAB- $\text{Al}^{(3+)}$ -MXFX and determination of moxifloxacin, *Health Sci.* (2010), [http://en.cnki.com.cn/Article\\_en/CJFDTOTAL-HNKX201002013.htm](http://en.cnki.com.cn/Article_en/CJFDTOTAL-HNKX201002013.htm), accessed date March 2013.
- [88] K.V.S.P. Rao, L.D. Srinivas, P. Ravikumar, P. Yesupadam, G. Prabhakar, A note on the estimation of moxifloxacin in bulk and pharmaceutical formulations by precipitation reagents, *E-J. Chem.* 3 (2006) 5–8.
- [89] S.M. Al-Ghannam, Atomic absorption spectroscopic, conductometric and colorimetric methods for determination of some fluoroquinolone antibacterials using ammonium reineckate, *Spectrochim. Acta A Mol. Biomol. Spectrosc.* 69 (2008) 1188–1194.

- [90] S.K. Sahu, M.A. Azam, D. Sahu, M. Banarjee, Visible spectrophotometric estimation of moxifloxacin in bulk and its pharmaceutical formulations, *Pharmacology (Online)* 3 (2011) 1223–1233.
- [91] L.M. Abdellaziz, M.M. Hosny, Development and validation of spectrophotometric, atomic absorption and kinetic methods for determination of moxifloxacin hydrochloride, *Anal. Chem. Insights* 6 (2011) 67–78.
- [92] A. Mahmood, A.H. Chaudhry, K.M. Ashfaq, T.A. Malik, R. Mahmood, Spectrophotometric determination of moxifloxacin HCl in pure and blood sample, *Am. J. PharmTech Res.* 2 (2012) 363–370.
- [93] J.A. Ocaña, F.J. Barragán, M. Callejón, Spectrofluorimetric determination of moxifloxacin in tablets, human urine and serum, *Analyst* 125 (2000) 2322–2325.
- [94] S.T. Ulu, Spectrofluorimetric determination of fluoroquinolones in pharmaceutical preparations, *Spectrochim. Acta A Mol. Biomol. Spectrosc.* 72 (2009) 138–143.
- [95] J. Shah, M.R. Jan, M.N. Khan Inayatullah, Micellar-enhanced spectrofluorometric quantification of moxifloxacin in pharmaceutical formulations, human urine and plasma samples, *Afr. J. Pharm. Pharm.* 5 (2011) 616–624.
- [96] M. Kamruzzaman, A. Al-Mahmud, S.H. Lee, D. Ragupathy, Y.H. Kim, S.-R. Park, S.H. Kim, Spectrofluorimetric study of the interaction between europium(III) and moxifloxacin in micellar solution and its analytical application, *Spectrochim. Acta A Mol. Biomol. Spectrosc.* 86 (2012) 375–380.
- [97] X. Wang, R. Feng, H. Zhao, S. Chen, X. Wang, S. Meng, The study of fluorescence properties about system of yttrium (III)-moxifloxacin ligand and its analytical application, *Anal. Lab.* (2005), [http://en.cnki.com.cn/Article\\_en/CJFDTOTAL-FXSY200501010.htm](http://en.cnki.com.cn/Article_en/CJFDTOTAL-FXSY200501010.htm), accessed date March 2013.
- [98] H.-P. Xi, Q. Meng, X.-H. Shi, Fluorescence resonance energy transfer quenching method for determination of moxifloxacin, *Phys. Test. Chem. Anal. B Chem. Anal.* (2011), [http://en.cnki.com.cn/Article\\_en/CJFDTOTAL-LHJH201110017.htm](http://en.cnki.com.cn/Article_en/CJFDTOTAL-LHJH201110017.htm), accessed date March 2013.
- [99] H.-Z. Cai, H.P. Xi, H.X. Guo, Fluorometric determination of moxifloxacin with calcein-congo red, *Chin J. Anal. Lab.* (2011) [http://en.cnki.com.cn/Article\\_en/CJFDTOTAL-FXSY201104023.htm](http://en.cnki.com.cn/Article_en/CJFDTOTAL-FXSY201104023.htm), accessed date March 2013.
- [100] J.A. Ocaña, F.J. Barragán, M. Callejón, F. De la Rosa, Application of lanthanide-sensitised chemiluminescence to the determination of levofloxacin, moxifloxacin and trovafloxacin in tablets, *Microchim. Acta* 144 (2004) 207–213.
- [101] M.M. Karim, C.W. Jeon, S.M. Wabaidur, H.Y. Chung, H.W. Park, S.O. Jin, S.H. Lee, Chemiluminescence determination of moxifloxacin using  $\text{Ru}(\text{bpy})_3^{2+}$ -Ce(IV) system, *Appl. Chem.* 11 (2007) 433–436.
- [102] S.H. Lee, G.E. Kim, S.M. Alam, M. Kang, J.H. Choi, T. Ferdous, Y.S. Suh, Flow-injection chemiluminescence determination of moxifloxacin using tris(2,2-bipyridyl) ruthenium(II)-Ce(IV) system, *Sens. Lett.* 9 (2011) 247–251.
- [103] S.A. Shah, I.S. Rathod, B.N. Suhagia, M.V. Baldaniya, High performance thin layer chromatographic method for estimation of moxifloxacin in tablet dosage form, *Indian J. Pharm. Sci* 67 (2005) 112–115.
- [104] S.K. Motwani, R.K. Khar, F.J. Ahmad, S. Chopra, K. Kohli, S. Talegaonkar, Application of a validated stability-indicating densitometric thin-layer chromatographic method to stress degradation studies on moxifloxacin, *Anal. Chim. Acta* 582 (2007) 75–82.
- [105] D. Vandana, A.K. Chaudhary, A validated HPTLC method for estimation of moxifloxacin hydrochloride in tablets, *Afr. J. Pharm. Sci. Pharm.* 1 (2010) 74–84.
- [106] U. Hubicka, B. Żuromska-Witek, J. Krzek, M. Walczak, M. Żylewski, Kinetic and thermodynamic studies of moxifloxacin hydrolysis in the presence and absence of metal ions in acidic solutions, *Acta Polon. Pharm. Drug Res.* 69 (2012) 821–831.

- [107] P.J. Vyas, J.B. Dave, C.N. Patel, Application of HPTLC and HPLC methods for the simultaneous determination of moxifloxacin HCl and bromfenac sodium in eye drops, *Invent. Rapid Pharm. Anal. Qual. Assur.* (2012) <http://www.inventi.in/Article/ppaqa/450/12.aspx>, accessed date March 2013.
- [108] H. Stass, A. Dalhoff, Determination of BAY 12-8039, a new 8-methoxyquinolone, in human body fluids by high-performance liquid chromatography with fluorescence detection using on-column focusing, *J. Chromatogr. B* 702 (1997) 163–174.
- [109] C.M. Tobin, J. Sunderland, L.O. White, A.P. MacGowan, D.S. Reeves, An isocratic high performance liquid chromatography (HPLC) assay for moxifloxacin, a new 8-methoxyquinolone, *J. Antimicrob. Chemother.* 42 (1998) 278–279.
- [110] J.-G. Möller, H. Stass, W. Mück, Advances in bioanalytical methodology used to characterise clinical pharmacokinetics of moxifloxacin, *Drugs* 2 (1999) 237–238.
- [111] H.M. Siefert, A. Domdey-Bette, H. Henninger, F. Hucke, C. Kohlsdorfer, H.H. Stass, Pharmacokinetics of the 8-methoxyquinolone, moxifloxacin: a comparison in humans and other mammalian species, *J. Antimicrob. Chemother.* 43 (1999) 69–76.
- [112] T. Lemoine, D. Breilh, D. Ducint, J. Dubrez, J. Jougon, J.F. Velly, M.C. Saux, Determination of moxifloxacin (BAY 12-8039) in plasma and lung tissue by high-performance liquid chromatography with ultraviolet detection using a fully automated extraction method with a new polymeric cartridge, *J. Chromatogr. B* 742 (2000) 247–254.
- [113] B.B. Ba, R. Etienne, D. Ducint, C. Quentin, M.-C. Saux, Determination of moxifloxacin in growth media by high-performance liquid chromatography, *J. Chromatogr. B* 754 (2001) 107–112.
- [114] K. Vishwanathan, M.G. Bartlett, J.T. Stewart, Determination of moxifloxacin in human plasma by liquid chromatography electrospray ionization tandem mass spectrometry, *J. Pharm. Biomed. Anal.* 30 (2002) 961–968.
- [115] B. Zhu, C.Q. Hu, S.J. Jiang, L.H. Yin, Determination of moxifloxacin preparations by high performance liquid chromatography, *Chin. J. Antibiot.* (2002) [http://en.cnki.com.cn/Article\\_en/CJFDTTotal-ZKSS200208004.htm](http://en.cnki.com.cn/Article_en/CJFDTTotal-ZKSS200208004.htm), accessed date March 2013.
- [116] H.A. Nguyen, J. Grellet, B.B. Ba, C. Quentin, M.-C. Saux, Simultaneous determination of levofloxacin, gatifloxacin and moxifloxacin in serum by liquid chromatography with column switching, *J. Chromatogr. B* 810 (2004) 77–83.
- [117] C.-L. Zhang, H.N. Charles, P.N. David, A reverse phase high performance liquid chromatographic assay for determination of moxifloxacin in special growth media, *Chin. Pharm. J.* (2004) [http://en.cnki.com.cn/Article\\_en/CJFDTTotal-ZGYX200409025.htm](http://en.cnki.com.cn/Article_en/CJFDTTotal-ZGYX200409025.htm), accessed date March 2013.
- [118] Y.R. Kumar, V.V.N.K.V.P. Raju, R.R. Kumar, S. Eswaraiah, K. Mukkanti, M.V. Suryanarayana, M.S. Reddy, Structural identification and characterization of impurities in moxifloxacin, *J. Pharm. Biomed. Anal.* 34 (2004) 1125–1129.
- [119] J.A. Ocaña, M.C. Mochón, F.J.B. de la Rosa, Simultaneous determination of cefepime and the quinolones garenoxacin, moxifloxacin and levofloxacin in human urine by HPLC-UV, *Microchim. Acta* 151 (2005) 39–45.
- [120] F.L.B. Guerra, C.S. Paim, M. Steppe, E.E.S. Schapoval, Biological assay and liquid chromatographic method for analysis of moxifloxacin in tablets, *J. AOAC Int.* 88 (2005) 1086–1092.
- [121] M. Ferdig, A. Kaleta, W. Buchberger, Improved liquid chromatographic determination of nine currently used (fluoro)quinolones with fluorescence and mass spectrometric detection for environmental samples, *J. Sep. Sci.* 28 (2005) 1448–1456.
- [122] A. Laban-Djurđević, M. Jelikić-Stankov, P. Djurđević, Optimization and validation of the direct HPLC method for the determination of moxifloxacin in plasma, *J. Chromatogr. B* 844 (2006) 104–111.

- [123] S. Schulte, T. Ackermann, N. Bertram, T. Sauerbruch, W.D. Paar, Determination of the newer quinolones levofloxacin and moxifloxacin in plasma by high-performance liquid chromatography with fluorescence detection, *J. Chromatogr. Sci.* 44 (2006) 205–208.
- [124] S. Esposito, S. Noviello, G. D'Errico, G. Motta, D. Passali, C. Aimoni, S. Pilucchi, S. Fallani, M.I. Cassetta, T. Mazzei, A. Novelli, Concentration of moxifloxacin in plasma and tonsillar tissue after multiple administration in adult patients, *J. Antimicrob. Chemother.* 57 (2006) 789–792.
- [125] K.P. Chan, K.O. Chu, W.W.-K. Lai, K.W. Choy, C.C. Wang, D.S.-C. Lam, C.P. Pang, Determination of ofloxacin and moxifloxacin and their penetration in human aqueous and vitreous humor by using high-performance liquid chromatography fluorescence detection, *Anal. Biochem.* 353 (2006) 30–36.
- [126] D. Huang, B. Zhang, B. Li, L. Ding, J. Qi, X. Zhao, Determination of 2 kinds of components in compound moxifloxacin nasal drops by HPLC, *Chin. Pharm* (2007) [http://en.cnki.com.cn/Article\\_en/CJFDTotals-ZGYA200713021.htm](http://en.cnki.com.cn/Article_en/CJFDTotals-ZGYA200713021.htm), accessed date March 2013.
- [127] D. He, J. Yu, Determination of moxifloxacin in human serum by RP-HPLC, *Chin. Pharm.* (2007), [http://en.cnki.com.cn/Article\\_en/CJFDTotals-ZGYA200732017.htm](http://en.cnki.com.cn/Article_en/CJFDTotals-ZGYA200732017.htm), accessed date March 2013.
- [128] S.T. Ulu, High-performance liquid chromatography assay for moxifloxacin: pharmacokinetics in human plasma, *J. Pharm. Biomed. Anal.* 43 (2007) 320–324.
- [129] N. Srinivas, L. Narasu, B.P. Shankar, R. Mullangi, Development and validation of a HPLC method for simultaneous quantitation of gatifloxacin, sparfloxacin and moxifloxacin using levofloxacin as internal standard in human plasma: application to a clinical pharmacokinetic study, *Biomed. Chromatogr.* 22 (2008) 1288–1295.
- [130] W. Li, C.-Q. Hu, Spectral correlation of high-performance liquid chromatography-diode array detection data from two independent chromatographic runs peak tracking in pharmaceutical impurity profiling, *J. Chromatogr. A* 1190 (2008) 141–149.
- [131] R.N. Rao, N. Venkateswarlu, R. Narsimha, Determination of antibiotics in aquatic environment by solid-phase extraction followed by liquid chromatography-electrospray ionization mass spectrometry, *J. Chromatogr. A* 1187 (2008) 151–164.
- [132] P. Djurdjevic, A. Ciric, A. Djurdjevic, M.J. Stankov, Optimization of separation and determination of moxifloxacin and its related substances by RP-HPLC, *J. Pharm. Biomed. Anal.* 50 (2009) 117–126.
- [133] J. De Smet, K. Boussery, K. Colpaert, P. De Sutter, P. De Paepe, J. Decruyenaere, J.V. Bocxlaer, Pharmacokinetics of fluoroquinolones in critical care patients: a bio-analytical HPLC method for the simultaneous quantification of ofloxacin, ciprofloxacin and moxifloxacin in human plasma, *J. Chromatogr. B* 877 (2009) 961–967.
- [134] D.J. Hutchinson, C.E. Johnson, K.C. Klein, Stability of extemporaneously prepared moxifloxacin oral suspensions, *Am. J. Health-Syst. Pharm.* 66 (2009) 665–667.
- [135] Y. Chen, J. Shi, M. Jin, Determination of concentration of moxifloxacin in human serum by high-performance liquid chromatography coupled with ion trap mass spectrometry, *Chin. J. Clin. Pharm* (2009) [http://en.cnki.com.cn/Article\\_en/CJFDTotals-LCZZ200906008.htm](http://en.cnki.com.cn/Article_en/CJFDTotals-LCZZ200906008.htm), accessed date March 2013.
- [136] D.Q. Huang, F.H. Yi, Determination of moxifloxacin hydrochloride and dexamethasone acetate in compound moxifloxacin ear drops by HPLC, *West Chin. J. Pharm. Sci* (2009), [http://en.cnki.com.cn/Article\\_en/CJFDTotals-HXYO200902034.htm](http://en.cnki.com.cn/Article_en/CJFDTotals-HXYO200902034.htm), accessed date March 2013.
- [137] A.K.H. Kumar, G. Ramachandran, Simple and rapid liquid chromatography method for determination of moxifloxacin in plasma, *J. Chromatogr. B* 877 (2009) 1205–1208.
- [138] N. Sultana, M.S. Arayne, M. Akhtar, S. Shamim, S. Gul, M.M. Khan, High-performance liquid chromatography assay for moxifloxacin in bulk, pharmaceutical

- formulations and serum: application to in-vitro metal interactions, *J. Chin. Chem. Soc.* 57 (2010) 708–717.
- [139] A.D. Pranger, J.-W.C. Alfenaar, A.M.A. Wessels, B. Greijdanus, D.R.A. Uges, Determination of moxifloxacin in human plasma, plasma ultrafiltrate, and cerebrospinal fluid by a rapid and simple liquid chromatography-tandem mass spectrometry method, *J. Anal. Toxicol.* 34 (2010) 135–141.
- [140] K.M. Venkatachari, C. Saravanan, R. Subbaiah, B. Jayakar, Method development and validation for estimation of moxifloxacin HCl in tablet dosage Form by RP-HPLC method, *Int. Res. J. Pharm.* 1 (2010) 333–336.
- [141] Y.H. Xu, D. Li, X.Y. Liu, Y.Z. Li, J. Lu, High performance liquid chromatography assay with ultraviolet detection for moxifloxacin: validation and application to a pharmacokinetic study in Chinese volunteers, *J. Chromatogr. B* 878 (2010) 3437–3441.
- [142] L.T. Davis, N. Kumar, L.M. Nijm, L.J. Ulanski II, E.Y. Tu, R.G. Fiscella, R.J. Peterson, R.D. Glickman, An adaptable HPLC method for the analysis of frequently used antibiotics in ocular samples, *J. Chromatogr. B* 878 (2010) 2421–2426.
- [143] M. Sher, M.A. Hussain, S. Jahan, A.R. Mufti, M.A. Shaheen, M.N. Hassan, S. Bashir, Bioequivalence of two oral formulations of moxifloxacin and its analytical study by HPLC-UV method, *Pak. J. Sci.* 62 (2010) 84–88.
- [144] J. Zhu, X. Kan, D. Lou, J. Dong, G. Hu, Determination of moxifloxacin in rat plasma by HPLC and its application in pharmacokinetic study, *Zhongguo Xiandai Yingyong Yaxue (Chin. J. Mod. Appl. Pharm.)* 28 (2011) 759–762.
- [145] A.K.H. Kumar, V. Sudha, R. Srinivasan, G. Ramachandran, Simple and rapid liquid chromatography method for determination of moxifloxacin in saliva, *J. Chromatogr. B* 879 (2011) 3663–3667.
- [146] A.P. Dewani, B.B. Barik, S.K. Kanungo, B.R. Wattyani, A.V. Chandewar, Development and validation of RP-HPLC method for the determination of moxifloxacin in presence of its degradation products, *Am. Eurasian J. Sci. Res.* 6 (2011) 192–200.
- [147] N. Sultana, M. Akhtar, S. Shamim, S. Gul, M.S. Arayne, Simultaneous determination of moxifloxacin and H<sub>2</sub> receptor antagonist in pharmaceutical dosage formulations by RP-HPLC: application to in vitro drug interactions, *Quim. Nova* 34 (2011) 683–688.
- [148] G. Lin, G. Zhu, Z. Wang, X. Cui, X. Lin, Determination of moxifloxacin concentration in human plasma by RP-HPLC, *Chin. Pharm* (2011), [http://en.cnki.com.cn/Article\\_en/CJFDTotat-YYGZ201122026.htm](http://en.cnki.com.cn/Article_en/CJFDTotat-YYGZ201122026.htm), accessed date March 2013.
- [149] X.V. Doorslaer, K. Demeestere, P.M. Heynderickx, H.V. Langenhove, J. Dewulf, UV-A and UV-C induced photolytic and photocatalytic degradation of aqueous ciprofloxacin and moxifloxacin: reaction kinetics and role of adsorption, *Appl. Catal. B* 101 (2011) 540–547.
- [150] X. Yang, Q. Liu, X. Ding, Y. Li, HPLC assay of R-isomer in moxifloxacin hydrochloride, *Yaowu Fenxi Zazhi (Chin. J. Pharm. Anal.)* 32 (2012) 92–94.
- [151] C.M. Modi, S.K. Mody, H.B. Patel, Disposition kinetics of long acting moxifloxacin following intravenous administration in sheep, *Vet. World* 5 (2012) 517–521.
- [152] M. Sturini, A. Speltini, F. Maraschi, A. Profumo, L. Pretali, E.A. Irastorza, E. Fasani, A. Albini, Photolytic and photocatalytic degradation of fluoroquinolones in untreated river water under natural sunlight, *Appl. Catal. B* 119–120 (2012) 32–39.
- [153] S.K. Pankaja, M.S. Niranjana, K.C. Chaluvajru, C.E. Rajendra, Method development and validation for simultaneous estimation of moxifloxacin hydrochloride and ornidazole by RP-HPLC, *Int. J. Pharm. Res. Dev.* 4 (2012) 129–134.
- [154] C.K. Shah, D. Umalkar, K.S. Rajesh, Development of an RP-HPLC method for simultaneous estimation and force degradation of cefixime and moxifloxacin in bulk and pharmaceutical dosage form, *Int. J. Pharm. Res. Bio-Sci.* 1 (2012) 128–147.



- [155] R. Respaud, S. Grayo, E. Singlas, S. Dubouch, A. Le Monnier, M.-C. Lott, High-performance liquid chromatography assay for moxifloxacin in brain tissue and plasma: validation in a pharmacokinetic study in a murine model of cerebral listeriosis. *J. Anal. Methods Chem* (2012), <http://dx.doi.org/10.1155/2012/436349>, accessed date March 2013.
- [156] S.N. Razzaq, I.U. Khan, M. Ashfaq, I. Mariam, Stability indicating HPLC method for simultaneous determination of moxifloxacin hydrochloride and ketorolac tromethamine in pharmaceutical formulations, *Quim. Nova* 35 (2012) 1216–1221.
- [157] H. Ogino, K. Kido, M. Tsuchiya, J. Kizu, S. Hori, Simple determination of fluoroquinolones with high-performance liquid chromatography, *Nippon Kagaku Ryoho Gakkai Zasshi* (Jap. J. Chemother.) 53 (2005) 619–622.
- [158] C. Chamseddin, T. Jira, Comparison of the chromatographic behavior of levofloxacin, ciprofloxacin and moxifloxacin on various HPLC phases, *Pharmazie* 66 (2011) 244–248.
- [159] L. Li, W. Shi, T.-F. Chen, S.-X. Liu, Determination of moxifloxacin in human of pulse high volume hemofiltration serum urine and displacement liquid, *J. Prac. Med.* (2011) [http://en.cnki.com.cn/Article\\_en/CJFDTotal-SYYZ201111008.htm](http://en.cnki.com.cn/Article_en/CJFDTotal-SYYZ201111008.htm), accessed date March 2013.
- [160] U. Hubicka, J. Krzek, B. Żurowska, M. Walczak, M. Żylewski, D. Pawłowski, Determination of photostability and photodegradation products of moxifloxacin in the presence of metal ions in solutions and solid phase. Kinetics and identification of photoproducts, *Photochem. Photobiol. Sci.* 11 (2012) 351–357.
- [161] M. Ibáñez, C. Guerrero, J.V. Sancho, F. Hernández, Screening of antibiotics in surface and wastewater samples by ultra-high-pressure liquid chromatography coupled to hybrid quadrupole time-of-flight mass spectrometry, *J. Chromatogr. A* 1216 (2009) 2529–2539.
- [162] G.K. Jain, N. Jain, S.A. Pathan, S. Akhter, S. Talegaonkar, P. Chander, R.K. Khar, F.J. Ahmad, Ultra high-pressure liquid chromatographic assay of moxifloxacin in rabbit aqueous humor after topical instillation of moxifloxacin nanoparticles, *J. Pharm. Biomed. Anal.* 52 (2010) 110–113.
- [163] G.N.K. Reddy, V.V.S.R. Prasad, N.J. Maiti, D. Nayak, P.K. Maharana, Development and validation of a stability indicating UPLC method for determination of moxifloxacin hydrochloride in pharmaceutical formulations, *Pharm. Anal. Acta* 2 (142) (2011), [org/10.4172/2153-2435.1000142](http://en.cnki.com.cn/Article_en/CJFDTOTAL-LHJH201106007.htm).
- [164] J.-H. Zhao, W.-F. Wu, X.P. Zheng, Y. Zheng, J. Lin, C. Yu, J.-H. Zhang, Simultaneous UHPLC-MS/MS determination of gatifloxacin, moxifloxacin and levofloxacin in aquatic products, physical testing and chemical analysis, *Chem. Anal. B* (2011), [http://en.cnki.com.cn/Article\\_en/CJFDTOTAL-LHJH201106007.htm](http://en.cnki.com.cn/Article_en/CJFDTOTAL-LHJH201106007.htm), Accessed date March 2103 (Summary in English form SciFinder®).
- [165] M.H. Warsi, G.K. Jain, S.A. Pathan, M. Anwar, N. Mallick, N. Ahmad, S. Talegaonkar, F.J. Ahmad, R.K. Khar, UPLC/Q-TOF-MS/MS method for evaluation of moxifloxacin loaded nanoplexes as vehicles for ocular drug delivery, *J. Liq. Chromatogr. Related Technol.* 35 (2012) 1826–1841.
- [166] J.-G. Möller, H. Staß, R. Heinig, G. Blaschke, Capillary electrophoresis with laser-induced fluorescence: a routine method to determine moxifloxacin in human body fluids in very small sample volumes, *J. Chromatogr. B* 716 (1998) 325–334.
- [167] Y. Fan, Z. Tian, W. Qin, Quick and sensitive determination of fluoroquinolones by capillary electrophoresis–potential gradient detection, *Anal. Lett.* 42 (2009) 1057–1069.



- [168] Z. Yang, W. Qin, Separation of fluoroquinolones in acidic buffer by capillary electrophoresis with contactless conductivity detection, *J. Chromatogr. A* 1216 (2009) 5327–5332.
- [169] H. Stass, A. Dalhoff, D. Kubitz, U. Schühly, Pharmacokinetics, safety, and tolerability of ascending single doses of moxifloxacin, a new 8-methoxy quinolone, administered to healthy subjects, *Antimicrob. Agents Chemother.* 42 (1998) 2060–2065.
- [170] G. Ruckdeschel, A. Dalhoff, The in-vivo activity of moxifloxacin against *Legionella* species and the effect of medium on susceptibility test results, *J. Antimicrob. Chemother.* 43 (1999) 25–29.
- [171] A.P. MacGowan, K.E. Bowker, M. Wootton, H.A. Holt, Exploration of the in-vitro pharmacodynamic activity of moxifloxacin for *Staphylococcus aureus* and *Streptococci* of lancefield groups A and B, *J. Antimicrob. Chemother.* 44 (1999) 761–766.
- [172] V. Rodriguez-Cerrato, C.C. McCoig, I.C. Michelow, F. Ghaffar, H.S. Jafri, R.D. Hardy, C. Patel, K. Olsen, G.H. Mccracken, Pharmacodynamics and bactericidal activity of moxifloxacin in experimental *Escherichia coli* meningitis, *Antimicrob. Agents Chemother.* 45 (2001) 3092–3097.
- [173] J. Sunderland, C.M. Tobin, A.J. Hedges, A.P. MacGowan, L.O. White, Antimicrobial activity of fluoroquinolone photodegradation products determined by parallel-line bioassay and high performance liquid chromatography, *J. Antimicrob. Chemother.* 47 (2001) 271–275.
- [174] G.P. Allen, G.W. Kaatz, M.J. Rybak, Activities of mutant prevention concentration-targeted moxifloxacin and levofloxacin against *Streptococcus pneumoniae* in an in vitro pharmacodynamic model, *Antimicrob. Agents Chemother.* 47 (2003) 2606–2614.
- [175] J. Strahilevitz, A. Lev, I. Levi, E. Fridman, E. Rubinstein, Experimental pneumococcal pleural empyema model: the effect of moxifloxacin, *J. Antimicrob. Chemother.* 51 (2003) 665–669.
- [176] M.L. Devi, K.B. Chandrasekhar, A validated, specific stability-indicating RP-LC method for moxifloxacin and its related substances, *Chromatographia* 69 (2009) 993–999.
- [177] M. Misra, A.K. Misra, G.M. Panpalia, A.K. Dorle, Compatibility screening of some diluents with newer fluoroquinolone: moxifloxacin HCl, *Int. J. Pharm. Res. Innovation* 2 (2011) 9–17.
- [178] P.K. Pawar, R. Katara, D.K. Majumdar, Design and evaluation of moxifloxacin hydrochloride ocular inserts, *Acta Pharm.* 62 (2012) 93–104.
- [179] P. Bosché, H.F. Mahler, C. Weisemann, Pharmaceutical moxifloxacin preparation, United States Patent US6610327, 2003.
- [180] E. Fernández-Varón, P. Marín, A. Espuny, L. Villamayor, E. Escudero, C. Cárcelos, Stability of moxifloxacin injection in peritoneal dialysis solution bags (Dianeal PD1 1.36%® and Dianeal PD1 3.86%®), *J. Clin. Pharm. Therap* 31 (2006) 641–643.
- [181] M. Palumbo, B. Gatto, G. Zagotto, G. Palú, On the mechanism of action of quinolone drugs, *Trends Microbiol.* 1 (1993) 232–235.
- [182] A. Uzunović, E. Vranić, Influence of type and neutralisation capacity of antiacids on dissolution rate of ciprofloxacin and moxifloxacin from tablets, *Bosn. J. Basic Med. Sci.* 9 (2009) 89–93.
- [183] P. Djurdjević, R. Jelić, L. Joksović, I. Lazarević, M. Jelikić-Stankov, Study of solution equilibria between gadolinium (III) ion and moxifloxacin, *Acta Chim. Slov.* 57 (2010) 386–397.
- [184] M. Imran, T. Kokab, S. Latif, M. Llvui, Z. Mahmood, Synthesis, characterization and in vitro antibacterial studies of ternary complexes using quinolone antibiotics as primary ligand, *J. Chem. Soc. Pak.* 32 (2010) 223–228.
- [185] CMPH/EMA Opinion on Avelox® and Associated Names INN: Moxifloxacin, Background Information, 2008.

- [186] CDER. Approval Letter (NDA 21-085) to Bayer Corporation, Rockville, Maryland, December 10, 1999.
- [187] CHMP/EMA Opinion on Avelox<sup>®</sup> and Associated Names - Annex III: Summary of Product Characteristics, London, October 13, 2008.
- [188] Avelox<sup>®</sup> Full Prescribing Information. Bayer HealthCare Pharmaceuticals Inc., Wayne, NJ, U.S.A. Reference ID: 3180115, August, 2012.
- [189] CDER. Approval Letter (NDA 21-598) to AlconInc, Rockville, Maryland, April 15, 2003.
- [190] Vigamox Label. Alcon, Inc., Fort Worth, TX, U.S.A. Reference ID: 3025484, 2011.
- [191] H. Stass, Absorption and bioavailability of moxifloxacin, *Drugs* 58 (1999) 227-228.
- [192] J.A.B. Balfour, L.R. Wiseman, Moxifloxacin, *Drugs* 57 (1999) 363-373.
- [193] H. Stass, D. Kubitz, Basic pharmacokinetics of moxifloxacin, *Drugs* 58 (1999) 225-226.
- [194] R. Lindstrom, S. Lane, S.A. Cottingham, S. Smith, K. Sall, L. Shettle Silverstein, T. Walters, R. Faulkner, P. Cockrum, N. Teuscher, Conjunctival concentrations of a new ophthalmic solution formulation of moxifloxacin 0.5% in cataract surgery patients, *J. Ocul. Pharmacol. Therap.* 26 (2010) 591-595.
- [195] H. Stass, Distribution and tissue penetration of moxifloxacin, *Drugs* 58 (1999) 229-230.
- [196] H. Stass, Metabolism and excretion of moxifloxacin, *Drugs* 58 (1999) 231-232.
- [197] J.A. Balfour, H.M. Lamb, Moxifloxacin: a review of its clinical potential in the management of community-acquired respiratory tract infections, *Drugs* 59 (2000) 115-139.
- [198] W.A. Petri, Chapter 52: sulfonamides, trimethoprim-sulfamethoxazole, quinolones, and agents for urinary tract infections, in: B.A. Chabner, B.C. Knollmann, L.L. Brunton (Eds.), *The Pharmacological Basis of Therapeutics*, 12th ed., Goodman & Gilman's, New York, 2011.



# Pravastatin Sodium

**Abdullah A. Al-Badr, Gamal A.E. Mostafa**

Department of Pharmaceutical Chemistry, College of Pharmacy, King Saud University, P.O. Box 2457, Riyadh, Kingdom of Saudi Arabia

## Contents

1. Description	434
1.1 Nomenclature	434
1.2 Formulae	435
1.3 Elemental analysis	435
1.4 Solubility	435
1.5 Appearance	436
1.6 Partition coefficient	436
2. Uses and Applications	436
3. Methods of Preparation	436
4. Physical Characteristics	447
4.1 X-ray powder diffraction	447
4.2 Thermal methods of analysis	448
4.3 Ultraviolet spectroscopy	448
4.4 Vibrational spectroscopy	448
4.5 Nuclear magnetic resonance spectrometry	452
4.6 Mass spectrometry	454
5. Methods of Analysis	456
5.1 Compendial methods	456
5.2 Spectrophotometric methods	474
5.3 Electrochemical methods	476
5.4 Chromatographic methods	477
5.5 Immunoassay methods	497
6. Pharmacokinetics	499
7. Metabolism	501
8. Stability	505
9. Reviews	506
Acknowledgments	506
References	506



## 1. DESCRIPTION

### 1.1. Nomenclature

#### 1.1.1 Systematic chemical names

- 3 $\beta$ -Hydroxycompactin sodium.
- $\beta R, \delta R, 1S, 2S, 6S, 8S, 8aR$ )-1,2,6,7,8,8a-Hexahydro- $\beta, \delta, 6$ -trihydroxy-2-methyl-8-[(2S)-2-methyl-1-oxobutoxy]-1-naphthaleneheptanoic acid.
- Sodium (+)-(3R,5R)-3,5-dihydroxy-7-[(1S,2S,6S,8S,8aR)-6-hydroxy-2-methyl-8-[(S)-2-methylbutyryloxy]-1,2,6,7,8,8a-hexahydro-1-naphthyl]heptanoate.
- Sodium(+)(3R,5R)-3,5-dihydroxy-7-{(1S,2S,6S,8S,8aR)-6-hydroxy-2-methyl-8-[(S)-2-methylbutyryloxy]-1,2,6,7,8,8a-hexahydro-1-naphthyl}heptanoate.
- 1-Naphthalene heptanoic acid, 1,2,6,7,8,8a-hexahydro- $\beta, \delta, 6$ -trihydroxy-2-methyl-8-(2-methyl-1-oxobutoxy)-, monosodium salt, [1S-[1 $\alpha$ ( $\beta S^*$ ,- $\delta S^*$ )-2 $\alpha, 6\alpha, 8\beta$ ( $R^*$ ),8a $\alpha$ ]].
- [1S-[1 $\alpha$ ( $\beta S^*, \delta S^*$ ),2 $\alpha, 6\alpha, 8\beta$ -( $R^*$ ),8a $\alpha$ ]]-1,2,6,7,8,8a-Hexahydro- $\beta, \delta, 6$ -trihydroxy-2-methyl-8-(2-methyl,1-oxobutoxy)-1-naphthalene heptanoic acid monosodium salt.
- (3R,5R)-7-[(1S,2S,6S,8S,8aR)]-1,2,6,7,8,8a-hexahydro-6-hydroxy-2-methyl-8-[(S)-2-methylbutyryloxy-1-naphthyl]-3,5-dihydroxyheptanoate.
- Sodium (+)-(3R,5R)-3,5-dihydroxy-7-{(1'S,2'S,6'S,8'S,8'aR)-6'-hydroxy-2'-methyl-8'-[(S)-2-methylbutyryloxy]-1',2'-6'-7'-8',8'a-hexahydro-1'-naphthyl}heptanoate.
- Sodium (+)( $\beta R, \delta R, 1S, 2S, 6S, 8S, 8aR$ )-1,2,6,7,8,8a-hexahydro- $\beta, \delta, 6, 8$ -tetrahydroxy-2-methyl-1-naphthalene heptanoate, 8[(2S)-2-methylbutyrate].
- 1,2,6,7,8,8a-Hexahydro-6-hydroxy-2-methyl-8-((2-methylbutyryloxy)-1-naphthyl)-3,5-dihydroxynaphthoate [1-3].

#### 1.1.2 Nonproprietary names

Pravastatin sodium; Pravastatina; Pravastatine; Pravastatinum; Eptastatin sodium, CS 514, SQ-31000 [1-3].

#### 1.1.3 Proprietary names

Aplactin, Bristacol, Compactin, Elisor, Lipemol, Liplat, Lipostat, Liprevil, Mevalotin, Mevastatin, Mevinolin, Oliprevin, Pralidon, Praredut, Prasterol,

Prava, Pravachol, Pravacol, Pravaselect, Pravasin, Pravasine, Sanaprav, Selectin, Selectine, Selipran, Vasten [1–3].

## 1.2. Formulae

### 1.2.1 Empirical formula, molecular weight, CAS-number [1]

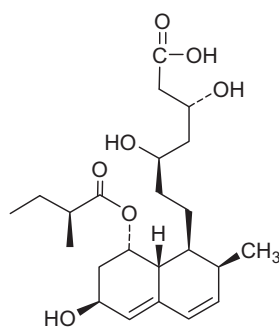
Pravastatin

$C_{23}H_{36}O_7$	425.5	[81093-37-0]
-------------------	-------	--------------

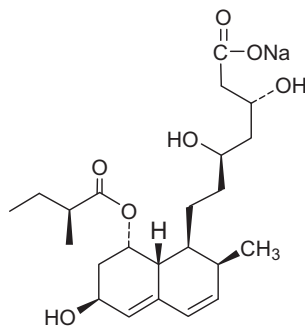
Pravastatin sodium

$C_{23}H_{35}O_7 Na$	446.52	[81131-70-6]
----------------------	--------	--------------

### 1.2.2 Structural formula [1]



Pravastatin



Pravastatin sodium

## 1.3. Elemental analysis

Pravastatin [1]

C 65.07 %	H 8.55%	O 26.38%
-----------	---------	----------

Pravastatin sodium [1]

C 61.87%	H 7.90%	O 25.08%	Na 5.15%
----------	---------	----------	----------

## 1.4. Solubility

Pravastatin is freely soluble in water and methanol, relatively insoluble in chloroform, ether, acetone and acetonitrile [1–3].

## 1.5. Appearance

Pravastatin sodium is a hygroscopic white to off-white crystalline powder. Pravastatin lactone is colorless plate-like crystal [1–3].

## 1.6. Partition coefficient

Log *P* (octanol/water), −0.23 (pravastatin sodium) [3].



## 2. USES AND APPLICATIONS

Pravastatin, 3-hydroxy-3-methylglutaryl coenzyme A (HMG-CoA) reductase inhibitor (a statin), is a lipid-regulating drug with actions on plasma lipids similar to those of simvastatin. Pravastatin is used in the treatment of hypercholesterolemia, particularly in the types IIa and IIb hyperlipoproteinemias. It is also given prophylactically in hypercholesterolemic patients for both primary and secondary prevention of ischemic heart disease. It is also used in patients with a previous myocardial infarction to reduce the risk of stroke. Pravastatin is given by mouth as the sodium salt in usual doses of 10–40 mg once daily at bedtime. The dose may be adjusted at intervals of not less than 4 weeks [2].



## 3. METHODS OF PREPARATION

Terahara *et al.* [4,5] isolated pravastatin as a metabolite of compactin through enzymatic hydroxylation by means of microorganisms.

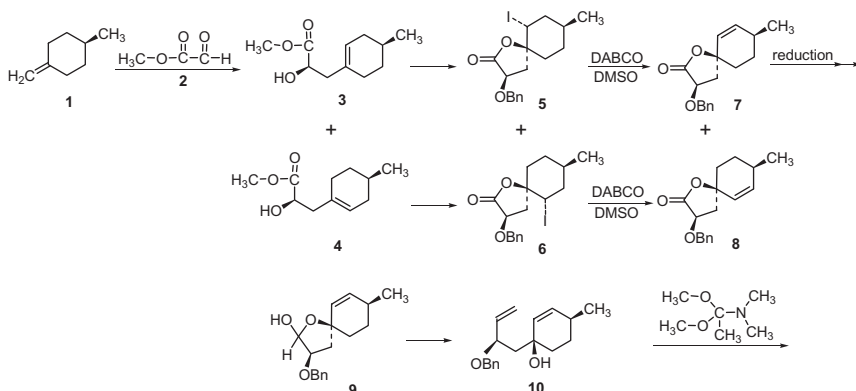
Daniewski *et al.* [6] described the following total synthesis of pravastatin:

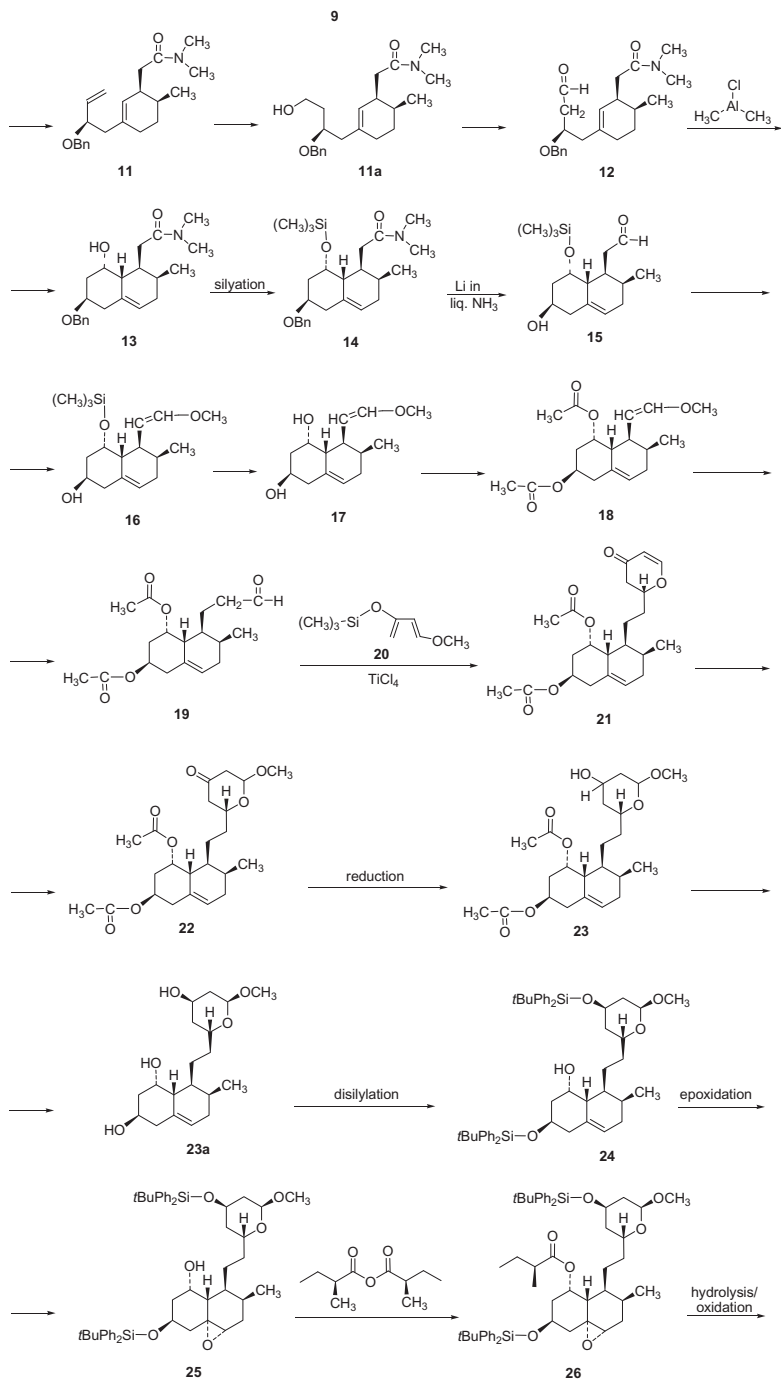
1-Methyl-4-methylenecyclohexane **1** reacted with methyl glyoxylate **2** to form an inseparable mixture of two diastereomers **3** and **4** in 68:32 ratio in 72% yield. Without separation, the mixture **3** and **4** was carried through benzylation of the hydroxyl group (80%), hydrolysis and iodolactonization to **5** and **6** (82% yield) followed by dehydroiodination with 1,4-diazabicyclo [2,2,2]-octane (DABCO) in DMSO (99%) to give **7** and **8** as a chromatographically separable mixture. The lactone **7** was reduced to the lactol **9** followed by Wittig methylenation to give **10** (75% yield for the two steps). Heating compound **10** with the dimethyl acetal of *N,N*-dimethylacetamide produced the amide **11** in 92% yield. Hydroboration and oxidation provided the aldehyde **12**. While the intramolecular ene reaction of **12** with dimethyl aluminum chloride produced the desired ene product **13**

regioselectively and stereospecifically, it was accompanied by substantial amount of simple methyl addition to the aldehyde. Silylation of **13–14** followed by the simultaneous benzyl group cleavage and amide reduction with lithium in liquid ammonia produced hydroxy aldehyde **15** (64%). The one-carbon extension was accomplished by methoxy methylenation of the aldehyde **15**, and the subsequent conversions under standard conditions **16–19** to give the required acetoxy aldehyde **19** in good overall yield.

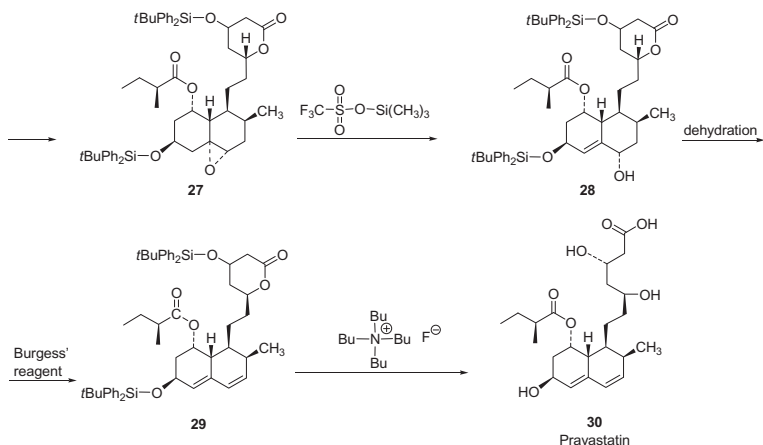
The reaction of **19** with the diene **20** catalyzed with  $\text{TiCl}_4$  produced, after acidity workup, the desired enone **21** in 62% yield accompanied by its diastereomer in 92:8 ratio. Without separation, this mixture **21** was allowed to undergo the 1,4 addition of methanol in the presence of trimethylamine and gave, after purification, acetal **22** in 66% yield. Stereoselective reduction with tri-*sec*-butylborohydride gave alcohol **23** (86%), which after removal of the acetate groups **23a** and regioselective desilylation provided alcohol **24**. The stereospecific hydroxyl-assisted epoxidation of alcohol **24** provided, as required for the diene formation epoxide **25** which was esterified directly with (*S*)-2-methylbutyric anhydride to give **26** in excellent overall yield. Hydrolysis and concomitant oxidation of the acetal **26**, accomplished in one operation with chromium trioxide in methylene chloride/aqueous acetic acid, afforded lactone **27**.

The epoxide to diene transformation was effected smoothly by two-stage protocol involving elimination of the epoxide to the allylic alcohol **28** with trimethylsilyl triflate followed by dehydration with Burgess' reagent to give the silylated pravastatin derivative **29**. Final desilylation of this acid-sensitive diene ether with buffered tetrabutylammonium fluoride produced pravastatin **30**.

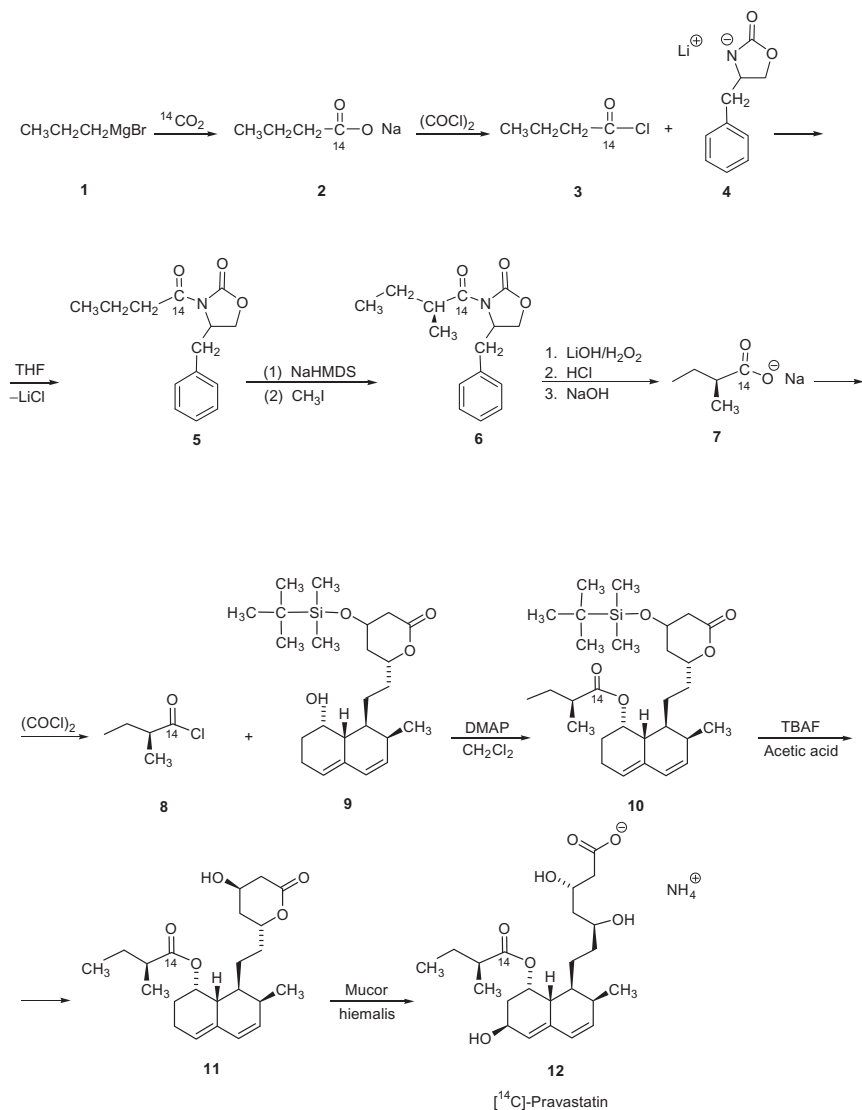






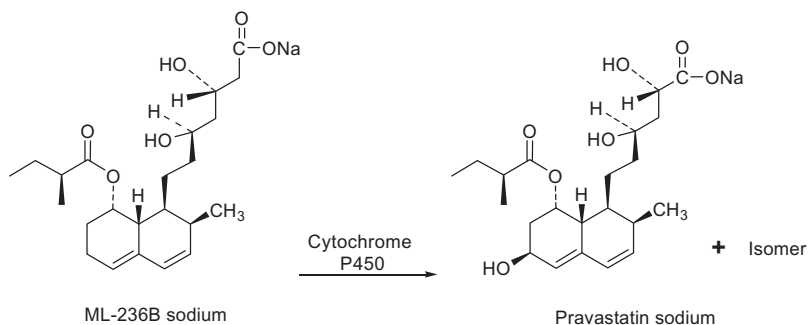


Wallace *et al.* [7] outlined a method for the synthesis of [ $^{14}\text{C}$ ]-labeled pravastatin. Reaction of propyl magnesium bromide **1** with  $^{14}\text{CO}_2$  gives [ $^{14}\text{C}$ ]-butyric acid sodium salt **2**, which was converted to the corresponding acyl chloride **3** by reaction with oxalyl chloride. The condensation of compound **3** with 4(*S*)-benzyloxazolidin-2-one **4** in THF yields the corresponding acylation product **5**, which is methylated with sodium hexamethyldisilazide (NaHMDS) and methyl iodide to afford a mixture of tautomeric *N*-4(*S*)-benzyl-3-[2-(*R* and *S*)-methylbutyryl]oxazolidin-2-ones, which are separated by preparative high-performance liquid chromatography (HPLC) to obtain the optically pure diastereomer **6**. The oxidative cleavage of compound **6** with  $\text{H}_2\text{O}_2$  and LiOH, followed by acidification and treatment with sodium hydroxide, yields sodium 2(*S*) methylbutyrate **7**, which is treated with oxalyl chloride to afford the corresponding acyl chloride **8**. The condensation of compound **8** with 4(*R*)-(*tert*-butyldimethylsilyloxy)-6(*R*)-[2-[8(*S*)-hydroxy-2(*S*)-methyl-1,2,6,7,8,8*a*(*R*)-hexahydronaphth-1(*S*)-yl]ethyl]-tetrahydropyran-2-one **9** by means of 4-dimethylamino-pyridine (DMAP) in methylene dichloride give the esterified compound **10**, which is deprotected with tetrabutylammonium fluoride (TBAF) in acetic acid, yielding the hydroxylated pyrone **11**. Finally, this compound is submitted to an asymmetric hydroxylation with a culture broth of *Mucor hiemalis* MF-5021. The final product **12** is extracted from the culture broth and purified by preparative HPLC to give a final radiochemical purity of 95% of [ $^{14}\text{C}$ ]-pravastatin.



Matsuoka *et al.* [8] used cytochrome P450 enzymes for preparing pravastatin and other related hydroxylated compounds from ML-236B sodium.

Emonds [9] used a novel and versatile approach to the total asymmetric total synthesis of pravastatin. The method is based on the annulation of



chiral cyclohexenones. Both 5-(trimethylsilyl)cyclohex-2-en-1-one and 5-(dimethylphenylsilyl)cyclohex-2-en-1-one could be stereospecifically annulated. 5-(Dimethylphenylsilyl)cyclohex-2-en-1-one is the new cyclohexanone synthon specifically developed for this study. The four-step annulation methods, consisting of a conjugate addition of a (tributylstannyl)vinyl cuprate, side-chain extension via a Stille coupling, cyclopropanation, and cyclization, led to the production of bicyclo[4.4.0]decene systems, which were ideally set up for further elaboration in the mevinic acids. The one chiral center of the cyclohexenone directed the four additional chiral centers with essentially complete diastereoselectivity. Variations in the structure of the cyclization precursor and in the amount of the fluoride used to induce cyclization caused wide and reproducible variation in the type and amounts of product formed. One annulation product was transformed in a single step into an extremely versatile enone synthon to be used to synthesize a wide variety of mevinic analogs. As a demonstration of the usefulness of this methodology, the enone synthon was transformed into a known precursor of a dihydropravastatin analog.

Narula *et al.* [10] prepared the sodium salt of pravastatin from its lactone form according to the following procedure: Five grams of the lactone form of pravastatin, isolated as a crude product from fermentation broth of a species of *Streptomyces*, is suspended in 15 ml of methanol:water (1:2) mixture containing about 3% (w/v) sodium hydroxide. The reaction mixture is warmed to 35 °C and stirred for 40–60 min until the hydrolysis is complete. The pH of the solution is adjusted to pH 4 using concentrated hydrochloric acid. The hydroxy acid form of pravastatin is extracted in ethyl acetate by stirring for 20–30 min and dried over anhydrous sodium sulfate. Stoichiometric quantity of sodium 2-ethyl hexanoate is added to the ethyl acetate layer and stirred gently at room temperature for 2 h until the precipitate of sodium salt of pravastatin appears. The slurry is cooled to 5–10 °C, further

stirred for 60 min, and the product is filtered, washed, and dried to afford about 2.8 g of pravastatin sodium salt as a dry powder.

Lee *et al.* [11] prepared pravastatin from new saccharothrix isolates by fermentation of saccharothrix (18–48 h) under the presence of compactin (1–2 g). The process of production of pravastatin using saccharothrix isolates is provided.

Abe [12] provided a DNA sequence of a gene cluster from *Penicillium citrinum*. The gene cluster can be used for the biosynthesis of pravastatin precursor, compactin.

Kumar *et al.* [13] prepared pure pravastatin by microbial hydroxylation of compactin. The microorganism is species of the genus *Streptomyces*, such as *Streptomyces carbophilus*. The conditions capable of converting compactin to pravastatin include the fermentation production medium containing glucose at a concentration level of about 15–25 g/l, Soya bean meal, cotton seed meal, corn steep liquor, sodium chloride, and calcium carbonate at a certain concentration levels. The conditions also include the maintenance of temperature at about 18–50 °C and pH from 5 to 10.

Jekkel *et al.* [14] used a new microbial process: *Mortierella maculata* for the preparation of pravastatin sodium from compactin sodium.

Mei *et al.* [15] used *Micropolyspora roseoalba* for preparation of pravastatin. *M. roseoalba* is useful for manufacturing pravastatin sodium at low cost. The physiological and morphological characteristics of *M. roseoalba* were given.

Keri and Melczer [16] described a method for synthesizing and purifying pravastatin. This work encompasses methods of synthesizing pravastatin comprising less than about 0.1% by weight pravastatin C comprising (a) purification of compactin containing compactin C until the amount of compactin C is less than about 0.16% by weight, and (b) synthesizing pravastatin using compactin from (a). The work also encompasses compactin prepared according to the crystallization process and the pharmaceutical formulations comprising thereof.

Klaassen *et al.* [17] used Recombinant *Escherichia coli* cells and compactin hydrolases for preparation of the pharmaceutically active  $\beta$ -variant of pravastatin. *Amycolatopsis orientalis* is capable of converting compactin into pravastatin with 100% efficiency. The gene (cmpH) encoding the cytochrome P450 enzyme capable of hydroxylating compactin to pravastatin was isolated from *A. orientalis* gene library and cloned into *E. coli*. A number of synthetic genes encoding derivatives of compactin hydroxylase were tested in *E. coli* and shown to improve the compactin into pravastatin

conversion. This method produces pravastatin with a 90–95%: 5–10% ratio of  $\beta$ -variant to the  $\alpha$ -variant.

A process [18] for the preparation of pravastatin or its salts is disclosed. A mutant strain of *S. carbophilus* FERM BP 1145 capable of converting compactin or its salt into pravastatin or its salts is also disclosed.

Mei *et al.* [19] produced pravastatin sodium from mevastatin or mevastatin salt by hydroxylation in microorganism known as *M. roseoalba* CGMCC0624.

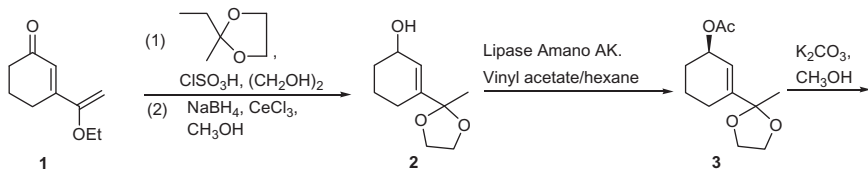
Sato and Kawasaki [20] described an efficient method for preparation of pravastatin its salt or lactone with cytochrome P450 3A by converting compactin salt or lactone. The microsomal fraction of cells producing cytochrome P450 3A is used. Transgenic cells producing both cytochromes P450 3A and NADPH cytochrome P450 reductase are preferred. Transgenic human or insect cells expressing cytochrome *b*<sub>5</sub> gene in addition to cytochrome P450 3A gene and NADPH cytochrome P450 reductase gene gave a better conversion rate.

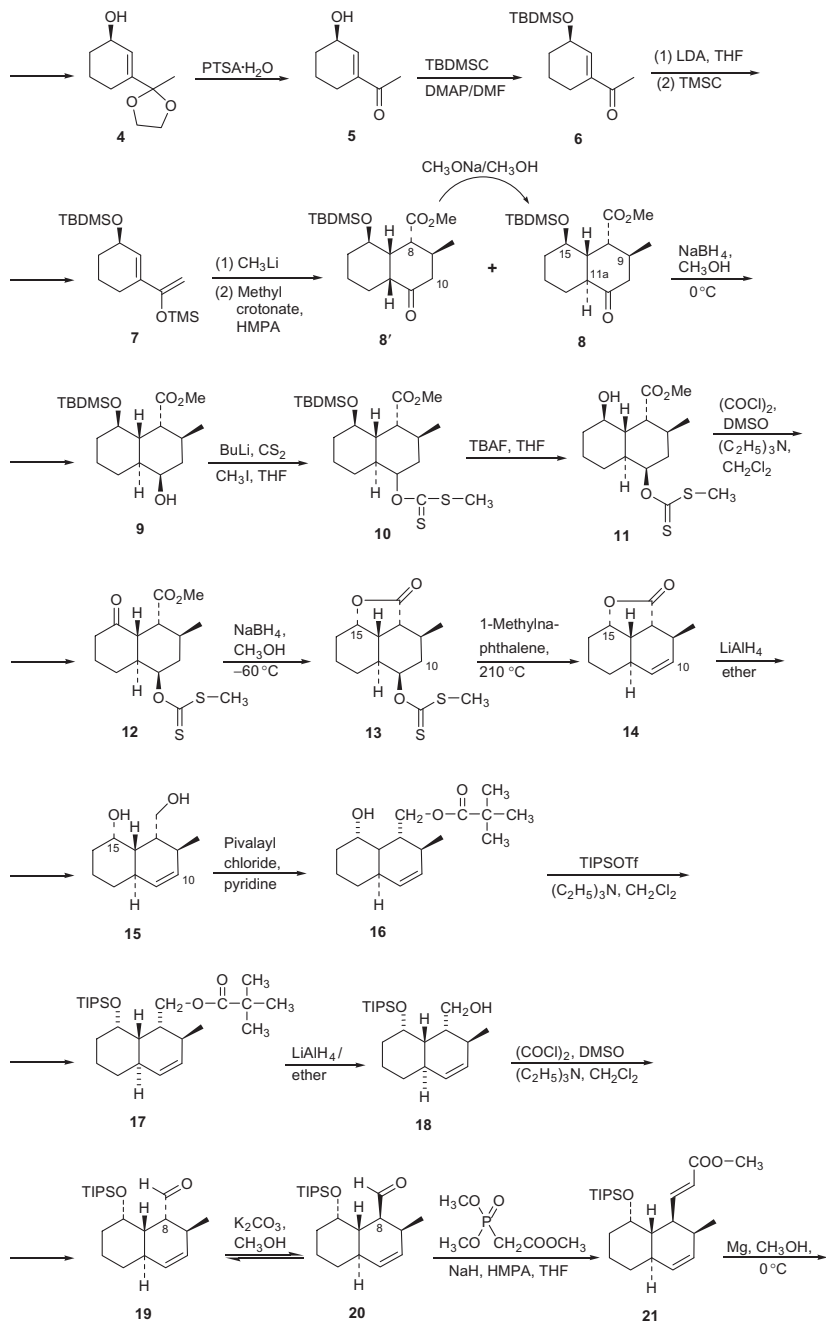
Hagiwara *et al.* [21] described the following total synthesis of (+)-compactin from which pravastatin is prepared by enzymatic hydroxylation [4,5,8–20].

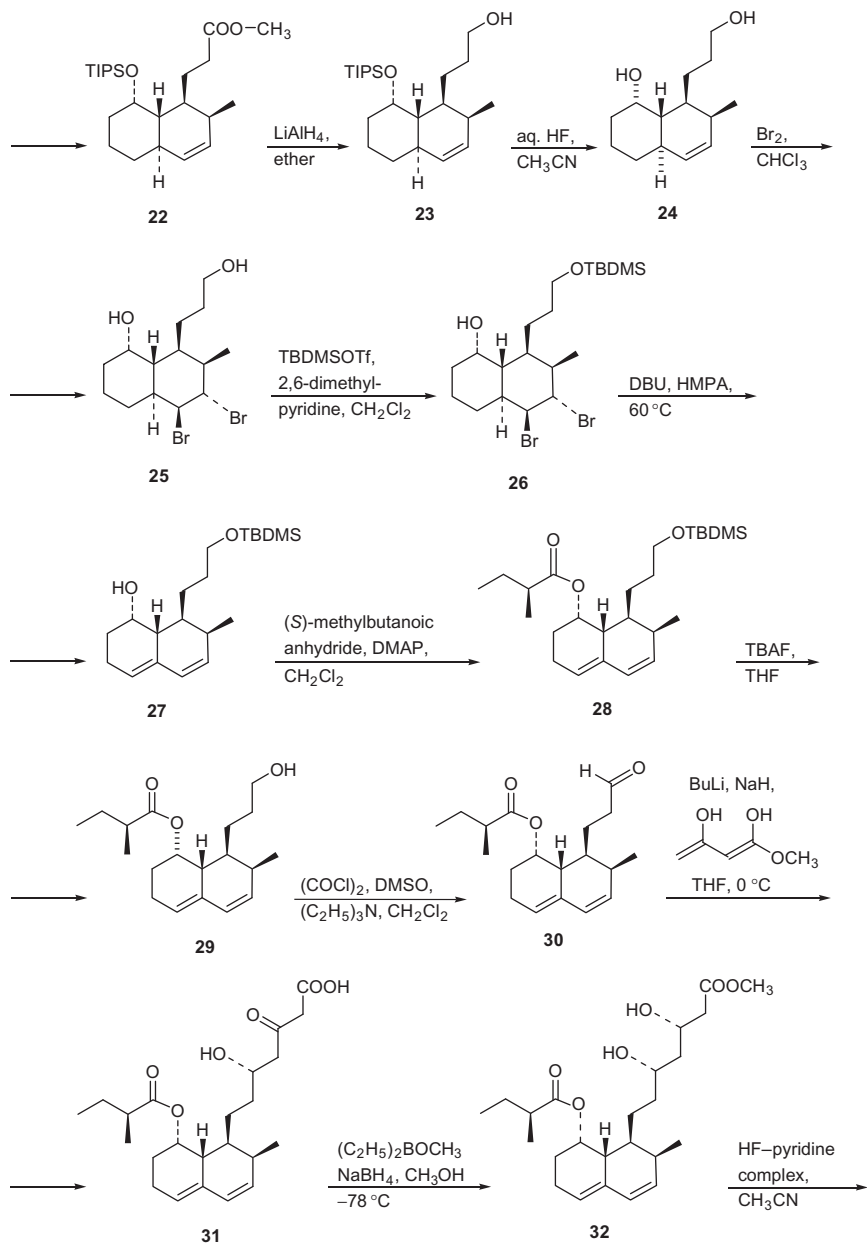
Treatment of the vinyl ether **1** with 2-ethyl-2-methyl-1,3-dioxolane with chlorosulfonic acid in ethylene glycol followed by reduction with sodium borohydride and cerium chloride in methanol gives the alcohol **2**. Alcohol **2** is converted to the (*R*)-cyclohexenol acetate **3** using Lipase Amano AK, with vinyl acetate in hexane. The acetate **3** was treated with potassium carbonate in methanol to produce the alcohol **4** which was refluxed with *p*-toluene sulfonic acid (PTSA·H<sub>2</sub>O) in aqueous acetone to give **5**. The alcohol **5** was treated with *tert*-butyldimethyl silyl chloride (TBDMSC) and dimethylamino-pyridine (DMAP) in DMF to produce **6**. The ketone **6** was reduced with lithium diisopropyl amide (LDA) in tetrahydrofuran at –78 °C and was then treated with trimethyl silyl chloride (TMSC) from –78 to 0 °C and gave **7**. Treatment of compound **7** with methyl lithium and methyl crotonate in the presence of two equivalent of hexamethyl phosphoric triamide (HMPA) afforded a mixture of *cis*-decalone and *trans*-decalone **8'** and **8**. The mixture of isomers was converted to *trans*-decalone by refluxing with sodium methoxide in methanol for 2 h to yield *trans*-decalone **8**. *trans*-Decalone **8** was reduced with sodium borohydride at 0 °C to produce the axial alcohol **9** which was converted to the xanthate **10** by treatment with butyl lithium, carbon disulfide, and methyl iodide in tetrahydrofuran. Deprotection of the *tert*-butyl dimethyl silyl group gives **11** which was subjected to Swern oxidation afforded the ketone **12**. Reduction of ketone **12** with sodium borohydride at –60 °C gave a

mixture of hydroxy ester and lactone **13**. Lactone **13** was heated at 210 °C with 1-methylnaphthalene to introduce the double bond **14**. The resulting olefinic lactone **14** was reduced with lithium aluminum hydride to give the diol **15**. The primary alcohol of the diol **15** was protected as the pivalate ester to afford **16** and the secondary alcohol as the triisopropyl silane (TIPS) ether to produce the silyl ether **17**. Removal of the pivaloyl group with lithium aluminum hydride gives **18** and treatment of **18** with Swern oxidation gave the aldehyde **19**.

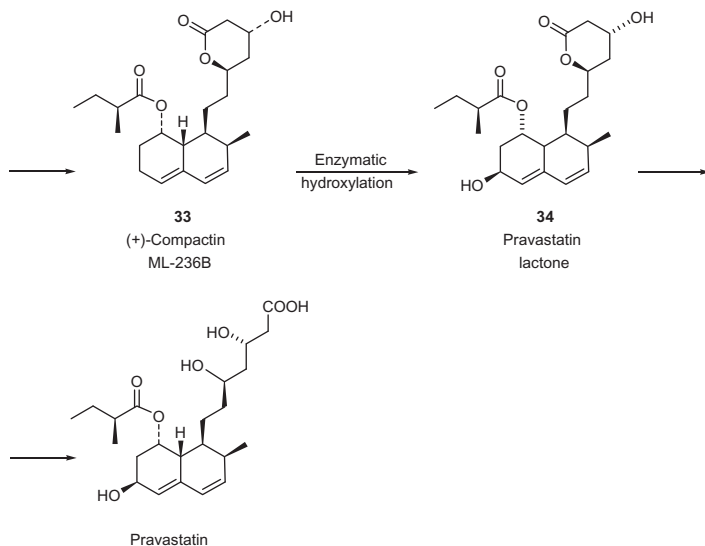
Treatment of the aldehyde **19** with potassium carbonate in methanol provided an equilibrium mixture of isomeric aldehyde **20** along with the recovered aldehyde **19**. These two aldehydes **19** and **20** were separated by medium pressure liquid chromatography enabling easy recycling. Elongation of the two carbon atom unit from the aldehyde **20** was performed by Horner–Emmons reaction leading to the  $\alpha$ – $\beta$ -unsaturated ester **21**. The double bond of **21** was reduced with magnesium in methanol to give the methyl ester **22** which was reduced with lithium aluminum hydride to the alcohol **23**. Deprotection of *tert*-butyldimethylsilyl group of the alcohol **23** gives the diol **24** quantitatively. The diene moiety was introduced by bromination–dehydrobromination sequence. The diol **24** was treated with a solution of bromine in chloroform to give the dibromide **25**. After selective protection of the primary alcohol of the dibromide **25**, the silyl ether **26** was produced. Treatment of **26** with diazabicycloundecene (DBU) furnished the diene **27**. Esterification of **27** with (*S*)-2-methyl butanoic anhydride provided the ester **28** which was deprotected to give hydroxy ester **29** quantitatively. Swern oxidation of **29** proceeded to give the aldehyde **30**. Aldol condensation of the dianion of methyl acetoacetate proceeded to give the aldol product **31** which were an inseparable mixture of epimers. The carbonyl group in **31** was reduced by sodium borohydride in the presence of diethyl methoxy borane to afford the diol **32** quantitatively. Treatment of the diol **32** with HF–pyridine complex in acetonitrile gave the desired product, compactin **33**. Enzymatic hydroxylation of (+)-compactin (ML-236B) afforded pravastatin lactone **34** which is finally converted to pravastatin.











## 4. PHYSICAL CHARACTERISTICS

### 4.1. X-ray powder diffraction

X-ray powder diffraction (XRD) pattern of pravastatin sodium was performed using a Simmon XRD-5000 diffractometer (Figure 8.1).

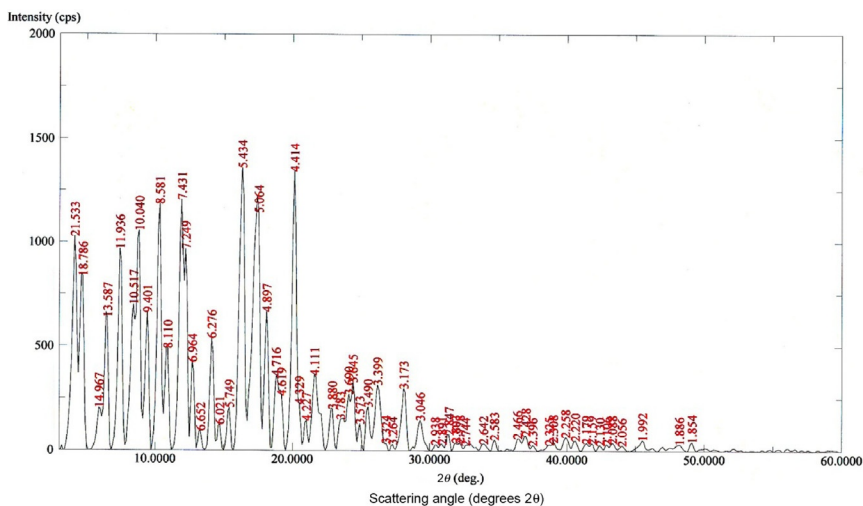


Figure 8.1 The X-ray powder diffraction pattern of pravastatin sodium.

Table 8.1 shows the values for the scattering angles ( $^{\circ}2\theta$ ), the interplanar  $d$ -spacing ( $\text{\AA}$ ), and the relative intensities (%) observed for the major diffraction peaks of the pure sample of pravastatin sodium drug substance.

Keri *et al.* [22] prepared a new crystalline form of pravastatin sodium and studied the X-ray powder diffraction data, the differential scanning calorimetry and thermogravimetric analysis, and other experiments for the drug form.

## 4.2. Thermal methods of analysis

### 4.2.1 Melting range

140–142  $^{\circ}\text{C}$ .

### 4.2.2 Differential scanning calorimetry

Differential scanning calorimetry (DSC) studies were carried out using differential scanning calorimeter equipped with an intercooler (Shimadzu DSC-60, Shimadzu Corporation, Koyoto, Japan). Indium/zinc standards were used to calibrate the temperature and enthalpy scale. The samples were hermetically sealed in an aluminum pans and heated at a constant rate of 10  $^{\circ}\text{C}/\text{min}$  over a temperature range of 25–300  $^{\circ}\text{C}$ . Inert atmosphere was maintained by purging nitrogen gas at a flow rate of 50 ml/min (Figure 8.2).

## 4.3. Ultraviolet spectroscopy

The ultraviolet (UV) absorption spectrum of pravastatin sodium in aqueous ethanol, shown in Figure 8.3, was recorded using a Shimadzu UV–Vis spectrophotometer 1601 PC. Pravastatin exhibited three maxima at 230, 238, and 246 nm.

Clark [3] reported the following for pravastatin sodium: methanol: 230, 237, and 245 nm; aqueous acid: 238 nm; basic: 238 nm; lactone in methanol: 230, 237, and 245 nm.

## 4.4. Vibrational spectroscopy

The infrared (IR) absorption spectrum of pravastatin sodium, shown in Figure 8.4, was obtained in a KBr pellet using a Perkin–Elmer IR spectrophotometer. The assignments of principal peaks of the IR major absorption bands are listed in Table 8.2.

**Table 8.1** Data deduced from X-ray powder diffraction pattern of pravastatin (Figure 8.1)

Peak no.	Diffraction angel ( $2\theta$ )	<i>d</i> -Value	<i>I</i> / <i>I</i> <sub>o</sub>	Peak no.	Diffraction angel ( $2\theta$ )	<i>d</i> -Value	<i>I</i> / <i>I</i> <sub>o</sub>
1	4.100	21.5333	76	31	24.900	3.5729	10
2	4.700	18.7856	62	32	25.500	3.4902	16
3	5.900	14.9672	16	33	26.200	3.3985	24
4	6.500	13.5869	47	34	26.800	3.3238	3
5	7.400	11.9364	72	35	27.300	3.2640	3
6	8.400	10.5175	52	36	28.100	3.1729	23
7	8.800	10.0403	78	37	29.300	3.0456	11
8	9.400	9.4007	49	38	30.400	2.9379	3
9	10.300	8.5812	88	39	30.900	2.8915	3
10	10.900	8.1102	37	40	31.400	2.8466	6
11	11.900	7.4308	89	41	31.900	2.8031	3
12	12.200	7.2487	72	42	32.200	2.7776	3
13	12.700	6.9645	32	43	32.600	2.7445	2
14	13.300	6.6516	8	44	33.900	2.6421	3
15	14.100	6.2759	40	45	34.700	2.5830	5
16	14.700	6.0211	10	46	36.400	2.4662	5
17	15.400	5.7490	16	47	37.000	2.4276	6
18	16.300	5.4335	100	48	37.500	2.3963	2
19	17.500	5.0635	85	49	38.700	2.3248	3
20	18.100	4.8970	50	50	39.000	2.3076	4
21	18.800	4.7162	27	51	39.900	2.2576	5
22	19.200	4.6189	20	52	40.600	2.2202	4
23	20.100	4.4140	99	53	41.400	2.1792	3
24	20.500	4.3288	17	54	41.800	2.1592	3
25	21.000	4.2268	11	55	42.400	2.1301	3
26	21.600	4.1108	27	56	42.900	2.1064	3
27	22.900	3.8803	15	57	43.300	2.0878	3
28	23.500	3.7825	12	58	44.000	2.0562	2
29	24.100	3.6897	20	59	45.500	1.9919	4
30	24.400	3.6450	25	60	48.200	1.8864	3

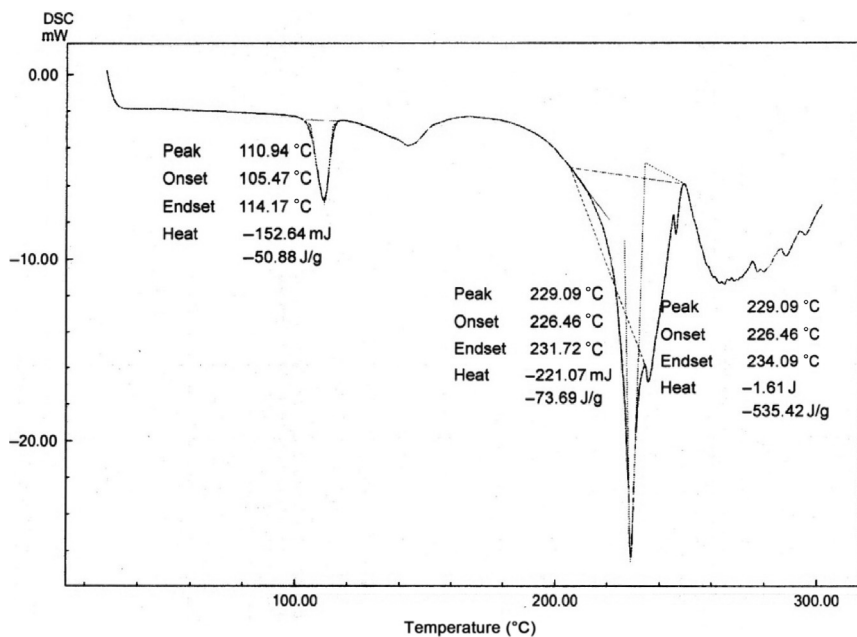


Figure 8.2 The differential scanning calorimetry thermogram of pravastatin sodium.

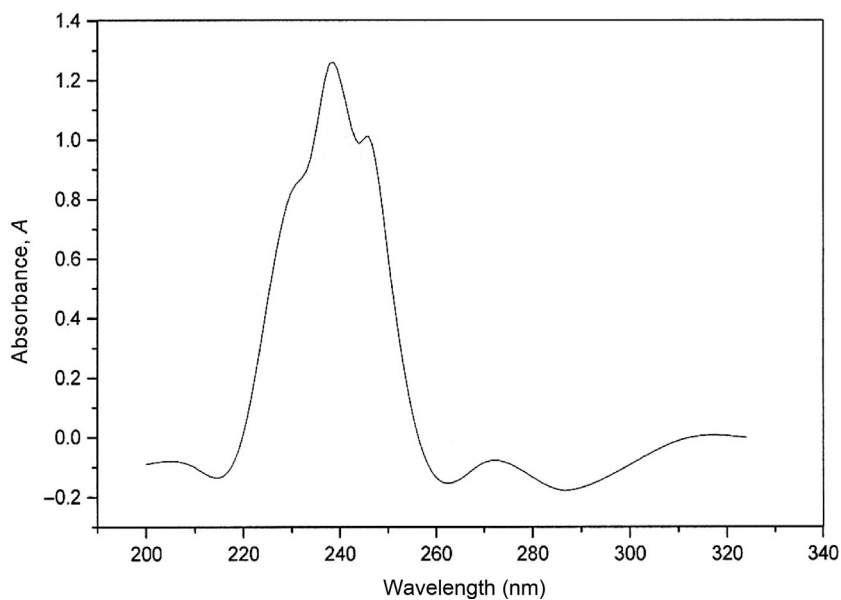
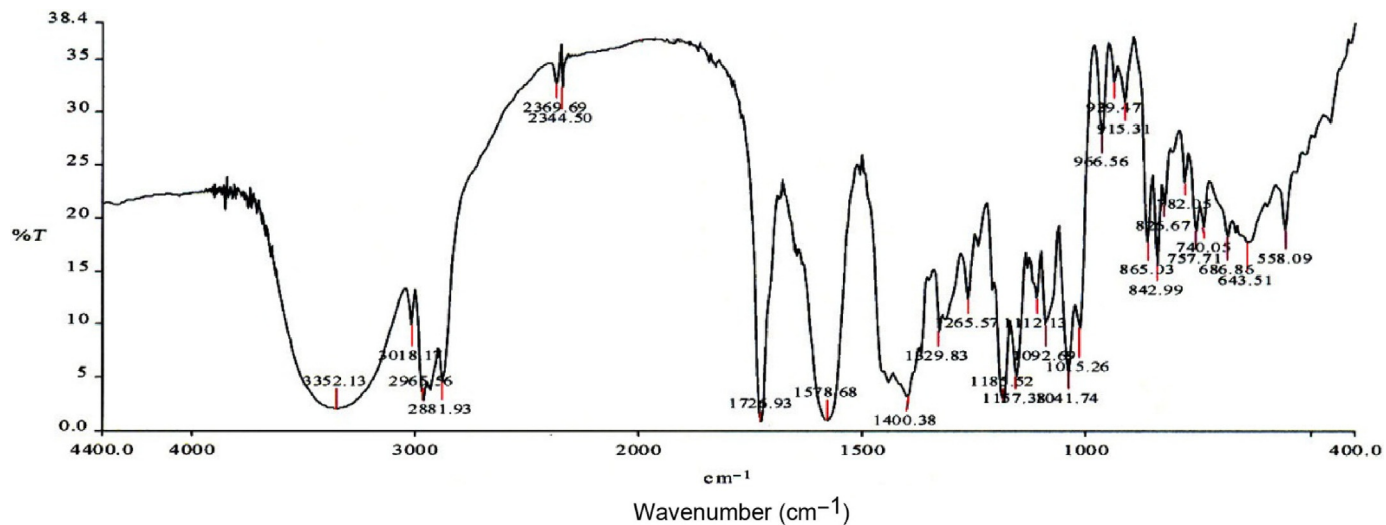


Figure 8.3 The UV absorption spectrum of pravastatin sodium in aqueous ethanol.



**Figure 8.4** The infrared absorption spectrum of pravastatin sodium (KBr disk).

**Table 8.2** Vibrational assignments for pravastatin sodium infrared absorption bands

Frequency ( $\text{cm}^{-1}$ )	Assignments
3352	O—H stretch
2965, 2881	$\text{CH}_3$ and $\text{CH}_2$ stretch
1725	$\text{C}=\text{O}$ stretch
1578	$\text{C}=\text{C}$ stretch
1400, 1329	$\text{CH}_2$ bending
1187	CH bending
1015	$\text{C}-\text{O}$ stretch
865	CH bending

Clarke [3] reported the following: Pravastatin sodium salt (KBr disk). Principal peaks at wavenumbers 1727, 1579, and  $1187\text{ cm}^{-1}$ .

## 4.5. Nuclear magnetic resonance spectrometry

### 4.5.1 $^1\text{H}$ NMR spectrum

The proton nuclear magnetic resonance ( $^1\text{H}$  NMR) spectra of pravastatin sodium were obtained using a Bruker Instrument Operating at 300, 400, or 500 MHz. Standard Bruker software was used to execute the recording of DEPT, COSY, and HETCOR spectra. The sample was dissolved in  $\text{CD}_3\text{OD}$  and all resonance bands were referenced to tetramethylsilane (TMS) as internal standard. The  $^1\text{H}$  NMR spectra of pravastatin sodium are shown in Figures 8.5–8.7 and the COSY  $^1\text{H}$  NMR is shown in Figure 8.8. The assignments for the pravastatin sodium are listed in Table 8.3.

### 4.5.2 $^{13}\text{C}$ NMR spectrum

The  $^{13}\text{C}$  NMR spectra of pravastatin sodium were obtained using a Bruker Instrument Operating at 75, 100, and 125 MHz. The sample was dissolved in  $\text{CD}_3\text{OD}$  and TMS was added to function as the internal standard. The  $^{13}\text{C}$  NMR spectra are shown in Figure 8.9 and the DEPT 90 and DEPT 135 are shown in Figures 8.10 and 8.11, respectively. The HSQC and the HMBC NMR are shown in Figures 8.12 and 8.13, respectively. The assignments of the observed resonance bands associated with the various carbons are listed in Table 8.4.

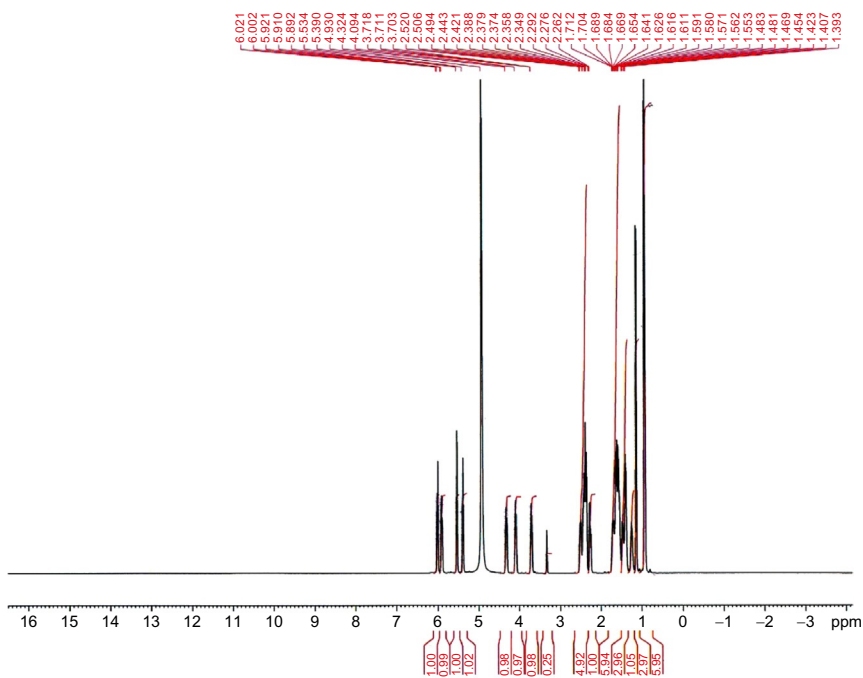


Figure 8.5 The  $^1\text{H}$  NMR spectrum of pravastatin sodium in  $\text{CD}_3\text{OD}$ .

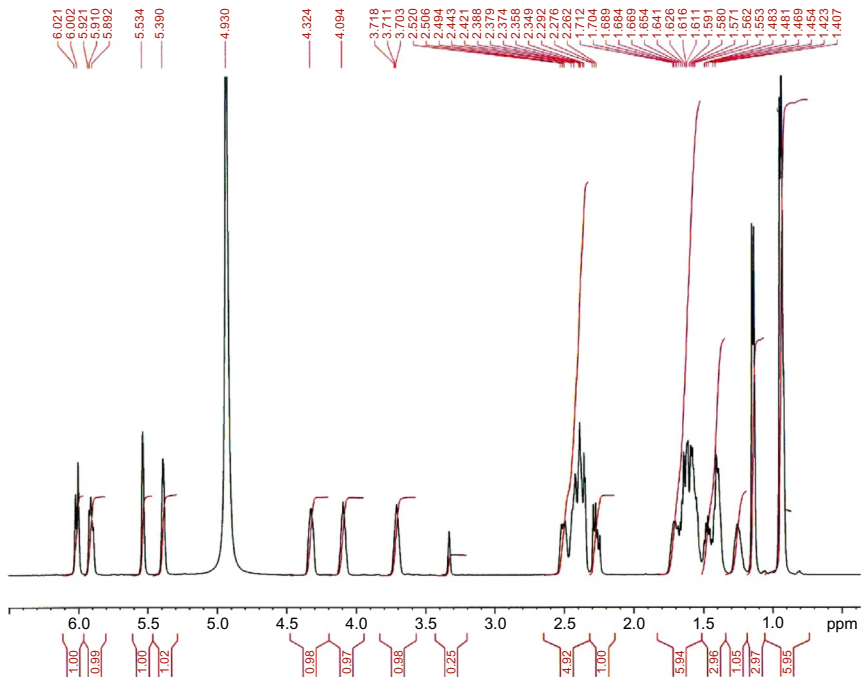
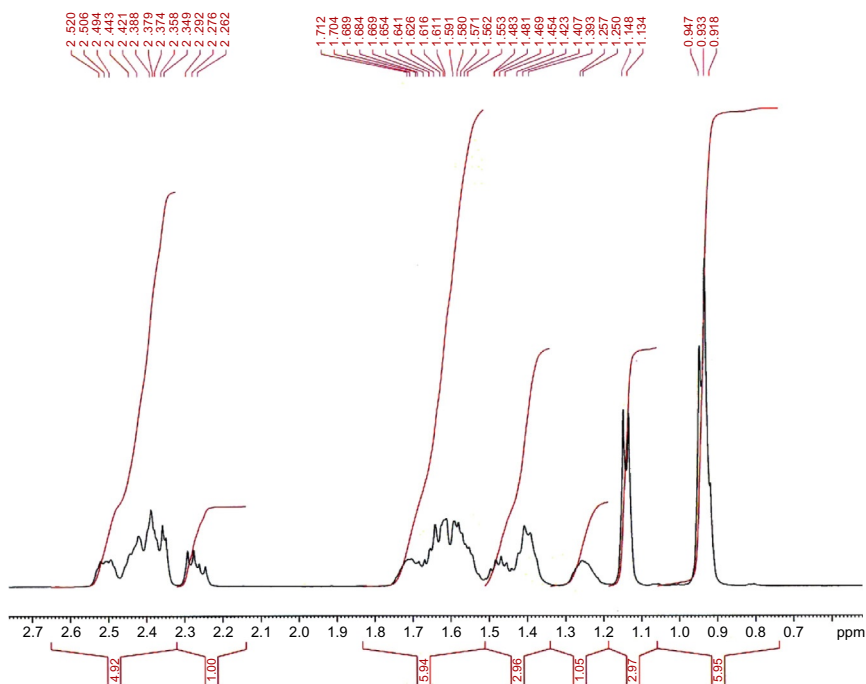


Figure 8.6 The expanded  $^1\text{H}$  NMR spectrum of pravastatin sodium in  $\text{CD}_3\text{OD}$ .



**Figure 8.7** The expanded  $^1\text{H}$  NMR spectrum of pravastatin sodium in  $\text{CD}_3\text{OD}$ .

Bacher *et al.* [23] reported the complete assignments of the  $^1\text{H}$  and  $^{13}\text{C}$  NMR data of pravastatin derivatives.

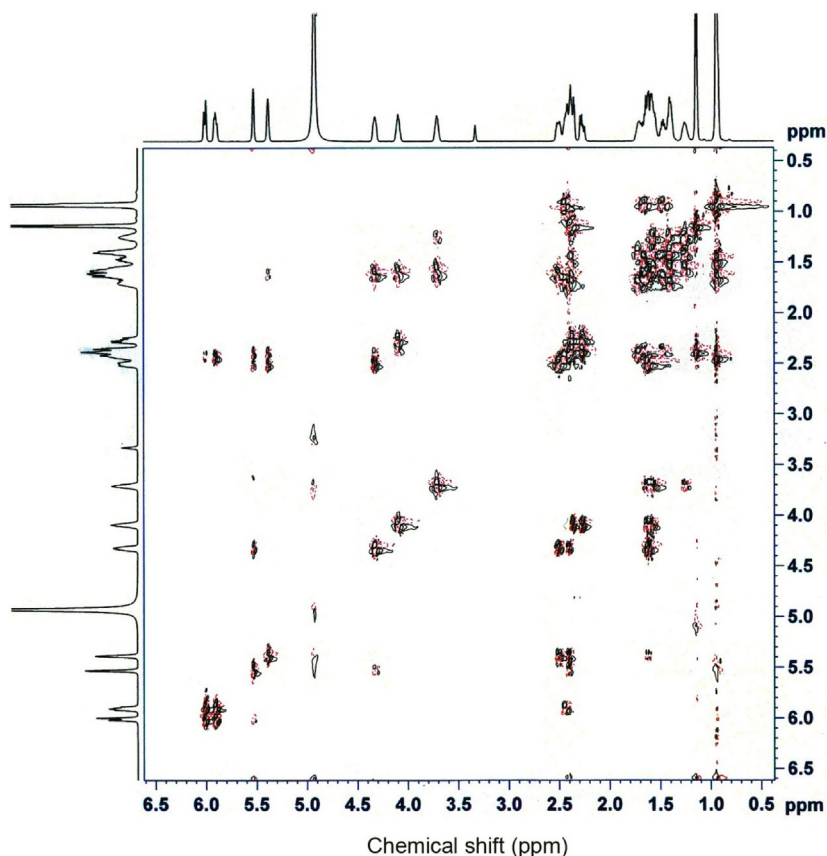
#### 4.6. Mass spectrometry

The mass spectrum of pravastatin sodium was obtained using an Agilent 6410 triple quadrupole LC/MS in the negative mode. Figure 8.14 shows the mass fragmentation pattern of the drug substance, and Table 8.5 lists the assignments of the mass fragments.

Lateef [24] separated the in process impurities in pravastatin using Agilent 6410 tripe quadrupole LC/MS in the negative ion mode.

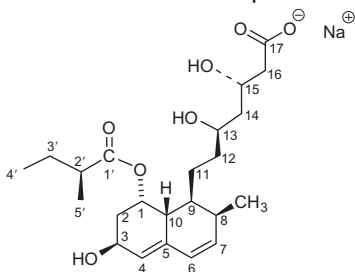
Kocijan *et al.* [25] identified an impurity in pravastatin by application of collision-activated decomposition mass spectra. Pravastatin is produced by two-step fermentation. Mevastatin and 6-*epi*-pravastatin are the main





**Figure 8.8** The COSY  $^1\text{H}$  NMR spectrum of pravastatin sodium in  $\text{CD}_3\text{OD}$ .

impurities in the fermentation broth as well as in final product. An unknown impurity with  $m/z$  437 for  $(\text{M}-\text{H})^-$  was detected in analysis of pravastatin sodium sample by reversed phase HPLC-MS. CAD spectrum of the impurity was obtained using HPLC-MS/MS equipped with negative APCI. The collision-activated decomposition mass spectra of impurity were similar with collision-activated decomposition mass spectra of statins. The structure of an impurity was finally determined on the basis of proposed fragmentation mechanisms for statins.

**Table 8.3** Proton NMR spectrum of pravastatin sodium in CD<sub>3</sub>OD

Chemical shift $\delta$ (ppm)	Multiplicity	Number of protons	Assignment hydrogen at carbon number
0.92–0.95	m	6 H	4', 18 2 CH <sub>3</sub>
1.14	d $J=7$	3 H	5' CH <sub>3</sub>
1.25–1.26	m	1 H	8
1.39–1.42	m	2 H	11
1.45–1.48	m	1 H	9
1.55–1.75	m	6 H	12, 14, 17
2.26–2.29	m	1 H	10
2.35–2.44	m	4 H	2, 3'
2.49–2.52	m	1 H	2'
3.70–3.72	m	1 H	13
4.09	m	1 H	15
4.32	s	1 H	3
5.39	s	1 H	1
5.53	s	1 H	4
5.89–5.92	m	1 H	7
6.01	d $J=9.9$	1 H	6



## 5. METHODS OF ANALYSIS

### 5.1. Compendial methods

#### 5.1.1 British pharmacopoeia methods [26]

##### Identification

- A.** Specific optical rotation, this test should be carried out as described in the general procedure (2.2.7) (see Tests).

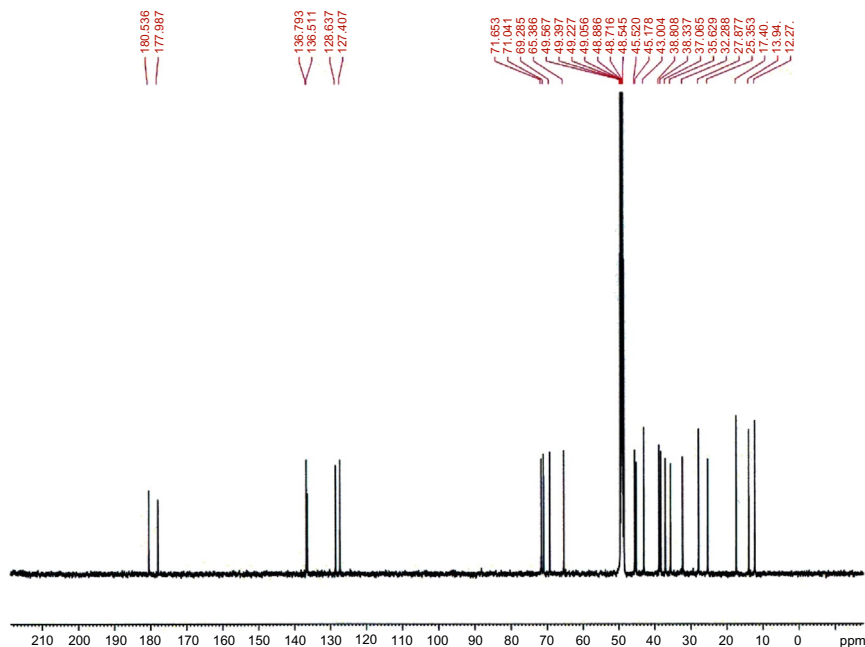


Figure 8.9 The  $^{13}\text{C}$  NMR spectrum of pravastatin sodium in  $\text{CD}_3\text{OD}$ .

- B.** Infrared absorption spectrophotometry: Carry out this test according to the general procedure (2.2.24) and compare with a *Ph. Eur. reference spectrum of pravastatin sodium*.
- C.** 1 ml of solution *S* gives reaction (a) of sodium according to the general procedure (2.3.1) (see Tests)

#### Tests

##### Solution *S*

Dissolve 1 g in *carbon dioxide free water R* and dilute to 20 ml with the same solvent.

##### Appearance of solution

When the test is carried out according to the general procedure (2.2.1), the solution is clear and not more intensely colored than reference solution  $\text{BY}_6$  which was carried out according to the general test (2.2.2, *Method II*).

Dilute 2 ml of solution *S* to 10 ml with *water R*.

**pH** Carry out the test according to the general procedure (2.2.3). 7.2–9.0 for solution *S*.

**Specific optical rotation** This test should be carried out according to the general procedure (2.2.7).

+153 to +159 (anhydrous and ethanol-free substance).

Dilute 2 ml of solution *S* to 20 ml with *water R*.

#### Related substances

Liquid chromatography	Carry out this test according to the general procedure (2.2.29).
Solvent mixture	Mix 9 volumes of <i>methanol R</i> with 11 volumes of <i>water R</i> .
Test solution (a)	Dissolve 0.1 g of pravastatin sodium in the solvent mixture and dilute to 100 ml with the solvent mixture.
Test solution (b)	Dilute 10 ml of test solution (a) to 100 ml with the solvent mixture.
Reference solution (a)	Dissolve 5 mg of pravastatin sodium and 5 mg of <i>pravastatin impurity A CRS</i> in the solvent mixture and dilute to 50 ml with the solvent mixture.
Reference solution (b)	Dilute 2 ml of test solution (a) to 100 ml with the solvent mixture. Dilute 1.0–10 ml of the solvent mixture.
Reference solution (c)	Dissolve 12.4 mg of <i>pravastatin 1,1,3,3-tetramethylbutylamine CRS</i> in the solvent mixture and dilute to 100 ml with the solvent mixture.
<b>Column:</b>	
– size:	$l = 0.15 \text{ m}$ , $\varnothing = 4.6 \text{ mm}$
– stationary phase:	<i>Octadecylsilyl silica gel for chromatography R</i> (5 $\mu\text{m}$ )
– temperature:	25 °C
Mobile phase:	<i>Glacial acetic acid R</i> , <i>triethylamine R</i> , <i>methanol R</i> , <i>water R</i> (1:1:450:550 <i>V/V/V/V</i> ).
Flow rate:	1.3 ml/min.
Detection:	Spectrophotometer at 238 nm.
Injection:	10 $\mu\text{l}$ ; inject test solution (a) and reference solutions (a) and (b).
Run time:	2.5 times the retention time of pravastatin.
Relative retention with reference to pravastatin (retention time = about 21 min): impurity B = about 0.2; impurity A = about 0.6; impurity C = about 2.1.	

System suitability:	Reference solution (a):
– <i>Resolution</i> :	minimum 7 between the peaks due to impurity A and to pravastatin.
Limits:	
– <i>impurity A</i> :	not more than 1.5 times the area of the principal peak in the chromatogram obtained with reference solution (b) (0.3%),
– <i>any impurity</i> :	not more than the area of the principal peak in the chromatogram obtained with reference solution (b) (0.2%),
– <i>total</i> :	not more than 3 times the area of the principal peak in the chromatogram obtained with reference solution (b) (0.6%),
– <i>disregard limit</i> :	0.25 times the area of the principal peak in the chromatogram obtained with reference solution (b) (0.05%).
<b>Ethanol</b>	Carry out this test according to the general procedure (2.4.24, <i>System A</i> ).
Maximum	3% <i>m/m</i> .
<b>Heavy metals</b>	Carry out this test according to the general procedure (2.4.8).
Maximum	20 ppm.
Dissolve 2 g of pravastatin sodium in a mixture of 15 volumes of <i>water R</i> and 85 volumes of <i>methanol R</i> and dilute to 20 ml with the same mixture of solvents. 12 ml of this solution complies with limit test B. Prepare the standard using lead standard solution (2 ppm Pb) prepared by diluting <i>lead standard solution (100 ppm Pb) R</i> with a mixture of 15 volumes of <i>water R</i> and 85 volumes of <i>methanol R</i> .	
<b>Water</b>	Carry out this test according to the general procedure (2.5.12). Maximum 4%, determined on 0.5 g.

### Assay

Liquid chromatography Carry out this test according to the general procedure (2.2.29) as described in the test for related substances.

*Injection*: Test solution (b) and reference solution (c).

Calculate the percentage content of  $C_{23}H_{35}NaO_7$  using the chromatogram obtained with reference solution (c) and the declared content of pravastatin in *pravastatin 1,1,3,3-tetramethylbutylamine CRS*.

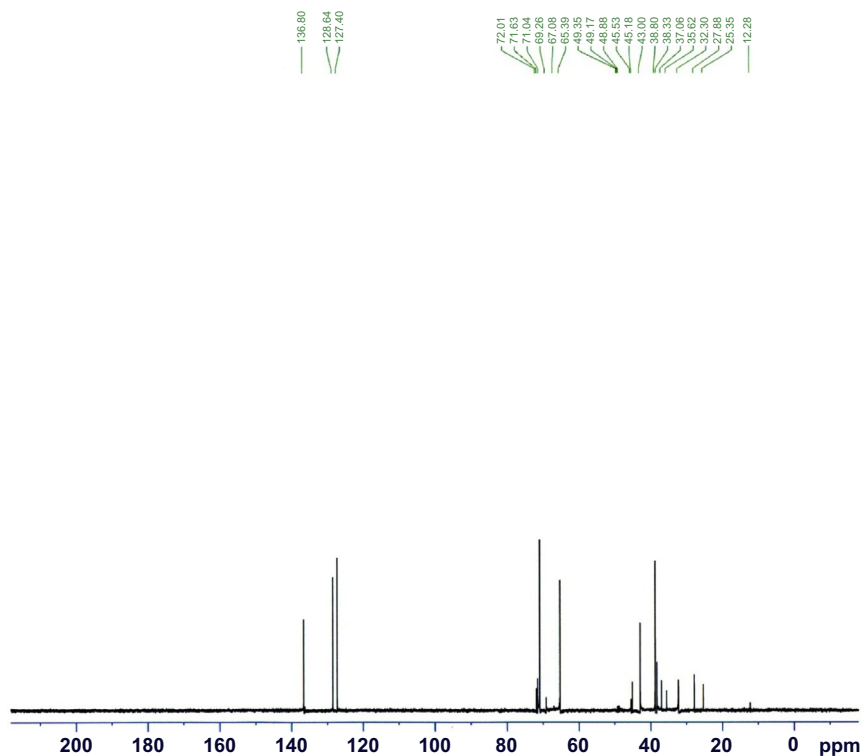


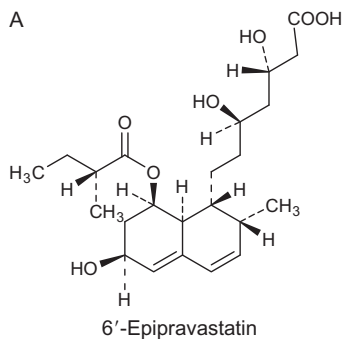
**Figure 8.10** The DEPT 90  $^{13}\text{C}$  NMR spectrum of pravastatin sodium in  $\text{CD}_3\text{OD}$ .

1 mg of pravastatin is equivalent to 1.052 mg of pravastatin sodium.

Storage

In an airtight container.

Impurities



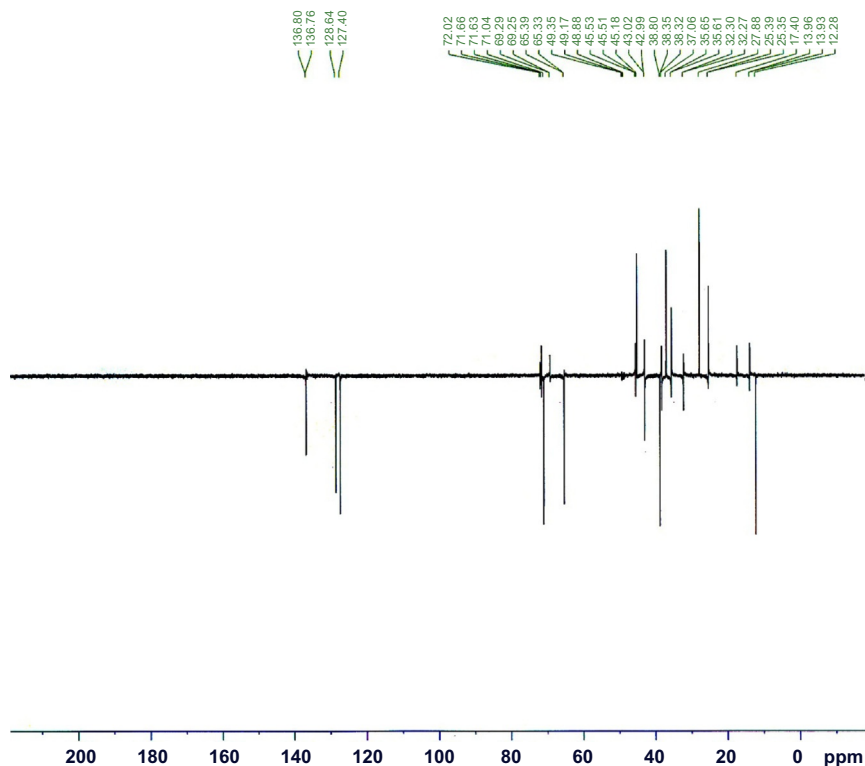
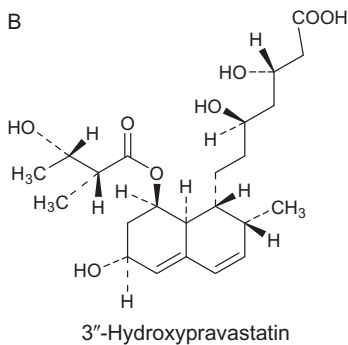


Figure 8.11 The DEPT 135  $^{13}\text{C}$  NMR spectrum of pravastatin sodium in  $\text{CD}_3\text{OD}$ .

- A. (3*R*,5*R*)-3,5-dihydroxy-7-[(1*S*,2*S*,6*R*,8*S*,8*aR*)-6-hydroxy-2-methyl-8-[[[(2*S*)-2-methylbutanoyl]oxy]-1,2,6,7,8,8*a*-hexahydronaphthalen-1-yl] heptanoic acid. (6'-epipravastatin),



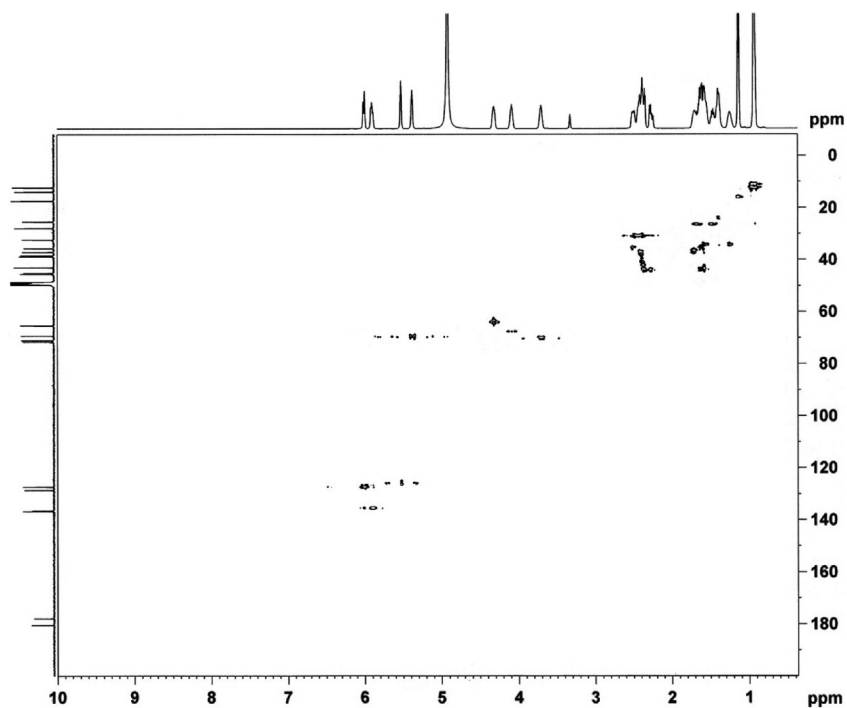


Figure 8.12 The HSQC NMR experiment of pravastatin sodium in  $\text{CD}_3\text{OD}$ .

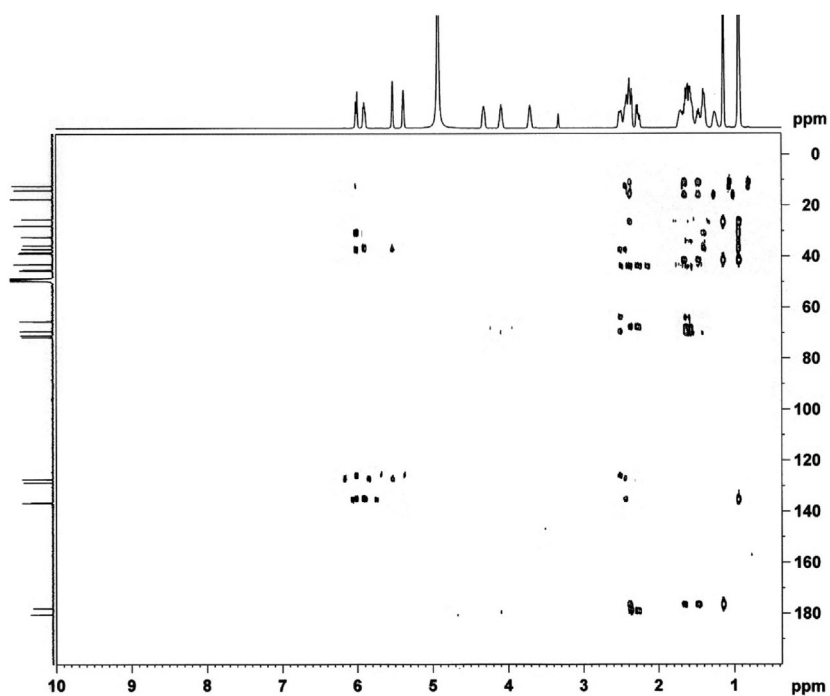
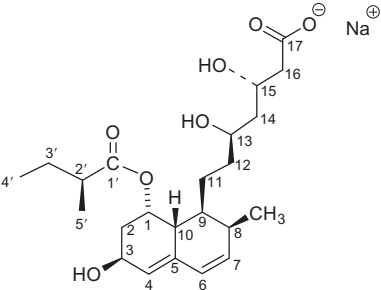


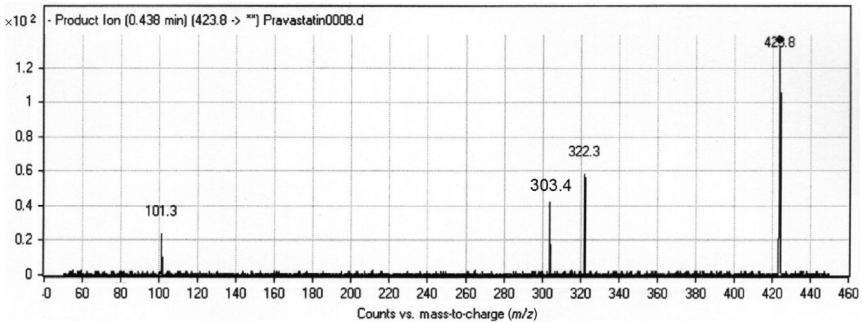
Figure 8.13 The HMBC NMR experiment of pravastatin sodium in  $\text{CD}_3\text{OD}$ .



**Table 8.4** Carbon-13 spectrum of pravastatin sodium in CD<sub>3</sub>OD

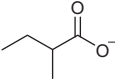
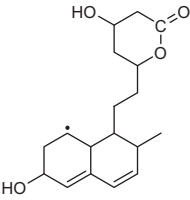
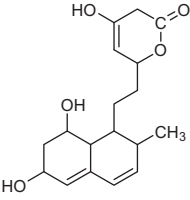
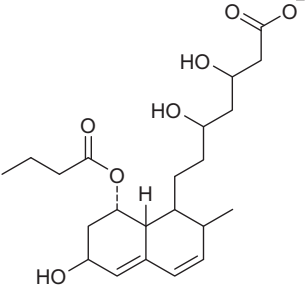


Chemical shift $\delta$ (ppm)	Assignment	Chemical shift $\delta$ (ppm)	Assignment
12.27	C <sub>4</sub>	45.52	C <sub>16</sub>
13.94	C <sub>18</sub>	65.39	C <sub>3</sub>
17.40	C <sub>5</sub>	69.29	C <sub>1</sub>
25.35	C <sub>11</sub>	71.04	C <sub>15</sub>
27.88	C <sub>3'</sub>	71.65	C <sub>13</sub>
32.29	C <sub>8</sub>	127.4	C <sub>4</sub>
35.63	C <sub>12</sub>	128.64	C <sub>6</sub>
37.07	C <sub>2</sub>	136.51	C <sub>5</sub>
38.34	C <sub>9</sub>	136.79	C <sub>7</sub>
38.83	C <sub>10</sub>	177.99	C <sub>1'</sub>
43.00	C <sub>2'</sub>	180.54	C <sub>17</sub>
45.18	C <sub>14</sub>		

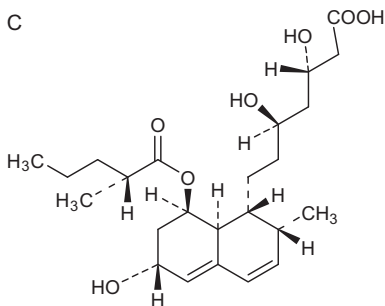


**Figure 8.14** Electrospray mass spectrum of pravastatin sodium.

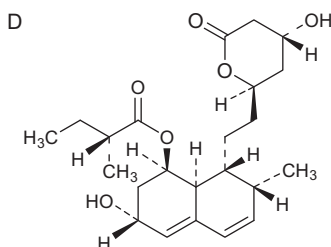
**Table 8.5** Assignments of fragmentation ions observed in the mass spectrum of pravastatin sodium

<i>m/z</i>	Relative intensity (%)	Fragment	
		Formula	Structure
101.1	20	C <sub>5</sub> H <sub>9</sub> O <sub>2</sub>	
303.4	32	C <sub>18</sub> H <sub>35</sub> O <sub>4</sub>	
322.3	42	C <sub>18</sub> H <sub>26</sub> O <sub>5</sub>	
423.5	100	C <sub>23</sub> H <sub>35</sub> O <sub>7</sub>	

**B.** (3*R*,5*R*)-3,5-dihydroxy-7-[(1*S*,2*S*,6*S*,8*S*,8*aR*)-6-hydroxy-8-[[[(2*S*,3*R*)-3-hydroxy-2-methylbutanoyl]oxy]-2-methyl-1,2,6,7,8,8*a*-hexahydronaphthalen-1-yl]]heptanoic acid. (3''-hydroxy pravastatin),



- C. (3*R*,5*R*)-3,5-dihydroxy-7-[(1*S*,2*S*,6*S*,8*S*,8*aR*)-6-hydroxy-2-methyl-8-[[*(2S)*-2-methylpentanoyl]oxy]-1,2,6,7,8,8*a*-hexahydronaphthalen-1-yl]heptanoic acid.



Pravastatin lactone

- D. (1*S*,3*S*,7*S*,8*S*,8*aR*)-3-hydroxy-8-[2-[(2*R*,4*R*)-4-hydroxy-6-oxotetrahydro-2*H*-pyran-2-yl]ethyl]-7-methyl-1,2,3,7,8,8*a*-hexahydronaphthalen-1-yl (2*S*)-2-methylbutanoate (pravastatin lactone).

### 5.1.2 United States Pharmacopoeia methods [27]

#### 5.1.2.1 Pravastatin sodium

Pravastatin sodium contains not less than 97.5% and not more than 102% of  $C_{23}H_{35}NaO_7$ , calculated on the anhydrous and solvent-free basis.

**Packaging and storage**—Preserve in tight containers. Store as per labeling instructions. Possible storage conditions could include the following, in the presence of stability data supporting the condition: Store under nitrogen in a cold place. Store at room temperature.

**USP Reference standards**—See the general procedure ⟨11⟩ the USP reference standards are *USP Pravastatin 1,1,3,3-Tetramethylbutylamine RS*, *USP Pravastatin Sodium RS*, and *USP Pravastatin-Related Compound A RS*.

#### Identification

**A: Infrared absorption** When this test is carried out according to the general procedure ⟨197K⟩. The infrared absorption spectrum of a KBr dispersion of pravastatin sodium previously dried exhibits maxima only at the same wavelength as that of similar preparation *USP Pravastatin Sodium RS*.

**B:** It meets the requirements of the pyroantimonate precipitation test for *Sodium* as described in the general procedure ⟨191⟩.

**Specific rotation** Carry out this test according to the general procedure ⟨781⟩: between +150° and +160° (at 20°), calculated on the anhydrous and solvent-free basis.

*Test solution:* 5 mg/ml in water.

**pH** Carry out this test according to the general procedure (791): between 7.2 and 9.0, in a solution (1 in 20).

**Water, Method I** Carry out this test according to the general procedure (921): not more than 4.0%.

**Heavy metals** Carry out this test according to the general procedure *Method II* (231): 0.002%.

**Limit of alcohol** (*if present*)

*Test solution*—Transfer about 0.2 g of pravastatin sodium, accurately weighed, to a 20-ml volumetric flask, dilute with water to volume, and mix. Pipet 5 ml of this solution into a vial fitted with a septum and a crimp cap, add 1 ml of water, seal the vial, and mix. Heat the sealed vial at 80° for 60 min.

*Standard solution*—Pipet 2 ml of dehydrated alcohol into a 100-ml volumetric flask, dilute with water to volume, and mix. Pipet 10 ml of this solution into a 100-ml volumetric flask, dilute with water to volume, and mix. Pipet 1 ml of this solution into a vial fitted with a septum and a crimp cap, and calculate the amount of alcohol,  $W_A$ , added, in g, the specific gravity of dehydrated alcohol being 0.79 g/ml. Add 5 ml of the *Test solution* to the same vial, seal the vial, and mix. Heat the sealed vial at 80 °C for 60 min.

*Blank solution*—Pipet 6 ml of water into a vial fitted with a septum and a crimp cap, and seal the vial. Heat the sealed vial at 80 °C for 60 min.

*Chromatographic system* (see *Chromatography*, in the general procedure (621))—The gas chromatograph is equipped with a flame-ionization detector and a 0.53-mm  $\times$  30-m fused-silica capillary column coated with a 3- $\mu$ m film of stationary phase G43. The carrier gas is helium, with a split ratio of 1:5, and flowing with a linear velocity of about 35 cm per second. The chromatograph is programmed as follows. The column temperature is maintained at 40 °C for 20 min, and then the temperature is increased at a rate of 10 °C per minute to 240 °C and maintained at 240 °C for 20 min. The transfer line temperature is maintained at 85 °C, the injection port temperature is maintained at 140 °C, and the detector is maintained at 250 °C. Chromatograph the *Blank solution* and record the peak responses as directed for *Procedure*: no interfering peaks are observed.

*Procedure*—Separately inject equal volumes (about 1 ml) of headspace gas of the *Standard solution* and the *Test solution* into the chromatograph, record the chromatograms, and measure the area responses for the major peaks.

Calculate the percentage (w/w) of alcohol in the portion of pravastatin sodium taken by the formula:

$$100 (W_A/W)(V/5)[r_U/(r_s - r_U)]$$

in which  $W_A$  is the amount of the alcohol added in g;  $W$  is the weight, in g, of pravastatin sodium taken to prepare the *Test solution*;  $V$  is the volume, in ml, of the *Test solution*; 5 is the volume, in ml, of the *Test solution* taken; and  $r_U$  and  $r_s$  are the peak area responses of alcohol obtained from the *Test solution* and the *Standard solution*, respectively: not more than 3% is found.

**Chromatographic purity**—[Note: The *Standard solution* and the *Test solution* are maintained at 15 °C until injected into the chromatograph.]

*Diluent*—Prepare a mixture of methanol and water (1:1).

*Buffer pH 7*—Prepare a 0.08 M phosphoric acid solution, adjust with triethylamine to a pH of 7, and mix.

*Solution A*—Prepare a filtered and degassed mixture of water, *Buffer pH 7*, and acetonitrile (52:30:18).

*Solution B*—Prepare a filtered and degassed mixture of acetonitrile, *Buffer pH 7*, and water (60:30:10).

*Mobile phase*—Use variable mixtures of *Solution A* and *Solution B* as directed for *Chromatographic system*. Make adjustments if necessary (see *System Suitability under Chromatography* (621)).

*Standard solution*—Dissolve an accurately weighed quantity of USP Pravastatin 1,1,3,3-Tetramethylbutylamine RS in *Diluent*, and dilute quantitatively, and stepwise if necessary, with *Diluent* to obtain a solution having a known concentration of about 1.25 µg of pravastatin 1,1,3,3-tetramethylbutylamine per ml.

*System suitability solution*—Dissolve accurately weighed quantities of USP Pravastatin 1,1,3,3-Tetramethylbutylamine RS and USP Pravastatin-Related Compound A RS in *Diluent* to obtain a solution containing about 0.6 mg of USP Pravastatin 1,1,3,3-tetramethylbutylamine RS and 0.001 mg of USP Pravastatin-Related Compound A RS per ml. [Note: USP Pravastatin-Related Compound A RS is a sodium salt of 3α-hydroxyisocompactin acid.]

*Test solution*—Transfer about 50 mg of pravastatin sodium, accurately weighed, to a 100-ml volumetric flask, dissolve in and dilute with *Diluent* to volume, and mix.

*Chromatographic system* (see *Chromatography in the general procedure* (621))—The liquid chromatograph is equipped with a 238-nm detector and a 4.6-mm  $\times$  7.5-cm column that contains 3.5- $\mu$ m packing L1. Alternatively, a 4-mm  $\times$  10-cm column that contains 3- $\mu$ m packing L1 can be used. The flow rate is about 1 ml/min. The chromatograph is programmed as follows.

Time (min)	Solution A (%)	Solution B (%)	Elution
0–3	100	0	Isocratic
3–26.5	100 $\rightarrow$ 0	0 $\rightarrow$ 100	Linear gradient
26.5–26.6	0 $\rightarrow$ 100	100 $\rightarrow$ 0	Linear gradient
26.6–30	100	0	Reequilibration

Chromatograph the *System suitability solution* and record the peak responses as directed for *Procedure*: the relative retention times are about 1 for pravastatin and 1.1 for pravastatin-related compound A; and the resolution, *R*, between pravastatin and pravastatin-related compound A is not less than 2. Chromatograph the *Standard solution* and record the peak responses as directed for *Procedure*: the relative standard deviation for replicate injections is not more than 10%.

*Procedure*—Separately inject equal volumes (about 10  $\mu$ l) of the *Standard solution* and the *Test solution* into the chromatograph, record the chromatograms, identify the impurities listed in Table 8.6, and measure the peak

**Table 8.6** The limits of impurities of pravastatin, 1

Name	Relative retention time	Limit (%)
3''-Hydroxy pravastatin	0.33	0.2
6'-Epipravastatin	0.92	0.3
3 $\alpha$ -Hydroxyisocompactin <sup>a</sup>	1.1	0.2
Pentanoyl impurity <sup>b</sup>	1.2	0.2
Pravastatin lactone	1.8	0.2
Compactin	3.1	0.2

<sup>a</sup>Sodium (3*R*,5*R*)-3,5-dihydroxy-7-[(1*S*,2*S*,3*S*,8*S*,8*aR*)-3-hydroxy-2-methyl-8-[[[(2*S*)-2-methylbutanoyl]oxy]-1,2,3,7,8,8*a*-hexahydronaphthalen-1-yl]heptanoate (pravastatin-related compound A).

<sup>b</sup>(3*R*,5*R*)-3,5-dihydroxy-7-[(1*S*,2*S*,6*S*,8*S*,8*aR*)-6-hydroxy-2-methyl-8-[[[(2*S*)-2-methylpentanoyl]oxy]-1,2,6,7,8,8*a*-hexahydronaphthalen-1-yl]heptanoic acid.

responses. Calculate the percentage of each impurity in the portion of pravastatin sodium taken by the formula:

$$100 \times (446.51/553.78)C(V/W)(r_i/r_s)$$

in which 446.51 and 553.78 are the molecular weights of pravastatin sodium and pravastatin 1,1,3,3-tetramethylbutylamine, respectively;  $C$  is the concentration, in mg/ml, of pravastatin 1,1,3,3-tetramethylbutylamine in the *Standard solution*;  $V$  is the volume, in ml, of the *Test solution*;  $W$  is the weight, in mg, of pravastatin sodium taken to prepare the *Test solution*;  $r_i$  is the peak response for each impurity obtained from the *Test solution*; and  $r_s$  is the pravastatin peak response obtained from the *Standard solution*, in addition to not exceeding the limits for each impurity specified in Table 8.6 not more than 0.1% of any other individual impurity is found, and not more than 0.6% of total impurities is found.

#### Assay

**Solution A**—Prepare a 0.08 M phosphoric acid solution, adjust with a 25% sodium hydroxide solution to a pH of 5, mix, filter, and degas.

**Solution B**—Use acetonitrile.

**Mobile phase**—Use variable mixtures of *Solution A* and *Solution B* as directed for *Chromatographic system*. Make adjustments if necessary (see *System Suitability* under *Chromatography* (621)).

**Standard preparation**—Dissolve an accurately weighed quantity of USP Pravastatin 1,1,3,3-Tetramethylbutylamine RS in methanol, and dilute quantitatively, and stepwise if necessary, with methanol to obtain a solution having a known concentration of about 0.25 mg of pravastatin 1,1,3,3-tetramethylbutylamine per ml.

**System suitability preparation**—Dissolve accurately weighed quantities of USP Pravastatin 1,1,3,3-Tetramethylbutylamine RS and USP Pravastatin-Related Compound A RS in methanol to obtain a solution containing about 0.25 mg of USP Pravastatin 1,1,3,3-Tetramethylbutylamine RS and 0.001 mg of USP Pravastatin-Related Compound A RS per ml.

**Assay preparation**—Transfer about 20 mg of pravastatin sodium, accurately weighed, to a 100-ml volumetric flask, dissolve in and dilute with methanol to volume, and mix.

**Chromatographic system** (see *Chromatography* (621))—The liquid chromatograph is equipped with a 238-nm detector and a 4-mm × 10-cm column that contains 3-μm packing L1. The flow rate is about 1 ml/min. The chromatograph is programmed as follows.

Time (min)	Solution A (%)	Solution B (%)	Elution
0–7	80 → 72	20 → 28	Linear gradient
7–10	72 → 50	28 → 50	Linear gradient
10–17	50	50	Isocratic
17–17.1	50 → 80	50 → 20	Linear gradient
17.1–20	80	20	Reequilibration

Chromatograph the *System suitability preparation* and record the peak responses as directed for *Procedure*: the relative retention times are about 1 for pravastatin and 1.2 for pravastatin-related compound A; the resolution,  $R$ , between pravastatin and pravastatin-related compound A is not less than 1.2; and the relative standard deviation for replicate injections for the pravastatin peak is not more than 2%.

*Procedure*—Separately inject equal volumes (about 10  $\mu$ l) of the *Standard preparation* and the *Assay preparation* into the chromatograph, record the chromatograms, and measure the responses for the pravastatin peaks. Calculate the quantity, in mg, of  $C_{23}H_{35}NaO_7$  in the portion of pravastatin sodium taken by the formula:

$$(446.51/553.78)VC(r_U/r_s)$$

in which 446.51 and 553.78 are the molecular weights of pravastatin sodium and pravastatin 1,1,3,3-tetramethylbutylamine, respectively;  $V$  is the volume, in ml, of the *Assay preparation*;  $C$  is the concentration, in mg/ml, of pravastatin 1,1,3,3-tetramethylbutylamine in the *Standard preparation*; and  $r_U$  and  $r_s$  are the responses of the pravastatin peak obtained from the *Assay preparation*; and the *Standard preparation*, respectively.

#### 5.1.2.2 Pravastatin sodium tablets

Pravastatin sodium contains not less than 90% and not more than 110% of the labeled amount of pravastatin sodium ( $C_{23}H_{35}NaO_7$ ).

**Packaging and storage**—Preserve in tight containers. Protect from moisture and light. Store at controlled room temperature.

**USP Reference standards**: See the general procedure, USP Reference standard are  $\langle 11 \rangle$ —USP *Pravastatin-Related Compound B RS*, USP *Pravastatin Sodium RS*, and USP *Pravastatin 1,1,3,3-Tetramethylbutylamine RS*.



## Identification

**A:** The retention time of the major peak in the chromatogram of the *Assay preparation* corresponds to that in the chromatogram of the *Standard preparation*, as obtained in the *Assay*.

**B: Ultraviolet Absorption** Carry out this test as directed in the general procedure (197U)—Finely powder a number of tablets and extract with water a portion equivalent to about 10 mg of pravastatin sodium. The UV absorption spectrum of a solution of pravastatin sodium in water containing about 10 µg/ml exhibits maxima at the same wavelength as that of a similar solution of USP Pravastatin Sodium RS, concomitantly measured between 220 and 340 nm.

**Dissolution** Carry out this test as directed in the general procedure (711)—*Medium*: water; 900 ml.

*Apparatus 2*: 50 rpm.

*Time*: 30 min.

*Procedure*—Determine the amount of  $C_{23}H_{35}NaO_7$  dissolved by employing UV absorption at the wavelength of maximum absorbance at about 238 nm on filtered portions of the solution under test, suitably diluted with *Medium*, if necessary, in comparison with Standard solution having a known concentration of USP Pravastatin 1,1,3,3-Tetramethylbutylamine RS in the same *Medium*. [Note: To express the concentration of the Standard solution as pravastatin sodium, use the conversion factor of (446.51/553.78), in which 446.51 and 553.78 are the molecular weights of pravastatin sodium and pravastatin 1,1,3,3-tetramethylbutylamine, respectively.]

*Tolerances*—Not less than 80% (Q) of the labeled amount of  $C_{23}H_{35}NaO_7$  is dissolved in 30 min.

**Uniformity of dosage units** Carry the test as directed in the general procedure (905): meet the requirements.

Related compounds—

*Mobile Phase and Chromatographic system*—Proceed as directed in the *Assay*.

*Test solution*—Use the *Assay preparation*, prepared as directed in the *Assay*. [Note: Use this solution within 24 h of preparation.]

*Procedure*—Inject a volume (about 20 µl) of the *Test solution* into the chromatograph, record the chromatograms for up to 4 times the retention time of the pravastatin peak, identify the impurities listed in Table 8.7, and measure the peak responses. Calculate the percentage of each impurity in the portion of tablets taken by the formula:

$$100(r_i/r_s)$$

**Table 8.7** The limits of impurities of pravastatin, 2

Name	Relative retention time	Limit (%)
Oxidation impurity <sup>a</sup>	0.5	1
Pravastatin sodium	1.0	n/a
Specified unknown impurity 1	1.6	0.2
Specified unknown impurity 2	1.8	0.2
Pravastatin lactone	2.1	2
Specified unknown impurity 3	2.8	0.2
Specified unknown impurity 4	3.2	0.2
Specified unknown impurity 5	3.8	0.2

<sup>a</sup>Sodium (3*R*,5*R*)-3,5-dihydroxy-7-((1*S*,2*S*)-6-hydroxy-2-methyl-1,2-dihydronaphthalen-1-yl)heptanoate.

in which  $r_i$  is the peak response of the individual impurity, and  $r_s$  is the sum of the responses of all the peaks obtained from the *Test solution*. In addition to not exceeding the limits of each impurity in Table 8.7, not more than 0.2% of any unspecified individual impurity is found and not more than 3% of total impurities are found. Disregard the peak due to pravastatin-related compound B that elutes at the relative retention time of about 0.7 and the peak due to 3''-hydroxy pravastatin at the relative retention time of about 0.3, as these impurities are controlled in the drug substance monograph. Disregard any impurity that is less than 0.05%.

**Assay**—[Note: The *Standard preparation*, *Assay stock preparation*, and *Assay preparation* can be stored for up to 7 days at room temperature.]

**Mobile phase**—Prepare a filtered and degassed mixture of methanol, water, glacial acetic acid, and triethylamine (500:500:1:1). Make adjustments if necessary (see *System Suitability* under *Chromatography* <621>).

**Diluent 1**—Transfer 16.4 g of anhydrous sodium acetate into a 2000-ml volumetric flask. Add 1600 ml of water, adjust with glacial acetic acid to a pH of 5.6, dilute with water to volume, and mix.

**Diluent 2**—Prepare a mixture of *Diluent 1* and methanol (80:20).

**Standard preparation**—Transfer an accurately weighed quantity of USP Pravastatin 1,1,3,3-Tetramethylbutylamine RS to a suitable volumetric flask and dissolve in *Diluent 1* using sonication to obtain a solution having a known concentration of about 0.6 mg of pravastatin 1,1,3,3-tetramethylbutylamine per ml. Dilute 5.0 ml of this solution with *Diluent 2* to 25 ml and mix.

*Assay stock preparation*—Transfer not fewer than five tablets to a suitable volumetric flask with at least a  $NL \times 2$  ml capacity,  $N$  being the number of tablets transferred, and  $L$  being the label claim per tablet, filled to at least 80% capacity with *Diluent 1*. [Note: It is necessary to fill the flask to 80% capacity to maintain the correct pH throughout the preparation.] Shake for at least 1 h and sonicate for at least 15 min with periodic shaking of the flask by hand, until the tablets have completely disintegrated. Allow to cool, and dilute with *Diluent 1* to volume. Centrifuge a portion of the solution for 15 min at 2000 rpm or filter.

*Assay preparation*—Dilute approximately 5 ml of the *Assay stock preparation* with *Diluent 2* to obtain a solution having an expected concentration of about 0.1 mg/ml, based on the label claim.

*Resolution solution*—Transfer about 2 mg of USP Pravastatin-Related Compound B RS to a 10-ml volumetric flask. Dissolve in and dilute with methanol to volume. Transfer 0.1 ml of this solution and 1 ml of the *Standard preparation* to a small tube and mix. [Note: Pravastatin-related compound B is the 6'-epipravastatin sodium.]

*Chromatographic system* (see *Chromatography* (621))—The liquid chromatograph is equipped with a 238-nm detector and a 4.6-mm  $\times$  5-cm column that contains end-capped packing L1. Alternatively, a 3.9-mm  $\times$  7.5-cm column containing end-capped packing L1 can be used. The flow rate is about 1 ml/min. Chromatograph the *Resolution solution* and record the peak responses as directed for *Procedure*: the relative retention times are about 0.7 for pravastatin-related compound B and 1 for pravastatin; the resolution,  $R$ , between the pravastatin-related compound B and the pravastatin peaks is not less than 3. Chromatograph the *Standard preparation* and record the peak responses as directed for *Procedure*: the relative standard deviation for replicate injections is not more than 2%.

*Procedure*—Separately inject equal volumes (about 20  $\mu$ l) of the *Standard preparation* and the *Assay preparation* into the chromatograph, record the chromatograms, and measure the peak response for pravastatin. Calculate the percentage of pravastatin sodium ( $C_{23}H_{35}NaO_7$ ) in the portion of tablets taken by the formula:

$$100(446.51/553.78)(CVD/NL)(r_U/r_s)$$

in which 100 is the conversion factor to percentage; 446.51 and 553.78 are the molecular weights of pravastatin sodium and pravastatin 1,1,3,3-tetramethylbutylamine, respectively;  $C$  is the concentration, in mg/ml, of

pravastatin 1,1,3,3-tetramethylbutylamine in the *Standard preparation*;  $V$  is the volume, in ml, of the *Assay stock preparation*;  $D$  is the dilution factor of the *Assay preparation*;  $N$  is the number of tablets taken to prepare the *Assay stock preparation*;  $L$  is the label claim, in mg of pravastatin sodium per tablet; and  $r_U$  and  $r_s$  are the pravastatin peak responses obtained from the *Assay preparation* and the *Standard preparation*, respectively.

## 5.2. Spectrophotometric methods

Rao *et al.* [28] developed a simple and reproducible spectrophotometric method for the estimation of pravastatin sodium. The method is based on the reaction of the drug with ferric chloride and potassium ferricyanide which form a green chromogen exhibiting absorption maxima at 737 nm.

Lotfy *et al.* [29] developed two spectrophotometric methods for the determination of pravastatin in the presence of its degradation products. The first method depends on derivative spectrophotometry (1D and 2D) by measuring the peak amplitude of the first derivative curve of pravastatin at 249 nm. This method determined pravastatin in the concentration range (3–21  $\mu\text{g/ml}$ ) with mean percentage recovery of 100.90% for first derivative spectrophotometry and 100.30% for second derivative spectrophotometry. The second method depended on the quantitative densitometric evaluation of the thin-layer chromatography of pravastatin in the presence of its degradation products without any interference. Toluene:methanol:ethyl acetate:acetic acid (68:40:28:0.7) were used as the mobile phase for pravastatin and the chromatograms were scanned at 238 nm. This method detected pravastatin in the concentration range of 1–10 ng/spot with mean percentage recovery of 100.20%.

Balaji and Khatteboina [30] developed and validated a novel, simple, and rapid UV spectrophotometric method for the determination of pravastatin sodium in tablets. The method shows the maximum absorbance at 240 nm. Beer's law was obeyed in the concentration range of 2–18  $\mu\text{g/ml}$ . The method was validated in terms of linearity, precision, accuracy, and specificity. The method is precise, accurate, sensitive, and reproducible and can be used for routine quality control (QC) testing of marketed formulations.

Kalvikkarasi *et al.* [31] developed two spectrophotometric methods for estimation of pravastatin sodium in pure and in pharmaceutical formulations. Method A is based on the reduction of ferric to ferrous ions followed by complexation with 2,2'-piprydil to produce an orange-red chromogen at 522 nm, and Method B is based on the reduction of ferric to ferrous ions

followed by complexation with 1,10-phenanthroline to produce an orange-red chromogen at 510 nm and both obeyed Beer's linearity in the concentration range of 50–250 µg/ml for method A and 20–100 µg/ml for Method B. Both methods were extended to pharmaceutical formulation.

Farouk *et al.* [32] presented an accurate, precise, rapid, and reproducible spectrophotometric method for determination of pravastatin in the presence of its acid degradates by third derivative spectrophotometry, first derivative of ratio spectra, and first derivative of pH-induced difference spectrophotometry. The methods were validated according to the ICH guidelines and were applied for the determination of the drug in pure form, in laboratory prepared mixtures, and in pharmaceutical formulations.

Ashour *et al.* [33] described a new, accurate, and reliable spectrophotometric method for the assay of pravastatin sodium in pure form and pharmaceutical formulations. The method involves the oxidative coupling reaction of pravastatin with 3-methyl-2-benzothiazolinone hydrazone hydrochloride monohydrate (MBTH) in the presence of Ce(IV) in an acidic medium to form colored products at 664 nm. Beer's law was obeyed in the ranges of 7.0–30.0 µg/ml for pravastatin–MBTH. Molar absorptivities for the above three methods were found to be  $0.68 \times 10^4$  l/mol/cm. Statistical treatment of the experimental results indicates that the method is precise and accurate. The method has been applied to the determination of the components in commercial forms with no interference from the excipients. A comparative study between the suggested procedure and the official method for these compounds in the commercial forms showed no significant difference between the two methods.

Ashour and Khateeb [34] described a simple and sensitive kinetic spectrophotometric method for the quantitative analysis of pravastatin sodium in pure and in pharmaceutical formulations. The method is based on the formation of colored products between pravastatin and 4-chloro-7-nitrobenzo-2-oxa-1,3-diazole in acetone medium at  $55 \pm 2$  °C. The reaction was followed spectrophotometrically by measuring the increase in absorbance at 462 nm as a function of time. The initial rate and fixed-time methods were adopted for constructing the calibration curves. The linearity ranges were 15–50 and 10–70 µg/ml for initial rate and fixed-time methods, respectively. The limit of detection for initial rate and fixed-time methods was 0.029 and 0.08 µg/ml, respectively. Both methods were applied for the estimation of pravastatin in commercial dosage forms with no interference from excipients. The results are compared with the HPLC pharmacopoeial method.

Frag *et al.* [35] described a sensitive extractive spectrophotometric method for the determination of pravastatin in pharmaceutical formulations. The method involves the formation of colored ion pairs between the drug and the Mo(V)-thiocyanate binary complex followed by their extraction with 1,2-dichloroethane and quantitative determination at 470 nm. The experimental conditions were optimized to obtain the maximum color intensity. The method permits the analysis of pravastatin over a concentration range of 10–150 µg/ml with a detection limit of 0.26 µg/ml.

### 5.3. Electrochemical methods

#### 5.3.1 Polarographic methods

Coskun *et al.* [36] used a differential pulse polarographic method for the determination of pravastatin sodium in tablets. Ground pravachol tablets were extracted with methanol by shaking for 30 min, the filtered extract was mixed with 1 M tetramethylammonium bromide and diluted with water, and the solution was deaerated with nitrogen before differential pulse polarography between  $-1.6$  and  $-2.6$  V versus Ag/AgCl. The height of the peak at  $-2.1$  V was measured and referred to a calibration graph for the range of 80–240 µM pravastatin sodium. The relative standard deviation for 10 mg of the drug in tablets was 1.61%. The results agreed with those obtained by UV spectrophotometry.

#### 5.3.2 Voltammetric methods

Nigović [37] studied the electrochemical reduction and adsorptive voltammetric behavior of pravastatin by means of cyclic and square-wave voltammetry at a hanging mercury-drop electrode in electrolytes of different pH. Within the entire pH range (2–9) in Britton–Robenson buffer, pravastatin gave rise to a single voltammetric peak in the potential interval from  $-1.22$  to  $-1.44$  V, depending on pravastatin concentration. It was found that the reduction of pravastatin proceeds via a relatively stable intermediate, which is transformed to the final electroinactive product by a coupled chemical reaction or can be reoxidized back to pravastatin. The rate of chemical transformation is controlled by the proton concentration. The electrode mechanism has the properties of a surface redox reaction. A sensitive analytical method for trace analysis of pravastatin based on the adsorptive stripping technique has been developed. The calibration plot was linear in the range of  $8 \times 10^{-8}$ – $5 \times 10^{-7}$  mol/l. Application of the square-wave voltammetric method to the determination of pravastatin in a

pharmaceutical dosage form, without sample pretreatment, resulted in acceptable deviation from the stated concentration.

Neves *et al.* [38] studied the electro-oxidative behavior of pravastatin in aqueous media by square-wave voltammetry at a glassy-carbon electrode and at a screen-printed carbon electrode. Maximum peak current intensities in a pH 5 buffer were obtained at +1.3 V versus AgCl/Ag and +1 V versus Ag for the glassy-carbon electrode and the screen-printed carbon electrode surface, respectively. Validation of the developed methodologies revealed good performance characteristics and confirmed their applicability to the quantitation of pravastatin in pharmaceutical products without significant sample pretreatment.

## 5.4. Chromatographic methods

### 5.4.1 Thin-layer chromatographic methods

Chaudhari *et al.* [39] developed a high-performance thin-layer chromatographic method for the separation and quantitation of pravastatin sodium and two other statins in tablet dosage forms. The stationary phase was precoated silica gel 60 F<sub>254</sub>. The mobile phase was a mixture of chloroform–methanol–toluene (6:2:2). The method has been validated and proved to be rugged. Calibration curves were linear over the studied ranges with correlation coefficient greater than 0.999. The drugs were extracted from tablets using methanol. The percentage recoveries ranged from 98 to 101 for pravastatin. The limit of detection for pravastatin was 8 ng/spot and the limit of quantitation was 100 ng/spot for pravastatin. The method is useful in the QC of the bulk manufacturing and tablet dosage forms.

Ahmed *et al.* [40] established and validated a stability-indicating high-performance thin-layer chromatographic method for the simultaneous analysis of pravastatin and mevastatin in fermentation broth. Compounds were separated on aluminum foil TLC plates precoated with silica gel 60 F<sub>254</sub>. The mobile phase was toluene–ethyl acetate–formic acid 3:2:1, which gave compact bands of pravastatin and mevastatin ( $R_f$   $0.31 \pm 0.02$  and  $0.48 \pm 0.02$ , respectively). Detection at 237 nm resulted in  $r=0.995$  and 0.994 for pravastatin and  $r=0.992$  and 0.995 for mevastatin, for peak height and peak area, respectively. The limit of detection and quantification for pravastatin 19.2 and 58.3 ng/band and 20.1 and 60.8 ng/band for mevastatin. The method enabled effective quantification of both drug in the fermentation broth of *Actinomadura macra* and can be used as a stability-indicating method for routine analysis of these compounds during bioconversion.

#### 5.4.2 Gas chromatography/mass spectrometric methods

Funke *et al.* [41] determined pravastatin sodium and its major metabolites in human serum and plasma by capillary gas chromatography–negative-ion chemical ionization mass spectrometry. Serum or plasma samples (1 ml) plus tetrahydropravastatin and the dihydrotriol metabolite of pravastatin sodium as internal standards was applied to a Bond Elut C<sub>18</sub> extraction column preactivated by passage of methanol, dil. phosphate buffer of pH 7, and heptane. The adsorbed compounds were eluted with acetone (5 ml) and the solvent was evaporated under nitrogen at 50 °C. The compounds were derivatized with pentafluorobenzyl bromide at 40 °C and, after adding propionic acid to remove surplus pentafluorobenzyl bromide, with bis(trimethylsilyl)trifluoroacetamide. The derivatives were determined with a Hewlett–Packard 5985 B GC–MS apparatus with a fused-silica column (5.5 m × 0.23 mm) of CP SIL 19CB bonded phase (0.12 µm). Temperature programmed from 210 (held for 1 min) to 290 °C at 30 °C/min and ammonia as reagent gas. Pravastatin sodium and its major 3-hydroxy- and triol metabolites could be determined down to 0.3 ng/ml in serum.

Pan *et al.* [42] investigated the oral bioavailability of pravastatin and lovastatin. Serum specimens were assayed by gas chromatography/mass spectrometry for pravastatin or lovastatin acid and by bioassay for active inhibitor concentration and, after hydrolysis of the lactones, for total inhibitor concentration. The systemic bioavailabilities of the total inhibitors of the two drugs were different, with the mean AUC value for lovastatin being 50% higher than that for pravastatin (mean ± SEM) AUC 0–24 values of 285 ± 25 and 189 ± 13 ng equiv. h/ml, respectively. Pravastatin, which is administered as the monosodium salt, is present in the systemic circulation as the open acid; lovastatin, which is administered as the lactone, is present as both the open acid active metabolites (62%) and closed-ring lactone metabolites (38%), which are potentially active. Based on mean AUC values, pravastatin accounted for 75% of the active inhibitors from a pravastatin dose.

Kawabata *et al.* [43] quantified pravastatin and its metabolites in human biological fluids using automated gas chromatographic/mass spectrometry. The method was applied to pharmacokinetic studies in volunteers and patients. The method relies upon a simple extraction and purification of the sample on a C<sub>8</sub> solid-phase extraction column, and derivatization with diazomethane ester, and pentafluorobenzyl ester, followed by an automated gas chromatography/electron impact negative ion chemical ionization mass spectrometric quantitative analysis. The method was used in human pharmacokinetic studies.



Morris *et al.* [44] determined pravastatin in plasma by gas chromatography–chemical ionization mass spectrometric method. Pravastatin present in human plasma as hydroxylactone and the corresponding free hydroxyacid were extracted as the corresponding potassium salts and derivatized with pentafluorobenzyl bromide in *N,N*-diisopropylethylamide and with *N*-methyl-*N*-trimethylsilyltrifluoroacetamide. The derivatized material was dissolved in 20 ml tetradecane. 6'-beta-Hydroxymethylsimastatin (5 ng in acetonitrile) was used as an internal standard. Samples (1  $\mu$ l) were analyzed in the splitless mode on a Hewlett-Packard (HP) 5890A GC with an HP 7673A autoinjector at 280 °C and an Ultra 2 column (12 m  $\times$  0.2 mm) of methyl–5% phenyl (0.11  $\mu$ m) with temperature programming from 210 (held for 1 min) to 300 °C at 10 °C/min and chemical ionization mass spectrometry. Calibration graphs were rectilinear from 1 to 50 ng/ml of pravastatin.

Cai *et al.* [45] described a gas chromatography–mass spectrometry method for the quantitative determination of pravastatin in plasma. Plasma (1 ml) was mixed well with 0.5 ml sodium chloride and 0.2 M phosphate buffer of pH < 4 for 20 min and the mixture was extracted with 4 ml ethyl acetate for 5 min and centrifuged for 15 min. The supernatant solution was evaporated to dryness, the residue was methylated and silanized, and the excess solvents were evaporated. The residue was dissolved in diethyl ether, and portions were analyzed for pravastatin TMS methyl ester by GC on a column (12 m  $\times$  0.2 mm i.d.) coated with HP-1 (0.32  $\mu$ m) operated with temperature programming from 18 (held for 0.5 min) to 300 °C (held for 10 min) at 20 °C/min and 70 eV electron impact mass spectrometry detection operating with selective-ion monitoring at  $m/z$  462. The calibration graph was linear from 1 to 60 ng/ml of pravastatin and the detection limit was 0.015 ng. Recoveries were  $\sim$ 90% with relative standard deviation ( $n=5$ ) of <7.7%. No interference was observed.

#### 5.4.3 High-performance liquid chromatographic methods

Whigan *et al.* [46] determined pravastatin sodium and its isomeric metabolite in human urine by HPLC with UV detection. Urine ( $\leq$ 0.5 ml), treated with 1  $\mu$ g of 9-fluoro-11 $\beta$ -hydroxy-16 $\alpha$ ,17 $\alpha$ -(1-methylethylidenedioxy)-3-oxoandrosta-1,4-diene-17-carboxylic acid (internal standard), was applied to a Bond Elut cyclohexyl cartridge. Elution was with acetone (3 ml) and the eluate was evaporated to dryness at 50 °C under nitrogen. The residue was dissolved in 1 ml of mobile phase (pH > 3). Separation was achieved on a column (25 cm  $\times$  4.6 mm) of alkylphenyl (5  $\mu$ m) with a precolumn of silica gel (37–53  $\mu$ m) and aq. 0.1 M acetic acid buffer

(pH 3)–acetonitrile–propan-2-ol (31:15:4) as the mobile phase (0.8 ml/min) at 15 °C, with detection at 239 nm. The calibration graph was rectilinear up to 1.5 µg/ml of pravastatin sodium and its isomeric metabolite, with a detection limit of 0.1 µg/ml in urine for both. Recoveries were quantitative. Intra- and interday coefficients of variation were  $\leq 10.0\%$  for pravastatin sodium and its metabolite.

Muramatsu *et al.* [47] developed a highly sensitive method by using immobilized antibody column extraction followed by HPLC for the determination of pravastatin sodium in plasma. The analyte was monitored by a laser-induced fluorescence detector after fluorogenic derivatization with dansyl ethylenediamine.

Iacona *et al.* [48] developed a HPLC method for determination of pravastatin in plasma. Plasma (1 ml) was mixed with 1 ml of 0.1 M potassium dihydrogen phosphate of pH 7.2 and applied to a C2 Bond Elut extraction column which was washed with 2 ml of water before elution was effected with 500 µl of aq. 25% acetonitrile. The eluate was vacuum-dried and the residue was dissolved in 80 µl of internal standard solution [2 ml of methanolic simvastatin  $\beta$ -hydroxyacid solution (0.1 mg/ml) mixed with 1 ml of methanol and 1 ml of aq. 0.1 M potassium dihydrogen phosphate of pH 5]. A 50 µl portion of the resulting solution was analyzed on a column (5 cm  $\times$  4.6 mm i.d.) of 3 µm LC-18 equipped with a 2 cm long Supelguard LC-18 precolumn and operated at 50 °C with 0.05 M ammonium phosphate of pH 3.5/acetonitrile (37:13) as the mobile phase (1.6 ml/min) and detection at 238 nm. The calibration graph was linear for 5–200 ng/ml of pravastatin with a detection limit of 2 ng/ml. The relative standard deviation was  $\leq 10\%$  and the recovery was 75%.

Dumousseaux *et al.* [49] tested a highly sensitive and specific method for the determination of pravastatin sodium in plasma by HPLC with laser-induced fluorescence detection after immobilized antibody extraction. Plasma (1 ml) was applied to an immobilized antibody column and washed with 2  $\times$  4 ml water, 4 ml phosphate buffer saline, and 2  $\times$  4 ml water. Elution was effected with 4 ml methanol and the eluate was treated with 0.1 ml aqueous internal standard solution (R-416; 100 ng/ml) and evaporated to dryness. The residue was dissolved in 100 µl DMF and derivatized with 100 µl each of triethylamine (47.7 µl/ml in dioxane), diethyl phosphorocyanidate (51.8 µl/ml in dioxane), and *N*-dansylethylenediamine (100 µg/ml in dioxane). The mixture was stirred for 10 min and then allowed to stand for 10 min. A 10 µl portion of the mixture was analyzed by column-switching HPLC on a 300-C4 column (15 cm  $\times$  4.6 mm i.d.)

with 10 mM citric acid of pH 2.4/acetonitrile (7:3) as the mobile phase (1 ml/min) and a second column of 5C<sub>18</sub>-AR (15 cm × 6 mm i.d.) with 5 mM citric acid of pH 2.6/acetonitrile (1:1) as the mobile phase (1 ml/min) with laser-induced fluorescence at 325 nm. The separation time was 20 min with an introduction time from the first to the second column of 7.5–10 min. The calibration range was 0.5–100 ng/ml with detection and quantitation limits of 2 and 100 pg/ml, respectively; relative standard deviation was <8%.

Otter and Mignat [50] developed an HPLC with ultraviolet detection for the determination of pravastatin in human plasma. A 100 µl sample of pravastatin (I) and triamcinolone acetonide (internal standard) in methanol, extracted from plasma by solid-phase extraction, was analyzed by HPLC on a Purospher RP-18 (5 µm) end-capped column (25 cm × 4 mm i.d.). Analytes were eluted (1 ml/min) with 20 mM potassium dihydrogen phosphate buffer containing 1 mM sodium dodecyl sulfate/acetonitrile (7:13) and detection at 239 nm. The calibration graph was linear from 2 to 200 ng/ml of pravastatin with a detection limit of 4 ng and quantitation limit of 2 ng/ml. Intra- and interday relative standard deviations ( $n=6$ ) were <6 and <17%, respectively, over the calibration range with a mean recovery of  $69.2 \pm 6.7\%$  for pravastatin from plasma.

Siekmeier *et al.* [51] developed a simple and reliable HPLC method for the determination of pravastatin plasma concentrations under clinical routine conditions. Samples were prepared by solid-phase extraction on cyclohexyl Bond Elut Cartridge. Chromatography was carried out on an octyl matrix. Triamcinolone acetonide was used as the internal standard. The method was linear within the range of 5–200 µg/l pravastatin. The coefficient of variation depended on the concentration of the drug, but was less than 10% throughout. The pharmacokinetics of the drug were determined in healthy individuals. Peak plasma concentration of pravastatin was found between 60 and 120 min after oral administration of 60 mg and reached values between 37 and 126 µg/l.

Wang [52] determined pravastatin and compactin in fermentation liquor by reversed-phase HPLC (RP-HPLC) at 237 nm on Spherisorb C<sub>18</sub> column with methanol: 0.2 M ammonium acetate (53:47) as the mobile phase. The results showed that the method was convenient, rapid, and effective and may be used for online monitoring fermentation process.

Bastarda *et al.* [53] developed a fast HPLC method to separate and quantify the products of the isomerization. Hypersil ODS, 3 µm (15 cm × 4.6 mm) column with a mobile phase consisted of 2.5 mM phosphate buffer, pH 7:

acetonitrile (80:20) and 2.5 mM phosphate buffer, pH 7:acetonitrile (20:80). Flow rate was 1.5 ml/min and UV detection at 235 nm.

Bauer *et al.* [54] estimated pravastatin in human plasma and urine sample by HPLC. The preparation of samples was performed by automated solid-phase extraction using clonazepam as the internal standard. The compounds were separated by isocratic RP-HPLC ( $C_{18}$ ) and detected at 239 nm. The method was linear up to concentrations of 200 ng/ml in plasma and 2000 ng/ml in urine. The intra-assay variability for pravastatin in plasma ranged from 0.9% to 3.5% and from 2.5% to 5.3% in urine. The interassay variability ranged from 9.1% to 10.2% in plasma and from 3.9% to 7.5% in urine. The validated limits of quantification were 1.9 ng/ml for plasma and 125 ng/ml for urine estimation. The method characteristics allowed the determination of the pharmacokinetic parameters of pravastatin after administration of therapeutic doses.

Kawabata *et al.* [55] developed and validated a liquid chromatography–mass spectrometric method for rapid and sensitive analysis of pravastatin and R-416, the main metabolite of pravastatin, in human plasma. The analytes were extracted from plasma samples by a solid-phase extraction method using a Bond Elut<sup>®</sup> C8. The method involved the use of liquid chromatography coupled with atmospheric pressure chemical ionization (APCI) and selected reaction monitoring mass spectrometry. A pravastatin analog, R-122798, was used as the internal standard (IS). Separation of pravastatin, R-416, and the IS was accomplished using an RP column ( $C_{18}$ ). The components eluted were ionized by the APCI source (negative ion) and subsequently detected by a highly selective triple quadrupole mass spectrometer in the SRM mode. Linear standard curves were obtained from 0.1 ng/ml (lower limit of quantification, LLOQ) to 100 ng/ml. The intra-assay precisions (coefficient of variation) for the samples at the LLOQ were 1.8% for pravastatin and 1.6% for R-416. The intra-assay accuracy values were 95.8–107.6% for pravastatin and 92.6–109.0% for R-416, respectively. Precision and accuracy of QC samples were determined at concentrations of 0.5, 10, and 80 ng/ml for all analytes. The intra- and interassay precisions calculated from QC samples were within 10% for pravastatin and within 11% for R-416. The overall recoveries for pravastatin and R-416 were 75.7–82.1% and 68.6–74.3%, respectively. Pravastatin and R-416 were stable in human plasma for 3 weeks at  $-20^{\circ}\text{C}$  in a freezer, up to 6 h at room temperature, and up to 48 h at  $6^{\circ}\text{C}$ . This assay method was used to evaluate the pravastatin and R-416 levels in healthy volunteers following oral administration of Mevalotin<sup>®</sup>.

Kocijan *et al.* [56] developed an HPLC and capillary electrophoresis methods for the determination of pravastatin in production media. The analyses were performed on particle column, monolithic column, and silica capillary filled with borate buffer, pH 9.3, containing 20 mM sodium dodecyl sulfate. All three methods successfully separate pravastatin from interfering compounds (matrix, mevastatin, and 6-epipravastatin) and runtimes are less than 1 min. Solvent consumptions for methods using small particle column, monolith column, and MECK were 132, 510, and 1.5 ml/h. The most sensitive was the method using particle column (LOD was about  $10^{-5}$  mg/ml) followed by the system using monolith column (LOD was  $2 \times 10^{-4}$  mg/ml) and the MECK method (LOD was about 0.02 mg/ml).

Rani and Reddy [57] developed an HPLC method for estimation of pravastatin sodium in tablets. Chromatography was carried out on an ODS column using a mixture of acetonitrile and water (50:50) as the mobile phase at a flow rate of 1 ml/min. Nimesulide was used as the internal standard and detection was carried out at 230 nm. The retention time of the drug was 2.16 min. The method produced linear responses in the concentration range of 0.5–40 µg/ml of pravastatin sodium. The method was applicable for determination of the drug in tablets.

Pasha *et al.* [58] developed and validated a specific, accurate, precise, and reproducible HPLC method for the simultaneous quantitation of pravastatin, and other statin, in pharmaceutical formulations and extended the application to *in vitro* metabolism studies of these statins. Ternary gradient elution at a flow rate of 1 ml/min was employed on an Intertisl ODS 3V column ( $4.6 \times 250$  mm, 5 µm) at ambient temperature. The mobile phase consisted of 0.01 M ammonium acetate (pH 5), acetonitrile, and methanol. Theophylline was used as an internal standard (IS). The drugs and their metabolites were monitored at a wavelength of 237 nm. Drugs were found to be 89.6–105.6% of their label's claim in the pharmaceutical formulations. For *in vitro* metabolism studies, the reaction mixtures were extracted with simple liquid–liquid extraction using ethyl acetate. Baseline separation of statins and their metabolites along with IS free from endogenous interferences was achieved. Nominal retention times of IS were 7.5 min. The method is simple, selective, and could be applicable for routine analysis of the statins in pharmaceutical preparations as well as *in vitro* metabolism studies.

Onal and Sagirli [59] developed and validated a stability-indicating HPLC method for pravastatin sodium in tablets. The separation was achieved isocratically on a C<sub>18</sub> column (15 cm  $\times$  4.6 mm) using

methanol-phosphate buffer (pH 7, 0.02 M) (57:43) as a mobile phase at a flow rate of 1 ml/min with UV detection at 238 nm. A linear response was observed in the range of 1–5 µg/ml. The method showed good recovery (100.5%) and the relative standard deviation for intra- and interday was 1.4%. The method can be used for QC assay of the drug in tablets and for stability studies as the method separates pravastatin from its degradation products and tablet excipients.

Campos-Lara *et al.* [60] developed an HPLC method for the estimation of pravastatin in human serum samples to monitor the dyslipidemic patients. The validation parameters were linearity 10–200 ng/ml, correlation coefficient 0.99, mean recovery 0.73, quantification limit 10 ng/ml, and the limit of detection 5 ng/ml. The method was applied for pravastatin determination in human serum from Mexican dyslipidemic patients. Pravastatin values found for three studied patients were 73, 57, and 10 ng/ml, indicating the importance of the monitoring, due to the metabolic variability of the patients.

Xie [61] used an HPLC method for the determination of dissolution of pravastatin sodium capsule. The drug was analyzed using Diamonsil™ C<sub>18</sub> (5 µm, 20 cm × 4.6 mm) and a mobile phase of methanol-phosphate buffer solution (60:40), pH 3.5 ± 0.05, at a flow rate of 1 ml/min and detection at 238 nm. The linear range of pravastatin sodium was 3–12 µg/ml. The average recovery of pravastatin sodium was 99.86%.

Ashour *et al.* [62] described an HPLC formulation assay method for pravastatin. Separation was achieved using a Tecknokroma C<sub>8</sub> (5 µm, 25 cm × 4.6 mm) column and a mobile phase consisting of 10 mM ammonium acetate:methanol:triethylamine (40:60:0.17) with a flow rate of 1 ml/min. Pravastatin was detected at 239 nm and was eluted 2.15 min after injection. Linearity range for pravastatin was 0.4–1000 mg/ml. The determination of intra- and interday precision was less than 2.94% and 2.97% at all concentration levels. The method was applied to the determination of the component in commercial tablets with no interference for the excipient.

Brain-Isasi *et al.* [63] developed and applied an HPLC stability-indicating method to study the hydrolytic behavior of pravastatin in different pHs and temperature. From the system suitability test, the selected chromatographic conditions were a C<sub>18</sub> column, acetonitrile–30 mmol/l phosphate buffer solution pH 2 (28.72) as the mobile phase, 40 °C temperature column, a flux of 1 ml/min, and 239 nm as wavelength detection. The method exhibited an adequate repeatability and reproducibility and a recovery higher than 98%.

Campos-Lara and Mendoza-Espinoza [64] developed a selective extraction method for pravastatin quantification in tablets using HPLC with ultraviolet detection. The mobile phase consisted of acetonitrile and phosphate buffer (7:3), pH 2, and was delivered at the rate of 1 ml/min and detected at 238 nm. Retention time was 7.3 min and this peak was analyzed with mass spectroscopy. The method was fully validated and validation parameters were linearity 10–200 ng/ml, correlation coefficient 0.999, mean recovery 99%, limit of quantitation 5 ng/ml, and limit of detection 5 ng/ml. The method can be used for QC assay.

Gomes *et al.* [65] developed and validated an HPLC method for the determination of pravastatin sodium in pharmaceuticals. Two stability-indicating HPLC methods were developed with a small change (10%) in the composition of the organic modifier in the mobile phase. An RP-18 column was used with mobile phases consisting of methanol–water 60:40 for pravastatin. The pH of the mobile phase was adjusted to 3 with orthophosphoric acid and the flow rate was 1 ml/min.

He *et al.* [66] developed an HPLC-UV with solid-phase extraction method for the determination of pravastatin and relative bioavailability in plasma. Sample separation was based on solid-phase extraction. The compounds were separated on a Hypersil Gold C<sub>18</sub> column (4.6 mm × 15 cm, 5 μm) with a mixture of acetonitrile (solvent A) and 20 mmol/l sodium dihydrogen phosphate–1 mmol/l sodium dodecyl sulfate (pH: 2.45) (solvent B) as the mobile phase at a 0.8 ml/min. The gradient elution program was A: B = 29:71 (0–11 min), A: B = 40:60 (11–15 min), and A: B = 29:71 (15–18 min), and the detection wavelength was 239 nm. The plasma samples were obtained and determined by the HPLC method, and the pharmacokinetic and bioavailability was studied. The calibration curve for pravastatin was linear at 2–256 ng/ml, with limit of quantity of 2 ng/ml and recoveries were 102.5–108.6%. The method is sensitive, selective, and rapid.

Sparidans *et al.* [67] developed and validated a bioanalytical assay method for pravastatin and two isomeric metabolites, 3'α-isopravastatin and 6'-epipravastatin. Mouse plasma and tissue homogenates from liver, kidney, brain, and heart were pretreated using protein precipitation with acetonitrile containing deuterated internal standards of the analytes. The extract was diluted with water and injected into the chromatographic system. This system consisted of a polar-embedded octadecyl silica column using isocratic elution with formic acid in a water:acetonitrile mixture. The eluate was transferred to an electrospray interface using negative ionization, and the

analytes were detected and quantified with the selected reaction monitoring mode of a triple quadrupole mass spectrometer. The assay was validated in a 3.4–7100 ng/ml concentration range for pravastatin, 1.3–2200 ng/ml for 3'-isopravastatin, and 0.5–215 ng/ml for 6'-epipravastatin using only plasma for calibration. For plasma samples, subjected to full validation, within- and between-day precisions were 1–7% (9–18% at the lower limit of quantitation level) and accuracies were between 91% and 103%. For tissue homogenates, subjected to partial validation, within- and between-day precisions were 2–12% (6–19% at the lower limit of quantitation level) and accuracies were between 87% and 113% (81% and 113% at the lower limit of quantitation level). Drug and metabolites were shown to be chemically stable under most relevant analytical conditions. Finally, the assay was applied for a pilot study in mice. After intravenous administration of the drug, all isomeric compounds were found in plasma; however, in liver and kidney homogenate, only the parent drug showed levels exceeding the lower limit of quantitation.

Abdullah [68] developed an RP-HPLC method for the determination of pravastatin and two other statins. The method involves the use of a 15 cm × 4.6 mm of Zorbax Extend C<sub>18</sub> column (5 μm) and different chromatographic conditions for the separation of the drugs. Linearity range was 10–60 μg/ml for pravastatin. The method was used for the determination of the drugs in spiked human plasma samples.

Sultana *et al.* [69] developed a validated RP-HPLC method for the simultaneous determination of pravastatin, lisinopril, and other statins in active pharmaceutical ingredients, formulations, and human serum. A Purospher star C<sub>18</sub> (5 μm, 25 cm × 4.6 mm) column was used with mobile phase consisting of acetonitrile:water (60:40, pH 3) with flow rate of 1 ml/min, and the quantitative evaluation was performed at 225 nm. The retention time was 2 min for lisinopril and 3.1 min for pravastatin. Suitability of this method for the quantitative determination of the drugs was proved by validation in accordance with the requirements laid down by International Conference on Harmonization guidelines. The method was applied to the determination of the drugs in active pharmaceutical ingredients and in pharmaceutical preparations, with high percentage of recovery, good accuracy, and precision.

Sampath *et al.* [70] developed and validated an ultra-flow liquid chromatography-tandem mass spectrometric method for the estimation of pravastatin in human plasma. Pravastatin and omeprazole (internal standard) were extracted from human plasma using a solid-phase extraction procedure



with Strata X cartridge. Samples were chromatographed on Hypurity Advance C<sub>18</sub>, 5 cm × 4.6 mm, 5 μm column using a mobile phase consisting of (80:20) acetonitrile and 2 mM ammonium formate. Pravastatin and omeprazole (IS) were ionized using the electrospray interface operating in the negative ion mode. The characteristic ion dissociation transitions  $m/z$  423.1 → 321.2 and  $m/z$  344 → 193.8 were monitored for pravastatin and omeprazole (IS), respectively. The assay was robust, sensitive, and highly specific with no interference from human plasma. The method is suitable for supporting clinical studies and applied to the analysis of samples from a bioequivalence study.

Huang *et al.* [71] developed a single *in vitro* dissolution method for a combination trilayer tablet formulation of pravastatin and clopidogrel. A robust and discriminating HPLC method for the analysis of the two drugs simultaneously in dissolution samples was developed and validated. The RP-HPLC method utilizes a Phenomenex Synergi Hydro-RP column (4 μm, 5 cm × 4.6 mm) maintained at 30 °C with a mobile phase of water–methanol–trifluoro acetic acid (45:55:0.025), a flow rate of 1 ml/min, and UV detection at 238 nm.

Harisa *et al.* [72] developed and used a reversed-phase ultra performance liquid chromatographic method for the assay of pravastatin. The mobile phase consists of acetonitrile and water (35:65), the flow rate was 0.5 ml/min. The analyte separation was carried out using C<sub>18</sub> column under temperature 40 °C using ultraviolet detector at 237 nm.

Kadikar and Shah [73] developed and validated an RP-HPLC method for the simultaneous estimation of pravastatin and coenzyme Q10 in pure and formulated dosage form. The quantification was carried out using symmetry C<sub>18</sub> column, (25 cm × 4 mm, 5 μm) column, in isocratic mode, with mobile phase compressing acetonitrile and tetrahydrofuran (80:20). The flow rate was 1 ml/min and the detection by UV at 254 nm. Retention times were 6.45 and 3.64 for coenzyme Q10 and pravastatin, respectively.

Silva *et al.* [74] developed and validated a simple and fast RP-HPLC method in the linear range of 28–52 μg/ml for the determination of pravastatin in bulk drug or dosage form. The drug was determined using C<sub>8</sub> end-capped column (25 cm × 4 mm, 5 μm) column, isocratic mobile phase of acetonitrile and 0.1% phosphoric acid (65:35), 30 °C, ultraviolet diode array detection at 238 nm, and 1 ml/min flow rate for pravastatin sodium. The method shows appropriate linearity, accuracy, precision, and selectivity toward placebo and/or degradation products in very similar chromatographic conditions for the drug.

#### 5.4.4 High-performance liquid chromatography/mass spectrometric methods

Kawabata *et al.* [75] described an automated method for the simultaneous determination of pravastatin and its main metabolite in human plasma by HPLC–atmospheric pressure chemical ionization mass spectrometry. Plasma (1 ml), spiked with 100  $\mu$ l R 1437 (800 ng/ml, internal standard), was adjusted to pH 6 with phosphate buffer of pH 4, and the mixture was applied to a preconditioned Bond Elut C8 solid-phase extraction cartridge. Pravastatin and its main metabolite R-416 were eluted with 1.5 ml propan-2-ol, and the eluate was evaporated at 40 °C under reduced pressure. The residue was dissolved in 300  $\mu$ l mobile phase, and portions were analyzed by HPLC on a 5- $\mu$ m Inertsil ODS-2 column (15 cm  $\times$  4.6 mm i.d.) with acetonitrile/0.01 M ammonium acetate (3:2), containing 0.2% anhydrous acetic acid and 0.06% triethylamine, as the mobile phase (1 ml/min) and atmospheric–pressure chemical ionization mass spectrometric detection. The mass spectrometer was operated in selected-ion monitoring mode at  $m/z$  423 and 466, respectively, for pravastatin and R-416. Optimization of the MS interface is described. The calibration graph was linear up to 80 ng/ml for each drug. Intra-assay relative standard deviations ( $n=5$ ) were 0.4–9.7% and 16.8–19.7%, respectively, for 1.25–8 and 0.625 ng/ml of pravastatin and R-416. Inter-assay relative standard deviations ( $n=5$ ) were 0.4–8.3%. Results correlated well ( $r \geq 0.969$ ) with those by GC–MS.

Zhu and Neirinck [76] developed an HPLC/ion electrospray (negative ion) MS for the determination of pravastatin in human plasma. Plasma samples were prepared by a solid-phase extraction on C<sub>18</sub> Bond Elut cartridge. Chromatography was carried out with a Zorbax C8 column. Simple isocratic chromatography conditions were used. The method has been validated in a linear range of 0.25–300 ng/ml with a coefficient of variation of 0.6–3.4%. The overall recovery was 90.5% for pravastatin and 90.8% for the internal standard  $\beta$ -hydroxylovastatin. The method is simple and reliable with a total run time of less than 2 min.

Deng *et al.* [77] determined both pravastatin and its main metabolite, 3' $\alpha$ -isopravastatin in human plasma by HPLC–MS method. After addition of mycophenolic acid (internal standard), the analytes in plasma samples were extracted with solid-phase extraction and then separated on a Discovery C<sub>18</sub> (5  $\mu$ m, 15 cm  $\times$  4.6 mm) column with a mobile phase of methanol–acetonitrile–6 mmol/l ammonium acetate solution (20:30:50) at a flow rate of 0.4 ml/min. HPLC–ESI–MS was performed in the selected-ion

monitoring mode using target ions at  $m/z$  423.4 (pravastatin and 3' $\alpha$ -isopravastatin) and  $m/z$  319.2 (internal standard). The blank plasma did not interfere with the determination of the analytes. The linear concentration ranges of the calibration curves for pravastatin and 3' $\alpha$ -isopravastatin were both 1.25–200 ng/ml. The limits of quantitation of pravastatin and 3' $\alpha$ -isopravastatin were both 1.25 ng/ml. The extraction recovery was more than 80%. The method is suitable for pharmacokinetics study of the drug and its main metabolite.

Vlckova *et al.* [78] reported a simple and reproducible ultra HPLC-tandem mass spectrometric method for the determination of pravastatin and its lactone in rat plasma and urine using deuterium-labeled internal standard for the quantification. Separation of the analytes was performed on BEH C<sub>18</sub> analytical column (5 cm  $\times$  2.1 mm, 1.7  $\mu$ m) using gradient elution by mobile phase consisting of acetonitrile and 1 mM ammonium acetate at pH 4. Run time was 2 min. Quantification of the analytes was performed using the selected reaction monitoring experiment in electrospray ionization negative ion mode for pravastatin and in electrospray ionization positive-ion mode for pravastatin lactone. Sample treatment consisted of a protein precipitation by acetonitrile and microextraction by packed sorbent for rat plasma. Simple microextraction by packed sorbent procedure was sufficient for rat urine. Microextraction by packed sorbent was implemented using the C<sub>8</sub> sorbent inserted into a microvolume syringe, an eVol hand-held automated analytical syringe, and a small volume of sample (50  $\mu$ l). The analytes were eluted by 100  $\mu$ l of the mixture of acetonitrile:0.01 M ammonium acetate, pH 4.5 (90:10). The method was validated and demonstrated good linearity in the range of 5–500 nmol/l for plasma and urine samples. Recovery was within 97–109% for plasma samples and 92–101% for urine samples. The method was applied for the measurement of pharmacokinetic plots of pravastatin and its lactone in rat plasma and urine samples.

Li *et al.* [79] determined pravastatin in rat muscle by RP-HPLC. Pravastatin was extracted from muscle homogenate with solid-phase extraction and analyzed by RP-HPLC with a UV detector. The lowest detection limit of the drug was 0.4 ng and the quantitation limit was 5 ng/g of muscles. The linearity range was 5100 ng/g of muscle and the solid-phase extraction recovery was 52.66%. The precision of the method was 61.8%. The method is sensitive with good precision to assay pravastatin in rat muscle. A pharmacokinetic application to determine the drug in muscle has been practiced.

Li *et al.* [80] established an RP-HPLC method for the analysis of pravastatin in rat liver. An aliquot of 5 g liver homogenate, spiked with triamcinolone acetonide (internal standard), was extracted by solid-phase extraction with Bond Elut C<sub>18</sub> column. Chromatography was performed using a C<sub>18</sub> reversed-phase column with mobile phase of disodium hydrogen phosphate buffer solution (0.035 mmol/l, pH 3)–acetonitrile (155:42). The linear equation was  $Y = 0.1843X - 4.238 \times 10^{-3}$  ( $r = 0.9934$ ) in the range of 0.05–10 µg/g liver. The limit of detection for pravastatin was 13 ng/ml and the limit of quantification for pravastatin in liver homogenate was 50 ng/g liver. The average extraction recovery of the drug from liver at different concentrations was 80.8% and the average interday precision was 11%. This procedure was applied to the assay of pravastatin in rat liver, which was collected from Lewis rats at different times after administration of pravastatin (i.e. 20 mg/kg). The method was sensitive and feasible for pharmacokinetic and distribution study of the drug.

Li *et al.* [81] determined pravastatin in rat plasma by solid-phase extraction and RP-HPLC. The drug in an aliquot of 1 ml plasma, spiked with internal standard, was extracted by solid-phase extraction with Bond Elut C<sub>18</sub> column and determined by HPLC. Chromatography employed a Purospher RP-C<sub>18</sub> reversed-phase column (5 µm, 25 cm × 4 mm), a Lichrospher 100 RP-C<sub>18</sub> precolumn (5 µm, 4 mm × 4 mm) as the analytical column, and the mixture of phosphate buffer (0.035 mmol/l disodium hydrogen phosphate, pH adjusted to 3 with phosphoric acid)–acetonitrile (13:7) as the mobile phase with a flow rate of 1 ml/min. Pravastatin was detected with a UV detector at 239 nm. The column temperature was set at 40 °C. The linearity range was 10–400 ng/ml with limits of detection and quantitation being 2 and 10 ng/ml, respectively. The average extraction recovery of pravastatin at different concentrations was 71.48%. Average intra- and interday precisions were 13% and 19%, respectively. The method was applied to the determination of pravastatin in rat plasma. The method is practical and can be used for pharmacokinetic study of the drug.

Delhi-Raj *et al.* [82] used a simple RP-HPLC method for the determination of pravastatin in tablet dosage form. The method used phenomendex<sup>®</sup> Luna 5 µm C<sub>18</sub> (15 cm × 4.6 mm) column and a mobile phase consisting of acetonitrile:potassium dehydrogen orthophosphate (0.02 M) (30:70) adjusted to pH 3 with orthophosphoric acid, a flow rate of 1.5 ml/min with ultraviolet detection at 240 nm. The correlation coefficient for calibration curves within the detection range of 35.22–65.4 µl/ml

is 0.9993. The within- and between-day precisions were determined for both retention time and peak area.

Sultana *et al.* [83] developed and validated an RP-HPLC method for the estimation of pravastatin in the presence of ceftriaxone in formulation and human serum. The separation was conducted on prepacked Purospher star C<sub>18</sub> (5  $\mu$ m, 25 cm  $\times$  4.6 mm) column at room temperature using methanol: water:acetonitrile (70:15:20) as the mobile phase, pH adjusted at 2.8 with orthophosphoric acid, and at a flow rate of 1 ml/min, while UV detection was performed at 240 nm. The results obtained showed a good agreement with the declared content. The method may be used for the quantitative analysis of pravastatin alone or in combination with ceftriaxone from raw material and dosage formulations and in serum. The method is rapid, accurate, selective, sensitive, and reproducible.

#### 5.4.5 Liquid chromatography/mass spectrometric methods

Matsushima *et al.* [84] developed a liquid chromatography/APCI mass spectrometric method, to study the pharmacokinetics of the drug. The method is highly sensitive and good for quantitation and can be used for determination of plasma samples automatically. The method was validated and compared with a quantitation method for pravastatin using automated gas chromatography/mass spectrometry.

Jemal *et al.* [85] developed a high-flow HPLC coupled with positive and negative ion electrospray tandem mass spectrometry for quantitative bioanalysis via direct injection of the plasma/serum samples of pravastatin. Plasma or serum was mixed with an internal standard and injected onto a column (5 cm  $\times$  1 mm i.d.) packed with 30  $\mu$ m OASIS particles, and matrix components were eluted with an aqueous mobile phase (3–4 ml/min). After the cleanup stage was complete, the mobile phase was switched to an organic one with a flow rate of 0.5–0.8 ml/min, to elute the analytes, and the column effluent was directed to a mass spectrometer. The method was applied to rat plasma containing compound **1** and human serum containing pravastatin and SQ-31906. Rat plasma (50  $\mu$ l) was mixed 1:1 with water containing internal standard prior to analysis; the column temperature was 40 °C. The first mobile phase was 20 mM formic acid (4 ml/min; 1 min) and the second was acetonitrile (0.8 ml/min; 2 min). The calibration graph was linear from 1 to 1000 ng/ml compound I. Human serum (200  $\mu$ l) was mixed 4:1 with water containing internal standard; the column temperature was 40 °C, the first mobile phase was 1 mM formic acid (3 ml/min; 1.1 min), and the second was acetonitrile/1 mM formic acid (0.5 ml/min;

2.8 min). The column was coupled with a 5  $\mu\text{m}$  C<sub>18</sub> column (5 cm  $\times$  3.9 mm i.d.) during the second stage. The calibration graph was linear from 0.5 to 100 ng/ml pravastatin and SQ-31906. For both methods, the analysis time was  $\leq 5$  min/sample and relative standard deviation was  $<10\%$ .

Mulvana *et al.* [86] developed and validated a turbo ion spray LC-MS/MS method for the quantitative determination of pravastatin and its biotransformation products in human serum. Serum samples (0.5 ml) were acidified and extracted by a solid-phase extraction procedure to isolate all five analytes from human serum. Sample extracts were reconstituted and analyzed by turbo ion spray LC-MS/MS in the positive-ion mode. The total run time was 9 min between injections. The assay demonstrated a lower limit of quantitation of 0.5 ng/ml for all five analytes. The calibration curves were linear from 0.5 to 100 ng/ml for all five analytes. The coefficients of determination of all calibration curves were  $>0.999$ . Precision and accuracy QC samples were prepared at concentrations of 2, 30, 80, and 500 ng/ml for all analytes. The intra- and interassay precisions calculated from QC samples were within 8% for all analytes. The interassay accuracy calculated from QC samples was within 8% for all analytes. The extraction recoveries were  $<90\%$  for all analytes. Bench-top stability experiments in an ice-water bath ( $\leq 10^\circ\text{C}$ ) demonstrated that over time, pravastatin lactone hydrolyzes to pravastatin in serum. Pravastatin and pravastatin-*d*<sub>5</sub> and SQ-31906 and SQ-31906-*d*<sub>5</sub> were stable under these conditions for up to 24 h. Hydrolysis was minimized by buffering the serum to pH 4.5 and maintaining the serum sample in an ice-water bath. All analytes were stable after three freeze/thaw cycles and in reconstitution solution after 1 week at  $4^\circ\text{C}$ . Stability of all analytes in human serum was demonstrated after storage at  $-70^\circ\text{C}$  for 77 days. The bench-top ( $\leq 10^\circ\text{C}$ ) stability of pooled study samples was also investigated, and the results were comparable to those obtained from serum QC samples.

Miao and Metcalfe [87] determined pravastatin and three other statins using liquid chromatography-electrospray ionization tandem mass spectrometry with methylammonium acetate as an additive in the mobile phase. Protonated atorvastatin, methylammonium-adducted lovastatin, pravastatin, and simvastatin were selected as precursor ions, and product ions were detected by selected reaction monitoring in positive-ion mode. The instrumental detection limits of atorvastatin, lovastatin, pravastatin, and simvastatin are 0.7, 0.7, 8.2, and 0.9 pg, respectively. A solid-phase extraction method was developed to enrich the analytes from aqueous samples. All of

the statins were detected in an untreated sewage sample at 4–117 ng/l and in a treated sewage sample at 1–59 ng/l.

Kawabata and Urasaki [88] developed a liquid chromatography-APCI tandem mass spectrometric method for the quantitative determination of pravastatin and its main metabolite (R-416) in human plasma with a fully automated online solid-phase extraction system. The method employed the direct online injection of human plasma into the Prospekt-2 system for extraction of the analytes followed by column-switching introduction of analytes to the LC/APCI-MS/MS system. The use of online solid-phase extraction system resulted in reducing the sample preparation time and decreasing endogenous interfering substances in the extract. The lower limit of quantification for the assay was 0.1 ng/ml for pravastatin and its metabolite R-416 on a 100  $\mu$ l plasma sample. The calibration curves were linear for concentrations ranging from 0.1 to 100 ng/ml for both analytes. The intra- and interassay precision was less than 4%. The method provided an automated sample analysis in a total cycle time of 6 min, allowing analysis of many plasma samples to be conducted with increased throughput and improved robustness.

Jain *et al.* [89] described a rapid, specific, and sensitive LC-MS/MS assay method using solid-phase extraction for the determination of pravastatin, in human plasma. The plasma filtrate obtained after solid-phase extraction, using a polymer base, a hydrophilic-lipophilic balance cartridge, was submitted directly to short-column liquid chromatography-tandem mass spectrometric (LC-MS/MS) assay, with negligible matrix effect on the analysis. For validation of the method, the recovery of the free analytes was compared with that from an optimized extraction method, and the analyte stability was examined under conditions mimicking the sample storage, handling, and analysis procedures. The extraction procedure yielded extremely clean extracts with a recovery of 107.44% and 98.93% for pravastatin and internal standard, respectively. The intra- and interassay precisions for the samples at the lower limit of quantitation were 3.30% and 7.31%, respectively. The calibration curves were linear for the dynamic range 0.5–200 ng/ml with correlation coefficient  $r \geq 0.9988$ . The intra- and interassay accuracy ranged from 95.87% to 112.40%. The method is simple and reliable with a total run time of 3 min. This validated method was applied to the pharmacokinetic study in human volunteers receiving a single oral dose of 40 mg immediate release formulation.

Deng *et al.* [90] developed a liquid chromatography and tandem mass spectrometry (LC-MS/MS) method for determining pravastatin or

pitavastatin in plasma. Pravastatin, pitavastatin, and the internal standard fluvastatin were extracted from plasma with solid-phase extraction columns and eluted with methanol. After drying the organic layer, the residue was reconstituted in mobile phase (acetonitrile:water, 90:10, v/v) and injected onto an RP-C<sub>18</sub> column. The isocratic mobile phase was eluted at 0.2 ml/min. The ion transitions recorded in multiple reaction monitoring mode were  $m/z$  423  $\rightarrow$  101, 420  $\rightarrow$  290, and 410  $\rightarrow$  348 for pravastatin, pitavastatin, and fluvastatin, respectively. The coefficient of variation of the assay precision was less than 12.4%, and the accuracy exceeded 89%. The limit of detection was 1 ng/ml for all analytes. This method was used to measure the plasma concentration of pitavastatin or pravastatin from healthy subjects after a single 4 mg oral dose of pitavastatin or 40 mg oral dose of pravastatin. The method is a simple, sensitive, and accurate and can be used to determine the pharmacokinetic profiles of pitavastatin or pravastatin.

Wang and Wang [91] developed and validated a high-throughput bioanalytical method for simultaneous quantitation of pravastatin and its metabolite in human serum. Online extraction following liquid chromatography-tandem mass spectrometry was used. The online extraction was accomplished by direct injection of a 50  $\mu$ l serum sample, mixed 4:1 with an aqueous internal standard solution, into one of the extraction columns with aqueous 1 mM formic acid at flow rate of 3 ml/min. The separation and analysis were achieved by back eluting the analytes from the extraction column and the analytical column to the mass spectrometer with an isocratic mobile phase consisting of 62% aqueous 1 mM formic acid and 38% acetonitrile at a flow rate of 0.8 ml/min. The second extraction column was being equilibrated, while the first column was being used for the analysis and vice versa. The standard curve range was 0.5–100 ng/ml for pravastatin and metabolite.

Mertens *et al.* [92] developed a liquid chromatography combined with diode array and tandem mass spectrometry LC-DAD-MS/MS detection for the simultaneous quantitative determination of pravastatin, its main metabolite, and fenofibric acid in human plasma. An automated solid-phase extraction on disposable extraction cartridge is used to isolate compounds from the biological matrix and to prepare a cleaner sample before injection and analysis in the LC-DAD-MS/MS system. Online LC-DAD-MS/MS system using an atmospheric pressure ionization (TurbolonSpray) was developed for the simultaneous determination of pravastatin, 3-hydroxy isomeric metabolite, pravalactone, and fenofibric acid. The separation was obtained



on an end-capped dodecyl silica-based stationary phase using a mobile phase consisting of a mixture of acetonitrile, methanol, and 5 mM ammonium acetate solution (30:30:40). Sulindac and triamcinolone were used as internal standards. The detection of fenofibric acid and sulindac was achieved by means of a DAD system. The MS/MS ion transitions monitored were  $m/z$  442.2  $\rightarrow$  269.1, 442.2  $\rightarrow$  269.1, 424.3  $\rightarrow$  183, and 435.2  $\rightarrow$  397.2 for pravastatin, 3-hydroxy metabolite, pravalactone, and triamcinolone, respectively. The method was validated for stability, selectivity, extraction efficiency, response function, trueness, precision lower limit of quantitation, and matrix effect.

Tan *et al.* [93] described an LC-MS/MS method for the determination of pravastatin in human plasma. After the addition of rosuvastatin as an internal standard, pravastatin in plasma samples was extracted with solid-phase extraction column. The analysis involved a Hypurity C<sub>18</sub> (15 cm  $\times$  2.1 mm, 5  $\mu$ m) column. The mobile phase consisted of acetonitrile:water (1000 ml water added 2 ml formic acid) (85:15), the flow rate was 0.2 ml/min, the column temperature was 40 °C. ESI<sup>+</sup> was performed in the MRM mode using target ions at  $m/z$  447  $\rightarrow$  327 (pravastatin) and  $m/z$  482  $\rightarrow$  272 (rosuvastatin). The peak area of pravastatin in plasma showed good linearity within the range between 2.52 and 660  $\mu$ g/l. The lower limit of quantitation in plasma was 2.52  $\mu$ g/l. The extracted recovery was 70% and the relative recovery was 98–102%. The intra- and interday relative standard deviation was 15%. The method is simple, sensitive with good recovery, and can be used in analyzing the drug in biological samples.

Zhang *et al.* [94] established an LC-MS/MS method for the determination of pravastatin in human plasma. After the addition of rosuvastatin as an internal standard with liquid–liquid extraction, the analysis involved an Inertsil ODS-3 (2.1 mm  $\times$  50 mm, 5  $\mu$ m) column. The mobile phase consisted of acetonitrile:1 mmol/l ammonium formate water solution (include 0.1% formic acid) (60:40) at a flow rate of 0.2 ml/min, and the column temperature was set at 40 °C. ESI<sup>+</sup> was performed in the MRM mode using target ions at 448  $\rightarrow$  327.7 (pravastatin) and  $m/z$  483.2–258.6 (rosuvastatin). The peak area of pravastatin in plasma showed good linearity in the range of 0.957–510 ng/ml, and the lower limit of quantitation of pravastatin in plasma was 0.957 ng/ml. The extracted recovery was 75%, the relative recovery was 80–120%, and the intra- and interday relative standard deviation was 15%. The method can be used for the determination of pravastatin sodium tablets plasma concentration and its pharmacokinetic study.

Pilli *et al.* [95] developed and validated a simple, rapid, and sensitive liquid chromatography/tandem mass spectrometry method for the quantitation of pravastatin in human plasma. Topiramate was used as the internal standard. The analytes were extracted from human plasma samples by liquid–liquid extraction. The reconstituted samples were chromatographed on a C<sub>18</sub> column by using a 90:10 mixture of acetonitrile and 5 mM ammonium acetate as the mobile phase at a flow rate of 1 ml/min. The method is applicable to clinical studies.

#### 5.4.6 Capillary electrophoresis methods

Kircali *et al.* [96] described a capillary electrophoretic method for the determination of pravastatin in pharmaceutical tablet formulations. Pravastatin and lansoprazole (internal standard) were well migrated in the background electrolyte of 10 mM borate buffer (pH 8.5) and 10% acetonitrile using a fused-silica capillary. Separation was achieved by applying 27.5 kV, detecting at 200 nm, and injecting the sample for 0.5 s and with an average migration time for pravastatin and internal standard of 4.7 and 3.9 min, respectively, at ambient temperature. The results were precise and repeatable. The method was applied to the determination of pravastatin in the pharmaceutical tablets.

Nigovic and Vegar [97] developed and validated a capillary zone electrophoresis method for the determination of pravastatin. Rapid migration of negatively charged pravastatin molecule was obtained in alkaline buffer by the application of electric field of 30 kV. The influence of pH value and ionic strength of running buffer, applied voltage, and capillary temperature on mobility and sensitivity was evaluated. Detection wavelength was set to 237 nm. The method was applied to the determination of the drug in pharmaceutical dosage form. Pravastatin is a  $\delta$ -hydroxy acid which is prone to lactonize and epimerize in a pH-dependent manner. Micellar electrokinetic chromatographic approach was chosen to develop a method able to separate pravastatin and its degradation products in acid media. The method allows baseline separation of hydroxy acid and neutral lactone forms of the drug that appear as interconversion products depending on the pH value.

Damic and Nigovic [98] introduced a universal micellar electrokinetic capillary chromatographic method with diode array detection for the simultaneous and short-time analysis of pravastatin and five other statins. Optimized conditions were found to be a 25 mM borate buffer pH 9.5 with 25 mM sodium dodecyl sulfate and 10% methanol added as an organic modifier, an applied voltage of 23 kV, and a separation temperature of 30 °C.

Ketoprofen was used as an internal standard. The linearity of the detector response for each statin was within the concentration range from 10 to 100 µg/ml with a correlation coefficient greater than 0.9994. Analysis of pravastatin and the other statins in pharmaceutical samples were carried out in only 5 min. Recovery values were in the range of 98.04–100.8%, and the interference of the tablet sample matrix was not observed.

### 5.5. Immunoassay methods

Wang-Iverson and Cohen [99] used bioanalytical approaches, including quantitative mass spectrometry, for pravastatin and two other statins. Radioenzyme assay measured the inhibition of HMG-CoA reductase *in vitro*. Serum samples containing pravastatin were added to rat liver microsomes, various cofactors, and  $^{14}\text{C}$ -HMG-CoA as reductase. The amount of  $^{14}\text{C}$ -mevalomolactone generated served as a measure of the reductase activity, the standard curve being linearized; the lower limit of quantitation was 3 ng/ml for the drug, with a range up to 200 ng/ml. Radioimmunoassay measured pravastatin and its 6-hydroxy major metabolite, SQ-31906. This method has a very high sample throughput and proved to be very rugged. Gas chromatography–negative ion chemical ionization–mass spectrometry (GC–NICI–MS) required sample preparation, particularly solid-phase extraction of the serum, and pentafluorobenzyl derivatization. The lower limit of quantitation was 0.5 ng/ml and linearity was up to 120 ng/ml. The advantage of the GC–NICI–MS technique over REA and RIA was its ability to measure the analyte of interest.

Muramatsu *et al.* [100] used an enzyme immune assay method for pravastatin in blood. The determination pravastatin in blood involves, reacting test pravastatin in the sample using a standard curve. The detection range was 600 pg to 200 ng/ml. The competitive enzyme immune assay is simple and specific. Preparation of 5-dehydroxy pravastatin–bovine serum albumin complex for antibody production is described.

Muramatsu *et al.* [101] developed and validated an enzyme immunoassay (EIA) for the determination of pravastatin sodium (I) in human plasma samples. Microtiter plates were coated with goat anti-rabbit IgG (IgG fraction), blocked with human serum albumin (HSA), and washed with phosphate buffer saline containing 0.05% Tween 20 (buffer A). Rabbit antiserum (50 µl) to pravastatin diluted in phosphate buffer saline containing 0.1% HSA, 50 µl horseradish peroxidase-labeled antigen diluted to 200–1000 or 100–500 ng/ml for methods A and B, respectively, and sample (50 µl)

were incubated in the wells at 4 °C for 20–24 h. After washing with buffer A, 200 µl 0.01% tetramethylbenzidine in 50 mM acetate/citrate buffer of pH 5.5 containing 3% DMSO and 0.002% hydrogen peroxide was added for 30 min, followed by 0.05 M sulfuric acid, and the absorbance was measured at 450 nm. The antisera were obtained using bovine serum albumin conjugates of the  $\beta$ -alanine derivative of pravastatin (for method A) or the *S*-deoxy derivative of pravastatin for method B. At optimal antiserum/labeled antigen dilutions, pravastatin could be determined in the range of 5–500 pg/well with an  $IC_{50}$  of 36–130 pg/well. The detection limit for method A was 500 pg/ml pravastatin, and the relative standard deviation at 5 ng/ml was 4.5%.

Darwish *et al.* [102] developed and validated a new highly sensitive EIA for the determination of pravastatin in human plasma samples. Pravastatin was coupled to keyhole limpet hemocyanin and bovine serum albumin via its terminal carboxylic acid group by carbodiimide reagent. Pravastatin–keyhole limpet hemocyanin conjugate was used as an immunogen for raising anti-pravastatin polyclonal antibody in rabbits. The generated anti-pravastatin antibody recognized pravastatin with high affinity and selectivity. Pravastatin–bovine serum albumin conjugate was immobilized onto microwell plates and used as a solid phase. The assay involved a competitive binding reaction between pravastatin, in plasma sample, and the immobilized pravastatin–bovine serum albumin for the binding sites on a limited amount of the anti-pravastatin antibody. The anti-pravastatin antibody bound to the plate wells was quantified with horseradish peroxidase-labeled anti-immunoglobulin second anti-rabbit IgG antibody and 3,3',5,5'-tetramethylbenzidine as a substrate for the peroxidase enzyme. The concentration of pravastatin in the sample was quantified by its ability to inhibit the binding of the anti-pravastatin antibody to the immobilized pravastatin–bovine serum albumin and subsequently the color development in the assay wells. The conditions of the enzyme immune assay method were investigated, and the optimum conditions were employed in the determination of pravastatin in plasma samples. The assay limit of detection was 0.2 ng/ml, and the effective working range at relative standard deviation of  $\leq 5\%$  was 0.5–20 ng/ml. The mean analytical recovery of pravastatin from spiked plasma was  $100.9 \pm 2.98\%$ . The precision of the assay was satisfactory; relative standard deviation was 2.61–3.70% and 3.96–4.17% for intra- and interassay precision, respectively. The analytical procedure is convenient, and one can analyze approximately 200 samples per working day, facilitating the processing of large-number batch of samples. The enzyme immune assay

method has a great value in the routine analysis of pravastatin in plasma samples for its therapeutic monitoring and pharmacokinetic studies.



## 6. PHARMACOKINETICS

In a two-way crossover study, eight healthy male subjects each received an intravenous and an oral dose of [ $^{14}\text{C}$ ]-pravastatin sodium. The oral absorption of [ $^{14}\text{C}$ ] activity from pravastatin sodium was about 34%, and the oral bioavailability was about 18%, suggesting first-pass metabolism of the drug. After intravenous dose, the recovery of radioactivity averaged 60% and 34% in urine and feces, respectively. Corresponding values were 20% (urine) and 71% (feces) for oral dose [103].

Biotransformation profile of pravastatin in pooled human urine, plasma, and feces from healthy male volunteers given single oral dose or single intravenous doses of [ $^{14}\text{C}$ ]-pravastatin were determined by HPLC. The drug-related component in urine, plasma, and feces corresponds to the intact pravastatin in the pooled urine samples. Pravastatin constituted 29% and 69% of the radioactivity after the oral and the intravenous doses, respectively [104].

The disposition and metabolism of pravastatin sodium in rats, dogs, and monkeys have been studied using [ $^{14}\text{C}$ ]-labeled compound. Absorption was about 70% in rat and 50% in dogs. Tissue distribution examined by both whole-body autoradiography, and radiography measurement demonstrated that the drug was selectively taken up by the liver and excreted via bile mainly in unchanged form [105].

The effect of oral contraceptive steroids on the pharmacokinetics of pravastatin in young women was evaluated. Normal healthy male and female were subjected to receive a single dose of pravastatin after an overnight fast. The pharmacokinetic profiles of pravastatin and SQ-31906 in young and elderly subjects of men and women differed little. Concomitant administration of oral contraceptives in young women did not affect the pharmacokinetics of pravastatin and SQ-31906. No difference was detected between the disposition of the parent drug or its metabolite in men and women [106].

Pravastatin differs from other statins because of its greater hydrophilicity due to the hydroxy group attached to its decalin ring. The hydrophilic nature of pravastatin accounts for its minimal penetration into the intracellular space of nonhepatic tissues, including an apparent inability to cross the blood-brain barrier. The drug is well tolerated and is rapidly absorbed and excreted. Pravastatin does not accumulate in plasma even with repeated administration. The drug is taken up into the liver by an active transport

carrier system. The hepatic excretion ratio is high (0.66). Pravastatin and metabolites are cleared through both hepatic and renal routes. The drug is 50% protein bound [107].

The single dose and steady-state pharmacokinetics of pravastatin and its two metabolites, SQ-31906 and SQ-31945, were evaluated in hemodialysis patients. No statistical differences in the pharmacokinetics of pravastatin or SQ-31906 were evident when comparing the first and last days of oral dosing with pravastatin. The pharmacokinetic parameters of pravastatin and SQ-31906 were similar to those of healthy volunteers. SQ-31945, the inactive polar metabolite, accumulated in dialysis patients. Pravastatin can be administered in the usual dosages to subjects with renal failure on hemodialysis and no change of dosing is necessary [108].

Many of the *in vivo* and *in vitro* human and animal studies suggest that an active transport mechanism is involved in the pharmacokinetics of pravastatin. The drug is rapidly absorbed from the upper part of the small intestine, via proton-coupled carrier-mediated transport, and then taken up by the liver by a sodium-independent bile acid transporter [109].

Co-administration of pravastatin with gemfibrozil leads to the inhibition of human organic anion transporter 3-mediated pravastatin transport and the metabolites in humans. It causes a decrease in renal clearance of the drug by about 40% in healthy volunteers. An uptake study was undertaken of pravastatin using human organic anion transporter-expressing  $S_2$  cells. Human organic anion transporter 3 and human organic anion transporter 4 transported pravastatin in a saturable manner with Michaelis–Menten constant of 27.7 and 257  $\mu\text{M}$ , respectively. Human organic anion transporters 1 and 2 did not transport pravastatin [110].

Pharmacokinetic properties of pravastatin in Mexicans were studied in health adult volunteers. To evaluate the pharmacokinetic properties of pravastatin in healthy Mexican mestizo's volunteers and to compare them with those in white and Japanese populations described in the literature. Twenty-four subjects (15 women, 9 men; mean age, 30.6 years) participated in the study. The mean (SD)  $C_{\text{max}}$  was 9.5 (2.4) ng/ml;  $T_{\text{max}}$ , 0.8 (0.3) h;  $\text{AUC}_{0-\infty}$ , 35.7 (19.7) ng/ml;  $t_{1/2}$ , 2.7 (1.1) h; and mean residence time, 3.1 (1.1) h. One volunteer (4%) had an AUC value that differed substantially from the rest of the study population, producing a bimodal distribution of the pharmacokinetic parameters. No adverse events were observed or reported during the trial [111].

Studies compared the multiple-dose pharmacokinetic interaction profiles of pravastatin when co-administered with four inhibitors of cytochrome P450-3A4 isoenzymes in healthy subjects was studied. Compared with

pravastatin alone, co-administration of verapamil, mibefradil, or itraconazole with pravastatin was associated with no significant changes in pravastatin pharmacokinetics. Pravastatin has a neutral drug interaction profile relative to cytochrome P450-3A4 inhibitors [112].



## 7. METABOLISM

Iwabuchi *et al.* [113] reported that, in rat, pravastatin was metabolized to two metabolites. After incubation of one of the metabolites with rat hepatocytes, a glutathione conjugate was found. Metabolic pathways for pravastatin were proposed.

Everett *et al.* [104] studied the biotransformation profiles pravastatin in pooled urine, plasma, and feces from healthy males given single 19.2 mg oral or 9.9 mg intravenous doses of [ $^{14}\text{C}$ ]-pravastatin and determined them by HPLC. The main drug-related component in urine, plasma, and feces corresponded to intact pravastatin. Twelve metabolites were isolated and identified as unchanged pravastatin **1**, 3 $\alpha$ -*iso*-pravastatin **2**, 6-*epi*-pravastatin **3**, desacyl pravastatin **4**, pravastatin glucuronide **5**, 5,6-epoxy 3 $\alpha$ -*iso*-pravastatin **6**, 3'(*S*)-OH-pravastatin **7**, unknown conjugate of metabolite **9**, tetranor of 3'(*S*)-OH-pravastatin **8**, tetranor analog of 3'(*S*)-OH-pravastatin **9**, 3-keto-5,6-dihydroxy derivative of pravastatin **10**, 7-OH-3 $\alpha$ -*iso*-pravastatin **11**, and triol metabolite of pravastatin **12**. Figure 8.15 shows the biotransformation pathways of pravastatin in human.

Muramatsu *et al.* [114] studied the metabolic fate of pravastatin sodium in isolated rat hepatocytes. Two polar metabolites were isolated and identified as a glutathione conjugate and a dehydrodiol. Both metabolites were formed via an epoxide which has been identified as the 4' $\beta$ ,5' $\beta$  epoxide on the decalin moiety. Formation of the glutathione conjugate was enzymic, while the dehydrodiol was formed by nonenzymic hydrolysis of the epoxide accompanied by the intramolecular migration of the double bond.

Nakamura *et al.* [115] determined the structures, including stereochemistry, of the two major metabolites of pravastatin sodium in an isolated rat hepatocyte system, 4- $\alpha$ -glutathione conjugates, and 3',5'-dehydrodiol by one- and two-dimensional NMR spectroscopy. The structures of two synthetic pravastatin epoxides, possible precursors of the metabolites, were established. One of the synthetic epoxides, 4' $\alpha$  beta, 5'beta epoxide, was converted to the pravastatin metabolite, 4' $\alpha$ -glutathione conjugate by a rat liver cytosol system, and is proposed as the common metabolic intermediate between pravastatin sodium and the two metabolites.

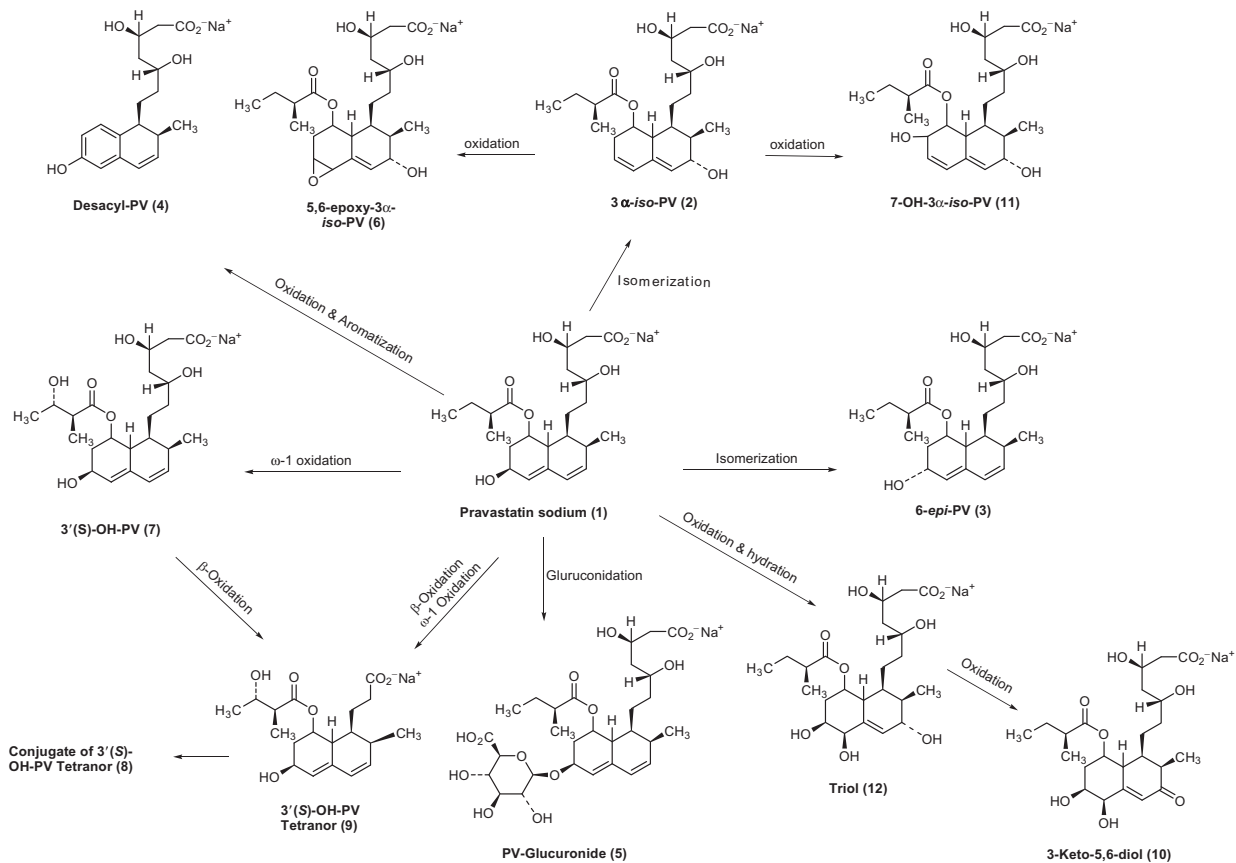


Figure 8.15 Biotransformation pathways for pravastatin in humans [104].



Komai *et al.* [105] studied the disposition and the metabolism of pravastatin in rat, dogs and monkeys using [ $^{14}\text{C}$ ]-labeled compound. The extent of absorption was approximately 70% in rats and 50% in dogs. Tissue distribution examined by both whole-body autoradiography and radioactivity measurement demonstrated that the drug was selectively taken up by the liver, a target organ of the drug, and excreted via bile mainly in unchanged form. Since pravastatin excreted by the bile was reabsorbed, the enterohepatic circulation maintained the presence of unchanged pravastatin in the target organ. The profiles of metabolites of pravastatin were studied in various tissues and excreta, and the main metabolic pathway of pravastatin sodium is shown in Figure 8.16.

Kitazawa *et al.* [116] stated that a major metabolite R-416 of pravastatin sodium and a minor metabolite R-418 were produced in rat liver cytosol in the presence of adenosine-3'-phosphate-5'-phosphosulfate as a cofactor. The reactions were inhibited by the inhibitors for sulfotransferase, and  $^{18}\text{OH}$  was introduced to the 3'- $\alpha$  and 6'- $\alpha$  positions of R-416 and R-418, respectively, by incubation with  $\text{H}_2^{18}\text{O}$ . Pravastatin was, therefore, metabolically activated by sulfation at the 6'- $\beta$ -hydroxy group by sulfotransferase, followed by nucleophilic attack of hydroxy anions at 3- $\alpha$  or 6- $\alpha$  positions, to give R-416 or R-418, respectively (Figure 8.17).

Muramatsu *et al.* [117] studied the metabolism of pravastatin sodium by 3 $\alpha$ -hydroxysteroid dehydrogenase. When incubated with isolated rat hepatocytes, pravastatin sodium yields a small amount of a metabolite in addition to two metabolites. The metabolite was found to be formed by at first being enzymatically dehydrogenated to 6'-keto intermediate (R-195) through spontaneous deesterification with accompanying aromatization. The pravastatin-6'- $\beta$ -hydroxydehydrogenase activity was localized in cytosolic fraction and required NADP, preferentially over NAD, as a cofactor. The formation of R-195 by rat liver cytosol was strongly inhibited by indomethacin. The results and high substrate specificity of purified pravastatin-6'- $\beta$ -hydroxy dehydrogenase toward 3 $\alpha$ -hydroxysteroids suggested that the enzyme is identical to 3 $\alpha$ -hydroxysteroid dehydrogenase.

Jacobsen *et al.* [118] compared the intestinal metabolism of lovastatin and pravastatin *in vitro*. Incubation of pravastatin with human small intestinal microsomes resulted in the generation of 3' $\alpha$ ,5' $\beta$ ,6' $\beta$ -trihydroxy pravastatin and hydroxy pravastatin, as in the liver, pravastatin was metabolized in the small intestine by sulfation and subsequent degradation to its main metabolite 3' $\alpha$ -*iso*-pravastatin.

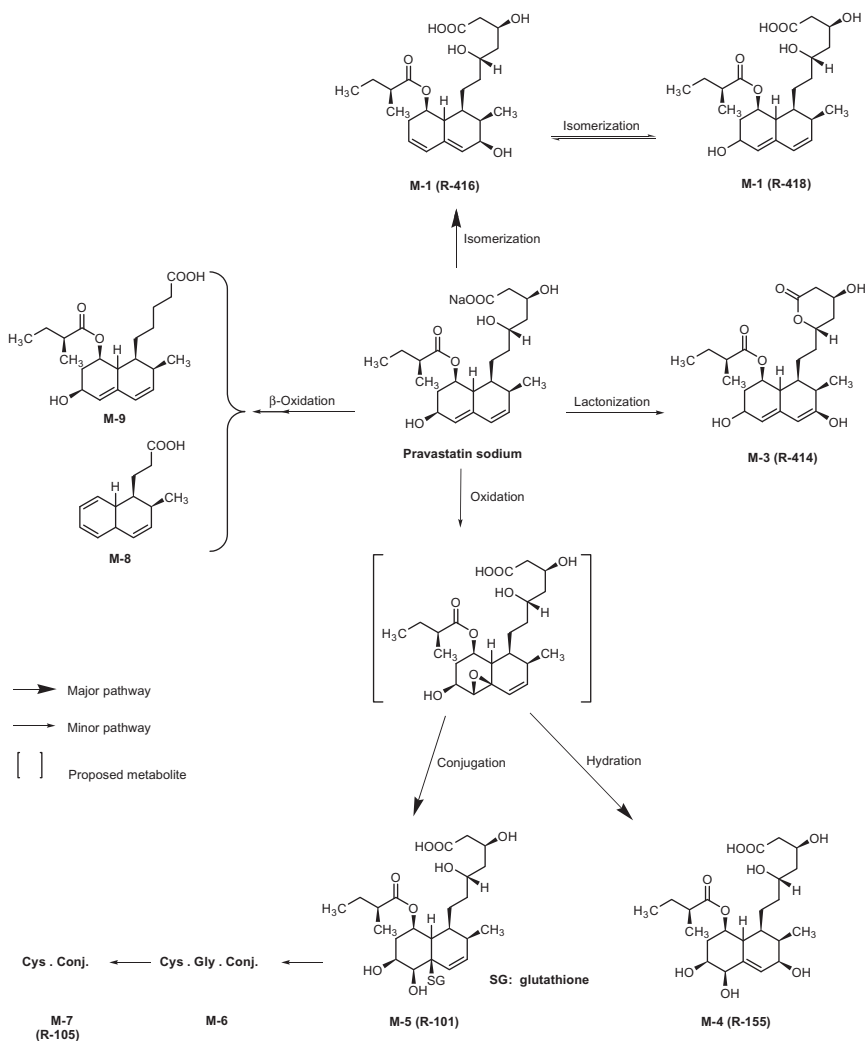


**Figure 8.16** Main metabolic pathway of pravastatin sodium [105].

Jacobsen *et al.* [119] also compared the *in vivo* cytochrome P450 3A-dependent metabolism and drug interaction of lovastatin and pravastatin. Incubation of pravastatin with human liver microsomes resulted in the generation of 3' $\alpha$ ,5 $\beta$ ,6 $\beta$ -trihydroxy pravastatin and hydroxy pravastatin.

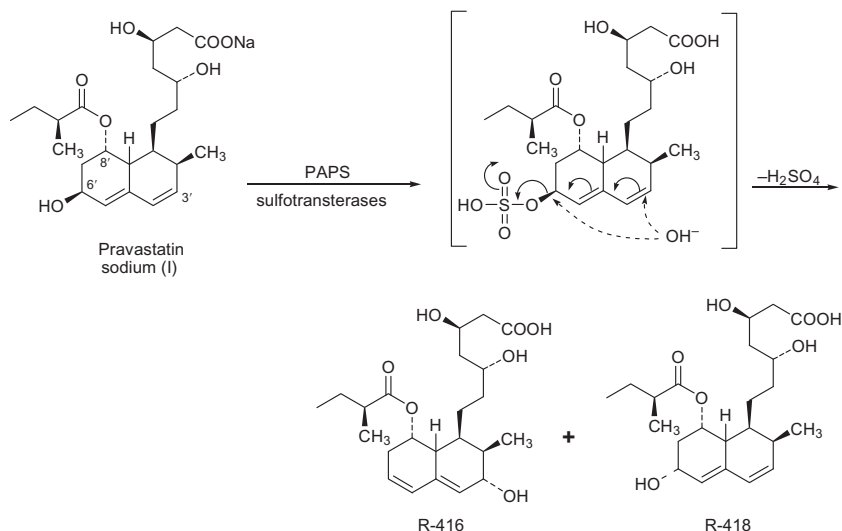


**Figure 8.17** Plausible metabolic pathway of pravastatin sodium to R-416 and R-418 [116].

## 8. STABILITY

Deng *et al.* [120] found that pravastatin was unstable under the simulated stomach conditions. Brain-Isasi *et al.* [63] reported that degradation of pravastatin is dramatically influenced on both pH and temperature and that stability of pravastatin increases with the increase of pH. Lotfy *et al.* [121] studied the stability of pravastatin sodium under acidic hydrolytic conditions. Polagani *et al.* [122] conducted a stability test to evaluate analyte stability in stock solutions and in plasma samples under different conditions. Stock solutions were found to be stable for 23 days at 2–8 °C. Pilli *et al.* [95] studied the stability of pravastatin in human plasma and found that the drug is stable for 30 days at 2–8 °C. Bastarda *et al.* [53] studied the chemical stability of pravastatin in aqueous media at pH between 1 and 7. Due to the presence of a highly sensitive diene alcohol and 3-hydroxy-8-lactone, pravastatin showed very characteristic chemical behavior. In the acidic media of pH 1–3, pravastatin undergoes isomerization of 6 $\alpha$ -hydroxy group in the hexahydronaphthalene ring forming a mixture of 6 $\alpha$ -, 6 $\beta$ -, 3 $\alpha$ -, and 3 $\beta$ -hydroxyl isomers. Each isomer may also undergo lactonization of the hydroxy acid chain to form the corresponding lactone. Thus in acidic media pravastatin sodium could convert to the following seven different

compounds: Pravastatin lactone, 3- $\beta$ -OH-pravastatin lactone, 3- $\alpha$ -OH-pravastatin lactone, 6- $\alpha$ -OH-pravastatin lactone, 3- $\alpha$ -OH-pravastatin sodium, 3- $\beta$ -OH-pravastatin sodium, and 6- $\alpha$ -OH-pravastatin sodium.



## 9. REVIEWS

Serizawa [123] presented a review on two-stage manufacturing pravastatin by fermentation. It comprises the manufacturing of (+)-compactin, ML-236B, fermentation of pravastatin with microorganisms, and future perspective.

Arai *et al.* [124] presented a review on the production, chemistry, enzyme inhibition, and animal studies, metabolic studies, of pravastatin.

Erturk *et al.* [125] presented a review on the analytical methods for the quantitative determinations of pravastatin and four other statins in biological fluids. Almost all the assays reviewed are based on HPLC or gas chromatography. Some purification steps (liquid–liquid extraction, solid-phase extraction, etc.) have been used before they are submitted to separation of chromatographic procedures and are detected by various detection method such as ultraviolet, fluorescence, and mass spectrometry. The review showed that most methods may be used for quantitative determination of statin in plasma and are suitable for therapeutic monitoring of these drugs.

Nirogi *et al.* [126] presented a review on chromatography–mass spectrometry methods for the quantitation of pravastatin and six other statins in biological samples. HPLC in combination with tandem mass spectrometry is the analytical technique of choice for the quantification of these compounds in biological samples. This review envisages that most of the methods used for quantification of pravastatin and the other statins are in plasma and they are suitable for therapeutic drug monitoring of these drugs.

## ACKNOWLEDGMENTS

The authors wish to thank Mr. Tanvir Ahmed Butt, Pharmaceutical Chemistry Department, College of Pharmacy, King Saud University for his secretarial assistance in preparing this profile.

## REFERENCES

- [1] S. Budavari (Ed.), *The Merck Index*, 12th ed., Merck and Co, New Jersey, 2004, p. 1323.
- [2] Sean C. Sweetman (Ed.), *Martindale: The Complete Drug Reference*, 32nd ed., Pharmaceutical Press, London, 2002, p. 1277.
- [3] A.C. Moffat (Ed.), *Clarke's Analysis of Drugs and Poisons*, 3rd ed., The Pharmaceutical Press, London, 2004, pp. 1469–1470.

- [4] A. Terahara, M. Tanaka, ML-236B derivatives and their preparation, United States Patent, 4,346,227, 1982.
- [5] A. Terahara, M. Tanaka, ML-236B derivatives, United States Patent, 4,448,979, 1984.
- [6] A.R. Daniewski, P.M. Wovkulich, M.R. Uskokovic, Remote diastereoselection in the asymmetric synthesis of pravastatin, *J. Org. Chem.* 57 (1992) 7133–7139.
- [7] M.A. Wallace, D.C. Dean, R.F. White, R.L. Ellsworth, D.G. Melillo, T. Marks, The synthesis of carbon-14 labeled pravastatin, *J. Label. Compd. Radiopharm.* 33 (1993) 967.
- [8] T. Matsuoka, and S. Miyakoshi, Cytochrome P-450 enzymes, US Patent US 5,179,013, 1993.
- [9] M.V.M. Emonds, A novel and versatile approach to the asymmetric total synthesis of pravastatin, related mevinic acid, and analogs, Ph. D. Thesis, University of Michigan, USA, 1993.
- [10] P. Narula, S. Raman, M.L. Kumar, P. Kumar, Process for the preparation of sodium salts of statins, WO 01/44144 A2, 2001.
- [11] F. Lee, M. Li, A.G. Hong, S. Chu, Preparation of pravastatin from *Sacharothrix* isolates and its use as inhibitor of HMG-CoA reductase, *Jpn Kokai Tokkyo Koho*, UP 2003250532 A 20030909, 2003.
- [12] Y. Abe, DNA sequence of gene cluster from *penicillium citrinum* and its use for preparation of pravastatin precursor ML-136B, *Jpn Kokai Tokkyo Koho*, JP 2003116567 a 20030422, 2003.
- [13] P. Kumar, V. Katial, P. Gigras, S. Kumar, A. Shukla, Fermentation process for the preparation of pravastatin, Patent WO 2004/087935 A2, 2004.
- [14] A. Jekkel, A. Konya, I. Barta, E. Ilkoy, G. Somogyi, G. Ambrus, G. Horvath, K. Albrecht, I. Szabo, J.M.N. Suto, J. Salat, A. Andor, L. Birinesik, S. Boros, I. Lang, M.B.N. Igloy, Microbial process for preparing pravastatin, United States patent US 6,750,366 B2, 2004.
- [15] M. Mei, X. Ji, X. Gao, F. Zheng, Y. Chen, *Micropolyspora roseoalba* for preparation of pravastatin, PTC Inc. Appl., WO 2005005618 A1 20050120, 2005.
- [16] V. Keri, I. Melczer, Method of synthesizing and purifying pravastatin, US Pat Appl. Publ. US 2005113446 A1 20050526, 2005.
- [17] P. Klaassen, A.W.H. Vollebregt, M.A. Van Den Berg, M. Hans, J.M. Van der laan, Compactin hydroxylase from *Amycolatopsis orientalis* and its derivatives and their use for fermentative preparation of pravastatin by recombinant *Escherichia coli*, PCT Int. Appl. WO 2008071673 A1 20080619, 2008.
- [18] Anonymous, Process for the preparation of pravastatin, *IP.com J.* 8 (2008) 18.
- [19] M. Mei, X. Ji, X.Gao, Y.Chen, Y. Li, Y. Yao, Z. Zhuo, J. Xu, Microorganisms and the process for preparation of pravastatin sodium, United States Patent, US 7.582.464 B2, 2009.
- [20] T. Sato, N. Kawasaki, Preparation of pravastatin with cytochrome p-450 3A for use as therapeutic for hyperlipidemia, *Jpn. Kokai Tokkyo Koho*, JP 11235147 A 1990831, 1999.
- [21] H. Hagiwara, T. Nakano, M. Kon-no, H. Uda, Total synthesis of (+)-compactin by a double Michael protocol, *J. Chem. Soc., Perkin Trans. 1* 7 (1995) 777–783.
- [22] V. Keri, A. Nagyne, Z. Czovek, A. Kovacsne-Mezsei, I.V. Katai, Methods of making pravastatin sodium, Patent WO 2006/086680 A1, 2006.
- [23] M. Bacher, K. Baumann, H. Knapp, A. Steck, S. Teibl, Complete assignment of  $^1\text{H}$  and  $^{13}\text{C}$  NMR data of pravastatin derivatives, *Magn. Reson. Chem.* 47 (2009) 71–83.
- [24] S. Lateef, Assessments of in-process impurities in pravastatin using the Agilent 6410 triple quadrupole LC/MS in negative mode, Application notes [www.agilent.com/chem/QQQ](http://www.agilent.com/chem/QQQ), 2008, pp. 1–7.
- [25] A. Kocijan, R. Grahek, L. Zupancic-Kralj, Identification of an impurity in pravastatin by application of collision-activated decomposition mass spectra, *Acta Chim. Slov.* 53 (2006) 464–468.

- [26] British Pharmacopoeia 2005, vol. 2, Her Majesty Stationary Office Publication Ltd, London, 2005, 1636.
- [27] United States Pharmacopoeia 31, United States Pharmaceutical Convention, Inc, Rockville, MD, 2008, pp. 3053–3056.
- [28] Y.S. Rao, G. Haritha, P. Nayana Tara, K.P.R. Chowdary, J.V.L.N. Seshagiri Rao, Estimation of pravastatin sodium by spectrophotometric method, *Int. J. Chem. Sci.* 1 (2003) 368–370.
- [29] H.M. Lotfy, H.F. El-Sanabary, Z.A. El-Sherif, M.G. El-Bardicy, Stability-indicating methods for the determination of two hypolipidemic drugs, *Bull. Facul. Pharm. (Cairo Univ.)* 44 (2006) 143–158.
- [30] S. Balaji, S. Khatteboina, Development of spectrophotometric method for determination of pravastatin sodium in bulk and tablet formulations, *J. PharmTech. Res.* 1 (2009) 1017–1019.
- [31] S. Kalvikkarasi, V. Vaidhyalingam, V. Niraimathi, A. Aruna, Spectrophotometric determination of pravastatin sodium in pharmaceutical oral solid dosage forms, *Asian J. Chem.* 21 (2009) 1648–1650.
- [32] M. Farouk, O. Abdel-Aziz, R. Nagi, L. Abdel-Fattah, Validated spectrophotometric methods for determination of some anti-hyperlipidemic used drugs, *J. Biomed. Sci. Res.* 2 (2010) 202–211.
- [33] S. Ashour, M. Bahbouh, M. Khateeb, A novel use of oxidative coupling reactions for determination of some statins (cholesterol-lowering drugs) in pharmaceutical formulations, *Spectrochim. Acta A* 78 (2011) 913–917.
- [34] S. Ashour, M. Khateeb, Kinetic spectrophotometric determination of pravastatin in drug formulations *via* derivatization with 4-chloro-7-nitrobenzo-2-oxa-1,3-diazole (NBD-Cl), *Arabian J. Chem.* 4 (2011) 299–305.
- [35] E.Y.Z. Frag, G.G. Mohamed, M.H. Gaber, Sensitive extractive spectrophotometric method for the determination of some statin drugs in pharmaceutical preparations, *Insight Pharm. Sci.* 1 (2011) 39–46.
- [36] N.Y. Coskun, S. Aycan, S. Sungur, Differential pulse polarographic determination of pravastatin sodium in tablets, *Pharmazie* 52 (1997) 485–486.
- [37] B. Nigović, Electrochemical properties and square-wave voltammetric determination of pravastatin, *Anal. Bioanal. Chem.* 384 (2006) 431–437.
- [38] M.M.P.S. Neves, H.P.A. Nouws, C. Delerue-Matos, Carbon surfaces for the oxidative quantification of pravastatin: glassy-carbon *vs* screen-printed carbon electrodes, *J. Food Drug Anal.* 18 (2010) 353–357.
- [39] B.G. Chaudhari, N.M. Patel, P.B. Shah, Determination of simvastatin, pravastatin sodium and rosuvastatin calcium in tablet dosage forms by HPTLC, *Indian J. Pharm. Sci.* 69 (2007) 130–132.
- [40] A. Ahmed, B.P. Panda, M. Mujeeb, A validated stability-indicating method for simultaneous analysis of mevastatin and pravastatin in formulation broth during bioconversion by *Actinomadura macra*, *Acta Chromatogr.* 23 (2011) 121–131.
- [41] P.T. Funke, E. Ivashkiv, M.E. Arnold, A.I. Cohen, Determination of pravastatin sodium and its major metabolites in human serum and plasma by capillary gas chromatography-negative-ion chemical ionization mass spectrometry, *Biomed. Environ. Mass Spectrom.* 18 (1989) 904–909.
- [42] H.Y. Pan, A.R. DeVault, D. Wang-Iverson, E. Ivashkiv, B.N. Swanson, A.A. Sugerman, Comparative pharmacokinetics and pharmacodynamics of pravastatin and lovastatin, *J. Clin. Pharmacol.* 30 (1990) 1128–1135.
- [43] K. Kawabata, K. Hoshiyama, S. Satsuki, T. Nitani, S. Kunihiro, Quantitative methods of pravastatin and its metabolites in human biological fluids using automated gas chromatographic/mass spectrometry and their application to pharmacokinetic

- studies in volunteers and patients, *Nippon Iyo Masu Supekutoru Gakkai Koenshu* 16 (1991) 149–152.
- [44] M.J. Morris, J.D. Gilbert, J.Y.-K. Hsieh, B.K. Matuszewski, H.G. Ramjit, W.F. Bayne, Determination of the HMG-CoA reductase inhibitors, simvastatin, lovastatin, and pravastatin in plasma by gas chromatography-chemical ionization mass spectrometry, *Biol. Mass Spectrom.* 22 (1993) 1–8.
- [45] K.H. Cai, B.Y. Tan, Z.Y. Feng, Z.W. Li, M. Huang, X.L. Zhao, The quantitative determination of pravastatin in plasma by a gas chromatograph-mass spectrometry method, *Seppu* 14 (1996) 121–123.
- [46] D.B. Whigan, E. Ivashkiv, A.I. Cohen, Determination of pravastatin sodium and its isomeric metabolite in human urine by HPLC with UV detection, *J. Pharm. Biomed. Anal.* 7 (1989) 907–912.
- [47] S. Muramatsu, C. Dumousseaux, W. Takasaki, H. Takahagi, Highly sensitive determination of pravastatin sodium in plasma by laser-induced fluorescence detection, *Kuromatogurafi* 14 (1993) 54–55.
- [48] I. Iacona, M.B. Regazzi, I. Buggia, P. Villani, V. Fiorito, M. Molinaro, E. Guarnone, High performance liquid chromatography determination of pravastatin in plasma, *Ther. Drug Monit.* 16 (1994) 191–195.
- [49] C. Dumousseaux, S. Muramatsu, W. Takasaki, H. Takahagi, Highly sensitive and specific determination of pravastatin sodium in plasma by high performance liquid chromatography with laser-induced fluorescence detection after immobilized antibody extraction, *J. Pharm. Sci.* 83 (1994) 1630–1636.
- [50] K. Otter, C. Mignat, Determination of pravastatin in human plasma by high-performance liquid chromatography with ultraviolet detection, *J. Chromatogr. B Biomed. Sci. Appl.* 708 (1998) 235–241.
- [51] R. Siekmeier, W. Gross, W. Marz, Determination of pravastatin by high performance liquid chromatography, *Int. J. Clin. Pharmacol. Ther.* 38 (2000) 419–425.
- [52] J. Wang, Determination of pravastatin by HPLC, *Zhongguo Kangshengsu Zazhi* 26 (2001) 254–255.
- [53] A. Bastarda, R. Granek, A. Kocijan, Chemical stability of pravastatin in acidic media, in: *International Symposium, Advances in Analytical Separation Science*, (Portschach/Worthersee, Austria), vol. 7, 2002.
- [54] S. Bauer, J. Mwinyi, A. Stoeckle, T. Gerloff, I. Roots, Quantification of pravastatin in human plasma and urine after solid phase extraction using high performance liquid chromatography with ultraviolet detection, *J. Chromatogr. B* 818 (2005) 257–262.
- [55] K. Kawabata, N. Samata, Y. Urasaki, Quantitative determination of pravastatin and R-416, its main metabolite in human plasma, by liquid chromatography-tandem mass spectrometry, *J. Chromatogr. B* 816 (2005) 73–79.
- [56] A. Kocijan, R. Grahek, A. Bastarda, L.Z. Kralj, Fast analysis of pravastatin in production media, *J. Chromatogr. B* 822 (2005) 311–315.
- [57] B.S. Rani, P.V. Reddy, Estimation of pravastatin sodium in tablets by HPLC, *Acta Ciencia Indica Chem.* 32 (2006) 409–412.
- [58] M.K. Pasha, S. Muzeeb, S.J.S. Basha, D. Shashikumar, R. Mullangi, N.R. Srinivas, Analysis of five HMG-Co-reductase inhibitors, atorvastatin, lovastatin pravastatin rosuvastatin and simvastatin: pharmacological, pharmacokinetic and analytical overview and development of a new method for use in pharmaceutical formulations analysis and in-vitro metabolism studies, *Biomed. Chromatogr.* 20 (2006) 282–293.
- [59] A. Onal, O. Sagirli, Development of a selective LC method for the determination of pravastatin sodium, *Chromatographia* 64 (2006) 157–162.
- [60] M. Campos-Lara, R. Pinto-Almazan, M.V. Oropeza, J.A. Mendoza-Espinoza, Optimization of a pravastatin quantification method using HPLC with ultraviolet detection

- in human serum for monitoring dyslipidemic patients, *J. Liq. Chromatogr. Relat. Technol.* 31 (2008) 667–674.
- [61] H. Xie, HPLC Determination of Dissolution of Pravastatin Sodium Capsule, Lishizhen Medicine and Materia Medica Research, 2006.
- [62] S. Ashour, H. Nakshbandi, S. Omar, Quantitative determination of pravastatin in pharmaceutical dosage forms by high performance liquid chromatography with ultraviolet detection, *Int. J. Biomed. Sci.* 4 (2008) 135–139.
- [63] S. Brain-Isasi, C. Requena, A. Alvarez-Lueje, Stability study of pravastatin under hydrolytic conditions assessed by HPLC, *J. Chil. Chem. Soc.* 53 (2008) 1684–1688.
- [64] M. Campos-Lara, J.A. Mendoza-Espinoza, Development of a selective extraction method for pravastatin quantification in tablets using HPLC with ultraviolet detection, *J. Liq. Chromatogr. Relat. Technol.* 31 (2008) 619–623.
- [65] F.P. Gomes, P.L. Garcia, J.M.P. Alves, A.K. Singh, E.R.M. Kedor-Hackmann, M.I.R.M. Santoro, Development and validation of stability-indicating HPLC methods for quantitative determination of pravastatin, fluvastatin, atorvastatin, and rosuvastatin in pharmaceuticals, *Anal. Lett.* 42 (2009) 1784–1804.
- [66] Q. He, J. Tian, Y. Zhang, J. Ding, Determination of pravastatin and relative bioavailability in the plasma by HPLC with solid-phase extraction, *Zhongnan Yaoxue* 7 (2009) 840–843.
- [67] R.W. Sparidans, D. Iusuf, A.H. Schinkel, J.H. Schellens, J.H. Beijnen, Liquid chromatography-tandem mass spectrometric assay for pravastatin and two isomeric metabolites in mouse plasma and tissue homogenates, *J. Chromatogr. B* 878 (2010) 2751–2759.
- [68] O.M. Abdullah, RP-HPLC determination of three anti-hyperlipidemic drugs in spiked human plasma and dosage forms, *E-J. Chem.* 8 (2011) 753–761.
- [69] N. Sultana, M.S. Arayne, N. Safila, Validated method for the simultaneous determination of lisinopril, pravastatin, atorvastatin and rosuvastatin in API, formulation and human serum by RP-HPLC, *Clin. J. Chem.* 29 (2011) 1216–1220.
- [70] K. Sampath, N. Ramesh, S. Kumar, S.L. Sasijith, J.D. Terish, Method development and validation of pravastatin sodium in human plasma by using LCMS/MS, *J. Bioequiv. Bioavailab.* 3 (2011) 48–51.
- [71] Z. Huang, R. Lozano, R. Francis, A.F. Aubry, A. Steckbeck, D.O. Sciascia, Development of a single in vitro dissolution method for a combination trilayer tablet formulation of clopidogrel and pravastatin, *Dissolution Technol.* 18 (2011) 12–19.
- [72] G.E.I. Harisa, M.F. Ibrahim, F.K. Alanazi, Characterization of human erythrocytes as potential carrier for pravastatin: an in-vitro study, *Int. J. Med. Sci.* 8 (2011) 222–230.
- [73] H.K. Kadikar, R. Shah, RP-HPLC method for simultaneous estimation of pravastatin and coenzyme Q10 in their combined formulated dosage form, *Int. J. Pharm. Res. Biosci.* 1 (2012) 102–111.
- [74] T.D. Silva, M.A. Oliveira, R.B. de Oliveira, C.D. Vianna Soares, Development and validation of a simple and fast HPLC method for determination of lovastatin, pravastatin and simvastatin, *J. Chromatogr. Sci.* 50 (2012) 831–838.
- [75] K. Kawabata, N. Matsushima, K. Sasahara, An automated method for the simultaneous determination of pravastatin and its main metabolite in human plasma by high performance liquid chromatography/atmospheric pressure chemical ionization mass spectrometry, *Biomed. Chromatogr.* 12 (1998) 271–275.
- [76] Z.M. Zhu, L. Neirinck, High-performance liquid chromatography coupled with negative ion tandem mass spectrometry for determination of pravastatin in human plasma, *J. Chromatogr. B* 783 (2003) 133–140.
- [77] M. Deng, H. Liu, H. Xue, J. Liu, Simultaneous determination of pravastatin and its main metabolite, 3'- $\alpha$ -isopravastatin in human plasma by HPLC-MS, *Chin. J. Pharm. Anal.* 25 (2005) 160–164.



- [78] H. Vlckova, M. Rabatinova, A. Miksova, G. Kolouchova, S. Micuda, Determination of pravastatin and pravastatin lactone in rat plasma and urine using UHPLC-MS/MS and microextraction by packed sorbent, *Talanta* 90 (2012) 22–29.
- [79] X. Li, T. Yao, S. Zeng, Determination of pravastatin in rat muscle by RPHPLC, *J. Zhejiang Univ. (Med. Sci.)* 28 (1999) 110–113.
- [80] X. Li, K. Otter, A. Ziegler, Determination of pravastatin in rat liver by RP-HPLC, *Yao Xue Xue Bao* 36 (2001) 123–126.
- [81] X. Li, J.H. Xu, S. Zeng, Determination of pravastatin in rat plasma by solid phase extraction and RP-HPLC, *Yaowu Fenxi Zazhi* 21 (2001) 384–387.
- [82] N. Delhi-Raj, S. Kumaravel, R. Murugan, S.S. Narayanan, R. Vijayalakshmi, Reversed phase HPLC method for the determination of pravastatin in tablet dosage forms, *Int. J. Res. Pharm. Sci.* 1 (2010) 187–189.
- [83] N. Sultana, M.S. Arayne, W. Shazad, Simultaneous determination of ceftriaxone sodium and statin prodrugs in pharmaceutical formulations and human serum by RP-HPLC, *J. Chil. Chem. Soc.* 55 (2010) 193–198.
- [84] N. Matsushima, K. Kawabata, T. Nitandai, K. Sasahara, Automated and simultaneous determination of pravastatin and its main metabolite in human plasma by LC/APCI-MS and its application to pharmacokinetic studies in volunteers and patients, *Nippon Iyo Masu Supekutoru Gakkai Koenshu* 18 (1993) 169–172.
- [85] M. Jemal, Y. Qing, D.B. Whigan, The use of high-flow high performance liquid chromatography coupled with positive and negative ion electrospray tandem mass spectrometry for quantitative bioanalysis via direct injection of the plasma/serum samples, *Rapid Commun. Mass Spectrom.* 12 (1998) 1389–1399.
- [86] D. Mulvana, M. Jemal, S. Coates-Pulver, Quantitative determination of pravastatin and its biotransformation products in human serum by turbo ion spray LC/MS/MS, *J. Pharm. Biomed. Anal.* 23 (2000) 851–866.
- [87] X.S. Miao, C.D. Metcalfe, Determination of cholesterol-lowering statin drugs in aqueous samples using liquid chromatography–electrospray ionization tandem mass spectrometry, *J. Chromatogr. A* 998 (2003) 133–141.
- [88] K. Kawabata, Y. Urasaki, Automated sensitive method for determination of pravastatin and its metabolite in human plasma by LC/APCI-MS/MS with Prospekt-2 on-line solid-phase extraction, *J. Mass Spectrom. Soc. Jpn.* 53 (2005) 79–87.
- [89] D.S. Jain, G. Subbaiah, M. Sanyal, V.K. Jain, P. Shrivastav, A rapid and specific approach for direct measurement of pravastatin concentration in plasma LC-MS/MS employing solid-phase extraction, *Biomed. Chromatogr.* 21 (2007) 67–78.
- [90] J.W. Deng, K.B. Kim, I.S. Song, J.H. Shon, H.H. Zhou, K.H. Liu, J.G. Shin, Determination of two HMG-CoA reductase inhibitors, pravastatin and pitavastatin, in plasma samples using liquid chromatography–tandem mass spectrometry for pharmaceutical study, *Biomed. Chromatogr.* 22 (2008) 131–135.
- [91] X. Wang, Y. Wang, On-line extraction coupled with liquid chromatography tandem mass spectrometry for quantitation of pravastatin and its metabolite in human serum, *Biomed. Chromatogr.* 22 (2008) 719–726.
- [92] B. Mertens, B. Cahay, R. Klinkenberg, B. Streel, An automated method for the simultaneous determination of pravastatin, 3-hydroxy isomeric metabolite, pravallactone and fenofibric acid in human plasma by sensitive liquid chromatography combined with diode array and tandem mass spectrometry detection, *J. Chromatogr.* 1189 (2008) 493–502.
- [93] Z. Tan, D. Ouyang, G. Zhou, D. Guo, Y. Chen, C. Xiao, L. Peng, H. Chen, Y. Chen, L. Zhang, Y. Han, H. Zhou, A simple and sensitive LC-MS/MS method for determination of pravastatin in human plasma, *Chin J. New Drugs* 17 (2008) 1150–1153.

- [94] M. Zhang, Z. Tan, H. Chen, Y. Chen, D. Guo, H. Zhou, LC-MS/MS determination of pravastatin in human plasma, *Chin. J. Pharm. Anal.* 29 (2009) 58–61.
- [95] N.R. Pilli, J.K. Inamadugu, V.K. Karra, S.R. Polagani, J.V.L.N. Seshagiri Rao, Rapid liquid chromatographic-tandem mass spectrometric method for the quantitation of pravastatin in human plasma, *Der. Pharm. Lett.* 4 (2012) 142–151.
- [96] K. Kircali, M. Tuncel, H.Y. Aboul-Enein, Determination of pravastatin in tablets by capillary electrophoresis, *Il Farmaco* 59 (2004) 241–244.
- [97] B. Nigovic, I. Vegar, Capillary electrophoresis determination of pravastatin and separation of its degradation products, *Croat. Chem. Acta* 81 (2008) 615–622.
- [98] M. Damic, B. Nigovic, Fast analysis of statins in pharmaceuticals by MEKC, *Chromatographia* 71 (2010) 233–240.
- [99] D. Wang-Iverson, A.I. Cohen, Bioanalytical approaches, including quantitative MS, for pravastatin, lovastatin and simvastatin, *Methodol. Surv. Bioanal. Drugs* 23 (1994) 127–139.
- [100] S. Muramatsu, W. Takasaki, H. Takahagi, EIA of pravastatin in blood, *Jpn Kokai Tokkyo Koho*, JP 03289564 A 19911219, 1991.
- [101] S. Muramatsu, W. Takasaki, M. Uchiyama, Y. Komokata, Y. Tanaka, H. Takahagi, Enzyme-linked immunosorbent assay of pravastatin, a HMG-CoA reductase inhibitor, in human plasma, *J. Immunoassay* 17 (1996) 13–27.
- [102] I.A. Darwish, A.R.M. Al-Obaid, H.A. Al-Malaq, New highly sensitive enzyme immunoassay for the determination of pravastatin in human plasma, *Talanta* 79 (2009) 1478–1483.
- [103] S.M. Singhvi, H.Y. Pan, R.A. Morrison, D.A. Willard, Disposition of pravastatin sodium, a tissue-selective HMG-CoA reductase inhibitor, in healthy subjects, *Br. J. Clin. Pharmacol.* 29 (1990) 239–243.
- [104] D.W. Everett, T.J. Chando, G.C. Didonato, S.M. Singhvi, H.Y. Pan, S.H. Weinstein, Biotransformation of pravastatin sodium in humans, *Drug Metab. Dispos.* 19 (1991) 740–748.
- [105] T. Komai, K. Kawai, T. Tokui, Y. Tokui, C. Kuroiwa, E. Shigehara, M. Tanaka, Disposition and metabolism of pravastatin sodium in rats, dogs and monkeys, *Eur. J. Drug Metab. Pharmacokinet.* 17 (1992) 103–113.
- [106] H.Y. Pan, A.P. Wacławski, F.T. Funke, D. Whigan, Pharmacokinetics of pravastatin in elderly versus young men and women, *Ann. Pharmacother.* 27 (1993) 1029–1033.
- [107] J.A. Quin, P.H. Jones, Clinical pharmacokinetics of pravastatin, *Clin. Pharmacokinet.* 27 (1994) 94–103.
- [108] T.W.B. Gehr, D.A. Sica, P.H. Slugg, J.L. Hammett, R. Raymond, N.F. Ford, The pharmacokinetics of pravastatin in patients on chronic hemodialysis, *Eur. J. Clin. Pharmacol.* 53 (1997) 117–121.
- [109] T. Hatanaka, Clinical pharmacokinetics of pravastatin: mechanism of pharmacokinetic events, *Clin. Pharmacokinet.* 39 (2000) 397–412.
- [110] R. Nakagomi-Hagihara, D. Nakai, T. Tokui, Inhibition of human organic anion transporter 3 mediated pravastatin transport by genfibrozil and the metabolites in humans, *Xenobiotica* 37 (2007) 416–426.
- [111] Y. Escobar, C.R. Venturelli, C. Hoyo-Vadillo, Pharmacokinetic properties of pravastatin in Mexicans: an open-label study in healthy adult volunteers, *Curr. Ther. Res.* 66 (2005) 238–246.
- [112] T.A. Jacobson, Comparative pharmacokinetic interaction profiles of pravastatin, simvastatin, and atorvastatin when coadministered with cytochrome p-450 inhibitors, *Am. J. Cardiol.* 94 (2004) 1140–1146.
- [113] H. Iwabuchi, K. Miyaguchi, T. Nakamura, M. Uchiyama, A. Kitagawa, S. Muramatsu, T. Kinoshita, H. Takahagi, E. Kirazawa, Metabolic study of pravastatin

- sodium (IV). Structure elucidation of metabolites and possible metabolic pathways, *Nippon Iyo Masu Supekutoru Gakkai Koenshu* 14 (1989) 205–208.
- [114] S. Muramatsu, K. Miyaguchi, H. Iwabuchi, Y. Matsushita, T. Nakamura, T. Kinoshita, M. Tanaka, H. Takahagi, Metabolism of pravastatin sodium in isolated rat hepatocytes. I. Glutathione conjugate formation reaction, *Xenobiotica* 22 (1992) 487–498.
- [115] T. Nakamura, K. Yoda, H. Kuwano, K. Miyaguchi, S. Muramatsu, H. Takahagi, T. Kinoshita, Metabolism of pravastatin sodium in isolated rat hepatocytes. II. Structure elucidation of the metabolites by n.m.r. spectroscopy, *Xenobiotica* 21 (1991) 277–293.
- [116] E. Kitazawa, N. Tamura, H. Iwabuchi, M. Uchiyama, S. Muramatsu, H. Takahagi, M. Tanaka, Biotransformation of pravastatin sodium (I). Mechanisms of enzymic transformation and epimerization of an allylic hydroxyl group of pravastatin sodium, *Biochem. Biophys. Res. Commun.* 192 (1993) 597–602.
- [117] S. Muramatsu, Y. Komokata, Y. Tanaka, H. Takahagi, Metabolism of pravastatin sodium by 3- $\alpha$ -hydroxysteroid dehydrogenase, *Biol. Pharm. Bull.* 20 (1997) 1199–1203.
- [118] W. Jacobsen, G. Kirchner, K. Hallensleben, L. Mancinelli, M. Deters, I. Hackbarth, K. Baner, L.Z. Benet, K.-F. Sewing, V. Christians, Small intestinal metabolism of the 3-hydroxy-3-methylglutaryl-Coenzyme A reductase inhibitor lovastatin and comparison with pravastatin, *J. Pharmacol. Exp. Ther.* 291 (1999) 131–139.
- [119] W. Jacobsen, G. Kirchner, K. Hallensleben, L. Mancinelli, M. Deters, I. Hackbarth, L.Z. Benet, K.-F. Sewing, V. Christians, Comparison of cytochrome p-450-dependent metabolism and drug interaction of the 3-hydroxy-3-methylglutaryl-CoA reductase inhibitors, lovastatin and pravastatin in the liver, *Drug Metab. Dispos.* 27 (1999) 173–179.
- [120] M. Deng, H.-C. Liu, Study on stability of pravastatin under simulated in-vivo conditions, *Chin. J. Hosp. Pharm.* 26 (2006) 37–39.
- [121] H.M. Lotfy, H.F. El-Sanabary, Z.A. El-Sherif, M.G. El-Bardicy, Stability study of simvastatin and pravastatin sodium under acidic hydrolytic conditions assessed by high performance liquid chromatography, *Anal. Chem.* 9 (2010) 172–184.
- [122] S.R. Polagani, N.R. Pilli, V. Gandu, High performance liquid chromatography mass spectrometric method for the simultaneous quantification of pravastatin and aspirin in human plasma: pharmacokinetic application, *J. Pharm. Anal.* 2 (2012) 206–213.
- [123] N. Serizawa, Dual stage production of HMG-CoA reductase inhibitor pravastatin, *Shin Tanpatiusuitsu Oyo Kogaku* (1996) 628–635.
- [124] M. Arai, N. Serizawa, A. Terahara, Y. Tsujita, M. Tanaka, H. Masuda, S. Ishikawa, Pravastatin sodium (cs-514), a novel cholesterol-lowering agent which inhibits HMG-CoA reductase, *Sankyo Kinkusho Nenpo* 40 (1988) 1–38.
- [125] S. Erturk, A. Onal, S.M. Cetin, Analytical methods for the quantitative determination of 3-hydroxy-3-methylglutaryl coenzyme A reductase inhibitors in biological samples, *J. Chromatogr. B Anal. Technol. Biomed. Life Sci.* 793 (2003) 193–205.
- [126] R. Nirogi, K. Mudigonda, V. Kandikere, Chromatography-mass spectrometry methods for the quantitation of statins in biological samples, *J. Pharm. Biomed. Anal.* 44 (2007) 379–387.



# Vardenafil Dihydrochloride

**Abdelkader E. Ashour<sup>\*</sup>, A.F.M. Motiur Rahman<sup>†</sup>,  
Mohammed G. Kassem<sup>†</sup>**

<sup>\*</sup>Department of Pharmacology and Toxicology, College of Pharmacy, King Saud University, Riyadh, Saudi Arabia

<sup>†</sup>Department of Pharmaceutical Chemistry, College of Pharmacy, King Saud University, Riyadh, Saudi Arabia

## Contents

1. Introduction	515
1.1 Nomenclature	516
1.2 Formula	516
1.3 Physical properties	517
2. Methods of Preparation	518
3. Physical Properties	522
3.1 Spectroscopy	522
3.2 Nuclear magnetic resonance spectrometry	523
3.3 Mass spectrum	526
4. Methods of Analysis	528
4.1 Chromatographic methods	528
4.2 Voltammetric method	535
4.3 Immunoassay methods	535
5. Pharmacology of Vardenafil	536
5.1 Pharmacodynamics	536
5.2 Pharmacokinetics	539
Acknowledgment	540
References	540



## 1. INTRODUCTION

Vardenafil (Levitra<sup>®</sup>) is a potent and highly selective inhibitor of cGMP-specific phosphodiesterase type 5 (PDE-5), the most prominent PDE in the penile corpus cavernosum. It has been proven to be safe and effective treatment for erectile dysfunction (ED). This action can result in smooth muscle relaxation that is needed for a penile erection [1]. Vardenafil is 5–10 times more potent than sildenafil, the classic PDE-5 inhibitor [2]. The drug is generally well tolerated, with a favorable safety profile. Its use

is associated with few treatment-related side effects, most notably headache, flushing, indigestion and nasal congestion [3,4]. Vardenafil has a rapid onset of action, and ED patients can gain erections sufficiently rigid for eventual intercourse completion as early as 10–15 min after drug intake [5,6]. It is hepatically metabolized into more than 14 metabolites, the most important of which is *N*-desethyl vardenafil (M1). Interestingly, this metabolite is pharmacologically active [7,8].

## 1.1. Nomenclature

### 1.1.1 Systematical chemical names

- 2-(2-Ethoxy-5-((4-ethylpiperazin-1-yl)sulfonyl)phenyl)-5-methyl-7-propylimidazo[5,1-f][1,2,4]triazin-4(1H)-one (free base) [8].
- 2-[2-Ethoxy-5-(4-ethylpiperazine-1-sulfonyl)phenyl]-5-methyl-7-propyl-1H,4H-imidazo[4,3-f][1,2,4]triazin-4-one (IUPAC, free base) [9].
- 2-{5-Ethoxy-2-[(4-ethyl-1-piperazinyl)sulfonyl]phenyl}-5-methyl-7-propylimidazo[5,1-f][1,2,4]triazin-4(1H)-one (free base) [10].
- 2-{2-Ethoxy-5-[(4-ethyl-1-piperazinyl)sulfonyl]phenyl}-5-methyl-7-propylimidazo[5,1-f][1,2,4]triazin-4(1H)-one dihydrochloride (ACD/IUPAC name) [11].
- 2-{2-Ethoxy-5-[(4-ethylpiperazin-1-yl)sulfonyl]phenyl}-5-methyl-7-propylimidazo[5,1-f][1,2,4]triazin-4(1H)-one dihydrochloride [11].

### 1.1.2 Nonproprietary names

Synonyms: VDN (free base) [12].

### 1.1.3 Proprietary names

Levitra [11], Staxyn , Staxyn ODT, Vivanza.

## 1.2. Formula

### 1.2.1 Empirical formula, molecular weight, obtained mass, and CAS number

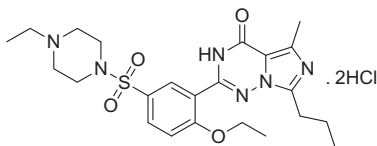
Chemical formula:  $C_{23}H_{32}N_6O_4S \cdot 2HCl$ ;  $C_{23}H_{34}Cl_2N_6O_4S$

Molecular weight: 561.53

Monoisotopic mass: 560.17395 Da, molecular weight: 488.60, monoisotopic mass: 488.220581 Da (free base), exact mass: 488.22, exact mass: 488.22,  $m/z$  488.9  $[M+H]^+$  (obtained),

CAS number 224789-15-5, CAS number 224785-90-4 (free base) [9,12].

### 1.2.2 Structural formula



Vardenafil dihydrochloride (**1**) [12]

### 1.2.3 SMILES

Cl.Cl.O=C2\N=C(/Nn1c(nc(c12)C)CCC)c3cc(ccc3OCC)S(=O)(=O)N4CCN(CC)CC4 [11].

CCCC1=NC(C)=C2N1NC(=NC2=O)C1=C(OCC)C=CC(=C1)S(=O)(=O)N1CCN(CC)CC1 (free base) [13].

### 1.2.4 InChI

InChI=1S/C23H32N6O4S.2ClH/c1-5-8-20-24-16(4)21-23(30)25-22(26-29(20)21)18-15-17(9-10-19(18)33-7-3)34(31,32)28-13-11-27(6-2)12-14-28;/h9-10,15H,5-8,11-14H2,1-4H3,(H,25,26,30);2\*1H [11].

InChI=1S/C23H32N6O4S/c1-5-8-20-24-16(4)21-23(30)25-22(26-29(20)21)18-15-17(9-10-19(18)33-7-3)34(31,32)28-13-11-27(6-2)12-14-28/h9-10,15H,5-8,11-14H2,1-4H3,(H,25,26,30) (free base) [13].

## 1.3. Physical properties

### 1.3.1 Appearance

White crystalline powder

### 1.3.2 Solubility

Water solubility: 0.11 mg/mL (HCl salt) [13].

### 1.3.3 Melting point

241 °C, 192 °C (free base) [3], 214–216 °C [9], 224–239 °C [14].

### 1.3.4 Stability

30 °C/75% relative humidity [15].

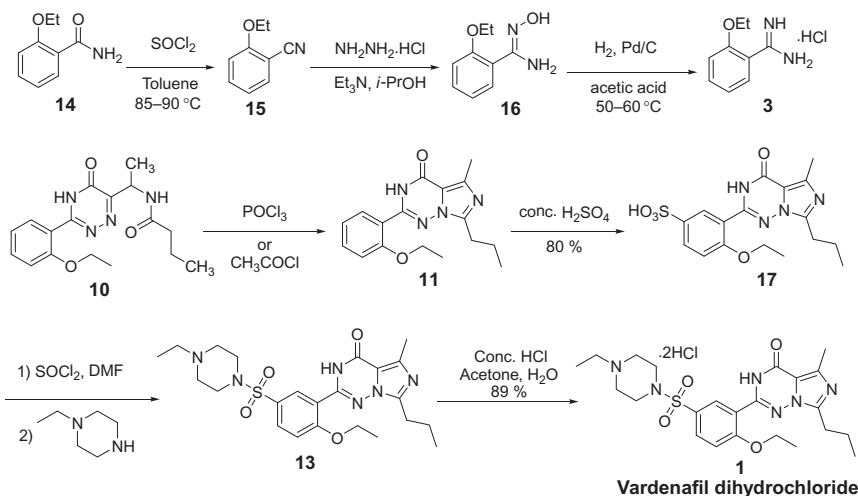
### 1.3.5 Dissociation constant

$pK_{a1}$  = 4.72;  $pK_{a2}$  = 6.21 (tertiary amine)/estimated (free base) [16].



A solution of crude **9** in ethanol was added to carboximidohydrazide **4**, formed *in situ* by addition of hydrazine hydrate to amidine **3** in ethanol, and the mixture was heated at 70 °C for 4 h to give the condensation product **10**. Intermediate **10** was cyclized to the imidazotriazinone **11** using phosphorous oxychloride. Compound **11** was formed in 28% yield from **3** and **7**, when intermediates **4**, **9**, and **10** were taken to the next step without purification. Reaction of **11** with chlorosulfonic acid provided the sulfonyl chloride **12**, which was treated with *N*-ethylpiperazine to obtain vardenafil (**13**) followed by salt formation using hydrochloric acid in ether furnished vardenafil dihydrochloride (**1**). A modified synthesis of vardenafil dihydrochloride (**1**) on a multikilogram scale has recently been reported by the same authors [22] (Scheme 9.2). Benzamide **3** was prepared in a different manner than what is described in Scheme 9.1, because it is difficult to use triethyl-aluminum on a large scale. Thus, 2-ethoxybenzamide (**14**) was dehydrated with thionyl chloride to give 2-ethoxybenonitrile (**15**), which was treated with hydroxylamine hydrochloride to afford the *N*-hydroxybenzimidine (**16**), which was treated with hydroxylamine hydrochloride to afford the *N*-hydroxybenzimidine (**16**).

Catalytic hydrogenation of **16** provided benzamidine **3**. Intermediate **9** was condensed with the imidohydrazide intermediate **4** in a similar manner as that described in Scheme 9.1 to give **10**. Compound **10** was cyclized using phosphorous oxychloride or acetyl chloride to deliver **11**. Compound **11** was sulfonated with H<sub>2</sub>SO<sub>4</sub> to furnish the sulfonic acid **17**. Treatment of **17** with thionyl chloride and DMF provided the sulfonyl chloride, which



Scheme 9.2 Large scale synthesis of vardenafil dihydrochloride.

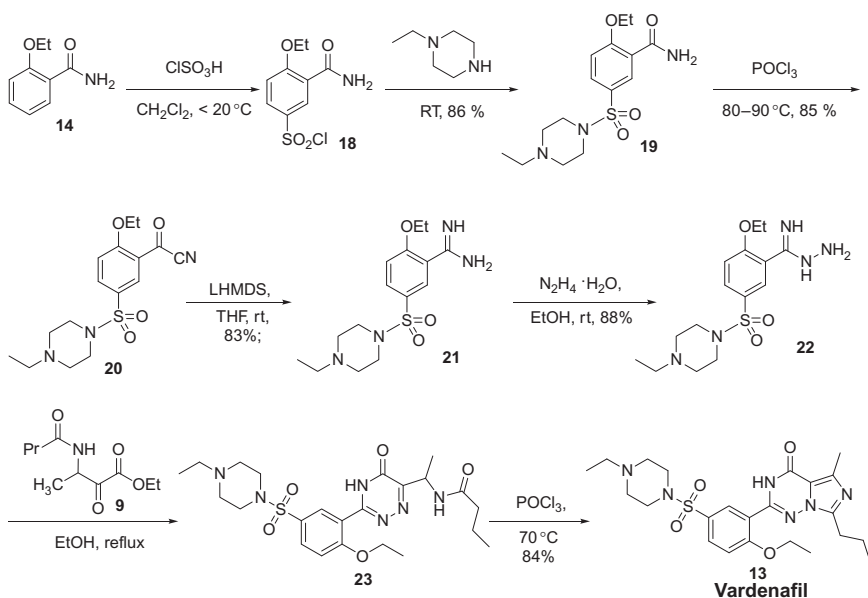


was reacted with *N*-ethylpiperazine in the same pot to give vardenafil (**13**) in 93 % yield. The vardenafil dihydrochloride (**1**) salt of vardenafil (**13**) was prepared using concentrated HCl in acetone and water.

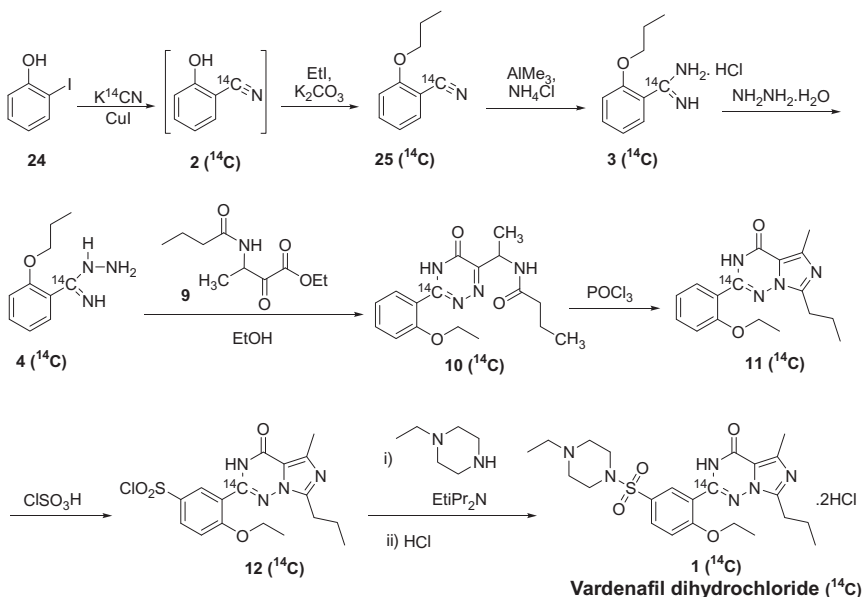
Recently, in 2009, Yongjun Mao *et al.* [18] presented an improved synthetic route (Scheme 9.3) for the synthesis of vardenafil (**13**). In this scheme, compound **5** was treated with chlorosulfonic acid to obtain sulfonyl chloride substituted product **18**, which was then treated with 1-ethylpiperazine to provide **19**, followed by POCl<sub>3</sub> treatment to give the benzonitrile **20**.

The benzamidine **21** was afforded by the reaction of **20** with lithium hexamethyldisilazane. Then benzamidine **21** was treated with hydrazine hydrate in ethanol to convert the benzamidine **21** to the benzamidrazone **22**. Compound **22** [19] was then reacted with **9** to afford the intermediate **23** which was directly transformed into the title vardenafil (**13**).

For the synthesis of vardenafil (**13**), imidazole **26** was prepared according to the reported procedure [23–25]. Aminolysis of imidazole **26**, followed by



**Scheme 9.3** Improved synthetic route for the synthesis of vardenafil dihydrochloride [21].

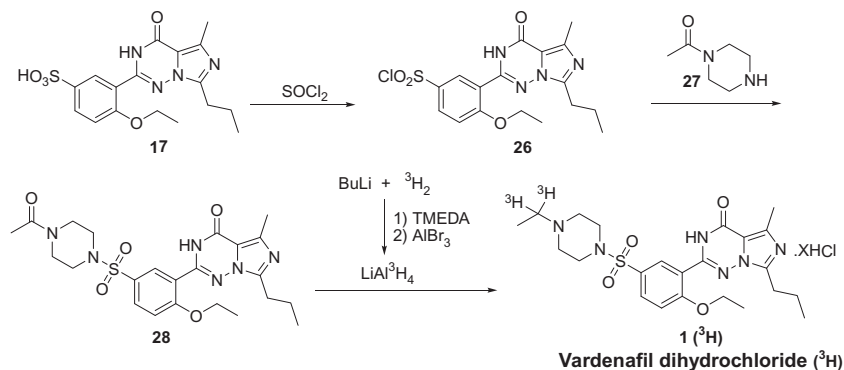


**Scheme 9.4** Synthesis of [ $^{14}\text{C}$ ]-labeled vardenafil hydrochloride [27].

N-amination produced aminoimidazole carboxamide **28** (Scheme 9.4). Aminoimidazole carboxamide **28** was then acylated with 2-ethoxybenzoyl chloride (**14**) and provided the 3-(2-ethoxybenzoylamino)-imidazole **29** [26]. Compound **31** was cyclized in presence of potassium *tert*-butoxide in *tert*-butyl alcohol in a sealed tube at 160 °C and produced compound **11**. Compound **11** was then preceded to next steps as explained in Scheme 9.1 and produced vardenafil (**13**).

[ $^{14}\text{C}$ ]-labeled vardenafil hydrochloride was synthesized as depicted in Scheme 9.4. Starting [ $^{14}\text{C}$ ]-labeled 2-hydroxybenzonitrile **2**( $^{14}\text{C}$ ) was synthesized from 2-hydroxy iodobenzene (**24**) using [ $^{14}\text{C}$ ]-labeled KCN in presence of copper iodide (CuI). Next steps were performed according to the literature procedure as explained earlier in Scheme 9.1.

In Scheme 9.5, [ $^3\text{H}$ ]-labeled vardenafil dihydrochloride was synthesized using [ $^3\text{H}$ ]-labeled lithium aluminum hydride isotope. 2-[2-Ethoxy-5-(4-acetylpiperazine-1-sulfonyl)-phenyl]-5-methyl-7-propyl-3H-imidazo[5,1-f][1,2,4]triazin-4-one (**28**) was synthesized from known sulfonic acid **17** in



**Scheme 9.5** Synthesis of [ $^3\text{H}$ ]-labeled vardenafil dihydrochloride [28].

two steps. In the first step, sulfonic acid **17** was treated with thionyl chloride to obtain **26**. Compound **26** was then treated with *N*-acetylpiperazine (**27**) and gave **28**. Reduction of carbonyl group of compound **28** was then performed using [ $^3\text{H}$ ]-labeled lithium aluminum hydride to obtain [ $^3\text{H}$ ]-labeled vardenafil dihydrochloride ( $1[^3\text{H}]$ ).



## 3. PHYSICAL PROPERTIES

### 3.1. Spectroscopy

#### 3.1.1 Ultraviolet spectroscopy

The ultraviolet/visible (UV/VIS) absorption spectrum of vardenafil dihydrochloride was recorded for selecting the proper maximum absorption peak ( $\lambda_{\text{max}}$ ). The absorption spectrum of the compound in ethanol was scanned from 200 to 800 nm, using a UV/VIS spectrometer (Varian Cary 50 UV/VIS spectrophotometer). As shown in Figure 9.1, the  $\lambda_{\text{max}}$  of vardenafil dihydrochloride is located at 270 nm.

#### 3.1.2 Vibrational spectroscopy of vardenafil dihydrochloride

##### 3.1.2.1 IR Spectroscopy of vardenafil dihydrochloride

The IR absorption spectrum of vardenafil dihydrochloride was obtained in KBr plate, using a Shimadzu infrared spectrophotometer. The IR spectrum is shown in Figure 9.2. The principal peaks were observed at 3420.88, 2969.94, 2451.95, 1724.33, 1654.07, 1599.99, 1491.25, 1333.086,

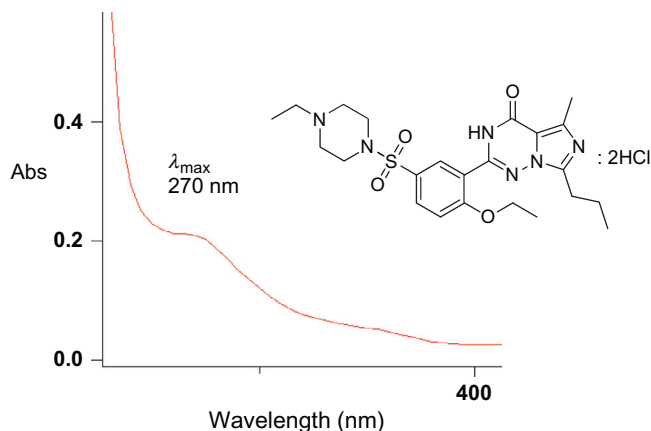


**Figure 9.1** UV spectrum of vardenafil dihydrochloride ( $5.8 \times 10^{-5}$  M solution in ethanol).

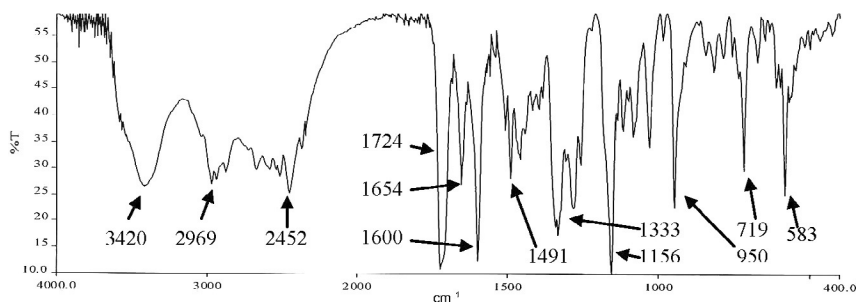
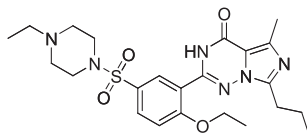


**Figure 9.2** Infrared spectroscopy (IR) spectra of vardenafil dihydrochloride in KBr pellet.

1281.50, 1156.50, 950.28, 719.82, and 583.54  $\text{cm}^{-1}$ . Assignments for the major IR absorption bands are provided in [Table 9.1](#).



### 3.2. Nuclear magnetic resonance spectrometry

$^1\text{H}$  and  $^{13}\text{C}$  nuclear magnetic resonance (NMR) spectra of vardenafil dihydrochloride were obtained using a Bruker 500 MHz Nuclear Magnetic Spectrometer. Chemical shifts were expressed in parts per million (ppm) ([Table 9.2](#)) with respect to the tetramethylsilane signal for  $^1\text{H}$  and  $^{13}\text{C}$  NMR ([Figures 9.3–9.5](#), respectively).

**Table 9.1** Infrared spectroscopic data for vardenafil dihydrochloride in KBr plate

Entry	Bond	Absorption peaks ( $\lambda_{\max}$ ) ( $\text{cm}^{-1}$ )	Appearance
1	C—N	719	Strong
2	C—O	1156	Strong
3	—C—H, HC=CH (aryl)	1600, 1491, 1333	Strong
4	C=O	1724	Strong
5	CH <sub>2</sub> , C—H (alkyl)	2970	Strong
6	N—H	3421	Broad

**Table 9.2** Comparative study of <sup>1</sup>H NMR spectra of vardenafil dihydrochloride with literature

Entry	Chemical shift (500 MHz, CD <sub>3</sub> OD)	Chemical shift <sup>a</sup> (500 MHz, CDCl <sub>3</sub> )	Chemical shift <sup>b</sup> (200 MHz, DMSO- <i>d</i> <sub>6</sub> )
1	—	—	12.45 (s, 1H, —NH)
	—	9.52 (s, 1H, —NH)	11.42 (s, 1H, —NH)
2	8.09 (s, 1H)	8.48 (d, 1H, <i>J</i> = 2.1 Hz)	
3	8.06 (d, <i>J</i> = 9 Hz)	7.88 (dd, 1H, <i>J</i> = 9.0, 2.1 Hz)	7.95 (m, 2H)
4	7.48 (d, <i>J</i> = 8.0 Hz, 1H)	7.15 (d, 1H, <i>J</i> = 9.0 Hz)	7.48 (d, 1H)
5	4.34 (d, <i>J</i> = 6.0 Hz, 2H)	4.32 (q, 2H, <i>J</i> = 6.9 Hz)	4.25 (q, 2H)
6	3.96 (d, <i>J</i> = 12.0 Hz, 2H)	3.15 (br, 4H)	3.70 (m, 2H)
7	3.68 (d, <i>J</i> = 11.5 Hz, 2H)	2.99 (t, 2H, <i>J</i> = 7.2 Hz),	3.50 (m, 2H),
8	3.28–3.23 (m, 6H)	2.64 (s, 3H)	3.08 (m, 6H)
9	2.95 (t, <i>J</i> = 11.5 Hz, 2H)	2.54 (br, 4H)	2.88 (m, 2H)
10	2.78 (s, 3H)	2.49 (q, 2H, <i>J</i> = 7.2 Hz)	2.61 (s, 3H)
11	1.94 (d, <i>J</i> = 6.5 Hz, 2H)	1.86 (m, 2H)	1.81 (sextet, 2H)
12	1.48 (t, 3H)	1.58 (t, 3H, <i>J</i> = 6.9 Hz)	1.36 (t, 3H)
13	1.39 (t, 3H)	1.08 (t, 3H, <i>J</i> = 7.2 Hz)	1.22 (t, 3H)
14	1.1 (t, 3H)	1.0 (t, 3H, <i>J</i> = 7.2 Hz)	0.99 (t, 3H)

<sup>a</sup>Free base [21].<sup>b</sup>HCl salt [16].

### 3.2.1 $^1\text{H}$ NMR spectrum of vardenafil dihydrochloride

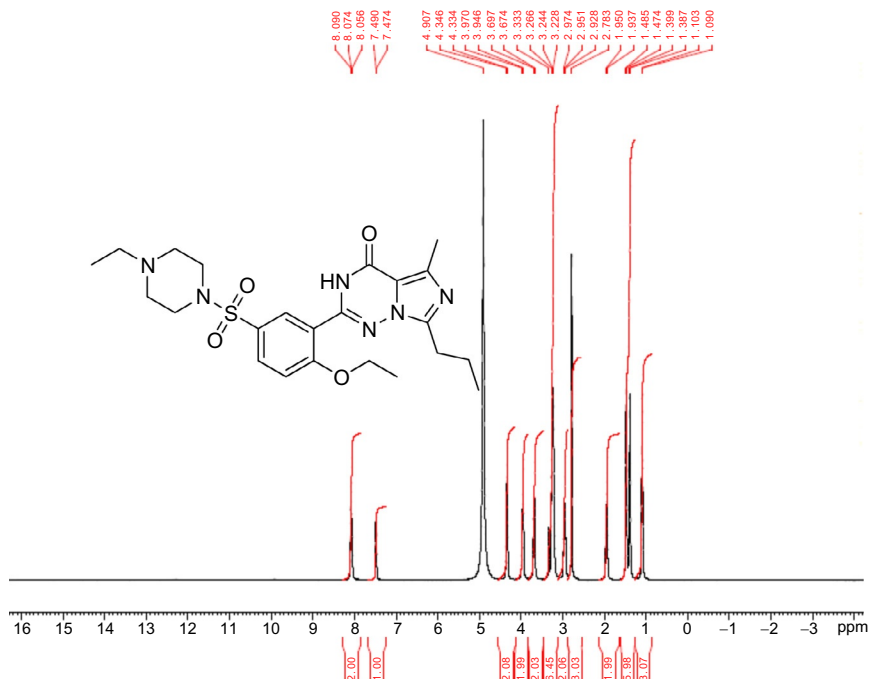


Figure 9.3  $^1\text{H}$  NMR spectra of vardenafil dihydrochloride in  $\text{CD}_3\text{OD}$ .

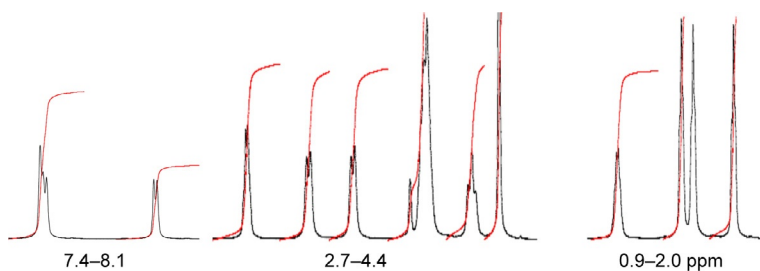


Figure 9.4 Expanded  $^1\text{H}$  NMR spectra of vardenafil dihydrochloride in  $\text{CD}_3\text{OD}$ .

### 3.2.2 $^1\text{H}$ NMR of vardenafil dihydrochloride in $\text{CD}_3\text{OD}$

$^1\text{H}$  NMR ( $\text{CD}_3\text{OD}$ , 500 MHz):  $\delta$  8.09 (s, 1H), 8.06 (d,  $J=9$  Hz), 7.48 (d,  $J=8.0$  Hz, 1H), 4.34 (d,  $J=6.0$  Hz, 2H), 3.96 (d,  $J=12.0$  Hz, 2H), 3.68 (d,  $J=11.5$  Hz, 2H), 3.28–3.23 (m, 6H), 2.95 (t,  $J=11.5$  Hz, 2H), 2.78 (s, 3H), 1.94 (d,  $J=6.5$  Hz, 2H), 1.48 (t, 3H), 1.39 (t, 3H), 1.1 (t, 3H) ppm.

### 3.2.3 $^{13}\text{C}$ NMR spectrum of vardenafil dihydrochloride

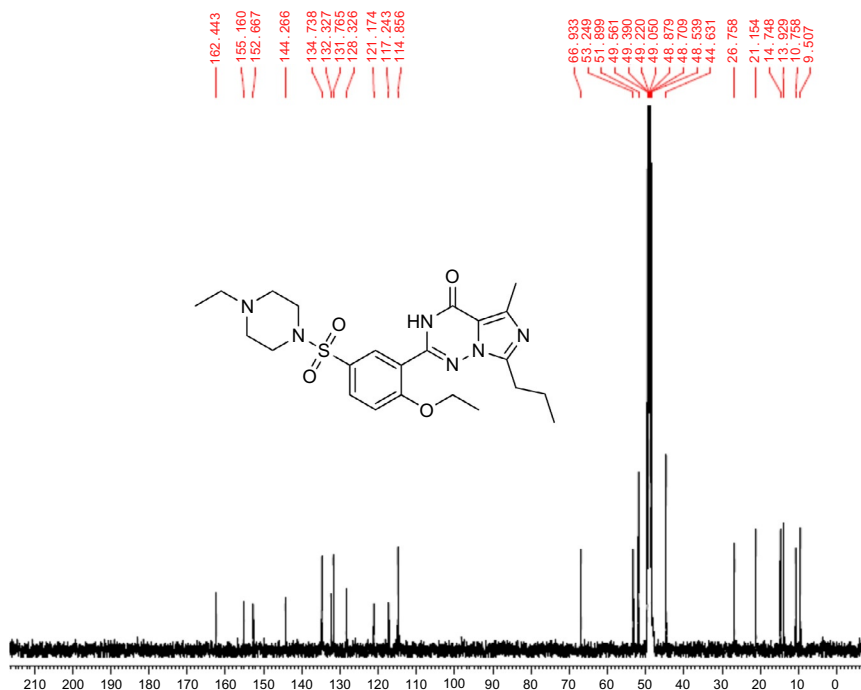


Figure 9.5  $^{13}\text{C}$  NMR spectra of vardenafil dihydrochloride in  $\text{CD}_3\text{OD}$ .

### 3.2.4 $^{13}\text{C}$ NMR of vardenafil dihydrochloride in $\text{CD}_3\text{OD}$

$^{13}\text{C}$  NMR ( $\text{CD}_3\text{OD}$ , 125 MHz):  $\delta$  162.44, 155.16, 152.67, 144.27, 134.74, 132.33, 131.76, 128.33, 121.17, 117.24, 114.86, 66.93, 53.25, 51.90, 44.63, 26.76, 21.15, 14.75, 13.93, 10.76, and 9.51 ppm.

## 3.3. Mass spectrum

Mass spectral studies of vardenafil dihydrochloride were carried out with an Agilent 6320 Ion Trap LC/MS system by infusion of 1  $\mu\text{g}$  of vardenafil dihydrochloride solution in  $\text{MeOH}:\text{H}_2\text{O}$  (1:1) without a column. Smart fragmentor and automatic optimization were performed to obtain the spectra and make fragmentation. The source parameters were as follows: temperature was 350 C, gas flow was 10 L/min, and nebulizer was 50 psi. Figure 9.6 shows the mass spectrum for the parent compound ( $m/z$  488.9), Figures 9.7 and 9.8 detail mass fragmentation pattern interpretation of the drug substance. The reported  $m/z$  for vardenafil dihydrochloride is 489 [29].

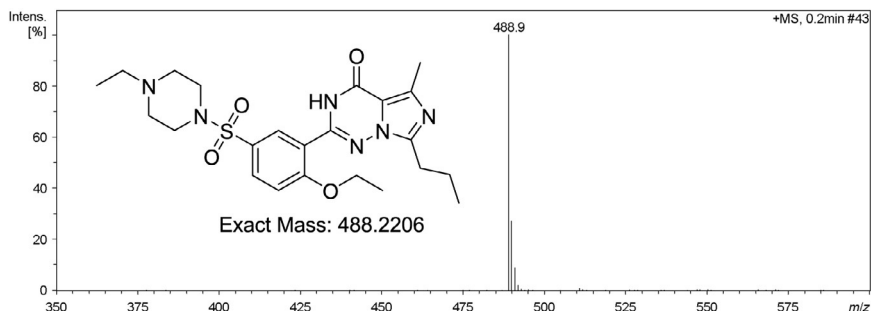


**Figure 9.6** Vardenafil dihydrochloride shows a  $m/z=88.9$   $[M+H]^+$  molecular ion peak in positive mode.

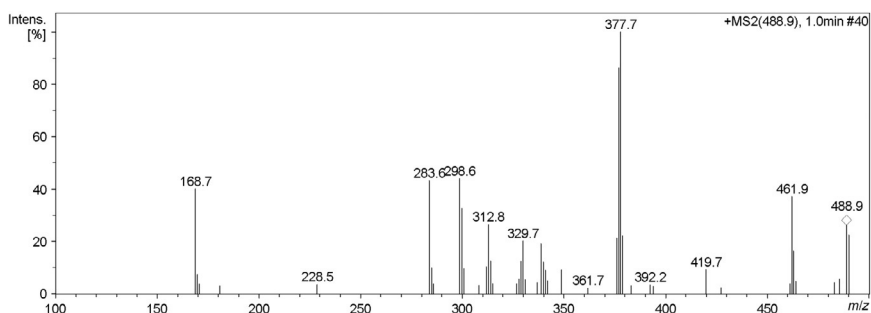


**Figure 9.7** MS/MS spectrum for  $m/z=488.9$  in positive mode.

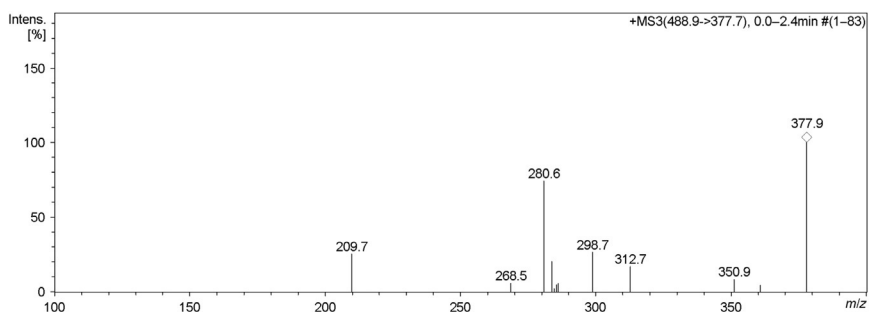
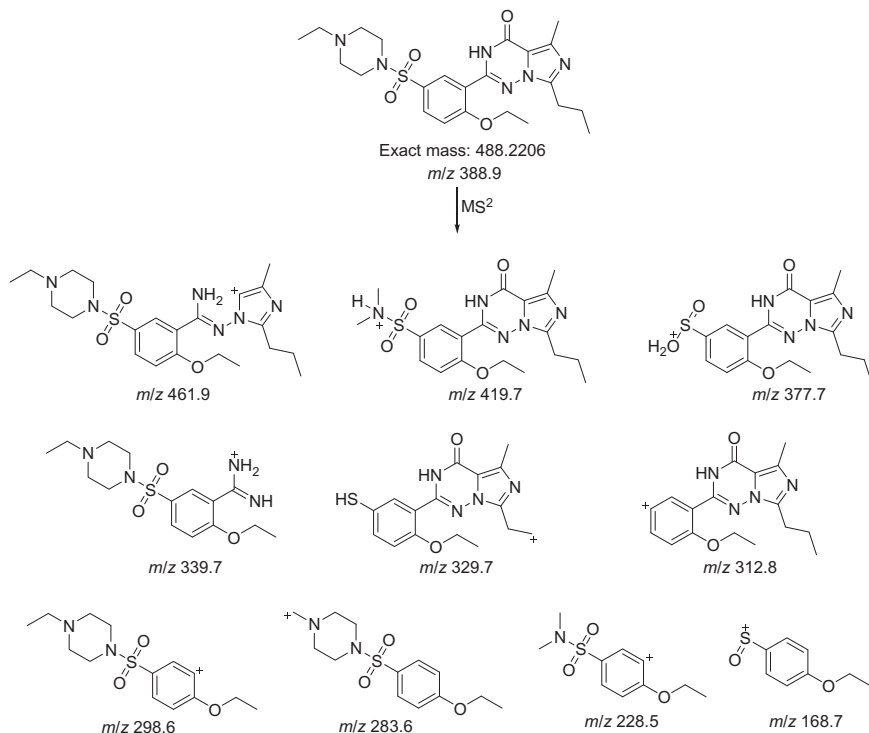


**Figure 9.8** MS/MS/MS spectra for  $m/z=399.9$  in positive mode.

### 3.3.1 Fragmentation pattern of vardenafil dihydrochloride

The MS/MS scan of the molecular ion peak gave fragments at  $m/z$  values of 461.9, 419.7, 377.7, 339.7, 329.7, 312.8, 298.6, 283.6, 228.5, and 168.7 (Figure 9.7; Scheme 9.6).





**Scheme 9.6** MS<sup>2</sup> scan for the vardenafil dihydrochloride at  $m/z$  = 488.9.

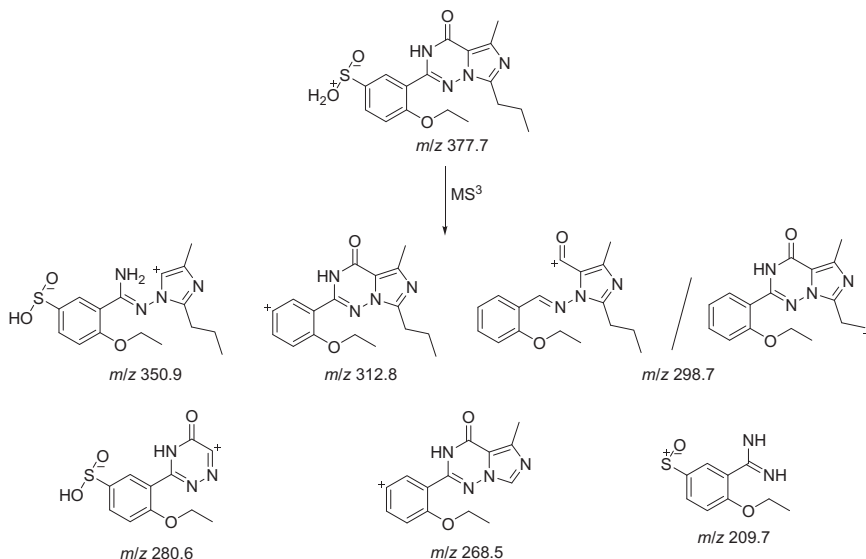
The MS/MS/MS scan of the fragment  $m/z$  377.9 gave number of peaks including  $m/z$  350.9, 312.7, 398.7, 280.6, 268.5, and 209.7. The fragments are shown in [Scheme 9.7](#).



## 4. METHODS OF ANALYSIS

### 4.1. Chromatographic methods

Literature surveys have revealed several chromatographic methods for determination of vardenafil in bulk drug and biological samples published by Kumar *et al.* [30], Subba Rao *et al.* [31], Carlucci *et al.* [32] Zhang *et al.* [33], Gratz *et al.* [34], Zou *et al.* [35], Di *et al.* [36] Bartosova *et al.* [37], Cheng *et al.* [38], Ku *et al.* [39], Lake *et al.* [40], Zhu *et al.* [41], Zhang *et al.* [42], and Man *et al.* [43].



**Scheme 9.7** Possible fragments for the MS/MS/MS scan of vardenafil dihydrochloride.

#### 4.1.1 High-performance liquid chromatography

##### 4.1.1.1 High-performance liquid chromatography/ultraviolet detection

A stability indicating RP-LC method has been developed by Kumar *et al.* [30] for the quantitative determination of vardenafil and its related impurities in both bulk drugs and pharmaceutical dosage forms. Effective chromatographic separation was achieved on a C18 stationary phase with a simple mobile phase combination delivered in a simple gradient program, and quantitation was accomplished by UV detection at 210 nm. The mobile phase consisted of a buffer and acetonitrile delivered at a flow rate 0.25 ml/min. The buffer consisted of 20 mM ammonium bicarbonate, where the pH was adjusted to 5.0 using orthophosphoric acid. In the developed UPLC method, the resolution between vardenafil and its four potential impurities was found to be greater than 2.0. Regression analysis showed a correlation coefficient greater than 0.999 for vardenafil and its four impurities. This method was capable of detecting all four impurities of vardenafil at a level of 0.25  $\mu\text{g/mL}$  with respect to a test concentration of 500  $\mu\text{g/mL}$  for a 2  $\mu\text{L}$  injection volume. The inter- and intraday precision values for all four impurities and for vardenafil were found to be within 2.0%. The method showed good and consistent recoveries for vardenafil in bulk drugs (98.8–100.9%), pharmaceutical dosage forms (100.5–101.5%), and its all

four impurities (99.8–102.5%). The test solutions were found to be stable in acetonitrile for 48 h.

The drug was subjected to stress conditions of hydrolysis, oxidation, photolysis, and thermal degradation. Considerable degradation was found to occur in peroxide hydrolysis. The stress samples were assayed against a qualified reference standard and the mass balance was found close to 99.9%. The developed RP-LC method was validated with respect to linearity, accuracy, precision, and robustness.

Another stability indicating LC method for vardenafil HCl has been developed by Subba Rao *et al.* [31] and Carlucci *et al.* [32] for the quantitative determination of vardenafil HCl in bulk drug and in pharmaceutical dosage forms used to treat ED. The developed method is also applicable for the determination of related substances. Efficient chromatographic separation was achieved on a C18 stationary phase with simple mobile phase combination delivered in a gradient mode, and quantification was carried out using UV detection at a flow rate of 1.0 mL/min. In the developed LC method, the resolution between vardenafil and its four potential impurities was found to be greater than 3.0. Regression analysis showed a correlation coefficient greater than 0.99 for vardenafil and its four impurities. This method was capable of detecting all four impurities of vardenafil at a level of 0.009% with respect to test concentration of 1.0 mg/mL for a 10  $\mu$ L injection volume. The method has shown good and consistent recoveries for vardenafil (98.4–100.6%) and its four impurities (93.5–106.2%). The test solution was found to be stable in the diluent for 48 h. Mass balance was found close to 99.4%.

A simple high-performance liquid chromatographic (HPLC) method with photometric detection was described by Giuseppe Carlucci *et al.* [32] for the determination of vardenafil hydrochloride in human plasma. Chromatographic separation of the analyte and internal standard was achieved on an analytical 250  $\times$  4.6 mm i.d. reversed-phase Kromasil KR 100 C18 (5- $\mu$ m particle size) column using a mobile phase of acetonitrile–potassium dihydrogen phosphate (30:70 v/v). The run time was less than 15 min. Column eluate was monitored at 230 nm. The linearity over the concentration range of 10–1500 ng/mL for vardenafil was obtained and the limit of quantification (LOQ) was 10 ng/mL. This method has been applied to analysis of vardenafil concentrations for application in pharmacokinetic studies.

HPLC coupled with liquid–liquid–liquid microextraction was developed by Zhaohui Zhang *et al.* [33] for the simultaneous determination of

sildenafil and vardenafil in human plasma. The effects of extraction solvent, the volume of organic solvent, drop size of acceptor phase, stirring rate, and extraction time on the enrichment factors of analytes were investigated. The optimized experimental conditions included 300  $\mu$ L toluene as the organic phase, 2  $\mu$ L of 0.2 mol/L HCl as the acceptor phase, a centrifugation speed of 600 r/min, and an extraction time of 40 min. Under these conditions, high enrichment factors were obtained. The linear range of studied analytes ranged from 5  $\mu$ g/L to 1.0 mg/L. The relative standard deviation (RSD) was lower than 5%. The limits of detection were 1  $\mu$ g/L for sildenafil and 0.5  $\mu$ g/L for vardenafil at a signal-to-noise ratio of 3. This method with little solvent consumption may provide high analyte preconcentration and excellent sample clean-up. It was also a sensitive and suitable method for simultaneous determination of the two substances in human plasma.

#### 4.1.1.2 High-performance liquid chromatography with UV detection and electrospray ionization–mass spectrometry method

A liquid chromatography–electrospray ionization–mass spectrometry (LC–ESI–MS) method was developed by Gratz *et al.* [34] to screen for the presence of synthetic PDE-5 inhibitors including sildenafil, tadalafil, and vardenafil. The method was applied to the analysis of dietary supplements and bulk herbal materials. Bulk powders or composites of tablets, capsules, or liquids were prepared, and an extraction of PDE-5 inhibitors was performed using a mixture of acetonitrile and water with sonication. Identification of sildenafil, vardenafil, or tadalafil was accomplished using a single quadrupole mass spectrometer coupled to a liquid chromatograph with an electrospray interface. Positive ion detection in the full scan mode was used while in-source collision-induced dissociation provided several structurally significant fragment ions to aid in the mass spectral identification. Approximately, half of the 40 botanical products analyzed were found to contain undeclared synthetic PDE-5 inhibitors. For products found to contain one of these three compounds by LC–MS, HPLC with UV detection was used for quantitation.

#### 4.1.1.3 High-performance liquid chromatography–diode array detection and liquid chromatography–electrospray ionization–tandem mass spectrometry method

A high-performance liquid chromatography–diode array detection (HPLC–DAD) method and a liquid chromatography–electrospray ionization–tandem mass spectrometry (LC–ESI–MS/MS) method were developed

by Zou *et al.* [35] to screen for the presence of synthetic PDE-5 inhibitors, including sildenafil, vardenafil, tadalafil, homosildenafil, acetildenafil, and hydroxyhomosildenafil. The methods were applied to premarket samples submitted to the Health Sciences Authority of Singapore for testing. One sample was in the form of capsules while six other samples were premixed bulk powder samples for dietary supplements to be repackaged or formulated into the final dosage forms (usually capsules). Identification of PDE-5 inhibitors was achieved by comparing individual peak retention times ( $t_R$ ), UV spectra, and mass spectra with those of reference standards. The seven samples were found to contain at least one of the following compounds: sildenafil, vardenafil, hydroxyhomosildenafil, homosildenafil, and acetildenafil. The five compounds were simultaneously determined by LC-ESI-MS/MS in multiple reactions monitoring (MRM) scan mode. The method has been validated for accuracy, precision, linearity, and sensitivity.

#### 4.1.1.4 High-performance liquid chromatography:

##### Chemiluminescence method

Di *et al.* [36] developed a flow method of HPLC separation and chemiluminescence (CL) detection for sensitive vardenafil analysis in dietary supplements. The vardenafil separation was achieved on a C18 column at 30 °C using ethanol-H<sub>3</sub>PO<sub>4</sub> and ethylenediaminetetraacetic acid disodium salt (Na<sub>2</sub>EDTA) aqueous solution (25:75, v/v%) as a mobile phase. The followed continuous CL detection was conducted based on the strong CL enhancement by the presence of vardenafil to luminol-K<sub>3</sub>Fe(CN)<sub>6</sub> reaction in alkaline medium. At the flow rate of 0.8 mL/min, the vardenafil  $t_R$  was 6.4 min. Factors that affected the HPLC resolution and CL detection were studied and optimized. The calibration curve obtained for vardenafil standard was linear in concentration range of  $8.0 \times 10^{-7}$  to  $\sim 1.0 \times 10^{-4}$  mol/L. The RSDs of intra- and interday precision were less than 3.5%. The proposed method was applied to the vardenafil determination in oral liquid, wine, and capsule samples.

#### 4.1.1.5 High-performance liquid chromatographic method with amperometric detection

An HPLC method with electrochemical detection employing a boron-doped diamond electrode for the determination of sildenafil, vardenafil, and their main metabolites, *N*-desmethyl sildenafil and *N*-desethyl vardenafil in human plasma was described by Bartošová *et al.* [37]. The assay

involved drug extraction by *tert*-butyl methyl ether and isocratic reversed-phase liquid chromatography with amperometric detection. Complete separation of all analytes was achieved within 12 min. The mobile phase consisted of 20 mM sodium dihydrogen phosphate with 40 mM sodium perchlorate/acetonitrile (70:30, v/v), pH 3.5. The electrode working potential was +1520 mV (vs. Pd/H<sub>2</sub>). Calibration curves were linear over the concentration range of 10–400 ng/mL. Phloretin was used as an internal standard. The limit of detection (LOD) and LOQ for the studied analytes were within the range of 2–4 ng/mL and 7.0–13.4 ng/mL, respectively. The developed method was applied to human plasma samples spiked with analytes at therapeutic concentrations. The study confirms the method's suitability for both pharmacokinetic studies and therapeutic monitoring.

#### 4.1.1.5 HPLC/fluorescence detection

An HPLC method with fluorescence detection was developed and validated by Cheng *et al.* [38] for the determination of vardenafil in small volumes of rat plasma and bile. The absorbance and fluorescence characteristics of vardenafil were studied and factors that affect the HPLC resolution and fluorescence intensity were examined and optimized. Vardenafil and the internal standard cisapride were extracted using acetonitrile. The separation was achieved on a C18 column at 35 °C using acetonitrile–50 mM ammonium acetate aqueous solution (pH 6.8) (40:60) as mobile phase. At a flow rate of 1 mL/min, the total run time was 18 min. Fluorescence was measured with excitation at 280 nm, and the emission was monitored at 470 nm. The calibration curves were linear from 10 to 1000 ng/mL and 0.2–100 µg/mL for plasma and bile samples, respectively. The intra- and interday imprecision did not exceed 10.8%, and the accuracy was within 9.6% deviation of the nominal concentration. The method was used successfully to investigate the disposition and biliary excretion of vardenafil in rats.

#### 4.1.1.6 High-performance liquid chromatographic with tandem mass spectrometry methods

LC–MS/MS has been used to identify vardenafil and the other PDE-5 inhibitors sildenafil and tadalafil in dietary supplements and bulk herbal materials. Gratz *et al.* [34], Zou *et al.* [35], Zhu *et al.* [41], and Ku *et al.* [39] published validated LC–MS/MS methods for the analysis of vardenafil and its metabolite, *N*-desethylvardenafil, in human plasma. A lower limit of quantitation of 0.5 ng/mL from 0.25 mL of plasma was reported, utilizing sildenafil as the internal standard. However, the biological

activity of the *N*-desethyl metabolite, as a percentage of the total pharmacological activity of vardenafil, was relatively low (estimated at approximately 7%).

An HPLC–MS/MS assay has been developed by Lake *et al.* [40] for the quantitative analysis of vardenafil in human plasma. Vardenafil and the internal standard, alprazolam, were extracted from 0.2 mL aliquots of alkalized plasma by a single solvent extraction into hexane:dichloromethane. Reversed-phase chromatographic separation was affected by gradient elution with mobile phases consisting of 10 mM ammonium formate (pH 7.0) (solvent A) and methanol (100%, solvent B), delivered at a flow rate of 0.4 mL/min. The analytes were detected by an electrospray ion source on a 4000 QTrap triple quadrupole mass spectrometer operating in positive ionization mode. The mass transitions were  $m/z$  489.3  $\rightarrow$  312.2 for vardenafil and  $m/z$  309.2  $\rightarrow$  281.0 for alprazolam. The assay was linear over the concentration range of 0.2–100 ng/mL, with correlation coefficients  $\geq 0.995$ . The intra- and interday precision was less than 5.4% in terms of relative standard deviation, and the accuracy was within 12.7% in terms of relative error. The lower limit of quantitation was found to be 0.2 ng/mL. The high sensitivity and acceptable performance of the assay allowed its application to the analysis of plasma samples obtained following the oral administration of vardenafil to healthy male volunteers in a pharmacokinetic study.

An HPLC method coupled with UV detection and electrospray ionization–mass spectrometry was developed by Zhu *et al.* [41] for simultaneous determination of banned additives (i.e., sildenafil, vardenafil, and tadalafil) in dietary supplements for male sexual potency. The separation was achieved on a C18 column with acetonitrile and aqueous solution (20 mmol ammonium acetate, 0.2% formic acid) as a mobile phase at a flow rate of 1 mL/min with a linear gradient program. UV detection was at 292 nm. Identification of drugs was accomplished using ESI–MS. Good linearity between response (peak area) and concentration was found over a concentration range of 0.8–80  $\mu\text{g/mL}$  for sildenafil, 2.25–225  $\mu\text{g/mL}$  for vardenafil, and 1.1–110  $\mu\text{g/mL}$  for tadalafil, with regression coefficients better than 0.999. The recovery of the method ranged from 93.3% to 106.1%, and the relative standard deviation varied from 2.0% to 5.6% ( $n=6$ ). The method has been successfully applied to the analysis of practical samples of natural dietary supplements.

A simple and sensitive HPLC–MS/MS method was developed by Y. Zhang *et al.* [42] for determination of illegal adulterants (yohimbine, sildenafil, vardenafil, and tadalafil) in dietary supplements. The separation was

achieved on a C18 column with the mobile phase consisting of acetonitrile and 0.1% acetic acid aqueous solution with a gradient elution at a flow rate of 0.5 mL/min. The analytes were quantified and identified by two characteristic transitions using the MRM mode. The recoveries of the analytes ranged from 77.5% to 109.3% with the RSD less than 8.1% ( $n = 6$ ). The method has been successfully applied to screen illegal adulterations of natural dietary supplements.

#### **4.1.2 Gas chromatograph–mass spectrometer assay**

Some dietary supplements, herbal preparations, and food products which have been claimed to enhance male sexual function have been found to be adulterated with PDE-5 inhibitors. A gas chromatograph–mass spectrometer (GC–MS) assay was developed by Man *et al.* [43] for identification of the drugs. In addition to good and short chromatographic separation that can be achieved within 6 min by using a short 10 m capillary column, the method does not require prior sample clean-up before GC–MS analysis, thus making this assay a cost-saving and rapid method. Furthermore, the assay is specific as the identification of sildenafil, tadalafil, and vardenafil was performed by detection of molecular ions;  $m/z$  474, 389, and 488 [corrected], respectively, and several other characteristic ions resulted from the mass fragmentation of individual molecules. Using currently developed assay, sildenafil and its analogues were successfully identified in food and herbal matrices.

#### **4.2. Voltammetric method**

The voltammetric behavior of vardenafil was studied by Uslu *et al.* [44] on glassy carbon electrode using cyclic, differential pulse, and Osteryoung square-wave voltammetric techniques. Vardenafil exhibited irreversible anodic waves over the pH range of 1.00–12.00 in different supporting electrolytes. The current–concentration plot was rectilinear over the range from  $4 \times 10^{-7}$  to  $2 \times 10^{-5}$  M with a correlation coefficient of 0.999. The wave was characterized as being irreversible and diffusion controlled. The developed procedure was successfully applied to the determination of vardenafil in tablets and in spiked human serum. Furthermore, results obtained by the proposed method have been compared with an HPLC method.

#### **4.3. Immunoassay methods**

1. To screen vardenafil and its analogues in herbal matrix rapidly, an immunoassay based on a group-specific monoclonal antibody (McAb) was developed by Carlucci *et al.* [32] and Guo *et al.* [45].



2. Glutaraldehyde was used to link vardenafil to immunogen and coating-antigen, respectively. Through the assessment of the structural specificity of eight anti-vardenafil McAbs, the McAb 4B9 was characterized as being specific to the common structure of vardenafil and its analogues. An indirect competitive enzyme-linked immunosorbent assay (ic-ELISA) was established based on this McAb, the LOD of vardenafil was 5.0 ng/mL, the calibration curve was linear from 5.0 to 40 ng/mL ( $R=0.952$ ) with an  $IC_{50}$  value of 18.2 ng/mL. In the extracts of 20 Chinese traditional drugs, the detection capability (CC $\beta$ ) of vardenafil was 0.08 mg/g, the recoveries were 76–116%, and the coefficients of variation were 9.7–16.2%. The ic-ELISA was in a good agreement with LC–UV for detection of herbal products containing vardenafil and its analogues. The method was a suitable tool for screening vardenafil and its analogues as illegal additives in herbal products.



## 5. PHARMACOLOGY OF VARDENAFIL

### 5.1. Pharmacodynamics

#### 5.1.1 An overview

Vardenafil (VAR) is a safe and well-tolerated treatment of men with ED. It is a highly potent and selective inhibitor of PDE-5, the most prevalent phosphodiesterase in the human penile corpus cavernosum, and thus increases intracellular cGMP levels in the cavernosum tissue of the penis [7]. It was the first second-generation PDE-5 inhibitor that received marketing approval in the United States. Unlike the other PDE-5 inhibitors, sildenafil and tadalafil, VAR was developed from the outset specifically for use as an erectogenic agent [46]. It is 5–10 times more potent than sildenafil, the classic PDE-5 inhibitor [2]. VAR has been shown to be efficacious in the treatment of ED in the doses of 10 and 20 mg taken on demand, prior to intercourse [47]. For most patients, the recommended starting dose is 10 mg, which according to US labeling information should be taken approximately 60 min prior to sexual activity [46]. Adverse effects associated with VAR are not severe, mostly dose dependent and tend to decrease with time. These include headache, flushing, dyspepsia, and rhinitis [8,48].

#### 5.1.2 Mechanism of action

VAR increases penile rigidity and tumescence via a mechanism of action similar to that of the other PDE-5 inhibitors, sildenafil and tadalafil. It facilitates penile erection by the inhibition of cGMP-specific PDE-5, the most

active PDE involved in the termination of cGMP signaling in the penile corpus cavernosum, the erectile tissue in the penis. This, in turn, potentiates endogenous increases in cGMP levels in the corpus cavernosum and the vessels supplying it, thus increasing dilatation of the corporeal sinusoids allowing more blood flow, which induces an erection. Interestingly, this occurs only in the presence of nitric oxide release with sexual arousal. Sexual stimulation causes the release of nitric oxide (NO) from neurons and endothelial cells in the corpus cavernosum. NO, in turn, activates the enzyme guanylyl cyclase, with the resultant conversion of guanosine triphosphate to cGMP. This results in activation of cGMP-dependent protein kinase, phosphorylation of several proteins and reduction of intracellular calcium levels, and a consequent smooth muscle relaxation and an increased arterial blood flow leading to enlargement of the corpus cavernosum. Because of the increased tumescence, veins are compressed between the corpus cavernosum and the tunica albuginea, leading to an erection [8,49–53]. Notably, VAR has no effect on NO release and is, thus, ineffective in causing erection in the absence of sexual arousal [54].

### **5.1.3 Efficacy and safety of VAR for the treatment of erectile dysfunction**

#### **5.1.3.1 Efficacy of VAR for the treatment of erectile dysfunction**

VAR has been reported to be highly effective in the treatment of ED in the broad population at doses of 10 and 20 mg taken in an on-demand fashion [55]. Efficacy and tolerability of VAR have been frequently reported. Rosen *et al.* [56] have reported that VAR was clearly efficacious in treating patients with mixed ED etiologies, achieving a high response rate with significant improvement in the scores measuring sexual function and satisfaction. The same study has also shown that VAR was safe and well tolerated with few patients reporting adverse events. These data have been supported by the recent findings of Tan *et al.* [57], Rosen *et al.* [58], and Porst *et al.* [59] who demonstrated that VAR was a highly effective and very well-tolerated treatment for patients with ED. Several clinical studies have shown that VAR is effective in men with ED originating from various underlying organic causes and severities, including traditionally difficult-to-treat men with diabetes or a history of radical prostatectomy [60–62]. Further, Porst *et al.* [60] have confirmed the efficacy of VAR in ED regardless of organic, psychogenic, or mixed causes, the baseline severity of the condition and patient age.

With regard to potency, VAR has been shown to be the most potent and specific of the commercially available PDE-5 inhibitors [54]. Potency can be

determined by measuring the concentration of a particular PDE-5 inhibitor *in vitro* that inhibits PDE-5 activity by 50% and is known as IC<sub>50</sub>. Assuming all other factors are equal, the higher the potency of a PDE-5 inhibitor for PDE-5, the lower the expected dose of the inhibitor that will be needed [63]. *In vitro* studies have demonstrated that IC<sub>50</sub> of VAR is 0.7 nM, which is much lower than that of sildenafil (3.9 nM) and tadalafil (5 nM) [64]. In addition, Blount *et al.* [65] have reported that VAR binds more rapidly to PDE-5 and has a slower dissociation from the enzyme than sildenafil and tadalafil, and that the VAR–PDE-5 complex is more stable than the complex formed between PDE-5 and the other PDE-5 inhibitors. This is confirmed by the reported rapid onset of action of VAR (as early as 10 min after dosing) [5] and the extended duration of action (8–12 h) [66].

#### 5.1.3.2 Safety of VAR in the treatment of erectile dysfunction

VAR is generally well tolerated, with a favorable safety profile and few treatment-related side effects. Most side effects are related to the vasodilatory properties of VAR. The accompanying headache, flushing, rhinitis, and indigestion are usually mild and transient in nature [3,4]. Stief *et al.* [67] have reported that the frequency of such side effects was numerically greater in patients treated with 20 mg VAR compared with those receiving 10 mg VAR. Similar to other PDE-5 inhibitors, drug-related side effects have been reported to be greatest during the first weeks of therapy and to rapidly decrease during long-term use of VAR with no cardiovascular safety concerns [67]. Stief *et al.* also have shown that few patients reported drug-related abnormal vision. Importantly, in this 2-year study, assessment of vital signs and ECG recordings revealed no cardiovascular safety concerns with VAR. In a prospective clinical trial, VAR significantly improved erectile function in patients with ED and arterial hypertension treated with multiple antihypertensives and was well tolerated and did not significantly affect blood pressure [68].

In a double-blind, crossover study involving men with reproducible stable exertional angina due to ischemic coronary artery disease (CAD), VAR 10 mg had no effect on ECG, exercise tolerance, or time to onset of angina, while increasing the time to ischemic threshold compared with placebo [69]. These findings supported the conclusion that in men with CAD, VAR did not exacerbate myocardial ischemia in response to exercise at a level similar to that of sexual intercourse. In addition, the observed increase in the time to ischemic threshold on exercise tolerance testing in the previous study might suggest that VAR has a beneficial effect in terms of cardiovascular risk.

Nitrate preparations are commonly prescribed for the prevention and treatment of angina pectoris, and the actions of these drugs are terminated by cGMP hydrolysis in blood vessels [64]. Thus, PDE-5 inhibitors, including VAR, could increase the effects of the nitrates, and this may result in severe vasodilatation and hypotension. In fact, the patient information sheet for VAR states that in 18 healthy subjects pretreated with VAR 20 mg, there was an additional reduction in blood pressure and increase in heart rate with nitroglycerin administration, and it is recommended that nitrate preparations not be taken until at least 24 h after VAR, due to significant, potentially life-threatening hypotension [64,70,71]. Due to its effect on Q-T interval, VAR is also not recommended in patients taking type 1A (such as quinidine and procainamide) or type 3 antiarrhythmics (such as amiodarone and sotalol) or in patients with congenitally prolonged Q-T syndrome [70,72]. In addition,  $\alpha$ -adrenergic receptor blockers, such as doxazosin, should only be combined with PDE-5 inhibitors, including VAR, with special caution and close monitoring of blood pressure [71].

## 5.2. Pharmacokinetics

### 5.2.1 An overview

In addition to pharmacodynamic properties discussed above, pharmacokinetic properties of VAR (ingestion/food interaction, movement in the circulation, tissue uptake, elimination) have great impact on efficacy. In this context, Klotz *et al.* [73] have studied the pharmacokinetic and pharmacodynamic properties of VAR in 21 ED patients. The results showed that single doses of 10 and 20 mg VAR led to a rapid rise in the plasma concentrations of VAR, with a  $t_{\max}$  (the time required to achieve maximum plasma concentration) of 0.9 and 0.7 h and a mean  $C_{\max}$  (the maximum plasma concentration) of 9.1 and 20.9 ng/mL, respectively. In the post-absorptive phase, the concentrations declined with an average half-life of 4.2 and 3.9 h, respectively. VAR is extensively metabolized by CYP3A4 and to a small extent by CYP3A5 and CYP2C isoforms into more than 14 metabolites. The major metabolite, *N*-desethyl VAR (M1), is pharmacologically active. It has 28% of VAR's potency for PDE-5 inhibition and its contribution to the overall VAR activity is 7%. The elimination half-life of VAR and its major metabolite M1 is about 4–5 h and independent of the dose. VAR is primarily excreted as metabolites in the feces and to a small extent in urine. Only 1% of the administered VAR dose is excreted into urine in an unchanged form [8,46].

### 5.2.2 Comparison of VAR with other PDE-5 inhibitors from the pharmacokinetic perspective

Even though VAR shares the same mechanism of action and selectivity for PDE-5 with sildenafil and tadalafil, there are noted pharmacokinetic disparities that largely affect the efficacy profiles of the three drugs [74]. The three PDE-5 inhibitors are rapidly absorbed after oral administration and have a rapid onset of action. However, the absolute bioavailability for VAR and sildenafil is limited to only 15% and 40%, respectively, because of extensive presystemic metabolism in the gut wall and liver via CYP3A4 and/or CYP3A5 pathways. The absolute bioavailability of tadalafil has not been reported to date [64,72]. The half-life of tadalafil is 17.5 h, compared to 3.9 h for VAR, and 3.8 h for sildenafil [64]. Consequently, the duration of action of VAR and sildenafil is found to be about 8–12 h [6,75], whereas that of tadalafil is about 36 h [76]. The  $C_{\max}$  of VAR (20.9 ng/mL) is significantly lower than that for sildenafil (450 ng/mL) and tadalafil (378 ng/mL), which might be expected based on its lower bioavailability [55]. VAR and sildenafil have broadly similar  $t_{\max}$  of about 0.8 h which predicts a similar time of onset of action, whereas tadalafil has a  $t_{\max}$  of about 2 h [77]. A high-fat meal has been found to have no significant effect on the rate and extent of tadalafil absorption, but delayed the absorption of VAR and sildenafil, possibly affecting the onset of action [72,78]. Consequently, sildenafil and VAR package inserts state that efficacy may be delayed following a high-fat meal, independently from the type of formulation, while tadalafil can be administered independently of food intake [72].

## ACKNOWLEDGMENT

This work was supported by a grant from the National Plan of Science, Technology, and Innovation (Grant No. 10-MED1188-02) King Saud University, Riyadh, Saudi Arabia.

## REFERENCES

- [1] G.M. Keating, L.J. Scott, Vardenafil: a review of its use in erectile dysfunction, *Drugs* 63 (2003) 2673–2703.
- [2] I. Saenz de Tejada, J. Angulo, P. Cuevas, A. Fernandez, I. Moncada, A. Allona, E. Lledo, H.G. Korschen, U. Niewohner, H. Haning, E. Pages, E. Bischoff, The phosphodiesterase inhibitory selectivity and the in vitro and in vivo potency of the new PDE5 inhibitor vardenafil, *Int. J. Impot. Res.* 13 (2001) 282–290.
- [3] E. Chung, G.B. Broc, A state of art review on vardenafil in men with erectile dysfunction and associated underlying diseases, *Expert Opin. Pharmacother.* 12 (2001) 1341–1348.
- [4] J.M. Young, Vardenafil, *Expert Opin. Invest. Drugs* 11 (2002) 1487–1496.
- [5] F. Montorsi, H. Padma-Nathan, J. Buvat, H. Schwaibold, M. Beneke, E. Ulbrich, T.J. Bandel, H. Porst, Earliest time to onset of action leading to successful intercourse

- with vardenafil determined in an at-home setting: a randomized, double-blind, placebo-controlled trial, *J. Sex. Med.* 1 (2004) 168–178.
- [6] L. Valiquette, F. Montorsi, W.J. Hellstrom, F. Giuliano, M. Homering, T. Taylor, I. Eardley, Penetration and maintenance of erection with vardenafil: a time-from-dosing analysis, *Can. J. Urol.* 12 (2005) 2687–2698, discussion 2699.
- [7] U. Gresser, C.H. Gleiter, Erectile dysfunction: comparison of efficacy and side effects of the PDE-5 inhibitors sildenafil, vardenafil and tadalafil—review of the literature, *Eur. J. Med. Res.* 7 (2002) 435–446.
- [8] D. Ormrod, S.E. Easthope, D.P. Figgitt, Vardenafil, *Drugs Aging* 19 (2002) 217–227, discussion 228–219.
- [9] S. Sweetman, Martindale: The Complete Drug Reference, 36th ed., Pharmaceutical Press, London, 2009.
- [10] <http://www.chemspider.com/Chemical-Structure.21513317.html?rid=269f812c-2bfe-4000-9f5a-0772600f39cb>.
- [11] <http://www.chemspider.com/Chemical-Structure.129930.html>.
- [12] <http://www.drugbank.ca/drugs/DB00862>.
- [13] J.M. O'Neil, Merck & Co. (Eds.), The Merck Index, an Encyclopedia of Chemicals, Drugs, and Biologicals, 14th ed., Merck & Co., Inc., Whitehouse Station, NJ, USA, 2006, p. 1706.
- [14] E. Sajja; R.R. Koppera; S. Revu, V.R. Vajrala, V.R. Kanumathi, Polymorphic forms of Vardenafil, US 0197535 A1, 2007.
- [15] Assessment Report, European Medicines Agency, 2010. [http://www.ema.europa.eu/docs/en\\_GB/document\\_library/EPAR\\_-\\_Assessment\\_Report\\_-\\_Variation/human/000475/WC500097073.pdf](http://www.ema.europa.eu/docs/en_GB/document_library/EPAR_-_Assessment_Report_-_Variation/human/000475/WC500097073.pdf).
- [16] <http://pubchem.ncbi.nlm.nih.gov/summary/summary.cgi?cid=110634>.
- [17] U. Niewohner, M. Es-Sayed, H. Haning, T. Schenke, K.-H. Schlemmer, J. Keldenich, E. Bischoff, E. Perzborn, K. Dembowski, P. Serno, M. Nowakowski, 2-phenyl substituted imidazotriazinones as phosphodiesterase inhibitors, US 6362178, 2002.
- [18] Y. Mao, G. Tian, Z. Liu, J. Shen, J. Shen, An improved synthetic route for preparative process of vardenafil, *Org. Process Res. Dev.* 13 (2009) 1206–1208.
- [19] M. Nowakowski, R. Gehring, W. Heilman, K.H. Wahl, Method for producing sulfonamide-substituted imidazotriazinones, *Chem. Abstr.* 137 (2002) 47233. PCT Int. Appl. WO 200250076, 2002.
- [20] H. Haning, U. Niewohner, T. Schenke, M. Es-Sayed, G. Schmidt, T. Lampe, E. Bischoff, Imidazo[5,1-f]triazin-4(3H)-ones, a new class of potent PDE 5 inhibitors, *Bioorg. Med. Chem. Lett.* 12 (2002) 865–868.
- [21] L.A. Sorbera, L. Martín, X. Rabasseda, J. Castañer, Vardenafil. Treatment of erectile dysfunction, *Drugs Fut.* 26 (2001) 141–144.
- [22] M. Nowakowski, R. Gehring, W. Heilmann, K.-H. Wahl, WO 02/50076, 2006.
- [23] B.C. Ross, D. Middlemiss, D.I.C. Scopes, T.I.M. Jack, K.S. Cardwell, M.D. Dowle, D.B. Judd, European Patent EP0514216A1-Antihypotensive benzofuran derivatives with N-linked 1H-imidazolyl-methyl-5-carboxamide substituents, 1992.
- [24] A. Heim-Riether, D.P. Rotella, Methods for synthesizing imidazotriazinones, US Patent Appl. Publ. (2006) US 20060264624 A1.
- [25] D.B. Judd, M.D. Dowle, D. Middlemiss, D.I. Scopes, B.C. Ross, T.I. Jack, M. Pass, E. Tranquillini, J.E. Hobson, T.A. Panchal, et al., Bromobenzofuran-based non-peptide antagonists of angiotensin II: GR138950, a potent antihypertensive agent with high oral bioavailability, *J. Med. Chem.* 37 (1994) 3108–3120.
- [26] A. Heim-Riether, J. Healy, A novel method for the synthesis of imidazo[5,1-f][1,2,4] triazin-4(3H)-ones, *J. Org. Chem.* 70 (2005) 7331–7337.
- [27] D. Seidel, P. Brehmer, Y. Schoof, U. Weinberg, M. Nowakowski, Synthesis of [14C]-labelled vardenafil hydrochloride and metabolites, *J. Labelled Compd. Radiopharm.* 46 (2003) 1019–1032.

- [28] U. Pleiss, Synthesis of [3H] vardenafil, Levitra<sup>®</sup>, using a new labeling technique, *Labelled Compd. Radiopharm.* 46 (2003) 1241–1247.
- [29] S. Singh, B. Prasad, A.A. Savaliya, R.P. Shah, V.M. Gohil, A. Kaur, Strategies for characterizing sildenafil, vardenafil, tadalafil and their analogues in herbal dietary supplements, and detecting counterfeit products containing these drugs, *Trends Anal. Chem.* 28 (2009) 13–28.
- [30] K.K. Kumar, C.K. Rao, Y.R.K. Reddy, K. Mukkanti, A validated rapid stability-indicating method for the determination of related substances in vardenafil hydrochloride by ultra-performance liquid chromatography, *Am. J. Anal. Chem.* 3 (2012) 59–66.
- [31] D.V. Subba Rao, K.V. Surendranath, P. Radhakrishnanand, M.V. Suryanarayana, P. Raghuram, A stability indicating LC method for vardenafil HCl, *Chromatographia* 68 (2008) 829–835.
- [32] G. Carlucci, P. Palumbo, P. Iuliani, G. Palumbo, Development of a method for the determination of vardenafil in human plasma by high performance liquid chromatography with UV detection, *Biomed. Chromatogr.* 23 (2009) 759–763.
- [33] Z. Zhang, S. Kang, M. Xu, M. Ma, B. Chen, S. Yao, Determination of sildenafil and vardenafil in human plasma by high performance liquid chromatography coupled with liquid-liquid-liquid microextraction *Se Pu* 23 (2005) 358–361.
- [34] S.R. Gratz, C.L. Flurer, K.A. Wolnik, Analysis of undeclared synthetic phosphodiesterase-5 inhibitors in dietary supplements and herbal matrices by LC-ESI-MS and LC-UV, *J. Pharm. Biomed. Anal.* 36 (2004) 525–533.
- [35] P. Zou, S.S. Oh, P. Hou, M.Y. Low, H.L. Koh, Simultaneous determination of synthetic phosphodiesterase-5 inhibitors found in a dietary supplement and pre-mixed bulk powders for dietary supplements using high-performance liquid chromatography with diode array detection and liquid chromatography-electrospray ionization tandem mass spectrometry, *J. Chromatogr. A* 1104 (2006) 113–122.
- [36] Y. Di, M. Zhao, Y. Nie, F. Wang, J. Lv, A high-performance liquid chromatography: chemiluminescence method for potential determination of vardenafil in dietary supplement, *J. Autom. Methods Manag. Chem.* 2011 (2011) 982186.
- [37] Z. Bartosova, D. Jirovsky, A. Horna, High-performance liquid chromatographic method with amperometric detection employing boron-doped diamond electrode for the determination of sildenafil, vardenafil and their main metabolites in plasma, *J. Chromatogr. A* 1218 (2011) 7996–8001.
- [38] C.L. Cheng, G.J. Kang, C.H. Chou, Development and validation of a high-performance liquid chromatographic method using fluorescence detection for the determination of vardenafil in small volumes of rat plasma and bile, *J. Chromatogr. A* 1154 (2007) 222–229.
- [39] H.Y. Ku, J.H. Shon, K.H. Liu, J.G. Shin, S.K. Bae, Liquid chromatography/tandem mass spectrometry method for the simultaneous determination of vardenafil and its major metabolite, N-desethylvaridenafil, in human plasma: application to a pharmacokinetic study, *J. Chromatogr. B Analyt. Technol. Biomed. Life Sci.* 877 (2009) 95–100.
- [40] S.T. Lake, P.M. Altman, J. Vaisman, R.S. Addison, Validated LC-MS/MS assay for the quantitative determination of vardenafil in human plasma and its application to a pharmacokinetic study, *Biomed. Chromatogr.* 24 (2010) 846–851.
- [41] X. Zhu, S. Xiao, B. Chen, F. Zhang, S. Yao, Z. Wan, D. Yang, H. Han, Simultaneous determination of sildenafil, vardenafil and tadalafil as forbidden components in natural dietary supplements for male sexual potency by high-performance liquid chromatography-electrospray ionization mass spectrometry, *J. Chromatogr. A* 1066 (2005) 89–95.
- [42] Y. Zhang, Z. Huang, L. Ding, H. Yan, M. Wang, S. Zhu, Simultaneous determination of yohimbine, sildenafil, vardenafil and tadalafil in dietary supplements using

- high-performance liquid chromatography-tandem mass spectrometry, *J. Sep. Sci.* 33 (2010) 2109–2114.
- [43] C.N. Man, N.M. Nor, R. Lajis, G.L. Harn, Identification of sildenafil, tadalafil and vardenafil by gas chromatography-mass spectrometry on short capillary column, *J. Chromatogr. A* 1216 (2009) 8426–8430.
- [44] B. Uslua, B. Dogana, S.A. Özkana, H.Y. Aboul-Enein, Electrochemical behavior of vardenafil on glassy carbon electrode: determination in tablets and human serum, *Anal. Chim. Acta* 552 (2005) 127–134.
- [45] J.B. Guo, Y. Xu, Z.B. Huang, Q.H. He, S.W. Liu, Development of an immunoassay for rapid screening of vardenafil and its potential analogues in herbal products based on a group specific monoclonal antibody, *Anal. Chim. Acta* 658 (2010) 197–203.
- [46] M. Gupta, A. Kovar, B. Meibohm, The clinical pharmacokinetics of phosphodiesterase-5 inhibitors for erectile dysfunction, *J. Clin. Pharmacol.* 45 (2005) 987–1003.
- [47] S. Markou, P. Perimenis, K. Gyftopoulos, A. Athanasopoulos, G. Barbalias, Vardenafil (Levitra) for erectile dysfunction: a systematic review and meta-analysis of clinical trial reports, *Int. J. Impot. Res.* 16 (2004) 470–478.
- [48] J. Pryor, Vardenafil: update on clinical experience, *Int. J. Impot. Res.* 14 (Suppl. 1) (2002) S65–S69.
- [49] K.E. Andersson, G. Wagner, Physiology of penile erection, *Physiol. Rev.* 75 (1995) 191–236.
- [50] J.D. Corbin, Mechanisms of action of PDE5 inhibition in erectile dysfunction, *Int. J. Impot. Res.* 16 (Suppl. 1) (2004) S4–S7.
- [51] C.S. Lin, G. Lin, T.F. Lue, Cyclic nucleotide signaling in cavernous smooth muscle, *J. Sex. Med.* 2 (2005) 478–491.
- [52] N.N. Kim, Y.H. Huang, I. Goldstein, E. Bischoff, A.M. Traish, Inhibition of cyclic GMP hydrolysis in human corpus cavernosum smooth muscle cells by vardenafil, a novel, selective phosphodiesterase type 5 inhibitor, *Life Sci.* 69 (2001) 2249–2256.
- [53] R.C. Rosen, K.E. McKenna, PDE-5 inhibition and sexual response: pharmacological mechanisms and clinical outcomes, *Annu. Rev. Sex Res.* 13 (2002) 36–88.
- [54] K.R. Rice, R.C. Dean, Vardenafil: efficacy, tolerability and future directions, *Expert Opin. Drug Metab. Toxicol.* 5 (2009) 553–562.
- [55] I. Eardley, C. Donatucci, J. Corbin, A. El-Meliegy, K. Hatzimouratidis, K. McVary, R. Munarriz, S.W. Lee, Pharmacotherapy for erectile dysfunction, *J. Sex. Med.* 7 (2010) 524–540.
- [56] H. Porst, R. Rosen, H. Padma-Nathan, I. Goldstein, F. Giuliano, E. Ulbrich, T. Bandel, The efficacy and tolerability of vardenafil, a new, oral, selective phosphodiesterase type 5 inhibitor, in patients with erectile dysfunction: the first at-home clinical trial, *Int. J. Impot. Res.* 13 (2001) 192–199.
- [57] H.M. Tan, C.M. Chin, C.B. Chua, E. Gatchalian, A. Kongkanand, C.L. Moh, F.C. Ng, K. Ratana-Olarn, D. Serrano, A. Taher, I. Tambi, A. Tantiwong, M.W. Chen, W.C. Yip, Efficacy and tolerability of vardenafil in Asian men with erectile dysfunction, *Asian J. Androl.* 10 (2008) 495–502.
- [58] R. Rosen, R. Shabsigh, M. Berber, P. Assalian, M. Menza, L. Rodriguez-Vela, R. Porto, K. Bangerter, M. Seger, F. Montorsi, Efficacy and tolerability of vardenafil in men with mild depression and erectile dysfunction: the depression-related improvement with vardenafil for erectile response study, *Am. J. Psychiatry* 163 (2006) 79–87.
- [59] H. Porst, G. Lungimayr, Efficacy and tolerability of vardenafil within the time window of 6 hours after administration and beyond. Results of a clinical study carried out in 233 urological offices, *MMW Fortschr. Med.* 147 (Suppl. 1) (2005) 27–32.
- [60] H. Porst, J.M. Young, A.C. Schmidt, J. Buvat, Efficacy and tolerability of vardenafil for treatment of erectile dysfunction in patient subgroups, *Urology* 62 (2003) 519–523, discussion 523–514.



- [61] I. Goldstein, J.M. Young, J. Fischer, K. Bangerter, T. Segerson, T. Taylor, Vardenafil, a new phosphodiesterase type 5 inhibitor, in the treatment of erectile dysfunction in men with diabetes: a multicenter double-blind placebo-controlled fixed-dose study, *Diabetes Care* 26 (2003) 777–783.
- [62] G. Brock, A. Nehra, L.I. Lipshultz, G.S. Karlin, M. Gleave, M. Seger, H. Padma-Nathan, Safety and efficacy of vardenafil for the treatment of men with erectile dysfunction after radical retropubic prostatectomy, *J. Urol.* 170 (2003) 1278–1283.
- [63] J.D. Corbin, S.H. Francis, Pharmacology of phosphodiesterase-5 inhibitors, *Int. J. Clin. Pract.* 56 (2002) 453–459.
- [64] S. Doggrel, Do vardenafil and tadalafil have advantages over sildenafil in the treatment of erectile dysfunction? *Int. J. Impot. Res.* 19 (2007) 281–295.
- [65] M.A. Blount, A. Beasley, R. Zoraghi, K.R. Sekhar, E.P. Bessay, S.H. Francis, J.D. Corbin, Binding of tritiated sildenafil, tadalafil, or vardenafil to the phosphodiesterase-5 catalytic site displays potency, specificity, heterogeneity, and cGMP stimulation, *Mol. Pharmacol.* 66 (2004) 144–152.
- [66] H. Porst, G. Lunglmayr, Efficacy and tolerability of vardenafil within the time window of 6 hours after administration and beyond MMW *Fortschr. Med.* 147 (2005) 43.
- [67] C. Stief, H. Porst, I. Saenz De Tejada, E. Ulbrich, M. Beneke, Sustained efficacy and tolerability with vardenafil over 2 years of treatment in men with erectile dysfunction, *Int. J. Clin. Pract.* 58 (2004) 230–239.
- [68] H. van Ahlen, K. Wahle, W. Kupper, A. Yassin, T. Reblin, M. Neureither, Safety and efficacy of vardenafil, a selective phosphodiesterase 5 inhibitor, in patients with erectile dysfunction and arterial hypertension treated with multiple antihypertensives, *J. Sex. Med.* 2 (2005) 856–864.
- [69] U. Thadani, W. Smith, S. Nash, N. Bittar, S. Glasser, P. Narayan, R.A. Stein, S. Larkin, A. Mazzu, R. Tota, K. Pomerantz, P. Sundaresan, The effect of vardenafil, a potent and highly selective phosphodiesterase-5 inhibitor for the treatment of erectile dysfunction, on the cardiovascular response to exercise in patients with coronary artery disease, *J. Am. Coll. Cardiol.* 40 (2002) 2006–2012.
- [70] G. Corona, E. Razzoli, G. Forti, M. Maggi, The use of phosphodiesterase 5 inhibitors with concomitant medications, *J. Endocrinol. Invest.* 31 (2008) 799–808.
- [71] T. Reffellmann, R.A. Kloner, Sexual function in hypertensive patients receiving treatment, *Vasc. Health Risk Manag.* 2 (2006) 447–455.
- [72] G. Corona, N. Mondaini, A. Ungar, E. Razzoli, A. Rossi, F. Fusco, Phosphodiesterase type 5 (PDE5) inhibitors in erectile dysfunction: the proper drug for the proper patient, *J. Sex. Med.* 8 (2011) 3418–3432.
- [73] T. Klotz, R. Sachse, A. Heidrich, F. Jockenhovel, G. Rohde, G. Wensing, R. Horstmann, R. Engelmann, Vardenafil increases penile rigidity and tumescence in erectile dysfunction patients: a RigiScan and pharmacokinetic study, *World J. Urol.* 19 (2001) 32–39.
- [74] N. Mehrotra, M. Gupta, A. Kovar, B. Meibohm, The role of pharmacokinetics and pharmacodynamics in phosphodiesterase-5 inhibitor therapy, *Int. J. Impot. Res.* 19 (2007) 253–264.
- [75] C. Gingell, S.R. Sultana, M.B. Wulff, S. Gepi-Attee, Duration of action of sildenafil citrate in men with erectile dysfunction, *J. Sex. Med.* 1 (2004) 179–184.
- [76] H. Porst, H. Padma-Nathan, F. Giuliano, G. Anglin, L. Varanese, R. Rosen, Efficacy of tadalafil for the treatment of erectile dysfunction at 24 and 36 hours after dosing: a randomized controlled trial, *Urology* 62 (2003) 121–125, discussion 125–126.
- [77] S.H. Francis, J.D. Corbin, Molecular mechanisms and pharmacokinetics of phosphodiesterase-5 antagonists, *Curr. Urol. Rep.* 4 (2003) 457–465.
- [78] A.D. Seftel, Phosphodiesterase type 5 inhibitor differentiation based on selectivity, pharmacokinetic, and efficacy profiles, *Clin. Cardiol.* 27 (2004) 114–119.

# CUMULATIVE INDEX

Bold numerals refer to volume numbers.

## A

Acebutolol, **19**, 1  
Acetaminophen, **3**, 1; **14**, 551  
Acetazolamide, **22**, 1  
Acetohexamide, **1**, 1; **2**, 573; **21**, 1  
Acetylcholine chloride, **31**, 3, 21  
Acyclovir, **30**, 1  
Adenosine, **25**, 1  
Alendronate sodium, **38**, 1  
Allopurinol, **7**, 1  
Amantadine, **12**, 1  
Amikacin sulfate, **12**, 37  
Amiloride hydrochloride, **15**, 1  
Aminobenzoic acid, **22**, 33  
Aminogluthethimide, **15**, 35  
Aminophylline, **11**, 1  
Aminosalicylic acid, **10**, 1  
Amiodarone, **20**, 1  
Amitriptyline hydrochloride, **3**, 127  
Amlodipine besylate, **37**, 31  
Amobarbital, **19**, 27  
Amodiaquine hydrochloride, **21**, 43  
Amoxicillin, **7**, 19; **23**, 1  
Amphotericin B, **6**, 1; **7**, 502  
Ampicillin, **2**, 1; **4**, 518  
Apomorphine hydrochloride, **20**, 121  
Arginine, **27**, 1  
Aripiprazole, **38**, 35  
Ascorbic acid, **11**, 45  
Aspartame, **29**, 7  
Aspirin, **8**, 1  
Astemizole, **20**, 173  
Atenolol, **13**, 1  
Atorvastatin calcium, **35**, 1  
Atropine, **14**, 325  
Azathioprine, **10**, 29  
Azintamide, **18**, 1  
Azithromycin, **39**, 1  
Aztreonam, **17**, 1

## B

Bacitracin, **9**, 1  
Baclofen, **14**, 527

Benazepril hydrochloride, **31**, 117  
Bendroflumethiazide, **5**, 1; **6**, 597  
Benperidol, **14**, 245  
Benzocaine, **12**, 73  
Benzoic acid, **26**, 1  
Benzyl benzoate, **10**, 55  
Betamethasone dipropionate, **6**, 43  
Bretylum tosylate, **9**, 71  
Brinzolamide, **26**, 47  
Bromazepam, **16**, 1  
Bromcriptine methanesulfonate, **8**, 47  
Buclizine, **36**, 1  
Bumetanide, **22**, 107  
Bupivacaine, **19**, 59  
Busulphan, **16**, 53  
Butyl methoxy dibenzoylmethane, **38**, 87

## C

Caffeine, **15**, 71  
Calcitriol, **8**, 83  
Camphor, **13**, 27  
Candesartan cilexetil, **37**, 79  
Captopril, **11**, 79  
Carbamazepine, **9**, 87  
Carbenoxolone sodium, **24**, 1  
Carvedilol, **38**, 113  
Cefaclor, **9**, 107  
Cefamandole nafate, **9**, 125; **10**, 729  
Cefazolin, **4**, 1  
Cefdinir, **39**, 41  
Cefixime, **25**, 39  
Cefotaxime, **11**, 139  
Cefoxitin sodium, **11**, 169  
Ceftazidime, **19**, 95  
Ceftriaxone sodium, **30**, 21  
Cefuroxime sodium, **20**, 209  
Celiprolol hydrochloride, **20**, 237  
Cephalexin, **4**, 21  
Cephalothin sodium, **1**, 319  
Cephadrine, **5**, 21  
Chitin, **36**, 35  
Chloral hydrate, **2**, 85  
Chlorambucil, **16**, 85

Chloramphenicol, **4**, 47; **15**, 701  
Chlordiazepoxide, **1**, 15  
Chlordiazepoxide hydrochloride, **1**, 39;  
**4**, 518  
Chloropheniramine maleate, **7**, 43  
Chloroquine, **13**, 95  
Chloroquine phosphate, **5**, 61  
Chlorothiazide, **18**, 33  
Chlorpromazine, **26**, 97  
Chlorprothixene, **2**, 63  
Chlortetracycline hydrochloride, **8**, 101  
Chlorthalidone, **14**, 1  
Chlorzoxazone, **16**, 119  
Cholecalciferol, **13**, 655  
Cimetidine, **13**, 127; **17**, 797  
Ciprofloxacin, **31**, 163, 179, 209  
Cisplatin, **14**, 77; **15**, 796  
Citric Acid, **28**, 1  
Clarithromycin, **24**, 45  
Clidinium bromide, **2**, 145  
Clindamycin hydrochloride, **10**, 75  
Clioquinol, **18**, 57  
Clofazimine, **18**, 91; **21**, 75  
Clomiphene citrate, **25**, 85  
Clonazepam, **6**, 61  
Clonfibrate, **11**, 197  
Clonidine hydrochloride, **21**, 109  
Clopidogrel bisulfate, **35**, 71  
Clorazepate dipotassium, **4**, 91  
Clotrimazole, **11**, 225  
Cloxacillin sodium, **4**, 113  
Clozapine, **22**, 145  
Cocaine hydrochloride, **15**, 151  
Cocrystal Systems of Pharmaceutical  
Interest: 2007–2008, **35**, 373  
Cocrystal Systems of Pharmaceutical  
Interest: 2009, **36**, 361  
Codeine phosphate, **10**, 93  
Colchicine, **10**, 139  
Cortisone acetate, **26**, 167  
Creatine monohydrate, **34**, 1  
Crospovidone, **24**, 87  
Curcumin, **39**, 113  
Cyanocobalamin, **10**, 183  
Cyclandelate, **21**, 149  
Cyclizine, **6**, 83; **7**, 502  
Cyclobenzaprine hydrochloride, **17**, 41  
Cycloserine, **1**, 53; **18**, 567

Cyclosporine, **16**, 145  
Cyclothiazide, **1**, 65  
Cyproheptadine, **9**, 155  
Cytarabine, **34**, 37

## D

Dapsone, **5**, 87  
Dasatinib, **39**, 205  
Dexamethasone, **2**, 163; **4**, 519  
Diatrizoic acid, **4**, 137; **5**, 556  
Diazepam, **1**, 79; **4**, 518  
Dibenzepin hydrochloride, **9**, 181  
Dibucaine, **12**, 105  
Dibucaine hydrochloride, **12**, 105  
Diclofenac sodium, **19**, 123  
Didanosine, **22**, 185  
Diethylstilbestrol, **19**, 145  
Diflunisal, **14**, 491  
Digitoxin, **3**, 149; **9**, 207  
Dihydroergotoxine methanesulfonate, **7**, 81  
Diloxanide furoate, **26**, 247  
Diltiazem hydrochloride, **23**, 53  
Dioctyl sodium sulfosuccinate, **2**, 199;  
**12**, 713  
Diosgenin, **23**, 101  
Diperodon, **6**, 99  
Diphenhydramine hydrochloride, **3**, 173  
Diphenoxylate hydrochloride, **7**, 149  
Dipivefrin hydrochloride, **22**, 229  
Dipyridamole, **31**, 215  
Disopyramide phosphate, **13**, 183  
Direct Crystallization of Enantiomers and  
Dissociable Diastereomers, **36**, 331  
Disulfiram, **4**, 168  
Dobutamine hydrochloride, **8**, 139  
Donepezil, **35**, 117  
Dopamine hydrochloride, **11**, 257  
Dorzolamide hydrochloride, **26**, 283;  
**27**, 377  
Doxorubicine, **9**, 245  
Droperidol, **7**, 171

## E

Echothiophate iodide, **3**, 233  
Econazole nitrate, **23**, 127  
Edetic Acid (EDTA), **29**, 57  
Emetine hydrochloride, **10**, 289  
Enalapril maleate, **16**, 207

Ephedrine hydrochloride, **15**, 233  
Epinephrine, **7**, 193  
Ergonovine maleate, **11**, 273  
Ergotamine tartrate, **6**, 113  
Erthromycin, **8**, 159  
Erthromycin estolate, **1**, 101; **2**, 573  
Estradiol, **15**, 283  
Estradiol valerate, **4**, 192  
Estrone, **12**, 135  
Ethambutol hydrochloride, **7**, 231  
Ethynodiol diacetate, **3**, 253  
Etodolac, **29**, 105  
Etomidate, **12**, 191  
Etoposide, **18**, 121  
Eugenol, **29**, 149  
Ezetimibe, **36**, 103

## F

Famotidine, **34**, 115  
Fenoprofen calcium, **6**, 161  
Fenoterol hydrobromide, **27**, 33  
Flavoxate hydrochloride, **28**, 77  
Fexofenadine hydrochloride, **34**, 153  
Flecainide, **21**, 169  
Fluconazole, **27**, 67  
Flucytosine, **5**, 115  
Fludrocortisone acetate, **3**, 281  
Flufenamic acid, **11**, 313  
Fluorouracil, **2**, 221; **18**, 599  
Fluoxetine, **19**, 193  
Fluoxymesterone, **7**, 251  
Fluphenazine decanoate, **9**, 275; **10**, 730  
Fluphenazine enanthate, **2**, 245; **4**, 524  
Fluphenazine hydrochloride, **2**, 263; **4**, 519  
Flurazepam hydrochloride, **3**, 307  
Flurbiprofen, **37**, 113  
Flutamide, **27**, 115  
Fluvoxamine maleate, **24**, 165  
Folic acid, **19**, 221  
Furosemide, **18**, 153

## G

Gadoteridol, **24**, 209  
Gatifloxacin, **37**, 183  
Gefitinib, **39**, 239  
Gemifloxacin, **36**, 151  
Gentamicin sulfate, **9**, 295; **10**, 731  
Glafenine, **21**, 197

Glibenclamide, **10**, 337  
Glimepiride, **36**, 169  
Gluthethimide, **5**, 139  
Gramicidin, **8**, 179  
Griseofulvin, **8**, 219; **9**, 583  
Guaifenesin, **25**, 121  
Guanabenz acetate, **15**, 319  
Guar gum, **24**, 243

## H

Halcinonide, **8**, 251  
Haloperidol, **9**, 341  
Halothane, **1**, 119; **2**, 573; **14**, 597  
Heparin sodium, **12**, 215  
Heroin, **10**, 357  
Hexestrol, **11**, 347  
Hexetidine, **7**, 277  
Histamine, **27**, 159  
Homatropine hydrobromide, **16**, 245  
Hydralazine hydrochloride, **8**, 283  
Hydrochlorothiazide, **10**, 405  
Hydrocortisone, **12**, 277  
Hydroflumethazide, **7**, 297  
Hydroxyprogesterone caproate, **4**, 209  
Hydroxyzine dihydrochloride, **7**, 319  
Hyoscyamine, **23**, 155

## I

Ibuprofen, **27**, 265  
Imatinib mesylate, **39**, 265  
Imipramine hydrochloride, **14**, 37  
Impenem, **17**, 73  
Indapamide, **23**, 233  
Indinivar sulfate, **26**, 319  
Indomethacin, **13**, 211  
Iodamide, **15**, 337  
Iodipamide, **2**, 333  
Iodoxamic acid, **20**, 303  
Iopamidol, **17**, 115  
Iopanoic acid, **14**, 181  
Ipratropium bromide, **30**, 59  
Iproniazid phosphate, **20**, 337  
Isocarboxazid, **2**, 295  
Isoniazide, **6**, 183  
Isopropamide, **2**, 315; **12**, 721  
Isoproterenol, **14**, 391  
Isosorbide dinitrate, **4**, 225; **5**, 556

Isosuprine hydrochloride, **26**, 359  
Itraconazole, **34**, 193  
Ivermectin, **17**, 155

## K

Kanamycin sulfate, **6**, 259  
Ketamine, **6**, 297  
Ketoprofen, **10**, 443  
Ketotifen, **13**, 239  
Khellin, **9**, 371

## L

Lactic acid, **22**, 263  
Lactose, anhydrous, **20**, 369  
Lamotrigine, **37**, 245  
Lansoprazole, **28**, 117  
Leucovorin calcium, **8**, 315  
Levallorphan tartrate, **2**, 339  
Levarterenol bitartrate, **1**, 149; **2**, 573;  
**11**, 555  
Levodopa, **5**, 189  
Levothyroxine sodium, **5**, 225  
Lidocaine, **14**, 207; **15**, 761  
Lidocaine hydrochloride, **14**, 207; **15**, 761  
Lincomycin, **23**, 275  
Lisinopril, **21**, 233  
Lithium carbonate, **15**, 367  
Lobeline hydrochloride, **19**, 261  
Lomefloxacin, **23**, 327  
Lomustine, **19**, 315  
Loperamide hydrochloride, **19**, 341  
Lorazepam, **9**, 397  
Lornoxicam, **36**, 205  
Lovastatin, **21**, 277

## M

Mafenide acetate, **24**, 277  
Malic Acid, **28**, 153  
Magnesium Silicate, **36**, 241  
Maltodextrin, **24**, 307  
Mandelic Acid, **29**, 179  
Maprotiline hydrochloride, **15**, 393  
Mebendazole, **16**, 291  
Mebeverine hydrochloride, **25**, 165  
Mefenamic acid, **31**, 281  
Mefloquine hydrochloride, **14**, 157  
Melatonin: comprehensive profile, **38**, 159

Melphalan, **13**, 265  
Menadione, **38**, 227  
Meperidine hydrochloride, **1**, 175  
Meprobamate, **1**, 207; **4**, 520; **11**, 587  
Mercaptopurine, **7**, 343  
Mesalamine, **25**, 209; **27**, 379  
Mestranol, **11**, 375  
Metformin hydrochloride, **25**, 243  
Methadone hydrochloride, **3**, 365; **4**, 520;  
**9**, 601  
Methaqualone, **4**, 245  
Methimazole, **8**, 351  
Methixen hydrochloride, **22**, 317  
Methocarbamol, **23**, 377  
Methotrexate, **5**, 283  
Methoxamine hydrochloride, **20**, 399  
Methoxsalen, **9**, 427  
Methylclothiazide, **5**, 307  
Methylphenidate hydrochloride, **10**, 473  
Methypylon, **2**, 363  
Metipranolol, **19**, 367  
Metoclopramide hydrochloride, **16**, 327  
Metoprolol tartrate, **12**, 325  
Metronidazole, **5**, 327  
Mexiletine hydrochloride, **20**, 433  
Miconazole nitrate, **32**, 3  
Minocycline, **6**, 323  
Minoxidil, **17**, 185  
Mitomycin C, **16**, 361  
Mitoxanthrone hydrochloride, **17**, 221  
Morphine, **17**, 259  
Moxalactam disodium, **13**, 305  
Moxidectin, analytical profile, **38**, 315  
Moxifloxacin hydrochloride, **39**, 299

## N

Nabilone, **10**, 499  
Nadolol, **9**, 455; **10**, 732  
Nalidixic acid, **8**, 371  
Nalmefene hydrochloride, **24**, 351  
Nalorphine hydrobromide, **18**, 195  
Naloxone hydrochloride, **14**, 453  
Naphazoline hydrochloride, **21**, 307  
Naproxen, **21**, 345  
Natamycin, **10**, 513; **23**, 405  
Neomycin, **8**, 399  
Neostigmine, **16**, 403  
Niclosamide, **32**, 67

Nicotinamide, **20**, 475  
Nifedipine, **18**, 221  
Nimesulide, **28**, 197  
Nimodipine, **31**, 337, 355, 371  
Nitrazepam, **9**, 487  
Nitrofurantoin, **5**, 345  
Nitroglycerin, **9**, 519  
Nizatidine, **19**, 397  
Norethindrone, **4**, 268  
Norfloxacin, **20**, 557  
Norgestrel, **4**, 294  
Nortriptyline hydrochloride, **1**, 233;  
    **2**, 573  
Noscapine, **11**, 407  
Nystatin, **6**, 341

## O

Ofloxacin, **34**, 265  
Omeprazole, **35**, 151  
Ondansetron hydrochloride, **27**, 301  
Ornidazole, **30**, 123  
Oxamniquine, **20**, 601  
Oxazepam, **3**, 441  
Oxyphenbutazone, **13**, 333  
Oxytetracycline, **32**, 97  
Oxytocin, **10**, 563

## P

Paclitaxel, **34**, 299  
Pantoprazole, **29**, 213  
Papaverine hydrochloride, **17**, 367  
Parbendazole, **35**, 263  
Particle Size Distribution, **31**, 379  
Paroxetine hydrochloride, **38**, 367  
Paroxetine hydrochloride: polymorphs  
    and solvatomorphs, **38**, 407  
Penicillamine, **10**, 601; **32**, 119, 131, 149  
Penicillin-G, benzothine, **11**, 463  
Penicillin-G, potassium, **15**, 427  
Penicillin-V, **1**, 249; **17**, 677  
Pentazocine, **13**, 361  
Pentoxifylline, **25**, 295  
Pergolide Mesylate, **21**, 375  
Phenazopyridine hydrochloride, **3**, 465  
Phenelzine sulfate, **2**, 383  
Phenformin hydrochloride, **4**, 319; **5**, 429  
Phenobarbital, **7**, 359  
Phenolphthalein, **20**, 627

Phenoxymethyl penicillin potassium,  
    **1**, 249  
Phenylbutazone, **11**, 483  
Phenylephrine hydrochloride, **3**, 483  
Phenylpropanolamine hydrochloride, **12**,  
    357; **13**, 767  
Phenytoin, **13**, 417  
Physostigmine salicylate, **18**, 289  
Phytonadione, **17**, 449  
Pilocarpine, **12**, 385  
Pimozide, **37**, 287  
Piperazine estrone sulfate, **5**, 375  
Pirenzepine dihydrochloride, **16**, 445  
Piroxicam, **15**, 509  
Polymorphism 2004, **32**, 263  
Polythiazide, **20**, 665  
Polyvinyl alcohol, **24**, 397  
Polyvinylpyrrolidone, **22**, 555  
Povidone, **22**, 555  
Povidone-Iodine, **25**, 341  
Pralidoxine chloride, **17**, 533  
Pravastatin sodium, **39**, 433  
Praziquantel, **25**, 463  
Prazosin hydrochloride, **18**, 351  
Prednisolone, **21**, 415  
Primaquine diphosphate, **32**, 153  
Primidone, **2**, 409; **17**, 749  
Probenecid, **10**, 639  
Procainamide hydrochloride, **4**, 333;  
    **28**, 251  
Procaine hydrochloride, **26**, 395  
Procarbazine hydrochloride, **5**, 403  
Promethazine hydrochloride, **5**, 429  
Proparacaine hydrochloride, **6**, 423  
Propiomazine hydrochloride, **2**, 439  
Propoxyphene hydrochloride, **1**, 301;  
    **4**, 520; **6**, 598  
Propyl paraben, **30**, 235  
Propylthiouracil, **6**, 457  
Pseudoephedrine hydrochloride, **8**, 489  
Pyrazinamide, **12**, 433  
Pyridoxine hydrochloride, **13**, 447  
Pyrimethamine, **12**, 463

## Q

Quinidine sulfate, **12**, 483  
Quinine hydrochloride, **12**, 547

**R**

Ranitidine, **15**, 533  
Reserpine, **4**, 384; **5**, 557; **13**, 737  
Riboflavin, **19**, 429  
Rifampin, **5**, 467  
Risperidone, **37**, 313  
Rocuronium bromide, **35**, 285  
Rutin, **12**, 623

**S**

Saccharin, **13**, 487  
Salbutamol, **10**, 665  
Salicylamide, **13**, 521  
Salicylic acid, **23**, 427  
Scopolamine hydrobromide, **19**, 477  
Secobarbital sodium, **1**, 343  
Sertraline hydrochloride, **24**, 443  
Sertraline lactate, **30**, 185  
Sildenafil citrate, **27**, 339  
Silver sulfadiazine, **13**, 553  
Simvastatin, **22**, 359  
Sodium nitroprusside, **6**, 487; **15**, 781  
Sodium valproate, **32**, 209  
Solasodine, **24**, 487  
Sorbitol, **26**, 459  
Sotalol, **21**, 501  
Spironolactone, **4**, 431; **29**, 261  
Starch, **24**, 523  
Streptomycin, **16**, 507  
Strychnine, **15**, 563  
Succinylcholine chloride, **10**, 691  
Sucralose, **38**, 423  
Sulfacetamide, **23**, 477  
Sulfadiazine, **11**, 523  
Sulfadoxine, **17**, 571  
Sulfamethazine, **7**, 401  
Sulfamethoxazole, **2**, 467; **4**, 521  
Sulfasalazine, **5**, 515  
Sulfathiazole, **22**, 389  
Sulfisoxazole, **2**, 487  
Sulfoxone sodium, **19**, 553  
Sulindac, **13**, 573  
Sulphamerazine, **6**, 515  
Sulpiride, **17**, 607  
Sunitinib malate, **37**, 363

**T**

Tadalafil, **36**, 287  
Talc, **23**, 517  
Teniposide, **19**, 575  
Tenoxicam, **22**, 431  
Terazosin, **20**, 693  
Terbutaline sulfate, **19**, 601  
Terfenadine, **19**, 627  
Terpin hydrate, **14**, 273  
Testolactone, **5**, 533  
Testosterone enanthate, **4**, 452  
Tetracaine hydrochloride, **18**, 379  
Tetracycline hydrochloride, **13**, 597  
Theophylline, **4**, 466  
Thiabendazole, **16**, 611  
Thiamine hydrochloride, **18**, 413  
Thiamphenicol, **22**, 461  
Thiopental sodium, **21**, 535  
Thioridazine, **18**, 459  
Thioridazine hydrochloride, **18**, 459  
Thiostrepton, **7**, 423  
Thiothixene, **18**, 527  
Ticlopidine hydrochloride, **21**, 573  
Timolol maleate, **16**, 641  
Titanium dioxide, **21**, 659  
Tobramycin, **24**, 579  
 $\alpha$ -Tocopheryl acetate, **3**, 111  
Tolazamide, **22**, 489  
Tolbutamide, **3**, 513; **5**, 557; **13**, 719  
Tolnaftate, **23**, 549  
Tramadol hydrochloride, **38**, 463  
Tranlycypromine sulfate, **25**, 501  
Trazodone hydrochloride, **16**, 693  
Triamcinolone, **1**, 367; **2**, 571; **4**, 521; **11**, 593  
Triamcinolone acetonide, **1**, 397; **2**, 571; **4**, 521; **7**, 501; **11**, 615  
Triamcinolone diacetate, **1**, 423; **11**, 651  
Triamcinolone hexacetonide, **6**, 579  
Triamterene, **23**, 579  
Triclobisonium chloride, **2**, 507  
Trifluoperazine hydrochloride, **9**, 543  
Triflupromazine hydrochloride, **2**, 523; **4**, 521; **5**, 557  
Trimethaphan camsylate, **3**, 545

Trimethobenzamide hydrochloride,  
    **2**, 551  
Trimethoprim, **7**, 445  
Trimipramine maleate, **12**, 683  
Trioxsalen, **10**, 705  
Tripeleennamine hydrochloride, **14**, 107  
Triprolidine hydrochloride, **8**, 509  
Tropicamide, **3**, 565  
Tubocurarine chloride, **7**, 477  
Tybamate, **4**, 494

## V

Validation, Analytical Methods,  
    **37**, 439  
Validation, Chromatographic Methods,  
    **32**, 243  
Valproate sodium, **8**, 529  
Valproic acid, **8**, 529; **32**, 209  
Vardenafil dihydrochloride, **39**, 515  
Varenicline, **37**, 389  
Verapamil, **17**, 643  
Vidarabine, **15**, 647

Vigabatrin, **35**, 309  
Vinblastine sulfate, **1**, 443; **21**, 611  
Vincristine sulfate, **1**, 463; **22**, 517  
Vitamin D3, **13**, 655

## W

Warfarin, **14**, 423

## X

X-Ray Diffraction, **30**, 271  
Xylometazoline hydrochloride, **14**, 135

## Y

Yohimbine, **16**, 731

## Z

Zaleplon, **35**, 347  
Zidovudine, **20**, 729  
Zileuton, **25**, 535  
Zolpidem tartrate, **37**, 413  
Zomepirac sodium, **15**, 673